University of Southampton

Faculty of Environmental and Life Sciences

School of Biological sciences

Beyond the Synapse: Exploring CSPα's Role in Proteostasis, SNAP-25 Stability, and Cellular Differentiation in PC12 cells

by

Lucy Laura Scullard

ORCID ID 0000-0002-5423-5003

Thesis for the degree of Doctor of Philosophy

March 2026

University of Southampton

Abstract

Faculty of Environmental and Life Sciences

School of Biological Sciences

Thesis for the degree of Doctor of Philosophy

Beyond the Synapse: Exploring CSPα's Role in Proteostasis, SNAP-25 Stability, and Cellular Differentiation in PC12 cells

by

Lucy Laura Scullard

The Cysteine String Protein alpha (CSPα) is a presynaptic co-chaperone that is essential for the maintenance of synapses and for presynaptic proteostasis. CSPα, via its interactions with the Heat shock cognate 70 (Hsc70) and the Small Glutamate Tetrapeptide repeat protein (SGT) acts to maintain the conformation of client proteins, including key regulators of exo- and endocytic reactions, SNAP-25 and Dynamin-1. CSPα is described as having "antineurodegenerative properties" and has been implicated in a number of neurodegenerative disorders, including Alzheimer's, Parkinson's, Huntington's, and Motor neuron disease. CSPα -/- mice have a reduced life span and associated neurodegeneration and progressive loss of synapses. The CSPα -/- neurons have increased levels of misfolded proteins and ubiquitination.

Increased levels of ubiquitination and ubiquitin-induced degradation of SNAP-25 have been detected in CSPα -/- mice. There must be an E3 ligase responsible for the ubiquitination and associated degradation; as such, we planned to identify E3 ligases that interact with SNAP25 and have the potential to lead to its increased degradation in the absence of CSPα. As such, the first aim was to identify E3 ligases by a bioinformatics-based approach and use two biochemical approaches: a BioID proximity-dependent labelling protocol and Myc pull-down to identify potential E3 ligase-SNAP-25 interacting proteins. This approach evidenced known interactions with SNARE proteins and also showed a new interaction with E3-ligase Parkin. This interaction with SNAP-25 was independent of Parkin's E3 ligase activity, as an interaction between the Myc-BioID -SNAP-25 construct and both WT-HA-Parkin and the ligase-dead C431S-HA-Parkin was observed.

Secondly, CRISPR Cas was utilised to generate two independent CSPα-deficient PC12 cell lines, which were characterised with the aim of investigating SNAP-25-E3 ligase interactions in this context.

Before using these reagents, we observed that knockdown of CSPα led to hyperproliferation. This was associated with a loss of neurotrophin responsiveness and corresponding loss of differentiation ability and an alteration in the expression of Trk A and Trk B, the plasma membrane receptors for the neurotrophic factors NGF and BDNF. This unexpected consequence of CSPα was investigated using label-free whole-cell proteomics. This identified large-scale protein alterations between the parental and CSPα-deficient lines. The phenotypic and proteomic changes observed in the absence of CSPα provide insight into potential roles for CSPα beyond its neuronal chaperone function. They implicate an apparent critical role in cellular homeostasis that controls signalling and metabolic fluxes that regulate proliferation. My observation is consistent with an emerging nascent literature that describes clear potential for a role of this co-chaperone beyond the role of maintenance of proteostasis, supporting transmitter release in differentiated neurons.

Table of Contents

Table of Contents i
Table of Tables xii
Table of Figures xiv
Research Thesis: Declaration of Authorship 19
Acknowledgements 20

Definitions and Abbreviations 24
Chapter 1 Introduction 26
1.1 Protein homeostasis 26
1.2 Maintenance of synaptic structure and function 26
1.3 Issue of protein folding stability 27
1.4 Molecular chaperones and CO-chaperones 27
1.4.1 Classes of molecular chaperones involved in the vesicle cycle 28
1.5 Cysteine String Protein α (CSPα) 28
1.5.1 ATP cycle in the context of the CSPa-Hsc70 chaperone complex 30
1.5.2 CSPα mutation in humans 30
1.5.3 CSPα in neurodegeneration 31
1.5.4 CSPα in animal models 31
1.5.5 Known CSPα interactors and clients 33
1.5.6 Dyn-1 is a client of the CSPα chaperone complex 33
1.5.7 SNAP-25 is a client of the CSPα chaperone complex 34
1.5.8 Proteins affected by a lack of CSPα 34
1.5.9 Additional non-client- chaperone role of CSPα in neuronal cells 37
1.5.10 Effects of CSPα in non-neuronal cellular models 38
1.6 SNARE complexes 39
1.7 Synaptosome-associated protein 25 (SNAP-25) 41
1.7.1 SNAP-25 family 41
1.7.2 SNAP25 lifecycle 42
1.7.3 Additional roles of SNAP25's role at the pre-synapse 44
1.7.4 Roles of SNAP25's at the post-synapse 44
1.7.5 Association of SNAP-25 in neurological disorders 45
1.8 Ubiquitination and the ubiquitin-proteasome system 46

1.8.1 Components required for ubiquitination and the UPS 47
1.8.2 Diversity in ubiquitin modification code 47
1.8.3 Protein degradation by 26S proteasome 49
1.8.4 Alteration and dysregulation of ubiquitination in neurodegeneration and neurodevelopmental disorders 50
1.8.5 Synaptic ubiquitination 50
1.8.6 How hyper-ubiquitinated SNAP-25 can be used to discover ligases(s) responsible for ubiquitination at the pre-synapse 52
1.9 Aims 53

Chapter 2 Materials and Methods 54

2.1 Materials 54
2.2 Bioinformatics methods 54

2.2.1 Literature association bioinformatic approach to identify candidate SNAP-25 E3 ligases 55
2.2.2 BioGRID and Human E3 ubiquitin ligase database for the identification of SNAP-25- E3 ubiquitin ligase Interactors 55
2.2.3 PubMed database for the identification of E3 ligases that interact with SNAP25 56
2.2.4 Predictive bioinformatic approach to identify E3 ligases 57
2.2.5 Use of Ubi-Browser to predict E3 ligases that have the potential to interact with SNAP-25 57
2.2.6 Use of Human Protein Atlas to identify neuronal protein expression 58
2.2.7 Identification of E3 ligases that interact with proteins with structural similarity to SNAP-25 58
2.2.8 Disease association bioinformatic approach to support identified E3 ligases which may interact with SNAP-25 60
2.2.9 Interrogation of literature to identify proteomic screens of candidate E3 ligases 61
2.2.10 AlphaFold Multimer used for the prediction of interaction between SNAP-25 and Parkin 61

2.3 Molecular biology 62

2.3.1 Genomic DNA extraction from cells 62
2.3.2 RNA extraction from cells 62
2.3.3 RNA Quality Assessment 62
2.3.4 cDNA synthesis 63

2.3.5 Primer design for end-point cDNA and genomic PCR 64
2.3.6 End-point Polymerase Chain Reaction (PCR) 65
2.3.7 Polymerase chain reaction (PCR) for cDNA cloning. 66
2.3.8 Agarose gel electrophoresis 67
2.3.9 PCR/Gel Clean-up of amplified cDNA 67
2.3.10 Determining DNA concentration 67
2.3.11 Annealing of oligos 67
2.3.12 Restriction digest of DNA insert and plasmid backbone 68
2.3.13 Ligation reaction of the vector and insert 68
2.3.14 Bacterial Agar Plate Preparation 69
2.3.15 Bacterial transformation 69
2.3.16 Plasmid expression and mini-prep 70
2.3.17 Restriction digest screening 70
2.3.18 Generation of Myc BioID constructs 70
2.3.19 Generation of Myc-BioID-SNAP-25 71
2.3.20 Generation of Myr-Myc-BioID 72

2.4 Generation of reagents for CRISPR cell line generation 74

2.4.1 Designing sgRNAs for genetic knockdown in Cell lines 74
2.4.2 Cloning to generate Lenti CRISPR V1 plasmid containing sgRNA 74
2.4.3 Ligation and test digest of Lenti CRISPR V1 plasmid 75
2.4.4 Sequencing 77

2.5 Cell culture 77

2.5.1 Preparation of glass coverslips 77
2.5.2 Maintenance of HEK293FT Cells 77
2.5.3 PC12 cells maintenance 77
2.5.4 PC12 cells differentiation 78
2.5.5 Lipofectamine transfection of PC12 cells 78
2.5.6 Polyethyleneimine (PEI) Transfection of HEK293FT cells 79
2.5.7 MG-132 proteasome blocking 79
2.5.8 Generation of CSPα Knockdown cells PC12 cells 79
2.5.9 Cell proliferation assay 80

2.6 Imaging and Microscopy 80

2.6.1 Plating cells for Immunocytochemistry of immortal cell lines 80
2.6.2 Plasma membrane staining of cells 81

2.6.3 Fixing and immunocytochemistry staining of immortal cell lines 81
2.6.4 Fluorescence microscopy 82
2.6.5 Image analysis 82
2.7 Protein preparation and analysis 83
2.7.1 Preparation of Cell lysate from immortal cells 83
2.7.2 Homogenisation of CSPα brain tissue 83
2.7.3 Protein assay 83
2.7.4 Sample preparation for SDS PAGE 83
2.7.5 SDS-polyacrylamide gel electrophoresis (SDS-PAGE) 84
2.7.6 Coomassie gel staining 84
2.7.7 Electroblotting of proteins to nitrocellulose membrane.....85
2.7.8 Immunolabelling of transferred proteins 85
2.7.9 Detection of Biotin on proteins transferred to nitrocellulose 86
2.7.10 Analysis of immunoblotting of proteins 90
2.7.11 Streptavidin pull-down and Myc-Immunoprecipitation 90
2.7.12 HEK293FT and PC12 streptavidin pull-down with Myc BioID constructs. 90
2.7.13 PC12 Myc Immunoprecipitation with Myc BioID constructs 90
2.8 Cell maintenance and preparation for Mass spectroscopy 91
2.8.1 Protein extraction from cells to generate samples for Mass spectroscopy..91
2.8.2 Preparation of protein sample for mass spectroscopy 92
2.8.3 In solution digestion sample preparation for Mass spectroscopy 93
2.8.4 Separation of samples for mass spectroscopy 93
2.8.5 Mass spectroscopy analysis of parental and CSPα-deficient cell lines.....94
2.8.6 Proteomic Data Analysis 96
2.8.6.1 PEAK studio label-free quantification parameters and statistics 96
2.8.7 Differential Protein Expression 97
2.8.7.1 Determining vector ratio distribution to set fold change of relative abundance 98
2.8.7.2 Retention time m/z shift distribution 98
2.8.8 Missing values and ID-transfer 99
2.8.9 Data visualisation and summary 100
2.9 GO term and Pathway analysis of proteomic data 101

2.9.1 PANTHER Overrepresentation Test for enrichment of GO biological processes 101

2.9.2 STRING database used to annotate the pathways altered in CSPα knockdown PC12 cells as determined by proteomic mass spectroscopy.....103

2.9.3 Use of SYNGO to determine changes in synaptic proteins in the proteomic readout of CSPα knock-out PC12 cells 103

Chapter 3 A bioinformatics approach to identify candidate E3-ubiquitin ligases for SNAP-25 105

3.1 Introduction 105

3.1.1 SNAP-25 ubiquitination and turnover 105

3.1.2 SNAP-25 lysine residues that support ubiquitination 105

3.2 E3 ligases in neurons.....106

3.2.1 E3 ubiquitin ligase classes 107

3.2.2 RING family of E3 ligases 107

3.2.3 HECT family of E3 ligases 108

3.2.4 RBR family of E3 ligases 109

3.2.5 RING-Cys-Relay (RCR) family 109

3.2.6 Known ubiquitination of SNAP-25 109

3.3 Aims 110

3.4 Results 110

3.4.1 Literature-based approach to identify E3 ubiquitin ligases that may interact with SNAP-25 110

3.4.1.1 BioGRID search for the identification of SNAP-25 E3 ligase candidates 111

3.4.1.2 PubMed search for the identification of SNAP-25 E3 ligase candidates 111

3.4.2 Predictive approach 112

3.4.2.1 Motifs for interaction with ubiquitin. 113

3.4.2.2 Ubibrowser: A bioinformatics platform for investigation into the human E3 ubiquitin ligase-substrate interaction network 114

3.4.2.3 Testing ubibrowser 1.0 and 2.0 for known synaptic E3 ligase-substrate interactions 114

3.4.2.4 E3 ligases which have been predictive to interact with SNAP-25 based on specific domains and motifs using Ubibrowser 115

3.4.2.5 E3 ligases identified by Ubibrowser 1.0 filtering 116

3.4.2.6 E3 ligases identified by Ubibrowser 2.0 filtering 116
3.4.2.7 Mapping of Ubibrowser predicted E3 ligase candidates on SNAP-25 sequence 117
3.4.2.8 E3 ligases that interact with SNAP family proteins 119
3.4.2.9 Sequence identity between SNAP family proteins 119
3.4.2.10 Identification of E3 ligases known to interact with SNAP family proteins 121
3.4.2.11 Filtering of E3 ligases identified to interact with SNAP family proteins 121
3.4.2.12 Identification of E3 ligase interaction domains and motifs in SNAP-family proteins 122
3.4.2.13 E3 ligases identified to be of interest from the predictive approach 124
3.4.2.14 E3 ligases with disease-related support for interaction with SNAP-25 124
3.4.3 Screens of E3 ligases of interest 124
3.5 Discussion 129
3.5.1 Discussion high-priority E3 ligases 130
3.5.1.1 TRIM9 was identified as an interacting partner of SNAP-25 130
3.5.1.2 FBX07 identified as an interacting partner of SNAP-25 131
3.5.1.3 Parkin is a promising candidate to interact with SNAP-25 133
3.5.2 E3 ligases to test with a medium priority 134
3.5.3 E3 ligases to test with a lower priority 135
3.5.4 Limitations of methods and databases used 135
3.5.4.1 Algorithm mismatching prediction and data. 135
3.5.4.2 Unutilised bioinformatics resources 135
3.5.4.3 E3 ligases that would be included retrospectively 136
3.6 Summary 137
Chapter 4 Investigating the validity of predicted SNAP-25-interacting E3 ligase candidates in cellular models HEK293FT and PC12 138
4.1 Introduction 138
4.1.1 Detecting protein-protein interactions 138

4.1.2 Proximity-dependent biotin identification (BioID) to identify protein-protein interactions 138
4.1.3 Development of BioID 139
4.1.4 Limitations of BioID 139
4.1.5 Using protein-protein interaction detection techniques in parallel 140
4.2 Aims 140
4.3 Methods 140
4.3.1 Designing experimental controls 140
4.4 Results 141
4.4.1 PC12 cells as a model for the identification of synaptic E3 ligases 141
4.4.2 Expression of key synaptic proteins across PC12 differentiation.....141
4.4.3 Confirmation of expression of BioID Constructs in HEK293FT 145
4.4.4 Localisation of recombinantly expressed BioID constructs in HEK293FT cells 147
4.4.5 Localisation of recombinantly expressed Myc-BioID constructs in PC12 cells 148
4.4.6 Biotinylation by Myc-BioID constructs in HEK293FT cells. 149
4.4.7 Optimisation of biotinylation timings 151
4.4.8 Pull down in HEK293FT cells as a proof of concept. 151
4.4.9 BioID pull-downs in PC12 cells using Myc-BioID-SNAP-25 as bait 154
4.4.10 Identification of proximity between SNAP-25 and established binding partners 156
4.4.11 Investigation candidate E3 ligases interaction with SNAP-25 by proximity labelling.....157
4.4.12 Investigation into the specificity of Myc-BioID-SNAP-25 proximity labelling of Parkin 158
4.4.13 BioID proximity labelling of HA Wild-Type and mutant C431S Parkin 159
4.4.14 Myc Pulldowns to identify direct interaction of Myc BioID SNAP-25 160
4.4.15 Investigation into if candidate E3 ligases immunoprecipitated with SNAP-25 162
4.5 Discussion.....165
4.5.1 E3 ligases identified by bioinformatic approaches tested for interaction with SNAP-25 165
4.5.2 Myc BioID constructs were generated and expressed in HEK293FT and PC12 cells 165

4.5.3 Myc-BioID-SNAP-25 bound to known interactors but not TRIM9 and FBXO7 165
4.5.4 BioID used to identify proximity between Myc BioID SNAP-25 and E3 ligase Parkin 166
4.5.5 Bioinformatic support for an interaction between Parkin and SNAP-25 ...167
4.5.6 Literature Support for an Interaction between SNAP-25 and Parkin 168
4.5.7 Potential non E3 ligase-substrate roles of a SNAP-25 – Parkin interaction..169
4.6 Summary 170

Chapter 5 Generation of a CRISPR CSPα Deficient PC12 Model 171

5.1 Introduction 171

5.1.1 Using CRISPR-Cas technology 171
5.1.2 Using CRISPR-Cas technology to generate knockout cell lines 172
5.1.3 Identifying CRISPR knockdowns 173
5.1.4 Using PC12 cells to study neuronal proteins 173
5.1.5 Trk Neurotrophins and the Epidermal Growth Factor Receptors 173
5.1.6 Label-free proteomics to investigate changes in protein expression 174

5.2 Aims 176

5.3 Results 176

5.3.1 Identification of alteration of protein levels of CSPα in PC12 lines transfected with sgRNAs targeting CSPα 176
5.3.2 Molecular description of CRISPR genomic disruption in CSPα-deficient lines.....177
5.3.3 Phenotypic changes in CSPα-deficient cells 179
5.3.3.1 Detailing the Alterations in the growth rate of CSPα-deficient cells 179
5.3.3.2 CSPα-deficient lines don't differentiate in the presence of NGF or BDNF 181
5.3.4 Neurotrophin receptor expression in CSPα knockdown models 183
5.3.4.1 Investigating expression of neurotrophins in CSPα -/- mouse forebrain tissue 183
5.3.5 Alteration of neuronal CSPα clients SNAP-25 and Dyn-1 in the CSPα-deficient cells 184
5.3.5.1 Immunodetection of CSPα clients in CSPα-deficient cells 184

5.3.5.2 Immunostaining of SNAP-25 in CSPα-deficient cells 187
5.3.5.3 Investigation into turnover of SNAP-25 in CSPα deficient cells 188
5.3.6 Preliminary investigation into alternative protein removal pathways 189
5.3.7 Evidence of proteomic disorder in the CSPα-deficient cells 190
5.3.8 Label-free proteomics to determine global changes in the CSPα-deficient cell lines 192
5.3.8.1 Quantification and visualisation of Mass spectroscopy proteomic data 193
5.3.8.2 Statistical significance of quantified protein alterations 194
5.3.9 Investigation into GO term enrichment of up- and down-regulated proteins in CSPα-deficient PC12 cells.....196
5.3.10 Pathway analysis of proteomic changes in CSPα-deficient cells 200
5.3.10.1 Pathway analysis of downregulated proteins 201
5.3.10.2 Pathway analysis of upregulated proteins 203
5.3.10.3 Verification of the reported downregulated protein 206
5.3.10.4 Verification of the reported upregulated proteins 207
5.4 Discussion.....209
5.4.1 Summary 209
5.4.2 Observed changes in phenotype in CSPα-deficient PC12 cells 209
5.4.2.1 Alteration in Trk and EGF receptor expression in CSPα models 210
5.4.2.2 Loss of HSP40 proteins affecting the stability of other proteins 210
5.4.2.3 CSPα's role in cellular proliferation 210
5.4.3 Proteomic investigation into the result of a knockdown of CSPα in the PC12 cells 211
5.4.3.1 Scale protein changes in CSPα deficiency determined by label-free Proteomics.....212
5.4.3.2 Comparison of proteomic readout with previous CSPα knockout Studies.....212
5.4.3.3 GO term and pathway analysis of up and downregulated proteins in the CSPα-deficient cells relating to an increase in proliferation 213
5.5 Future work 213
Chapter 6 General discussion and future directions 214
6.1 Summary of findings 214

6.2 Investigation into candidate E3 ubiquitin ligases suggests an E3 ligase independent interaction between SNAP-25 and Parkin 215

6.2.1 SNAP-25 and Parkin may interact in an E3 ligase-independent fashion 215

6.2.2 Functional implications of a Parkin-SNAP-25 interaction 218

6.2.3 Additional E3 ligases with the potential to ubiquitinate SNAP-25 218

6.3 Consequences of an absence of CSPα in PC12 cells 219

6.3.1 Alterations in several proteins lead to loss of PC12 differentiation 219

6.3.2 Could loss of differentiation ability in the CSPα-deficient PC12 cells be due to a loss of SNAP-25 221

6.4 Cell-type-specific function of CSPα.....223

6.4.1 A potential model of CSPα-deficiency in PC12 cells 225

6.4.2 Evidence of proteasomal disorder in the CSPα-deficient cell lines suggestive of cellular stress 225

6.5 Future Work.....225

6.5.1 Characterisation of SNAP-25- E3 ligase Parkin interaction 225

6.5.2 CSPα deficiency directs cell phenotype 226

6.6 Summary and Overall Conclusions 227

Appendix A Bioinformatics data 229

A.1 Identification of E3 ligases that interact with SNAP-25 from the literature-based approach 229

Appendix B :BioID development and cloning of constructs 241

B.1.1 Investigating if Myc-BioID-SNAP-25 can form a SNARE complex. 241

B.1.2 Time dependence of cellular biotinylation across varying incubation times.243

B.1.3 Patterns of biotinylation in proteins extracted from Myc-BioID-transfected cells reveal construct-selective biotinylation 244

B.1.4 Probing pull-down samples for known interactors of SNAP-25; TRIM9.....245

B.1.5 Setting up BioID for SNAP-25 in PC12 cells 247

B.1.6 Secondary only staining of Myc immunoprecipitations 248

Appendix C : Generation of CSPα-deficient PC12 cells 249

C.1 Genomic sequencing attempts.....249

C.2 CD3 cDNA sequencing example 251

C.3 Preliminary investigation into alternative protein disposal pathways 251

C.4 Quantification of protein altered in the cellular lysates submitted for label-free proteomics 252
C.5 Alterations in the expression of neuronal-associated proteins 253
C.6 Label-free proteomic readout 255
Bibliography 266

Table of Tables

Table 1.1: CSPα -/- models……...36

Table 1.2: Proteins with decreased expression levels in CSPα knock-out synapses..39

Table 1.3: Selected ubiquitination identified at the specific subcellular neuronal compartments……..55

Table 2.1: Databases used for the identification of E3 ubiquitin ligases that interact with SNAP-25 via the literature-based searches.……..60

Table 2.2: Databases used for the identification of E3 ubiquitin ligases that interact with SNAP-25 via structure-based searches……..63

Table 2.3: Additional Databases used for the identification of E3 ubiquitin ligases that interact with SNAP-25 via disease association-based searches.……65

Table 2.4: Components and Volumes required for reverse transcription……..67

Table 2.5: Conditions required for reverse transcription using thermocycler ……..68

Table 2.6: Primer pairs for end-point identification PCR experiments for murine samples and PC12 samples……..69

Table 2.7: Components and volumes of reagents used in end-point PCR reactions……70

Table 2.8. Conditions for RED TAQ PCR reactions.……70

Table 2.9: Volumes of reagents used for PCR reaction to generate inserts for molecular cloning……..70

Table 2.10: Conditions used for PCR reaction when using Q5 polymerase……..71

Table 2.11: Components required for the annealing and phosphorylation of oligos….72

Table 2.12: Reagents and volumes used for restriction digest reactions……73

Table 2.13: Components required for ligation reaction of vector and insert……..…73

Table 2.14: Primers and restriction enzymes used to generate Bio-ID reagents……75

Table 2.15: Guide RNA used for the generation of CSPα knockout PC12 cells……79

Table 2.16: Cell plating format and lipofectamine transfection reagent quantities……83

Table 2.17: cDNA plasmids used for transfection of PC12 cell cultures……..84

Table 2.18: WGA conjugates used for binding to cell surface sugars.……..86

Table 2.19: Primary antibodies used for immunostaining……87

Table 2.20: Secondary antibodies and fluorophore conjugates……87

Table 2.21: Components of the SDS-PAGE gels used for running protein samples……89

Table 2.22: Antibody table used for Western blotting ……92

Table 2.23: Secondary antibodies and dyes used for Western blotting……95

Table 2.24: Parameters used in PEAKS for quantification of proteins identified in label-free mass spectrometry.……102

Table 3.1: Examples of ubiquitination events identified in specific neuronal compartments……112

Table 3.2: Subfamily and example members of the HECT E3 ligase family……114

Table 3.3: The literature approach led to the identification of two proteins known to be binding partners of, or part of a SNAP-25 containing protein complex……117

Table 3.4: E3 ubiquitin ligases with motifs they recognise in substrate proteins……120

Table 3.5: E3 ligases predicted to interact with SNAP-25 by ubibrowser and be localised to human brain regions.……123

Table 3.6: E3 ligases identified by BioGrid which have been shown to interact with SNAP proteins which have structural homology with SNAP-25.……128

Table 3.7: Identified interactions screens undertaken in the literature……132

Table 3.8: Bioinformatic protein-protein interaction identification tools……144

Table 5.1: Description of observed differentials between Parental and PC12 CSPα deficit CD3 and CD5 cells lysis run on a Coomassie gel.……200

Table 5.2: Selected GO terms investigated due to the changes in phenotype observed in the CSPα-deficient lines……205

Table 5.3: PANTHER Overrepresentation for enrichment of GO biological processes..206

Table 6.1: Canonical and ubiquitin-independent functions of E3-ubiquin ligases……230

Table 6.2: PC12 knockdown lines which have lost the ability of differentiate in response to NGF……234

Table of Figures

Figure 1.1: Structure of mammalian CSPα. ……33

Figure 1.2: CSPα's known interacting clients at the presynaptic membrane……37

Figure 1.3: CSPα non-client- chaperone role in neuronal cells……42

Figure 1.4: SNARE complex formation……44

Figure 1.5: Structure of vertebrate SNAP-25 protein family members……46

Figure 1.6: SNAP-25 life cycle……47

Figure 1.7: SNAP-25 function at the pre- and post-synapse……49

Figure 1.8: Schematic depicting the changes in SNAP-25 expression identified in neurological diseases and disorders……50

Figure 1.9: Ubiquitination pathway……51

Figure 1.10: Examples of consequences of ubiquitination……53

Figure 1.11: The effect the presence and absence of CSPα has on SNAP-2 ubiquitination and subsequent degradation……56

Figure 2.1: Bioinformatics workflow to identify candidate SNAP-25 E3 ligases..58

Figure 2.2: BioGrid load-up page ……59

Figure 2.3: Ubibrowser look-up pages for iterations 1.0 and 2.0 for the prediction of E3 ligase–substrate interactions ……62

Figure 2.4: RNA Quality Assessment……67

Figure 2.5: Generation of the p-MycBioIDSNAP-25 plasmid via cloning of the SNAP-25 insert from PRSF vector backbone into the Myc-BioID vector……76

Figure 2.6: Molecular cloning of the Myc-Myr-BioID construct. ……78

Figure 2.7: Position of guide RNA in the context of the CSP gene and encoded protein. ……80

Figure 2.8: *Generation of the Lenti* CRISPR *P-vectors* plasmid. ……81

Figure 2.9: Identification of CSPα knockdown ……85

Figure 2.10: SDS-PAGE gel-nitrocellulose transfer sandwich.……91

Figure 2.11: Schematic depicting the extraction and preparation of cells for label-free mass spectroscopy……98

Figure 2.12: The Soluble fraction from the cell lysate submitted for mass

spectroscopy was a good representation of total protein……99

Figure 2.13: Sequential steps in the process by which data from mass-spectroscopy spectra features is used to identify peptides ……101

Figure 2.14: The distribution of feature vector ratio……104

Figure 2.15: (A) RT shift distribution; (B) M/Z shift distribution.……104

Figure 2.16: Percentage of missing values in each sample with or without ID transfer.105

Figure 2.17: Summary information of an identified protein altered from label-free mass spectroscopy……107

Figure 2.18: PANTHER upload page for PANTHER overrepresentation Test for enrichment of GO terms for biological processes using Fisher's exact test. ……108

Figure 2.19: STRING load up page ……109

Figure 2.20: SYNGO load-up page ……110

Figure 3.1: SNAP-25 sequence with likely ubiquitination sites highlighted……111

Figure 3.2: E3 ligase classes, structures and archetypical ubiquitination reaction……113

Figure 3.3: Workflow of the literature-based approach ……116

Figure 3.4: Workflow for predictive pathway to investigate E3 ligases that can interact and ubiquitinate SNAP-25……119

Figure 3.5: E3 ligases which are predicted to interact with SNAP-25 ……122

Figure 3.6: Filtering approach applied to E3 ligases predicted to interact with SNAP-25 by ubibrowser 1.0……123

Figure 3.7: SNAP-25 amino acid sequence with inferred recognition domains and motifs of E3 ligases predicted by Ubibrowser 1.0 and 2.0……125

Figure 3.8: Sequence alignment and structural homology of the SNAP family SNARE proteins……128

Figure 3.9: SNAP family members amino acid sequences; SNAP-23, SNAP-29 and SNAP-47……128

Figure 3.10: Summary of E3 ligases with the potential to interact with and ubiquitinate SNAP-25……137

Figure 3.11: Protein ubiquitination pathway for TRIM9……138

Figure 3.12: Features of SNAP-25 structure……139

Figure 3.13: Protein ubiquitination pathway for FBXO7 in SCF complex, ……140

Figure 3.14: Protein ubiquitination pathway for Parkin…… 142

Figure 3.15: Schematic of potential SNAP-25- E3 ligase pre-synaptic interaction subcellular localisations……..145

Figure 4.1: Schematic depicting the Myc BioID constructs ……..149

Figure 4.2: Relative Expression of key synaptic proteins and E3 ligases across PC12 differentiation time points……151

Figure 4.3: Quantification of selected protein expression across NGF-induced differentiation in PC12 cells.……..152

Figure 4.4: Recombinant expression of Myc-BioID constructs in HEK293FT cells ……...154

Figure 4.5: Immunofluorescence of HEK293 FT cells transfected with Myc-BioID- SNAP25 Myc-BioID and Myr-Myc-BioID constructs……156

Figure 4.6: Immunolocalisation of Myc-BioID construct expression in PC12 cells……..157

Figure 4.7: Immunocytochemical localisation of BioID-generated biotinylation in cells transfected with Myc-tagged BioID constructs. ……158

Figure 4.8: Streptavidin pull-down of Myc BioID constructs and biotinylated proteins in HEK293FT cells……160

Figure 4.9: Streptavidin pull-down of Myc BioID constructs and biotinylated proteins in PC12 cells……..163

Figure 4.10: Known SNAP-25 interacting proteins are BioID proximity-labelled in PC12 cells using Myc-BioID-SNAP-25 as bait.……..165

Figure 4.11: The E3 ligase Parkin shows BioID proximity-dependent labelling in PC12 cells transfected with Myc-BioID-SNAP-25 bait.……..166

Figure 4.12: Syntaxin and Parkin are selectively Biotinylated by Myc BioID SNAP-25 ….167

Figure 4.13: Parkin is selectively pulled down by Myc-BioID-SNAP-25 in an E3 ligase-independent manner. ……..168

Figure 4.14: Immunoprecipitation of Myc-BioID constructs in PC12 cells……169

Figure 4.15: Investigating established SNAP-25 interacting partners via immunoprecipitation of Myc BioID SNAP-25 from PC12 cell lysates.……170

Figure 4.16: Investigating candidate SNAP-25 interacting partners in PC12 cells via immunoprecipitation of Myc BioID SNAP-25.……171

Figure 4.17: Syntaxin and Parkin association with Myc-BioID-SNAP-25……172

Figure 4.18: AlphaFold prediction of Parkin-SNAP-25 interaction with Parkin's linker region……176

Figure 5.1: General approach of Label-free quantitative proteomics……183

Figure 5.2: PC12 cells transfected with Lenti CRISPR plasmids containing guides sgRNA_3 and sgRNA_5 led to a knockdown in CSPα.……185

Figure 5.3: Determining the molecular events that generated CSPα-deficient lines....187

Figure 5.4: PC12 CSPα-deficient CD3 and CD5 cells proliferate more quickly than the Parental line ……188

Figure 5.5: PC12 CSPα-deficient CD3 and CD5 cells fail to show signature differentiation in response to NGF ……190

Figure 5.6: TRK and EGF receptor levels are altered in PC12 CSPα-deficient CD3 and CD5 cells ……192

Figure 5.7: CSPα-deficient lines have a selective reduction of CSPα clients……..193

Figure 5.8: CRISPR CSPα-deficient PC12 cell lines have a reduction of CSPα client SNAP-25……195

Figure 5.9: Blocking the Proteasome does not restore SNAP-25 protein levels in PC12 CSPα-deficit CD3 and CD5 cells ……197

Figure 5.10: Investigation of global protein expression and relative ubiquitination in the PC12 CSPα-deficient CD3 and CD5 cells……199

Figure 5.11: Quantitative mass spectroscopy profiling of PC12 parental and PC12 CSPα deficit CD3 and CD5 cells……202

Figure 5.12: CRISPR Cas knockout of CSPα leads to alteration of the expression of a large number of proteins……204

Figure 5.13: STRING clustering of down-regulated alterations between Parental and PC12 CSPα-deficit CD3 and CD5 cells ……213

Figure 5.14: STRING clustering of up-regulated alterations between Parental and PC12 CSPα deficit CD3 and CD5 cells ……216

Figure 5.15: Validation of proteins downregulated due to the CSPα CRISPR knockdown in the PC12 cells determined by Mass spectroscopy ……219

Figure 5.16: Validation of proteins upregulated due to the CSPα CRISPR knockdown in the PC12 cells determined by Mass spectroscopy ……220

Figure 5.17: Both CD3 and CD5 SNAP-25 sequences align to RAT SNAP-25……221

Figure 6.1: Parkin protein domain structure with location of known interactions and functions……229

Figure 6.2: The role of dysfunctional mitophagy at the presynapse in neurodegenerative disease……..232

Figure 6.3: Roles of CSPα in neuronal post-mitotic cell models ……238

Figure 6.4: Roles of CSPα in non-neuronal pre-mitotic cell lines ……239

Research Thesis: Declaration of Authorship

Print name: Lucy Laura Scullard

Title of thesis: Beyond the Synapse: Exploring CSPα's Role in Proteostasis, SNAP-25 Stability, and Cellular Differentiation in PC12 cells.

I declare that this thesis and the work presented in it are my own and has been generated by me as the result of my own original research.

I confirm that:

1. This work was done wholly or mainly while in candidature for a research degree at this University;
2. Where any part of this thesis has previously been submitted for a degree or any other qualification at this University or any other institution, this has been clearly stated;
3. Where I have consulted the published work of others, this is always clearly attributed;
4. Where I have quoted from the work of others, the source is always given. With the exception of such quotations, this thesis is entirely my own work;
5. I have acknowledged all main sources of help;
6. Where the thesis is based on work done by myself jointly with others, I have made clear exactly what was done by others and what I have contributed myself;
7. None of this work has been published before submission

Signature: ..... Date: .....

Acknowledgements

Firstly, I would like to express my thanks to my supervisors, Prof Vincent O'connor and Prof Katrin Deinhardt, for their guidance, patience and mentorship. I would also like to thank all members of the Worm and Cellneuro bio labs for their help and encouragement.

I am very grateful to the Gerald Kerkut Charitable Trust for their financial support and the opportunities to present and discuss my work.

I would also like to thank Dr David Tumbarello and Prof Nullin Divecha for their generous gifts of plasmids and valuable scientific input. In addition, I would also like to thank Prof Paul Skipp, for his help with proteomics and Dr Kif Liakath-Ail for his discussion of proteomic data.

Finally, a thank you to Andrew, my parents, grandmothers and Julie, who, without their ongoing support, I would not be where I am today and finally to my two grandads, whilst not here today, always provided encouragement and always reminded me to always just try my best.

Definitions and Abbreviations

AD	Alzheimer's disease
ADHD	Attention-deficit hyperactivity disorder
ADNCL	Adult neuronal ceroid lipofuscinosis
ADP	Adenosine diphosphate
ALS	Amyotrophic lateral sclerosis
AS	Angelman syndrome
ATP	Adenosine triphosphate
BDNF	Brain-derived neurotrophic factor
BFA	Brefeldin A
BLAST	Basic Local Alignment Search Tool
BRF	Biomedical Research Facility
BSA	Bovine serum albumin
CD3	CSPα-deficient PC12 Exon 3
CD5	CSPα-deficient PC12 Exon 5
CSF	Cerebrospinal fluid
CSPα	Cysteine string protein alpha
DIV	Days *in vitro*
DLB	Dementia with Lewy bodies
dNTPs DPBS	Deoxynucleoside triphosphates
DUBs	Dulbecco's Phosphate Buffered Saline
DYN-1	Deubiquitinases
E15	Dynamin-1
EDTA	Embryonic day 15
FDR	Ethylenediaminetetraacetic acid
GAPDH	False-discovery rate
GFP	Glyceraldehyde 3-phosphate dehydrogenase
GluK5-KAR	Green fluorescent protein kainite-type
GM130	glutamate receptor 5
GST	Golgi membrane 130
GTP	Glutathione S-transferase
GDP	Guanosine-5'-triphosphate
GWAS	Genome-wide association studies
HECT	Homologous to E6AP C-terminus (HECT)-type E3 ubiquitin
HEPES	(4-(2-hydroxyethyl)-1-piperazineethanesulfonic acid)
HS	House serum
HSC70	Heat shock cognate 70
HSPs	Heat shock proteins
HSP70	Heat shock protein 70
INSOL	Triton-x-100 insoluble fraction
ISR	Integrated Stress Response
KD	Knock down
KO	Knock Out
LAMP1	Lysosomal-associated membrane protein 1
LC-MS LC-3	Liquid chromatography- mass spectroscopy Microtubule-
mRNA NEB	associated protein 1A/1B-light chain 3
	Messager Ribonucleic acid
	New England Biolabs

NEDD	Neural precursor cell expressed developmentally down-regulated protein
NGS	Next generation sequencing
np-40	nonyl phenoxypolyethoxylethanol -40
NSF	N-ethylmaleimide-sensitive fusion
MS	Mass spectroscopy
OUT	Ovarian tumour proteases
P1	Pellet 1 a nuclear pellet that is separated from a Homogenate by centrifugation
P2	Pellet 2 a crude synaptosomal fraction that contains intact plasma membrane profiles
P15	Postnatal day 15
PAM	Protospacer adject motif
PCR	Polymerase chain reaction
PD	Parkinson's disease
PDL	Poly-D-lysine
PEI	Polyethylenimine
PKA	Protein kinase A
PKC	Protein kinase C
PMSF	Phenylmethylsulfonyl fluoride
polyQ	Polyglutamine
PSD95	Postsynaptic density 95
PTM	Post-translational modification
pTM	Predicted template modelling
RBR	RING-IBR-RING E3 ligase family
RCFT	Rey Complex Figure Task
RCR	RING-Cys-Relay
RE	Restriction enzyme
RING	Really interesting new gene
RIPA	Radioimmunoprecipitation assay buffer
S1	Supernatant 1 suspension that remains above a pellet 1 after centrifugation
SDS	Sodium Dodecyl Sulfate
SDS PAGE	Sodium dodecyl-sulfate polyacrylamide gel electrophoresis
SGT	Small glutamine-rich tetratricopeptide repeat protein
SLM	Short linear motifs
SNAP-25	Synaptosomal-Associated Protein, 25kDa
SNARE	Soluble N-ethylmaleimide-sensitive factor attachment protein receptors
SNP	Single nucleotide polymorphisms
SOD1	Superoxide dismutases-1
TAE	Tris acetate EDTA
TBS	Tris-buffered saline
TDP-43	TAR DNA-binding protein 43
TIC	Total Ion Current
TSF	Triton-x-100 soluble fraction
UCH	Ubiquitin C-terminal hydrolases
UIM	Ubiquitin-Interacting Motif
UPR	Ubiquitin-proteasome response
UPS	Ubiquitin-proteasome system
USP	Ubiquitin-specific proteases
WT	Wildtype
α-Syn	Alpha-synuclein

Chapter 1 Introduction

1.1 Protein homeostasis

Protein homeostasis, or proteostasis, is the highly regulated network of processes that maintains the functional proteome. It is dependent on regulatory mechanisms that modulate the synthesis, folding, trafficking, localisation, and degradation of proteins (Sin and Nollen, 2015). Dysregulation of protein homeostasis can trigger the ubiquitin-proteasome response and autophagy, which degrades misfolded proteins, halts protein translation, and increases the pool of molecular chaperones to maintain the stability of cellular proteins (Walter and Ron, 2011). Disruption of the balance of proteostasis contributes to the pathogenesis of numerous diseases (Sharma et al., 2025). Neurodevelopmental and neurodegenerative pathologies and diseases have an associated change in protein turnover, whilst hyper- or hypo-ubiquitination leads to protein loss or an accumulation, respectively (Zheng et al., 2016, Cheon et al., 2019). As such, understanding the regulatory mechanisms of proteostasis is critical for understanding the determinants of cellular phenotype and its underpinning of function and dysfunction (Verma et al., 2021, Heard et al., 2018).

1.2 Maintenance of synaptic structure and function

Synapses are neuronal junctions that allow the passage of an electrical or chemical signal from the presynaptic axon of one neuron to either the postsynaptic dendrite of another neuron or a target cell (e.g muscle). For signals to be transmitted, synaptic vesicles containing neurotransmitters are repeatedly used and recycled in a process termed the synaptic vesicle cycle (Heuser and Reese, 1973, Fesce et al., 1994, Chanaday et al., 2019).

Maintenance of synapses is required to keep neuronal networks signalling and the networks active throughout life. Loss of synapses are seen in the early stages of neurodegenerative diseases such as Alzheimer's disease (AD) and Parkinson's disease (PD) (Bae and Kim, 2017). Within these diseases, it is likely that disrupted normal synaptic maintenance mechanisms are an initiator or a consequence of upstream diseases, triggering significant disease progression (Taoufik et al., 2018). Regulation of protein turnover is a critical component of synaptic function for both neuronal health and disease (Alvarez-Castelao and Schuman, 2015).

1.3 Issue of protein folding stability

Most proteins are required to adopt a defined 3D structure and remain within flexible functional states (Kulkarni et al., 2025), with the native conformational state required to carry out their function (Kim et al., 2003). The stability and 3D structure of a protein are determined by the amino acid sequence that defines intra- and intermolecular interactions (Anfinsen *et al.*, 1961; Jaenicke, 1991) and controls the kinetics and dynamics of the folding process. The folding of a protein to its native state is a balance between thermodynamic stability and flexibility, as such proteins often fail to fold to their native conformation due to factors such as errors in translation, mutations or external factors such as chemical or physical stress (Clausen et al., 2019). Un- or misfolded proteins are more susceptible to forming aggregates due to the exposure of hydrophobic regions, as observed in neurodegenerative diseases (Chiti and Dobson, 2006). Whilst some newly translated proteins can spontaneously fold, a large proportion are intrinsically disordered and require assistance to achieve their native folding state (Cooper, 2000).

1.4 Molecular chaperones and co-chaperones

Protein chaperones are essential regulators of proteostasis across all living organisms. They are involved in the mediation of folding newly synthesised peptides, refolding misfolded proteins, assembly of protein complexes and the trafficking of proteins between cellular compartments (Hartl, Bracher and Hayer-Hartl, 2011). Chaperones induce conformational changes in substrate proteins by utilising energy from ATP hydrolysis (Liberek et al., 2008). A molecular chaperone is defined as any protein that interacts with or aids the stability or functional activation of another protein but is not present in the functional structure (Hartl, 1996).

Chaperones are highly conserved between species and are essential in dealing with proteome disruptions in response to stress. Chaperones tend to operate on a wide range of substrates and within all cellular compartments (Saibil, 2013, Storey and Storey, 2023). The largest and most well-characterised group of chaperones are termed the heat-shock proteins (HSPs) due to their upregulation in aggregation-prone cellular stressed environments. These chaperones are named due to their corresponding molecular weights:
HSP40, HSP60, HSP90 and HSP100 (Zhao, Raines and Huang, 2020).

Co-chaperones act as regulators and guides for chaperones, influencing both a chaperone's interaction with its client and the client protein's folding. Co-chaperones can have chaperone activity and can bind to both another chaperone and the client simultaneously (Caplan, 2003). There are over 100 mammalian co-chaperones divided into two categories: the J-domain (Hsp70 and Hsp40)

(Zhang et al., 2023) and the tetratricopeptide repeat (TPR) proteins, which interact with Hsp70 and Hsp90 (Blatch and Lässle, 1999, Pokhrel et al., 2025).

1.4.1 Classes of molecular chaperones involved in the vesicle cycle

Chaperone proteins are a key component in the regulation of the synaptic vesicle cycle and maintenance of the functional state of synaptic proteins (Zinsmaier and Bronk, 2001). The major classes of chaperone complexes involved in the vesicle cycle are auxilin/Hsc70 and CSPα/Hsc70/SGT.

The CSPα/Hsc70/SGT chaperone complex is involved in the maintenance of SNAP-25 a SNARE protein. The SNARE protein family are essential for intracellular membrane fusion, for neurotransmitter release and vesicle transport (See Section 1.6 for further description). The SNAP/NSF complex is involved in the breakdown of the SNARE complex after fusion of synaptic vesicles, allowing the SNARES to be primed for subsequent fusion events (Littleton et al., 2001). The auxilin/Hsc70 complex is important during endocytosis in the clathrin uncoating of vesicles (Sousa and Lafer, 2015). Whilst HSC70 ATPase activity is enhanced by binding to co-chaperone CSPα and SGT, which is harnessed during the fusion step of the vesicle cycle (Tobaben et al., 2003). Chaperone complexes are essential to maintaining the correct conformation of proteins, as well as in the assembly and disassembly of complexes, which are critical for the maintenance of normal synaptic function (Gorenberg and Chandra, 2017). The function of chaperone complexes has been suggested to be dysregulated in a number of neurodegenerative disorders, which are caused by an accumulation of misfolded proteins (Roodveldt et al., 2017).

1.5 Cysteine String Protein α (CSPα)

The cysteine string protein α (CSPα) encoded by the DnaJ homolog subfamily C member 5 (DNAJC5) gene is a presynaptic co-chaperone that is essential for regulated exocytosis underpinning presynaptic proteostasis and maintenance of synapses (Figure 1.2) (Fernández-Chacón et al., 2004). CSPα contains a DNA-J domain, which is typical of heat shock-40 (HSP40) like cochaperones (Figure 1.1). CSPα is initially targeted to the surface of synaptic vesicle membranes via its palmitoylated cysteine string domain (Chamberlain and Burgoyne, 1998). The J domain of heat shock type 40 co-chaperones binds to the nucleotide-binding region of heat shock protein cognate 70 (HSC70) members (Zhang et al., 1999) and the Small glutamine-rich tetratricopeptide repeat protein (SGT) via its C-terminal domain to act as an active chaperone complex located on synaptic vesicles (Figure 1.2) (Tobaben et al., 2001). This complex formation stimulates the ATPase activity of HSC70, which is required for the chaperoning of client SNAP-25(Chamberlain and Burgoyne, 1997).

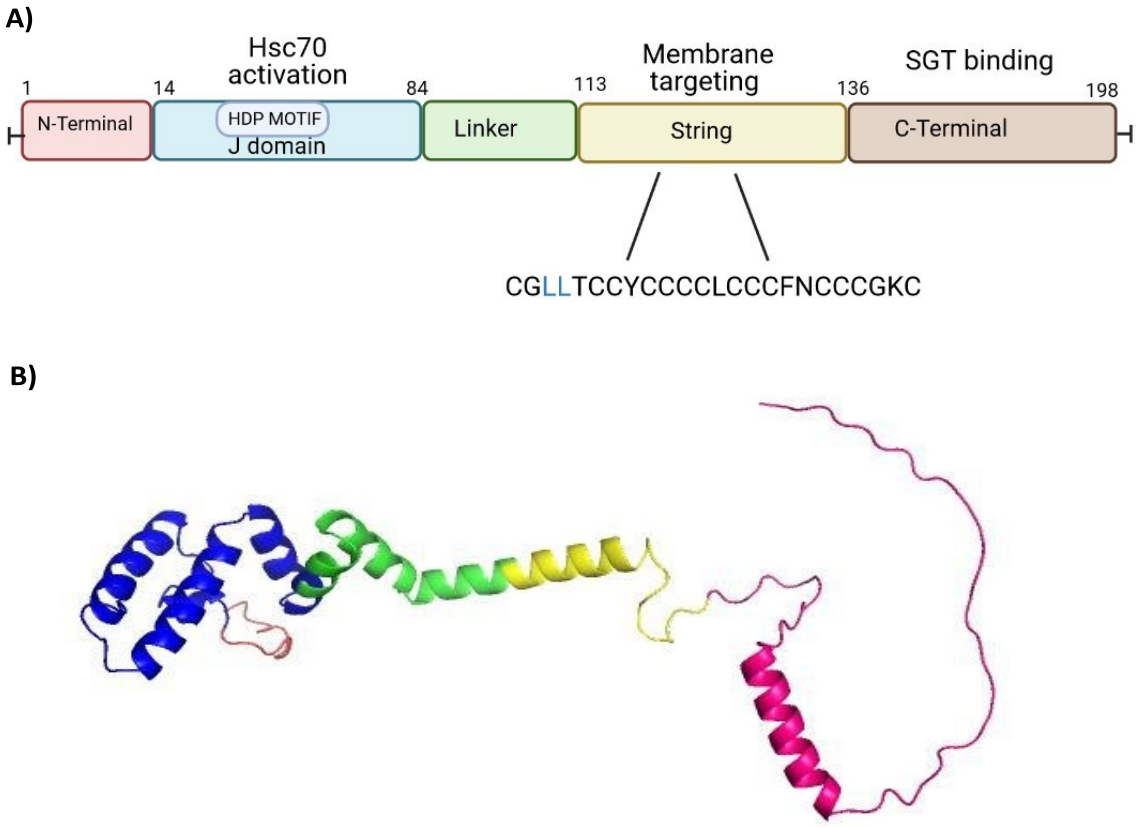

Figure 1.1: Structure of mammalian CSPα. A) Domain structure with a small variable N terminus. HSC70 binding-HPD motif of the J-domain. A hydrophobic linker domain. The cysteine-rich string domain with cysteine residues available for palmitoylation for membrane targeting, and the C-terminal domain. LL highlighted in the string domain corresponds to amino acids mutated in Adult Neuronal Ceroid Lipofuscinosis (ADNCL). B) Ribbon model of full-length human CSPα (Q9H3Z4) predicted by AlphaFold, with each domain labelled corresponding to the domain model. N-terminal domain, Red; J domain, Blue; Linker domain, Green; cysteine-string, yellow; C-terminal domain, Pink.

The cysteine string protein is named after the presence of 11 consecutive cysteine residues present in the cysteine string domain (Figure 1.1) (Zinsmaier et al., 1990). The string has a role in membrane targeting, most of the cysteine residues are post-translational modified by the addition of fatty acyl groups, which are required for membrane targeting (Gundersen, 2020) and may have a role in catalysing the fusion of membranes (Gundersen et al., 1995) or regulation of synaptotagmins at the membrane (Gundersen and Umbach, 2013). Recently, CSP has been suggested to act as a mediator of misfolding-associated protein secretion, and in micro-autophagy, re-routing proteins for disposal (Fontaine *et al.*, 2016. Deng *et al.*, 2017, Xu *et al.*, 2018).

Vertebrates have three CSP isoforms: α, β, and γ, encoded by the DNAJC5a, b and g genes (Evans et al., 2003). In mammals, CSPα is coded for by the DNAJC5a gene, and splicing of this gene leads to two CSPα species at the level of cDNA. The CSP1 cDNA encodes CSPα, and CSP2 encodes carboxyl (C)-terminally truncated CSPα, which is not normally expressed in cells (Coppola and Gundersen, 1996, Chamberlain and Burgoyne, 1996). Early work, now disputed, suggested that both the β and γ forms were expressed exclusively in the testes based on studies in mice (Fernández-Chacón et al., 2004); as such, most research in the CSP family has focused on CSPα. Data available from the human protein atlas suggests that there is a large-scale distribution of CSPα across human tissue, but there has been little work on a non-neuronal function (DNAJC5 protein expression summary - The Human Protein Atlas).

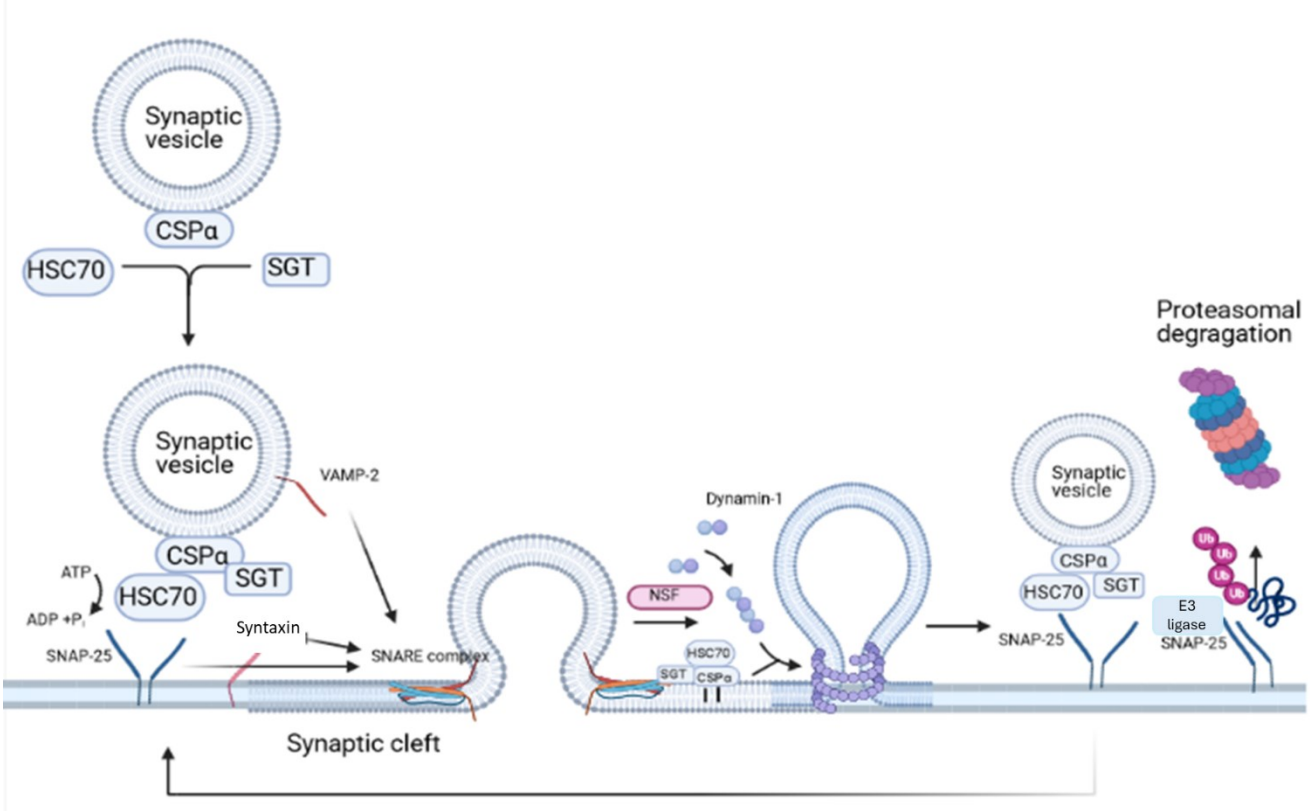

Figure 1.2: **CSPα's key players in synaptic proteostasis.** SNAP-25 interacts with the HSC70 to be maintained in a conformation that is able to form SNARE complexes, whilst Dyn-1 interacts with CSPα, which facilitates Dyn-1 polymerisation. In the absence of CSPα, SNAP-25 is increasingly ubiquitinated by an unknown E3 ligase and degraded by the proteasome.

1.5.1 ATP cycle in the context of the CSPa-HSC70 chaperone complex

Through HSC70, the CSPα chaperone complex couples protein binding and ATPase activity. HSC70 recognises hydrophobic surfaces in unfolded proteins and interacts with them, leading to a conformational change in the substrate protein in parallel with the progress of HSC70 through the ATPase cycle (Figure 1.2) (Mayer and Bukau, 2005). The HSC70 ATPase cycle alternates between an ATP state with low affinity for the fast exchange rates of substrates and the ADP state with high affinity for substrates (Young, 2010). CSPα enhances the ATPase activity of HSC70 in a dose-dependent manner (Braun et al., 1996) which may lead to more efficient chaperoning and a consequential reduction in ubiquitination or aggregation of substrates (Figure 1.2).

1.5.2 CSPα mutation in humans

A dominant mutation in the DNAJC5a gene causes the human autosomal neurodegenerative condition Adult neuronal ceroid lipofuscinosis (ADNCL) characterised by progressive neuronal dysfunction and reduction in life expectancy (Naseri, Sharma, and Velinov, 2021). ADNCL is primarily associated with two mutations (L115R and L116Δ) within CSPα's string domain (Figure 1.1), which disrupt CSPα palmitoylation and consequently its ability to target membranes (Nosková et al., 2011). In mouse models, it has been shown that whilst the mutations L115R and L116Δ led to lipofuscinosis, neither conventional or conditional knockout mice lacking CSPα/DNAJC5 exhibited any signs of it (López-Begines et al., 2025).

1.5.3 CSPα in neurodegeneration

CSPα -/- mouse neurons progressively develop a neurodegenerative phenotype, with highly active synapses affected more severely (Burgoyne and Morgan, 2015) this is characterised by defective neuron-muscular junctions with post-synaptic terminals being less mature and being occupied by fewer presynaptic nerve branches in CSPα -/- mice than in litter mate controls which is suggested to be a result of degradation rather than a lack of development (Fernández-Chacón et al, 2004).

Whilst the number of pre-synaptic active zones have been shown to not be significantly different between CSPα +/+ and -/-. In CSPα -/- 42% of terminals were shown to contain vacuoles and/or multilamellar bodies at all ages which are markers of both degeneration of synapses and a defect in protein processing, degradation and trafficking (Fernández-Chacón et al, 2004).

CSPα has also been investigated and implicated in several human neurodegenerative conditions (Burgoyne and Morgan, 2015), including in the early stages of Alzheimer's disease, where its reduction contributes to synapse loss (Tiwari et al., 2015, Sharma et al., 2012, Rupawala et al., 2022

), frontotemporal dementias and Lewy body disease in the presence of amyloid plaques (Rupawala et al., 2022), Parkinson's disease (Sharma et al., 2012, Chandra et al., 2005a, Caló, et al., 2021), Huntington's disease (Miller et al., 2003, Swayne, Beck and Braun, 2006, Shirasaki et al., 2012) and Amyotrophic Lateral Sclerosis (Coyne et al., 2017).

1.5.4 CSPα in animal models

Invertebrates have a single CSP gene, in contrast to the three vertebrate genes (Evans, Morgan and Burgoyne, 2003). In *Drosophil*a, three splice variants are derived from a single CSP gene. The consequences of CSP null mutants have different effects in different animal models (Table 1.1). In CSPα -/- mice and *Drosophila*, there is evidence of synaptic loss that is activity-dependent. This means that neuronal loss is thought to be more marked in frequently firing neurons as exemplified by parvalbumin GABAergic neurons (Schmitz et al., 2006, García-Junco-Clemente et al., 2010, Leal et al., 2023, López-Begines et al., 2025).

In *Drosophila*, CSPα is essential for synaptic maintenance, and a knockout leads to temperature-sensitive paralysis and a shortened life span. In *C. elegans* some studies have shown there is a mild or no phenotype to a knockout of homologue *DNJ-14*. This may be because *Drosophila* have a more complex and active nervous system in comparison to *C. elegans* (Zheng et al., 2018, Kapulkin et al., 2005).

Table 1.1: CSPα -/- models: Genetic disruption of CSP in distinct animal models, knockout phenotypes, genes expressed in the wildtype model and the reduction seen in the absence of the CSP gene.

Model	**Phenotype**	**CSPα gene/ protein**	**Reduction in life span**
Drosophila melanogaster	Shaking, spastic jumping, temperature-sensitive paralysis (Zinsmaier et al., 1990).	Single CSP gene, with three splice variants	Only 4% of mutant flies survive to adulthood (Umbach et al., 1994).
C. elegans	The *C. elegans* CSP homologue, *dnj-14,* has been implicated in an impairment in synaptic function. *Dnj-14* is expressed in various non-neuronal tissues, including the intestine, pharynx, spermathecae, and vulva/uterus (Barker et al., 2024)	Single CSP gene	The mean life span of *dnj-14* (*ok237* deletion mutation of the whole *dnj-14* gene and into the first exon of a neighbour gene *glit-1*) is 13.3 days, compared to 18.7 days for wild-type N2 strains (Kashyap et al., 2014). Another study focusing on the mutation *tm3223, which disrupts the just dnj-14 gene,* observed no reduction in lifespan or any deficits in neuromuscular-dependent behaviour in ageing of *dnj-14* mutant worms (Mulcahy et al., 2019) A third study produced a homozygous *dnj-14* null which have significantly shorter lifespans of 12.95 days compared with N2 controls, 17.16 days (Barker, Morgan and Barclay, 2023)
Mice	CSPα -/- pups resemble CSPα -/+ and +/+ until 2 weeks after birth. Impairment of synaptic transmission leading to severe motor and sensory impairments, causing paralysis, blindness and premature death (Schmitz et al., 2006) (García-Junco-Clemente et al., 2010).	3 DNJC5 genes a,b and γ encodes α, β, and γ. CSPα is the most widely expressed of the three and is expressed in most neurons.	CSPα -/- survive no more than 80 days (Fernández-Chacón et al., 2004).

1.5.5 Known CSPα interactors and clients

CSPα has a role in membrane trafficking and protein folding (Evans, Morgan and Burgoyne, 2003). Both SNAP-25 (Synaptosomal-Associated Protein, 25 kDa) and Dynamin-1 are clients of the CSPα-Hsc70 chaperone complex (Figure 1.2). To date, Dynamin-1 is the only protein to be identified as a

client of the CSPα-Hsc70 chaperone complex which directly binds to CSPα, as there is still debate over whether SNAP-25 interacts with the complex via CSPα or HSC70 (Figure 1.2) (Chandra et al., 2005; Y.-Q. Zhang et al., 2012).

1.5.6 **Dyn-1 is a client of the CSPα chaperone complex**

Dyn-1 is an endocytic GTPase involved in synaptic vesicle endocytosis (Figure 1.2). Zhang et al suggested that the CSPα-HSC70 complex was involved in the oligomerisation of Dyn-1 required for endocytosis of synaptic vesicles (Y.-Q. Zhang et al., 2012) due to a reduction of higher order Dyn-1 species but not in Dyn-1 monomers in CSPα -/-. The change in oligomerisation but not mono dynamin expression suggests that CSPα facilitates self assembly of Dyn-1 by switching its conformation, but does not affect total levels of Dyn-1.
Dyn-1 isn't increasingly ubiquitinated or aggregating in CSPα -/- (Y.-Q. Zhang et al., 2012). Dynamin-1 heterozygous mice have a total reduction of about 50% in Dyn-1 expression. Yet, are observed to be phenotypically normal and display no defects with synaptic vesicle endocytosis (Ferguson et al., 2007). Leading to the suggestion that the dysfunction observed in CSPα -/- is unlikely to be via its regulation of Dyn-1.

1.5.7 SNAP-25 is a client of the CSPα chaperone complex

SNAP-25 is a SNARE protein (soluble N-ethylmaleimide-sensitive factor attachment protein receptors) (See Section 1.6) located on the synaptic plasma membrane required for presynaptic transmitter release (Gonzalo et al., 1999). SNAP-25 has been identified as a client of the CSPα complex (Figure 1.2) based on the observed increase in ubiquitination and protein loss in the absence of CSPα (Sharma et al., 2011).

Deletion of CSPα leads to the formation of an abnormal conformer of SNAP-25, which is ubiquitinated and degraded by the proteasome, leading to a ~50% reduction of SNAP-25 levels (Chandra et al., 2005b). This leads to a reduction in its competency to form SNARE complexes (Sharma et al., 2011).

Inhibiting the proteasome with epoxomicin and lactacystin (10 μM) increases levels of SNAP-25 and subsequently SNARE complexes by 200% in CSPα -/-mouse cortical neurons. CSPα /- mice treated with proteasome inhibitors showed the alleviation of the symptoms of neurodegeneration, reversal of the impairment of the SNARE complex and increasing median life spans by an extra 10 days with lactacystin and 15.5 days with epoxomicin (Sharma, Burré and Südhof, 2012), suggesting that a key component of the CSPα -/- phenotype is dysregulated proteostasis.

1.5.8 Proteins affected by a lack of CSPα

The expression of additional proteins is affected by a loss of CSPα (Table 1.2). In an unbiased quantitative comparison of the synaptic proteome of CSPα +/+ vs -/- mouse synaptosomes, 37 proteins were found to be affected by a loss of CSPα; these proteins were mostly presynaptic, chaperones or involved in exocytic, endocytic, cytoskeletal or synaptic signalling pathways (see Table 1.2) (Zhang et al., 2012).

Table 1.2: Proteins with decreased expression levels in synapses from CSPα knock-out mice compared to wild type, identified either by DIGE or iTRAQ at P28, adapted from (Zhang et al., 2012)

Protein	Fold change	Fraction	Role
Chaperones			
CSPα	-4.18	Vesicle/ membrane	Regulation of the synaptic vesicle cycle and chaperonemediated protein folding
HSP90 (inducible and constitutive)	-1.80	Cytosol	Chaperone protein
Hsp70-5/GRP78	-1.78	Membrane/ Cytosol	Glucose-regulated protein, UPR regulator
Hsp70	-1.67	Vesicle/Membrane/Cytosol	ATPase protein chaperone
Hsp 105/110	-1.71	Cytosol	ATPase protein chaperone
HOP	-1.54	Cytosol	Hsp70-Hsp90 Organizing Protein
Hsp70-4 like	-1.47	Cytosol	ATPase protein chaperone
Hip	-1.40	Cytosol	Hsc70 interacting protein
Chaperonin TriC	-1.44	Cytosol	ATPase protein chaperone
Exocytosis			
Snap-25b	-3.26	Vesicle/Membrane/Cytosol	SNARE complex
Calcium channel β4	-1.64	Membrane	Calcium transmembrane transport
NSF	-2.32	Membrane	Disassembly of SNARE complexes
Complexin 1	-1.46	Cytosol	SNARE binding protein
Endocytosis			

Dynamin 1	-2.44	Vesicle/Membrane	GTPase severs membranes during endocytosis
Necap 1	-1.61	Vesicle	Role in clathrin-mediated endocytosis
Cytoskeletal			
Crmp3	-2.34	Vesicle	Axon guidance, neuronal growth cone collapse and cell migration
Septin 3	-2.20	Vesicle	GTPase required for cytokinesis
Septin 5	-1.97	Vesicle/Membrane	Nucleotide binding protein, regulate cytoskeletal organization
Septin 7	-1.90	Vesicle	Filament-forming cytoskeletal GTPase, organization of actin cytoskeleton
Septin 6	-1.64	Vesicle	Cytokinesis
BASP1	-1.50	Vesicle	Transcription corepressor
Dpysl2	-1.41	Cytosol	Semaphorin signal transduction pathway, involved in growth cone collapse in neural development
Signalling			
Diazepam binding inhibitor	-2.00	Vesicle	Lipid metabolism
Adenylate kinase 1	-1.94	Vesicle	Kinase involved in adenine nucleotide metabolism
Protein phosphatase 1c	-1.68	Vesicle	Ubiquitous serine/threonine phosphatase
PAFacetylhydrolase lBα	-1.60	Vesicle	Subunit of platelet-activating factor acteylhydrolase.
Visinin-like	-1.47	Cytosol	Neuronal calcium sensor protein
Rabconnectin 3β	-1.46	Cytosol	Forms the beta subunit of rabconnectin-3 regulator of Rab3 small G proteins involved in calciumdependant exocytosis of neurotransmitters

ARF-GEP	-1.42	Cytosol	Role in Arf6 signalling and Endocytosis
Other proteins			
Sec24b	-2.44	Vesicle	Vesicle trafficking, cargo binding protein involved in transport of secretory proteins from ER to golgi
PSD-95	-1.67	Vesicle	Membrane-associated guanylate kinase, component of scaffold for the clustering of receptors, ion channels, and associated signalling proteins at post synapse.
Proteolipid protein 1	-1.91	Membrane	Component of myelin
Myelin basic protein	-1.68	Membrane	Constituent of myelin sheath
Dynein light chain 2	-1.57	Vesicle	Cytoskeletal binding protein involved in motor activity
α-Synuclein	-1.49	Vesicle	Selective Inhibition of phospholipase D2
β-Synuclein	-1.43	Cytosol	Selective Inhibition of phospholipase D2

This investigation (Table 1.2) was carried out at P28, which is after the age where CSPα -/- resemble CSPα +/+. Two methods were used to detect changes: DIGE (2-D fluorescence Difference Gel Electrophoresis) and iTRAQ (Isobaric Tag for Relative and Absolute Quantitation), but many proteins were only detected by one of the methods used. Proteins with changes less than 40% were disregarded, leading to the potential that alterations were either missed due to the detection methods or due to the strict cutoff.

1.5.9 Additional non-client- chaperone role of CSPα in neuronal cells

In addition to CSPα acting as a chaperone for its client proteins (Section 1.5.5), CSPα has a number of other roles. CSPα is involved in Misfolded-Associated Protein secretion (MAPS) and endosomal uptake of misfolded protein, which promotes the unconventional secretion of misfolded cytosolic proteins such as α-synuclein, tau and TDP-43 through late endosomes and lysosomes (Almeida et al., 2023). This is not facilitated through CSPα's classical client chaperoning pathway. But in the case of MAPs via CSPα-associated to membranes proximal to the late endosomes and lysosomes allowing

for CSPα to facilitate the secretion of misfolded proteins (Xu et al., 2018b) and endosomal-associated CSPα, promoting ESCRT dependent microautophagy (Lee et al., 2023) (Figure 1.3).

CSPα influences calcium homeostasis via interaction with voltage-gated P/Q and N-type calcium channels, which may affect the function and localisation of these channels, influencing the calcium influx during synaptic activity (Magga *et al.*, 2000) (Figure 1.3).

CSPα also interacts with Gαs proteins localised on secretory vesicles, leading to the suggestion that CSPα may regulate G protein signalling (Magga et al., 2000, Bai et al., 2007) CSPα modulates G protein function by targeting the inactive GDP-bound form of G alpha(s) and promoting activating GDP/GTP exchange, leading to the termination of G Protein signalling (Natochin et al., 2005) (Figure 1.3).

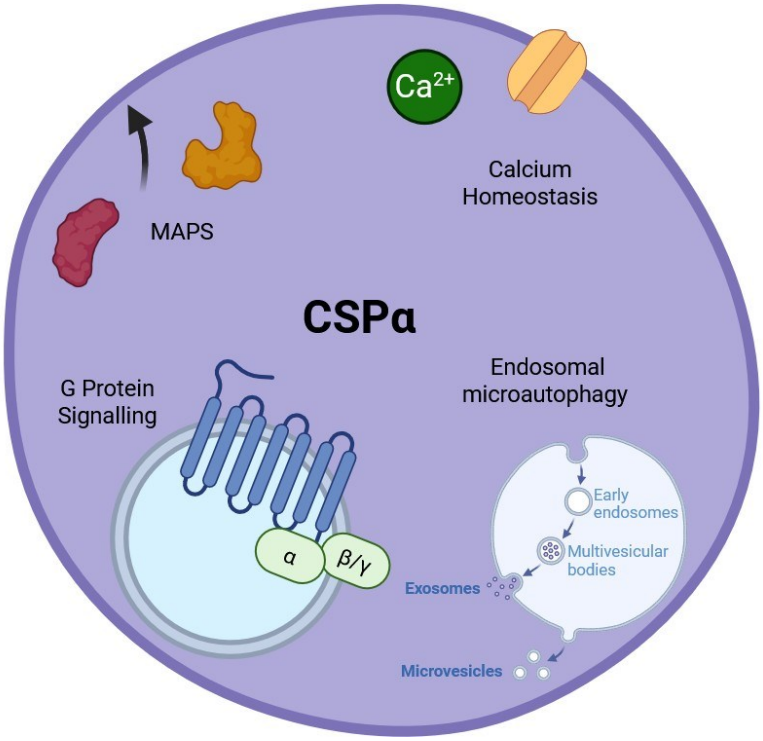

Figure 1.3: CSPα non-client- chaperone role of in neuronal cells, CSPα has been evidenced to be involved in Misfolded-Associated Protein secretion (MAPS), endosomal uptake of misfolded protein, regulation of calcium homeostasis via G-protein signalling and Endosomal microautophagy.

1.5.10 Effects of CSPα in non-neuronal cellular models

The majority of work undertaken on CSPα has been done in neuronal post-mitotic cells. Emerging work suggests that CSPα may have alterative roles and functions in non-neuronal cells in a cell-type specific manner (Table 1.3).

Table 1.3: **Phenotype of CSPα loss in non-neuronal cell models**

Cell line or model	**Effect of a loss of CSPα**	**Reference**
Mouse embryonic hepatic cell BNL cl.2	Inhibition of cell viability in a dose dependent manner	(Kang et al., 2008)
Glial cells: Astrocytes, Microglia, Oligodendrocytes, endothelial cells, and vascular-associated cells.	Transcriptional alterations Effect on the regulation of autophagy	(Wang et al., 2024)
Red blood cell, leukocyte, and megakaryocyte.	Role in platelet secretion, regulation of biogenesis. decrease in dense- and α-granule release without affecting levels of SNAP-25/23	(Smith et al., 2025)
RGL neural stem cells	Hypo-proliferation and depletion of neural stem cell pool via regulation of proliferation via hyperactivation of mTOR signalling	(Nieto-González et al., 2019)

Recent work undertaken in neuronal stem cells has suggested that an absence of CSPα can lead to hyperproliferation. Nieto-González et al found that mouse CSPα knockout hippocampal radial glia-like (RGL) neural stem cells, postnatally, lose quiescence and experience a period of increased proliferation, which leads to a depletion of the radial glial pool. Work in culture led to the identification that the absence of CSPα led to hyperactivation of the mechanistic target of rapamycin (mTOR) signalling pathway, causing the neurogenesis deregulation observed (Nieto-González et al., 2019).

CSPα has recently been identified as being required for platelet secretion, loss of CSPα in mice led to significate bleeding and effected the bone marrow progenitor cells leading to a reduction in red blood cell, leukocyte, and megakaryocyte numbers suggested to be due to an alteration in both their biogenesis and function in response to the loss of CSPα (Smith et al., 2025). Nieto-González et al and Smith et al suggest that CSPα may also play an important role in regulating the behaviour of non-neuronal stem cells, potentially via its chaperone ability, affecting protein homeostasis or impacting cellular stress responses.

Similarly, work undertaken in *C. elegans* found a widespread distribution of CSPα orthologue *DNJ-14* with an increased expression in the intestine under starvation, supporting a role in cellular stress responses and metabolic regulation (Barker et al., 2024).

Recent work investigating the CSPα transcriptomic signature using single-nucleus RNA sequencing to profile the cell types from the cortex of CSPα -/-, including; Excitatory neurons, Inhibitory neurons. Glial cells: Astrocytes, Microglia and Oligodendrocytes and endothelial cells and vascular-associated cells identified 1,772 genes with altered expression in CSPα Knock Out brains. Revealing that all neural cell classes showed signs of loss of synaptic pathways with an upregulation of autophagy-related genes, whilst microglia exhibited activation, and astrocytes and oligodendrocytes displayed signs of reactive gliosis, suggestive of an inflammatory response. The study highlighted the interplay between neurons and glial cells in the response to synaptic instability caused by a loss of CSPα (Wang et al., 2024).

CSPα exhibits oncogenic properties, promoting cell proliferation and migration in lung adenocarcinoma and hepatocellular carcinoma by elevating EGFR trafficking (H. Wang et al., 2021, Chen et al., 2025). Whilst interference with CSPα in the mouse embryonic hepatic cell BNL cl.2 led to a decrease in cell viability (Kang et al., 2008). In hepatocellular carcinoma, the microRNA (miRNA) miR-342-3p has been shown to interact with and inhibit CSPα in response to the long non-coding RNA (lncRNA) LINC00624, leading to apoptosis and proliferation (Xu et al., 2024).

These recent advances highlight that the effects of CSPα on cellular proliferation and fate are cell-type specific and that the regulation of CSPα expression and both the canonical cochaperone and novel functions are still not fully understood. As such new non-neuronal functions of CSPα need to be further investigated to gain a fuller understanding of its range of roles in a wide variety of cellular environments.

1.6 SNARE complexes

The SNARE complex is a protein complex which is essential for membrane fusion in eukaryotic cells, required for neurotransmitter release and vesicle trafficking. The complex is formed by the interaction of SNARE proteins localised to opposing membranes, which facilitates bringing the two membranes proximal to each other and facilitates fusion (Hu et al., 2003, Zhou et al., 2015, Yoon and Munson, 2018, Jahn et al., 2024)

The SNARE complex, formed of SNAP-25, Vesicle-associated membrane protein (VAMP-2)/ Synaptobrevin, and Syntaxin-1, is essential for exocytosis (Figure 1.4). The SNARE protein complex continuously cycles between a non-assembled state and a more stable assembled state (Söllner, Bennett, et al., 1993). The initial complex forms a coiled-coil quaternary structure. SNAP-25 contributes two α-helices, and VAMP-2 and Syntaxin-1 contribute one helix each. The α-helix of VAMP-2 binds to SNAP25 C-terminal helix, and Syntaxin-1 binds to SNAP-25's N-terminal helix. The formation of the SNARE complex is exergonic and provides the energy required for the membrane fusion event. Once the vesicle has fused with the membrane, the SNARE complex is dissociated by the ATPase N-ethylmaleimide-sensitive fusion (NSF) protein, inducing a conformational change in Syntaxin (Otto et al., 1997). Synaptic transmission is often high frequency, and as such, the SNAREs continuously cycle through this process (Figure 1.4).

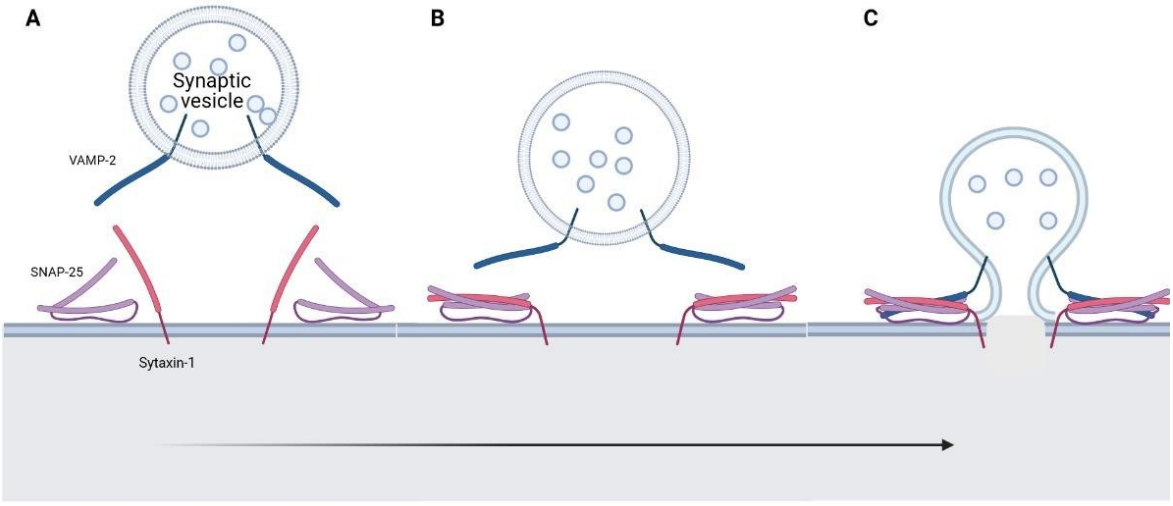

Figure 1.4: SNARE complex formation, core fusion machinery comprised of SNAP-25, VAMP-2 and Synatxin-1 required for the docking of a synaptic vesicle. VAMP-2 (a v-SNARE protein) interacts with the cytosolic domains of the t-SNARE proteins SNAP25 and Syntaxin1, forming a stable coiled-coil SNARE complex. This holds the synaptic vesicle close to the target membrane, allowing fusion of the two membranes to take place.

1.7 Synaptosome-associated protein 25 (SNAP-25)

SNAP-25 (Synaptosome-associated protein 25) is a t-SNARE protein that is highly expressed at the neuronal plasma membrane (Winkle and Gupton, 2016). Functioning at this location as a component of the SNARE complex required for synaptic vesicle exocytosis (Goda, 1997). The SNARE proteins are divided into T- and R-SNAREs, defined by each protein's position within the four-helical SNARE bundle. SNAP-25 knockout is perinatally lethal in homozygous mice, whilst heterozygotes do not display any alteration in phenotype (Washbourne et al., 2002).

1.7.1 SNAP-25 family

The Synaptosomal-Associated Protein proteins (SNAP) make up a sub-family of SNARE proteins consisting of: SNAP-25, SNAP-23, SNAP-29 and SNAP-47, named for their corresponding molecular weight. The SNAP family is made up of a short N-terminus a 60-70 amino acid SNARE motif (Q_b), a linker region, and a second SNARE motif (Q_c) (Fasshauer et al., 1998) see Figure 1.5. In vertebrates, the linker region contains four palmitoylated cysteine residues, allowing plasma membrane attachment. SNAP-25 has two isoforms a and b, which differ by 9 amino acids in the linker region due to alternative splicing of exon 5 of the *snap-25* gene (Figure 1.5). SNAP-25a is expressed during development, whilst SNAP-25b becomes the predominant isoform postnatally (Bark et al., 1995). SNAP-23 is the most closely related member of the family to SNAP-25 (Araki *et al.*, 1997), like SNAP-25, SNAP-23 has palmitoylated cysteines, providing membrane targeting capabilities (Vogel and Roche, 1999). Whilst SNAP-29 and SNAP-47 both have longer linker domains, and are found widely on intracellular membranes in mammals and close to the Golgi but lack the palmitoylated cysteines (Figure 1.5) (Steegmaier *et al.*, 1998; Holt *et al.*, 2006).

Both SNAP-25 and SNAP-23 are involved in the regulation of exocytosis from synaptic vesicles. Cross-rescue experiments have shown that SNAP-25 and SNAP-23 can, in part, substitute for each other in their roles forming SNARE complexes, but SNAP-29 and SNAP-47 cannot (Salaün et al., 2005a). SNAP-29 is involved in autophagosome-to-lysosome function. SNAP-47 has a similar role and additional roles in the mediation of postsynaptic AMPA-receptor insertion (Kádková et al., 2019) and the regulation of the secretion of brain-derived neurotrophic factor (BDNF) (Münster-Wandowski et al., 2017; Shimojo et al., 2015).

For SNAP-25, the two SNARE motifs are essential for interaction with VAMP-2 and Syntaxin-1, required for SNARE complex formation (Otto et al., 1997).

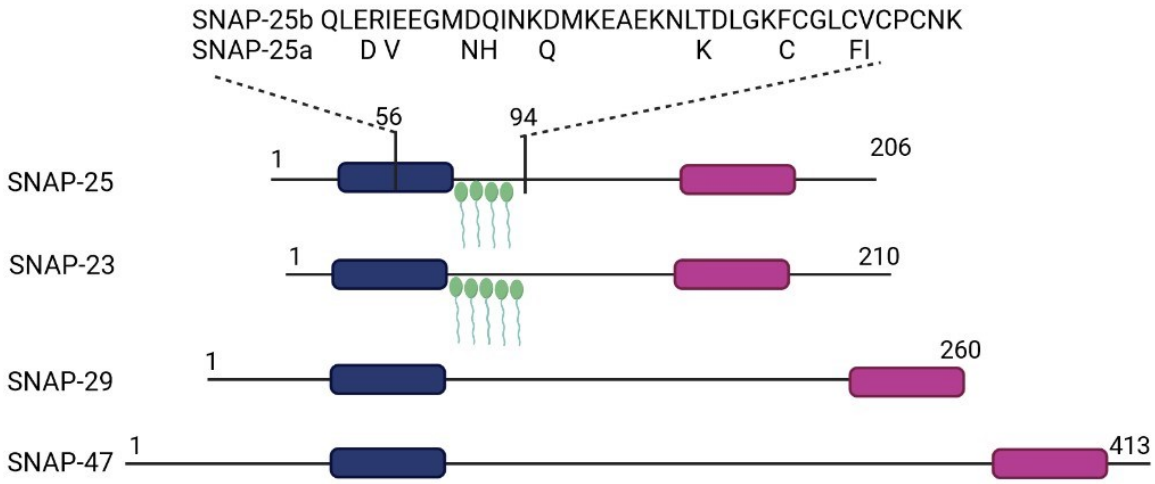

Figure 1.5: Structure of vertebrate SNAP-25 protein family members, SNAP-25 splice variants a and b at (top), which differ by nine amino acids in the C-terminus and linker region. The blue rectangle depicts the N-terminal SNARE motif (Q_b), whilst the purple rectangle depicts the second C-terminal SNARE motif (Q_c). Palmitoylated cysteines are depicted by green circles in SNAP-25 and SNAP-23, SNAP-29 and SNAP-47 do not contain any palmitoylated cysteines and maybe potentially become membrane-associated via interaction with other proteins, adapted from (Kádková et al., 2019).

1.7.2 SNAP25 lifecycle

When first synthesised in the cell, SNAP-25 is a soluble protein that undergoes palmitoylation about 20 minutes after synthesis, coinciding with an increase in protein stability (Figure 1.6) (Gonzalo and Linder, 1998).

Four SNAP-25 cysteines are palmitoylated by 3 members of the DHHC family, DHHC3, DHHC7, and DHHC17, which are localised to the Golgi. This modification recruits SNAP-25 to the Golgi from whence it is trafficked to the plasma membrane (Greaves et al., 2010). SNAP-25 binds to Q-SNARE protein Syntaxin, after which the two proteins form a complex that is then inserted into membranes (Vogel, Cabaniols and Roche, 2000). SNAP-25 is predominantly localised to the plasma membrane, with pools also found in the recycling endosomes and the trans-Golgi network (Greaves and Chamberlain, 2011).

In cerebellar granule neurons, the half-life of SNAP-25 was estimated at 16 hours, but this increased to 35 hours in mature neurons (Sanders, Yang and Liu, 1998). The age-dependent increase in the half-life suggests SNAP-25 becomes resistant to proteasome turnover in mature neurons (Sanders, Yang and Liu, 1998). SNAP-25 levels increase as neurons undergoing synaptogenesis *in vitro*, with a

major upregulation coinciding with the establishment of synapses in the latter stages of neuronal development (Catsicas et al., 1991).

Cycloheximide inhibition of protein synthesis causes a significant decrease in the degradation of SNAP-25, suggesting that synaptic activity affects the stability of SNAP-25 (Sharma et al., 2011).

SNAP-25 is poly-ubiquitinated as a normal part of its lifecycle, leading to proteasomal degradation (See Section 3.1.2 for details on ubiquitination sites) (Figure 1.6). This is increased in the absence of SNAP-25 chaperone CSPα (Sharma et al., 2012a). Currently, the compartment in which SNAP-25 is ubiquitinated in is unknown; there is the potential that SNAP-25 is ubiquitinated whilst anchored to the plasma membrane, during endocytosis or in the cytosol, either before SNAP-25 is input into the membrane or after extraction.

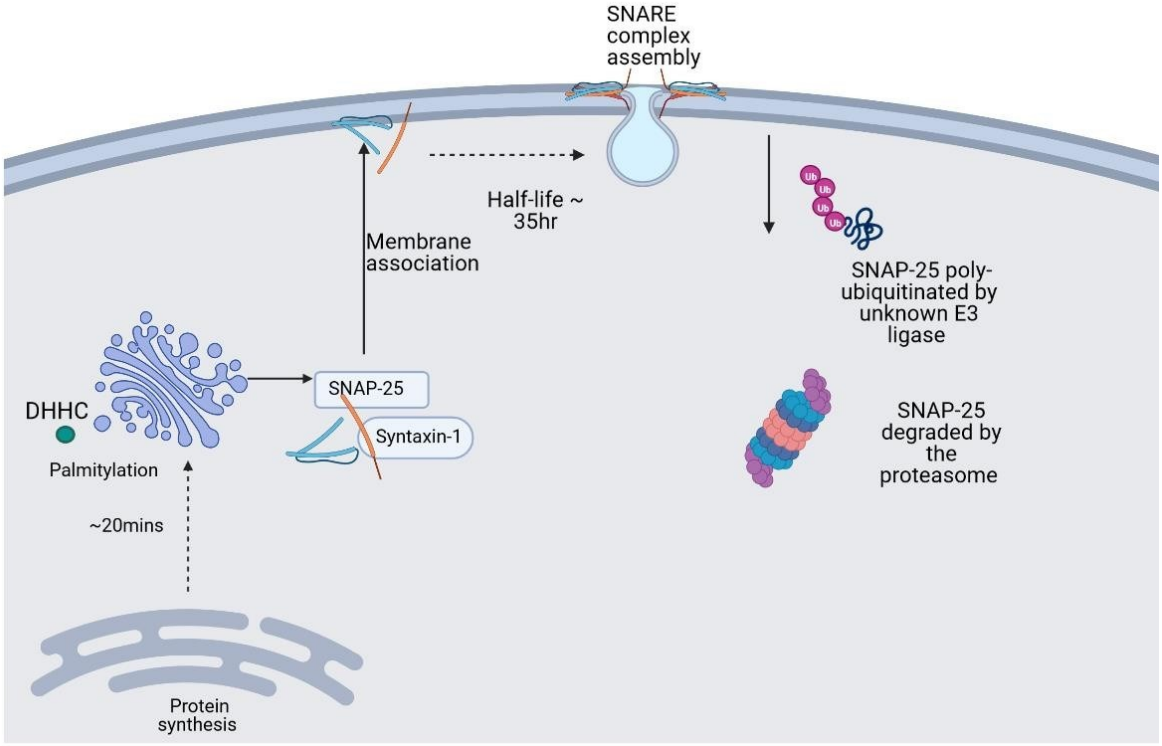

Figure 1.6: SNAP-25 life cycle. SNAP-25 is synthesised as a soluble protein and palmitoylated at the Golgi by DHHC. SNAP-25, whilst interacting with Syntaxin-1, is inserted into the presynaptic membrane, where, with syntaxin-1 and VAMP-2, it facilitates fusion of vesicles to the membrane as part of the synaptic vesicle cycle by the formation of SNARE complexes. At the end of SNAP-25's life or when it is unchaperoned, SNAP-25 is ubiquitinated and degraded by the proteasome, the site of which is still unknown.

1.7.3 Additional roles of SNAP25's role at the pre-synapse

In addition to SNARE complex formation, SNAP-25 is implicated in additional roles at the synapse. SNAP-25 interacts with synaptotagmin in a calcium-dependent fashion (Zhang et al., 2002), and SNAP-25 has a role in vesicle docking and priming (Mohrmann et al., 2010). SNAP-25 also interacts and modulates voltage-gated calcium channels (Toft-Bertelsen et al., 2016) via N-type (Sheng et al., 1996), P/Q-type (Martin-Moutot et al., 1996), L-type (Wiser et al., 1999) and T-type channels (Weiss et al., 2012). At hippocampal synapses, SNAP-25 has been shown to actively take part in slow clathrin-dependent endocytosis (Zhang et al., 2013) (Figure 1.7).

1.7.4 Roles of SNAP25's at the post-synapse

A postsynaptic role for SNAP-25 has also been suggested (Figure 1.7), due to SNAP-25 interacting with Protein Kinase C which implicates it in the control of NMDA (Lau et al., 2010) and kainate receptors (Selak et al., 2009). SNAP-25 may also play a role in postsynaptic spine morphogenesis and plasticity via interaction with the scaffold protein p140Cap located to dendritic spines (Tomasoni et al., 2013a) (Figure 1.7).

It is debated whether SNAP-25 localises to dendritic spines due to conflicting evidence from several studies (Figure 1.7); Immunofluorescence (Selak et al., 2009), ground state depletion microscopy (Tomasoni et al., 2013a) coimmunoprecipitation, electron microscopy (Hussain et al., 2019), bimolecular fluorescence complementation and biochemical fractionation (Fossati et al., 2015; Selak et al., 2009; Tomasoni et al., 2013a) studies have all suggested that SNAP-25 may be present at the postsynapse; however, conflicting studies, including immunogold labelling of synaptic boutons, showed exclusive presynaptic localisation of SNAP-25 (Holderith et al., 2012). The presynaptic population of SNAP-25 is likely to be in large excess, which may lead to difficulty in detecting and quantifying the postsynaptic pool if it is present (Tao-Cheng et al., 2000).

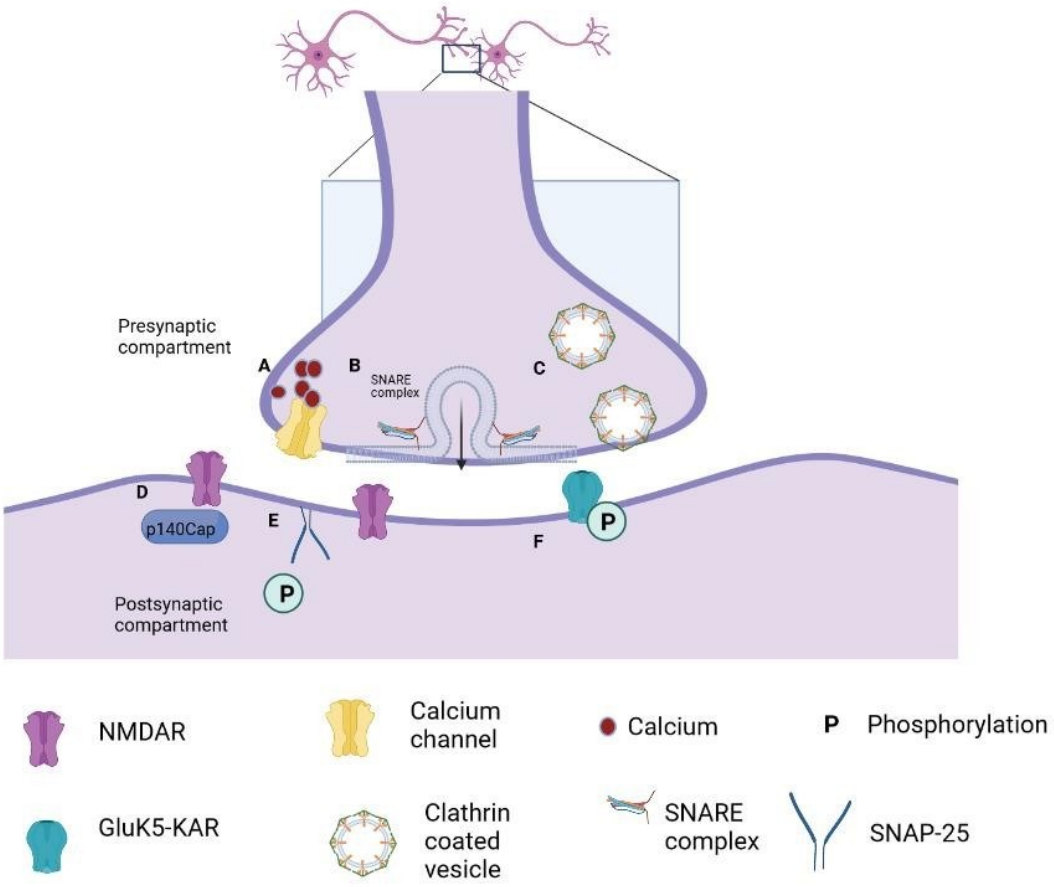

Figure 1.7: SNAP-25 function at the pre- and post-synapse. A: SNAP-25 interacts with Calcium ion channels, B: SNAP-25 forms a SNARE complex with VAMP-2 and Syntaxin-1 for docking and exocytosis of synaptic vesicles. A: SNAP-25 affects pre-synaptic calcium influx at calcium channels,. C: SNAP-25 has an active role in slow clathrin-mediated synaptic vesicle endocytosis by binding to the endocytic protein intersectin. D: SNAP-25 interacts with p140Cap, which forms a complex with PSD95, cortactin, Arp2,3 and F-actin involved in the organisation of the postsynaptic density protein network. E: Phosphorylation of SNAP-25 by PKC promotes the insertion of NMDA receptor-containing vesicles at the cell surface. F: SNAP-25 has a role in the removal of kainite receptors (KAR) from the cell surface when PKC phosphorylates of kainite receptor. Adapted from (Antonucci et al., 2016).

1.7.5 Association of SNAP-25 in neurological disorders

SNAP-25 is associated and potentially causative in a range of neurological disorders (Figure 1.8). Both up- and down-regulation of SNAP-25 has been observed in neurodevelopmental, neurodegenerative and psychiatric disorders. Assembly of the SNARE complex is a pivotal intermediate in synaptic function as it underpins the core process of transmitter release.

Both SNARE proteins and the complex are reduced in human post-mortem brain tissue from Alzheimer's and Parkinson's disease patients (Sharma, Burré and Südhof, 2012)

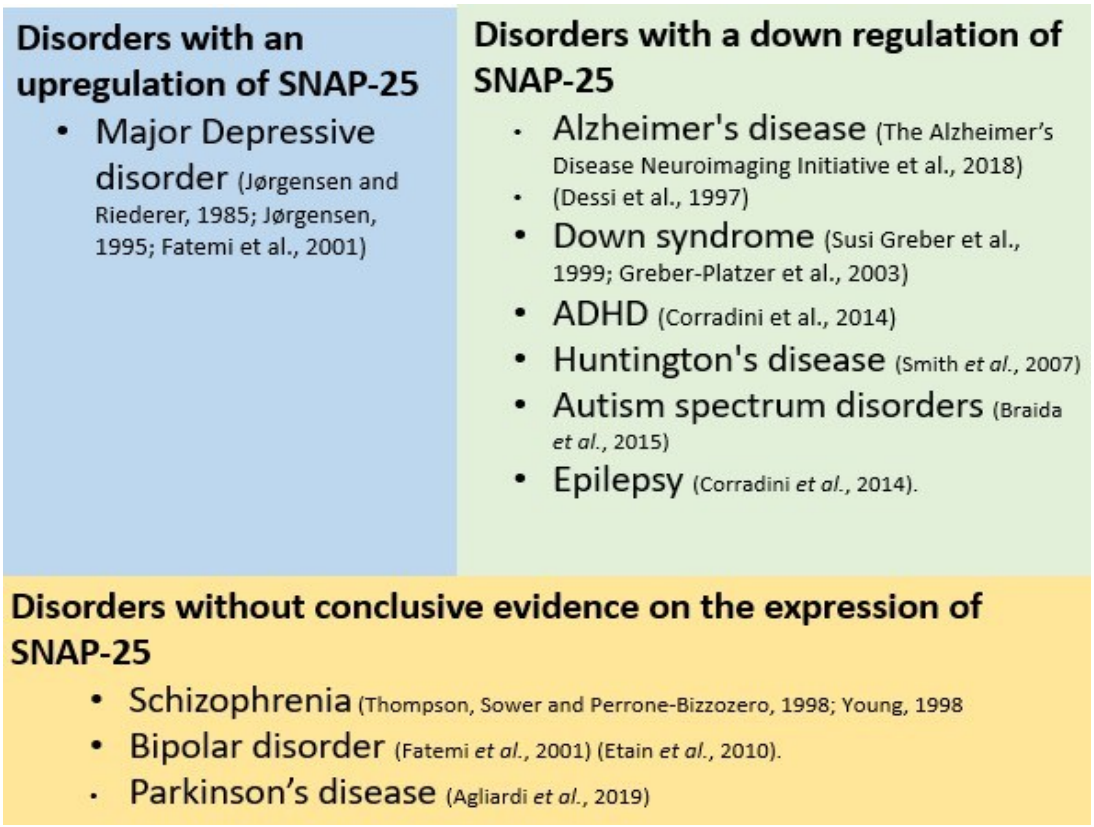

Figure 1.8: Schematic depicting the changes in SNAP-25 expression identified in neurological diseases and disorders. The blue column depicts disorders where there is an upregulation of SNAP-25, the green column depicts disorders with a downregulation of SNAP-25 and the orange column depicts disorders where there is inconclusive evidence of changes in SNAP-25 expression.

1.8 Ubiquitination and the ubiquitin-proteasome system

The ubiquitin-proteasome system (UPS) is a protein degradation system in eukaryotes mainly named for the modification of proteins with ubiquitin initiating degradation (Ciechanover and Schwartz, 1998). Ubiquitination is a posttranslational modification whereby ubiquitin, a protein formed of 76 amino acids is covalently bound to a lysine residue of a target protein substrate (Callis, 2014). Proteins can be both mono and poly ubiquitinated and modified at multiple residues (see section 1.8.2). Ubiquitination is a key regulator of protein degradation, proteostasis and cell signalling (Lecker et al., 2006).

1.8.1 Components required for ubiquitination and the UPS

A group of proteins termed ubiquitin ligases are required for ubiquitination, the process requires a number of highly regulated steps (Figure 1.9), the first of which is triggered by the ATP-dependent activation of ubiquitin by an E1 ubiquitin-activating enzyme. The activated ubiquitin is then able to

be transferred to the second enzyme, termed an E2 ubiquitinconjugating enzyme, which interacts and binds to an E3 ubiquitin ligase conjugated to a target substrate. E3 ubiquitin ligases are characterised by a specific defining motif which facilitates the ubiquitination of substrate proteins by ensuring that the E2 ligase and the substrate are proximal to the ubiquitin moiety to be transferred. E3 ligases give ubiquitination its specificity, with E3 ligases having selective cellular substrates (Pickart and Eddins, 2004).

In humans, there are two E1 ubiquitin ligases, about 40 E2 ubiquitin ligases, but over 600 genes encoding E3 ubiquitin ligases, which provide the specificity of ubiquitination for its target substrate (Callis, 2014; Yang et al., 2021).

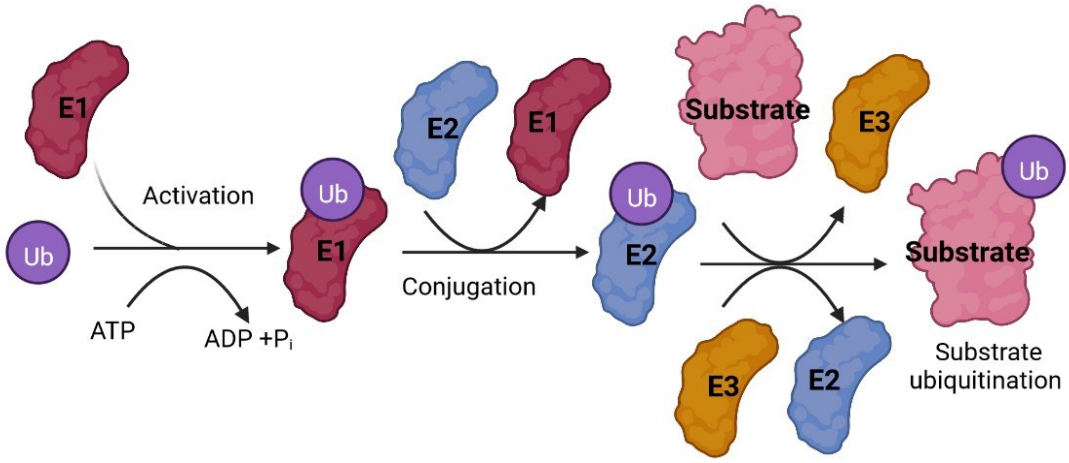

Figure 1.9: Ubiquitination pathway, conjugation of ubiquitin to the target substrate protein.

1) Ubiquitin is conjugated to E1 with a thioester linkage, activated by the breakdown of ATP. 2) Ubiquitin is transferred to an E2 ubiquitin ligase. 3) The E2-ubiquitin complex can then interact with specific E3 ligases, which facilitate the transfer of the ubiquitin molecule to a substrate protein. Adapted from (Pickart and Eddins, 2004)

1.8.2 Diversity in ubiquitin modification code

The hundreds of different mammalian E3 ubiquitin ligases provide diversity to ubiquitination; the E3 ligase-substrate relationship is highly complex as an individual E3 ligase can have multiple specific substrates and individual substrates can be ubiquitinated by multiple E3 ligases (O'Connor and Huibregtse, 2017).

A further level of diversity in ubiquitination is provided by the ubiquitin moiety itself and where it's placed (Figure 1.10). Ubiquitin can be conjugated to its substrate in a variety of configurations. Due to the presence of seven lysine residues and the N-terminal methionine residue in the ubiquitin

molecule, the ubiquitin chain can form seven isoforms; K6, K11, K27, K33, K48, K63 and M1 (Figure 1.10) (Akutsu et al., 2016).

Mono-ubiquitination is the attachment of a single ubiquitin molecule to a protein, which can be a consequence of being directly attached or due to trimming of polyubiquitinated chains by Deubiquitinases (DUBs). The addition of multiple ubiquitin moieties to different target sites in a substrate is termed multi-mono-ubiquitination (Ronai, 2016). Proteins can also become polyubiquitinated, which is the association of chains of ubiquitin on the terminal methionine residue or internal lysine residues (Pickart and Eddins, 2004). Polyubiquitination can further be divided into homotypic and heterotypic polyubiquitination (Grice et al., 2015). Different ubiquitin-chain linkages have different functions within the cell, leading to a change in cellular localisation, cell signalling, protein degradation, and DNA repair (Figure 1.10) (Li and Ye, 2008).

Ubiquitination can take place alongside other post-translational modifications (PTMs) such as phosphorylation (Song and Luo, 2019) and acetylation (Caron, Boyault and Khochbin, 2005), adding further regulation to the ubiquitin signalling pathways. Phosphorylation can modulate the binding affinity of the E3 ligase-substrate and affect the stability of a protein (Song and Luo, 2019).

In addition to trimming poly-ubiquitin chains, DUBs have a central role in maintaining ubiquitin homeostasis by releasing monoubiquitin from ubiquitinated substrate proteins, which have entered the proteasome once committed for degradation (Snyder and Silva, 2021). In addition, DUBs can also be used to remove mono-ubiquitin or trim poly-ubiquitin chains from proteins, allowing a change in protein inhibition, localisation or folding properties of substrates (Hagai and Levy, 2010; Xu and Jaffrey, 2011).

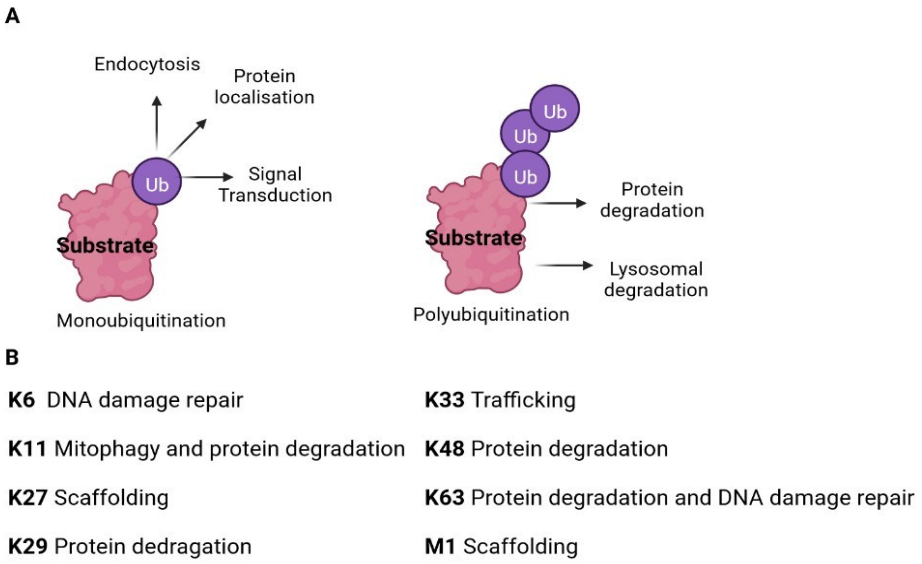

Figure 1.10: Examples of consequences of ubiquitination, A) Consequences due to mono and poly ubiquitination, B) Consequences of ubiquitination of different residues.

1.8.3 Protein degradation by 26S proteasome

The proteasome is a 2.5 MDa multi-subunit protease located in the cytosol and nucleus of eukaryotic cells, responsible for the degradation of ubiquitinated proteins (Marshall and Vierstra, 2019). The UPS has evolved to target soluble, short-lived nuclear and cytosolic proteins for degradation (Voges et al., 1999). The 26S proteasome is formed of a 20S core protease and a 19S regulatory cap (Groll et al., 1999; Schweitzer et al., 2016; Voges et al., 1999).

For a ubiquitinated protein to be degraded, the 19S regulatory unit associates with a ubiquitin-tagged protein, inducing a conformational change of the proteasome, causing the 19S ATPase translocation channel to be moved directly above the 20S gate, opening it for the substrate to unfold and translocate to the 20S core. Once committed for degradation, Rpn11 an integral proteasome-associated DUB located in the 19S complex, removes ubiquitin from substrates (Thibaudeau and Smith, 2019). ATPases bind to the protein and use ATP hydrolysis to unfold and translocate the protein into the 20S core (Lecker et al., 2006). The linearised polypeptide is cleaved, forming small peptides of 3-22 residues (Kisselev et al., 1999) which are released from the 20S and further digested by cytosolic endopeptidases and aminopeptidases, the resulting amino acids can then be reutilised in the synthesis of new proteins or metabolized (Reits *et al.*, 2004; Saric, Graef and Goldberg, 2004).

The Proteasome can be inhibited. Mg-132 (carbobenzoxyl-L-leucyl-L-leucyl-leucinal) is a reversible proteasome inhibitor which blocks the degradation of proteins by targeting and blocking the catalytic activity of the β-subunit of the 20S proteasome core (Lee and Goldberg, 1998, Guo and Peng, 2013) this allows for investigation into ubiquitinated proteins.

1.8.4 Alteration and dysregulation of ubiquitination in neurodegeneration and neurodevelopmental disorders

Alterations in the ubiquitin signalling pathway are associated with the pathogenesis of multiple diseases and genetic disorders. Errors in ubiquitination can result in defects in processes including autophagy, cell signalling and DNA repair mechanisms associated with neurodegeneration, cancer and autoimmune disorders (Haglund and Dikic, 2005; Sakai *et al.*, 2020; Li, Li and Wu, 2022).

Dysregulated ubiquitination and E3 ligases have been associated with a wide range of human neurodegenerative, neurodevelopmental and psychiatric disorders, including Alzheimer's disease (Kuzuhara *et al.*, 1988, Hu *et al.*, 2011, , Liu *et al.*, 2008, Potjewyd and Axtman, 2021, Wu et al, 2021), Down syndrome (Di Domenico *et al.*, 2013; Fortea *et al.*, 2021, Tramutola *et al.*, 2017). Huntington's disease (Sap and Reits, 2020, Steffan *et al.*, 2004), Bipolar disorder (Bousman *et al.*, 2010, Ryan *et al.*, 2006), Epilepsies (Engel et al., 2017), Rubio *et al.*, 2013), Autism spectrum disorders (Glessner et al., 2009) and in Major Depressive Disorder (Mouri *et al.*, 2012). There are also instances where E3 ligase defects are causative for human diseases; Angelman syndrome is a neurodevelopmental disorder caused by a de novo deletion of the UBE3A gene (Kishino, Lalande, and Wagstaff, 1997; Matsuura *et al.*, 1997; Clayton-Smith and Laan, 2003).

1.8.5 Synaptic ubiquitination

Ubiquitination is widely known to have a role in neuronal development, the formation and pruning of synapses (DiAntonio et al., 2001,Ding et al., 2007), and a role in both excitatory and inhibitory transmission (Colledge et al., 2003, Pinto et al., 2021).

A review by Hawabe and Stegmuller in 2021 highlighted the need to investigate further E3 ligases and how ubiquitination regulates the function of the synapses by acknowledging that whilst there has been a lot of work into the transcriptional and translational regulation of synapses, more work is required to uncover ubiquitination-dependent processes (Kawabe and Stegmüller, 2021a).

Targeted ubiquitination of multiple synaptic proteins has been described, and the effects of ubiquitination cover many aspects of neuronal function and dysfunction in the pre- and postsynapses and in both axons and dendrites (Table 1.3) (Ding and Shen, 2008).

Table 1.4: **Selected ubiquitination identified at the specific subcellular neuronal compartments**

Subcellular location	Ubiquitination events	References
Presynaptic	Regulates neurotransmission strength Size of the recycling synaptic vesicle pool Degradation of active zone proteins Ubiquitination of SNARE proteins	(Speese et al., 2003) (Willeumier et al., 2006) (Yao et al., 2007) (Chin et al., 2002a)
Postsynaptic	Regulation of neurotransmittergated ion channels. Trafficking of postsynaptic receptors Degradation of postsynaptic scaffold proteins Degradation signalling Functionally modulation signalling	(Lin and Man, 2013) (Christianson and Green, 2004) (Ehlers, 2003) (Haglund and Dikic, 2005)
Axon	Protein degradation in structural rearrangements of axon outgrowth. Ubiquitination by APC coordinates axon growth. RPM-1/ Highwire in axon differentiation.	(Campbell and Holt, 2001) (Konishi *et al.*, 2004) (H. Li et al., 2008)
Dendrites	Dendritic morphogenesis Promotes dendritic arbour formation. Regulation of dendrite length	(Choe et al., 2007) (Kim et al., 2009) (Kawabe et al., 2010)

1.8.6 How hyper-ubiquitinated SNAP-25 can be used to discover ligases(s) responsible for ubiquitination at the pre-synapse

Mutations and deletion of CSPα, SNAP-25 and proteins involved in the UPS including E3 ubiquitin ligases are associated with neurological disorders (Jiang and Beaudet, 2004). Evidence suggests that E3 ligases have crucial roles in neuronal functions including the formation and maintenance of synapses and synaptic transmission (Upadhyay et al., 2017).

SNAP-25 is ubiquitinated and degraded by the proteasome as a normal part of its life cycle (Figure 1.11). In wild-type mice models, SNAP-25 ubiquitination and degradation is regulated by synaptic activity; an overexpression of CSPα decreases the levels of SNAP-25 degradation (Sharma, Burré and Südhof, 2011). However, deletion of CSPα leads to the formation of an abnormal aggregating conformer of SNAP-25, subject to hyper-ubiquitination and degradation by the proteasome (Figure 1.11) (Sharma, Burré and Südhof, 2011). Suggesting that the expression and activity of SNAP-25 is in an equilibrium between being chaperoned by CSPα and being misfolded, ubiquitinated and degraded by the proteasome. This allows for a model to investigate ubiquitination in an environment with chaperone deficiency and dysregulated proteostasis.

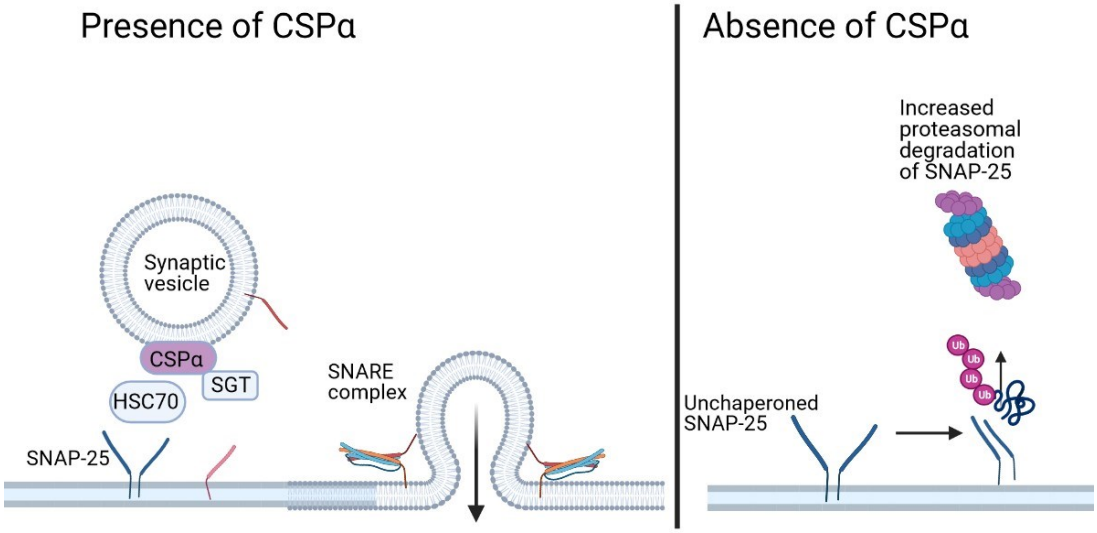

Figure 1.11: The effect of the presence and absence of CSPα on SNAP-25 ubiquitination and subsequent degradation. In the presence of CSPα, SNAP-25 is maintained in a conformation that is able to form SNARE complexes; in the absence of CSPα, the levels of SNAP-25 ubiquitination are increased along with subsequent degradation.

Identification of E3 ubiquitin ligases that hyper-ubiquitinate SNAP-25 will inform on the process of ubiquitination at the pre-synapse and the role ubiquitination has in the regulation of synaptic vesicle transport, which is dysregulated in a number of neurological disorders.

1.9 Hypothesis and Aims

Here I hypothesis that a lack of CSPα can be used to further our understanding of SNAP-25 ubiquitination.

I aim to use CSPα, SNAP-25 and synaptic function to investigate the wider issue of synaptic proteostasis:

1. Aim 1 of this project will investigate potential E3 ligases involved in the degradation of SNAP-25 via a bioinformatic and two biochemical approaches: a BioID proximitydependent labelling protocol and Myc immunoprecipitation. Using a Myc BioID SNAP-25 construct to identify E3 ligases that are located proximally which may be responsible for the increased levels of SNAP-25 ubiquitination observed in CSPα -/-.
2. Aim 2 of this project is to produce and characterise a CPSα knockdown PC12 line with the aim of increasing our knowledge of the role of CSPα in post-mitotic cells.

Chapter 2 Materials and Methods

2.1 Materials

All molecular biology reagents were supplied by New England Biolabs and Promega unless stated otherwise. All cell culture media and plastic consumables were sourced from Gibco ThermoFischer, Greiner Bio and Starlabs. For other cell culture experiments, reagents were obtained from Invitrogen unless stated otherwise. Reagents for protein preparation and staining were from Sigma Aldrich (Merck) or ThermoFischer unless otherwise noted. Primers were generated, and sequencing was carried out by Eurofins Genomics (Germany).

2.2 Bioinformatics methods

A three-part bioinformatics strategy was used to facilitate the investigation of candidate E3 ligases with the potential to ubiquitinate SNAP-25. This involved i. A literature, ii. A structural prediction approach (Figure 2.1). iii. Supplemented by literature-led interrogation of E3 ligases associated with disorders in which there is SNAP-25 dysfunction. Investigations into neuronal localisation and proteomic screen identification were carried out to filter and prioritise candidates for further investigation (Figure 2.1). Finally, the literature was reviewed to identify proteomic screens that had been carried out for each of the identified E3 ligases and to determine if SNAP-25 was found in these screens.

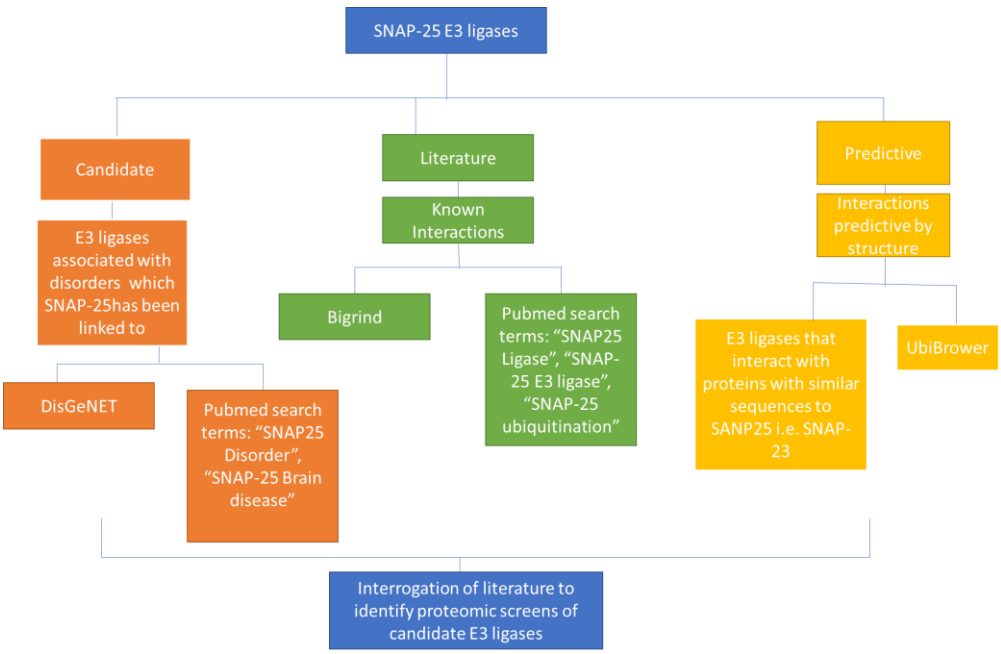

Figure 2.1: Bioinformatics workflow to identify candidate SNAP-25 E3 ligases. Literature approach (green) used to identify known and verified interactions of SNAP-25 and E3 ligases, the Predictive approach (yellow) used to identify potential interactions found by structural analysis, and the candidate approach (orange) was used to provide further support for E3 ligases due to an association with disorders SNAP-25 has been linked to.

2.2.1 Literature association bioinformatic approach to identify candidate SNAP-25 E3 ligases

The literature-based approach investigated deposited experimental data to probe existing literature evidence indicating a potential physical interaction between SNAP-25 and E3 ligases.

2.2.2 BioGRID and Human E3 ubiquitin ligase database for the identification of SNAP-25- E3 ubiquitin ligase Interactors

Figure 2.2: BioGrid load-up page used for the identification of literature-supported proteinprotein interactions.

The database BioGRID version 4.4 (https://thebiogrid.org/) (Accessed October 2021) (Figure 2.2, Table 2.1) was used to identify known SNAP-25 protein interactions. BioGRID is a literature depository database which produces a comprehensive list of protein-protein interactions with corresponding literature sources. The search term "SNAP25" Homo sapiens was used covering the terms (RIC-4, RIC4, SEC9, SNAP, SNAP-25, bA416N4.2, dJ1068F16.2) The protein interaction list generated for SNAP-25 was stored as a list in Excel, which was compared to the Human E3 ubiquitin ligase (https://hpcwebapps.cit.nih.gov/ESBL/Database/E3-ligases/) and Accessory Proteins databases lists (https://esbl.nhlbi.nih.gov/Databases/KSBP2/Targets/Lists/E3ligases/RelatedProteins.html) (Table 2.1) which were also saved in an excel format and conditional formatting for values duplicated between lists were used to identify SNAP-25 interactors that were present on the E3 ligase database. The literature sources from BioGRID for the proteins that were identified to have E3 ligase function were then evaluated for evidence of an interaction with SNAP-25. Finally, these proteins were

compared to the Human Protein Atlas version 20.1 (https://www.proteinatlas.org/) to identify if they were neuronally expressed.

2.2.3 PubMed database for the identification of E3 ligases that interact with SNAP25

PubMed (https://pubmed.ncbi.nlm.nih.gov/) (Accessed October 2021) (Table 2.1) was used to produce a list of SNAP-25-E3 ligase interactions. This was done using the search terms "SNAP-25 ligase", "SNAP-25 E3 ligases" and "SNAP-25 ubiquitination". Lists of potential E3 interacting partners were then compared to the Human E3 ubiquitin ligase.

Table 2.1: **Databases used for the identification of E3 ubiquitin ligases that interact with SNAP-25 via the literature-based searches.**

Database for Literature approach	Data collection methods	Data curation
BioGrid: The Biological General Repository for Interaction Datasets	Archives genetic and protein interactions from both model organisms; *S.cerevisiae, S. pombe, A.thaliana* and humans. Interactions are curated by primary literature, taking into account both high-throughput datasets and focused studies	Curation from database curators searching primary literature: CRISPR Database, HGNC, Alliance of Genome Resources, VEGA, OMIM, Entrez Gene, RefSeq, UniprotKB, Ensemble, HPRD.
PubMed	PubMed is an open-access database of citations from journals, online books and literature with a life science or biological theme.	Biomedical literature from MEDLINE, life science journals and online books
Human E3 ubiquitin ligase database	List of all predicted E3 ligase genes coded by the human genome, by manual curation of limited pre-existing lists.	Cell Signalling Technology Ubiquitin Ligase table, hUbiqutome database, Qiagen ubiquitin Ligase PCR array, UbiProt, DUDE v.1.0, and Ligases identified by Li et al within a Genome-Wide and Functional Annotation of Human Ubiquitin Ligases
Human E3 Ubiquitin Ligase Accessory Proteins Database	List of known E3 ligase accessory proteins coded by the human genome, by combining limited pre-existing lists	Supplementary Table 1 for Li et al with the additional inclusion of the Cullin proteins

Repeating the PubMed search with the above search terms in June 2025 produced two additional articles for the search term "SNAP-25 ligase", and six additional articles for the search term "SNAP-25 ubiquitination", which are discussed in Chapter 3.

2.2.4 Predictive bioinformatic approach to identify E3 ligases

The predictive approach utilised structural features of SNAP-25 and related SNAP-25-like proteins to produce a list of potential E3 ligases.

2.2.5 Use of Ubi-Browser to predict E3 ligases that have the potential to interact with SNAP-25

The database Ubibrowser (http://ubibrowser.bio-it.cn/ubibrowser/) (Accessed November 2021) (Table 2.2), which predicts E3 ligase-substrates interactions based on structural features and GO term annotation, was used to predict potential SNAP-25 E3 ligases.

Two iterations of the database were available (Figure 2.3) Ubibrowser 1.0 (http://ubibrowser.bio-it.cn/) predicted just human interactions using manual curation, protein orthologues, protein domains, protein motifs and network topology. Whilst UbiBrowser 2.0 (UbiBrowser_v2) has extended its database to include interactions for other eukaryotic species.

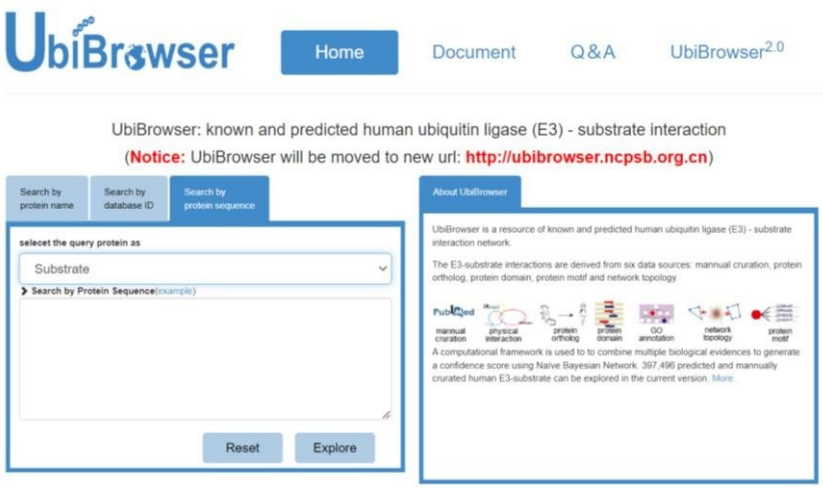

UbiBrowser_v2 (bio-it.cn)

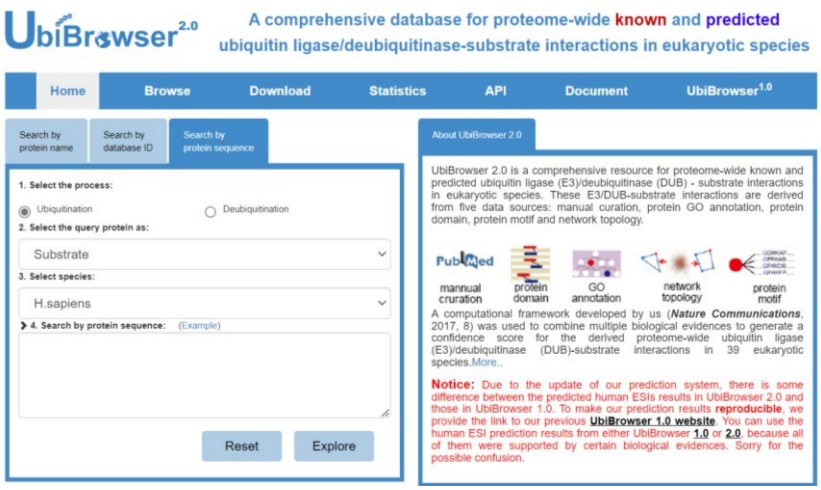

Figure 2.3: **Ubibrowser look-up pages for iterations 1.0 and 2.0 for the prediction of E3 ligase–substrate interactions**

P60880, Sequence SNP25_B_HUMAN used for the prediction of E3 ligase interactions:

MAEDADMRNELEEMQRRADQLADESLESTRRMLQLVEESKDAGIRTLVMLDEQGEQLERIEEGMD
QINKDMKEAEKNLTDLGKFCGLCVCPCNKLKSSDAYKKAWGNNQDGVVASQPARVVDEREQMAIS
GGFIRRVTNDARENEMDENLEQVSGIIGNLRHMALDMGNEIDTQNRQIDRIMEKADSNKTRIDEAN
QRATKMLGSG

Ubibrowser 1.0 and 2.0 search results were reassessed in June 2025, generating the same readout.

2.2.6 Use of Human Protein Atlas to identify neuronal protein expression

E3 ligases that were identified by Ubibrowser as being candidates for the ubiquitination of SNAP-25 were investigated for evidence of neuronal expression using the Human Protein Atlas. Each E3 ligase was individually searched by inputting the protein name, then the brain was chosen as the search location, and evidence of both RNA and Protein expression was assessed.

2.2.7 Identification of E3 ligases that interact with proteins with structural similarity to SNAP-25

Sequence and structural alignments of other human SNAP family members, which share sequence homology or predicted structural protein folds to SNAP-25, were carried out using BLAST (https://blast.ncbi.nlm.nih.gov/Blast.cgi)(Version: BLAST+ 2.12.0) (Accessed December 2021) (Table 2.2), Multalin (http://multalin.toulouse.inra.fr/multalin/) (Version 5.4.1) (Accessed December 2021), the RCSB PDB - Structure Pairwise Alignment Tool (https://www.rcsb.org/alignment) (Accessed November 2022) and UniProt https://www.uniprot.org/) (Version 2022_05) (Accessed November 2022) databases. BioGrid (https://thebiogrid.org/) (version 4.2.193) (Accessed December 2021) was then used for SNAP-23, 29 and 47 to identify all known interactors, which were then compared to the Human E3 ubiquitin ligase and Accessory Proteins databases to identify E3 ligase interactors as described in section 2.2.2. Ubibrowser was used to identify structural features, including domain pairs and E3 recognising motifs which would predict interaction with E3 ligases, which could be mapped onto the SNAP family amino acid sequence. Sequences for each of the SNAP family members are displayed below, and the combinations of outputs are displayed in Figure 3.9.

O00161, Sequence SNP23_HUMAN used for the prediction of E3 ligase interactions:

MDNLSSEEIQQRAHQITDESLESTRRILGLAIESQDAGIKTITMLDEQKEQLNRIEEGLDQINKDMRET
EKTLTELNKCCGLCVCPCNRTKNFESGKAYKTTWGDGGENSPCNVVSKQPGPVTNGQLQQPTTGA
ASGGYIKRITNDAREDEMEENLTQVGSILGNLKDMALNIGNEIDAQNPQIKRITDKADTNRDRIDIANA
RAKKLIDS

O95721, Sequence SNP29_HUMAN used for the prediction of E3 ligase interactions:

MSAYPKSYNPFDDDGEDEGARPAPWRDARDLPDGPDAPADRQQYLRQEVLRRAEATAASTSRSLA
LMYESEKVGVASSEELARQRGVLERTEKMVDKMDQDLKISQKHINSIKSVFGGLVNYFKSKPVETPPE
QNGTLTSQPNNRLKEAISTSKEQEAKYQASHPNLRKLDDTDPVPRGAGSAMSTDAYPKNPHLRAYH

QKIDSNLDELSMGLGRLKDIALGMQTEIEEQDDILDRLTTKVDKLDVNIKSTERKVRQL

Q5SQN1, Sequence SNP47_HUMAN used for the prediction of E3 ligase interactions:

MRAARRGLHCAGAERPRRRGRLWDSSGVPQRQKRPGPWRTQTQEQMSRDVCIHTWPCTYYLEPK

RRWVTGQLSLTSLSLRFMTDSTGEILVSFPLSSIVEIKKEASHFIFSSITILEKGHAKHWFSSLRPSRNVV

FSIIEHFWRELLLSQPGAVADASVPRTRGEELTGLMAGSQKRLEDTARVLHHQGQQLDSVMRGLDK

MESDLEVADRLLTELESPAWWPFSSKLWKTPPETKPREDVSMTSCEPFGKEGILIKIPAVISHRTESHV

KPGRLTVLVSGLEIHDSSSLLMHRFEREDVDDIKVHSPYEISIRQRFIGKPDMAYRLISAKMPEVIPILEV

QFSKKMELLEDALVLRSARTSSPAEKSCSVWHAASGLMGRTLHREPPAGDQEGTALHLQTSLPALSE

ADTQELTQILRRMKGLALEAESELERQDEALDGVAAAVDRATLTIDKHNRRMKRLT

Table 2.2: **Databases used for the identification of E3 ubiquitin ligases that interact with SNAP-25 via structure-based searches.**

Database for Predicting E3 ligases that interact	Data collection methods	Data collection sources
Ubibrowser 1.0 and 2.0	Ubibrowser is a comprehensive, evidencebased database used for the identification of known and predicted ubiquitin ligase/deubiquitinasesubstrate interactions in eukaryotic species.	Manual curation (PubMed), protein GO annotation, protein domain, protein motif and network topology
BLAST: Basic Local Alignment Search Tool	Basic Local Alignment Search Tool is used to compare sequence information, allowing DNA or protein query sequences to determine sequence homology.	Accession number(s), gi(s), or FASTA sequence(s) are inputted by the user and databases (PubMed, GenBank, and PMC)
UniProt	UniProt: open open-access protein sequences database.	Protein sequences from translations of coding sequences.

2.2.8 Disease association bioinformatic approach to support identified E3 ligases which may interact with SNAP-25

I created the disease-informed approach to extend known candidate interactions. I used literature to focus on E3 ligases implicated in disorders with which SNAP-25 has an established association. These were cross-referenced to investigate if there was a linkage between SNAP-25 and E3 ligase activity-related diseases.

Initially, the databases DisGenNET V7.0 (https://www.disgenet.org/) (Accessed December 2021) (Table 2.3) and PubMed (See Table 2.3 for further information) were utilised using the search terms "SNAP-25" for the former and "SNAP-25 disorder, SNAP-25 brain disease" for the latter. This produced two lists of disorders for which there is literature to support an association with SNAP-25. The list produced by DisGenNET V7.0 was then filtered for the terms mental disorders and nervous system disease, which were assigned by the database. The lists were assessed and the disordered ranked based on whether an association was a genetic, biochemical or an inferred association PubMed was then used again to identify E3 ligases for which there is evidence for a role in each of the disorders using the search term "(name of disorder) and E3 ligase". Initially, abstracts were searched then the articles were assessed for the literature for strength of association was then used to produce the final list of E3 candidates. The E3 ligases with the strongest supporting evidence of a genetic, biochemical or inferred association or that were involved in the most disorders with a downregulation of SNAP-25, were classed as strong candidates and were taken with evidence from other streams.

Table 2.3: **Additional Databases used for the identification of E3 ubiquitin ligases that interact with SNAP-25 via disease association-based searches.**

Database for Candidate Approach	Data collection methods	Data collection sources
DisGenNET V7.0	Human gene and variants associated with diseases. Integration of data is by means of gene and disease vocabulary mapping and the DisGeNET association type ontology	Data is integrated from curated repositories: UniProt, CTD, Orphanet, ClinGen, Genomics England, CGI, PsyGeNET. Animal models: RGD, MGD, CTD. Literature: LHGDN, BEFREE. Inferred: HPO, CliVar, GWAS catalogues, GWAS Database.

2.2.9 Interrogation of literature to identify proteomic screens of candidate E3 ligases

Once a list of E3 ligases that had the potential to interact with and ubiquitinate SNAP-25 had been produced (Sections 2.2.2 and 2.2.5). PubMed was used to investigate if there was literature to suggest a proteomic screen had been carried out on each protein using the search terms "E3 ligase name + proteomic screen" and "E3 ligase name + Screen". If a proteomic screen was identified for an individual E3 ligase, both the main paper and any supplementary data were investigated for evidence of SNAP-25 being included as a candidate interactor.

2.2.10 AlphaFold Multimer used for the prediction of interaction between SNAP-25 and Parkin

The protein sequences for SNAP-25 and Parkin were downloaded from Uniprot:
>Parkin (O60260)
MIVFVRFNSSHGFPVEVDSDTSIFQLKEVVAKRQGVPADQLRVIFAGKELRNDWTVQNCDLDQQSIV
HIVQRPWRKGQEMNATGGDDPRNAAGGCEREPQSLTRVDLSSSVLPGDSVGLAVILHTDSRKDSP
PAGSPAGRSIYNSFYVYCKGPCQRVQPGKLRVQCSTCRQATLTLTQGPSCWDDVLIPNRMSGECQ
SPHCPGTSAEFFFKCGAHPTSDKETSVALHLIATNSRNITCITCTDVRSPVLVFQCNSRHVICLDCFHL
YCVTRLNDRQFVHDPQLGYSLPCVAGCPNSLIKELHHFRILGEEQYNRYQQYGAEECVLQMGGVL
CPRPGCGAGLLPEPDQRKVTCEGGNGLGCGFAFCRECKEAYHEGECSAVFEASGTTTQAYRVDER
AAEQARWEAASKETIKKTTKPCPRCHVPVEKNGGCMHMKCPQPQCRLEWCWNCGCEWNRVCM
GDHWFDV

>SNAP25 (P60880)
MAEDADMRNELEEMQRRADQLADESLESTRRMLQLVEESKDAGIRTLVMLDEQGEQLERIEEGMD
QINKDMKEAEKNLTDLGKFCGLCVCPCNKLKSSDAYKKAWGNNQDGVVASQPARVVDEREQMAIS
GGFIRRVTNDARENEMDENLEQVSGIIGNLRHMALDMGNEIDTQNRQIDRIMEKADSNKTRIDEAN
QRATKMLGSG

The sequences were combined in a single FASTA, which was uploaded to the Alphafold2 Colabfold model v3 (Jumper et al., 2021) hosted by Cosmic[2] (Cianfrocco *et al*., 2017) (April 2025) Alpha fold predicted 5 models for Parkin and SNAP-25 to interact, all with low confidence, with regard to the predicted template modelling (pTM) score and the interface predicted template modelling (ipTM) score (EMBL-EBI, April 2025). The highest-ranked prediction was then visualised using the software PyMOL 3.1.4.1 and the domains of Parkin highlighted.

2.3 Molecular biology

2.3.1 Genomic DNA extraction from cells

Genomic DNA was extracted from cultured PC12 cells. 100 µl lysis buffer (NaCl 100mM, SDS 0.5%, EDTA 10 mM, Tris pH8 10 mM, protease K 0.4 mg/ml) was added to the cells, which were scraped and extracted into an Eppendorf tube that was heated to 54 °C for one hour. The samples were centrifuged (Sigma 1-14K microcentrifuge) for 10 minutes at 20,000 xg, and the supernatant was removed. 50 µl of isopropanol was added to 50 µl of the supernatant and mixed by pipetting. The samples were spun at 16000 xg for 5 minutes to pellet the genomic DNA. The supernatant was

removed, and the pellet was washed twice in 100 µl of 70% ethanol with pelleting. The ethanol was removed, and the pellet was then centrifuged for 5 minutes at 16000 xg. The pellet was air-dried and then resuspended in 50 µl RNAase-free water

2.3.2 RNA extraction from cells

RNA was extracted from cultured immortalised cell cultures using the RNeasy Mini kit (Qiagen). Briefly media was removed from the cells. For a 12-well plate, cells were lysed with 350 µl of RLT buffer, and for a 6-well 600 µl of RLT buffer. The lysate was removed and homogenised by vortexing (Vortex-Genie 2) for 1 minute at room temperature. The extracted RNA was purified using the RNeasy spin columns and eluted into 30 µl RNase-free water (Qiagen RNeasy kit). The RNA concentration was estimated using the nanodrop spectrophotometer (Thermo Fisher Scientific), and RNA integrity was determined by running 1 µg of RNA on a 1% agarose gel and determining the 28S:18S values.

2.3.3 RNA Quality Assessment

The RNA purity and yield were determined by spectroscopy with a Nanodrop2000®; 1 µl of eluted total or mRNA was measured between 230-280nm, with absorbance values used to calculate concentration. The ratios of absorbance at 260/230 nm and 260/280nm were used to assay purity. To assay RNA degradation, 1 µg of RNA was resolved on a 1% agarose gel with gel electrophoresis in TAE performed at 80V. The gel was then imaged on a UV imager and the 28:18S rRNA (ribosomal RNA) ratios were calculated with a ratio of ~2 considered good quality intact RNA (Figure 2.4).

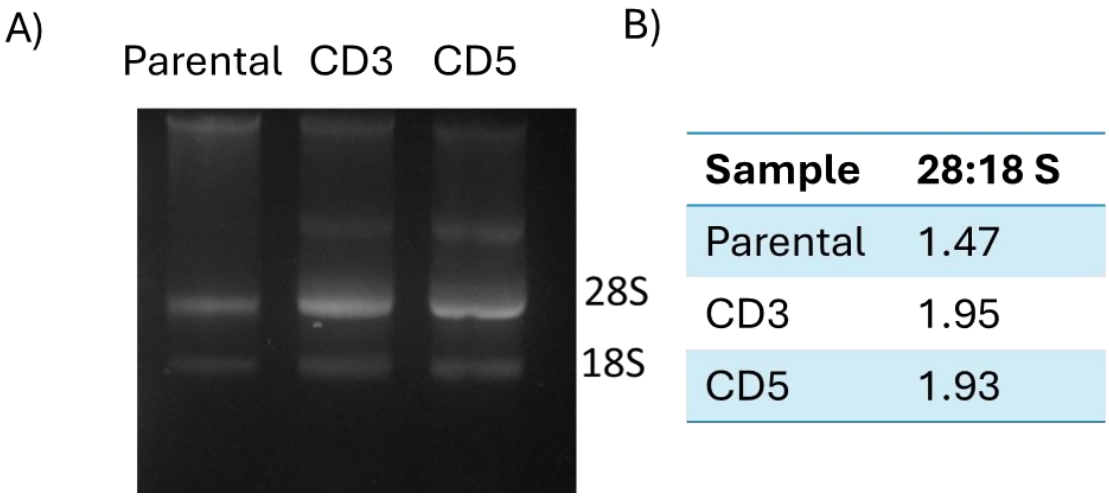

Figure 2.4: **RNA Quality Assessment.** RNA (1 µg) from parental and CSPα deficient PC12 cells visualisation of 28:18S rRNA on a 1% agarose gel. A) Gel electrophoresis of 1ug total RNA extracted from parental and CSPα-deficient 3 and 5 PC12 cells. B) The intensity of the 28:18S rRNA for the corresponding samples, indicating RNA integrity.

2.3.4 cDNA synthesis

200 ng of purified total RNA (section 2.3.2) was reverse transcribed with the Precision nanoScript 2 reverse transcription kit (Primer Design Eastleigh, UK) according to the manufacturer's instructions. These reactions were performed in thin-walled PCR tubes, carried out as indicated (Table 2.4). The reactions were incubated in the Applied Biosystems or BioRad T100 Thermal cycler under the conditions shown in Table 2.5. cDNA was stored at -20 °C.

Table 2.4: Components and Volumes required for reverse transcription

Components	Volume µl per reaction
NanoScript 2 4x buffer	5
NanoScript 2 enzyme	1
dNTP mix (10 mM)	3
Oligo-DT primer (0.2 nM)	1
Total RNA sample (200 ng)	Variable
Nuclease-free water	Variable
Total	20

Table 2.5: Conditions required for reverse transcription using thermocycler (GeneAmp PCR system 9700, Applied Biosystems, or BioRad T100 Thermal cycler)

Step	Temperature (°C)	Time (minutes)
Annealing	65	5
Extension	42	20
Heat inactivation	75	10

2.3.5 Primer design for end-point cDNA and genomic PCR

Primers (Eurofins genomic) (Table 2.6 for identification, Table 2.14 for cloning primers) were designed using the NCBI Primer Blast tool. The criteria used included: 18-24 bases in length (longer for cloning), melting temperature between 55°C – 65°C, ideally an amplicon size of between 70-200 bases and a guanine-cytosine content of between 40-70%. Oligonucleotide Analyser by IDTDNA was used to ensure the primers didn't contain hairpin structures or would self- or hetero dimerize. The cDNA primers were designed across exon-exon boundaries to allow the detection of genomic DNA

contamination. For genomic DNA, primers were designed in intronic regions. All primers were obtained from Eurofins Genomics.

Table 2.6: Primer pairs for end-point identification PCR experiments for murine samples and PC12 samples. Bp-base pair, FWD- forward primers, REV-reverse primer, T_A – annealing temperature.

Gene	Sequence 5-3 prime	Predicted amplicon size (bp)	T_A (°C)
SNAP-25 Mouse	FWD CTG GCT GAT GAG TCC CTG GAA AGC ACC C REV TCC CGG GCA TCA TTT GTT ACC CTG CGG	368	65
SNAP-25 Rat	FDW GCT GTG CTC TCC TCC AAT GT REV AGG AAG TCA GAA ACT GAG AGA TCC	138	64
GAPDH Mouse	FWD TGA ACG GGA AGC TCA CTG G REV TCC ACC ACC CTG TTG CTG TA	307	58
GAPDH RAT	FWD TGA ACG GGA AGC TCA CTG G REV ACA GGA GAC AAC CTG GTC CT	182	55
CSPα RAT cDNA	FWD ACT AAC CTA ACA TGG CTG ACC REV CAT GAT TCT AAG GTT GCA GTG GC	671	52
CSPα across sgRNA_3 Genomic	FWD AGT TAA CTT GTC AGA CAT GAC A REV GAT TAA AGG CAT TCG TCA CCA	402	50
CSPα across sgRNA_5 Genomic	FWD CTG GTT CCA GAG AGG TAG CCA G REV ACA AAC ACT CTC GGC ACA GTG	635	57
TRKB RAT	FWD GCT GAC GAG TTT GTG CAG GA REV TGG CTC CGT TGT AGA ACC AC	591	55
ACTIN RAT	FWD CAG CCT TCC TTC TTG GTA TG REV AGC TCA GTA ACA GTC CGC CT	360	52

2.3.6 End-point Polymerase Chain Reaction (PCR)

REDTaq Ready-mix PCR mix (Sigma-Aldrich) was used as the reagent for end-point reactions. A master mix was made according to Table 2.7. The master mix (24 µl) was aliquoted into each PCR

tube, and then 1 µl of cDNA template was added. The reaction was incubated (GeneAmp PCR system 9700, Applied Biosystems or BioRad T100 Thermal cycler) as described in steps outlined in Table 2.8.

Table 2.7: Components and volumes of reagents used in end-point PCR reactions.

Component	Volume per reaction µl
REDtaq Ready-mix PCR Reaction mix	12.5
Nuclease-free water	10.5
Indicated Forward Primer (10mM)	0.5 (0.2 mM)
Indicated Reverse Primer (10 mM)	0.5 (0.2 mM)
Indicated Template cDNA	1 (0.4 mM)
Total	25

Table 2.8. Conditions for RED TAQ end-point PCR reactions.

	Step	Temperature	Time
	Initial denaturation	94 °C	2 min
Variable number of cycles 25-35	Denaturation	94 °C	1 min
	Annealing	Variable (Table 2.6)	30 sec
	Extension	72°C	1 kb/ 30 sec
	Final Extension	72 °C	10 min
	Hold	10 °C	∞

2.3.7 Polymerase chain reaction (PCR) for cDNA cloning.

Primers (Eurofins genomic) were used to amplify cDNA (Section 2.3.4) for each primer pair, see Table 2.14. The PCR components are outlined in Table 2.9, and parameters are outlined in Table 2.10. The amplification was initially authenticated by resolving the products of the reaction using gel electrophoresis (Section 2.3.8)

Table 2.9: Volumes of reagents used for PCR reaction to generate inserts for molecular cloning.

Component	Volume (µl)
5 x Q5 Reaction Buffer	10
10 mM dNTPs	1 (0.2 nM)
10 µM Forward Primer	1 (0.2 mM)
10 µM Reverse Primer	1 (0.2 mM)
Template DNA	Variable
Q5 High-Fidelity DNA polymerase	0.5
Filtered- distilled water	Up to 50 µl

Table 2.10: Conditions used for PCR reaction when using Q5 polymerase

Step	Temperature (°C)	Time (seconds)
Initial denaturing	98	30
Denaturing	98	10
Primer Annealing (table)	60-72 (as indicated)	10-30
Extension	72	30 seconds/Kb*
Final Extension	72	600*
Hold	10	∞

*Optimal settings variable for different sets of primers

The conditions used for 25-35 cycles for PCR reactions with Q5 polymerase.

2.3.8 Agarose gel electrophoresis

Agarose powder (0.8 g) was suspended in 80ml of 1x TAE buffer (40mM Tris acetate and 1 mM EDTA), and the solution was heated in the microwave for ten-second intervals until fully dissolved. The molten agarose was allowed to cool until it could be held comfortably (~3-5 minutes), and 8 µl of Gel-red (10,000x stock in water, Biotium) was added. The gel was poured into a gel cassette with a comb inserted and allowed to solidify (Fisherbrand Verti-Gel Electrophoresis system). The gel was placed in an electrophoresis tank containing 1x TAE buffer. Samples were prepared by the addition of quick loading dye (Thermofisher Scientific 6x DNA loading dye). After solidifying, the comb was removed, and a DNA ladder (100 bp plus or 1KB plus gene ruler) and samples were loaded into individual wells. The gel was resolved using 120 volts (V) for between 45-90 minutes. The DNA sample gels were visualised at wavelength of 600 nm using a UV transilluminator and documented using the G: BOX (Syngene) imager.

2.3.9 PCR/Gel Clean-up of amplified cDNA

PCR products were purified directly from the PCR reactions (Section 2.3.6 or 2.3.7) or following purification through agarose gels. In the latter case, the PCR was run through a gel and visualised on a UV light box set to low illumination strength (Benchmark Accuris MyView Compact UV Transilluminator) (Section 2.3.8). A clean scalpel was used to excise the selected resolved DNA fragment. In both cases, the DNA was extracted and purified using Macherey-Nagel Nucleospin gel and PCR clean-up kit following the manufacturer's instructions (Macherey-Nagel).

2.3.10 Determining DNA concentration

The DNA concentration and quality of isolated plasmids and cDNA were estimated using a spectrophotometer (Thermo Fisher NanoDrop 2000c UV-Vis) with absorbance at 260 nm. Before measuring DNA concentration, the spectrophotometer was blanked with the 1 µl of the buffer the

DNA was dissolved in. Then, 1 µl of each sample was loaded onto the nanodrop to determine the concentration of the DNA.

2.3.11 Annealing of oligos

Oligonucleotides used for the generation of the guide RNA to be cloned in the P-Lenti CRISPR vector (source Addgene #52961) were annealed by combining the components listed in Table

2.11. The mixture was incubated at 37 °C for 30 minutes, then at 95 °C for 5 minutes before being allowed to cool down to 4 °C at a rate of 0.1 °C per second. The 10 µl reaction was then diluted in 250 µl of DDH_2O.

Table 2.11: Components required for the annealing and phosphorylation of oligos.

Component	Volume (Total 10 µl)
T4 PNK (10 U/µL)	0.5 µl (5 units)
DD water	6.5 µl
T4 ligase buffer (x10)	1 µl (1x)
Forward oligo (100 µm)	1 µl (10 µm)
Reverse oligo (100 µm)	1 µl (10 µm)

2.3.12 Restriction digest of DNA insert and plasmid backbone

A template for restriction digestion reactions was as listed in Table 2.12. The reaction mixtures were incubated at 37 °C for 60 minutes. Digested plasmids were resolved by gel electrophoresis (MultiSUB Choice, Horizontal electrophoresis system) and extracted from the gel (Sections 2.3.8 and 2.3.9) after visualisation. For specific reagents used in cloning reactions, see sections 2.4.

Table 2.12: Reagents and volumes used for restriction digest reactions* general volume used, volume dependent on the unit activity for the specific restriction enzyme.

Component	Quantities for 20 µl reaction (Promega)	Quantities for 10 µl reaction (NEB)
DNA	1 µg	1 µg
Restriction enzyme 1 (10 units/ 1µl)	0.5 µl* (5 units)	0.5 µl* (5 units)
Restriction enzyme 2 (10 units/ 1µl)	0.5 µl (5 units)	0.5 µl (5 units)
10X RE Buffer	2 µl (1x)	1 µl (1x)
Bovine serum albumin (BSA)	0.2 µl (0.1 mg/ml)	N/A
Filtered distilled water	Up to 20 µl	Up to 10 µl

2.3.13 Ligation reaction of the vector and insert

Purified restriction enzyme-digested vectors and PCR products (Section 2.3.9) were ligated with T4 DNA ligase (NEB) (Table 2.13). The molar ratios for each ligation were calculated using the formula in Equation 1. The T4 DNA ligase reaction mix was then incubated at RT for 15 minutes.

$$kb\ of\ insert \div kb\ of\ vector \times ng\ of\ vector = ng\ of\ insert\ needed\ for\ a\ 1{:}\ 1\ ratio$$

Equation 2.1 : Calculation to determine the amount of insert required for a 1:1 molar ratio

Table 2.13: Components and volumes required for ligation reaction of vector and insert.

* general volume used, volume dependent on specific reaction.

	Vector: Insert mole ratio			
Reagent	**Vector only control**	**1:1**	**1:3**	**1:5**
Vector (µl)	1	1	1	1
Insert (µl)	0	1*	3*	5*
10X T4 Ligase Buffer (µl)	1	1	1	1
T4 DNA Ligase (µl)	0.5	0.5	0.5	0.5
Filtered distilled water (µl)	Up to 10 µl	Up to 10 µl	Up to 10 µl	Up to 10 µl

2.3.14 Bacterial Agar Plate Preparation

Solid LB (Lysogeny Broth) agar (100 ml in water) from the media kitchen (School of Biological Sciences) was melted in the microwave once cooled to approximately 55°C either ampicillin (0.1%, 100 mg/ml) or kanamycin (0.1% 50mg/ml) antibiotic was added to the flask under sterile conditions to a final concentration of 100 µg/ml or 50 µg/ml respectively. The melted supplemented agar was poured into 10 cm sterile petri dishes and left to set. Once set, the plates were wrapped in Clingfilm and stored at 4 °C until required and used up to 14 days later.

2.3.15 Bacterial transformation

DH5α chemically competent *E. coli* cells (NEB) or STABLE 3 *E. coli* cells (Invitrogen) were placed on ice for 20 minutes and allowed to thaw. 2.5 µl of the ligation mix (Section 2.3.13) was put on ice, and 25 µl of thawed competent cells were added and mixed with the pipette tip. The cells were incubated on ice for 30 minutes, then heat shocked in a water bath at 42 °C for 30 seconds. The mixture was

then incubated on ice for a further 2 minutes. 150 µl Super Optimal broth with catabolite repression (SOC) growth media (NEB; 2% vegetable peptone, 0.5% yeast extract, 10 mM NaCl, 2.5 mM KCl, 10 mM $MgCl_2$, 10 mM $MgSO_4$, and 20 mM Glucose) was added and the mix was incubated at 37°C for DH5α or 30°C for STABLE 3 cells for one hour. The whole mix or aliquots thereof were spread on LB agar plates (Section 2.3.14), which had been pre-warmed to 37°C. The plates were left to dry before being incubated overnight at 37 °C for DH5α or 30°C for STABLE 3 cells.

2.3.16 Plasmid expression and mini-prep

Transformed bacterial colonies (Section 2.3.15) were identified based on growth on the indicated selective antibiotic. Candidates were picked from the plates and cultured in 3 ml LB media. The culture was incubated at 37 ^{o}C overnight in the shaking incubator. The culture was centrifuged at 4,000 x g for 5 minutes at 4 ^{o}C. The bacterial pellet was processed to extract plasmid DNA using the Macherey-Nagel NucleoSpin Plasmid DNA kit. After which, 50 µl of elution buffer was used to elute the DNA, which was quantified using absorbance at 260 nm (NanoDrop).

2.3.17 Restriction digest screening

Restriction digest (Section 2.3.12) was carried out to screen for correct plasmid subcloning.
The DNA isolated from colonies that displayed the predicted restriction digest were sent to Eurofins Genomic for Sanger sequencing in the forward and reverse directions. The chromatograms were inspected for precision, and the cDNA sequences were aligned with digital plasmid maps.

2.3.18 Generation of Myc BioID constructs

Cloning was carried out as depicted in the scheme in Figure 2.5 below to produce a MycBioID-SNAP-25 and Figure 2.6 for Myr-Myc-BioID constructs using the primers in Table 2.14.

Table 2.14: Primers and restriction enzymes used to generate Bio-ID reagents.

Gene	Sequence	Restriction enzyme	Expected size (bp)
p-mycSNAP-25BioID	FWD 5-GAT C**GA ATT C**TG CCG AAG ACG CAG ACA TGC GC-3 REV 3-GAT C**GT CGA C**TT AAC CAC TTC CCA GCA TC -5	EcoR1 Sal1	621
p-myc-MYR-BioID	FWD 5-GAT C**AC CGG T**TA TGG AAC AAA AAC TCA TCT CAG AA-3 REV 3-GAT C**GC GGC CGC** CTT CTC TGC GCT TCT CAG GGA GA-5	Agel 1 Not 1	996

2.3.19 Generation of Myc-BioID-SNAP-25

The SNAP-25 cDNA was amplified flanked by 5' and 3 ' sequences as described in Table 2.14. The insert and the Myc-BioID vector were digested with EcoR1 and Sal1, producing complementary overhangs. To screen for the production of the desired product from the cloning, a diagnostic restriction digest of the purified product using Sal1 and Ecor1 RE's, the Myc-BioID-SNAP-25 plasmid produced an insert of 600 bp, likely indicating successful generation of the construct, which was then confirmed by Sanger and whole plasmid sequencing (Figure 2.5).

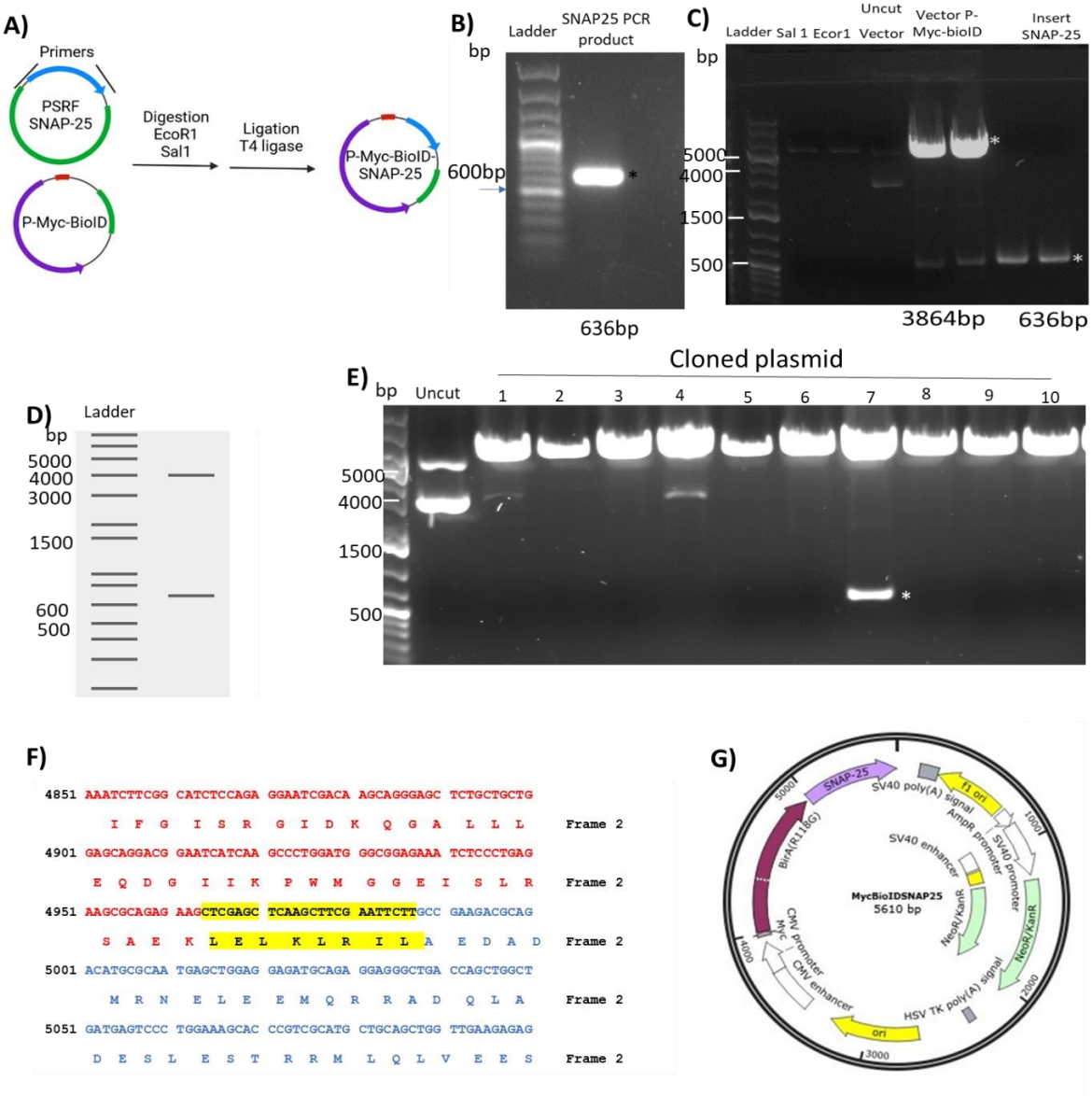

Figure 2.5: Generation of the p-Myc-BioID-SNAP-25 plasmid via cloning of the SNAP-25 insert from PRSF vector backbone into the Myc-BioID vector.

A) Schematic workflow of cloning strategies for the generation of p-Myc-BioID-SNAP-25. Forward and reverse primers were designed to amplify the SNAP-25, which was digested with the restriction enzymes indicated and ligated into the P-Myc BioID backbone. B) PCR amplification of the SNAP-25 insert, with amplified product marked with an asterisk. C) Digest of Myc-BioID vector and the SNAP-25 insert with Sal1 and EcoRI. D) Expected gel pattern when MycBioID-SNAP25 are digested in silico with Sal1 and Ecor1. E) Diagnostic test digest results for the cloned construct digested with Sal1 and Ecor1, with an asterisk sequencing of the insert. F) Sequenced results of the construct with red sequence depicting the end of the BioID construct, the yellow highlighted region the linker and the blue region highlighting the start of the SNAP-25 sequence. G) Plasmid map of P- Myc-BioID-SNAP25 construct generated from whole plasmid sequencing, SNAP25 is in frame with the Myctagged BioID construct.

2.3.20 Generation of Myr-Myc-BioID

The Myc-BioID sequence was amplified and isolated from p-Myc-BioID plasmid (primers in Table 2.14). The specific forward and reverse primers flanked the MYC-BioID region. The forward primer began with a GGATCC sequence, followed by an Agel1 restriction site, followed by a linker and 25 Nucleotides of the sense strand of the Myc BioID coding region. The reverse primer flanked the sequence with a Not1 restriction site, followed by a linker, then 23 nucleotides complementary to the antisense strand of the Myc BioID coding region.

Both the Myc-BioID insert and the Myr-GFP plasmid vector were digested with Agel1 and Not1, facilitating the removal of the GFP sequence to provide complementary overhangs. To screen for the production of the desired product from the cloning, a diagnostic restriction digest test was done on the purified product using Agel1 and Not1 RE's the Mry-Myc-BioID plasmid produced an insert to be cut out of 1004 bp, which was sent for sequencing whilst the plasmid containing the GFP would release an insert of 720 bp (Figure 2.6).

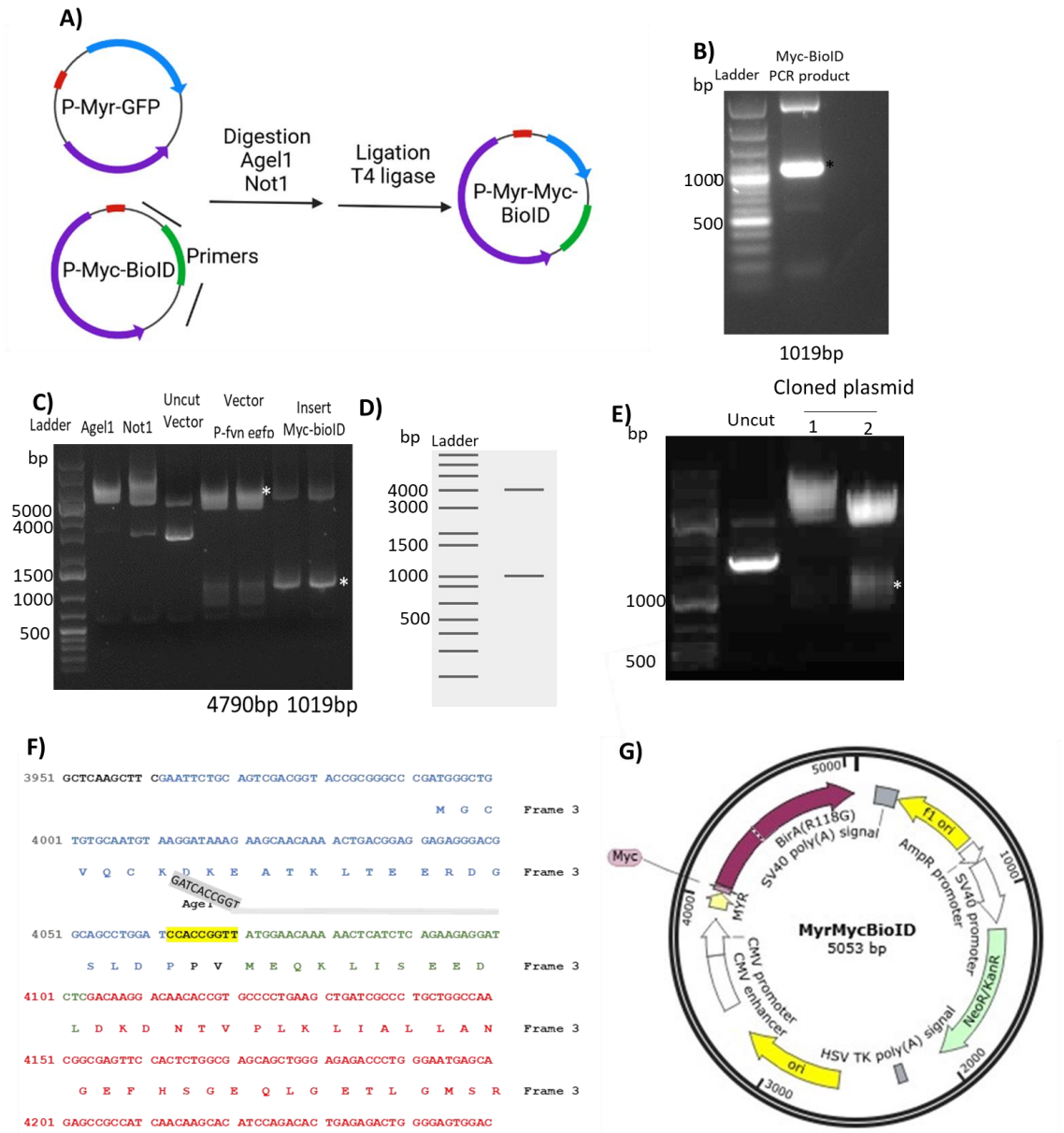

Figure 2.6: **Molecular cloning of the Myr-Myc-BioID construct.** A) Schematic workflow of cloning strategies for the generation of P-Myr-Myc-BioID. Forward and reverse primers were designed to amplify the Myc-BioID inserts from the p-Myc BioID vector backbone. Inserts of what were amplified using PCR, digested with the restriction enzymes indicated, were ligated into the P-Myr, which removed the GFP sequence. B) Gel depicting the amplified Myc BioID fragment with an asterisk. C) Digest of Myr-GFP vector and the Myc BioID insert with AgeI1 and Not1. D) In silico gel pattern when p-Myr Myc BioID was digested with AgeI1 and Not1. E) Diagnostic digest with AgeI1 and Not1, an asterisk indicating the presence of a band of 1004 bp consistent with successful production of Myr-Myc-BioID**.** F) Sequenced construct showing in blue Myr sequence, linker (yellow) between Myr and Myc, the green sequence corresponds to Myc tag and the red sequence is BioID. Forward Primer is depicted in grey. G) Plasmid map of p-Myr-Myc BioID, authenticated whole plasmid sequencing, Myr mysterilated protein in frame with the Myc-tagged BioID construct forming P-Myr-Myc-BioID.

2.4 Generation of reagents for CRISPR cell line generation

2.4.1 Designing sgRNAs for genetic knockdown in Cell lines

Optimal signal guide RNAs (sgRNAs) were selected based on established criteria (Doench et al., 2016). The software CRISPick was used to identify sites which could be used for the disruption of the DNAJ5C gene (Figure 2.7) in the *Rattus norvegicus* genome. SpyoCas, which identifies the PAM site NGG with Hsu, was input as the cutting enzyme and tracrRNA. Five potential sites (Figure 2.7) with no off-target homology or mismatches were mapped to the DNAJC5 gene: one in exon three, three in exon four and one in exon five.

Primers were designed to subclone the gRNAs into the lentiCRISPRv1 puro plasmid. CACC and AAAC were added to the sense and antisense primers, respectively, generating two BsmB1 sites to allow the required RNA sequences to be subcloned. All the selected oligomer sequences are 20 nucleotides long, but a G is added to increase the efficiency of Cas binding if there is not already one present (Table 2.15).

2.4.2 Cloning to generate Lenti CRISPR V1 plasmid containing sgRNA

Primer pairs for each of the indicated oligos in Table 2.15 were annealed and phosphorylated with T4 PNK (Section 2.3.11). With the naming of the oligos indicating which exon the guide is targeting, i.e, DNAJC5_sgRNA3 targeting exon 3 and DNAJC5_sgRNA5 targeting exon 5.

Table 2.15: **Guide RNA used for the generation of CSPα knockout PC12 cells,** with sequence and Forward and Reverse primers used to generate the oligos to clone into the PLenti CRISPR vector.

Guide RNA IDs	**RNA sequence** with the PAM sequence and the additional G if added.	**Forward primer**	**Reverse primer**
DNAJC5_sgRNA3	GAACATGGTATAACGATTCCCCGG	CACCGAACATGGTATAACGATTCCC	AAACGGGAATCGTTATACCATGTTC
DNAJC5_sgRNA4A	GATGACAAGTATGGCTCGCTGGGG	CACCGATGACAAGTATGGCTCGCTG	AAACCAGCGAGCCATACTTGTCATC
DNAJC5_sgRNA4B	GGCGTCTGTCAGGATTGCGTGGG	CACCGGCGTCTGTCAGGATTGCGT	AAACACGCAATCCTGACAGACGCC
DNAJC5_sgRNA4C	GCCAGCTGGAGAGTACGAAGTAGG	CACCGCCAGCTGGAGAGTACGAAGT	AAACACTTCGTACTCTCCAGCTGGC
DNAJC5_sgRNA5	GCAGGCGCTGTTCGTCGTCTGTGG	CACCGCAGGCGCTGTTCGTCGTCTG	AAACCAGACGACGAACAGCGCCTGC

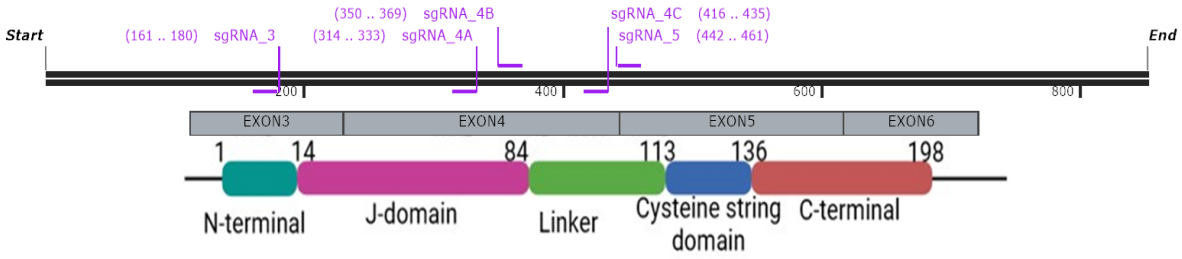

Figure 2.7: Position of guide RNA in the context of the CSP gene and encoded protein. Coding exons of DNAJC5 mapped to the protein domains of CSPα and the placement of guide sequences in the gene code.

2.4.3 Digestion of Lenti CRISPR V1 plasmid

The Lenti CRISPR V1 plasmid containing the Cas9 cassette was used to sub-clone the oligonucleotide sequences with the restriction enzyme BsmB1 (Section 2.3.12). The vector has two BsmB1 cut sites, which, upon overnight cleavage at 55°C, led to the loss of an 1885 bp fragment, resulting in a 11565 bp linear vector which was dephosphorylated with Shrimp Alkaline Phosphatase (rSAP).

2.4.3 Ligation and test digest of Lenti CRISPR V1 plasmid

Ligation was carried out as described in section 2.3.13 and transformed in NEB stable cells as described in section 2.3.15.

A test digest using BsmB1 was carried out with both an uncut control and a digest of the backbone. In the case of the backbone, this led to the formation of two fragments, one at 1885 bp and the other at 11565 bp. In the presence of the insert, the vector appeared uncut due to the absence of BsmB1 recognition sites. One of each plasmid identified to potentially contain the insert was sent for sequencing using a primer in the U6 promoter (GAG GGC CTA TTT CCC ATC ATT CC). The chromatograms containing each oligo sequence in-frame are highlighted in Figure 2.8.

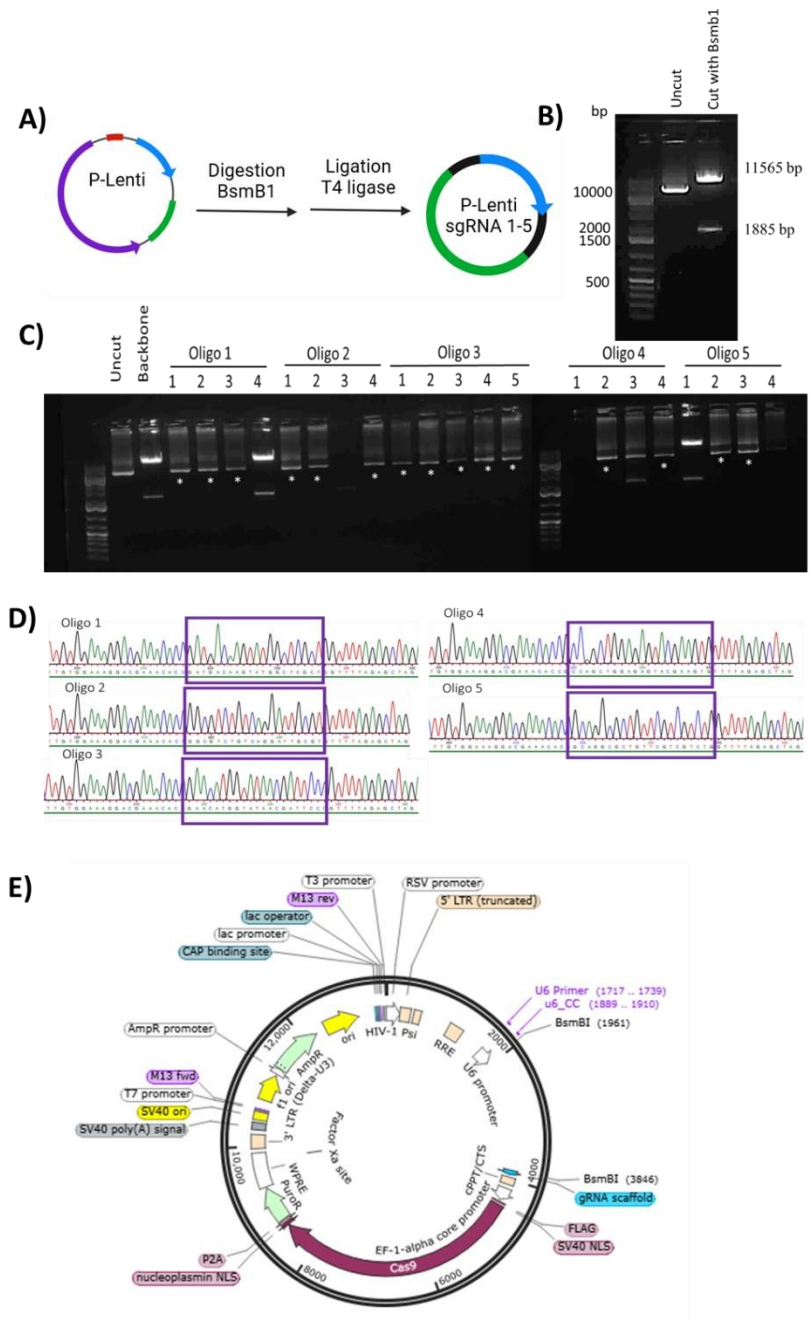

Figure 2.8: Generation of the Lenti CRISPR P-vectors plasmid. A) Schematic workflow of cloning strategies for the generation of P-Lenti with sgRNA 1-5 with 1 corresponding to sgRNA4A, 2: sgRNA4B, 3: sgRNA3, 4: sgRNA4C and 5: sgRNA5. B) Digest of the p-Lenti vector with BsmB1, generating a fragment at 1885bp and another at 11565bp. C) Diagnostic test digest to check for the presence of each of the guide RNAs cloned constructs using BsmB1. The White asterisk indicates the absence of digest, indicating the successful cloning of the oligos into the Lenti CRISPR V1 plasmid. E) Sequenced results of the construct; chromatogram depicting each guide cloned in frame into the Lenti CRISPR V1 plasmid.

2.4.4 Sequencing

Plasmids and PCR products were sent to Eurofins (Germany) for Sanger sequencing and/ or Next Generation sequencing (NGS) whole plasmid sequencing. FASTA sequences and base chromatograms were reviewed for quality and aligned to predicted sequences.

2.5 Cell culture

2.5.1 Preparation of glass coverslips

Glass coverslips (Dixon) were cleaned in 1N HCl by rocking agitation in a glass beaker for one hour. The coverslips were then washed three times for five minutes in double-distilled water. The washed coverslips were left on the rocker overnight in 70% ethanol, and fresh ethanol was added the following morning for prolonged storage. Coverslips were removed from storage and allowed to dry in cell culture plates. Dried coverslips were submerged in poly-D-lysine (PDL) (0.1 mg/ml) or Poly-L-Ornithine Solution (POL) (0.1 mg/ml) (Sigma) made up in double-distilled water and incubated at 37°C overnight. The PDL was removed, and the coverslips were washed three times in sterile water for five minutes. Washed coverslips were left to air dry inside the fume hood, then stored at -20°C in cell culture plates until required.

2.5.2 Maintenance of HEK293FT Cells

HEK93FT cells were used for all initial BioID experiments due to their ease of use and high rate of transfection For all experiments using HEK, HEK293FT cells (Oka et al., 2010). HEK293FT cells were maintained in 10 cm cell culture dishes in 10% FBS DMEM (with pyruvate, 4.5 g/l D-glucose and L-glutamine (4 mM)). Cells were passaged at 80-90% confluency, till passage 20. To passage, all conditioned media was removed and replaced with 5 ml of 1x PBS (phosphate-buffered saline) (without magnesium or calcium) to remove residual media. The PBS was removed, and cells were dissociated by incubation with 1 ml (Trypsin-EDTA solution 0.05% or 0.025%: Fischer Scientific) at 37 ^{0}C until the cells had visibly detached. The trypsin was inhibited by adding 7.5 ml 10% DMEM. The cells were dissociated by gently pipetting. The cell number was counted using a haemocytometer and diluted in 10% FBS DMEM, with 1 x 10^{6} plated in a 10 cm dish. Cells were maintained through recorded passages and discarded before passage 20.

2.5.3 PC12 cells maintenance

PC12 cells were used as they are widely used in synaptic research due to the ability to develop presynaptic-like structures, form synaptic vesicle clusters and they provide a neuronal like cell model which is easier and less costly to work with than Primary and IPSC cultures (Iwasaki et al., 1997)

were maintained in P75 cell culture flasks in 10% Horse serum, 5% FBS, DMEM (with pyruvate, 4.5 g/l D-glucose and L-glutamine (4 mM)). Cells were passaged every 2-3 days, the conditioned media was removed, and cells were washed with 5ml PBS till passage 20. The PBS was removed gently. 2 ml (Trypsin-EDTA solution 0.05% or 0.025%) (Fischer scientific) was added to the cells and incubated at 37 ^{0}C until they detached. The trypsin was inhibited with 7.5 ml 10% HS, 5% FBS and the cells were gently pipetted to disrupt cell clumps. Cells were split no more than 1 in 5 and generally at 1 in 2 or 1 in 3 for subsequent re-plating.

2.5.4 PC12 cells differentiation

Glass slides were placed in either a 10 cm dish or a 6-well plate and coated with PDL (Section 2.6.1). Cells are passaged as above and plated 2-3x10^{6} per 10cm dish and 5x10^{5} cells per well for a 6-well plate. Cells were left to grow for 24 hours before the media containing 10% HS and 5% FBS was removed and replaced with media containing 2% HS DMEM supplemented with 50 ng/ml NGF. The PC12 cells were then left for 3-5 days to differentiate before either the collection of lysate (Section 2.7.1) or cell fixation (Section 2.6.3).

2.5.5 Lipofectamine transfection of PC12 cells

PC12 cells were plated and allowed to adhere for 24 hours before being treated with Lipofectamine 2000 (Invitrogen) and DNA plasmid (Table 2.17). During transfection the amounts indicated in Table 2.16 were used. Lipofectamine and the DNA plasmids were diluted into two separate Eppendorf tubes in Opti-MEM. The Lipofectamine and DNA solutions were combined and mixed by gentle pipetting. The transfection mixture was incubated at room temperature (RT) for 35 minutes before adding the indicated volumes to the media. The cells were exposed to the transfection mix overnight at 37°C. The media containing the transfection mix was then removed and replaced with either fresh PC12 growth or PC12 differentiation media 2ml for a 6-well, 1 ml for a 12-well, 8 ml for a 10 cm dish. The cells were returned to incubate at 37 C until required. For transfection of the MycBioID constructs, PC12 cells were plated and transfected in a 10 cm dish, and the reagents were scaled accordingly.

Table 2.16: Cell plating format and lipofectamine transfection reagent quantities

Cell format	Lipofectamine	DNA plasmid	Total OPTI-MEM
6 well plate	6 µl	2 µg	400 µl
12 well plate	3 µl	1 µg	200 µl
10 cm dish	24 µl	8 µg	1.5 ml

Table 2.17: cDNA plasmids used for transfection of PC12 cell cultures

Construct	Encodes	Backbone	Resistance	Source
Myr-GFP	Myristoylated GFP	p-EGFP	Kanamycin	Ed Skolnik lab (NYU)
Myc-BioID	Myc- BioID	P-EGFP	Kanamycin	Ryan *et al.*, 2020
Myr-Myc-BioID	Myristoylated Myc-BioID	p-EGFP	Kanamycin	Section 2.3
Myc-BioIDSNAP-25	Myc-tagged BioID SNAP-25 construct	p-EGFP-C1	Kanamycin	Section 2.3
HA-WT-Parkin	HA-tagged wildtype Parkin construct	pIRESpuro2	Ampicillin	Ryan *et al.*, 2020
HA-C431S-Parkin	HA tagged C431S Parkin construct	pIRESpuro2	Ampicillin	Ryan *et al.*, 2020

2.5.6 Polyethyleneimine (PEI) Transfection of HEK293FT cells

For transfection of HEK293FT cells with Polyethyleneimine (PEI) and DNA, the two components were used in a 3:1 v/v ratio, for a 6-well plate based on 2 µg per well. DNA 2 µg was diluted in 100 µl serum-free DMEM or OptiMEM and incubated at room temperature for 10 minutes. PEI 6 µl was added and incubated for a further 10 minutes at room temperature. The transfection volume was removed from each well and replaced with the transfection solution, which was then left for 24-48 hours, depending on the experiment.

2.5.7 MG-132 proteasome blocking

PC12 cells were plated in a 6-well plate, and after 24 hours, MG-132 (10µM) was added and incubated for 2, 6 or 8 hours before cell lysis (Section 2.7.1) or fixing (Section 2.6.3).

2.5.8 Generation of CSPα Knockdown cells PC12 cells

PC12 cells with a stable expression of TrkB were plated in a 6-well plate, and 24 hours later, at ~70% confluency, they were transfected (Section 2.5.5) with the lentiCRISPRv1 puro sgRNA-containing plasmids generated in Section 2.4 using Lipofectamine. 24 hours later, the transfection media was removed and both the transfected cells and an untransfected control were grown in media supplemented with puromycin (2 µg/ml). Once all the cells in the un transfected control had died,

lines generated with the guides sgRNA_ 3, 4A, 4B, and 5 which survived the puromycin treatment and were maintained with the media being replaced every 3-4 days for 2 weeks before the cells were split into two populations one for maintenance and the other for lysing for Western blot (Figure 2.9). Once a knockdown in cell lines transfected with sgRNA3 and sgRNA5 was identified, these lines were termed PC12 CSPαdeficient exon3 (PC12 CD3) and PC12 CSPα-deficient exon5 (PC12 CD5). Stocks of these cells were frozen, and the cells were maintained in 10 cm dishes and passaged when they reached 80% confluence.

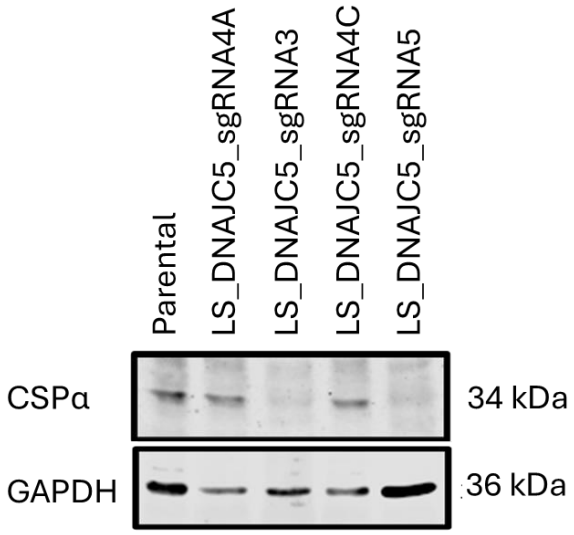

Figure 2.9 Identification of CSPα knockdown in two PC12 lines transfected with LS_DNAJC5_sgRNA guides in comparison to the parental line via Western blotting (Biological replicated N=1).

2.5.9 Cell proliferation assay

Parental PC12, Lenti Crispr, PC12 CSPα deficient cells 3 and 5 were plated at 250,000 cells each in triplicate and left to grow for 24, 48 or 72 hours before being detached and suspended in 1 ml of media, and live cells counted using trypan blue. The equation (number of cells counted dilution factor x 100,000)/ number of Squares counted was used to determine the number of cells present. The Malthusian growth nonlinear model was used to analyse proliferation, and data was plotted in GraphPad Prism version 9.

2.6 Imaging and Microscopy

2.6.1 Plating cells for Immunocytochemistry of immortal cell lines

HEK293FT and PC12 cells were plated in 6-well plates, containing 2 coverslips in each well for PC12 cells. POL (Poly-L-Ornithine Solution Sigma) was used to coat the coverslips before plating (Section 2.5.1).

2.6.2 Plasma membrane staining of cells

For plasma membrane staining, fluorescent Wheat germ agglutinin (WGA) conjugates, which act as a carbohydrate-binding molecule to cell surface sugars sialic acid and Nacetylglucosamine (Table 2.18), were diluted 1:1000 in ice-cold media and coverslips were incubated on ice with the stain for 15 minutes.

Table 2.18: WGA conjugates used for binding to cell surface sugars.

Dye	Dilution	Incubation	Supplier
WGA (Wheat Germ Agglutinin) Alexa 647 (1.0 mg/mL)	1:1000	15 mins on ice	Invitrogen™
WGA (Wheat Germ Agglutinin) Alexa 555 (1.0 mg/mL)	1:1000	15 mins on ice	Invitrogen™

2.6.3 Fixing and immunocytochemistry staining of immortal cell lines

The media was removed, and the cells were washed twice with 500 µl cold PBS. The PBS was removed, and the cells were fixed with 500 µl 4% PFA (paraformaldehyde in 1x PBS) (Sigma) for 15 minutes at room temperature. The incubation was quenched by the addition of 500 µL of NH_4Cl (50 mM) in Tris Buffered Saline (TBS) for 5 minutes at room temperature. Cells were incubated in 500 µL TBS containing 0.1 % Triton X-100 for 5 minutes at room temperature. This was removed, and the cells were then incubated in blocking buffer (TBS, 10% goat serum (v/v) 2% BSA (w/v)) at room temperature for 30 minutes. The coverslips were then incubated in primary antibody (Table 2.19) diluted in blocking buffer for 30 minutes at room temperature. The coverslips were washed with TBS three times for 5 minutes each. This was followed by incubating in the indicated secondary antibodies (and Alexa Fluor conjugate) (Table 2.20) (Alexa Fluor 488/555/647) diluted 1:1000 in blocking buffer solution and Hoechst stain diluted 1:5000 (Hoechst 33342 solution, Fisher Scientific) for 30 minutes. The cover slips were washed three times for five minutes in TBS before being mounted on T Epredia™ Frosted Microscope Slides, Ground 45,̊10-12 mm with ~8 µl Mowiol glue (Mowiol 4-88, Glycerol, 0.2 M Tris HCl pH 8.5, H_2O).

Table 2.19: Primary antibodies used for immunostaining

Antibody	Dilution	Incubation	Immunogen	Reactivity	Supplier
SNAP-25	1:1000	30min RT IF	Rabbit IgG AA 1 to 206 from rat SNAP25B	Rabbit	SYSY
Myc	1:1000	30min RT IF	Mouse / IgG1 AA 408 to 438 of human c-myc	Mouse	Santa Cruz Biotechnology
GFP	1:1000	30min RT IF	Mouse / IgG1 GFP from the jellyfish Aequorea Victoria N-terminal peptide-KLH conjugated.	Mouse	Santa Cruz Biotechnology
GM130	1:1000	30min RT IF	Mouse IgG1, κ Rat GM130 aa. 869-982	Mouse	BD biosciences

Table 2.20: Secondary antibodies and fluorophore conjugates used for immunostaining of HEK293FT and PC12 cells

Antibody	Dilution	Incubation	Isotype	Host species	Supplier
AlexaFluor488	1:1000	30mins RT	IgG Mouse	Goat (polyclonal)	Invitrogen (A-21121)
AlexaFluor488	1:1000	30mins RT	IgG Rabbit	Goat (polyclonal)	Invitrogen (A-11059)
AlexaFluor555	1:1000	30mins RT	IgG Mouse	Goat (polyclonal)	Invitrogen (A-21422)
AlexaFluor555	1:1000	30mins RT	IgG Rabbit	Goat (polyclonal)	Invitrogen (A21429)
AlexaFluor647	1:1000	30mins RT	IgG Mouse	Goat (polyclonal)	Invitrogen (A21235)
AlexaFluor647	1:1000	30mins RT	IgG Rabbit	Goat (polyclonal)	Invitrogen (A21245)
Streptavidin Alexa 555	1:1000	30 mins RT	Alexa Fluor dye		Invitrogen™

2.6.4 Fluorescence microscopy

Fixed cell fluorescence imaging was done on the Olympus IX83 Inverted Fluorescence Microscope that utilized an OptiMOS CMOS 1920 x 1080-pixel camera (Photometrics, USA). The offset, gain and binning settings were kept constant between experiments. Images were captured in the DAPI, FITC, TRITC, and Cy-5 channels, using an LED-based light source. Fixed and stained

Coverslips were stored at 4°C in the dark. For each experiment, at least 3 fields of view of each coverslip and 3 separate coverslips were imaged.

2.6.5 Image analysis

Composite images were reconstituted from multiple single images and analysed using Fiji processing package (Schindelin et al., 2012).

2.7 Protein preparation and analysis

2.7.1 Preparation of Cell lysate from immortal cells

Cells were placed on ice, and the media was removed from each well. The cells were washed twice with cold PBS (1 ml/well). On ice, 100 µl of lysis buffer (Tris pH 7.5 50 mM, NaCl 140 mM, EDTA 2 mM, NP-40 1%, glycerol 10%) was added one at a time. The cells were scraped off the dish with a pipette tip, and the lysates were stored at -20 C.

2.7.2 Homogenisation of CSPα brain tissue

Between 250-300 mg of pooled frozen hippocampus and cortex (n=4) from CSPα -/- and age matched littermate controls (p13-p18) were resuspended in 10 w/v of ice-cold Sucrose/ HEPES buffer (Sucrose 320mM, HEPES 10mM). The tissue was homogenised with 10 up/down strokes at 900 rpm with a glass Teflon homogeniser with 0.10-0.15 mm clearance.

2.7.3 Protein assay

Serial dilutions of the indicated samples (undiluted, 1:5, 1:25) were analysed for protein concentration using the Bio-Rad D_c protein assay method as described in the manufacturer's instructions. Protein concentration was estimated by comparing test samples against a bovine serum albumin (BSA) standard curve (2 mg/ml- 0.25 mg/ml) diluted in the same buffers as the samples. Each of the samples was tested in triplicate and incubated for 20 minutes in the dark at room temperature before the absorbance was read at 690nm using a UV-Vis Microplate Reader (BioTek ELx800UV).

2.7.4 Sample preparation for SDS PAGE

Samples were thawed on ice and diluted with water to the desired concentration before the addition of 5X sample buffer (312.5 mM Tris (pH 6.8), 10% w/v SDS, 50% v/v glycerol, 25% v/v β-Mercaptoethanol and 0.005% v/v bromophenol blue). This was done to give a final concentration of

0.3 mg/ml 1x Sample buffer concentration. The diluted samples were boiled at 95 °C for 5 minutes and centrifuged for 2 minutes at 16000 xg, before being loaded into wells in an SDS-PAGE gel.

2.7.5 SDS-polyacrylamide gel electrophoresis (SDS-PAGE)

The Fischer Scientific gel system was used for the casting and running of the SDS-PAGE gels. The backing and spacer 1.5 mm (Fisher) glass plates were cleaned with 70% ethanol prior to use, and were assembled into the casting frame. The SDS-PAGE gels were cast in two parts, the lower resolving layer (Table 2.21) was poured and overlaid with isopropanol to remove bubbles until the acrylamide polymerised. The isopropanol was then removed, and the stacking layer was overlaid, a 12-well comb was inserted, and the stacking gel was allowed to polymerise.

Once set, the glass plates containing the gels were transferred to an SDS-PAGE electrophoresis tank, which was then filled with 1 x Laemmli buffer (25 mM Tris, 192 mM glycine and 1% SDS. The comb was removed, and samples from section 2.7.4 were loaded into the SDS-PAGE gel alongside Page Ruler Plus Pre-Stained Protein ladder (Abcam), 5 µl. The gels were initially run at 20 mA for 15 minutes, which allowed the protein to stack, then ran at 35 mA for 90 minutes until the dye front reached the bottom of the separating gel using the Fisherbrand™ Power Supply system.

Table 2.21: Components of the SDS-PAGE gels used for running protein samples

Gel	8%	10%	12%	15%	Stacking gel
30% Acrylamide/ Bis-Acrylamide	2.14 ml	2.67 ml	3.2 ml	3.73 ml	0.35 ml
1.5 M tris +10 % SDS (pH 8.8)	2 ml	2 ml	2 ml	2 ml	-
0.5 M tris +10 % SDS (pH 6.8)	-	-	-	-	0.67 ml
H_2O	3.86 ml	3.33 ml	2.8 ml	2.27 ml	1.67 ml
Ammonium persulfate 10%	80 µl	80 µl	80 µl	80 µl	26.6 µl
Tetramethylenediamine	8 µl	8 µl	8 µl	8 µl	2.67 µl

2.7.6 Coomassie gel staining

After electrophoresis (Section 2.7.5), the resolving and attached stacking gel was fixed and stained in Coomassie gel stain (Brilliant blue G colloidal concentrate, Sigma Life Science) for 1 hour at room temperature. Subsequently, the gel was incubated in de-stain (10% v/v Acetic acid, 25% v/v methanol) overnight at room temperature with mild agitation on a rocking platform. Alternatively, for increased detection sensitivity, Bio-Rad QC Colloidal Coomassie Stain was used. Gels were placed in fixing solution (40% ethanol, 10% acetic acid) (50 ml) with agitation for 15 mins and rinsed in

deionised water. QC colloidal Coomassie (50 ml) was added to the washed gel and incubated with gentle agitation at room temperature overnight. The Coomassie was removed and the gel destained in deionised water with three changes for an hour.

The de-stained gels were scanned and imaged using the Syngene imager. The images were stored and processed with the line scan function of the ImageJ software. This scanned line and derived intensity were used to produce intensity profiles, which score global protein amounts within each lane as indicated (Schindelin et al., 2012).

2.7.7 Electroblotting of proteins to nitrocellulose membrane

For Western blotting following SDS-PAGE electrophoresis (Section 2.7.5), the resolving and attached stacking gel were used to transfer separated proteins to a nitrocellulose membrane (ThermoFisher). This was done by placing the acrylamide gel against a nitrocellulose membrane between a sandwich composed of Whatman filter paper and a support sponge. The organisation of this sandwich is depicted (Figure 2.10). The support material was pre-soaked in 1x Laemilli buffer containing 20% v/v methanol.

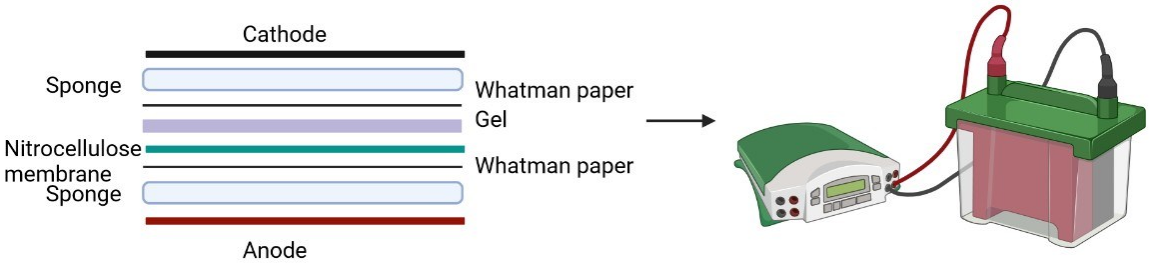

Figure 2.10: SDS-PAGE gel-nitrocellulose transfer sandwich. 2x outer sponge, 2x Whatman paper, the SDS-PAGE gel, a nitrocellulose membrane, another 2x Whatman paper, and another 2x sponges were placed in between plastic cassettes and inserted into the transfer tank. The nitrocellulose was placed adjacent to the anode, and the gel the cathode.

Proteins were transferred at 4°C for 1.5 hours at 150V in transfer buffer (Tris 0.5 M, glycine 0.4M, 10% methanol, double-distilled water). Protein transfer was confirmed by the presence of the coloured markers of the protein ladder run on the SDS-PAGE gel onto the nitrocellulose membrane.

2.7.8 Immunolabelling of transferred proteins

The nitrocellulose membranes harbouring transferred proteins were incubated with TBS-Tween (BSA (2%) (0.15M NaCl, 10 mM Tris pH 7.5 and 0.005% v/v Tween, 2% BSA) for 1 hour at room temperature. Membranes were then incubated with the indicated primary antibody diluted to an optimised concentration (Table 2.22) in TBS-Tween 2% BSA overnight at 4°C on the rollers set to 22 rpm. The nitrocellulose membranes were sequentially incubated for three x 5-minute TBS-Tween

washes before the nitrocellulose was incubated with the indicated secondary antibody (1:10,000) (Table 2.23) conjugated to a fluorophore (Alexa Fluor-680 or 800 Molecular probes from Licor) for 1 hour. Membranes were subsequently washed for three x 5-minute in TBS-Tween before being imaged with an Odyssey infrared imaging scanner (Licor) at wavelengths of either 700nm or 800nm, and the data processed using the Image Studio software.

2.7.9 Detection of Biotin on proteins transferred to nitrocellulose

For the detection of biotin after blocking the membrane in 2% BSA, the membrane was incubated with IRDye 800 CW streptavidin for 1 hour in the dark before imaging on the Licor and preceding to stain with primary and secondary antibodies.

Table 2.22: Antibody table used for Western blotting

Antibody	MW size of predicted immunoreactivity Da	Species	Supplier	Antibody dilution	Incubation conditions
Control antibodies					
GAPDH	37	Mouse (monoclonal)	Abcam (ab8245)	1:1000	RT 1 hour
CSPα and complex interacting partners					
CSPα	35	Rabbit	SYSY (154 003)	1:1000	4°C ON
HSC70	70	Mouse	Dr A Morgan	1:1000	4°C ON
SGT	36	Rabbit	Dr G Meyer	1:1000	4°C ON
Proteins known to be CSPα clients					
SNAP-25	25	Rabbit polyclonal IgG	SYSY (111 103)	1:1000	4°C ON
Dynamin 1	97	Mouse (IgG1)	BD Biosciences (610245)	1:1000	4°C ON
Proteins involved in vesicle endo/exocytosis					
VAMP-2	18	Mouse (69.1) C110.1	SYSY (104 211)	1:1000 weak signal	4°C ON
Syntaxin 1a/1b	33	Mouse (10H5)	Autogen Bioclear	1:1000	4°C ON
Synaptotagmin	64	Mouse (monoclonal)	SYSY (105.011)	1:1000	4°C ON
Synapsin	77	Rabbit IgG (D12G5)	Cell signalling (#5297)	1:1000	4°C ON
Markers of dysfunctional proteostasis					
LAMP-1	120	Mouse	Santa Cruz Biotechnology (sc-20011)	1:1000	4°C ON
LC-3	17	Rabbit	Santa Cruz biotech (sc-28266)	1:1000	4°C ON
Ubiquitin P4D1	-	Mouse A2813 IgG	Santa Cruz biotech (sc-8017)	1,1000 (weak signal) 1:200	4°C ON

RAB 7	23	Rabbit	Cell signalling (#2094)	1:1000	4°C ON
Subcellular marker proteins					
α-tubulin	50	Mouse (B512)	Sigma (T6074)	1:1000	4°C ON
Actin (AC40)	42	Mouse (Monoclonal)	Sigma (catalogue no: A4700)	1:1000	4°C ON
PSD95	95	Rabbit	Cell signalling (#3450)	1:1000	4°C ON
Synaptophysin	38	Rabbit (IgG) (D8F6H)	Cell signalling (#36406)	1:1000	4°C ON
E3 ubiquitin ligases					
TRIM9	70, 79	Rabbit	Cell signalling (#47990)	1:1000	4°C ON
FBX07	65-72	Rabbit (polyclonal) IgG	Proteintech (10696-1-AP)	1:1000	4°C ON
Parkin	50	Mouse	Cell signalling (#4211)	1:1000	4°C ON
Tags					
Myc	-	Mouse	Santa Cruz Biotechnology	1:1000 (1:1000 if)	4°C ON/30min RT IF
HA	-	Rabbit	Abcam (12CA5)	1:1000	4°C ON
GFP	27	Mouse	Santa Cruz Biotechnology	1:1000	4°C ON
Streptavidin IRdye 800	-	-	Licor		1hour RT
FLAG (M2)	-	Mouse	Sigma	1:1000	4°C ON
Neurotrophin receptors and neurotrophin signalling proteins					
Trk B	142 kDa	Rabbit	Millipore (07-225)	1:1000	4°C ON
Total TRK	~82 and 142 kDa	Rabbit	Santa cruz (C14 pan trk)	1:500	4°C ON
EGF receptor (D38B1)	175 kDa	Rabbit	Cell signalling (#4267)	1:1000	4°C ON
Total ERK	44 kDa	Rabbit	Cell signalling (#4695)	1:1000	4°C ON

P-ERK	44 kDa	Mouse	Cell signalling (#5726)	1:1000	4°C ON
Proteins identified in the proteomics of CSPα-deficient PC12 cells					
DJ-1	22 kDa	Rabbit	Cell signalling (2134)	1:1000	4°C ON
HSP90	90 kDa	Rabbit	Stressgen (spa-836)	1:1000	4°C ON
HSP40	40 kDa	Rabbit	Stressgen (spa400)	1:1000	4°C ON
EEF1A2	50 kDa	Mouse	Ptglab (4F3F4)	1:1000	4°C ON
SFRS3	19 kDa	Rabbit	Ptglab (10916-1-AP)	1:1000	4°C ON

Table 2.23: Secondary antibodies and dyes used for Western blotting

Secondary antibody	Supplier	Species	Dilution	Incubation conditions
Goat anti-mouse 680 (925-68070)	LI-COR	Goat (polyclonal)	1:10,000	1 hour, in the dark at room temperature
Goat anti-rabbit 680 (925-68071)	LI-COR	Goat (polyclonal)	1:10,000	1 hour, in the dark at room temperature
Goat anti-mouse 800 (926-32210)	LI-COR	Goat (polyclonal)	1:10,000	1 hour, in the dark at room temperature
Goat anti-rabbit 800 (925-32211)	LI-COR	Goat (polyclonal)	1:10,000	1 hour, in the dark at room temperature
IRDye® 800CW Streptavidin	Licor	N/A	1:1,000	1 hour, in the dark at room temperature

2.7.10 Analysis of immunoblotting of proteins

Statistical analysis was carried out using GraphPad Prism 9. The immunoreactivity of Immunoblotted proteins of interest and associated housekeeping proteins (Actin, Tubulin or GAPDH) as indicated, were measured in Image Studio Lite Version 5.2. These values were imported to GraphPad Prism 9, with each datapoint corresponding to a single measurement and then normalised to the housekeeping protein.

2.7.11 Streptavidin pull-down and Myc-Immunoprecipitation

HEK293FT or PC12 cells transfected with the biotin ligase as described in sections 2.5.6 and 2.5.5 were investigated. Biotin (50 µm) was added to the transfected cells expressing the indicated BioID variant for 24 hours before being washed twice in ice-cold PBS. After washing the biotin-treated cells were lysed in 500 µl buffer (Tris pH 7.5, 50 mM, NaCl 140 mM, 2 mM EDTA, 1% NP-40,10% glycerol) and used in the pull-down experiments as described below

2.7.12 HEK293FT and PC12 streptavidin pull-down with Myc BioID constructs

Pierce Streptavidin magnetic beads (Thermo Scientific) in a slurry of 75 µl were added to a clean 1.5 ml Eppendorf and washed twice with ice-cold lysis buffer. The beads were collected against the side of the Eppendorf with the magnet, and the wash lysis buffer was removed. The 500 µl cell lysate was homogenised and 10 % of this total lysate fraction was retained. The remaining fraction was centrifuged at 13,000 xg for 5 minutes, and a further 10 % fraction of supernatant was retained. The pellet fraction from this centrifugation was resuspended in lysis buffer and retained. The remaining lysate supernatant was added to the washed beads and incubated overnight at 4 C with head over end rotation. The beads were collected against the side of the Eppendorf with a magnet, and the unbound flow-through was removed and retained. The beads were washed twice with ice-cold 500 µl lysis buffer, and these washes were retained. Finally, the biotinylated proteins bound to the beads were eluted in 50 µl sample buffer (Section 2.7.4) after boiling at 95 C for 5 minutes. Samples were volume normalised, boiled, then run on gels for Coomassie staining (Section 2.7.6) or Western blot (Section 2.7.8)

2.7.13 PC12 Myc Immunoprecipitation with Myc BioID constructs

A slurry of 30 µl Pierce™ Anti-c-Myc magnetic beads (Thermo Scientific) were added to a clean 1.5 ml Eppendorf and washed twice with ice-cold lysis buffer. The beads were collected against the side of the Eppendorf with the magnet, and the buffer was removed. Cells transfected with the Myc BioID constructs (Section 2.4) were lysed (Section 2.7.1) and homogenised before 10 % of this total

lysate fraction was retained. The remaining fraction was centrifuged at 13,000 xg for 5 minutes and a 10 % fraction of supernatant was retained. The pellet was resuspended and retained to probe for detergent-insoluble material. The remaining supernatant was added to the 30 µl of prewashed Pierce™ Anti-c-Myc Magnetic Beads and incubated overnight at 4 C with head over end rotation. The beads were washed ˚twice in ice-cold 500 µl lysis buffer (washes retained). The bound proteins were eluted from the beads in 100 µl of 0.1 M glycine, pH 2, with rotation for 10 minutes. The beads were collected magnetically, and the eluate neutralised with 15 µl of Tris-base. Samples were boiled, then run on gels for Western blot (Section 2.7.7) orientation as described in (Section 2.10.1).

2.8 Cell maintenance and preparation for Mass spectroscopy

The parental and CSPα-deficient PC12 cells, exon_3 and exon_5 (CD3 and CD5) were maintained in four independent cell culture flasks. Each was plated in 10 cm dishes, such that they were at 80-90% confluent after 3 days. Cells were plated in PC12 growth media (DMEM 10% Horse serum, 5% FBS) for 48 hours, 18 hours before each culture was subjected to protein extraction, the PC12 growth media was removed and replaced with 2% HS DMEM.
At the point of protein extraction, the cells were imaged on the Invitrogen™ EVOS™ XL Core Imaging System to document cell density.

2.8.1 Protein extraction from cells to generate samples for Mass spectroscopy.

Samples for Mass spectroscopy were generated as described in figure 2.13. Each cell line (Parental, CD3, CD5) was sequentially extracted, and this pattern was repeated for each paired group of the quadruplicate cultures.
The cell culture media was removed from the cells and spun at 200 xg for 5 mins; this pellet, representing floating cells, was retained and the supernatant discarded. The adherent cells were covered in 1ml ice-cold Dulbecco's Phosphate Buffered Saline (DPBS) and scraped off the culture dish. Each dish was washed with a further 1 ml of DPBS to harvest the remaining cells. This combined volume from individual cultures was spun at 200 xg at 7 °C for 5 minutes and generated a combined floating and adhering cell pellet. The supernatant was removed, and the pellet was resuspended in fresh 1 ml DPBS. The pellet was spun at 2500 xg for 5 minutes before three further washes with 1 ml DPBS. The washed pellets were snap-frozen in liquid nitrogen and stored at -80 °C overnight (Figure 2.11).

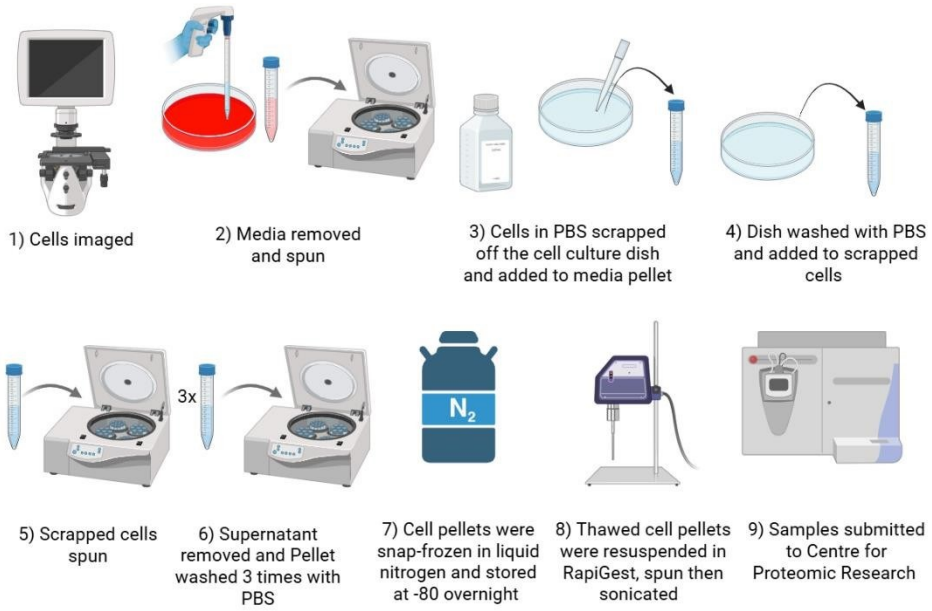

Figure 2.11: Schematic depicting the extraction and preparation of cells for label-free mass spectroscopy

2.8.2 Preparation of protein sample for mass spectroscopy

The 12-cell pellets from parallel culture types were thawed on ice and resuspended in 200 µl RapiGest (0.1% RapiGest (sodium 3-[(2-methyl-2-undecyl-1,3-dioxolan-4-yl)methoxy]-1propane sulfonate in 50 mM Ammonium Bicarbonate, pH 8.5). Each sample was sonicated (3 x 5 sec pulse (20 kHz) broken by 10 sec rest between each pulse). The sonicated samples were spun at 15,000 x g for 20 mins at 4 ◌̊C.

The supernatant fractions that were submitted for mass spectroscopy and corresponding pellet fractions were separated by SDS-PAGE and visualised with Coomassie to verify equivalent protein solubilisation (Figure 2.12). This revealed that whilst there was some protein present in the pelleted fraction, the majority of the cellular protein was extracted. This suggests that the samples sent for mass spectroscopy were representative of total cellular protein. The analysis by SDS-PAGE also indicated that there were some differences in the solubilisation between samples, particularly for low molecular weight proteins (<11 KDa) (Figure 2.12).

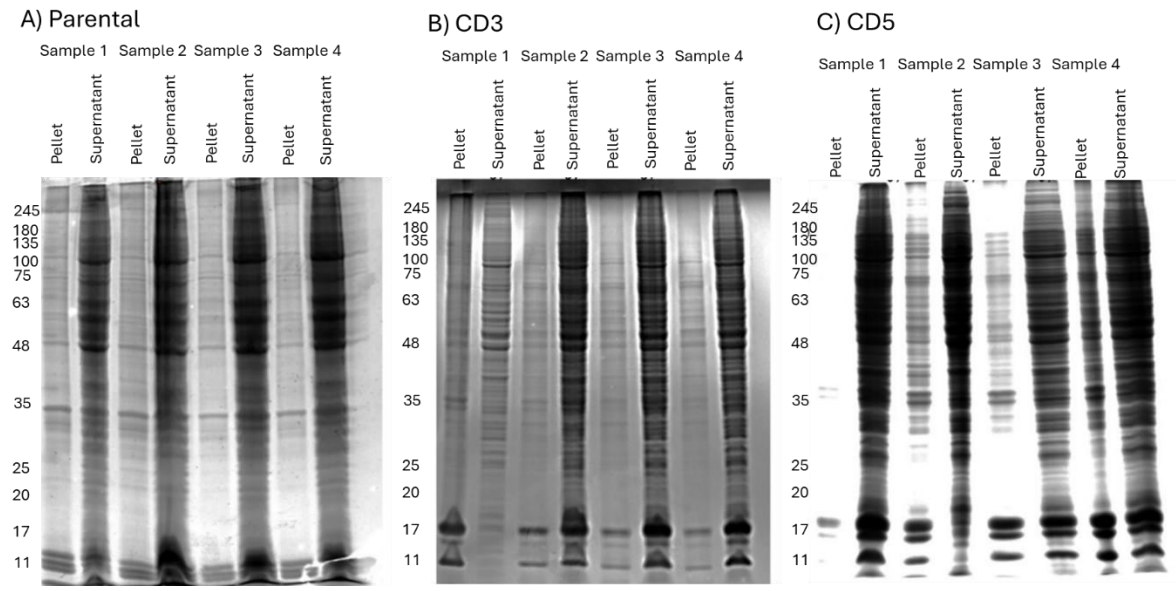

Figure 2.12: The Soluble fraction from the cell lysate submitted for mass spectroscopy was a good representation of total protein

Cell lysis supernatants and pellet fractions were run on an SDS-PAGE gel, then stained with Coomassie. A) Pellet and supernatant fractions for the four parental cultures lysed for mass spectroscopy. B) Pellet and supernatant fractions for the four CD3 cultures C) Pellet and supernatant fractions for the four CD5 cultures.

The DC Bio-Rad protein assay was used to estimate the protein concentration of each of the samples. These samples were diluted in RapiGest to give 1.5 microgram/microlitre.150 micrograms of sample, representing 100 microliters of each sample, was submitted to Professor Paul Skipp of the Centre for Proteomic Research at the University of Southampton

2.8.3 In solution digestion sample preparation for Mass spectroscopy

DTT was added to the 12 protein samples to a final concentration of 5 mM. The samples were heated at 60 C for 30 minutes and allowed to cool to room temperature. ° Iodoacetamide (15 mM) was added to these samples, which were placed in the dark for 30 mins. Digestion was performed using TPCK-modified trypsin (Sigma-Aldrich) in an enzyme: substrate ratio (W/W) of 1:25 at 37°C overnight. After this incubation, the samples were lyophilised.

2.8.4 Separation of samples for mass spectroscopy

Peptide extracts (1 □g on column) were separated on an Ultimate 3000 RSLC nano system (Thermo Scientific) using a PepMap C18 EASY-Spray LC column, 2 µm particle size, 75 µm x 75 cm column (Thermo Scientific) over a 140 min (single run) linear gradient of 3–25% buffer B (0.1%

formic acid in acetonitrile (v/v)) in buffer A (0.1% formic acid in water (v/v)) at a flow rate of 300 nL/min

2.8.5 Mass spectroscopy analysis of parental and CSPα-deficient cell lines

Peptides were introduced using an EASY-Spray source at 2000 V to a Fusion Tribrid Orbitrap mass spectrometer (Thermo Scientific). The ion transfer tube temperature was set to 275 °C.
Full MS spectra were recorded from 300 to 1500 *m/z* in the Orbitrap at 120,000 resolutions. This was performed using TopSpeed mode at a cycle time of 3 s. Peptide ions were isolated using an isolation width of 1.6 amu and trapped at a maximal injection time of 120 ms with an AGC target of 300,000. Higher-energy collisional dissociation (HCD) fragmentation was induced at an energy setting of 28 for peptides with a charge state of 2–4. Fragments were analysed in the Orbitrap at 30,000 resolutions.

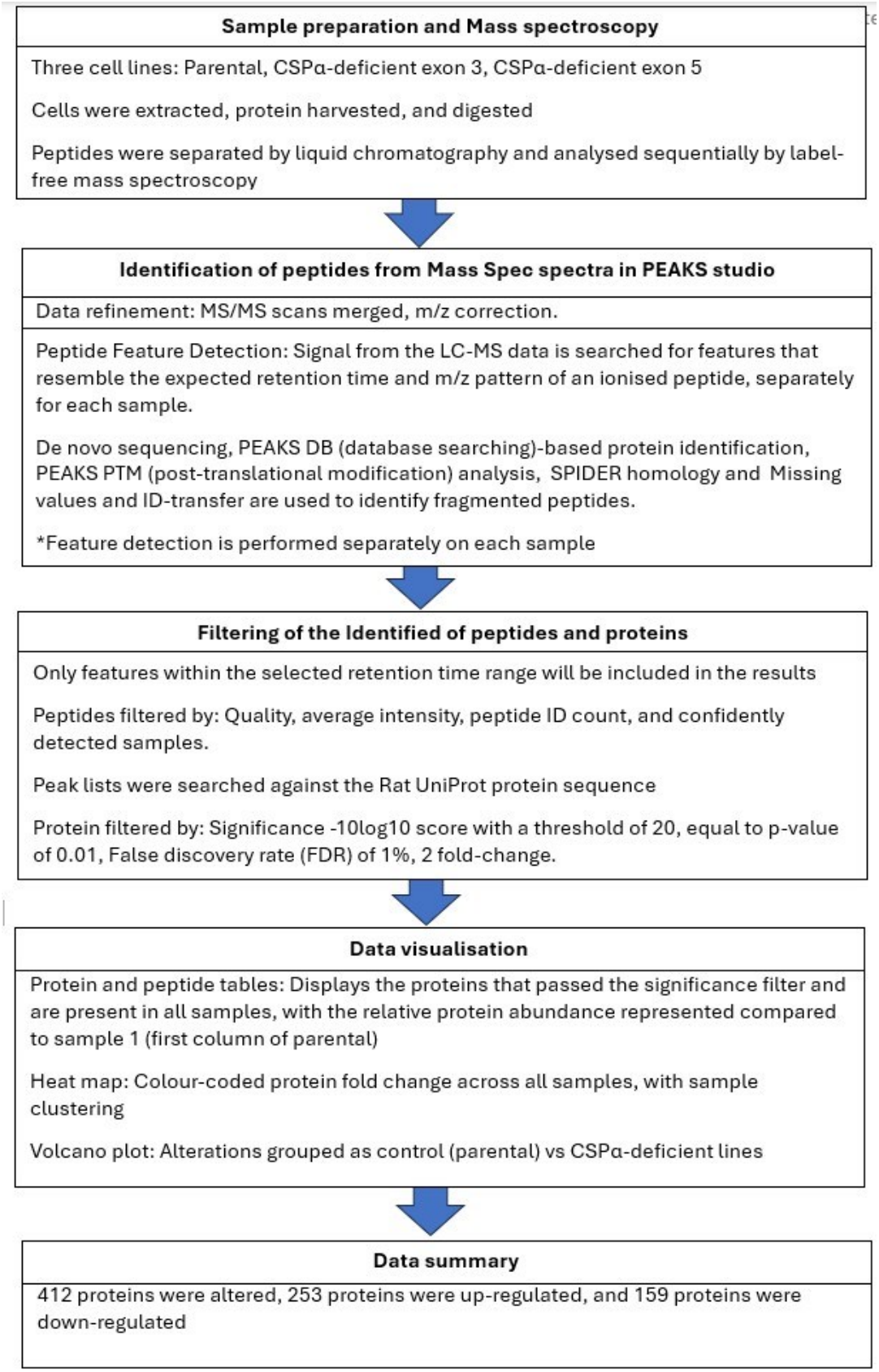

Figure 2.13: Sequential steps in the process by which data from mass-spectroscopy spectra features is used to identify peptides and, in turn protein alterations between control and CSPα-deficient lines (CD3 and CD5).

2.8.6 Proteomic Data Analysis

Raw spectrum files were analysed using Peaks Studio 10.0 and the data processed to generate reduced charge state and deisotoped precursor and associated product ion peak lists, which were searched against the UniProt database (20,350 entries, 2020-04-07). Parent mass error tolerance was set a 10ppm and fragment mass error tolerance at 0.6Da. Variable modifications were set for N-terminal acetylation (42.01 Da), methionine oxidation (15.99 Da), and carboxyamidomethylation (57.02 Da) of cysteine. A maximum of three variable modifications per peptide was set. The false discovery rate (FDR) was estimated with decoy fusion database searches and were filtered to 1% FDR.

Protein relative quantification in PEAKS was carried out by Professor Paul Skipp

2.8.6.1 PEAK studio label-free quantification parameters and statistics

The PEAKS peptide score (-10lgP) is calculated for every peptide precursor spectrum match reported by PEAKS DB, PEAKS PTM, and SPIDER. The score is derived from the p-value that indicates the statistical significance of the spectrum match. When a peptide feature is detected in multiple spectra, the peptide score is the maximum (J. Zhang et al., 2012). To determine the significance of the peptides detected the PEAKSQ method was used, whereby the statistical significance of each peak in the data set is determined, to distinguish true peaks from noise. The significance score is calculated as -10log10 of the significance testing p-value. With a significance score threshold of 20, equal to a significance testing p value of
0.01.

Table 2.24: Parameters used in PEAKS for quantification of proteins identified in label free mass spectrometry. A) The parameters used for the filtering of peptides identified in spectra. B) Lists the total number of features present in all spectra, the number of features which were identified, and the number of peptides identified. C) Lists the search parameters that were used for the identification of peptides from spectra generated by label-free mass spectroscopy.

A) **Result filtration parameters.**

Retention time lower bound	≥0
Retention time upper bound	≤250
Quality	≥0
Avg. Area	≥0E0
Charge lower bound	≥1
Charge upper bound	≤10
Confident number of samples per group	≥1
Peptide ID Count	≥1
Protein significance	≥20
Protein fold change	≥2

B) **Statistics of the filtered result.**

Features	96929
Features with ID	79352
Feature vectors	8365
Feature vectors with ID	8365
Protein groups	440
Significance method	PEAKSQ
Used Peptides	≥1
Normalization	Use TIC

C) **Search Parameters**

Quantification type: Label-free quantification

LFQ method: ID-directed LFQ

Coefficient of Variation filter: No

Do outlier removal: No

Mass Error Tolerance: 20.0 ppm

Retention Time Shift Tolerance: Auto detect

Dependent on PID: 31,34,37,39,41,43,45,47,49,51,53,55

FDR Threshold: 1%

Samples: 12 samples in 3 groups

Parent:

Sample 1, Sample 2, Sample 3, Sample 4.

CSPα deficient 3:

Sample 5, Sample 6, Sample 7, Sample 8.

CSPα deficient 5:

Sample 9, Sample 10, Sample 11, Sample 12.

Reference Sample: Sample 1 (auto detected)

Training Samples: Sample 9, Sample 11 (auto detected)

2.8.7 Differential Protein Expression

Label-free quantification using the Peaks Q module of Peaks Studio [1 & 2] yielding matrices of protein identifications as quantified by their normalised top 3 peptide intensities. Peaks corresponding to precursor ions were extracted with a minimum intensity threshold and retention times were aligned across all runs to correct for chromatographic drift. Label-free quantification was achieved by integrating the area under the curve of extracted ion chromatograms for each peptide feature. Peptide peak intensities were normalised against the total ion current. Protein-level quantitation was obtained by summing or averaging the intensities of unique peptides per protein group, with missing values imputed according to the software's default settings.

2.8.7.1 Determining vector ratio distribution to set fold change of relative abundance

Plots of the distribution (Figure 2.14) of the features present in all spectrums by A) Quality of the features detected and by the B) Average area. The plots described in Figure 2.14 are used to show how quantifiable a peptide is. This determines the threshold for the values for quality and intensity filters to obtain reliable peptide identification.

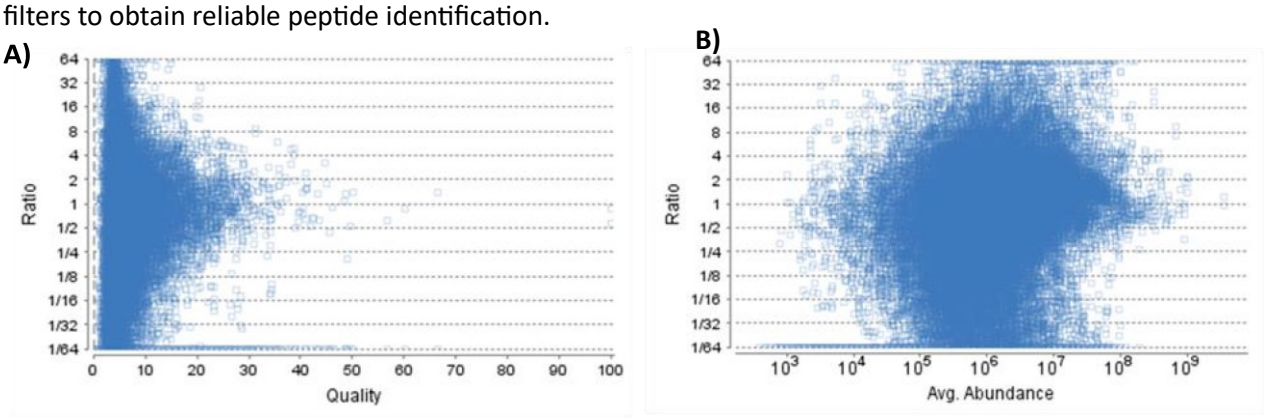

Figure 2.14. The distribution of feature vector ratio: (A) By quality; (B) By abundance, used to determine the threshold of the fold change.

2.8.7.2 Retention time m/z shift distribution

Plots of the A) retention time shift distribution to the reference sample (Figure 2.15) (Parental sample 1) B) The distribution of m/z of the reference sample. These figures are used to determine the retention time range that will be considered for a peptide to be included in the results. The red bars represent the range between all runs, which is then aligned and depicted as the blue bars, representing that most of the recordings are within 4 minutes, which was set as the Retention time upper bound.

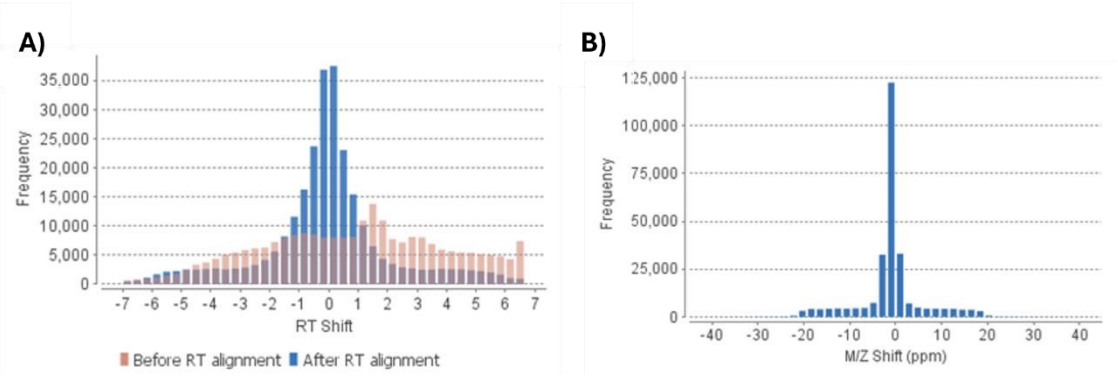

Figure 2.15. (A) RT shift distribution; (B) M/Z shift distribution.

2.8.8 Missing values and ID-transfer

Peptides of a particular protein may not be detected in all spectra for several reasons. Including the fact that Peptide fragmentation is not fully reproducible between runs, a fragmented spectrum may contain multiple signals from overlapping peptides, or spectral libraries may not contain information for all peptides, so some may be left unidentified. As such, to be able to interpret between runs, data ID transfer is required to reduce the number of missing peptides.

ID-transfer is a method where identification from spectra is transferred to another based on retention time and mass. Figure 2.16 depicts the percentage of unidentified peptides present in the dataset per sample before and after ID-transfer.

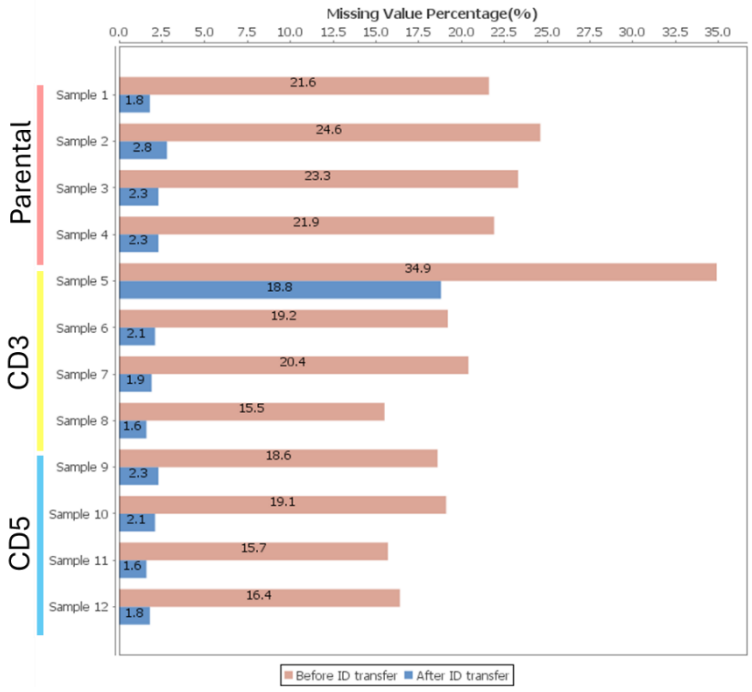

Figure 2.16: Percentage of missing values in each sample with or without ID transfer.

Whilst the percentage of missing values in each sample is largely consistent both before and after ID transfer, sample 5 (CD3) is an outlier in both before and after ID transfer. Whilst this was noted, this sample was not excluded from the analysis taken forward.

2.8.9 Data visualisation and summary

Data was summarised at the peptide and the protein level (Figure 2.17). For each protein identified, its Protein group, ID, Uniprot Accession, and a description were displayed (Figure 2.17, columns 1-3 and 12). The identified proteins were ordered based on the sum of the significance of distinguished peptide peaks identified above the spectral noise (Figure 2.17, A, column 4) Characterisation of the identified protein is summarised. The percentage of the total protein covered by identified peptides is listed, along with the number of peptides from the identified protein, and how many of these peptides are unique to the protein (Figure 2.17, A columns 5,6 and 7). The presence of post-translational modifications and the protein's average mass is listed (Figure 2.17, A, columns 8 and 9). The fold change between the control (parental) and each of the CD3 and CD5 samples: 1-12, and groups: Parental, CD3, CD5, were then summarised as colour-coded profiles. (Figure 2.17, A columns 10 and 11). At the peptide level, information about which peptides were used in abundance quantification was presented. (Figure 2.17, B) The identified peptides were mapped to the amino acid sequence of the corresponding protein, and the peptides were listed in a table below. The top three ranked peptides were involved in quantification, marked with a Y in (Figure 2.17, B) column 2, determined by the quality (Figure 2.17, B column 4) and the significance values (Figure 2.17, B column 5)

The detection parameters are listed in Figure 2.17, B, columns 6 and 7, with the average-ppm displaying the average mass error in ppm, whilst the average-area is the average area under the curve for each peptide.

The quantified change in abundance is displayed in Figure 2.17, B columns 8-12, with the sample and group profiles displaying relative peptide abundance to the average log2 depicted as a heatmap, and the group average abundance value is listed in the next column. The max ratio shows the maximum fold change between the control and the CSPα-deficient lines.

Vector shows the number of quantifiable features of a selected peptide (Figure 2.17, B, column 14) whilst the start and end are the first and last residue the peptide covers in the protein (Figure 2.17, B, columns 15-16), and lastly, the PTM column highlights the type and number of modifications present in the peptide (Figure 2.17, B, column 15).

A)

Protein Group	Protein ID	Accession	Significance	Coverage (%)	#Peptides	#Unique	PTM	Avg. Mass	Sample Profile	Group Profile	Description
50	24	P63039|CH60_RAT	200.00	12	8	8	Y	60956			60 kDa heat shock protein, mitochondrial OS=Rattus norvegicus OX=10116 GN=Hspd1 PE=1 SV=1

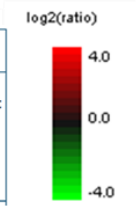

B)

P63039|CH60_RAT

| Protein Coverage | Supporting Peptides |

Protein Coverage:

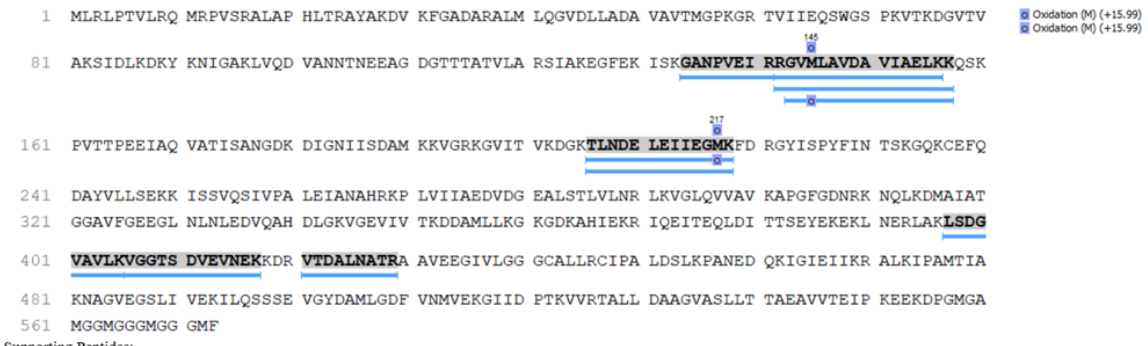

Supporting Peptides:

Peptide	Used	Candidates	Quality	Significance	Avg. ppm	Avg. Area	Sample Profile	Group Profile	Parent	Set3	Set5	Max Ratio	#Vector	Start	End	PTM
K.LSDGVAVLK.V	Y	Y	5.74	8.49	1.0	8.3766E7			2.5495E7	1.0842E8	1.1738E8	4.60	1	397	405	
K.VGGTSDVEVNEK.K	Y	Y	4.73	5.28	0.8	7.2153E7			2.6145E7	9.9054E7	1.1602E8	4.44	1	406	417	
R.VTDALNATR.A	Y	Y	4.50	4.25	2.5	7.0857E7			2.7692E7	7.0087E7	1.1479E8	4.15	1	421	429	
K.GANPVEIR.R	N	Y	5.21	5.25	0.6	5.3362E7			2.1224E7	7.155E7	8.5198E7	4.01	1	134	141	
K.TLNDELEIIEGMK.F	N	Y	4.70	2.68	1.8	4.9827E7			2.6498E7	6.8249E7	5.4733E7	2.58	1	206	218	
K.TLNDELEIIEGM(+15.99)K.F	N	Y	3.76	3.78	1.5	1.0746E7			3.4125E6	1.1244E7	1.758E7	5.15	1	206	218	Oxidation (M)
R.RGVMLAVDAVIAELKK.Q	N	Y	4.74	0.04	3.0	1.2218E6			1.2108E6	1.232E6	1.2227E6	1.02	1	142	157	
R.GVM(+15.99)LAVDAVIAELKK.Q	N	Y	3.91	1.04	0.7	4.9308E5			4.2613E5	4.8127E5	6.7837E5	1.59	1	143	157	Oxidation (M)
R.RGVMLAVDAVIAELK.K	N	Y	5.32	6.02	0.9	2.1775E5			9.8504E4	3.5972E5	1.9502E5	3.65	1	142	156	
total 9 peptides																

Figure 2.17: Summary information of an identified protein altered from label-free mass spectroscopy. A) Identified Protein and corresponding B) Peptide summary table, with protein identification and significance, and the relative abundance.

2.9 GO term and Pathway analysis of proteomic data

2.9.1 PANTHER Overrepresentation Test for enrichment of GO biological processes

The list of protein codes altered in the proteomics was covered to gene codes using the SYNGO ID mapping tool supported by the web service MyGene (MyGene.info | Gene Annotation as a Service, Dec 2024). The Panther knowledge base was used to carry out a PANTHER Overrepresentation Test for enrichment of GO biological processes using Fisher's Exact (Figure 2.18). Ranking GO terms by fold enrichment with corresponding raw P value and False Discovery Rate results for FDR $P < 0.05$ compared to a reference list of all genes present in the chosen organism (Rattus norvegicus). The fold enrichment is calculated by dividing the percentage of genes in the input list that are annotated with a specific GO term by the percentage of genes in the reference list annotated with the same GO term. A fold enrichment greater than 1 suggests overrepresentation, and enrichment over 100 indicates a significant overrepresentation,

whilst less than 1 indicates underrepresentation. The top 20 enriched GO terms for the up- and down-regulated terms are included in Chapter 5.

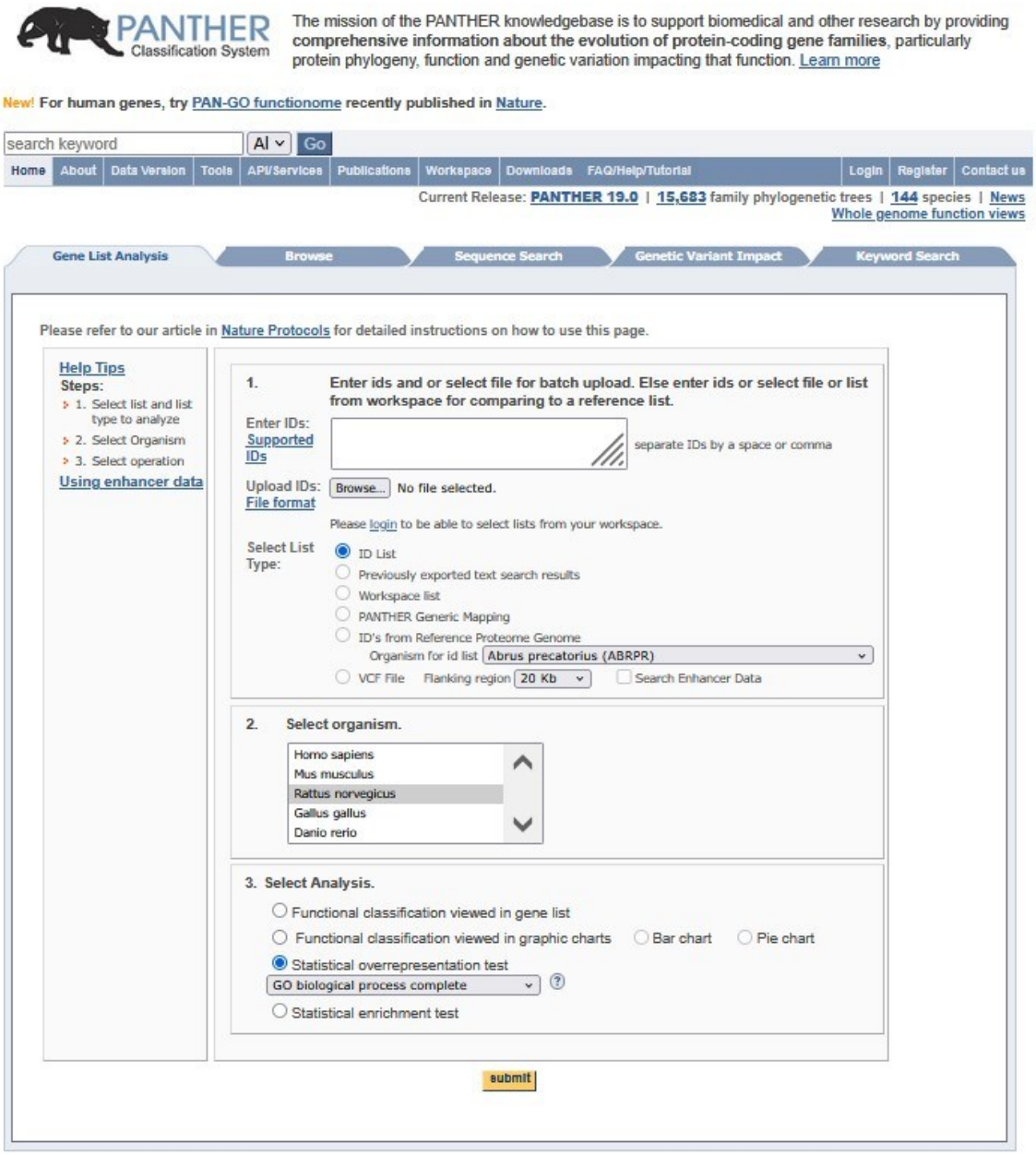

Figure 2.18: PANTHER upload page for PANTHER overrepresentation Test for enrichment of GO terms for biological processes using Fisher's exact test.

PANTHER Overrepresentation Test for enrichment of GO biological processes using Fisher's Exact. Displaying the top 20 enriched GO terms for the up- and down-regulated terms ranked by fold enrichment with corresponding raw P value and False Discovery Rate results for FDR $P < 0.05$.

2.9.2 STRING database used to annotate the pathways altered in CSPα knockdown PC12 cells as determined by proteomic mass spectroscopy.

String (version 12.0) (https://string-db.org/) (Accessed December 2024), which annotates protein-protein interactions indicating the strength or specificity of an interaction, was used to identify protein interaction networks in the proteins identified as being altered in the PC12 CSPα knockdown cells by Mass spectroscopy (Szklarczyk et al., 2023).

Up and down-regulated proteins (Appendix table C.4) were input into the database with the settings- Rattus norvegicus, full STRING network. With edges indicating both the function and the physical protein associations. The minimum required interaction score was set to medium confidence (0.400) or to high set at (0.700), and Markov Cluster Algorithm (MCL) clustering (find natural clusters based on the stochastic flow) was chosen with inflation parameters set to 3.

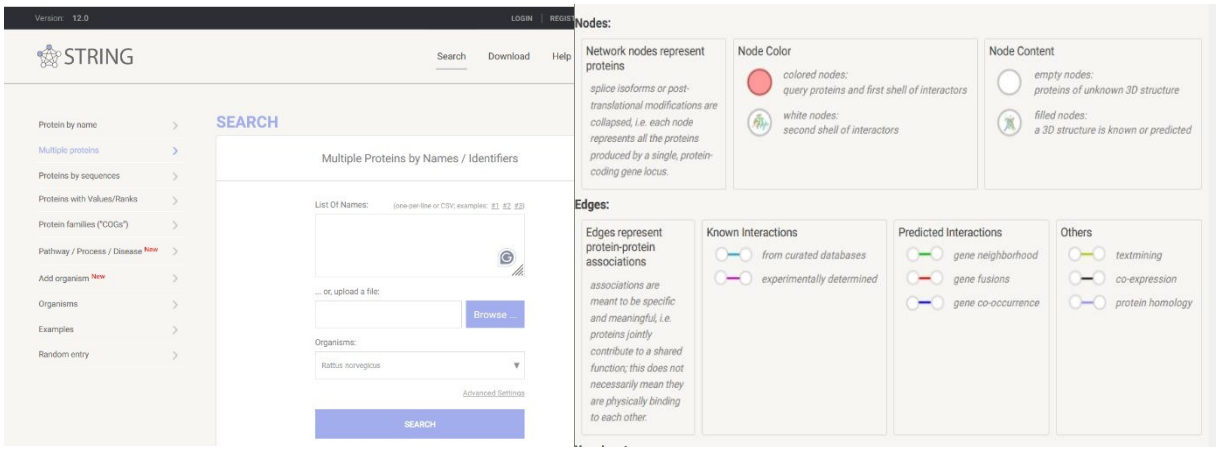

Figure 2.19: STRING load up page (left) for the pathway analysis of proteins altered between parental and CRISPR CSPα knockdown PC12 cells y. Legend STRING network (Right) with definition of network component.

2.9.3 Use of SYNGO to determine changes in synaptic proteins in the proteomic readout of CSPα knock-out PC12 cells

Prior to use of SYNGO protein symbols were converted to gene symbols using the SYNGO ID mapping tool supported by the webservice MyGene (*MyGene.info | Gene Annotation as a Service.*, Dec 2024) SYNGO (https://www.syngoportal.org/) (Accessed December 2024, version 1.2) was used to determine changes in synaptic protein expression between the parental and CD lines. SYNGO is an evidence-based, expert-curated resource for synaptic function, localisation and relationships between proteins (Koopmans et al., 2019). Up and down-regulated proteins were input, and either the domain of location or function was selected with enrichment analysis using -log10 Q value to produce a graphical readout and summary of the synaptic nature of the input list.

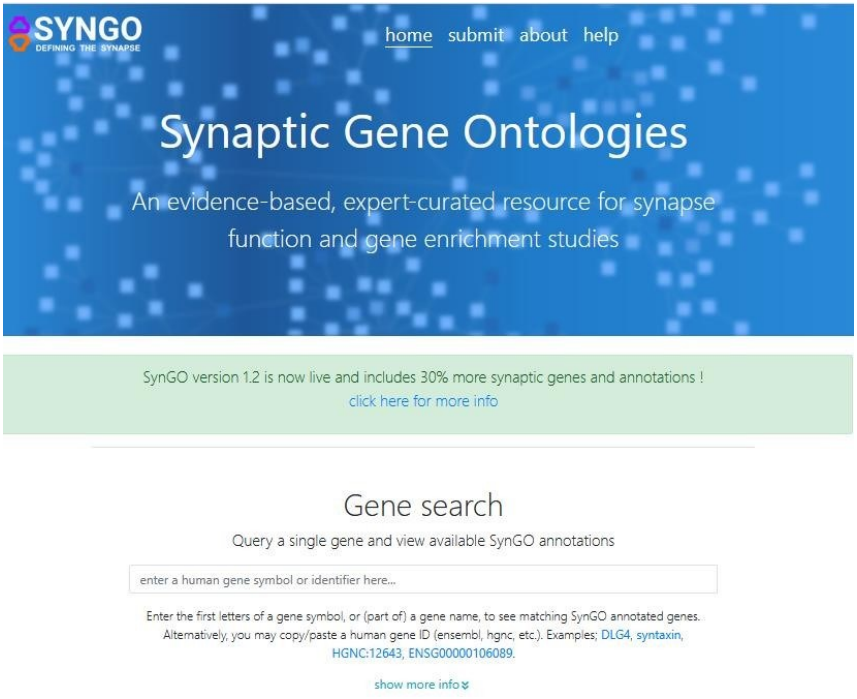

Figure 2.20: SYNGO load-up page used for the identification of the presence of synaptic proteins altered in the mass spectroscopy comparison of parental and CRISPR CSPα knockdown PC12 cells

Chapter 3 A bioinformatics approach to identify candidate E3-ubiquitin ligases for SNAP-25

3.1 Introduction

3.1.1 SNAP-25 ubiquitination and turnover

As described in the general introduction, SNAP-25's ubiquitination increases in the face of the proteostasis disruption caused by CSPα -/- (Section 1.8.6). Even with advances in elucidating how ubiquitin-proteasome pathways regulate synaptic protein composition (Ehlers, 2003, Haas and Broadie, 2008, Kawabe and Stegmüller, 2021) there is currently still limited knowledge of presynaptic ubiquitination and turnover; as such, SNAP-25 ubiquitination provides the possibility to identify compartment candidate E3 ligases.

3.1.2 SNAP-25 lysine residues that support ubiquitination

Lysine residue selection is important for generating specific substrate-ubiquitin interactions (Suryadinata et al., 2013). The proximity of the lysine(s) towards the E2 and E3 active sites is critical in the selection and ubiquitination of a specific residue (Sadowski and Sarcevic, 2010). SNAP-25 has 12 available lysine residues, with four ubiquitination positions identified by proteomic analyses from peptides extracted from mouse tissue at positions K40, K69, K72 and K103 (Figure 3.1) (Wagner et al., 2012).

Figure 3.1: **SNAP-25 sequence with likely ubiquitination sites highlighted.** Orange highlighted K are lysines identified to be likely ubiquitination targets. The palmitoylated membrane targeting region is highlighted in bold, and the SNARE motifs required for interaction with Syntaxin (1, N-terminal) and VAMP2 (2, C-terminal) are underlined.

3.2 E3 ligases in neurons

E3 ubiquitin ligases provide specificity to ubiquitination by selectively recognising a substrate (Pickart and Eddins, 2004). E3 ligases are differentially expressed in cells and across subcellular compartments, dependent on the localisation and function of target substrates as well as the scaffolding or selective organisation of a specific E3 ubiquitin ligase (Table 3.1) (Yang et al., 2021).

Table 3.1: **Examples of ubiquitination events identified in specific neuronal compartments**

Neuronal E3 ubiquitin ligases	Neuronal E3 ligase substrates
Ubiquitination at the presynapse	
Parkin	Glycosylated alpha-synuclein (Shimura et al., 2001) Synphilin-1 (Chung et al., 2001) Synaptotagmin 11 (Wang et al., 2018) Septin-5 (Y. Zhang et al., 2000)
APC	Liprin-α (synaptic growth) (van Roessel et al., 2004)
Highwire/ Rpm-1	MAPKKK, DLK (regulates synaptic growth) (Nakata *et al.*, 2005)
SCRAPPER	RIM-1 (priming for synaptic vesicle release) (Yao et al., 2007)
Staring	Syntaxin-1a/b (Chin et al., 2002b)
UBE3A	Arc, Tkv and SK2 (Dindot et al., 2008, Greer et al., 2010, (Li et al., 2016, Sun et al., 2015)
Ubiquitination at the post-synapse	
Parkin	DAT (Jiang et al., 2004) GluN1 (Zhu et al 2018) VPS35 (Williams et al., 2018)
Siah1A	GluR5 (Ishikawa et al., 1999)
MDM2	PSD-95 (Colledge *et al.*, 2003)
Ube3b	BCKDK (Cheon et al., 2019b) Ppp3cc (Ambrozkiewicz et al., 2021)
Ubiquitination in other neuronal compartments	
RPM-1 (axons)	GLO-4 (actin dynamics) and DLK-1 (microtubule dynamics) (Grill et al., 2007)
APP	Cdh1 (nuclear) (restrains axon outgrowth) (Konishi et al., 2004) Cdc20 (cytosolic) (regulates dendrite length) (Kim et al., 2009)

3.2.1 E3 ubiquitin ligase classes

There are five classes of E3 ubiquitin ligases (Figure 3.2), three of which have been extensively studied. The largest group, the Ring-finger type (Really Interesting New Gene (RING)-type) family, has more than 600 members (W. Li et al., 2008). The second most abundant group is HECT (homologous to E6AP C-terminus (HECT)-type E3 ubiquitin), with 28 members (Rotin and Kumar, 2009). Thirdly, the RBR: Ring between ring (RBR) E3 ubiquitin ligases family of 14 members (X. S. Wang et al., 2023). Then, the U-box type E3 ubiquitin ligase family which is structurally related to the RING family of E3 ligases. Finally, the RING Cys-Relay (RCR) family with one member (Yang et al., 2021) (Figure 3.2).

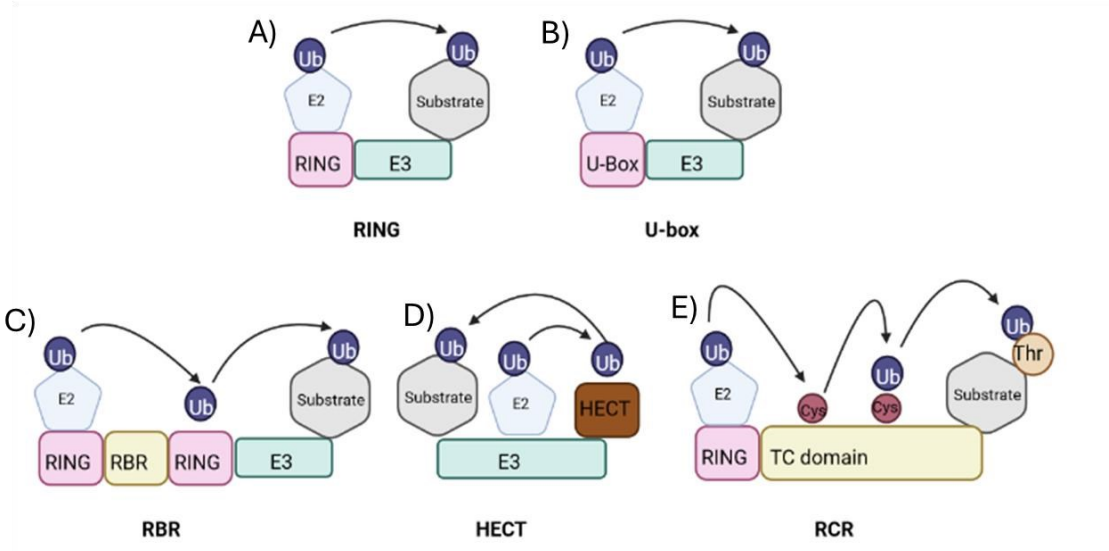

Figure 3.2: E3 ligase classes, structures and archetypical ubiquitination reaction.
A) Ring is representative of the Really Interesting New Gene (RING)-type family, B) U-box type E3 ubiquitin ligase family. C) RBR is representative of the Ring-between-ring E3 ubiquitin ligase family, D) HECT is representative of the homologous to E6AP C-terminus type E3 ubiquitin ligases family, and E) RCR is the RING-Cys-Relay family.

3.2.2 RING family of E3 ligases

The RING E3 ligase family are the major class of E3 ligases; they can provide a docking site for both the substrate protein and the E2-ubiquitin conjugate, with the RING domain facilitating the direct transfer of ubiquitin from the E2 ligase to the substrate protein (Figure 3.2, A) (Nguyen et al., 2017). The RING ligases act by coordinating two zinc^{2+} ions to form a platform in which E3 ubiquitin enzymes can bind (Deshaies and Joazeiro, 2009). The RING family have characteristic zinc chelating cysteine and histidine residues as part of their RING finger domain.

RING E3 ligases have a variety of substrates associated with DNA repair, tumour suppression and endocytosis (Metzger et al., 2014). Due to the variety of Ring type E3 substrates, the mechanisms of

substrate recognition are varied. Substrates can bind directly and indirectly to RING E3 ligases, which in turn can self-ubiquitinate or be ubiquitinated by heterologous
RING or HECT-type E3 ligases within the regulation of networks (Plechanovová et al., 2012).

3.2.3 HECT family of E3 ligases

HECT E3 ligases consist of a catalytic HECT domain at their C-terminus, and an E2 binding domain at the N-terminal, joined by a flexible hinge region which facilitates the transfer of ubiquitin from the bound E2 ligase (Figure 3.2, D) (Qian et al., 2020). Specificity of ubiquitin chain linkage is in the catalytic HECT domain. Ubiquitination requires an extra step in which an E3-ubiquitin intermediate is formed before ubiquitin is transferred to the substrate recruited by the HECT E3 ligase (Pickart, 2001). The HECT E3 ligases are divided into three subfamilies: the NEDD4 family, the HERC family and the "Other" HECT family (Table 3.2).

Table 3.2: **Subfamily and example members of the HECT E3 ligase family.**

Subfamily of HECT E3 ligases	Members	Structure
NEDD4	NEDD4, NEDD4-2, ITCH, WWP1, WWP2, SMURF2, SMURF1, HECW1, HECW2,	Lipid-binding/membrane domain, between two and four WW substrate recognition domains and a C-terminal HECT domain
HERC	HERC1, HERC2, HERC3, HERC4, HERC5, HERC6	Characterised by a regulator of chromatin condensation 1 (RCC)-like domain (RLD).
"other" HECT	E6AP, WUWE1, HACE1, TRIP12, UBR5, UBE3B, UBE3C, HECTD1, HECTD2, HECTD4, HECT3, G2E3, AREL1	Do not have a specific domain at their N terminus

U-box E3 ubiquitin ligases are a family of 21 ligases, named for a conserved U-box domain formed of 70 amino acids located at the C-terminus. The U-box domain interacts with an E2 ligase, allowing subsequent transfer of ubiquitin from the E2 ligase to the substrate (Figure 3.2, B) (Hatakeyama and Nakayama, 2003; Ohi *et al.*, 2003). U-box proteins are structurally related to the RING family, formed of a single polypeptide which makes use of zinc chelation, hydrogen bonds and disulfide bridges to transfer ubiquitin intermediates to the substrate (M.-S. Kim et al., 2021).

3.2.4 RBR family of E3 ligases

The RING-In-Between-RING (RBR) E3 ligases are characterised by a conversed catalytic region formed of a RING1 domain with a central in between-RINGS (IBR) domain and a RING2 domain. The RING1 is responsible for recruiting the E2 ligase, whilst the RING2 domain contains a catalytic cysteine required to accept a ubiquitin molecule (Spratt et al., 2014). RBR E3 ligases are involved in keeping

proteins in auto-inhibited states via intermolecular interactions (Chaugule *et al.*, 2011; Stieglitz *et al.*, 2012; Duda *et al.*, 2013). RBRs use a RING-HECT hybrid mechanism to carry out ubiquitination. The RING1 domain recruits the E2 ligase conjugated to ubiquitin, whilst a conserved cysteine residue in the RING2 domain accepts ubiquitin, which is transthiolated before it is transferred to the substrate (Figure 3.2, C) (Eisenhaber et al., 2007). Mutation of RING-type E3 ligases is linked to several human diseases, including Parkin, which has been shown to be involved in autosomal recessive juvenile Parkinsonism (Dawson and Dawson, 2010).

3.2.5 RING-Cys-Relay (RCR) family

The RING-Cys-Relay (RCR) family are a newly characterised family formed of one member, the neuron-associated E3 ligase MYCBP2, which is essential for neurodevelopment and regulates axon maintenance. MYCBP2 has both esterification and ubiquitination activity, containing two essential catalytic cysteine residues that relay ubiquitin to its required substrate via thioester intermediates (Figure 3.2, E). MYCBP2 has intrinsic selectivity for threonine over serine; non-lysine ubiquitination is rare, and this is the first case reported to have been identified in humans (Pao et al., 2018, Mabbitt et al., 2020, AlAbdi et al., 2023).

3.2.6 Known ubiquitination of SNAP-25

Whilst ubiquitination of SNAP-25 increases in CSPα-/-, currently, no E3 ubiquitin ligase has been found to be responsible for this, and to date, only one E3 ligase TFNAIP1, has been shown to ubiquitinate SNAP-25 in the context of postoperative cognitive dysfunction (W. Wang et al., 2023). Due to the fact that it is known that ubiquitination of SNAP-25 leads to its degradation, SNAP-25 is likely K48-linked polyubiquitinated when it is unchaperoned. Yet it is possible that SNAP-25 could also be mono- or K63-linked ubiquitinated to regulate its trafficking or recycling during the synaptic vesicle cycle (Hicke, 2001, Erpapazoglou, Walker and Haguenauer-Tsapis, 2014).

3.3 Aims

This chapter aims to leverage a bioinformatics approach to identify candidate E3-ligases that might be acting in the poly-ubiquitination of SNAP-25, which leads to its degradation. To this end, I used a combination of literature observations and structural predictions to generate a list of potential candidate E3 ubiquitin ligases. This is done with the aim of informing on the ubiquitination process of SNAP-25 and more broadly in the context of ubiquitination at the presynaptic nerve terminal.
To identify E3 ubiquitin ligases that potentially interact with SNAP-25, a literature-based approach looking for experimental evidence and a predictive-based approach based on structural features

were used. For full descriptions of the methods, databases, and filters used for this chapter, see Method Section 2.2.

3.4 Results

A bioinformatics approach was used to identify candidate E3 ligase activities as described and tabulated in Methods Section 2.2. Information on the database versions and the access dates can also be found here.

3.4.1 Literature-based approach to identify E3 ubiquitin ligases that may interact with SNAP-25

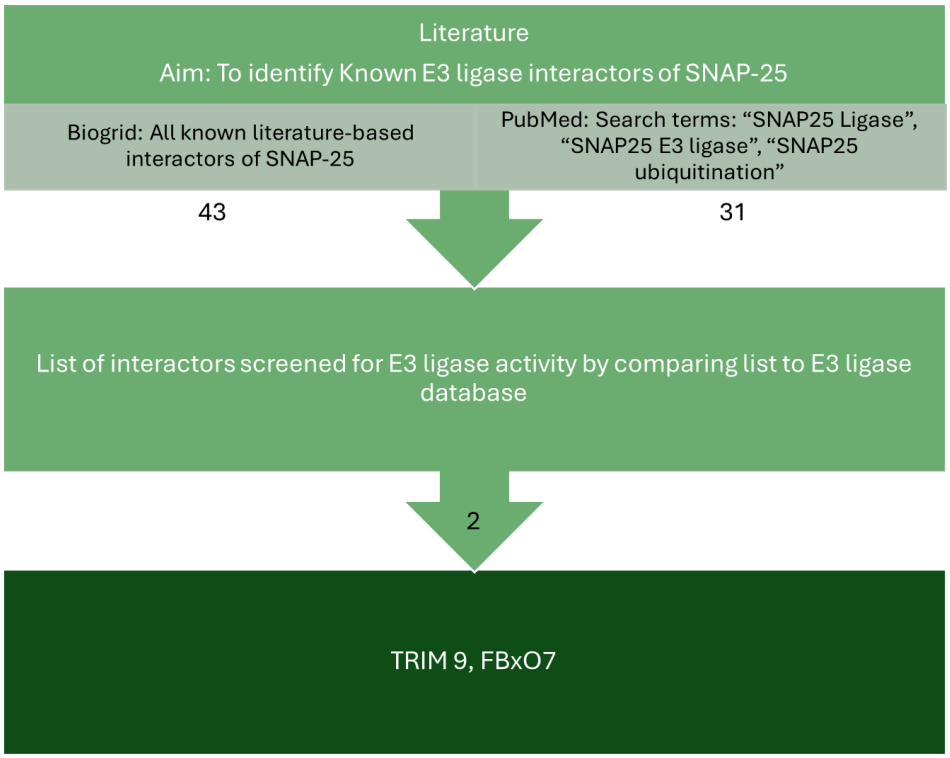

Figure 3.3: Workflow of the literature-based approach to identify E3 ligases that have been shown to interact with SNAP-25. With numbers highlighting the number of interactions returned from each stage of the approach.

The literature-based approach (Figure 3.3) was undertaken to extract existing candidates annotated as binding partners or associated in SNAP-25-containing protein complexes. For this reason, both the literature depositary database BioGRID and PubMed were used to facilitate this, utilising the search terms "SNAP-25 ligase", "SNAP-25 E3 ligase" and "SNAP25 ubiquitination".

3.4.1.1 BioGRID search for the identification of SNAP-25 E3 ligase candidates

BioGRID (https://thebiogrid.org/) (see method section 2.2.2 for details on the platform) returned 43 SNAP-25 interactions, including known SNAP-25 interacting proteins VAMP-2 and Synataxin-1. Of these interacting proteins, two were identified as having ligase activity (Li et al., 2017).

3.4.1.2 PubMed search for the identification of SNAP-25 E3 ligase candidates

For PubMed, the search term "SNAP25 Ligase" returned 11 papers, "SNAP25 E3 ligase" returned 8 papers and "SNAP25 ubiquitination" returned 31 papers. (See Appendix Table A.1). The final cohort of papers that emerged from these were read to investigate if their content provided evidence to support an interaction between SNAP-25 and proteins with E3 ligase activity.

TRIM9 was identified as a protein that interacted with SNAP-25 with confirmed E3 ubiquitin ligase activity as evidenced by subsequent BioGRID and PubMed searches, whilst FBX07 was identified via BioGRID but not PubMed (Table 3.3), potentially due to the fact that the data supporting an FBX07-SNAP-25 interaction was contained in the articles supplementary.

Table 3.3: The literature approach led to the identification of two proteins known to be binding partners of, or part of a SNAP-25 containing protein complex.

Gene symbol	Protein symbol	Uniprot number	Detection method	Function of SNAP-25 interaction	Source of interaction
FBX07	FBX7	Q9Y3I1	Biochemical activity assays of protein ubiquitination arrays	Evidence of SNAP-25 ubiquitination	(Teixeira et al., 2016a) *In vitro*
TRIM9	TRIM9	Q9C026	Affinity Capture-Western	Evidence of direct interaction	(Yankun Li et al., 2001; Menon et al., 2021; Winkle et al., 2014a)
			Yeast two-hybrid Interaction screen	negatively regulates	
			Proximity-dependent biotin exocytosis and ligase (BirA*)	SNAREmediated promiscuous labelling with axon branching in the absence of Netrin-1	

3.4.2 Predictive approach

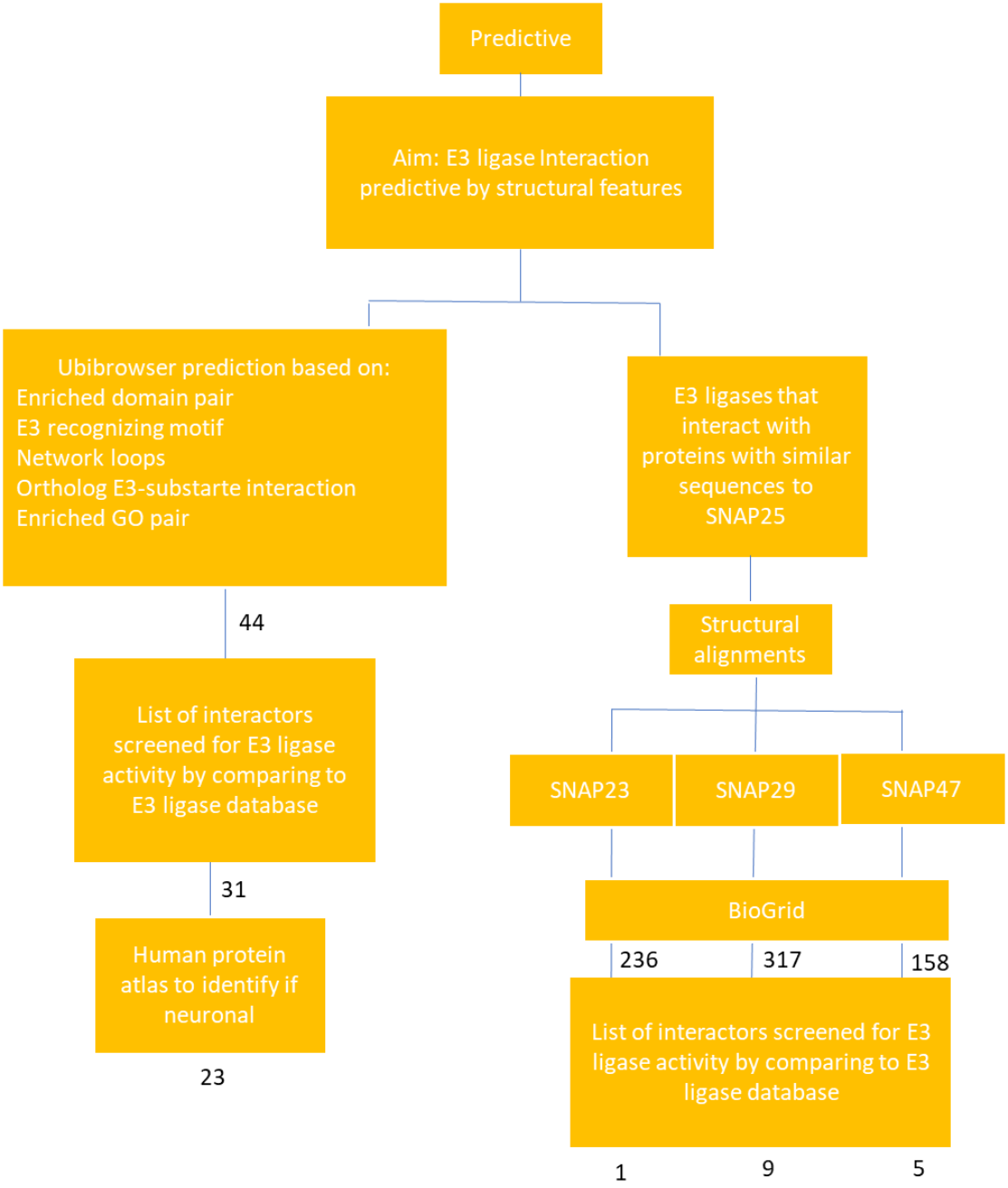

Figure 3.4: Workflow for predictive pathway to investigate E3 ligases that can interact and ubiquitinate SNAP-25. With the number of results returned for each stage of filtering.

The predictive approach used structural features to predict potential SNAP-25-E3 ligases interactions (Figure 3.4). The approach was developed around two routes. Firstly, two iterations of the prediction database, Ubibrowser predicted the likelihood of an E3 ligase-substrate interaction. The second route was rationalised on the basis that orthologues of SNAP-25 that serve as SNARE proteins in other vesicle trafficking reactions have sufficient structural and functional homology to be acted upon by shared or related E3 ligases. In this case, I used BioGrid (https://thebiogrid.org/) to identify interacting partners of these other SNAP-25 family members with an embedded E3-ligase activity

3.4.2.1 Motifs for interaction with ubiquitin.

Several different protein motifs are known to recognise and bind ubiquitin and can be used to predict candidate sites in proteins of interest (Lambrughi et al., 2021). A common motif for the interaction of ubiquitin with substrate proteins is the ubiquitin-interacting motifs (UIM) (Miller, Malotky and O'Bryan, 2004). Such short linear motifs (SLM) are often found in disordered regions of large proteins. The Ubiquitin-Interacting Motif (UIM) motifs, also termed the LALAL motif, is approximately 20 residues and often found in proteins involved in ubiquitination (Lambrughi *et al.*, 2021). In addition, ligase consensus sequences can be used to predict if a ligase of interest is likely to interact with a substrate under investigation (i.e. SNAP-25). Sequence motifs can be constitutively accessible to an E3 ligase or may only be formed after adding a post-translational modification such as palmitoylation (Hunter, 2007). The specificity of E3 ligases ensures they ubiquitinate targets with recognition motifs. For specific examples of E3 ubiquitin ligases, recognition motifs are listed in Table 3.4 and were used to guide my investigations. Using these guides, SNAP-25, SNAP-23, SNAP-47 and SNAP29 were interrogated for the existence of explicit ubiquitination target sequences.

Table 3.4: **Example E3 ubiquitin ligases with motifs they recognise in substrate proteins**

E3 ubiquitin ligase	Recognition motif	Source
NEDD4	WW domains recognise: PPxY, LPxY) (where x can be any amino acid) or Phosphor-threonine (pT) or phosphor-serine residues (pS)	(Aragón et al., 2012; Bobby et al., 2013; Escobedo et al., 2014; Qi et al., 2014)
ITCH	WW domain binds polypeptides with the PP xY consensus sequence (where x can be any residue)	(Qiu *et al.*, 2000; Zarrin par and Lim, 2000)
APC/C	Recognises D box's (RxxLxxI/VxN) present on substrates	(da Fonseca et al., 2011)

3.4.2.2 Ubibrowser: A bioinformatics platform for investigation into the human E3 ubiquitin ligase-substrate interaction network

Ubibrowser (http://ubibrowser.bio-it.cn/ubibrowser_v3/) was developed to facilitate an improved high-throughput way to identify candidate human E3 ligase-substrate interactions (Li *et al.*, 2017). The mUbiSiDa database of ubiquitination sites has over 30000 ubiquitination sites on over 5700 individual substrates (Chen *et al.*, 2014). Similarly, 900 human E3 ligase-substrate interactions have been collected into the E3Net database (Han *et al.*, 2012) as such responsible ubiquitin ligases are only assigned for a small number of ubiquitinated proteins. Ubibrowser was developed as a

database to allow the identification and prediction of E3 ligase-substrate interactions at the proteome scale.

Ubibrowser uses a naïve Bayesian classifier-based computational algorithm (a discriminant method which classifies based on the prior probability), to combine multiple different types of biological evidence to predict human E3 ligase-substrate interactions. Biological evidence, including homology E3 ligase-substrate interactions, enriched domain and Gene Ontology (GO) term pair, protein interaction network loops and inferred E3 recognition consensus motifs, is used to predict human E3 ligase-substrate interactions (Li *et al.*, 2017).

For Ubibrowser 1.0, each prediction is given a significance score that is calculated as a prediction's rank to the number of all the predicted pairs multiplied by the substrate number for the corresponding E3 ligase. Significance scores were defined as <0.001 as high confidence <0.01 as middle confidence , <0.05 as low confidence and >0.05 as a very low confidence interaction. For the 2.0 update, the predicted interactions were sorted into descending order of confidence score and the top 1% of interactions were assigned high confidence, and the remaining 99% were classified as low-confidence interactions and not displayed in the network.

3.4.2.3 Testing Ubibrowser 1.0 and 2.0 for known synaptic E3 ligase-substrate interactions

Ubibrowser versions 1.0 and 2.0 were used to identify E3 ligase interactions of PSD-95, which has been well characterised and is known to interact with Mdm2 (Colledge *et al.*, 2003) to determine if these interactions are identified by the Ubibrowser database.

Both iterations of the database identified the PSD-95-Mdm2 interaction as well as a known interaction between PSD-95 and UBE3A. Both versions of the database also predicted other likely E3-ligase-PSD-95 interactions, with iteration 1.0 returning 172 predicted results and version 2.0 returning 24 results. The difference in results returned is due to an update in how each interaction is ranked, as such, the 24 results returned by version 2.0 are ranked at a higher confidence.
The ubibrowser has the potential to be a valuable tool as a starting point to identify known E3 ligase-substrate interactions and make evidence-based predictions on potential E3 ligasesubstrate interactions, which can then be verified experimentally.

3.4.2.4 E3 ligases which have been predictive to interact with SNAP-25 based on specific domains and motifs using Ubibrowser

To identify E3 ligase-SNAP-25 potential interactions, both iterations of Ubibrowser were used. Ubibrowser 1.0 returned 44 predicted (Figure 3.5 and Appendix Table A1). Ubibrowser 2.0 returned one result for human interactions and a total of five for all eukaryotic species (summarised with biological evidence in Appendix Table A1.3). Neither search returned TRIM9 or FBX07 as interacting partners, which was unexpected due to literature-based searches already identifying them.

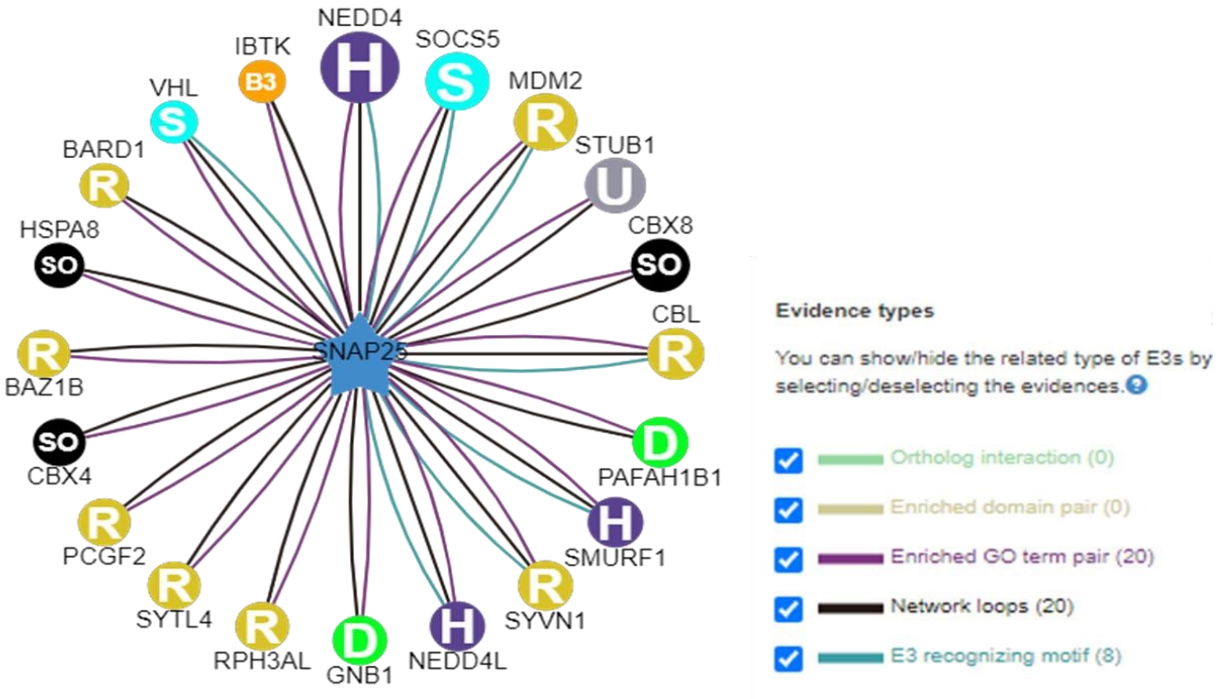

Figure 3.5: E3 ligases which are predicted to interact with SNAP-25 from Ubibrowser based on the likelihood of ortholog interactions, enriched domain pairs, enriched GO term pairs, network loops and E3 recognising motifs. The wheel depicting the ranked predicted interactions from Ubibrowser 1.0, with coloured arms connecting the centre of the wheel to the predicted E3 ligases, are coloured based on the evidence that supports the interaction; black represents evidence based on network loops, purple on enriched Go term pairs and blue on the presence of E3 recognising motifs.

3.4.2.5 E3 ligases identified by Ubibrowser 1.0 filtering

After collating E3 ligases, these were filtered by cross-checking against the Human E3 ubiquitin ligase database. The rationale here was to prioritise candidacy based on ensuring the identified proteins had E3 ubiquitin ligase activity and were not listed on Ubibrowser due to SUMO ligase or deubiquitinase activity.

This initial extraction included 44 proteins predicted by Ubibrowser 1.0 to interact with SNAP25. Deubiquitinating enzymes and SUMO ligases were removed, leaving a list of 31 candidate E3 ubiquitin ligases. Using the human protein atlas determined 23 proteins had evidence of brain localisation (Li *et al.*, 2017) (Table 3.5, Figure 3.6).

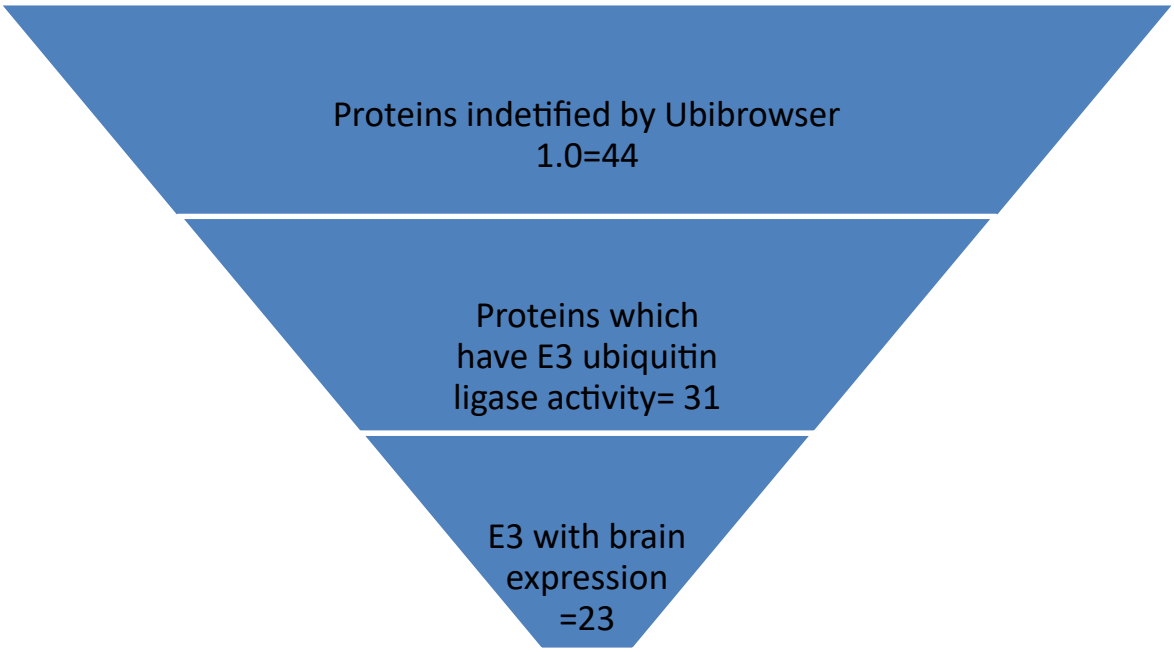

Figure 3.6: **Filtering approach applied to E3 ligases predicted to interact with SNAP-25 by Ubibrowser 1.0**.

3.4.2.6 E3 ligases identified by Ubibrowser 2.0 filtering

Of the 5 proteins predicted to interact with SNAP-25 across all mammalian species by Ubibrowser 2.0, all had known E3 ligase activity and all 5 are expressed in the human brain (Table 3.5).

Table 3.5: **E3 ligases predicted to interact with SNAP-25 by Ubibrowser and be localised to human brain regions.**

E3 ligases predicted to interact with SNAP-25 by Ubibrowser 1.0, with mRNA expressed in human brain regions listed in order of ranking.		E3 ligases predicted to interact with SNAP-25 by Ubibrowser 2.0, with mRNA expressed in human brain regions
NEDD4	PML	BTRC
SOCS5	TRIM27	BARD1
MDM2	TNFAIP1	ARIH1
STUB1	PPIL2	PRKN
CBL	WDTC1	RC3H2
SMURF1	SMURF2	
SYVN1	ASB2	
NEDD4L	PARK2	
HSPA8	CISH	
BARD1	FZR1	
MARCH 9	TTC3	
RNF216		

3.4.2.7 Mapping of Ubibrowser predicted E3 ligase candidates on SNAP-25 sequence

The Ubibrowser (http://ubibrowser.bio-it.cn/ubibrowser_v3/)predictions can be mapped onto SNAP-25's amino acid sequence to visually represent the domains that are expected to interact with specific E3 ligases (Figure 3.7). This highlights that different ligases are predicted to interact with different regions of the SNAP-25 structure and are likely to ubiquitinate at different lysine residues. Both HECT (NEDD4L recognition motif) and RING (BTRC and ASB2 motifs and HECT inferred recognition domain) inferred structure features were detected in SNAP-25, which suggests that members of either the RING or the HECT E3 ligase families may have the potential to interact with SNAP-25.

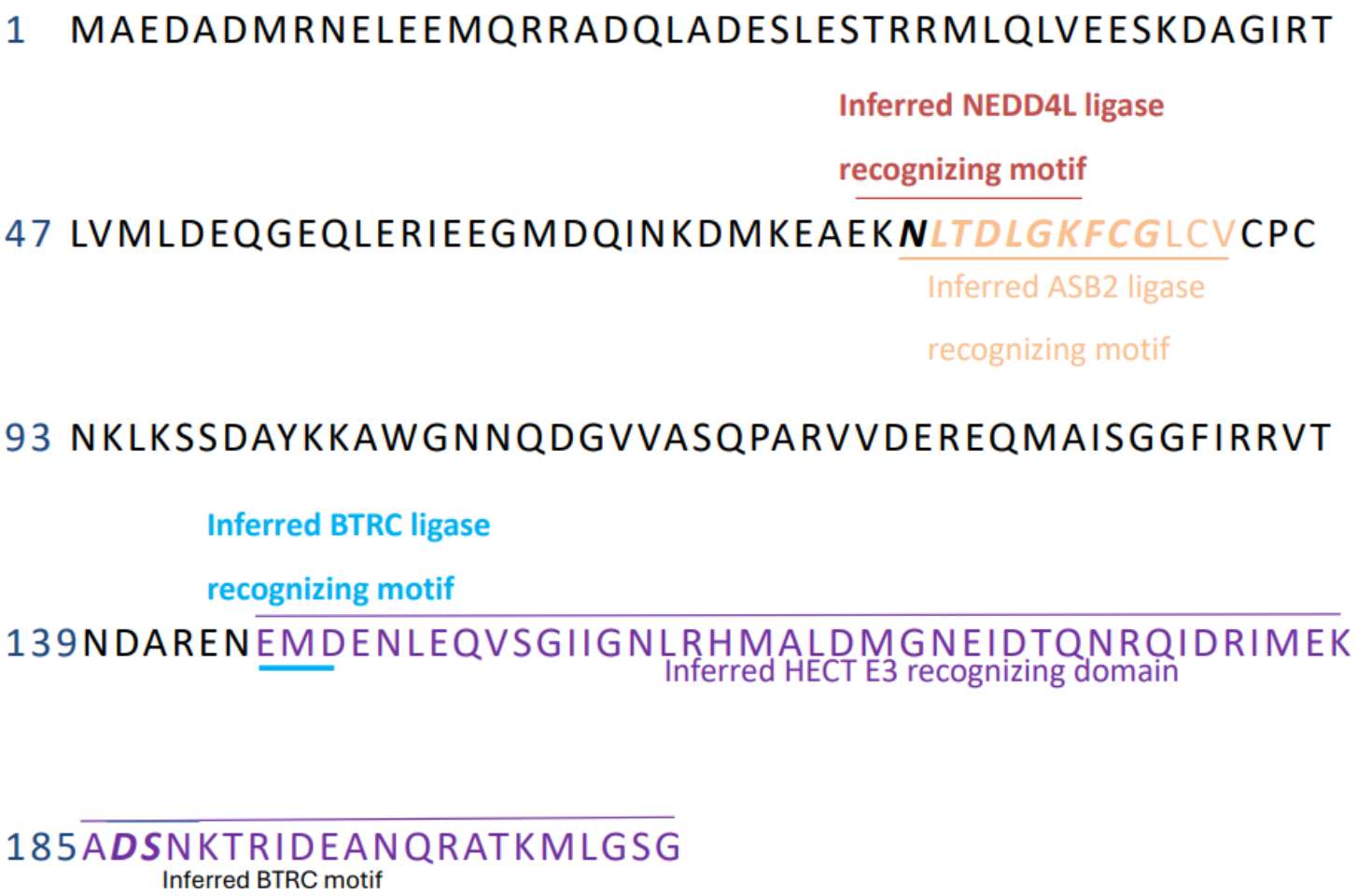

Figure 3.7: SNAP-25 amino acid sequence with inferred recognition domains and motifs of E3 ligases predicted by Ubibrowser 1.0 and 2.0

3.4.2.8 E3 ligases that interact with SNAP family proteins

Whilst the Ubibrowser database suggested domains and motifs that may increase the likelihood of interaction, none of the suggestions were based on known E3 ligase-substrate interactions for SNAP-25.

There are other SNAP family proteins present in vertebrates that SNAP-25 shares high homology with (Figure 3.8). I investigated whether any E3-ligases are known to interact with the other SNAP family proteins. Identifying domains and motifs in these sequences that facilitate these interactions, to determine whether these interactors could be possible for SNAP-25 also.

3.4.2.9 Sequence identity between SNAP family proteins

The amino acid sequences and 3D structures of the SNAP family proteins were compared and aligned to identify levels of homology (Figure 3.8). Structural overlays were done to identify conserved SNARE interaction domains, which harbour SNAP 25 lysine's and to determine if there is conservation in E3 ligase recognition motifs and domains between the family members. SNAP23 has ~60% sequence identity to SNAP25 at the amino acid. SNAP-29 has a longer N-terminal section than both SNAP-25 and SNAP-23, but has levels of homology throughout most of the sequence (Figure 3.8, B) . SNAP-29 had a 26% identity with SNAP-23 and a 32% identity with SNAP-25. The regions of highest homology of SNAP-29 to SNAP-23 and SNAP-25 reside in the amino- and carboxyl-terminal thirds of the SNAP-29 protein (Figure 3.8, C). SNAP-47 is the longest member of the SNAP protein family, and like SNAP-29, has longer linker domains and lacks the palmitoylated cysteines of SNAP-25 and SNAP-23. SNAP-47 alignment with the sequence of SNAP-25 revealed longer N and C-terminal sections with some levels of homology throughout the sequence (Figure 3.8,D), but to lower levels than that of SNAP-23 and SNAP29. The SNAP family proteins share conservation of the fold around the SNARE helices and linker unfolded regions, yet there is a large variation in the disordered regions (Figure 3.8). BioGRID (https://thebiogrid.org/) and Ubibrowser were then used to identify known or predicted E3-substrate interactions within the SNAP family protein sequences, which may be suggestive of the potential for interactions with SNAP-25.

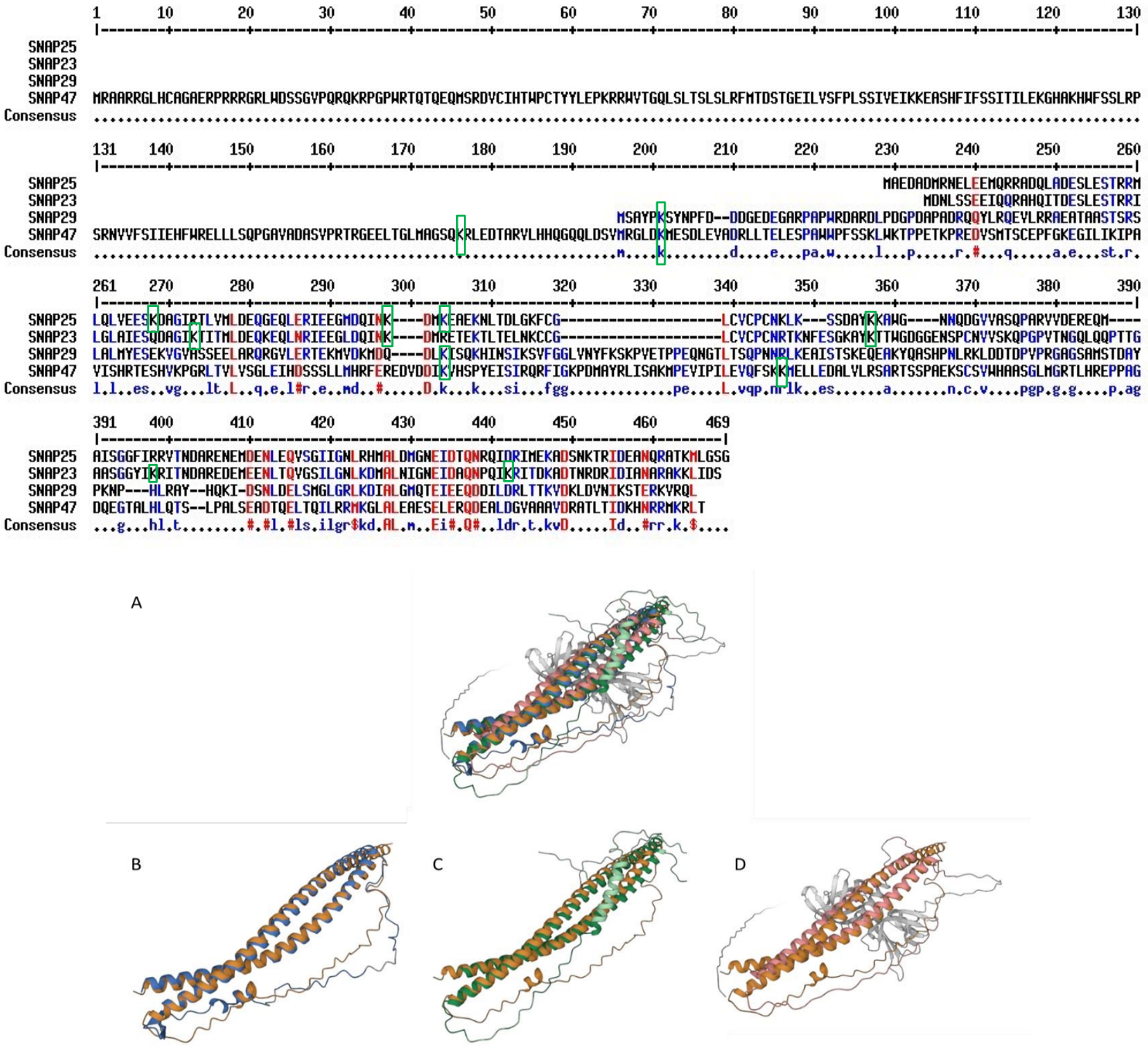

Figure 3.8: Sequence alignment and structural homology of the SNAP family SNARE proteins. Top alignment of the primary amino acid code of SNAP family proteins present in vertebrates (F. CORPET, 1988) Lysines (K), which have been shown experimentally to be ubiquitinated highlighted in green. Bottom A: overlay structural alignment of SNAP-25 (orange), SNAP-23 (blue), SNAP-29 (green) and SNAP-47 (pink). B: SNAP-25 (orange) and SNAP-23 (blue). C: SNAP-25 (orange) and SNAP-29 (green). D: SNAP-25 (orange) and SNAP-47 (pink/white) (*RCSB PDB - Structure Pairwise Alignment Tool*)

3.4.2.10 Identification of E3 ligases known to interact with SNAP family proteins

BioGRID (https://thebiogrid.org/) was used to identify known interactions of SNAP-23, SNAP-29 and SNAP-47. For SNAP-23, this produced a list of 236 interacting partners experimentally identified. Comparison to the Human E3 ubiquitin ligase database led to the identification of one E3 ubiquitin ligase, ZFPL1, and two accessory proteins to E3 ligases had ANKFY1 and KCTD7.
For SNAP-29, 317 interacting partners were identified, of which nine of the proteins, RFWD2, RNF183, RNF20, RNF40, TRAF3, TRAF6, TRIM26, TRIM62 and ZFPL1 had established E3 ubiquitin ligase activity, and one; KCTD7, was an E3 ligase accessory protein.
SNAP-47 produced a list of 158 interacting partners, of which five, MARCH 5, MID2, RNF170, TRIM59 and ZFPL1 had E3 ubiquitin ligase activity and one, KCTD7, functioned as an E3 ligase accessory protein.

3.4.2.11 Filtering of E3 ligases identified to interact with SNAP family proteins

The E3 ligases identified by BioGRID were filtered for neuronal expression and listed in Table 3.6. None of the E3 ligases identified to interact with SNAP-23, 29 or 47 (see Table 3.6) were predicted to interact with SNAP-25 by Ubibrowser or identified by BioGrid as being an interactor of SNAP-25. Yet it was identified that all of the SNAP-25 family members had a conserved Inferred HECT E3 recognition domain.
ZFPL1 was confirmed to interact with SNAP-23, SNAP-29 and SNAP-47 and due to the high levels of conservation between these family members and SNAP-25, may be a good candidate for an E3 ligase for SNAP-25.

Table 3.6: E3 ligases identified by BioGrid which have been shown to interact with SNAP proteins which have structural homology with SNAP-25.

SNAP-23 E3 ligases	SNAP-29 E3 ligases	SNAP-47 E3 ligases
ZFPL1	RFWD2	MARCH5
	RNF183	MID2
	RNF20	RNF170
	RNF40	TRIM59
	TRAF3	ZFPL1
	TRAF6	
	TRIM26	
	TRIM62	
	ZFPL1	

3.4.2.12 Identification of E3 ligase interaction domains and motifs in SNAP-family proteins

The Ubibrowser database was used to predict and visualise E3 ligase-interacting domains and motifs in the SNAP-family amino acid sequences (Figure 3.9).

From Ubibrowser version 1, SNAP-23, SNAP-29 and SNAP-25 shared an inferred HECT E3 recognition domain and 33 overlapping predicted E3 ligase interactions out of a total of 46 for SNAP-23 and 24 overlapping predicted E3 ligase interactions out of a total of 27 for SNAP-29. SNAP-47 does not share the Inferred HECT E3 recognition domain with the other SNAP family members but does share 13 overlapping predicted E3 ligase interactions out of a total of 20 with SNAP-25 in addition to inferred ASB2, NEDD4L, SYVN1 and RNF180 recognition motifs. All of the inferred motifs are in the C-terminal portions of each of the SNAP family members, which is the most conserved section, and whilst SNAP-25, 23, and 29 all share an inferred HECT E3 recognition domain, the sequences of each of these domains differ which may suggest that even through there is not full homology if an E3 binds to one SNAP family member there is the potential that it may be able to interact with other members.

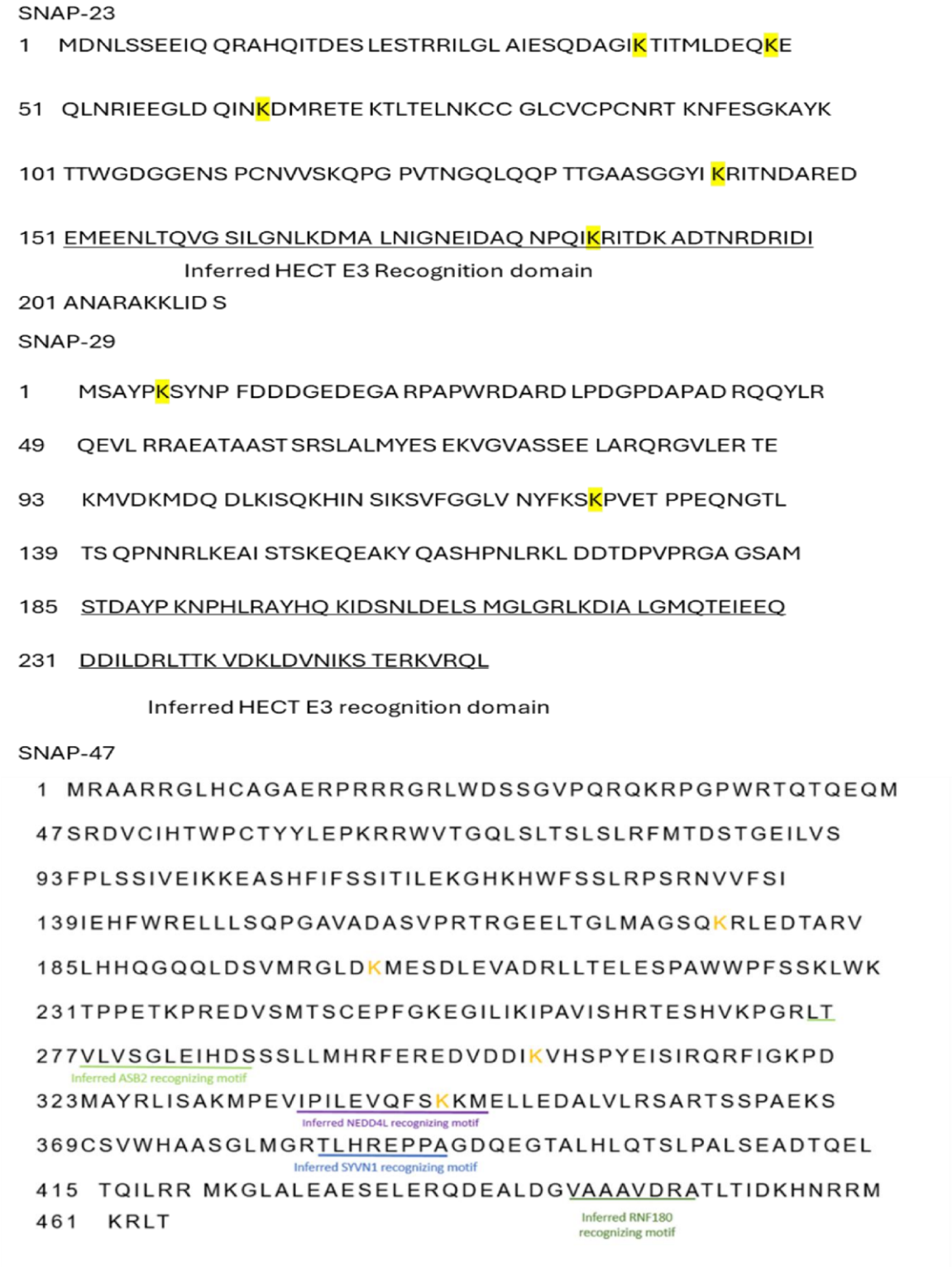

Figure 3.9: SNAP family members amino acid sequences; SNAP-23, SNAP-29 and SNAP-47. Amino acid sequences with experimentally verified ubiquitinated lysines highlighted in yellow and predicted inferred recognition motifs of E3 ligases underlined.

3.4.2.13 E3 ligases identified to be of interest from the predictive approach

All of the E3 ligases predicted by the Ubibrowser databases (Table 3.6) are ligases that could be interesting to test regarding interaction with and ubiquitination of SNAP-25. However, a more focused list of E3 ligases which have been identified to have neuronal expression and synaptic localisation would include:

- ASB2 is predicted to interact due to the presence of an interacting motif in SNAP-25
- BTRC is predicted to interact due to the presence of an interacting motif in SNAP-25
- NEDD4L is predicted to interact due to the presence of an interacting motif in SNAP-25
- BARD1 due to being predicted to interact by both iterations of the database due to enriched GO pair analysis and network loops.
- ZFPL1 due to interactions with all three SNAP family members (SNAP-23, 29 and 47)
- NEDD4 due to being the highest-ranked predicted interaction

3.4.2.14 E3 ligases with disease-related support for interaction with SNAP-25

Further ligases which were predicted to interact with a lower ranking but have evidence of involvement in disorders with an association of SNAP-25 (data not shown) may also be interesting to test these including: CUL3, FBXW7, STUB1, PARKIN, PRAJ-1, UBE3A, TTC3.

3.4.3 Screens of E3 ligases of interest

Once E3 ligases were identified by literature searches and/or structural predictions, it was investigated whether any proteomic screens had been carried out for each of the ligases to determine if an interaction with SNAP-25 had previously been identified in a high-throughput screen that had yet to be followed up (Table 3.7).
Proteomic studies for the identification of E3 ligase-substrate interactions often involve the use of either microarrays with ubiquitination assays or the extraction of protein samples from either tissue or cell types, followed by mass spectroscopy analysis to identify proteins which are ubiquitinated in an environment with an overexpression of an E3 ligase.

Interactions of E3 ligase-substrates or a change in ubiquitination require validation via further biochemical investigation, whilst ubiquitination microarray assays require investigation into where the interaction is likely to be biologically relevant.
It was investigated whether each of the prioritized E3 ligases had been used as bait in a Proteomic screen and whether this proteomic screen had taken place in a system where SNAP25 was present, and as such, an E3 ligase-SNAP-25 interaction would have been identified.

Table 3.7: Identified interactions screens undertaken in the literature

E3 ligase	Any proteomic screen undertaken	Was SNAP-25 looked for	Was SNAP-25 identified	Sources
E3 ligases identified in the predictive approach				
TRIM9	Yes BioID in primary cortical neurons	Yes	No	(Menon et al., 2021)
FBXO7	Yes *In vitro* ubiquitination screen of human microarray	Yes	Yes	(Teixeira *et al.*, 2016)
Priority E3 ligase identified in the predictive approach				
ZFPL1	No screens identified			
BTRC	No screens identified			
ASB2	Yes Nano-LC-ESI-LTQ-Orbitrap MS/MS Analysis of ASB2 expressing and non-expressing of PLB 985 cells (human blood cell line)	SNAP-25 is not predicted to be actively secreted into the blood	No	(Burande et al., 2009)
NEDD4	Yes *In vitro* ubiquitylation and binding assays using a microarray of human proteins	Yes	No	(Persaud et al., 2009)
NEDD4-2	Yes, *In vitro* Ubiquitylation and binding assays UPLC-MS/MS of isolated membrane fractions from Nedd4-2 +/+ and /- mouse whole brains	Yes	No No	(Persaud et al., 2009) (Eagleman et al., 2021)

BARD1	Yes, Quantitative proteomic mass spectroscopy	Mouse embryonic fibroblasts	No	(Song et al., 2011)
E3 ligases identified in predictive with a medium priority				
SOCS5	Yes, Affinity Capture-MS 293T cells and HCT116 cells	Yes	No	(Huttlin et al., 2021)
MDM2	Affinity Capture-Luminescence Affinity Capture-MS Proximity LabelMS	Yes	No	(Trepte et al., 2018) (Huttlin et al., 2015) (Kido et al., 2020)
CBL	Affinity Capture-MS Co-fractionation	Yes	No	(Erdem-Eraslan et al., 2015) (Golkowski et al., 2023) (Havugimana et al., 2022)
SMURF1	Affinity CaptureMS	Yes	No	(Huttlin et al., 2015) (Du et al., 2021) (Andrews et al., 2010)
SYVN1	Affinity Capture-MS Proximity LabelMS	Yes	No	(Fenech et al., 2020) (Huttlin et al., 2021)
E3 ligases identified in the predictive approach with lower priority				
CUL3	Protein extracts from E16.5 cortices from mutant cul3 analysed.	Yes	No	(Morandell et al., 2021)
FBXW7	Quantitative proteomics combined with degron motif searches in human colorectal cancer cell line *FBW7*	Expressed in some colon cell types	No	(Arabi et al., 2012)
STUB1	No screens identified			

PARKIN	Yes, BioUb strategy followed by MS in flies. diGly capture proteomics (diGly) HeLa^{PARKIN} cells	Yes Yes	Yes, SNAP-25 is more ubiquitinated but has less than 2-fold enrichment in parkin overexpression flies Yes	(Martinez et al., 2017) (Sarraf et al., 2013)
PRAJ-1	Protein microarray ubiquitylated using UBE2D3 as the E2 and Praja1 as the E3	Yes	No supplementary data available	(Loch et al., 2011)
UBE3A	AP-MS analysis of SH-SY5Y cells transfected with UBE3A constructs	Yes (Undifferentiated)	No	(Martínez-Noël et al., 2018)
TTC3	No screens identified			
HSPA8	Affinity Capture-MS Co-fractionation Cross-Linking-MS (XL-MS)	Yes	No	(Huttlin et al., 2021) (Havugimana et al., 2022) (Wheat et al., 2021)
MARCH	No highthroughput screens			
RNF216	No screens identified			
PML	Affinity CaptureMS	Yes	No	(Maillet et al., 2020)
TRIM27	Affinity CaptureMS	Yes	No	(Hein et al., 2015)
TNFAIP1	Affinity CaptureMS Negative Genetic	Yes	No	(Asmar et al., 2023) (Bennett et al., 2010) (Ito et al., 2021)
PPIL2	Affinity CaptureLuminescence	Yes	No	(Hegele et al., 2012) (Hart et al., 2015)
	Affinity CaptureMS			

WDTC1	Affinity CaptureMS Proximity LabelMS	Yes	No	(Bennett et al., 2010) (Raisch et al., 2023)
SMURF2	Affinity CaptureMS	Yes	No	(Huttlin et al., 2015)
CISH	Affinity CaptureMS Protein microarray	Yes	No	(Hüttenhain et al., 2019) (Jones et al., 2006)
FZR1	Affinity CaptureMS Proximity dependent labelling	Yes	No	(Oh et al., 2020) (Chen et al., 2014)
ARIH1	Affinity CaptureMS BioID in HEK293 cells	Yes	No	(Huttlin et al., 2015) (Coyaud et al., 2015)
RC3H2	Affinity CaptureMS Proximity LabelMS	Yes	No	(Huttlin et al., 2021) (Youn et al., 2018)

Some E3 ligases identified were removed from the list of E3 ligases to test based on proteomic screens not identifying SNAP-25 interactions (Table 3.7). Whilst both Need4 and Need4l were predicted to interact with SNAP-25 by Ubibrowser and had an association with several disorders where SNAP-25 is down-regulated in neither was identified to interact with SNAP-25 in proteomic screens in samples where SNAP-25 would have been present; this is also true for CUL3, FBXW7 and UBE3A.

Whilst TRIM9 and FBX07 identified as promising candidates via the literature-based approach, and Parkin identified via Ubibrowser, evidence from proteomic screens provides additional support for a potential interaction and as such, should be tested as high-priority candidates using the BioID assay developed in the next chapter.

3.5 Discussion

The aim of the work summarised in this chapter was to identify candidate E3 ligases with the potential to ubiquitinate SNAP-25. This bioinformatics approach was carried out in order to make informed decisions on candidate E3 ligases that should be taken forward to carry out experimental investigations.

It is known that SNAP-25 is ubiquitinated and that this contributes to SNAP-25's turnover and it can be blocked by inhibitors and seems sensitive to neuronal activity. Whilst SNAP-25 ubiquitination can happen as part of biogenesis, it seems particularly important in the context of the nerve terminals, essentially as dysfunctional turnover is implicated in disease processes, including models of degeneration and brain disease (Sharma, Burré and Südhof, 2011, Sheehan *et al.*, 2016). However, the details of this do not predict which or what the preferred ubiquitination mechanism of SNAP-25 is. All classes of E3 ligases are implicated in the turnover of SNAP-25 in neurons. Thus, we have an open mind on which E3 ubiquitin ligases could ubiquitinate SNAP-25.

The E3 ligases to take forward have been identified by bioinformatic approaches and have either been suggested to interact with SNAP-25 via a literature-based search or predictive modelling and identification in proteomic screens (Figure 3.10).

Priority E3 ligases
High priority
TRIM9, FBX07, Parkin
Medium priority
ASB2, BTRC, STUB1, PJA-1
Lower priority
ZFPL1
BARD1

Figure 3.10: Summary of E3 ligases with the potential to interact with and ubiquitinate SNAP-25. Priority to test the interactions experimentally ranked on the likelihood of an interaction taking place based on the evidence identified by the bioinformatics approaches.

3.5.1 Discussion high-priority E3 ligases

3.5.1.1 TRIM9 was identified as an interacting partner of SNAP-25

TRIM9 (RBCC tripartite motif-containing proteins), initially termed SPRING (a SNAP-25-interacting RING finger protein) is a RING Finger Protein formed of a RING finger domain with two B box motifs and a coiled-coil domain, making it part of the RING-B box coiled-coil (RBCC) subfamily of RING finger proteins. TRIM9 has two validated ubiquitination substrates, DCC and VASP (Y. Li *et al.*, 2001, Winkle *et al.*, 2014, Menon *et al.*, 2015) (Figure 3.11).

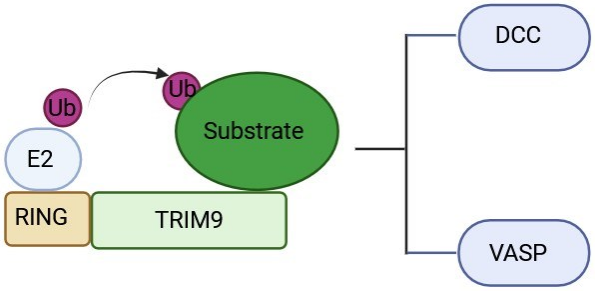

Figure 3.11: Protein ubiquitination pathway for TRIM9, with verified ubiquitination substrates DCC and VASP. DCC is ubiquitinated by TRIM9 to downregulate pathways responsible for axon branching and vesicle fusion. VASP is ubiquitinated, leading to a loss of localisation and a downregulation of filopodial stability and axonal guidance.

TRIM9 interacts with SNAP-25, in a yeast two-hybrid (Yankun Li et al., 2001). *In vitro* binding assays using recombinant His-tagged TRIM9 and GST-SNAP-25 independently verify the interaction between TRIM9 and SNAP-25. Importantly, TRIM9 did not interact with Syntaxin-1, VAMP-2 or SNAP-23. (Yankun Li et al., 2001). TRIM9 is expressed in the brain and enriched in neurons (Berti et al., 2002; Reymond et al., 2001; Tanji et al., 2010). Interestingly, the TRIM9 interaction with SNAP25 abolishes SNAP-25's ability to assemble into the SNARE complex (Yankun Li et al., 2001).
The binding domains of SNAP-25 and TRIM9 were investigated by Li et al using deletion analysis to identify the specific domains required for the association of the two proteins. Only GST-tagged SNAP-25 fusion proteins containing the N-terminal of the t-SNARE domain interacted with TRIM9 (Figure 3.12). The C-terminal t-SNARE domain and the central domain were not required for interaction. The N-terminal of SNAP-25 has previously been shown to be required for binding to Syntaxin-1, whilst both SNAP-25's N- and C-termini are required for binding to VAMP2. The B box C-terminal coiled-coil domain of TRIM9 was required to interact with SNAP25, whilst the RING finger, B Box domains, C-terminal and SPRY domains were not required (Yankun Li et al., 2001).

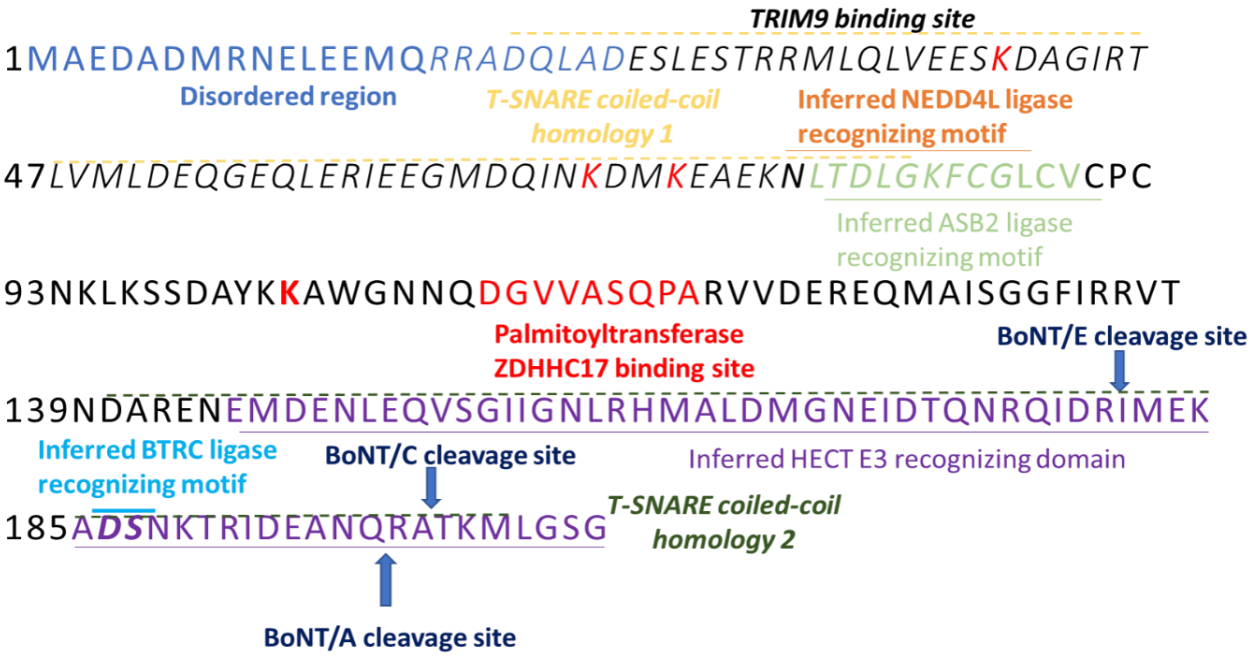

Figure 3.12: Features of SNAP-25 structure, including domains marked by dashed lines, known interacting sites of TRIM9 and Palmitoyltransferase ZDHHC17 responsible for SNAP-25 palmitoylation, inferred E3 ligase interacting sites determined by the predictive approach undertaken in this chapter and known BoNT cleavage sites.

TRIM9 synaptic localisation may position it to modulate synaptic vesicle exocytosis by preventing the formation of SNARE complexes and maintaining SNAP-25 in an inactive state. Whilst it has been confirmed that SNAP-25 and TRIM9 interact, no ubiquitination assays were reported, determining if SNAP-25 is ubiquitinated by TRIM9. The selectivity of interaction and the neuronal expression and sub-compartment enrichment raise interest in Trim9's potential to function as an E3 ligase in the case of SNAP-25

3.5.1.2 FBX07 identified as an interacting partner of SNAP-25

The second E3 ligase identified by the literature-based approach was RING-type FBX07, encoded by PARK15, a clinically relevant F-box protein which has been linked to cancer (Nelson et al., 2013) and early-onset autosomal recessive Parkinson's disease (Zhou et al., 2016, Zhong et al., 2023). The F-box proteins are the substrate-binding constituents of the four subunits of the ubiquitin protein ligase complex SKP1-cullin-F-box (SCFs) (Winston et al., 1999) and act as both the substrate recognition and binding domain. Currently, FBXO7 has 8 validated ubiquitination substrates; hepatoma up-regulated protein (HURP) (Hsu et al., 2004), cellular inhibitor of apoptosis protein 1 (c-IAP1) (Chang et al., 2006), TNF receptor-associated factor 2 (TRAF2) (Kuiken et al., 2012), Glycogen synthase kinase 3β (Gsk3β), translocase of outer mitochondrial membrane

20 (Tomm20) (Teixeira et al., 2016b), Ubiquitously expressed Transcript isoform 2 (UXTV2), (Spagnol et al., 2021), Neurotrophin Receptor-Interacting MAGE Homolog (NRAGE) (Kang and Chung, 2015) and phosphofructokinase (PFKP) (Harris et al., 2022). Ubiquitination of these substrates (summarised in Figure 3.13) leads to either the degradation of the substrate, regulation of substrate activity or regulation of localisation or regulation of the NF-κB signalling pathway.

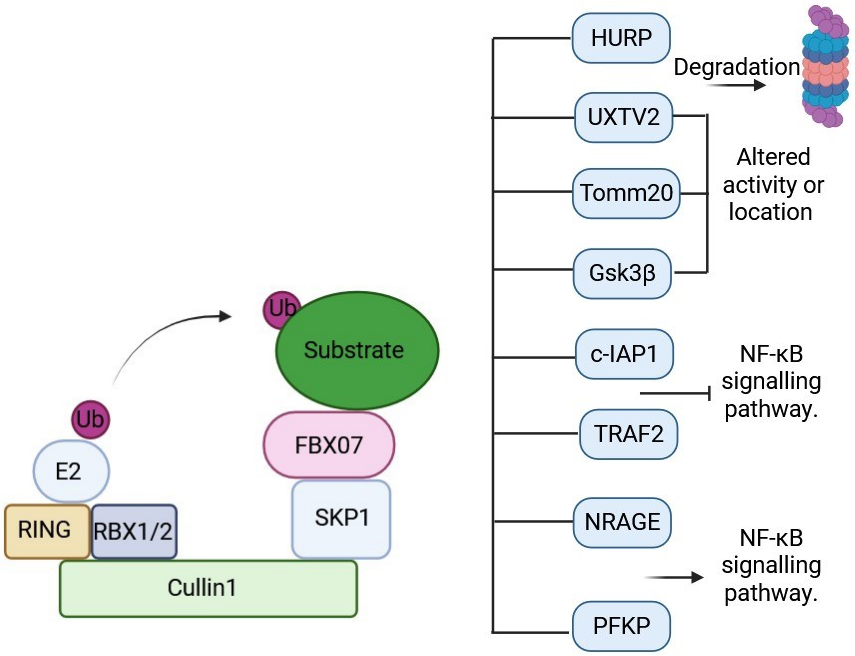

Figure 3.13: Protein ubiquitination pathway for FBXO7 in SCF complex, with Cullin1 acting as a protein scaffold, bound to RBX1 as the catalytic core and the substrate recognition module FBXO7 bound to SKP1. With the transfer of ubiquitin from an E2 to the bound substrate. The substrates of FBXO7: Ubiquitination of HURP and UXTV2 leads to their subsequent degradation, ubiquitination of UXTV2, Tomm20, and Gsk3β leads to alteration in their activity or localisation, ubiquitination of c-IAP1 and TRAF2 leads to inhibition of the NF-κB signalling pathway, whilst ubiquitination of NRAGE and PFKP leads to the upregulation of the NF-κB signalling pathway

SNAP-25 was identified to be one of 338 potential ubiquitinated substrates of SCFFbxo7 via a high-throughput screen using protein arrays to identify new candidate proteins that are ubiquitinated by the ligase complex. The interaction has not been independently validated (Teixeira et al., 2016a). Interestingly, FBXO7 and SNAP-25 are both on the University College London's Parkinson's disease-relevant priority protein list for annotation concerning disease relevance ('ebi.ac.uk/Parkinsons UK-UCL'). In the case of FBX07, the genetic association with disease warrants this, whilst SNAP-25 has a more causal link. Whilst no direct link has been validated between the two due to the identification

of SNAP-25 in the high-throughput screen and the established role FBXO7 has in synaptic proteostasis (Vingill *et al.*, 2016, J. Wang *et al.*, 2023, Kulkarni *et al.*, 2023), leads it to being a candidate that requires further research to explore a potential interaction.

3.5.1.3 Parkin is a promising candidate to interact with SNAP-25

Parkin, a HECT-like RBR E3 ubiquitin ligase, is predicted to interact with SNAP-25 by Ubibrowser. Parkin has a synaptic localisation and is involved in several disorders in which SNAP-25 is downregulated in. In addition to using the Ubibrowser prediction of Parkin, I interrogated the literature and identified 2 proteomic-based screens that provide evidence of an association of Parkin with SNAP-25 (Sarraf et al., 2013, Martinez et al., 2017). Parkin has a large and diverse number of substrates (Figure 3.14) this has led to the suggest that unlike some E3 ligases, Parkin does not require specific peptide sequences to be present in its substrates for recognition and ubiquitination, but instead Parkins ability to recognise substrates can be influenced by factors such as depolarization of the mitochondria, the presence of phosphorylated ubiquitin or the state and location of a specific protein (Walden and Martinez-Torres, 2012, Koyano *et al.*, 2019).
Parkin has been identified as a causal gene responsible for hereditary recessive early-onset Parkinsonism (Kitada et al., 1998) and has a well-established role in mitochondrial quality control by mediating mitophagy (Narendra et al., 2008). Other work has shown that Parkin also has a role in the maturation of endosomes, their sorting and their fusion with lysosomes for degradation by ubiquitinating endosomal proteins such as Rab7 and VPS35 (Song et al., 2016) and has been shown to interact and ubiquitinate with proteins present at the plasma membrane (Sassone et al., 2017) such as PSD 95 (L et al., 2002) and with synaptotagmin XI (Dp et al., 2003).

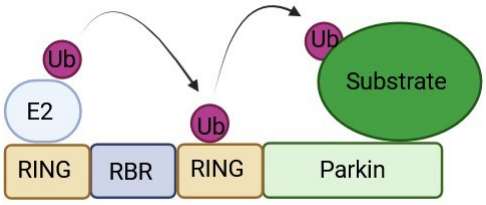

Mitofusins (MFN1 and MFN2)	Miro1	Pael-R	Synphilin-1
Voltage-Dependent Anion Channels (VDAC1, VDAC2, VDAC3)	Tom20	Cyclin E	Ataxin-3 and Ataxin-2
STEP61	α/β-tubulin	RanBP2	Ikkγ (NEMO)
TRAF2	PLCγ1	Eps15	Bcl-2
Drp1	PICK1	FBP1	α-Sp22
CDCrel-1 and CDCrel-2a	Synaptotagmin XI	p38	

Figure 3.14: Protein ubiquitination pathway for Parkin, which functions as a RING between RING E3 ubiquitin protein ligase and list of validated Parkin substrates List of Parkin substrates (Sarraf et al., 2013)

3.5.2 E3 ligases to test with a medium priority

E3 ligases that should be investigated as a medium priority include ASB2 and BTRC, which were predicted to interact with SNAP-25 due to motifs present in SNAP-25's structure. STUB1, which was predicted to interact by Ubibrowser and associated with four disorders, SNAP-25 is downregulated in, whilst PJA-1, which is associated with three disorders that SNAP-25 is downregulated in. Each of these four ligases has either not had a proteomic screen undertaken in a tissue type where SNAP25 is expressed, or the data is unavailable.

3.5.3 E3 ligases to test with a lower priority

Finally ZFPL1 and BARD1 are of potential interest, ZFPL1 was identified to interact with SNAP23, 29 and 47 so may have the potential to interact with SNAP-25 due to shared homology, whilst BARD1

was the only protein predicted to interact with SNAP-25 by both interactions of Ubibrowser but a screen undertaken in mouse fibroblasts did not identify SNAP-25 as an interactor.

3.5.4 Limitations of methods and databases used

3.5.4.1 Algorithm mismatching prediction and data.

I used both iterations of Ubibrowser. Whilst these represent iterations of an algorithm, they provided distinct results due to the weighting provided for the ranking of predictions. They are rationalised based on criteria set out in the Methods Section 2.2.5. Despite their ability to predict some experimentally verified E3 ligase interactions with other synaptic proteins I tested, I found no "known" literature-based interactions for SNAP-25. With ubibrowser 1.0, manual literature mining only included papers before the 1st January 2010, and only 913 E3 ligase substrate pairs were identified, which may explain why reported interactions of SNAP-25 were missing, such as SNAP-25-FBX07, which was published in 2016.

3.5.4.2 Loss of potential candidate E3 ligases by filtering

Ubibrowser ranked E3 ligases as high, medium and low confidence interactions, due to the large number of E3 ligases suggested with little evidence only high confidence ligase or those with further evidence were taken forward however since the resource was used a low confidence ranked E3 ligase TFNAIP1 has been investigated and shown to form a conjugate with SNAP-25 leading to SNAP-25 being 48-linked poly- ubiquitinated at SNAP-25 position K69 (W. Wang et al., 2023). In this work, SNAP-25 ubiquitination and downregulation were investigated in the context of cognitive dysfunction, and TNFAIP1 was followed up due to its role in neuroinflammation. Whilst in my work, it wasn't followed up due to other E3 ligases being more promising candidates based on our criteria set out above.

3.5.4.2 Unutilised bioinformatics resources

Since this bioinformatics work was conceived, there has been a large increase in the bioinformatics tools available (Table 3.8) for this type of protein-protein interaction prediction. These techniques may have increased the number of candidate E3 ligases initially identified but carrying out filtering would still be required as set out in this chapter to rank which to test experimentally due to experimental restraints.

Table 3.8: Bioinformatic protein-protein interaction identification tools and databases.

Approach	Tools/Databases	Strength	Limitation
Sequence motif search	DEGRONOPEDIA, (Szulc et al., 2024) UbPred (Radivojac et al., 2010)	Fast and scalable	Misses noncanonical interactions
Protein-Protein Interaction Network Analysis	STRING, (Szklarczyk et al., 2023) BioGRID,(Oughtred et al., 2021) UbiBrowser (Wang et al., 2022)	Integrates large data sets	Low specificity
Signal-pathway integration	PhosphoSitePlus, (Hornbeck et al., 2012) Signor (Lo Surdo et al., 2023)	Captures conditional interactions	Needs contextspecific data
Machine learning	UbiBrowser2.0, UniBind(G. Wang et al., 2023) PEPPI (Bell et al., 2022)	High-throughput prediction	Data-dependent; risk of false positives

3.5.4.3 E3 ligases that would be included retrospectively

The initial bioinformatics carried as described in this chapter was carried out in late 2021. Since then, further articles have been published, protein-protein interaction databases updated and there have been advances in machine learning. This leads to the likelihood that more candidate SNAP-25-E3 ligase interactions may be predicted now. Repeating the Ubibrowser 1.0 and 2.0 searches in June 2025 did not reveal any new predictions, but neither version of the database has been updated since June 2020.

Repeating the PubMed searches in June 2025 produced two additional articles for the search term "SNAP-25 ligase" and six additional articles for the search term "SNAP-25 ubiquitination". Including the 2023 paper describing an interaction between the E3 ligase TNFAIP1 and SNAP-25 (W. Wang et al., 2023) as discussed in Section 3.5.4.2.

In 2021, BioGrid returned 43 results with SNAP-25. As of June 2025, 58 verified SNAP-25 interactors were listed. Of these 15 newly added interactors, none were identified as having E3 ligase activity when compared to the Human E3 ligase database.

3.6 Summary

In summary, the bioinformatics approach set out in this chapter has provided evidence to investigate candidate E3 ligases. The evidence gathering highlights a virtue in bioinformatic platforming

experiments, but also highlights the need for systematic prioritisation with a view to experimental validation. This has provoked me to investigate candidates that operate within a neuronal context and provide evidence of potential synaptic function. On this basis, I have created a tabulation categorised by high, medium, and low priority candidates to facilitate experimental follow-up (Figure 3.10). This forms the basis for an approach in which the potential interaction and controlled ubiquitination of SNAP-25 by TRIM9, FBX07 and Parkin are investigated in the context of the pre-synapse (Figure 3.15 for potential subcellular localisation of an interaction between SNAP-25 and candidate E3 ligases).

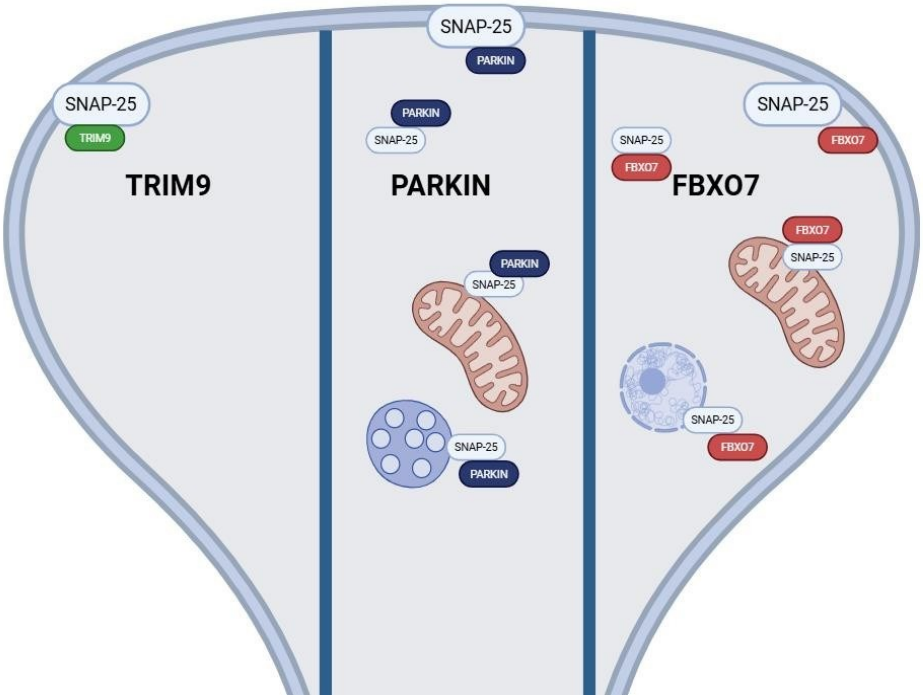

Figure 3.15: Schematic of potential SNAP-25- E3 ligase pre-synaptic interaction subcellular localisations. TRIM9 and SNAP-25 have been shown to localise to the plasma membrane. Parkin interacts with substrates at the plasma membrane, in the Cytoplasm, at the mitochondria and on endosomes. Whilst FBXO7 interacts with substrates at the plasma membrane, in the Cytoplasm, at the mitochondria and at the nucleus.

Chapter 4 Investigating the validity of predicted SNAP-25-interacting E3 ligase candidates in cellular models HEK293FT and PC12

4.1 Introduction

This chapter details an experimental approach and the reagents required to assess whether the E3 ligases identified bioinformatically in the last chapter (Chapter 3) have the ability to interact with SNAP-25.

4.1.1 Detecting protein-protein interactions

Detecting protein-protein interactions is key to understanding the functions of proteins. Historically, both biochemical and genetic techniques, such as co-immunoprecipitation and yeast two-hybrid (Fields and Song, 1989), have been used to verify or identify novel proteinprotein interactions (Rao et al., 2014). In addition, biochemically, both direct and proximitydependent technologies, whereby proteins have to be within a certain radius of each other to raise a likely interaction, can be employed (Pfeiffer et al., 2022).

4.1.2 Proximity-dependent biotin identification (BioID) to identify protein-protein interactions

The proximity labelling technique BioID is based on the use of a Biotin ligase fused to the protein or protein domain of interest. BioID was initially developed in 2012 (Roux et al., 2012) and to date has been adapted for use in vitro and *in vivo* (Kim and Roux, 2016, Khan *et al.*, 2018, Brudvig *et al.*, 2018). Since its development, BioID has been adapted in a number of ways, including the development of smaller versions of BioID, split-BioID studies and versions which biotinylate more quickly (Kim *et al.*, 2016, Schopp *et al.*, 2017, Branon *et al.*, 2018). BioID fusion proteins have been introduced into cells via transfection, viral infection and via CRISPR-Cas9 (Birendra Kc *et al.*, 2017, Long, Brown and Sibley, 2018).

4.1.3 Development of BioID

BioID utilises the BirA *Escherichia coli* biotin protein ligase, which specifically biotinylates acetyl-CoA. The mutant BirA* has a point mutation (R118G), causing it to act as a promiscuous biotin ligase (Cronan, 2005). BioID functions under the principle that when biotin (10-50 µM) is supplied to BirA*,

in the presence of ATP, BirA* binds to and activates the biotin, leading to the release of reactive biotinyl-AMP, which forms a covalent bond with primary amines on proximal lysine residues (Roux et al., 2012). This method assumes that if a recombinant protein with a fused BirA interacts, it will allow biotinylation of the partner protein. BioID can generate a history of potential candidate protein-protein interactions over a defined period under physiological conditions within living cells, unlike other methods that capture a snapshot of a single interaction (Sears et al., 2019). Targeting motifs attached to a particular protein can be used to target the BirA* to a particular subcellular compartment to localise the proximity labelling (Sears et al., 2019).

Proteins that become biotinylated by BioID can be classed into three categories: 1. Proteins that form direct stable or transient interactions with the protein of interest. 2. Proteins that interact indirectly with the protein of interest, or 3. Proteins that are within the proximal radius of the protein of interest but do not interact either directly or indirectly (Sears et al., 2019). The radius in which BioID can biotinylate is approximately 10-15 nm (Kim et al., 2014). As such, the use of robust controls is required to identify background proteins that have a high affinity for the promiscuous ligase but are not functionally relevant, or have a moderate affinity but are present in high abundance in the vicinity of the bait protein.

4.1.4 Limitations of BioID

BirA* has limitations, including the requirement for a Tag to bind the BioID ligase to the protein of interest, thereby modifying the protein. This can have consequences for protein localisation and function. Whilst BirA* is effectively expressed in bacterial systems, expression in mammalian cells can be challenging due to differences in codon usage, which can impact protein expression levels and the efficiency of biotinylation (Mechold et al., 2005). There is also the potential for non-specific biotinylation to take place with longer reaction times or under certain conditions (Chojnowski et al., 2018).

4.1.5 Using protein-protein interaction detection techniques in parallel

Due to the nature of E3-ligase-substrate interactions being weak (generally in the high nM to µM affinity range) and transient (Pierce *et al.*, 2009, Varshavsky, 2012, Coyaud *et al.*, 2015), they may not be detected in traditional direct binding assays. An advantage of proximity-dependent assays is that they can identify weak (super micro) and transient interactions. Some studies that have used both direct binding and proximity labelling in parallel have been shown to have only limited overlap between identified interactors (Gallo et al., 2023).

4.2 Aims

This chapter aims to:

1. Generate and characterise the Myc-BioID-SNAP-25 and control reagents required to carry out BioID using SNAP-25 as bait,
2. Characterise PC12s as a neuronal-like model to carry out BioID, and
3. Carry out BioID using SNAP-25 as bait in PC12 to determine if candidate E3 ligases identified as candidates by bioinformatics are found to be proximal to SNAP-25.

This work is intended to use independent biochemical evidence to validate an interaction with SNAP-25. This is a primer for experiments with the long-term view of increasing our understanding of the mechanisms that underlie the ubiquitination of SNAP-25.

4.3 Methods

4.3.1 Designing experimental controls

Two control constructs were designed alongside the BioID-SNAP-25 (Figure 4.1, A). In addition to the fusion of BioID to SNAP-25, the constructs expressed an N-terminal Myc tag. To control for the Myc-BioID-SNAP-25, a Myc-BioID construct that generates cDNA that encodes a soluble cytoplasmic BioID harbouring an N-terminal Myc tag, lacking the SNAP-25 fusion, was used in identifying nonspecific interactions (Figure 4.1, B).

SNAP-25 is localised at the plasma membrane in a steady state (Vogel et al., 2000). Thus, I generated a myristoylated Myr-Myc-BioID construct that encodes a Myr-Myc-BioID with a plasma membrane localisation signal. This was designed to detect potentially abundant interactions in the same compartment as SNAP-25 (Figure 4.1, C).

When referring to all three constructs collectively, they will be referred to as Myc-BioID constructs. In addition to experiments performed after transfection of the constructs described above, I routinely ran a non-transfected control in which biotin was fed to the cells. This was used to identify proteins which have an intrinsic ability to incorporate biotin, affinity for the streptavidin or non-specific binding to the solid phase used in downstream affinity purifications.

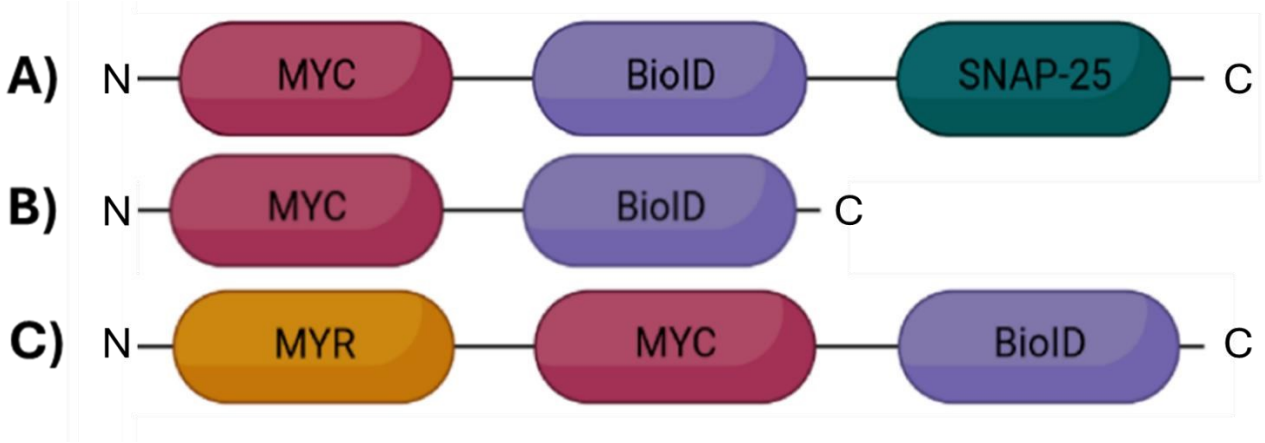

Figure 4.1: Schematic depicting the Myc-BioID constructs generated to carry out BioID. A) Myc-BioID-SNAP-25, B) Myc-BioID, C) Myr-Myc-BioID

4.4 Results

4.4.1 PC12 cells as a model for the identification of synaptic E3 ligases

PC12 cells are a good model for investigations of presynaptic sites and SNARE machinery (Chamberlain, Burgoyne and Gould, 2001, Salaün, Gould and Chamberlain, 2005). This has led to them being used to study the mechanisms of regulated release in the absence of full synaptic differentiation (Tao-Cheng *et al.*,1995, Chen *et al.*, 2001, Zhou *et al.*, 2006).

4.4.2 Expression of key synaptic proteins across PC12 differentiation

PC12 cells become more neuronal after differentiation *in vitro* upon the addition of NGF and a reduction in serum causing cessation of division and the extension of neurites via TrkA, the PI3K/Akt and ras/src pathways leading to changes in cytoskeletal structure and the alteration of neuronal gene expression (Jeon et al., 2010a). These protocols (Section 2.5.4) lead to the formation of neurite extensions and the emergence of transmitter release sites with increased expression and subcellular organisation of some synaptic proteins (Wiatrak et al., 2020). PC12 cells exhibit neuron-like features, including electrical excitability, neurite outgrowth, presynaptic-like ultrastructure, and protein clustering of synaptic markers but do not form fully functional synapses and lack fully formed presynaptic organisation as such whilst endocytosis is observed in neurites, exocytosis is absent (Wiatrak et al., 2020).

To determine when the proteins whose functions are supported by CSPα are expressed, we investigated the expression of key proteins upon neuronal differentiation of PC12 cells. Cells were differentiated for five days, and western blotting was carried out on the proteins extracted each day (Figures 4.2 and 4.3).

All proteins analysed were detectable in the undifferentiated PC12 cells. CSPα showed a trend for an increase in expression over the differentiation period. In contrast, SNAP-25, PSD95, Syntaxin-1 and VAMP-2 showed relatively stable expression across the differentiation time course. For the E3 ligases tested, TRIM9 and FBX07 demonstrated stable expression across the differentiation time course. Whilst Parkin displayed a trend for an increase in expression across differentiation. However, this expression was variable across biological repeats. Actin and Tubulin remained consistent across differentiation within 2-fold changes. As illustrated in the representative blot, Tubulin displays a trend for a reduction in expression across differentiation (Figures 4.2 and 4.3).

In summary, the key synaptic proteins and the E3 ligases to be investigated in this study were detectable in the undifferentiated PC12 cells, and interestingly, CSPα displayed the greatest differential and a clear increase in expression with neuronal-like differentiation.

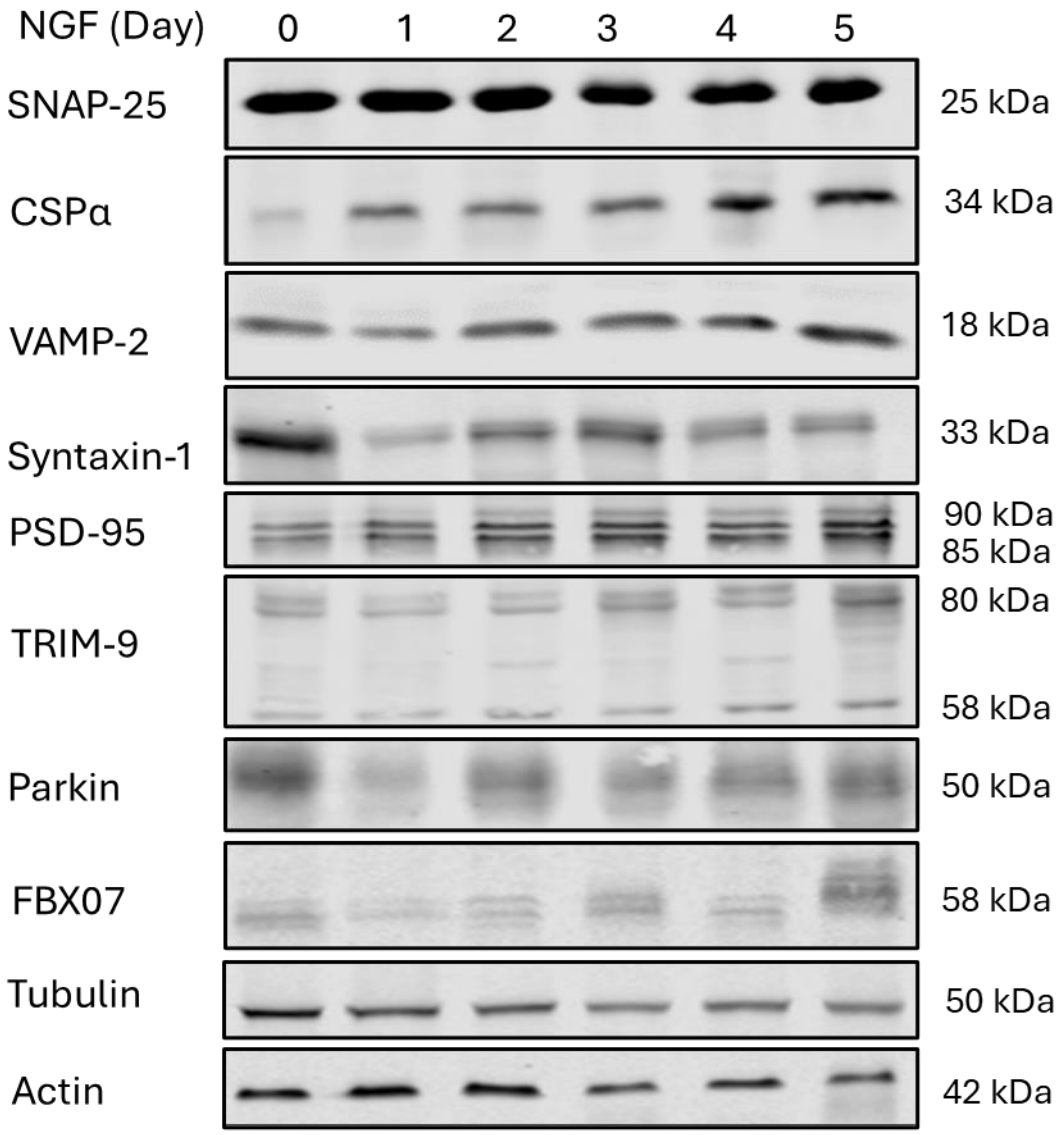

Figure 4.2: Relative Expression of key synaptic proteins and E3 ligases across NGF-induced PC12 differentiation.

PC12 cells were differentiated with NGF (50 ng/ml), and samples were lysed at the indicated time points up to Day 5. 10 µg of lysate protein was resolved by SDS-PAGE and immunoblotting of the indicated proteins was carried out, n = 3 for technical repeats from a clonal line.

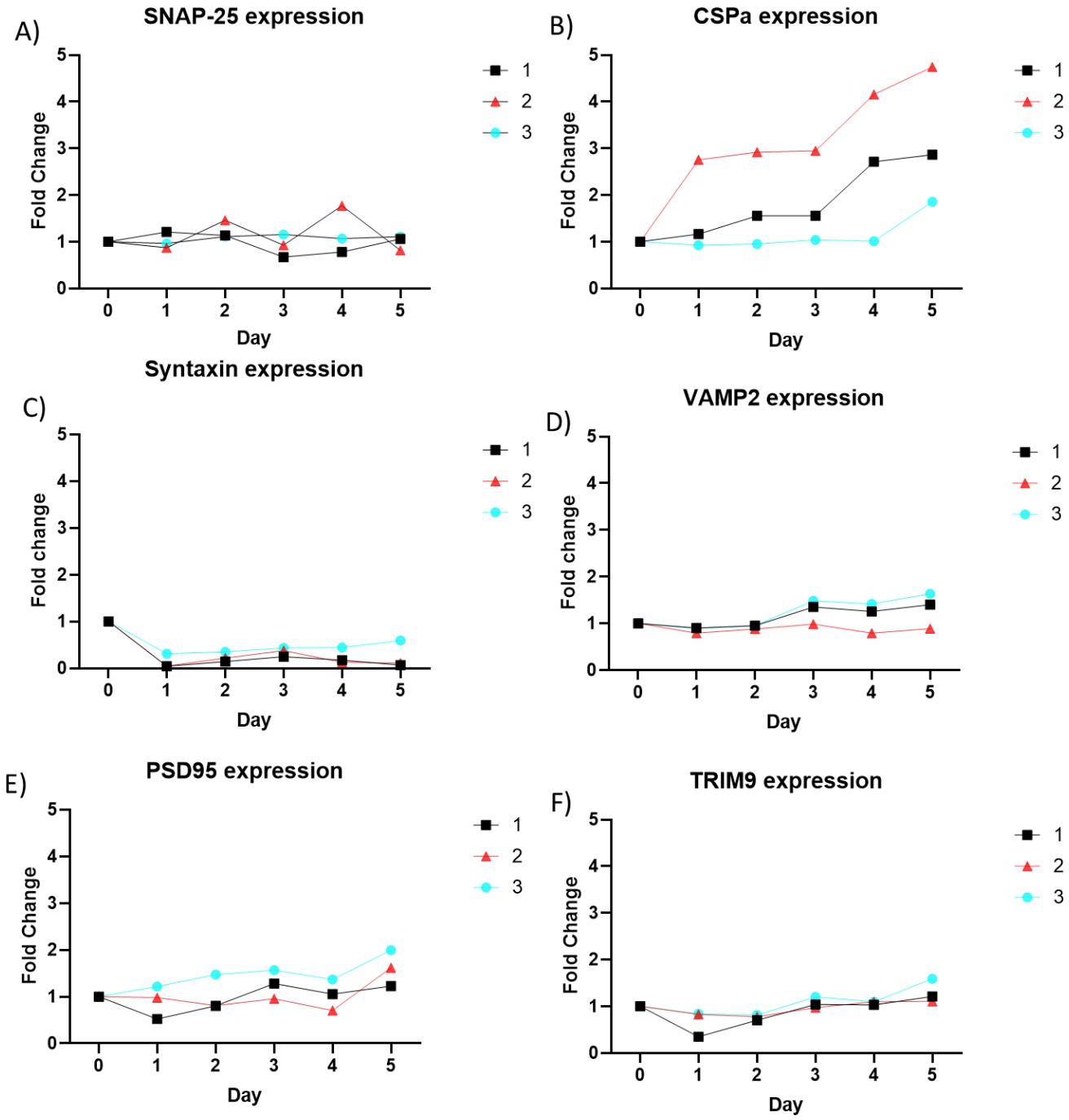
A)
SNAP-25 expression
Fold Change
Day
1
2
3
B)
CSPa expression
Fold Change
Day
1
2
3
C)
Syntaxin expression
Fold change
Day
1
2
3
D)
VAMP2 expression
Fold change
Day
1
2
3
E)
PSD95 expression
Fold Change
Day
1
2
3
F)
TRIM9 expression
Fold Change
Day
1
2
3

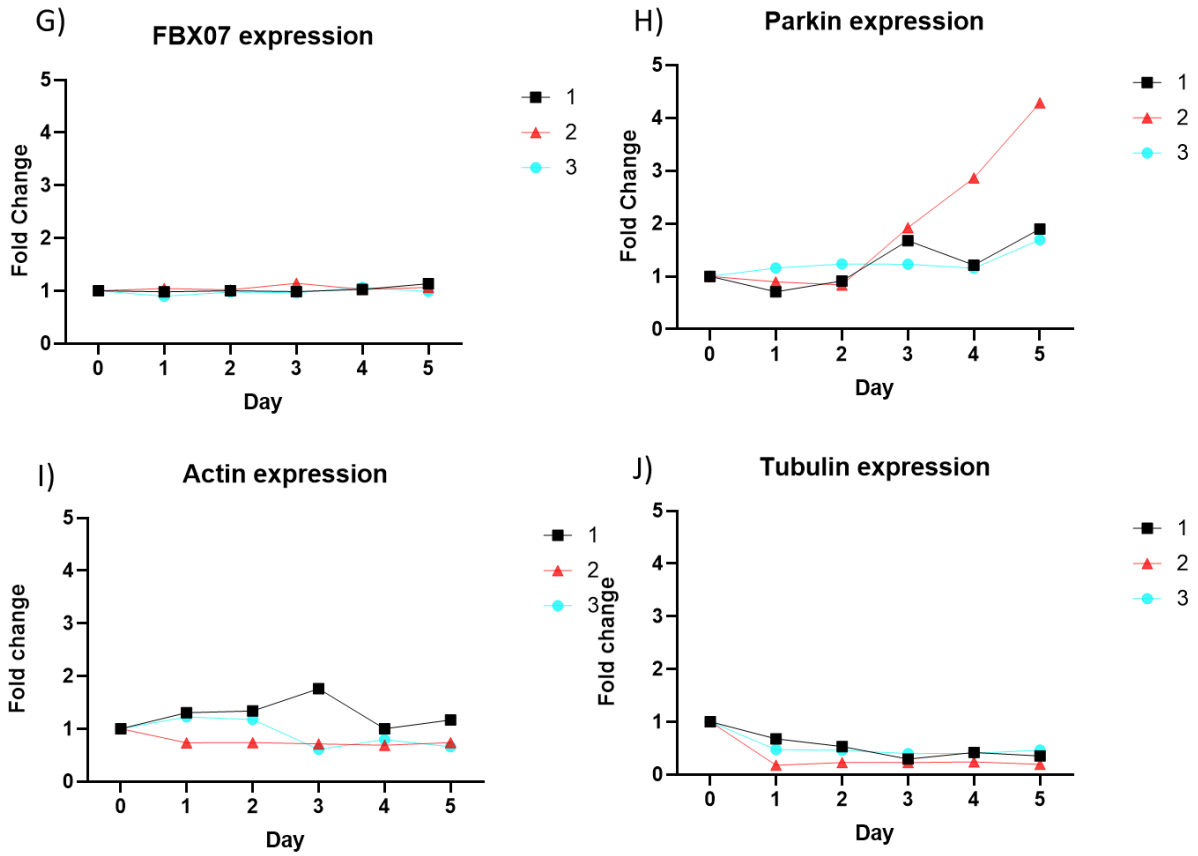

Figure 4.3: Quantification of selected protein expression across NGF-induced differentiation in PC12 cells.

Relative expression of the indicated immunolabelled protein extracted from PC12 cells at the indicated times across NGF differentiation (50 ng/ml). Immunolabeling Intensity for the protein bands were normalised to protein loading controls and plotted as a comparison based on the fold change to Day 0. N=3, where 1-3 corresponds to individual experimental repeats.

4.4.3 Confirmation of expression of BioID Constructs in HEK293FT

The Myc-BioID constructs were transfected into HEK293FT, which were then tested for their relative expression, localisation and associated biotin ligase activity. Initial experiments were carried out in HEK293FT cells due to there reported higher rates of transfection than PC12 cells.

Both transfected and untransfected cells were lysed 24 hours post-transfection. The cell lysates were resolved by SDS-PAGE, then subjected to Western blotting, and immunolabeled with a Myc antibody to detect the expression of the protein encoded by each construct (Figure 4.4). Untransfected lysates were run beside lysates from cells that had been transfected with each of

the constructs; no Myc immunoreactivity was present in the lysates from the untransfected cells.

The expression of Myc-BioID- SNAP-25 was investigated by probing for the immunoreactivity with a SNAP-25 antibody (K. Kim et al., 2021). This showed selective immunoreactivity at 25 kDa in both the untransfected lysate and lysate from cells transfected with Myc-BioID-SNAP-25, with a predicted additional immunoreactivity at 60 kDa. This immunoreactivity is explained by the endogenous SNAP-25 and the transfected Myc-BioID-SNAP-25 construct. This contradicts previous literature that states that SNAP-25 is not detectable by western blot in HEK293 cells (Scott et al., 2003).

In cells transfected with Myc-BioID-SNAP-25, probing for Myc immunoreactivity resolved a single major band at 60 kDa. In the case of Myc-BioID at 32 kDa and Myr-Myc-BioID at 35 kDa (Figure 4.4).

The absence of immunoreactivity of Myc in the untransfected cell lysate and the presence at the correct molecular weight for each construct confirmed the expression of Myc-BioID, MyrMyc-BioID and Myc-BioID-SNAP-25.

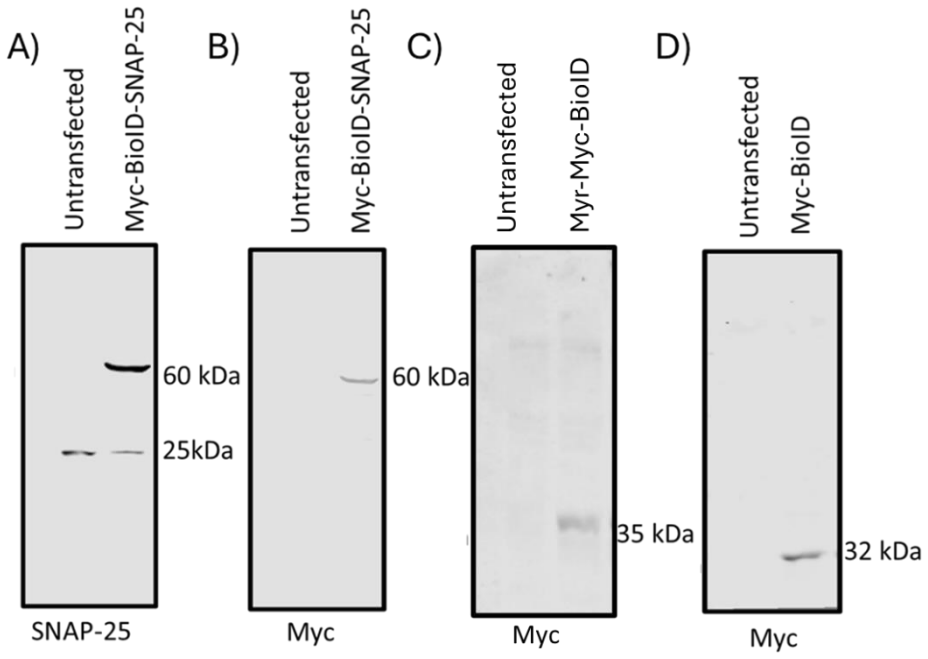

Figure 4.4: **Recombinant expression of the Myc-BioID constructs in HEK293FT cells**. Representative image of 3 independent transfections of HEK293FT cells transfected with MycBioID constructs. 10 µg of each lysate was resolved by SDS-PAGE and immunoblotted for the indicated proteins with Myc or SNAP-25, N=3.

4.4.4 Localisation of recombinantly expressed BioID constructs in HEK293FT cells

Transfection followed by immunofluorescent detection of Myc immunoreactivity staining was used to investigate the subcellular location of Myc-BioID, Myc-BioID-SNAP-25 and Myr-MycBioID proteins expressed in HEK293FT cells. Myc was used to detect the expression of the transfected constructs, Wheat Germ Agglutinin (WGA) was used to stain glycoproteins at the plasma membrane, and Hoechst was used as a nuclear stain (Figure 4.5).

Immunoreactivity of the protein encoded by the Myc-BioID-SNAP-25 construct was selectively found at the plasma membrane in the HEK293FT cells (Figure 4.5). Golgi staining with GM130 was also carried out to determine if there was a pool of the construct detectable in the Golgi, where SNAP-25 is palmitoylated (Greaves et al., 2010). Subsequent confocal microscope analysis did not resolve discernible intracellular co-localisation staining of SNAP-25 and GM130 at the Golgi in the transfected HEK293FT cells (Data not shown). This indicates that at steady state, SNAP-25 is localised at the plasma membrane.

The protein encoded by the Myr-Myc-BioID control localised to the plasma membrane. The immunoreactivity in the HEK293FT cells indicated it was present most intensely across the whole plasma membrane (Figure 4.5). The protein encoded by the Myc-BioID construct displayed immunoreactivity filling the cytoplasm of the cell, consistent with the expression of a soluble cytoplasmic protein (Figure 4.5).

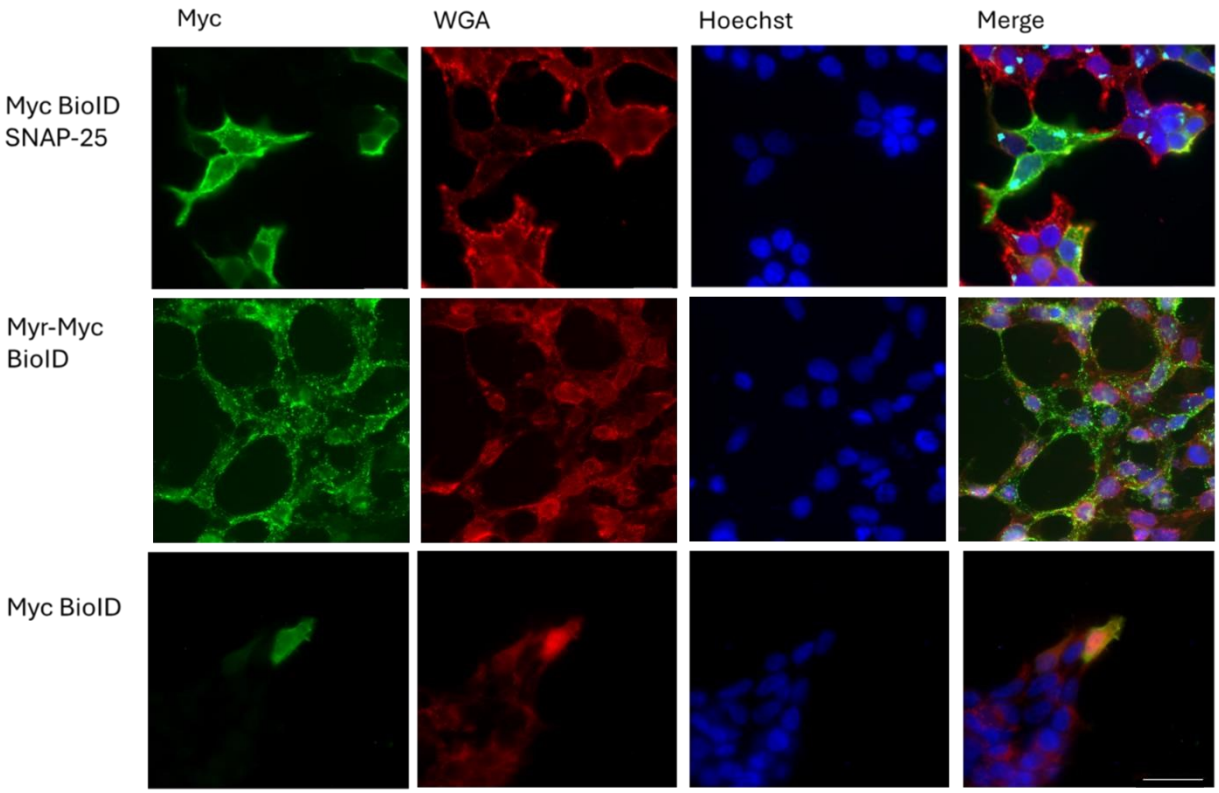

Figure 4.5: Immunofluorescence of HEK293 FT cells transfected with Myc-BioID- SNAP-25 Myc-BioID and Myr-Myc-BioID constructs.

Cells were incubated with Wheat Germ Agglutinin (WGA) (red channel), then fixed, permeabilised and probed for Myc immunoreactivity (green channel) and nuclear staining with Hoechst (blue channel). Scale bar 50 µM.

4.4.5 Localisation of recombinantly expressed Myc-BioID constructs in PC12 cells

Lipofectamine-based transfection of PC12s routinely generates below 20-25% transfection efficiency Figure 4.6, Lee et al., 2008). Myc immunostaining identified both a plasma membrane and potentially a peri-nuclear localisation of proteins encoded by each of the three Myc-BioID constructs. Whilst the Myc construct filled the cell there was localisation for the other two constructs, but this was not as plasma membrane defined as in the HEK293FT cells (Figure 4.5)..

Localisation of the SNAP-25 constructs at the plasma membrane suggests that the fusion of SNAP-25 to BioID does not disrupt the biosynthesis and the targeting of SNAP-25. This implies the expressed construct is palmitoylated, situated at the plasma membrane and correctly localised, leaving it well-placed to probe for endogenous protein-protein interactions. Whilst the peri-nuclear expression could be at the ER or the Golgi, which are sites of SNAP-25 maturation and transport, which could allow for the identification of interactions across SNAP-25's life course.

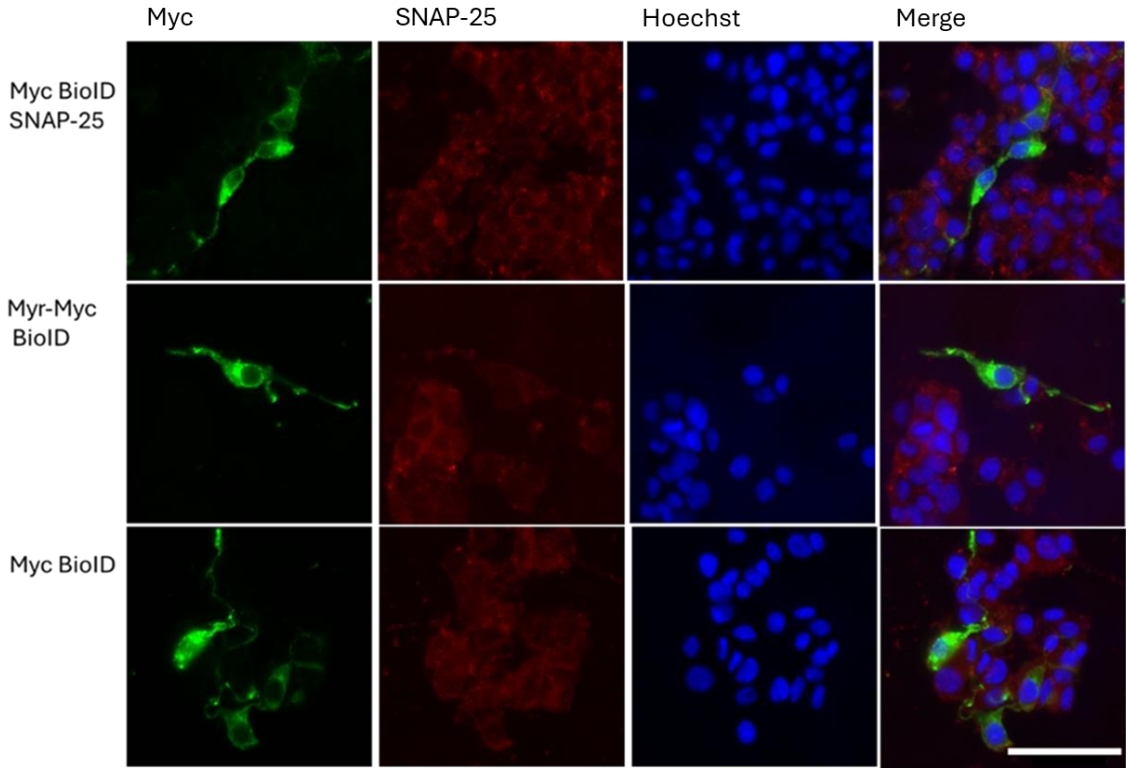

Figure 4.6: Immunolocalisation of Myc-BioID fusion constructs in PC12 cells.

Cells were transfected with Myc-BioID-SNAP, Myr-Myc-BioID and Myc-BioID constructs as indicated. Myc (green channel) SNAP-25 (red channel) immunoreactivity, and Hoechst staining are displayed as indicated in the (blue channel). The overlay in the merge image postprocessing. Scale bar 50 µM.

4.4.6 Biotinylation by Myc-BioID constructs in HEK293FT cells.

HEK293FT cells were transfected with the Myc-BioID-SNAP-25, Myr-Myc-BioID and Myc-BioID constructs and supplemented with Biotin (50 µM). 24 hours post-transfection, the cells were fixed and probed for Myc immunoreactivity, cellular streptavidin was labelled and Hoechst was used to stain nuclei. The expression of the proteins generated by each of the three constructs was identified

by Myc immunoreactivity in the expected locations (green channel, Figure 4.7). Importantly, the cells positive for Myc were also positive for streptavidin (purple channel, Figure 4.7) reactivity. This colocalization of the Myc-tagged biotin ligases and the biotinylated proteins decorated by streptavidin indicates cellular proximity labelling (Figure 4.7).

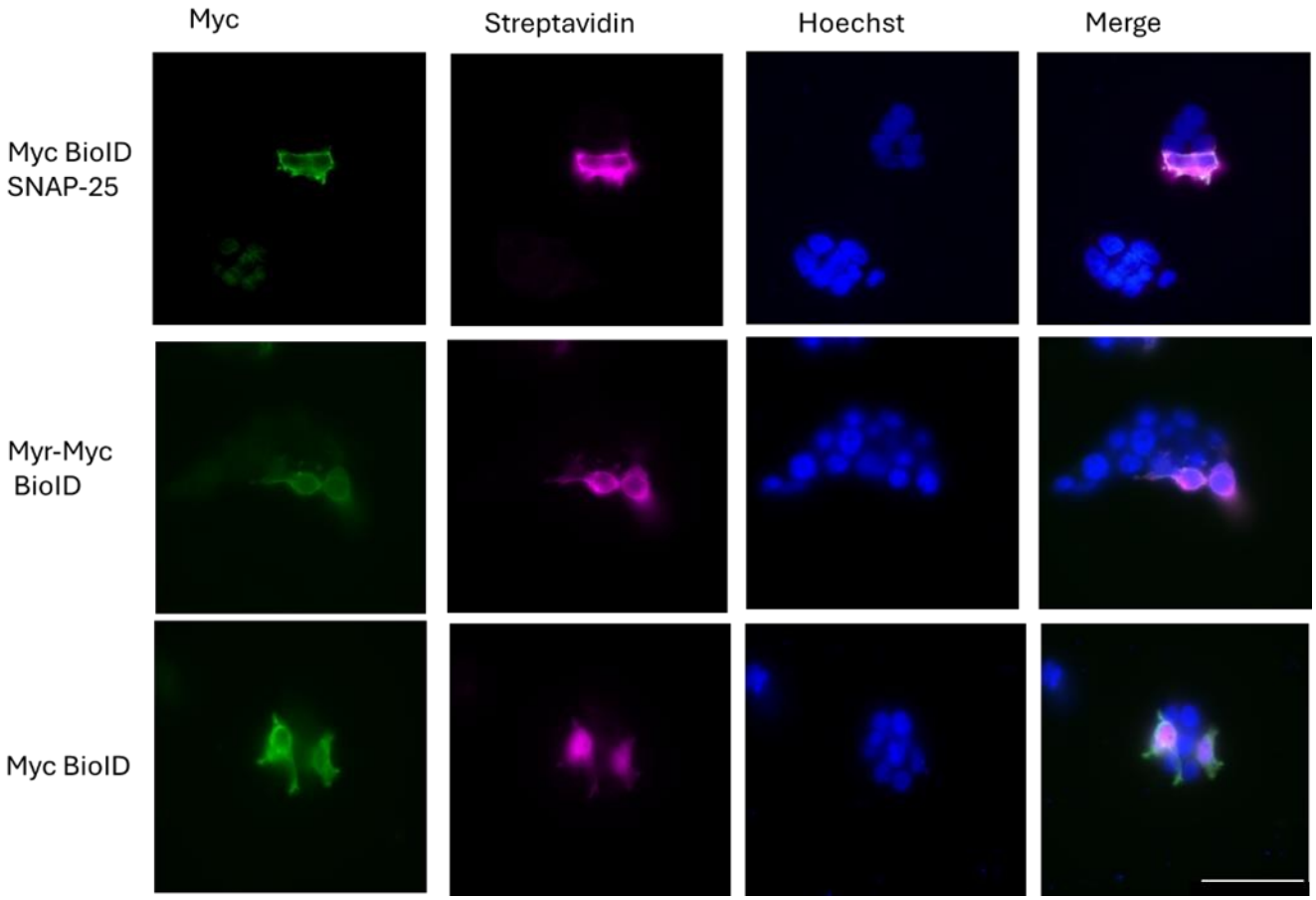

Figure 4.7: Immunocytochemical localisation of BioID-generated biotinylation in cells transfected with Myc-tagged BioID constructs.

Myc-BioID-SNAP-25, Myc-BioID and Myr-Myc-BioID constructs were transfected into HEK293FT cells and supplemented with biotin (50 µm). After 24 hrs, cellular biotinylation was detected by secondary incubation with fluorescent streptavidin Alexa 555 (purple channel). Cells were probed for Myc immunoreactivity (green channel), and Hoechst (blue channel). Scale bar 50 µM, N =3.

In addition, to immunofluorescent staining, an untransfected culture and cultures transfected with the Myc-BioID constructs incubated with or without biotin were lysed and resolved by

SDSPAGE. These resolved samples were Coomassie-stained to reveal the total protein extracted from each well was indistinguishable (Appendix Figure B.4).

Western blotting of the same lysates, followed by incubation with HRP-coupled streptavidin was used in parallel to investigate the cellular biotinylation in the absence and presence of exogenous biotin in cells expressing the distinct constructs. Streptavidin-labelled biotin revealed that in the untransfected cells, there was biotinylation of four major proteins at 220 kDa, 130 kDa, and two in the region of 70 kDa. With each of the constructs, transfected cells exhibited additional discrete biotin reactivity at the molecular weight corresponding to the migration of the corresponding recombinant construct. Lastly, within construct-transfected cultures, additional biotinylation was evident in the biotin-fed cultures in comparison to the cultures which just had the biotin available in the media (See Appendix B.4)

4.4.7 Optimisation of biotinylation timings

Before conducting biochemical investigation with the Myc-BioID constructs, I investigated optimised experimental conditions by varying the biotin incubation times after the Myc-BioID constructs were transfected into HEK239FT cells. The cells were transfected with each of the constructs and after 24 hours, the cultures were incubated with biotin (50 µM) and lysed 16, 18 or 24 hours later (Roux et al.,2012). There was no clear difference in the levels of cellular biotinylation or the emergence of additional immunoreactivity between 16, 18 and 24 hours. As such, cells were subsequently incubated with biotin for 16 hours (Appendix B.3).

4.4.8 Pull down in HEK293FT cells as a proof of concept.

A streptavidin pull-down from lysates generated from HEK293FT cells, as described above, was carried out. This was done to determine if biotinylated proteins could be isolated using the protocol outlined in Section 2.10.

HEK293FT cells transfected with the Myc-BioID constructs and an untransfected control were incubated with Biotin (50 µM), 16 hrs later, these cultures were lysed. After lysis, the samples were centrifuged. The detergent-solubilised cleared lysates were incubated with streptavidin beads, washed and eluted. The eluted proteins were resolved by SDS-PAGE and probed with HRP-coupled streptavidin (Figure 4.8).

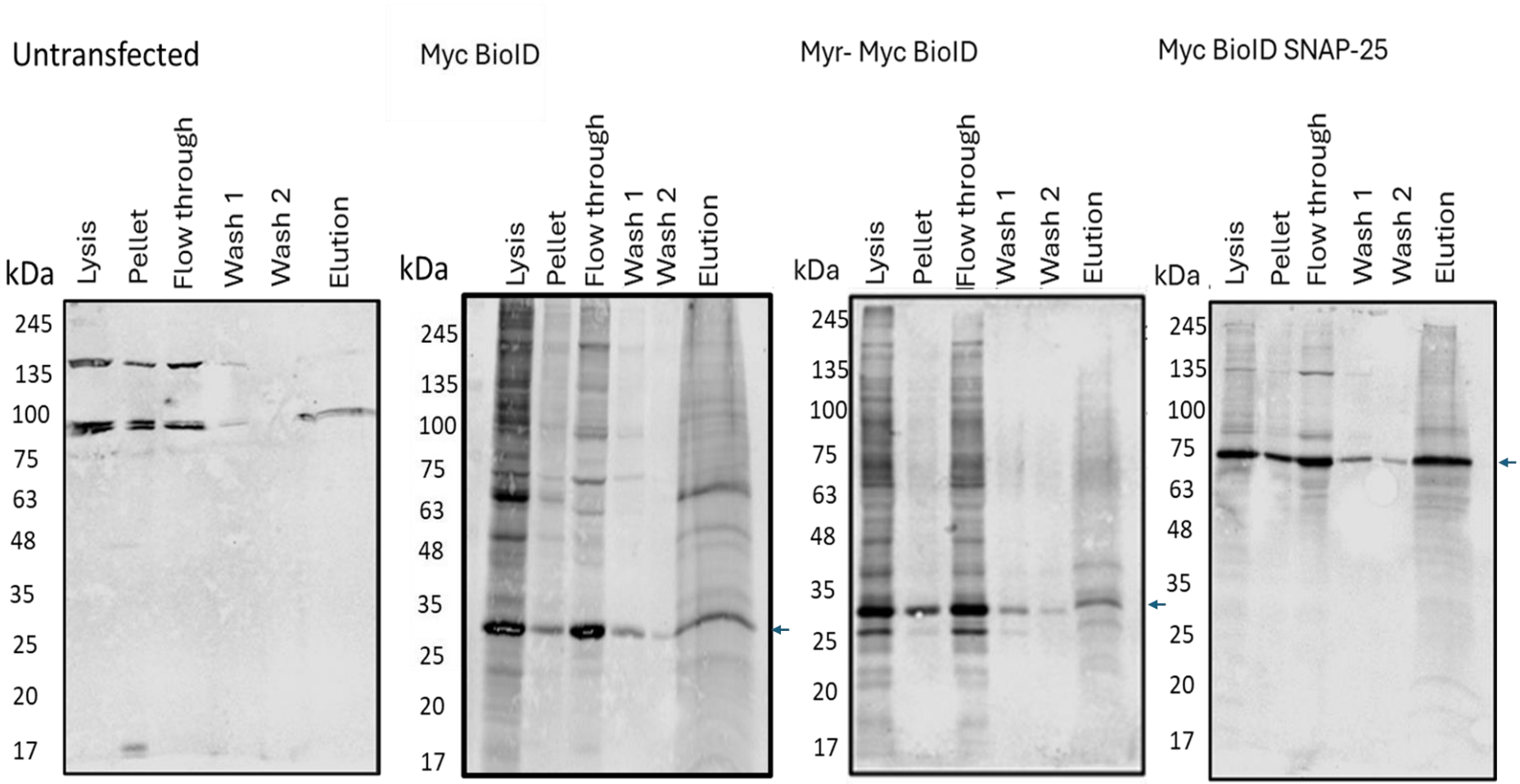

Figure 4.8: Streptavidin pull-down of Myc BioID constructs and biotinylated proteins in HEK293FT cells, Streptavidin pull-down in HEK293FT cells, lysates from untransfected cells, and cells transfected with Myc-BioID, Myr-Myc-BioID or Myc-BioID-SNAP-25 were resolved on SDS-PAGE gels and labelled with HRP-coupled streptavidin, with the expected molecular weight of each construct highlighted with a blue arrow N=1.

The pellet fraction clearly shows that the biotinylated proteins are largely soluble and thus available to be loaded onto the streptavidin beads (see Figure 4.8 Lysis and pellet for each).

In the untransfected cells, there was biotinylation of 4 major proteins at 220 kDa, 130 kDa and two bands in the region of 70 kDa, in the lysis, pellet, flowthrough, wash 1 and the elution. This reflects biotin's appearance within abundant mammalian carboxylases: CoA carboxylase (220 kDa), Pyruvate carboxylase (130 kDa), 3-methylcarotonyl CoA Carboxylase (75 kDa) and Propynyl CoA Carboxylase (72 kDa) (Figure 4.8, Untransfected). Accordingly, the four mammalian carboxylases are present in all the Myc-BioID-transfected cultures (Figure 4.8).

In comparison to the untransfected sample, each of the constructs generates an additional discrete major biotin-dependent reactivity across the sample fractions. The size of which corresponded to the molecular weight of each of the constructs: Myc-BioID (30 kDa), Myr-MycBioID (32 kDa) and Myc-BioID-SNAP-25 (60 kDa).

A comparison of the reactivity associated with the lysis and flow-through fraction for each of the transfections shows that none of the potential biotin-reacted proteins are quantitatively removed. The amount of protein loaded onto the beads (approx. 100-600 µg total with likely a low percentage of total protein being proximal to the biotin ligases) is within the beads' capacity of ~55µg biotinylated rabbit IgG/mg of beads.

Finally, the eluted fraction that follows two washes of the beads shows a specific association of a range of biotinylated proteins for each of the Myc-BioID constructs. The Intensity indicates that the Myc-BioID construct has the largest associated repertoire of protein interactions. Whilst there is a distinct labelling and pull-down for Myr-Myc-BioID and Myc-BioID-SNAP-25, suggesting that the distinct constructs have selective reactivity and show distinct patterns of proximity labelling (Figure 4.8).

Upon confirming that the streptavidin pull-down methodology was sufficient in extracting biotinylated proteins, the samples were probed for TRIM9 by tracking its immunoreactivity through the experimental extracts described above. The Lysate and elution fractions from untransfected cells, and cells transfected with Myc-BioID, Myr-Myc-BioID and Myc-BioIDSNAP-25 were resolved by SDS-PAGE and probed with a TRIM9 antibody. This analysis identified TRIM-9 immunoreactivity in the cell lysate fraction for each transfection, but there was no retention and/or elution in any of the conditions (Appendix B.5). This indicates that the recombinantly expressed SNAP-25 does not

support a protein interaction detected by proximity labelling with the TRIM-9 endogenously expressed HEK293FT cells.

4.4.9 BioID pull-downs in PC12 cells using Myc-BioID-SNAP-25 as bait

Setting up and carrying out the streptavidin pull-down in HEK293FT cells allowed for proof of concept that the biotinylation method carried out here allowed for specific labelling and extraction of biotinylated protein. Before the protocol was adapted for use in the PC12 cells, which contain more of the protein machinery which is likely to interact with SNAP-25.

PC12 cells were plated in 10 cm dishes, untransfected or populations transfected with Myc-BioID-SNAP-25, Myr-Myc-BioID or Myc-BioID, were compared after incubation with biotin (Section 2.7.11). The cell lysates were homogenised, and the soluble supernatants were loaded onto the streptavidin beads (Section 2.7.11).

After incubation with the streptavidin beads, the flow-through was removed, and the beads were washed. Samples were eluted by boiling in SDS-PAGE sample loading buffer (Method section 2.7.5).

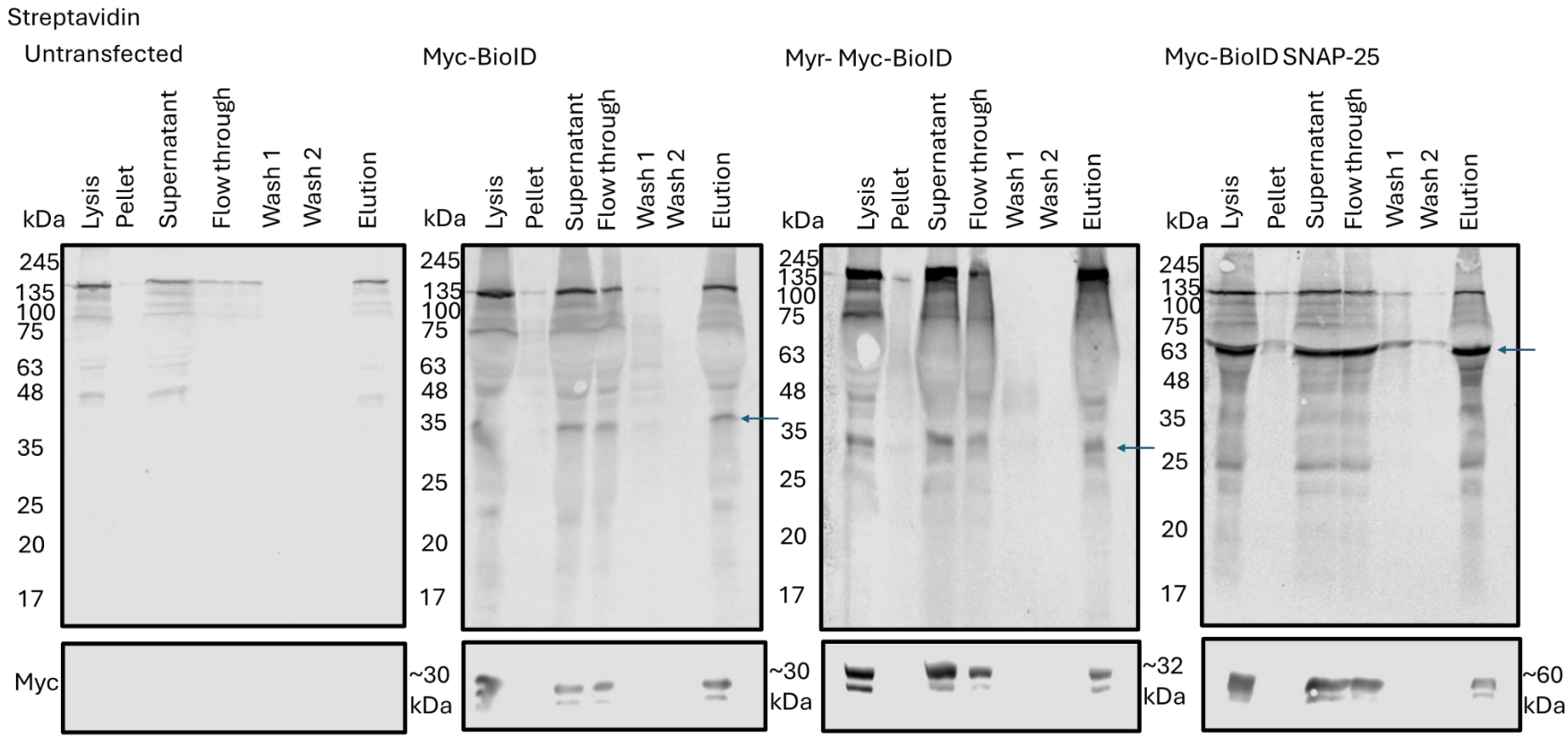

Figure 4.9: **Streptavidin pull-down of Myc BioID constructs and biotinylated proteins in PC12 cells**

Streptavidin pull-down in PC12 cells: Untransfected cells, cells transfected with Myc-BioID, Myr-Myc-BioID or Myc-BioID-SNAP-25, were incubated with biotin and lysed 16 hours later. Samples were resolved by SDS-PAGE and labelled with HRP-coupled streptavidin and Myc. N=1.

Probing for streptavidin reactivity identified biotinylated proteins present in the lysate, supernatant, flow-through and eluate of each condition, with some present in the washes of some of the conditions (Figure 4.10).

The presence of four bands were observed in the untransfected and Myc-BioID constructtransfected samples corresponding to known mammalian biotinylated proteins (As described in section 4.4.8). In addition, there was a large smear in the elution with an additional differential pattern in reactive proteins identified and purified from the distinct transfected cells.

Immunoreactivity for Myc was investigated and it showed that the constructs themselves were biotinylated and pulled down. This was shown by the presence of immunoreactivity at ~30 kDa for Myc-BioID, 32 kDa for Myr-Myc-BioID and at ~60 kDa for Myc-BioID-SNAP-25. (Figure 4.10).

4.4.10 Identification of proximity between SNAP-25 and established binding partners

The PC12 cells were transfected with Myc-BioID-SNAP-25 and the BioID pull-down protocol was carried out. The samples were resolved on SDS-PAGE gels and then immunolabeled with SNAP-25, Myc, VAMP-2 and Syntaxin. Immunoreactivity for all four proteins was detected in the cell lysis, supernatant, flow-through and the elute (Figure 4.10).

The presence of immunoreactivity in the lysate confirmed the expression of each protein, and the Myc ~60 kDa immunoreactivity confirmed that the cells were transfected. In the case of Syntaxin, VAMP-2 and Myc, the appearance of some immunoreactivity in the pellet was surprising and suggested incomplete solubilization of these samples. However, the majority of the immunoreactivity was in the supernatant, allowing purification of these proximity labelled proteins. In all cases, there was immunoreactivity in the elution fraction for all proteins investigated. This suggests proximity between the Myc-BioID-SNAP-25 construct and endogenous SNAP-25, VAMP-2 and Syntaxin (Figure 4.10). The proximity between the Myc-BioID-SNAP-25 construct and endogenous SNAP-25 is suggestive of the formation of SNAP-25 homodimers of which there is not previous literature evidence of. However, if SNAP-25 does form homodimers this may lead to competition between this formation and the formation of the SNAP-25-Syntaxin-1 dimer which is a critical step in the assembly of SNARE complex formation.

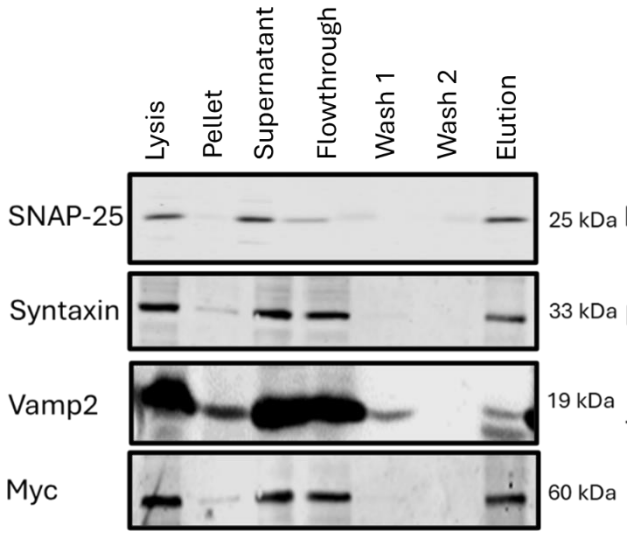

Figure 4.10: **Known SNAP-25 interacting proteins are BioID proximity-labelled in PC12 cells using Myc-BioID-SNAP-25 as bait.**

Lysates from PC12 cells transfected with Myc-BioID-SNAP-25 and pulled down with streptavidin beads and resolved by SDS-PAGE before being labelled with antibodies for SNAP25, Syntaxin, Vamp-2, and Myc, N=1.

4.4.11 Investigation candidate E3 ligases interaction with SNAP-25 by proximity labelling.

After known SNAP-25 binding partners were detected using BioID labelling with the Myc-BioIDSNAP-25 construct in the PC12 cells. This work was extended by investigating the three candidate E3 ligases, FBXO7, Trim9 and Parkin (Identified in Chapter 3).

FBXO7, Parkin and TRIM9 were extracted from PC12 cells transfected with Myc-BioID-SNAP-25, and immunoreactivity revealed they were all largely soluble (indicated by the expression in the lysis fractions, Figure 4.11). All were also present in the supernatant and the flow-through. TRIM9 and FBXO7 were not present in the elution, indicating no evidence for successful biotin proximity labelling. In contrast, tracking Parkin immunoreactivity identified that it is clearly found in the elution fraction. Thus, this suggests that Parkin can be proximity labelled by the Myc-BioID-SNAP-25 (Figure 4.11).

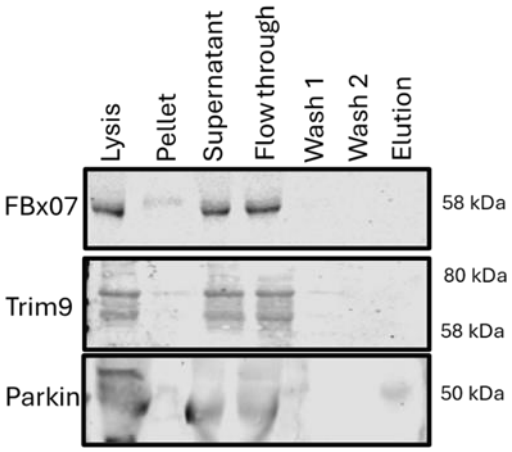

Figure 4.11: The E3 ligase Parkin shows BioID proximity-dependent labelling in PC12 cells transfected with Myc-BioID-SNAP-25 as bait.

Lysates from PC12 cells transfected with Myc-BioID-SNAP-25 and incubated with biotin were lysed and incubated with streptavidin beads. Affinity-purified peptides were resolved by SDSPAGE before being labelled with fluorophore-conjugated antibodies to label FBXO7, Trim9 and Parkin, N=3.

4.4.12 Investigation into the specificity of Myc-BioID-SNAP-25 proximity labelling of Parkin

To ensure that the immunoreactivity of Parkin (and known SNAP-25 interactor, Syntaxin) in the elute for the Myc-BioID-SNAP-25 transfected PC12 cells was selective, the BioID pull-down protocol was carried out on lysates from untransfected cells and cells transfected with MycBioID and Myr-Myc-BioID constructs.

Syntaxin and Parkin are present in the lysate of each of the samples described above but are only present in the elution of the Myc-BioID-SNAP-25 cells. This supports the selectivity of interaction of SNAP-25 with Parkin (Figure 4.12, A).

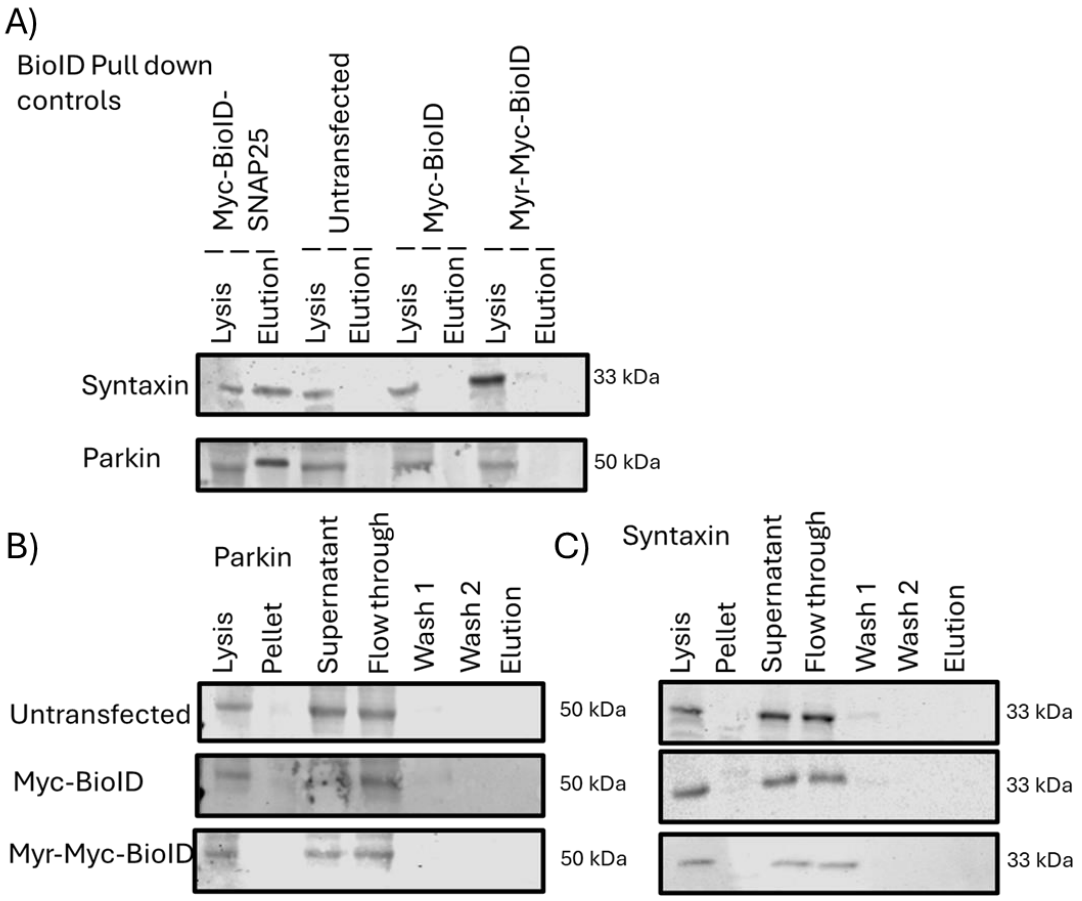

Figure 4.12: Syntaxin and Parkin are selectively Biotinylated by Myc BioID-SNAP-25

Lysates taken from either untransfected PC12 or cells transfected with Myc-BioID or Myr-MycBioID were incubated with streptavidin beads, then resolved by SDS-PAGE and labelled with antibodies for Syntaxin and Parkin, to identify if there was non-specific proximity labelling with the control Myc-BioID constructs, N=2.

4.4.13 BioID proximity labelling of HA Wildtype and mutant C431S Parkin

Having identified proximity labelling between endogenous Parkin and Myc-BioID-SNAP-25, I investigated whether Myc-BioID-SNAP-25 would biotinylate a transfected HA-Parkin construct. In addition, I compared this with a HA-Parkin C413S E3 ligase-deficient construct, which has been classified as an E3 ligase dead mutant due to the lack of ability to be recruited to the mitochondria and ubiquitinate substrates (Lazarou *et al.*, 2013a, Iguchi *et al.*, 2013).

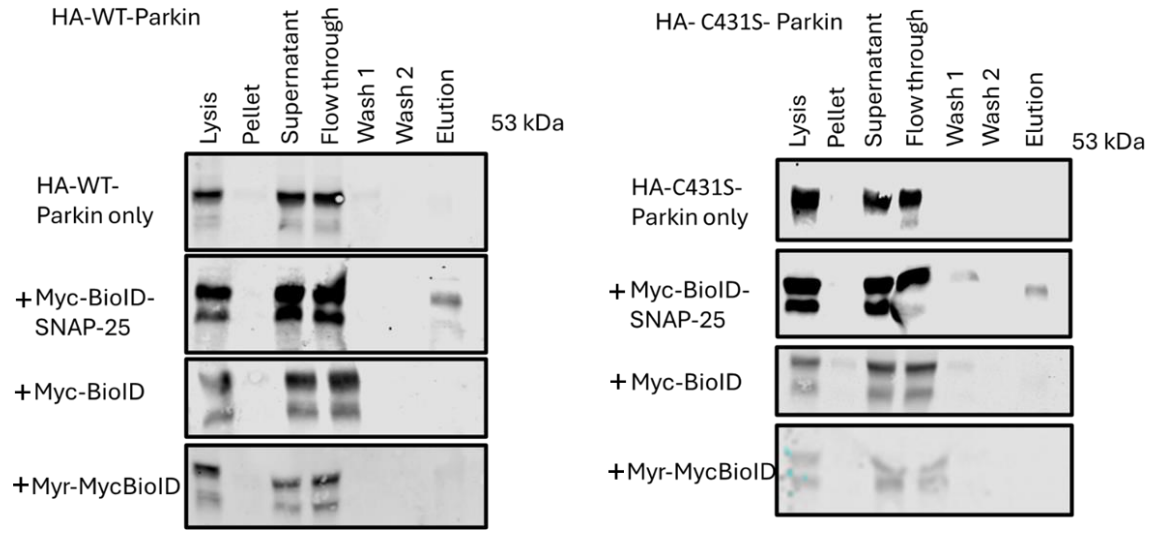

Figure 4.13: Parkin is selectively pulled down by Myc-BioID-SNAP-25 in an E3 ligase independent manner. Wild-type and E3 ligase-deficient Parkin are biotinylated and pulled down by Myc-BioID-SNAP-25. HA-wildtype and HA-C431S Parkin constructs were transfected into HEK293 FT cells either individually or in combination with Myc-BioID-SNAP-25, Myc-BioID or Myr-Myc-BioID in the presence of biotin, before being lysed and incubated with streptavidin beads. The proteins eluted from the beads were resolved by SDS-PAGE and labelled with a Parkin antibody, N=2.

Both the HA-WT Parkin and the HA-C431S Parkin were proximity biotinylated by the Myc-BioIDSNAP-25 construct. This is shown by the presence of Parkin (Figure 4.13) and HA-tagged (Data not shown) immunoreactivity in the elution fractions. No immunoreactivity was present in the elution fractions in the untransfected, Myc-BioID or Myr-Myc-BioID control conditions (Figure 4.13). This is suggestive of selective SNAP-25 proximity and the potential of an interaction between Parkin and SNAP-25, which is independent of Parkin's E3 ligase activity.

4.4.14 **Myc Pulldowns to identify direct interaction of Myc BioID SNAP-25**

Alongside the BioID pulldowns, I investigated the candidate SNAP-25-E3 ligase interactions using the encoded Myc-tag on the Myc-BioID constructs. Anti-c-Myc Magnetic Beads were used to immunoprecipitate the Myc-tagged proteins that can be identified in the Myc-BioID transfections. This provided an opportunity to investigate whether this distinct mode of protein interaction assay could evidence the interaction of SNAP-25 to probe the E3 ligases tested for proximity to SNAP-25

Initially, immunoprecipitation lysates from cells transfected with the Myc-BioID-SNAP-25 construct were resolved by SDS-PAGE and immunolabeled with Myc (Figure 4.14). Myc immunoreactivity was

present in the cell lysis, supernatant flow-through and elution fractions. This showed that the Myc-BioID-SNAP-25 construct was expressed and bound to the Myc beads.

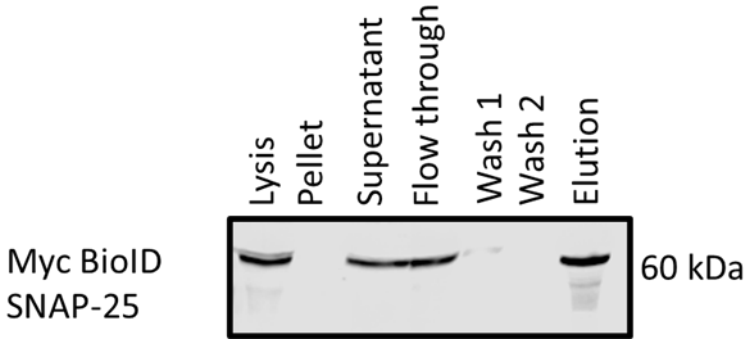

Figure 4.14: Immunoprecipitation of the Myc-BioID-SNAP-25 construct in PC12 cells

Myc pull-down in PC12 cells transfected with Myc-BioID-SNAP-25 and subjected to the Myc immunoprecipitation before samples were resolved by SDS-PAGE and labelled with a Myc antibody by Western blotting, N=1.

Following this, I investigated whether established interacting partners of SNAP-25 could be identified via this method. SNAP-25, VAMP-2 and Syntaxin immunoreactivity were investigated. Each of the proteins were identified in the lysate and elution fractions, indicating their association with Myc-BioID-SNAP-25 (Figure 4.15).

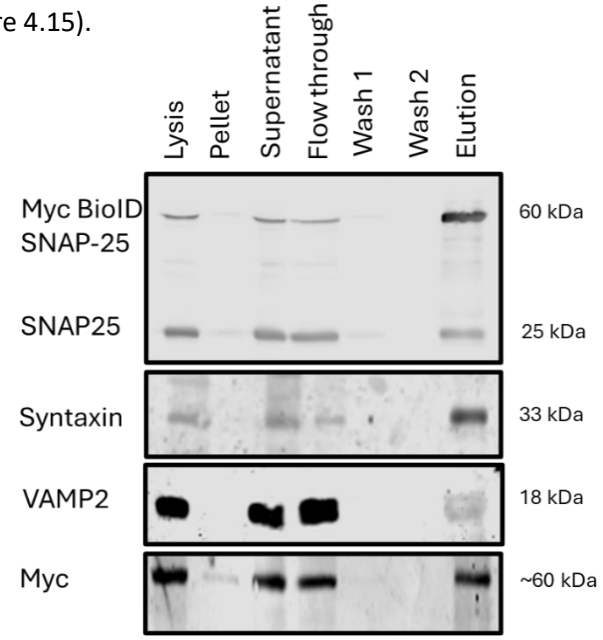

Figure 4.15: Investigating established SNAP-25 interacting partners via immunoprecipitation of Myc BioID-SNAP-25 from PC12 cell lysates. Samples of lysates from PC12 cells transfected with Myc-BioID- SNAP-25 were immunoprecipitated using Myc beads and eluted. The proteins were resolved by SDS-PAGE and labelled with antibodies for SNAP-25, Syntaxin, Vamp-2, Myc (control), N=3.

4.4.15 Investigation into if candidate E3 ligases immunoprecipitated with SNAP-25

Having established the credibility of Myc-directed immunoprecipitation to identify SNAP-25 binding partners, I investigated whether this approach could be used to investigate the predicted interaction between SNAP-25 and the E3 ligases FBXO7, TRIM9 or Parkin.

PC12 cells were transfected with the Myc-BioID-SNAP-25 construct, and the lysates were subjected to Myc-immunoprecipitation. The samples were resolved by SDS-PAGE and immunolabeled with TRIM9, FBXO7 and Parkin. Both TRIM9 and FBXO7 had immunoreactivity in the lysate, supernatant and flowthrough, but not in the elution fractions. This suggests there isn't a detectable direct interaction between Myc-BioID-SNAP-25 and either FBX07 or TRIM9 (Figure 4.16). Supporting my conclusion from BioID proximity-dependent experiments (Section 4.4.11).

Whilst blotting for established SNAP-25 interacting partners, it was noted that when mouse secondary antibodies were used, non-specific immunoreactivity was detected in the eluted fraction. This smeared immunoreactivity at 25 kDa and 50 kDa made a more specific resolution in this range challenging. Optimisation of the immunoprecipitation elution was attempted to reduce this by changing the elution buffer and protocol as described in (Appendix B.7). Whilst this reduced the non-specific immunoreactivity, it did not eliminate this confound if the resolved samples were probed for 2nd antibody only immunoreactivity. As such, identification of Parkin as a 50 kDa protein in the elution of Myc-pull downs was affected due to this nonspecific immunoreactivity.

When I investigated Parkin's interaction with Myc-BioID-SNAP-25 via Myc-immunoprecipitation, I identified immunoreactivity in the lysate, supernatant and flow-through and in the elution, where the immunoreactivity was present above the background to support the potential of a direct interaction between SNAP-25 and Parkin (Figure 4.16).

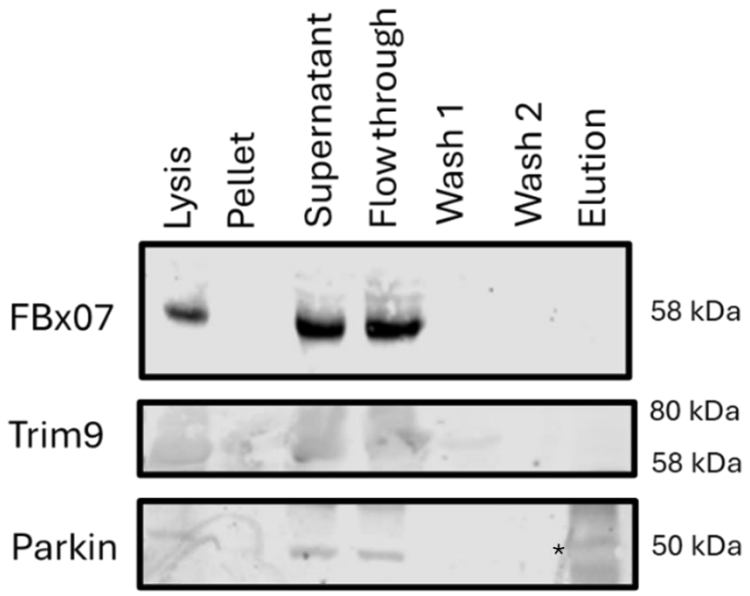

Figure 4.16: Investigating candidate SNAP-25 interacting partners in PC12 cells via immunoprecipitation of Myc BioID SNAP-25.

Lysates from PC12 cells transfected with Myc-BioID-SNAP-25 were subjected to Myc pull-down assays before samples were resolved by SDS-PAGE and labelled by Western blotting for FBXO7, Trim9 and Parkin (where an asterisk indicates where there may be immunoreactive specificity in the elution fraction), N=3.

Lastly, immunoprecipitations were carried out on un-transfected samples and samples transfected with Myc-BioID and Myr-Myc-BioID; these samples were then run as lysates and eluates side by side and probed for Syntaxin and Parkin immunoreactivity. Syntaxin was present in the lysate of each of the samples but was only present in the elute of the Myc-BioID-SNAP25-transfected samples, confirming the immunoprecipitation was specific for the Myc-BioIDSNAP-25 construct. For Parkin, immunoreactivity was present in the lysates of each sample, and there was immunoreactivity in the elution of the Myc-BioID-SNAP-25 transfected sample but not in the other conditions. This provides further support in addition to the evidence provided by BioID, indicating a specific interaction between SNAP-25 and Parkin (Figure 4.17).

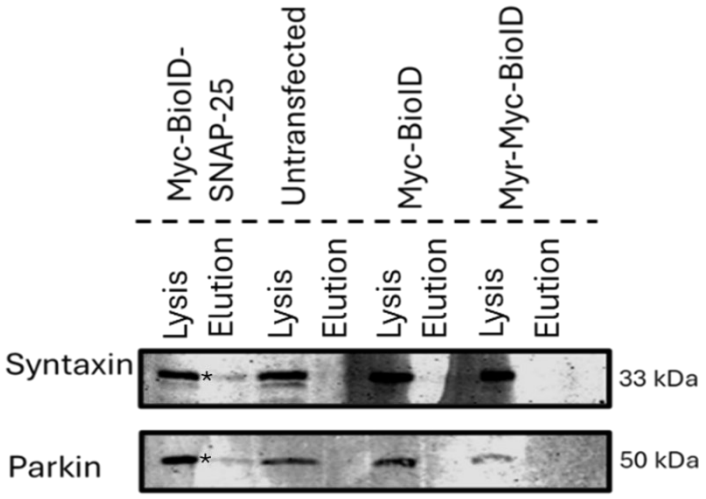

Figure 4.17: Comparison of Syntaxin and Parkin association with Myc-BioID-SNAP-25 in PC12 cells

Lysates taken from either untransfected PC12 or cells transfected with Myc-BioID-SNAP25, Myc-BioID or Myr-Myc-BioID of Syntaxin and Parkin were resolved by SDS-PAGE and labelled with antibodies by western blot to identify any non-specific immunoprecipitation of Syntaxin and Parkin. With specific immunoreactivity of Syntaxin and Parkin highlighted with an asterisk in elution of the Myc-BioID-SNAP-25 transfected samples (N=2).

4.5 Discussion

SNAP-25 is a presynaptic SNARE protein which is ubiquitinated and degraded as part of its normal life cycle and is increasingly degraded in the absence of its chaperone CSPα (Sharma et al., 2012a). There is a current lack of understanding of the proteins that are responsible for the ubiquitination and subsequent degradation of SNAP-25. Presynaptic ubiquitination is a key event in the in proteostasis (Tseng *et al.*, 2023, Sugiyama and Nishitoh, 2024). Therefore, I have developed approaches that focus on E3 ligases that might ubiquitinate SNAP-25 to further our understanding of proteostasis at the presynapse.

4.5.1 E3 ligases identified by bioinformatic approaches tested for interaction with SNAP-25

In the previous chapter, I used bioinformatics to predict potential E3 ligases that might have a role in the ubiquitination of SNAP-25. Here, I tested the three E3 ligases ranked as most likely to interact with SNAP-25 based on the findings of Chapter 3.

4.5.2 Myc-BioID constructs were generated and expressed in HEK293FT and PC12 cells

Within this chapter, I outlined the generation and validation of Myc-BioID constructs: MycBioID-SNAP-25, Myc-BioID and Myr-Myc-BioID, which have been used for proximity-dependent experiments in HEK293FT (Section 4.4.8) and PC12 cells (Section 4.4.11). The constructs were found to localise to expected domains and displayed distinct biotinylation activity consistent with differing localisation (Section 4.4.4-4.4.5). Plasma membrane localisation and confirmed proximity and interaction with established interacting partners suggest that the addition of the Myc-BioID cassette doesn't affect targeting or protein interaction of SNAP-25.

4.5.3 Myc-BioID-SNAP-25 bound to known interactors but not TRIM9 and FBXO7

BioID provided evidence for proximity between SNAP-25 established interactors (Figure 4.11) (Sutton et al., 1998) but there was no evidence of proximity via BioID pull-down for either TRIM9 or FBXO7 (Figure 4.12). Similarly, SNAP-25 and its established binding partners were shown to interact via an immunoprecipitation approach, but there was no evidence of an association between SNAP-25 and Trim9 or FBXO7.

In the case of TRIM9, this implies that these approaches have been unable to recapitulate previous findings, which provide evidence of a direct interaction with SNAP-25 in brain tissue and neuronal culture. Initially, a yeast two-hybrid screen identified an interaction between TRIM9 and SNAP-25 in rat brain. This was then followed up with affinity-capture and coimmunoprecipitation experiments in neurons, confirming a physical association between Trim9 and SNAP-25 (Yankun Li et al., 2001).

The TRIM family proteins have a broad range of biological functions. TRIM9 has E3 ubiquitin ligase activity and can self-ubiquitinate in the presence of the E2 ligase UbcH5b (Tanji et al., 2010). It also ubiquitinates VASP, but hasn't been shown to ubiquitinate SNAP-25 (Menon et al., 2015). The TRIM9 E3 ligase catalytic domain is not required for interaction with SNAP-25, suggesting that SNAP-25 and TRIM9 may interact in an E3 ligase-independent fashion (Y. Li *et al.*, 2001, Winkle *et al.*, 2014). TRIM9-SNAP-25 binding leads to SNAP-25 being sequestered and inhibited, regulating SNARE complex formation and exocytosis (Y. Li et al., 2001).

Not identifying any evidence of proximity between SNAP-25 and TRIM9 in either the HEK293FT or PC12 cells may suggest that the cellular system, environmental conditions or the presence of other proteins is required for the binary interaction between SNAP-25 and TRIM9. The expression levels of both proteins, the predominantly plasma membrane expression of the Myc-BioID-SNAP-25 or the

tagging of SNAP-25, may also contribute to an interaction not being identified. However, the N-terminal tagging of SNAP-25 does not disrupt its interaction with Syntaxin (Section 4.4.11).

Not identifying evidence for proximity between SNAP-25 and FBXO7 is less surprising. FBXO7 is an E3 ligase that was followed up here, as SNAP-25 was identified in a high-throughput screen as one of 338 potential ubiquitinated substrates of SCFFbxo7 in an *in vitro* ubiquitination assay, but the interaction has yet to be validated (Teixeira et al., 2016a). One suggestion is that SNAP25 is not a substrate of FBXO7, but alternative explanations could be that whilst FBXO7 has the potential to ubiquitinate SNAP-25, they may not interact in the PC12 cellular context or may require the presence of other proteins or stressors to drive the activated response.

4.5.4 BioID used to identify proximity between Myc BioID SNAP-25 and E3 ligase Parkin

The major finding of this work was evidence that SNAP-25 and Parkin interact in an E3 ligase independent fashion. The work evidenced that both endogenous (Section 4.4.11 and 4.4.13), HA-WT type and HA-C431S Parkin are found proximal to SNAP-25 and have the capacity to interact (Section 4.4.14).

4.5.5 Bioinformatic support for an interaction between Parkin and SNAP-25

To try and characterise potential interaction domains between Parkin and SNAP-25, I employed AlphaFold Multimer (Jumper *et al.*, 2021). Alpha fold predicted a model for Parkin and SNAP-25 to interact with a low confidence below 0.5 with regards to the predicted template modelling (pTM) score and the interface predicted template modelling (ipTM) score which means there are likely to be errors in the predicted structure (EMBL-EBI, April 2025), the ipTM score can be affected by disordered regions, such as the linker region of SNAP-25 which may reduce the confidence of the prediction (EMBL-EBI, April 2025).

In the model I generated, the linker region of Parkin between the UB1 and RING0 domains is predicted to loop around both the SNARE domains of SNAP-25. Part of the linker region in Parkin between the Ubl and RING0 domains is involved in interactions with other proteins, and is made up of hydrophobic residues, which act as a binding pocket for Parkin substrate Miro-1 (Koszela *et al.*, 2024). As such, if an interaction was confirmed, this may be a region in Parkin to investigate as a site of SNAP-25 interaction (Figure 4.18).

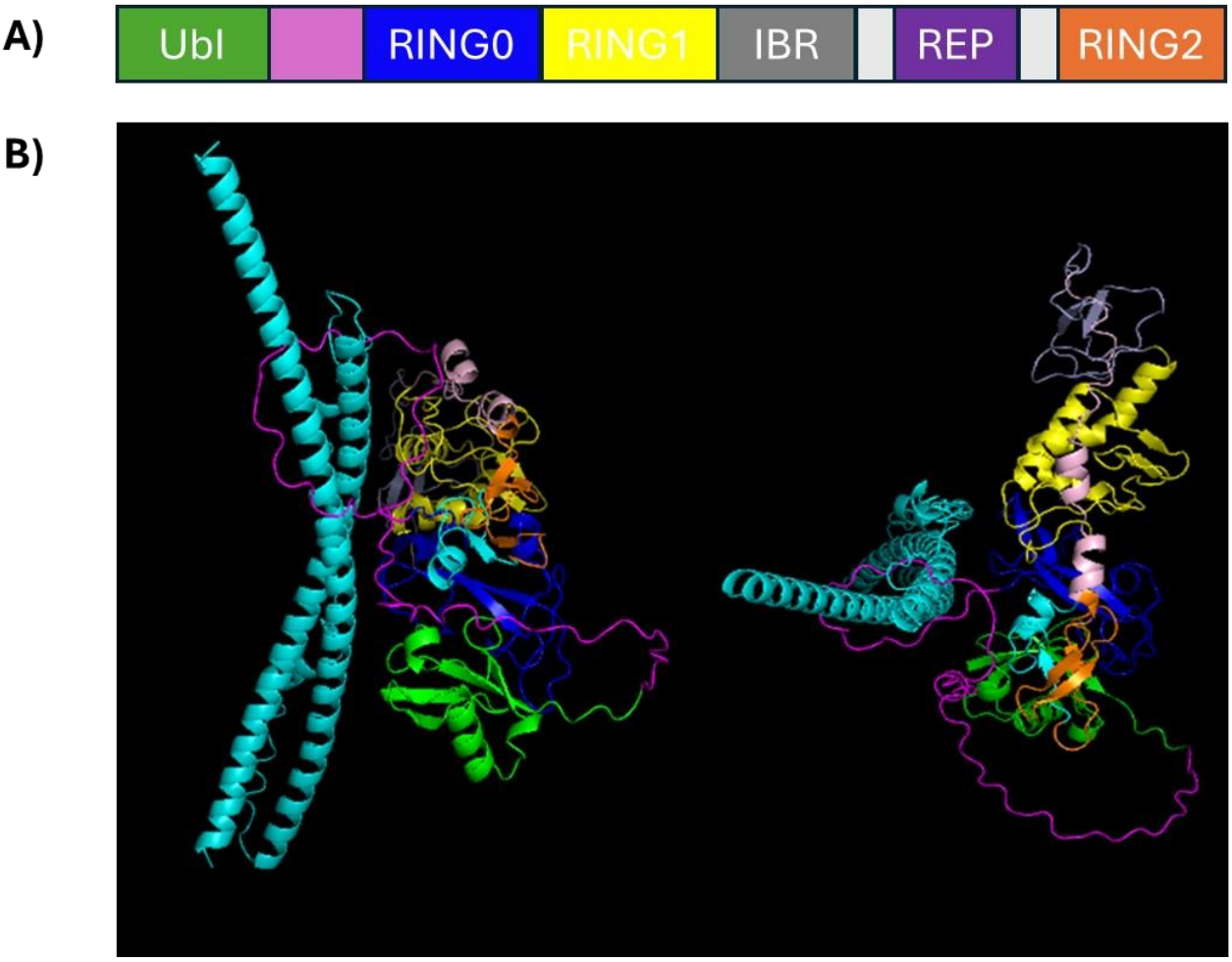

Figure 4.18: AlphaFold prediction of Parkin-SNAP-25 interaction in Parkin's linker region.

A) Domain architecture of Parkin with domains highlighted. B) A Ribbon representation of the top-ranked Alphafold2 Colabfold model of Parkin-SNAP-25 interaction, visualised with PyMol. A schematic of Parkin in it's autoinhibited conformation and SNAP-25. Parkin with its structural elements in sequence order: Ubl (Green), linker (magenta), RING0 (Blue), RING1 (Yellow), IBR (Grey), REP (Purple), RING2 (Orange) (colour coding corresponding to domains depicted in A). SNAP-25 in cyan is formed of two SNARE domains and a discorded region.

4.5.6 Literature Support for an Interaction between SNAP-25 and Parkin

SNAP-25 and Parkin are predicted to potentially interact by Ubibrowser (Section 3.4.2). However, no evidence for a direct interaction was identified. In addition, I used BioGrid to distil a list of known interactors of both SNAP-25 and Parkin. This didn't reveal any overlap between known interactors for the two proteins. This implies no obvious intermediate that could support proximity through an intermediate rather than a direct interaction.

My experiments suggest that the potential interaction between SNAP-25 and Parkin is E3 ligase independent. This could suggest that the interaction may have an alternative role outside ubiquitination and direct proteostasis. This would mirror the proposed regulatory role of the TRIM9-SNAP-25 interaction (Winkle et al., 2014b). An alternative explanation could be that Parkin and SNAP-25 don't directly interact but have proximity due to an interaction with a third party. Candidates could include PINK1, which binds Parkin, and SNAP-25 has been observed to facilitate PINK1-dependent mitophagy, with evidence that depletion of SNAP-25 destabilises PINK1 on mitochondrial membranes (Wang *et al*., 2023). TNFAIP1, which has been shown to ubiquitinate SNAP-25 and enhance the activity of Parkin/PINK1-dependent mitophagy (W. Wang et al., 2023). An alternative possibility could be HSC70, which interacts and chaperones SNAP-25 and can be mono-ubiquitinated by Parkin (Imai *et al.*, 2002, Moore *et al.*, 2008). To test if the interaction is direct, further experiments could be carried out, including GST-pulldowns and crosslinking reactions.

4.5.7 Potential non E3 ligase-substrate roles of a SNAP-25 – Parkin interaction

Parkin research has focused predominantly on its role as an E3 ligase at the mitochondria. However, emerging work is expanding this view with data supporting both lysosomal and endosomal functions and crosstalk with synaptic vesicles (Song and Krainc, 2024).

There is evidence to support Parkin localisation on (Kubo et al., 2001) or in close contact with the membranes of synaptic vesicles (Mouatt-Prigent et al., 2004). Although SNAP-25 is an abundant plasma membrane protein, it, like its partner SNARE proteins, undergoes dynamic trafficking onto endo membranes. Such that large pools exist on these membranes also (Walch-Solimena et al., 1995). Allowing for the possibility of SNAP-25 and Parkin being in the vicinity of each other. Parkin also interacts with or ubiquitinates proteins in the vicinity of SNAP25, such as CDCrel-1 and Synphilin-1, Synaptotagmin XI, Synaptojanin-1 and HSP/HSC70 (Zhang *et al.*, 2000, Chung *et al.*, 2001, Wang *et al.*, 2018, Song *et al.*, 2023, Song and Krainc, 2024, Moore *et al.*, 2008) (The roles Parkin has at the pre- and post-synapses are summarised in Table 3.1 in Chapter 3).
The presynaptic localisation of Parkin on the cytoplasmic surface of synaptic vesicles suggests that it may have the potential to interact with other proteins involved in the vesicle cycle, such as SNAP-25. There are a number of conditions where it could be hypothesised that SNAP-25 and Parkin may interact. 1. During oxidative stress or synaptic damage, if SNAP-25 undergoes misfolding, Parkin could potentially be recruited to ubiquitinate and lead to the removal of dysfunctional SNAP-25. This is supported by the fact that Parkin is found in synaptosomes and ubiquitinated synaptic proteins (Zhang *et al.*, 2000, Chung *et al.*, 2001, Kubo *et al.*, 2001) 2. The mitochondria cluster near the synaptic terminal (Graham *et al.*, 2017, Faitg *et al.*, 2021). Upon mitochondrial dysfunction near

active zones, Parkin may be recruited by PINK1 accumulation, potentially leading to proximity between SNAP-25 and Parkin, which could allow Parkin mediated remodelling of synaptic membrane components. 3. In times of high neuronal activity or plasticity, such as during activity-dependent remodelling or synaptic pruning, this could lead to an excess or a pool of inactive SNAP-25 needing to be degraded (Sheehan et al., 2016), for which Parkin may be involved in tagging. 4. In some diseased states, such as in models of Parkinson's disease, Parkin is sometimes overexpressed or mis-localised; as such, there is the potential that in diseased states, Parkin may become localised to the synaptic membranes and influence SNAP-25 turnover, which could contribute to the synaptic dysfunction observed in Parkinson's disease (Cookson *et al.*, 2003, Lebedeva *et al.*, 2023, Clausen *et al.*, 2024).

4.6 Summary

Whilst this study has not confirmed a direct interaction between SNAP-25 and an E3 ligase or confirmed any E3 ligase's specific ability to ubiquitinate SNAP-25, it has led to the suggestion that Parkin may either directly or indirectly interact with SNAP-25, which is an interesting avenue in light of the disease implications that alterations in both of the proteins have. (See Section 6.5 for future directions)

Chapter 5 Generation of a CRISPR CSPα Deficient PC12 Model

5.1 Introduction

To date, most work investigating CSPα has been undertaken in a neuronal post-mitotic context (Section 1.5). Mouse, *Drosophila* and *C. elegans* knock-out models have been generated (Section 1.5.4) with different phenotypic outcomes. Recently, work has been undertaken in proliferating stem cells and cancerous systems (Section 1.5.10), which have provided evidence of alternative and additional cell-type-specific roles of CSPα.

Whilst SNAP-25 hyper-ubiquitination has been well characterised in the CSPα -/- mouse model, E3 ligases have not been identified that may interact with SNAP-25 in this context. To carry out BioID using SNAP-25 with the reagents generated in the previous chapter, this system would require harvesting embryos from CSPα litters, performing genotyping, and generating single embryo cultures. It would then require transfection of these cultures with the reagents generated.

Due to the complications and the limitations around the number of cells able to be harvested for single-embryonic cultures and the low transfection rate of neurons, it was decided that a PC12 CRISPR Cas9 CSPα knockout model would be generated. Using CSPα knockdown PC12 cells would allow greater levels of flexibility and still allow for probing in a neuronal-like environment upon differentiation with NGF, and as such it could be used as a tool to carry out BioID of SNAP-25 to probe for SNAP-25 interactors in the chaperone-deficient environment.

5.1.1 Using CRISPR-Cas technology

CRISPR (Clustered Regularly Interspaced Short Palindromic Repeat) Cas is a genomic engineering technology that allows genomic changes that including knock out via deletion, base editing and knock-in of DNA sequences. This allows a versatile transformation of the system that allows the loss, alteration, correction or knock-in of a gene into cells and organisms (Hall et al., 2018, Lau et al., 2020).

CRISPR requires two components: a guide RNA (sgRNA) and a CRISPR-associated endonuclease (Cas) enzyme. The sgRNA is a short synthetic RNA formed of a 3-nucleotide sequence termed a Protospacer Adjacent Motif (PAM) site, which acts as a scaffold sequence required for Cas-binding, and a ~20-nucleotide sequence which defines the target to be modified that must be unique compared to the rest of the genome and adjacent to the PAM site (Jinek *et al.*, 2012, Ran *et al.*, 2013).

The CRISPR components can be introduced into cells by transduction of viral vectors such as adenovirus and lentivirus, via transfection of non-viral vectors and via physical methods such as via electroporation and microinjection (Liu et al., 2017, Milone and O'Doherty, 2018).

5.1.2 Using CRISPR-Cas technology to generate knockout cell lines

The sgRNA and the Cas9 protein form a ribonucleoprotein complex, causing an activating conformational change in Cas9, allowing DNA-binding (Anders et al., 2014). Once bound, the sgRNA sequence will begin to anneal to the target DNA, upon which Cas9 will undergo another conformational change where the opposite strand of DNA is cleaved, leading to a double strand break (DSB) in the target DNA ~3-4 nucleotides upstream of the PAM sequence.

The DSB is repaired by either non-homologous end joining (NHEJ), which is efficient but error prone, due to directly ligating the break ends (Chang et al., 2017) or homology-directed repair (HDR), which is less efficient but has high fidelity due to the DNA being copied directly from a matched template (Jasin and Rothstein, 2013). NHEJ frequently causes small nucleotide indels, insertions or deletions at the site of the DSB, leading to an array of mutations. Indels often result in amino acid deletions, insertions or frame shifts, leading to the formation of premature stop codons in an open reading frame (Chang et al., 2017).

HDR uses a homologous sequence as a template for the repair of the double-strand break and is a more accurate mechanism for repair than NHEJ. If the DNA template is identical to the original DNA, then the process is generally error-free (Smithies et al., 1985, Bollag et al., 1989, Jasin and Rothstein, 2013). HDR and NHEJ are not mutually exclusive and can both occur concurrently during DNA double-strand break repair. NHEJ is usually the predominant pathway, but HDR can be favoured under certain conditions or manipulations (Yang et al., 2020).

5.1.3 Identifying CRISPR knockdowns

In a situation where CRISPR is engineered to introduce a deletion that knocks out gene function by generating NHEJ and associated small nucleotide mutations, there is a propensity to cause frame shifts that lead to functional reduction or knockdowns.

Whilst CRISPR leads to the knockout of a specific protein via destroying an allele in a cell, if a cell culture is formed of mixed colonies, there is the possibility that there will be a mix of cells with some being wildtype and some null, leading to a knockdown rather than a complete knockout across the culture.

Generating knockdown cell lines with CRISPR-Cas technology is a well-established technique (Wang and Doudna, 2023). Identifying changes in mRNA expression can be carried out with RTqPCR or RNA-seq, and protein expression can be monitored by western blot, ELISA, flow cytometry or proteomics. Whilst sequencing allows characterisation of the editing events via DNA sequencing of the CRISPR targeted region, NGS or by sequencing followed by analysis with Tracks indels by decomposition (TIDE) software (Germini et al., 2018).

5.1.4 Using PC12 cells to study neuronal proteins

PC12 cells are a rat cell line derived from a pheochromocytoma of the adrenal medulla (Greene and Tischler, 1976). PC12 cells are used in research into neuronal function and can be induced to differentiate into neuron-like cells when exposed to neurotrophins (Greene and Tischler, 1976, Westerink and Ewing, 2008). These differentiated cells are a good model for the presynaptic site (Tao-Cheng et al., 1995)

5.1.5 Trk Neurotrophins and the Epidermal Growth Factor Receptors

Neurotrophins such as Nerve growth factor (NGF) are signalling molecules with roles in neuronal development and survival (Dechant et al., 1994). Neurotrophins bind to receptors named Trk (tyrosine kinase) receptors. TrkA binds NGF (Greene and Tischler, 1976, Wiesmann et al., 1999), TrkB binds brain-derived neurotrophic factor (BDNF) (Squinto *et al.*, 1991) and NT4 (Minichiello et al., 1998), and TrkC binds NT-3 (Urfer et al., 1994).

In PC12 cells, the addition of NGF acts through its Trk receptors, leading to sustained activation of the mitogen-activated protein (MAP) kinases, triggering the formation of neurite outgrowths and promoting neuronal-like differentiation (Pang et al., 1995, Kao et al., 2001). Knockout of TrkA in PC12

cells leads to a loss of NGF-responsiveness and an inability to induce neuronal like differentiation (Testa et al., 2022).

The Epidermal Growth Factor Receptor (EGFR) is a receptor for the epidermal growth factor family (EGF) (Rude Voldborg et al., 1997) involved in cell growth and differentiation (Boonstra et al., 1995). In PC12 cells, the addition of EGF leads to transient activation of the mitogen activated protein kinases (MAPKs). This transient activation does not promote neurite outgrowth that follows the sustained activation triggered by NGF but promotes cell growth and proliferation (Kao et al., 2001).

5.1.6 Label-free proteomics to investigate changes in protein expression

Alteration of particular proteins, such as via CRISPR knockdown, can lead to alterations in the expression of other proteins. These changes in protein expression can be investigated using techniques that compare the protein abundance between control and altered cell samples.

Proteomics is used to study the protein expression of a biological sample (Cui et al., 2022). Label-free proteomics is a quantitative method that doesn't require chemical or isotopic labelling of samples, relying instead on the abundance of peptides to determine absolute or relative quantities compared to a control (Anand *et al.*, 2017). Label-free proteomics advantages include a reduced cost and increased throughput compared to traditional labelled proteomics (Figure 5.1). Label-free proteomics can be performed by measuring chromatographic ion intensity changes as peptide peaks or by spectral counting the identified proteins (Zhu et al., 2010).

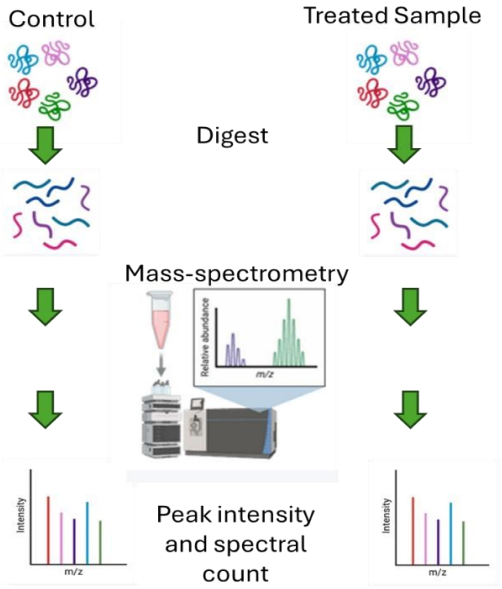

Figure 5.1: General approach of Label-free quantitative proteomics

Control and treated samples are harvested and are subjected to individual digestion; the digested peptides are then separated, and mass spectroscopy analysis is carried out. Quantification of the spectra from the control and the treated samples based on the comparison of peak intensity of the same peptide or the spectral count of the same protein is then carried out to determine the abundance change of peptides between the samples.
Adapted from Huang et al, 2010.

For label-free proteomics, proteins from the control and the treated sample are extracted from the cells or tissue and digested into their peptides. Peptides are separated by either gas or liquid chromatography and analysed by mass spectrometry (Figure 5.1), after which the peptides and corresponding protein identification and quantification are carried out using software such as OpenMS, MapQuant and PEAKS Q (Zhu et al., 2010).

Caveats surrounding label-free quantitative mass spectrometry include the fact that the analysis of protein abundance from biological samples can be complex, and peptide peak intensities can differ even between runs of the same sample due to preparation and sample injection, which leads to the requirement for normalisation to account for variation. The large amount of data generated from MS of complex protein mixtures needs to be automated to process the data. Whereby, the peptide peaks need to be distinguished from the background noise and other peptides, and the LC/GC-MS retention times adjusted to match peaks between sample runs (termed peak matching). Chromatographic peak intensity then needs to be calculated either by measuring the peak area or the peak height, and statistical analysis is carried out (Student's t-test) to determine the significance of changes between multiple samples (Zhu et al., 2010, Anand et al., 2017).

5.2 Aims

1. This chapter aimed to generate a CSPα knockdown PC12 line via CRISPR-Cas-9 technology to use it as a tractable model of synaptic proteasomal dysfunction.

2. Characterise the CSPα-deficient lines in comparison to the Parental and Lenti CRISPR control.

5.3 Results

5.3.1 Identification of alteration of protein levels of CSPα in PC12 lines transfected with sgRNAs targeting CSPα

Parental PC12-TrkB cells were transfected with either one of the 5 Lenti CRISPR sgRNA's plasmids (sgRNA_3 targeting exon 3, sgRNA_4A, B and C targeting exon 4 or sgRNA_5 targeting exon 5) or with an empty Lenti CRISPR control plasmid (Section 2.4). After transfection, the cells were selected with puromycin and allowed to recover. Western blotting for CSPα was carried out to determine if the sgRNA guides led to the knockdown of CSPα (Figure 5.2).

Two guides, sgRNA_3 targeting exon 3 and sgRNA_5 targeting exon 5, led to a clear reduction of CSPα protein compared to a Parental control and the empty Lenti CRISPR plasmid control. These have been termed PC12 CSPα deficient 3 (CD3) and PC12 CSPα deficient 5 (CD5). In contrast, the other sgRNA-transfected lines showed no alteration in expression levels of CSPα and were not pursued further in this thesis (Data not shown).

In an independent set of experiments, protein extracts were made from these four lines: Parental (Control), Lenti CRISPR (Control), CD3 and CD5. These extracts were then subjected to quantitative western blotting for CSPα (N=3). A reduction in CSPα of 82% was observed for cells transfected with guide sgRNA_3 and 95% in cells transfected with guide sgRNA_5 compared to the Parental PC12 line, normalised to GAPDH (Figure 5.2). The CSPα antibody used, Synaptic Systems 154 003, recognises the amino acids 182-198 in the C-terminal of CSPα, which is downstream of both CRISPR sites; as such, it is possible that if a truncated protein was formed, it would not be detected with this antibody.

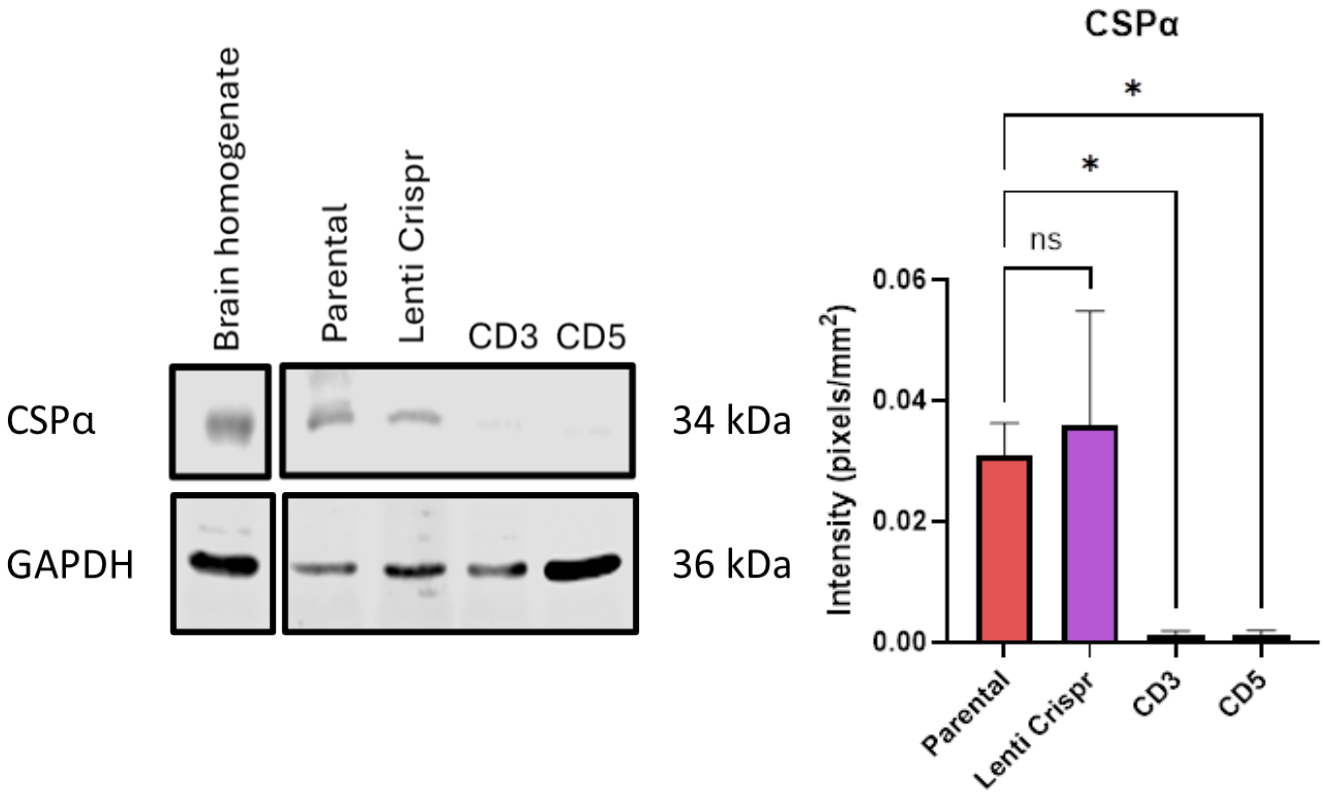

Figure 5.2: PC12 cells transfected with Lenti CRISPR plasmids containing guides sgRNA_3 and sgRNA_5 led to a knockdown in CSPα.

30 µg mouse brain homogenate (Adult female C57BL/6) and cell lysate from Parental, Lenti CRISPR, CD3 and CD5 were resolved by SDS-PAGE, western blotted and labelled with antibodies for CSPα and GAPDH. Intensity values of the immunofluorescent protein bands were normalised to the loading control GAPDH. A comparison between the Parental and each of the transfected conditions was made using ANOVA, with significance denoted as *p<0.05, N=4).

5.3.2 Molecular description of CRISPR genomic disruption in CSPα-deficient lines

To determine the molecular event that led to the generation of the CRISPR-mediated knockdown of the CSPα, Genomic DNA was extracted, and cDNA was made from extracted RNA from the Parental, Lenti CRISPR, CD3 and CD5 lines. SNAP-25 were amplified and sequenced from the genomic and cDNA from all 4 lines (Figure 5.3, A, Alignment Figure 5.17).

Primer pairs for amplification across the CD3 and the CD5 CRISPR-targeted regions were designed and generated for amplification from genomic DNA. The Primer pairs amplified fragments of the expected sizes in the Parental and the Lenti CRISPR lines. However, no amplification of CD3 and insufficient amplification of CD5 for sequencing were generated. This may suggest greater disruption

in the intronic regions surrounding the CRISPR events, but this was not determined as part of this work (See appendix C.1).

Primers depicted in (Figure 5.3, B) were used to amplify the region of DNAJC5 spanning exons 3-5 from cDNA. Amplification of DNAJC5 from cDNA produced two bands in the Parental, Lenti CRISPR, CD3 and CD5 as previously reported in cDNA generated from PC12 cells, chromaffin cells and from the spleen (Chamberlain and Burgoyne, 1996, Coppola and Gundersen, 1996). The lower band shares sequence identity with rat brain DNAJC5, whilst the upper band corresponds to a splice variant with an additional 72-base insert, based on work by (Coppola and Gundersen, 1996).

For CD3, there were low levels of amplification upon attempted amplification with the conditions optimised on the Parental line using 25 cycles (Figure 5.3, A). With 35 cycles, CD3 was amplified and sent for Sanger sequencing. The quality of the sequence generated in the PCR did not allow for the nature of the CRISPR disruption to be defined, as sequencing chromatograms depicted multiple overlapping sequences, potentially suggestive of the presence of a mixed culture after CRISPR (See appendix section C, Figure C.2 for chromatogram).

Via amplification of cDNA from the CD5 cell line, it was possible to map a loss of four bases starting 4 bases upstream of the PAM site used for recognition of sgRNA_5 (Figure 5.3, C). Translation of this sequence suggests this loss led to a shift, leading to an alteration in the transcript after the CRISPR site, predicting a translation of a CSPα protein with an altered frame harbouring a premature stop codon (Figure 5.3, D).

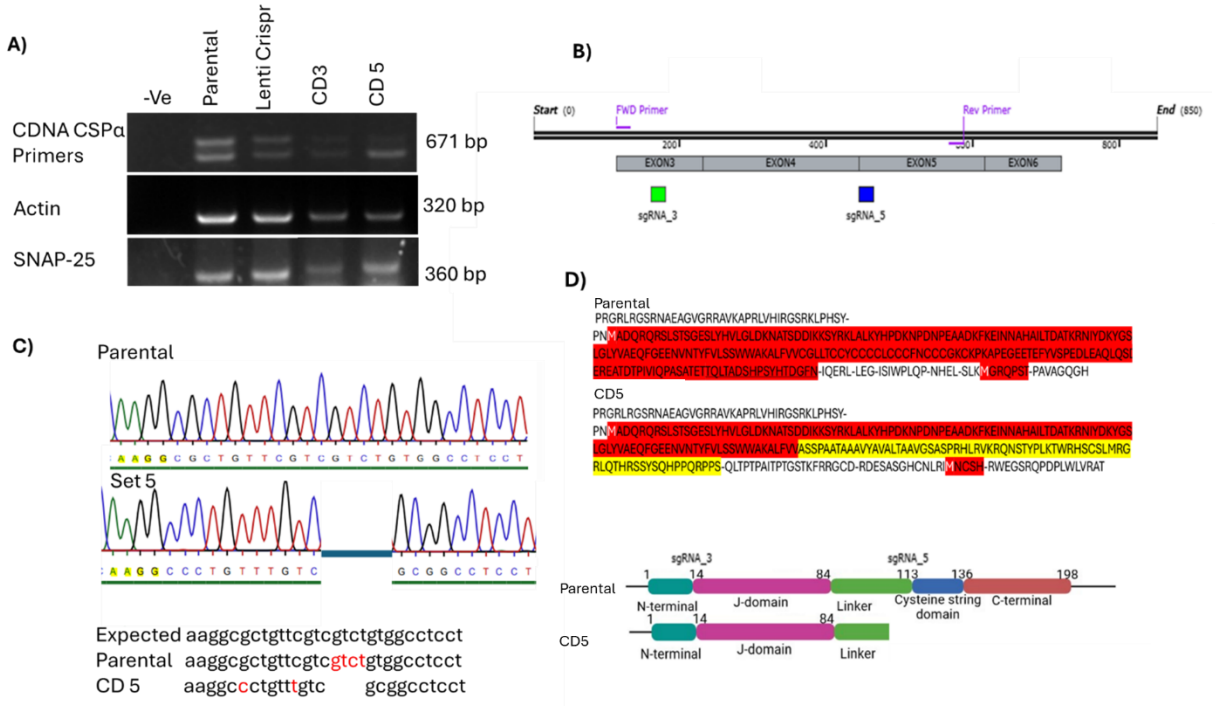

Figure 5.3: Determining the molecular events that generated CSPα-deficient lines. A) PCR amplifications of CSPα, Actin and SNAP-25 from cDNA from Parental, Lenti CRISPR only control, CSPα-deficient 3 and CSPα-deficient 5. PC12 cells B) CSPα cDNA schematic with localisation of primers used for amplification. C) Parental and CD5 sequencing chromatogram of site spanning the CRISPR region, with sequence below. D) Translation of Parental and CD5 sequences and schematic of corresponding Parental CSPα and CD5 protein.

5.3.3 Phenotypic changes in CSPα-deficient cells

5.3.3.1 Detailing the Alterations in the growth rate of CSPα-deficient cells

After recovery from the puromycin selection, it was observed that the CSPα-deficient lines (CD3 and CD5) were proliferating at an increased rate compared to the Parental and the Lenti CRISPR control lines. To quantify this qualitative observation, growth assays were carried out on the Parental, Lenti CRISPR and CSPα-deficient lines. After being seeded at a density of 250,000 cells, cells were counted over 3 Days to determine the growth rate.

Both CSPα-deficient lines showed increased growth rates in comparison to the Parental and Lenti CRISPR lines over the three-day time course (Figure 5.4). The Doubling Time of the Parental and the Lenti CRISPR lines was 3.1 and 3.6 days respectively, which was almost halved in the CSPα-deficient lines at 1.7 days for CD3 and 1.5 days for CD5. The reported rates for PC12 cells range from 1.6 to 3.8 days (PC-12- culturecollections.org, June 2025, Ds et al., 1999). When plated at a

density of 250,000, the Parental and the Lenti CRISPR cultures are about 40 % confluent by Day 2 and 80 % confluent by Day 3, whereas both CSPα deficient lines are at about 50-60 % confluent by Day 2 and 95-100 % confluent by Day 3. Two days after plating in culture, the control cells and the CSPα-deficient cells also appear to be growing differently, with the CSPα-deficient cells growing in tight clumps, whilst the control lines stay more spread, as illustrated below (Figure 5.4).

A)

B)

Line	Parental	Lenti CRISPR	CD3	CD5
Doubling Time Exponential (Malthusian) growth	3.083	3.636	1.743	1.590

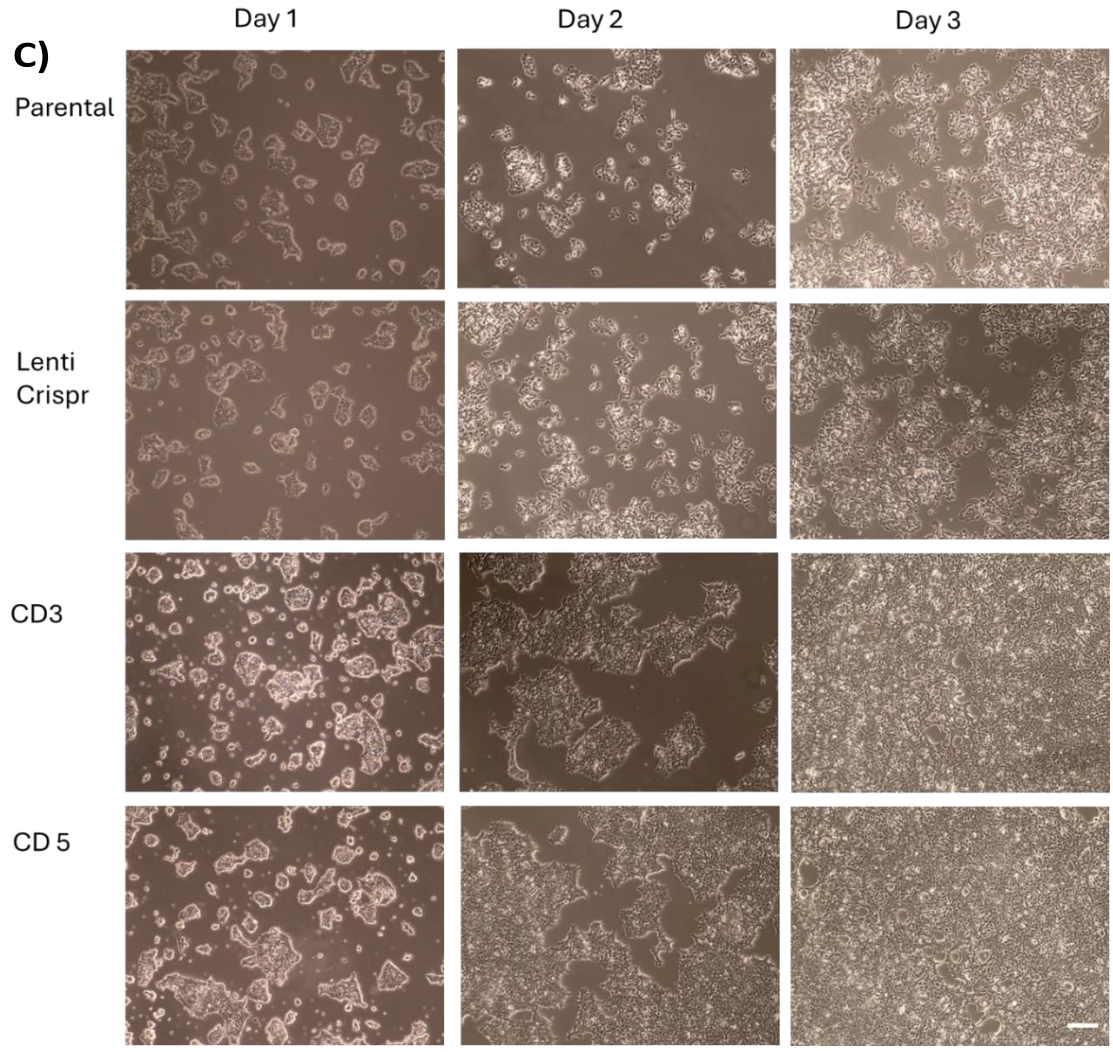

Figure 5.4: PC12 CSPα-deficient CD3 and CD5 cells proliferate more quickly than the Parental line

A) Parental (Control) (Red), Lenti CRISPR (Control) (Purple), CD3 (Blue) and CD5 (Black) cells (250,000 cells) were plated in triplicate and counted at 24, 48 and 72 hours post-plating, all data shown as ±SEM B) with the Doubling Time Exponential (Malthusian) growth rates tabulated below C) Representative images of the cells at each of the time points counted, Scale bar =50 µM. N=3 for each cell type at each time point.

5.3.3.2 CSPα-deficient lines don't differentiate in the presence of NGF or BDNF

Differentiation of PC12 cells is stimulated with a drop in serum levels and the addition of neurotrophins such as NGF (50 ng/ml) or BDNF (50 ng/ml) as described in Section 2.5.4.

In the control, Parental and Lenti CRISPR cell lines, the addition of NGF or BDNF led to a shift away from a proliferative state to one in which treated cells produced outgrowths with long, thin projections (Figure 5.5). When the same treatment was subjected to CD3 and CD5, the cell

populations failed to cease proliferation and did not produce outgrowths. Any projections formed were very short and triangular in comparison to the long, thin projections of the Parental and Lenti CRISPR cells (Figure 5.5).

Parental, Lenti CRISPR, CD3 and CD5 cells were plated at $5x10^5$ cells per well in a 6-well plate, and NGF (50 ng/ml) was added 24 hours later. Each of the cultures were imaged for three days, after which the CD cell lines started to become over-confluent and detach from the cell culture dish. At day one, none of the cultures display outgrowths, but by day two, the Parental and the Lenti CRISPR cultures start to exhibit projections developing from cells. By day three, outgrowths have developed in a large number of the Parental and the Lenti CRISPR cells. Whilst in the CD3 and CD5 lines, no outgrowths are present, and the cells continued to proliferate despite the addition of NGF or BDNF. As such, by Day three, CD3 and CD5 were confluent and went on to form overlying cell sheets, often with the potential to detach from the dish.

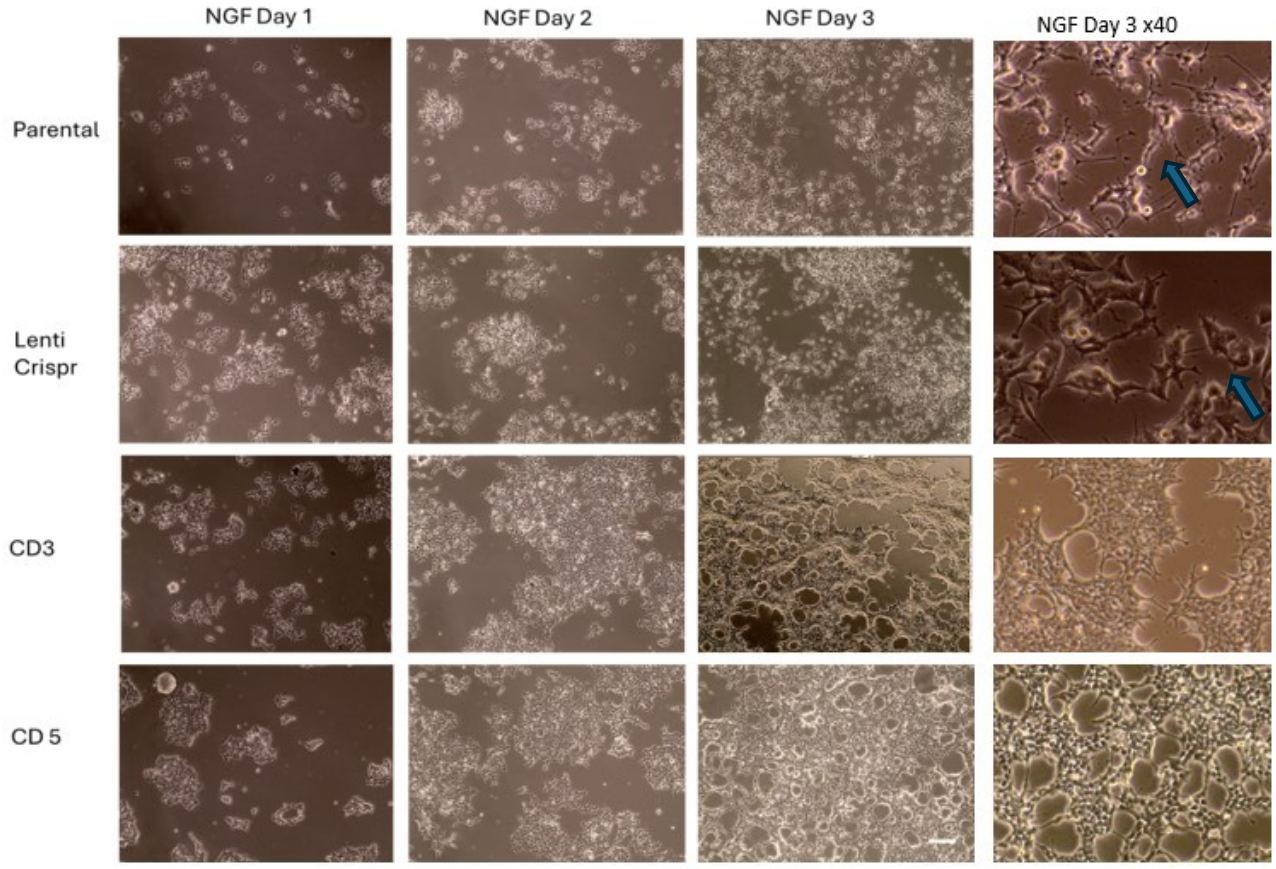

Figure 5.5: PC12 CSPα-deficient CD3 and CD5 cells fail to show signature differentiation in response to NGF Brightfield microscopy 10x magnification of Parental, Lenti CRISPR and PC12 CSPα-deficient CD3 and CD5 cells over three days after the addition of NGF (50 ng/ml), with arrows marking outgrowths observed in the Parental and Lenti CRISPR lines. N=3, Scale bar 50 µM.

5.3.4 Neurotrophin receptor expression in CSPα knockdown models

Due to the refractory PC12 differentiation and increased proliferation observed in the CD3 and CD5 cell lines, I investigated whether Trk and EGF receptors were expressed in the distinct cells.

TrkB and total Trk receptors (Trk A and B) were readily detected in the Parental line but not in the CSPα-deficient lines (CD3 and CD5) (Figure 5.6). This deficiency explains the lack of NGF and BDNF responsiveness observed in Section 5.3.3.

The EGF receptor was undetectable in the Parental cell line but was readily detected in the CSPα-deficient lines (CD3 and CD5). This corresponds to the increased proliferation observed in Section 5.3.3.

5.3.4.1 Investigating expression of neurotrophins in CSPα -/- mouse forebrain tissue

To determine if this intriguing observation was also observed in another CSPα knockdown model, CSPα +/+ and -/- mouse forebrain tissue from postnatal pups p15-18 was blotted using the same antibodies; in this tissue, the TrkB antibodies detected a doublet. This likely reflects a second band previously assigned to the glycosylated form of the Trk A receptor (Figure 5.6). Importantly, this immunoreactivity was not significantly different between the CSPα +/+ and -/- tissue, indicating no difference in the expression of these. In contrast, there was a doubling of the relative abundance of the EGFR in CSPα knockout forebrain tissue, potentially suggestive of a selective stabilisation of EGFR in the CSPα-deficient cells and mouse model.

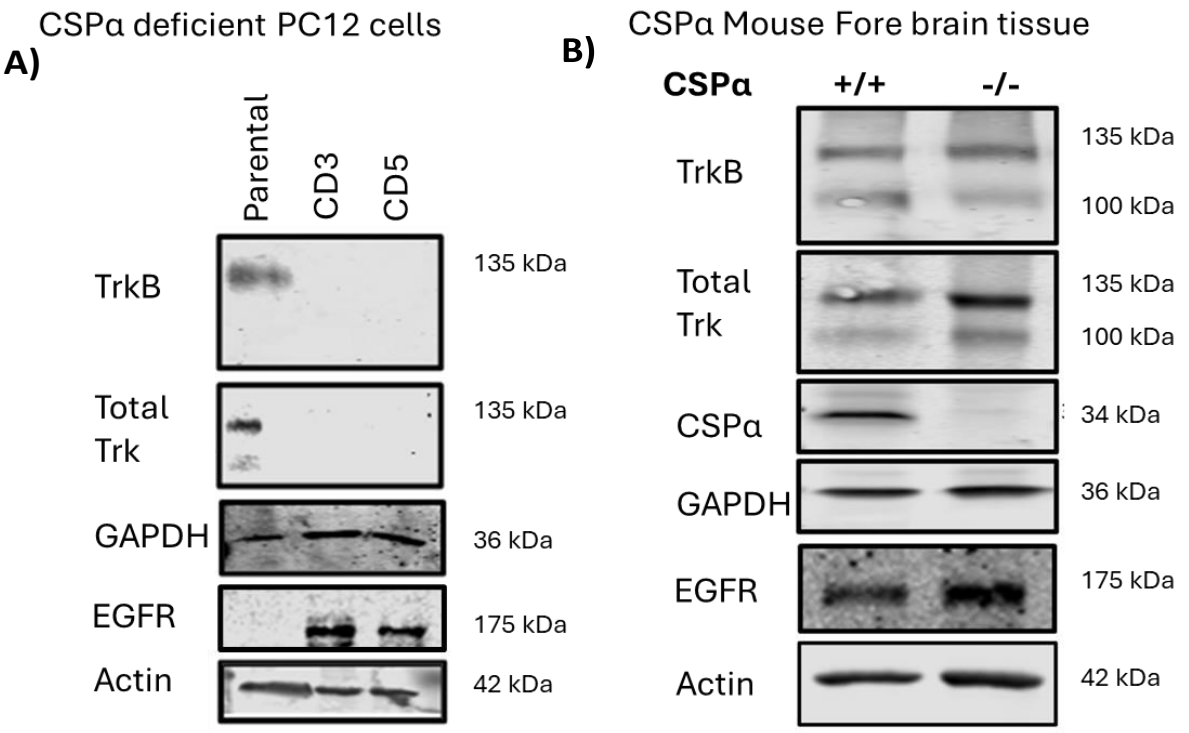

Figure 5.6: TRK and EGF receptor levels are altered in PC12 CSPα-deficient CD3 and CD5 cells

Levels of TRK and EGF receptors were investigated in the A) Parental and PC12 CSPα-deficient CD3 and CD5 cell lysates, and B) CSPα +/+ and -/- forebrain tissue. 20 µg of cell lysate or brain homogenate was resolved by SDS-PAGE, then labelled with the indicated antibodies by western blotting, N=3.

5.3.5 Alteration of neuronal CSPα clients SNAP-25 and Dyn-1 in the CSPα-deficient cells

5.3.5.1 Immunodetection of CSPα clients in CSPα-deficient cells

Protein extracts were made from the four lines (Parental, Lenti CRISPR, CD3 and CD5). These extracts were then subjected to quantitative western blotting for established neuronal CSPα clients SNAP-25 and Dyn-1and other neuronal proteins VAMP-2 and PSD95 (N=3).

A reduction of SNAP-25 was calculated to be 90.5% for CD3 and 99% for CD5, with a significance p-value of <0.0001. Whilst Dyn-1 was reduced by 50 %, 72% and 74% for CD3 across three repeats and 61%, 78% and 86% for CD5 across three repeats. Synaptic markers, VAMP-2 and

PSD95, were measured, and their relative expression between the Parental and Lenti CRISPR controls and CD3 and CD5 were quantifiably unchanged (Figure 5.7).

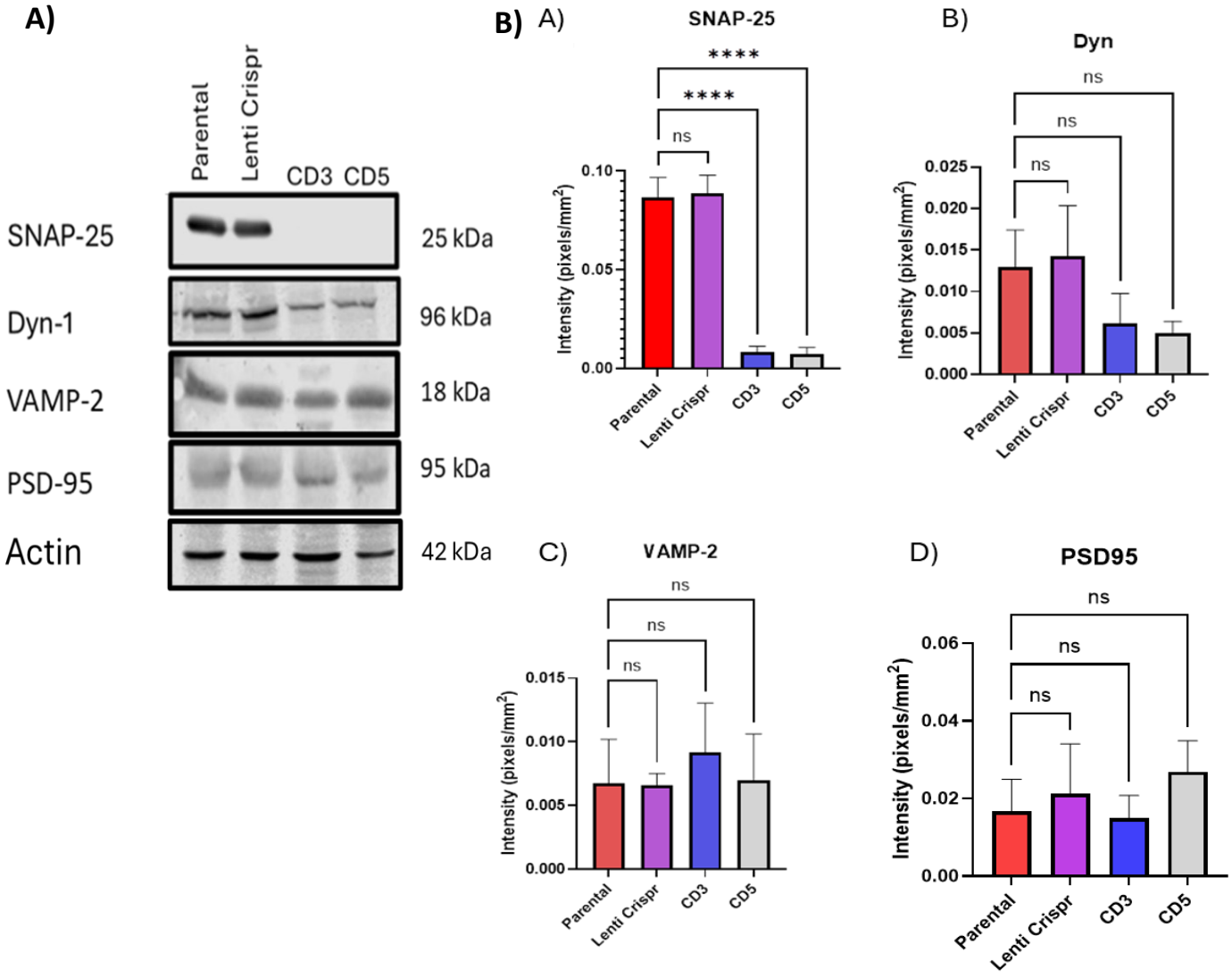

Figure 5.7: CSPα-deficient lines CD3 and CD5 have a selective reduction of CSPα clients. Blotting of CSPα client proteins SNAP-25 and Dynamin-1 with the quantified percentage reduction of expression, synaptic markers VAMP-2 and PSD95 in Parental, Lenti CRISPR and CSPα-deficient cells. A) Representative blots of CSPα clients and synaptic proteins. B) Quantification in SNAP-25, C) Dyn-1, D) VAMP-2 and E) PSD-95 expression in Parental, Lenti CRISPR, CD3, and CD5 cells, normalised to loading control Actin. A comparison of relative intensities between the Parental and each of the transfected conditions was made using ANOVA, with significance denoted as *p<0.05, ****P<0.0001, N=3.

5.3.5.2 Immunostaining of SNAP-25 in CSPα-deficient cells

To complement the western blots for CSPα clients, I subjected the Parental and the Lenti CRISPR controls and CD3 and CD5 cells to immunodetection staining for SNAP-25. Staining was carried out in both differentiated (Data not shown) and undifferentiated Parental and Lenti CRISPR cells, and the undifferentiated CSPα-deficient cells (See Section 5.3.3) (Figure 5.8).

In the Parental and Lenti CRISPR cells, all cells expressed a uniform plasma membrane SNAP-25 stain (Figure 5.8). In the CSPα-deficient cells (CD3 and CD5), a mosaic appearance of the SNAP-25 immunoreactivity was observed. The majority of cells had no SNAP-25 stain, with a minority of cells expressing SNAP-25 at the plasma membrane with an associated intense staining at the growth cone. An even smaller proportion of cells expressed SNAP-25 at lower levels. The knockdown cells with faint immunoreactivity could potentially be suggestive of the cells still expressing one copy of CSPα.

In the Parental and the Lenti CRISPR cells, 100% of cells expressed CSPα, whilst within the CSPα-deficient cell lines, 12% of cells were observed to be expressing SNAP-25 by immunofluorescence staining, corresponding to a lack of immunoreactivity detectable by western blot (Figure 5.8).

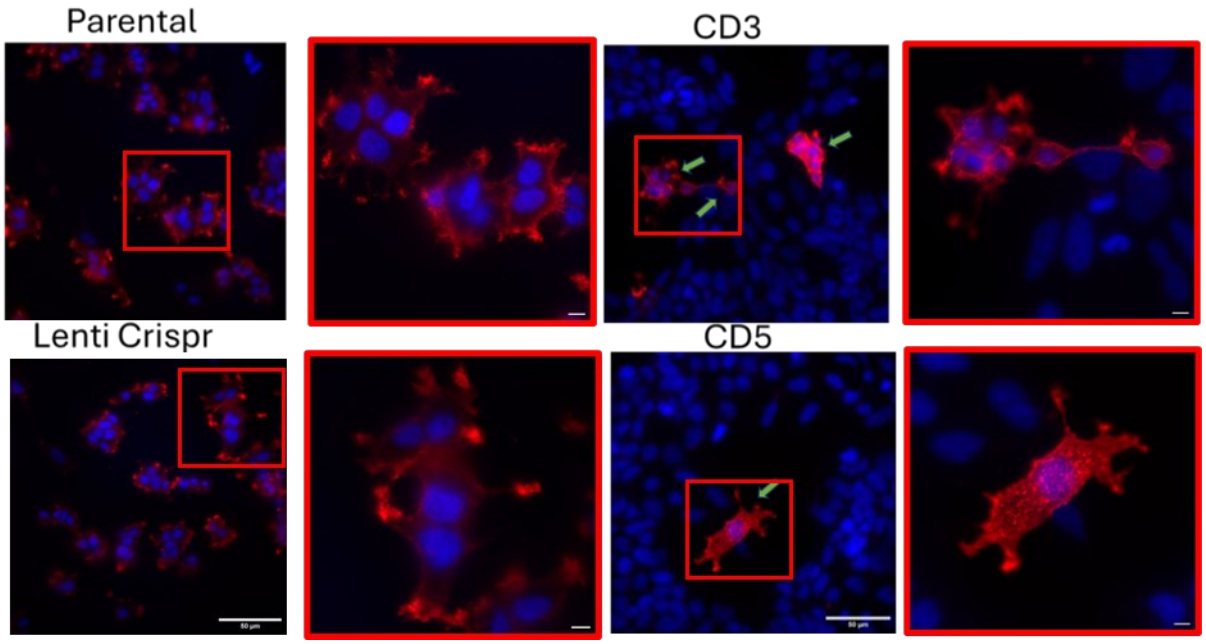

Figure 5.8: CRISPR CSPα-deficient PC12 cell lines have a reduction of CSPα client SNAP25. Parental, Lenti CRISPR, CD3 and CD5 cells were fixed, permeabilised and then probed for SNAP-25, represented in the red channel and Hoechst, represented in the blue channel. Scale bar 50 µM.

Cells positive for SNAP-25 in Parental, Lenti CRISPR, CD3 and CD5 (Indicated with arrow heads) were formed in tight clusters, with individual cells having small nuclei. While cells where SNAP-25 was not detected in the CD3 and CD5 cell lines had larger nuclei, and a potentially more epithelial-like phenotype with flatter cell morphology (Figure 5.8).

5.3.5.3 Investigation into turnover of SNAP-25 in CSPα deficient cells

To determine if blocking the proteasome rescues the loss of SNAP-25 observed in the knockdown cells, Parental PC12 cells and the CSPα-deficient cells (CD3 and CD5) were treated with proteasome inhibitor MG-132 (10mM) for 2, 6 and 8 hours. Cells were treated at these time points as generally proteasome inhibition is not evident before 3 hours which the 2 hour time point aligns with whilst protein accumulation is usually present within 4-8 hours without an effect on cell viability which the 6 and 8 hours time points fall within (Tarjányi et al., 2013, Tarjányi et al., 2022).

SNAP-25 is expected to be increasingly ubiquitin-conjugated in the PC12 CSPα-deficient model compared to the Parental line. We would hypothesise that in CSPα-deficient cells, where we see a reduction in SNAP-25, when treated with MG-132, we would see a restoration in SNAP-25 protein levels due to a block of its UPS degradation.

Immunofluorescence staining and western blotting were carried out to determine if there was a restoration of SNAP-25 levels. An increase of SNAP-25 was observed via western blot in the Parental line treated with MG-132 at each of the time points (2 hr and 6hr data not shown), but the reduction in SNAP-25 in the CSPα-deficient cells was not rescued, and no immunoreactivity for SNAP-25 was detected at any of the time points (Figure 5.9, A).

In the Parental cells, all cells had a plasma membrane-localised SNAP-25 immunoreactivity, which was unaltered in the cells treated with MG-132. In the untreated CSPα-deficient cells, few cells had a plasma membrane SNAP-25 stain consistent with the description of these cells above (See Section 5.3.5.2). In the CSPα-deficient cells, SNAP-25 immunoreactivity in the MG132-treated cells revealed a captured intracellular speckled staining. This immunoreactivity was present in the face of no clear plasma membrane staining. This implies SNAP-25 accumulates in a new compartment when the proteasome is blocked and/or the steady state capture of a distinct compartment that arises in the face of CSPα knockdown. This speckled stain was present in about 30% of cells (Figure 5.9, B).

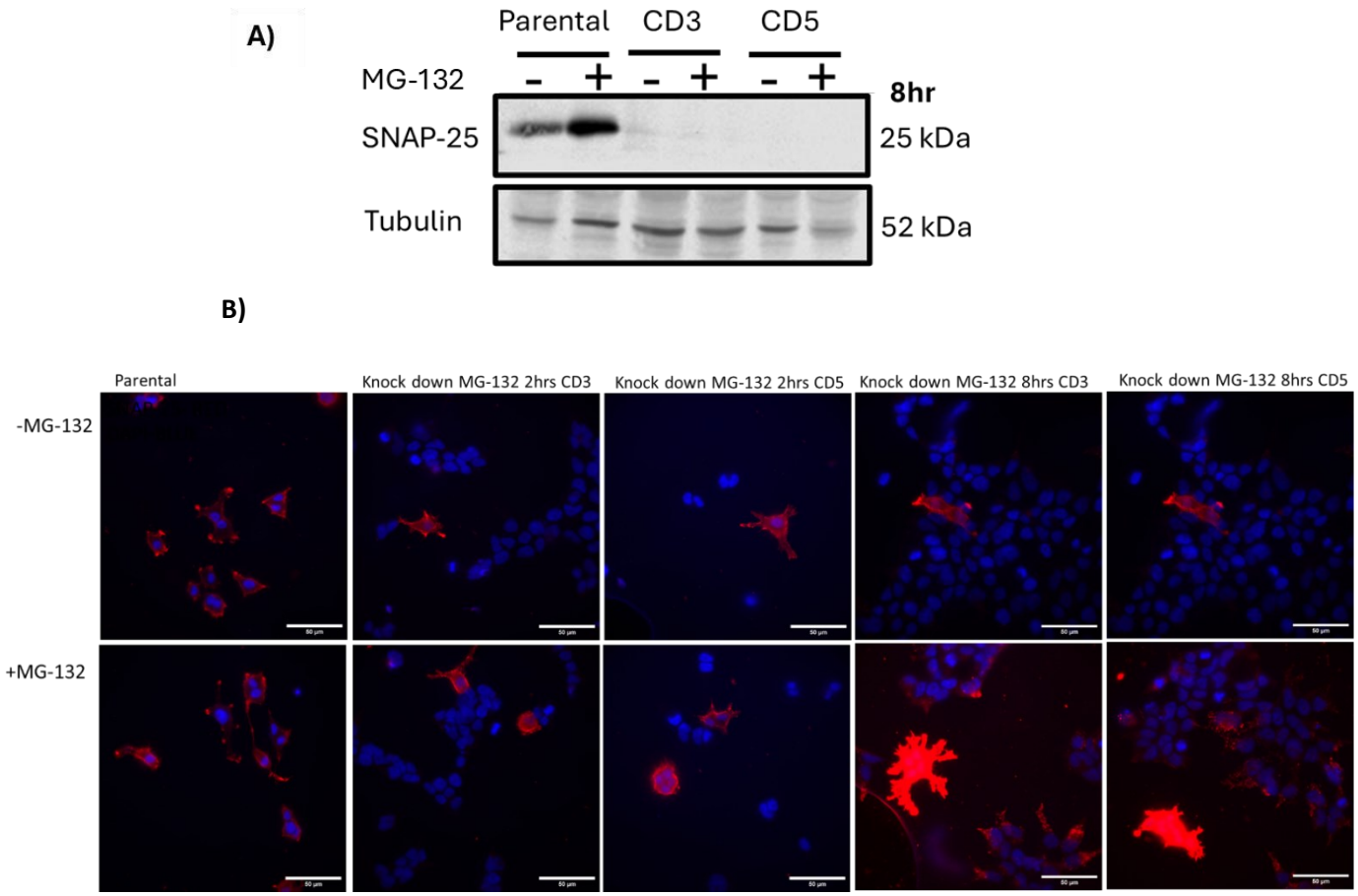

Figure 5.9: Blocking the Proteasome does not restore SNAP-25 protein levels in PC12 CSPα-deficit CD3 and CD5 cells

Parental and PC12 CSPα-deficient CD3 and CD5 cells were plated, then treated with MG-132 (10 µM) for 8 hours. A) 20 µg of lysate was resolved by SDS-PAGE and labelled with SNAP-25 and Tubulin antibodies to determine SNAP-25 levels. B) Representative immunofluorescent staining of SNAP-25, cells were fixed, permeabilised, and immunolabelled for SNAP-25 (red) and with Hoechst (blue), N=3.

5.3.6 Preliminary investigation into alternative protein removal pathways

To determine if the intracellular SNAP-25 staining observed upon the MG-132 treatment was likely to be processed by an alternative removal pathway, western blotted extracts with LC-3 (autophagy), LAMP-2 (lysosomes) and RAB7 9 (late endosome) Appendix Figure C.3. These blots suggested that there was no upregulation of these pathways in the CSPα-deficient lines in comparison to the parental controls. Future work would need to be carried out to aid in our understanding of what these SNAP-25 structures formed in the presence of the proteasomal blocker MG132 (Figure 5.9).

5.3.7 Evidence of proteomic disorder in the CSPα-deficient cells

In the CSPα -/- mouse brain, there is increased ubiquitination of selective proteins such as SNAP-25 (Sharma et al., 2012a) but there is no overall increase in ubiquitination. To determine if there was evidence of altered proteostasis in the CSPα-deficient PC12 lines more widespread than CSPα's clients, Coomassie staining was undertaken for total protein and blotting was undertaken for ubiquitin.

Lysates from the Parental and the CSPα-deficient samples were run on an SDS-PAGE gel and stained with colloidal Coomassie and silver stain to allow for identification of changes in global protein between the samples (Figure 5.10, A). Line scans of both the Coomassie and the Silver stained (data not shown) display a consistent pattern across all of the samples. This suggests that overall, there isn't a global difference in the proteome between the Parental and CSPα-deficient cell lines. However, further close visual inspection identified changes in some of the major proteins stained by this approach across distinct sample types. The position of the consistent differences across replicated samples are marked by an asterisk (Figure 5.10, A and summarised Table 5.1).

Additionally, the samples were resolved for ubiquitin immunoreactivity; the CSPα-deficient samples had increased levels of immunoreactivity to ubiquitin when compared to the Parental control. Ubiquitin levels in CD3 were 14-fold higher and in CD5 were 8-fold higher than in the Parental lines (Figure 5.10, C) which is suggestive of a change in both cellular proteostasis and the overall state of the cell.

When lysates from the Parental and the CSPα-deficient lines were run on a western blot, it was noted that in the CSPα-deficient lines, there was the presence of non-specific staining by secondary antibodies in the stacking gel, which isn't present in the Parental line. This may be suggestive of the presence of aggregating or misfolding proteins that do not enter the separating gel in these lines (Figure 5.10, B).

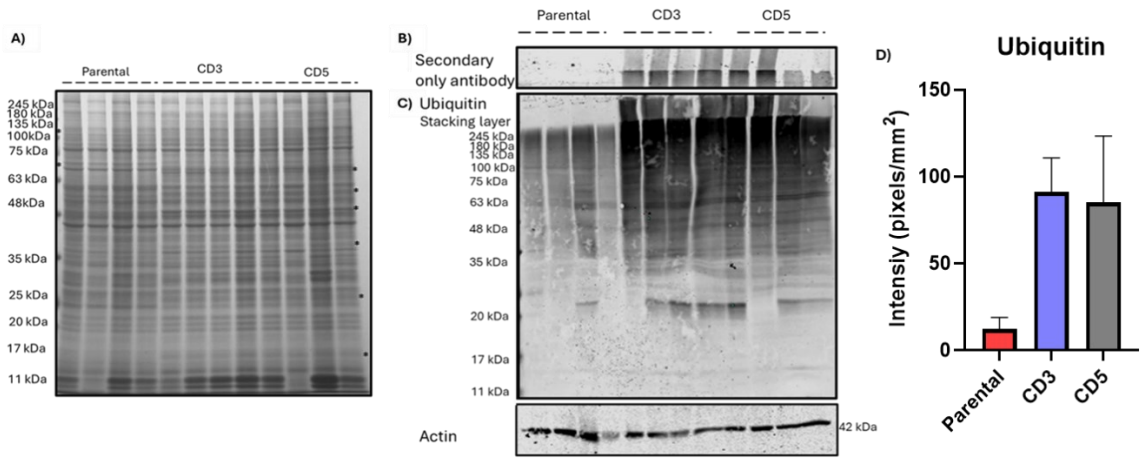

Figure 5.10: Investigation of global protein expression and relative ubiquitination in the PC12 CSPα-deficient CD3 and CD5 cells. A) Coomassie staining of the protein lysates. The major banding is similar between samples. Asterisks depict where replicated differentials are visualised in the Parental and PC12 CSPα-deficient CD3 and CD5 cells. B) Stacking gel with high molecular weight, potentially disordered protein present in PC12 CSPα-deficient CD3 and CD5 cells. C) and D) Ubiquitin levels in PC12 CSPα-deficient CD3 and CD5 lines are higher than in the Parental PC12 lines, N=4.

Table 5.1: Description of observed differentials between Parental and PC12 CSPα deficit CD3 and CD5 cells lysis run on a Coomassie gel.

Molecular weight	**Appearance/ disappearance in CRISPR lines**	**Description**
100 kDa	The upper band increases in intensity, and the disappearance of a lower band	The upper band becomes more defined, and the disappearance of a clear band below
~63-65 kDa	Disappearance	Doublet in Parental samples resolved to a less defined triplet in the CRISPR lines
~50 kDa	Appearance	Appearance of an undefined band
48 kDa	Appearance	Appearance of a defined band

~37 kDa	Appearance	Appearance of an undefined band
~25 kDa	Appearance	Appearance of an undefined band
17 kDa	Appearance	Appearance of a defined band
11 kDa	Differential expression of two bands across repeats of both the Parental and the CRISPR lines.	

5.3.8 Label-free proteomics to determine global changes in the CSPα-deficient cell lines

Due to the changes in the phenotype of the CSPα-deficient cells and unexpected changes identified by western blotting, whole cell proteomics was carried out. As the Parental and the Lenti CRISPR lines are alike in terms of phenotype and expression of CSPα, and its clients, proteomics were carried out comparing the Parental line to the two CSPα-deficient lines, CD3 and CD5.

Coomassie staining of all the pellet and supernatant (Methods section 2.8.2, Figure 2.12) confirmed that the majority of proteins present in the total cellular pool were present in the supernatant, suggesting good coverage of the total protein present in the samples. However, this analysis showed there is some differential in the pellet fraction within the same cell extraction, particularly at low molecular weights. This potential confound is highlighted by a triplet in the Parental line, which resolves to a doublet in both of the CSPα-deficient lines. At around 11 kDa, there is a large band inconsistently present in some samples of both the
Parental and the CSPα-deficient lines, which may be due to slight differences in solubilisation.

Peptides in the Parental, CD3 and CD5 identified by label-free mass-spectroscopy were analysed by PEAKS software (Methods section 2.8), which allowed for raw mass spectroscopy spectra to be analysed to identify candidate peptides. These were iterated through de novo sequencing, PEAKS DB (database searching)-based protein identification, PEAKS PTM (posttranslational modification) analysis, and a SPIDER homology search to identify the most likely peptide sequence that matches the given spectra.

This proteomic approach revealed a total of 412 proteins were altered between the Parental and the CPSα-deficient PC12 cell lines (CD3 and CD5), of which 253 proteins were upregulated and 159 proteins downregulated (see Appendix section C.4 for the full list).

5.3.8.1 Quantification and visualisation of Mass spectroscopy proteomic data

The heat map (Figure 5.11) displays the relative protein abundance in the control (Parental) and experimental conditions (CD3 and CD5) of proteins that passed the quality control filter, which excludes those designated peptides that fail to cross thresholds that resolve quality and quantity filtering (Section 2.8). The relative abundance in each condition is with respect to the abundance in the reference condition (Figure 5.11, Sample 1, first column Parental).

Altered proteins are clustered if they exhibit a similar expression across the samples, with the hierarchical clustering generated using a neighbour-joining algorithm with a Euclidean distance similarity measurement of log2 of the protein ratio of each sample relative to the average ratio.

The Heatmap displays individual proteins as either red, indicating upregulation, or green, indicating downregulation relative to Sample 1 (Figure 5.11, first column: Parental). The brighter the red or the green of a cell, the greater the fold change in the relative protein expression between the Parental and CPSα-deficient cell lines.

The alterations were consistent between repeats of the Parental, CD3 and CD5 cell lines. The CSPα-deficient cell lines were more alike to each other than the Parental and largely had similar changes in protein expression. In the case of CD3 sample 1 and for CD5 sample 2, there appears to be some disparity compared to the other samples of the same lines; an average of all samples in a group was taken in the final comparison of Parental to CSPα-deficient lines to assay overall relative protein change.

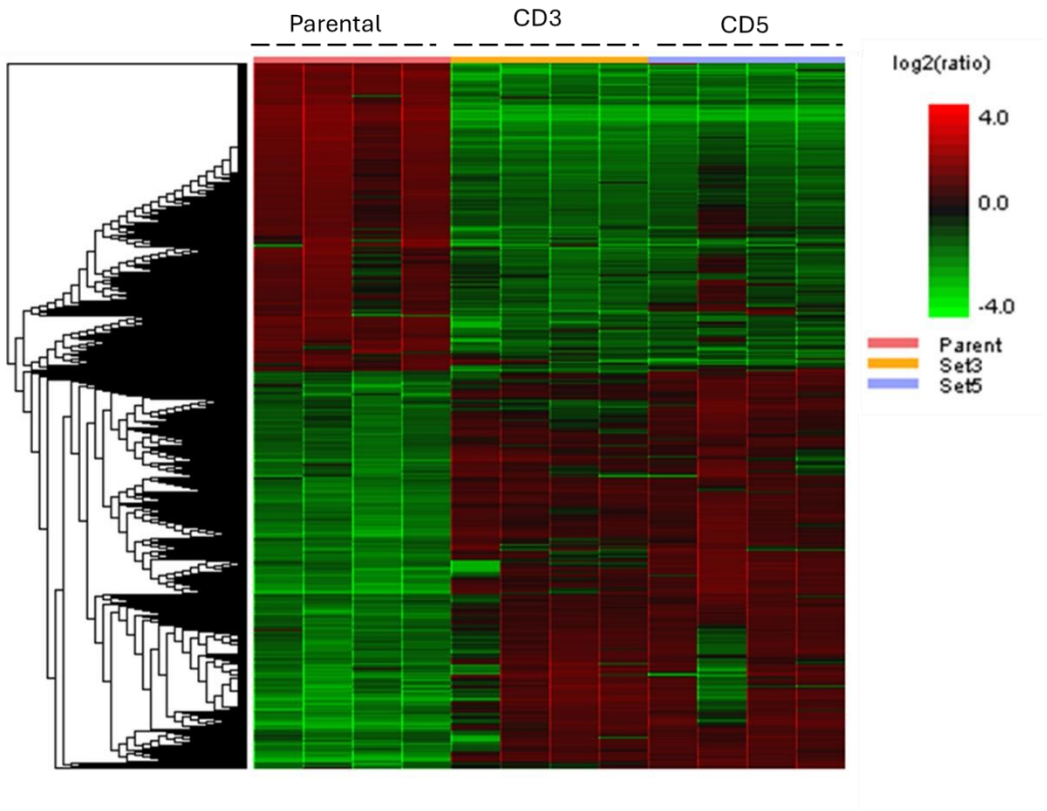

Figure 5.11: Quantitative mass spectroscopy profiling of PC12 Parental and PC12 CSPα deficit CD3 and CD5 cells

Protein profile heatmap cell colour represents the log2(ratio) to the average abundance across different samples from four independent Parental, and PC12 CSPα deficit CD3 and CD5 cells.

5.3.8.2 Statistical significance of quantified protein alterations

For analysis of the differential protein expression and visualisation on a volcano plot, the Parental line samples were grouped as control, and both the CSPα-deficient lines, CD3 and CD5, were grouped as the experimental group

The volcano plot plots significance versus fold-change of a quantified protein (Figure 5.12). The plot combines statistical significance with the magnitude of the change to enable visual identification of those data points that display a large magnitude change and are also statistically significant. The horizontal broken grey lines mark the selected significance threshold, set to 20, whilst the vertical broken grey line marks the selected fold change threshold set to 2-fold (Figure 5.12).

These lines separate the graph into regions, of which data points located in the top-right (Red) and the top-left (green) sections correspond to proteins which are both statistically significant (see

section 2.8.7.1) and beyond the set fold change threshold (see section 2.8.7.2), and as such represent proteins which are most likely to be quantifiably important.

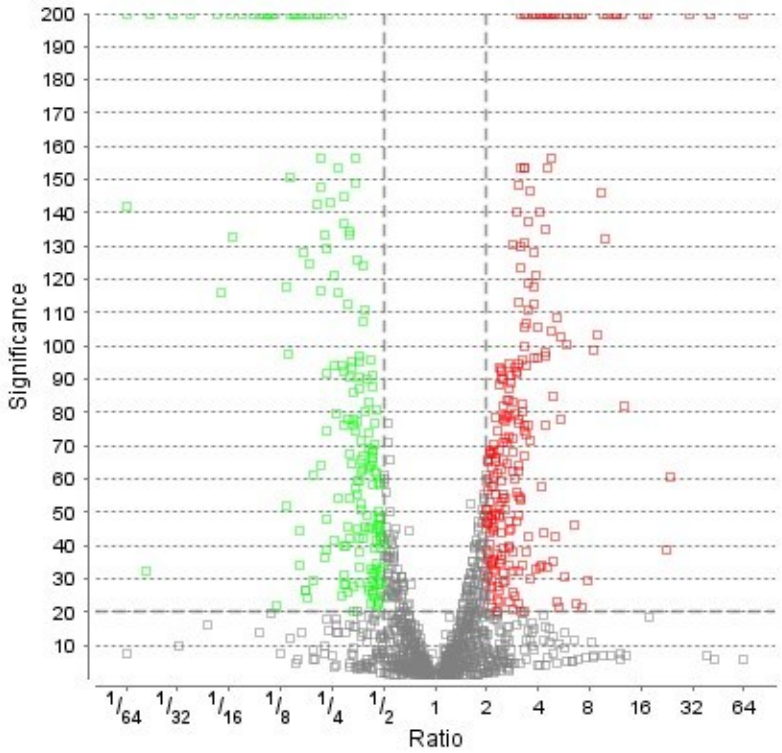

Figure 5.12: **CRISPR Cas knockout of CSPα leads to alteration of the expression of a large number of proteins.** Volcano plot for 2-fold down (green) and up (red) expressed proteins in CRISPR Cas CSPα-deficient PC12 cells compared to Parental control cells.

77 proteins had a 2-fold or greater alteration and had the maximum significance of 200, a further 61 with a significance between 100-200 and the remaining 274 proteins had a significance of between 20.10-100.

All proteins with a 2-fold or greater relative change and with a significance of between 20.10 and 200 were taken forward for subsequent interrogation and pathway analysis.

5.3.9 Investigation into GO term enrichment of up- and down-regulated proteins in CSPα-deficient PC12 cells

Initially, up- and down-regulated proteins were manually reviewed for their GO terms, for terms associated with biological functions that were of interest to investigate in the context of CSPαdeficiency. Alterations in Heat shock proteins were investigated as CSPα is a member of the Heat shock protein family, and in the CSPα -/- mouse, other Heat shock proteins are altered. CSPα

was the only member of the Heat shock proteins to be downregulated, whilst nine other heat shock proteins were upregulated in CD3 and CD5.

As blotting for ubiquitin showed an increase in the CD3 and CD5 lines, GO terms for ubiquitin associated proteins were investigated. Sixteen proteins were identified as being altered between the Parental and CD lines of these E3 ubiquitin ligases, hydrolases, modifiers and a proteasome regulatory subunit were altered. This could suggest that an upregulation of E3 ubiquitin ligase, a loss of hydrolases or a loss of regulation could all contribute to an overall increase in ubiquitin levels in the CSPα-deficient lines.

Lastly, due to the observed quantifiable increase in the cellular proliferation rate of the CSPαdeficient (CD3 and CD5) cell lines, proteins involved in proliferation were investigated. Six proteins were identified, which could, in part, lead to a dysregulation of cell proliferation in the CD lines (Table 5.2).

Table 5.2: Selected GO terms investigated due to the changes in phenotype observed in the CSPα-deficient lines, with the number of up- and down-regulated proteins with each GO term.

	Number of proteins with GO term	
GO term	**Up regulated**	**Down regulated**
Heat Shock Proteins- protein folding: GO:0031072	9	1
Ubiquitin associated: GO:0043130, GO:0016567, GO:0004842, GO:0061630	7	9
Proliferation and cell cycle GO:0008283, GO:0042127, GO:0051726	3	3

To unbiasedly identify enrichment in GO terms, both the up- and down-regulated lists of proteins were input into the Panther classification knowledgebase, which uses fold enrichment as a statistical measure to indicate the degree to which a specific phenotype is overrepresented in a particular gene or protein set. A fold enrichment of greater than one indicates overrepresentation, whilst greater than 100 indicates a strong overrepresentation.

Table 5.3 depicts the 20 most enriched GO terms for both the up- and down-regulated gene terms associated with the proteins identified as altered in the proteomics.

For down-regulated terms, two terms, regulation of late endosome to lysosome transport and the negative regulation of high voltage-gated calcium channel activity, have a fold enrichment of greater than 100. Both of these terms may be rationalised in terms of being affected by a loss of CSPα. A dysregulation of lysosomal homeostasis has previously been suggested in Neuronal ceroid lipofuscinosis caused by a lack of functional CSPα (Lee et al., 2022) Whilst CSPα has been shown to interact with N and P/Q type calcium channels (Ruiz et al., 2008, Lopez-Ortega et al., 2017). The rest of the top twenty include biosynthesis and metabolic processes (Table 5.3). which likely in part explains the alteration in proliferation rate observed (Section 5.3.3.1)

The upregulated terms have no enriched terms with a fold enrichment of greater than 100. The 20 GO biological processes that have the greatest fold enrichment are diverse, including terms corresponding to the introduction of the viral genome, regulation of signalling, metabolism, RNA localisation and chaperone-mediated protein folding (Table 5.3).

The GO term analysis revealed that the most upregulated GO terms involved the introduction of Viral components due to the use of a lentiviral plasmid to generate the CRISPR PC12 cell line (Table 5.3). Whilst using the Lenti Viral system allowed for stable knockdown of CSPα, using a viral system led to viral components being present in the cellular model, which can lead to insertional mutagenesis, whereby the vector may disrupt nearby genes, may cause aberrant splicing, cytotoxicity due to high viral loads or selection stress due to the requirement for the use of antibiotic resistance marker G418 (Shaw and Cornetta, 2014). Upregulation of GO terms relating to chaperone-mediated protein folding is expected since in response to the loss of one chaperone, other chaperone proteins are known to become upregulated (Saibil, 2013). Whilst the upregulation of signalling, metabolic pathways and RNA localisation, as well as the downregulation of biosynthesis and alternative metabolic processes, likely provides an explanation for the changes in cell states and phenotype observed and may be suggestive of a stressed cellular state.

Table 5.3 PANTHER Overrepresentation Test for enrichment of GO biological processes using Fisher's Exact. Displaying the top 20 enriched GO terms for the up- and down-regulated terms ranked by fold enrichment with corresponding raw P value and False Discovery Rate results for FDR $P < 0.05$.

Down regulation

Rank	GO biological process complete	Fold Enrichment	raw P value	FDR
1	Regulation of late endosome to lysosome transport	> 100	4.74E-05	5.92E-03
2	Negative regulation of high voltage-gated calcium channel activity	> 100	1.29E-06	4.52E-04
3	Glutamine catabolic process	96.5	1.42E-04	1.34E-02
4	Purine ribonucleoside diphosphate biosynthetic process	96.5	3.25E-08	2.59E-05
5	Purine nucleoside diphosphate biosynthetic process	96.5	3.25E-08	2.46E-05
6	Regulation of vacuolar transport	96.5	1.42E-04	1.33E-02
7	ADP biosynthetic process	86.85	3.20E-06	9.13E-04
8	Datp metabolic process	82.71	7.55E-08	4.75E-05
9	Isocitrate metabolic process	82.71	7.55E-08	4.56E-05
10	Negative regulation of hyaluronan biosynthetic process	72.37	2.82E-04	2.08E-02
11	Positive regulation of ryanodine-sensitive calcium-release channel Activity	*62.03*	*1.11E-05*	*2.39E-03*
12	Amyloid-beta clearance by transcytosis	62.03	1.11E-05	2.36E-03
13	Regulation of dopamine biosynthetic process	57.9	4.68E-04	3.02E-02
14	Adenine metabolic process	57.9	4.68E-04	3.01E-02

15	Purine deoxyribonucleoside triphosphate metabolic process	57.9	4.46E-07	1.87E-04
16	Ribonucleoside diphosphate biosynthetic process	52.64	6.97E-07	2.77E-04
17	Alditol biosynthetic process	48.25	6.99E-04	3.98E-02
18	Glutamate biosynthetic process	48.25	6.99E-04	3.97E-02
19	Asparagine metabolic process	48.25	6.99E-04	3.95E-02
20	UDP-alpha-D-glucose metabolic process	48.25	6.99E-04	3.94E-02

Upregulation

Rank	GO biological process complete	Fold Enrichment	Raw P value	FDR
1	Viral penetration into host nucleus	91.12	1.20E-04	9.39E-03
2	Entry of viral genome into host nucleus through nuclear pore complex via importin	91.12	1.20E-04	9.34E-03
3	Negative regulation of nitrosative stress-induced intrinsic apoptotic signalling pathway	91.12	1.20E-04	9.30E-03
4	Regulation of nitrosative stressinduced intrinsic apoptotic signalling pathway	91.12	1.20E-04	9.25E-03
5	Dendritic transport of messenger ribonucleoprotein complex	68.34	5.18E-06	5.84E-04
6	Glutamine catabolic process	60.74	3.57E-04	2.19E-02
7	Intracellular transport of virus	*60.74*	*3.57E*	*2.19E*
8	Telomere maintenance via semi-conservative replication	60.74	04	02

9	Positive regulation of establishment of protein localization to telomere	60.74	3.57E-04	2.17E-02
10	Transport of virus	60.74	3.57E-04	2.16E-02
11	Phosphocreatine metabolic process	45.56	7.09E-04	3.93E-02
12	Phosphagen metabolic process	45.56	7.09E-04	3.91E-02
13	Snorna localization	45.56	7.09E-04	3.90E-02
14	Mitochondrial translational elongation	45.56	7.09E-04	3.88E-02
15	Phosphagen biosynthetic process	45.56	7.09E-04	3.87E-02
16	Positive regulation by virus of viral protein levels in host cell	45.56	7.09E-04	3.86E-02
17	Phosphocreatine biosynthetic process	45.56	7.09E-04	3.84E-02
18	Positive regulation of nuclease activity	39.05	4.43E-05	3.86E-03
19	Chaperone mediated protein folding independent of cofactor	34.17	7.02E-05	5.86E-03
20	Positive regulation of Telomerase RNA localization to Cajal body	30.37	1.04E-04	8.40E-03

5.3.10 Pathway analysis of proteomic changes in CSPα-deficient cells

The STRING database, which compiles and integrates protein-protein association data, was used to visualise protein association clustering of the proteins altered in the label-free proteomics.

Of the 412 proteins altered in the label-free mass spectroscopy, 159 downregulated and 253 upregulated were mapped with the STRING network database to allow for clustering analysis. In the downregulated string clustering analysis, we see the pathway with the most downregulated members is the citrate acid cycle and regulation of calcium ions into the cytosol (Figure 5.13). In the upregulation string clustering analysis, we see that the most upregulated pathways are splicing factors, followed by protein folding factors (Figure 5.16).

5.3.10.1 Pathway analysis of downregulated proteins

The most downregulated clusters included components of isocitrate metabolism, 2oxocarboxylic acid metabolism and the Citric acid cycle (TCA cycle), which are three interconnected metabolic pathways that are involved in energy production and biosynthesis (Figure 5.13).

A)

color	cluster Id	gene count	description
	Cluster 1	5	- 1. Isocitrate metabolism 2. 2-Oxocarboxylic acid metabolism 3. Citric acid cycle (TCA cycle)
	Cluster 2	5	Regulation of release of sequestered calcium ion into cytosol by sarcoplasmic retic...
	Cluster 3	4	RHO GTPases activate IQGAPs
	Cluster 4	4	Translation initiation complex formation
	Cluster 5	3	U1 snRNP
	Cluster 6	3	- 1. 1-alkyl-2-acetylglycerophosphocholine esterase complex 2. Platelet-activating factor acetyltransferase activity
	Cluster 7	3	UBX domain, and UFD1-NPL4 complex
	Cluster 8	3	- 1. TBC/RABGAPs 2. Mixed, incl. Golgi vesicle fusion to target membrane, and GDP/GTP exchange factor Sec2p
	Cluster 9	3	Early phagosome
	Cluster 10	3	Podosome
	Cluster 11	3	Retromer complex

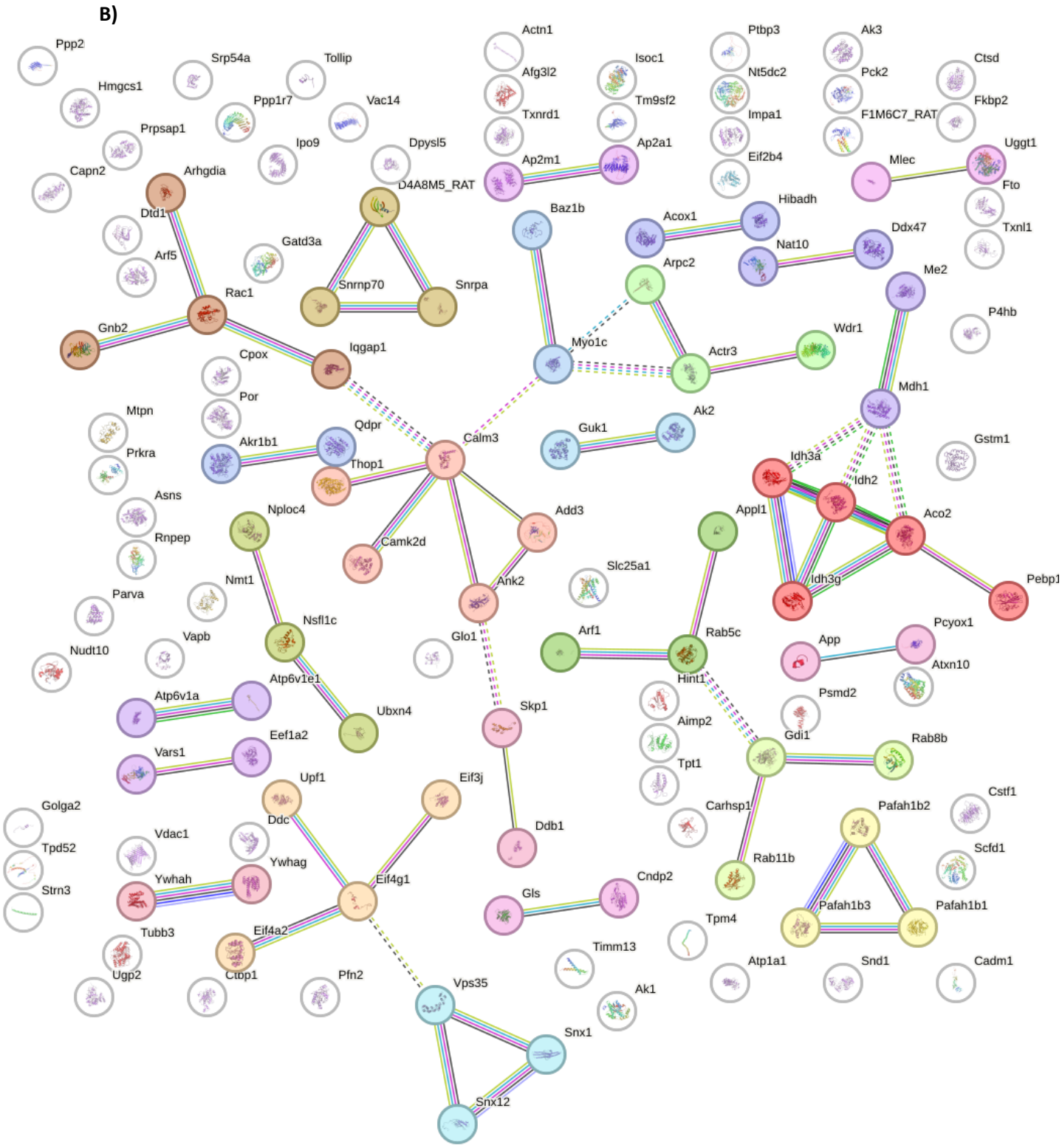

Figure 5.13: STRING clustering of down-regulated alterations between Parental and PC12 CSPα-deficit CD3 and CD5 cells with the high-confidence evidence-based analysis applied. A) Tabulation of down-regulated clusters altered in the PC12 CSPα-deficient CD3 and CD5 cells, with the number of members and cluster description and a schematic of STRING Pathway clusters for proteins down-

regulated in the CSPα-deficient lines. B) Graphical representation of STRING Clustering between down regulated proteins.

5.3.10.2 Pathway analysis of upregulated proteins

In the upregulated STRING analysis, the clusters largely fell into four Groups: 1. mRNA processing, 2. Protein folding, 3. DNA transcription, translation and processing and 4. Protein translocation (Figure 5.14).

The highest-ranking cluster with 28 members (Figure 5.13) was made up of mRNA splicing and spliceosome factors. This could be thought to be an unintended consequence of CRISPR Cas, which can induce off-target effects that impact mRNA splicing, exon skipping and alternative splicing (Mou et al., 2017, Chen et al., 2018, Zhang et al., 2020). Or it could be due to increased cellular stress (Biamonti and Caceres, 2009, Cui et al., 2024)

In addition to the highest-ranked cluster, other clusters ranked in the top ten also involved the regulation of RNA. The third most enriched cluster consists of RNA-binding proteins involved in promoting mRNA stability and preventing its degradation. The fourth was formed of the preribosome and DEAD/DEAH box proteins involved in the unwinding and rearrangement of RNA structures. Whilst Cluster 10 was formed of the supra-spliceosomal complex and proteins containing a double-stranded RNA binding motif.

The second most up-regulated cluster was protein folding and unfolded protein binding. This is expected due to CSPα's chaperoning role of binding to unfolded proteins and the precedent of other chaperone binding proteins to be up regulated upon the loss of one member (Zhang et al., 2012).

Four clusters largely group into upregulation of DNA processing, including cluster 5, Nuclear DNA replication, cluster 6, formation of the ternary complex and 43 complex, cluster 7, TP53 regulates transcription of DNA repair genes and RNA polymerase II transcription elongation and cluster 11, the Krüppel-associated box category of transcriptional repression domains.

Lastly, both Cluster 9 Nucleocytoplasmic carrier activity and Cluster 12 protein targeting to the mitochondrion and translocation are involved in the transport of protein around the cell.

All four of these groups can be upregulated during cellular stress, including mRNA splicing and DNA processing to facilitate repair and maintain genome stability, which is critical for adapting gene expression during cellular stress to maintain cellular homeostasis (Naro et al., 2015, Ainslie et al., 2015, Wickramasinghe and Venkitaraman, 2016). Similarly, an increase in unfolded protein binding

and increased protein translocation can also be a consequence of increased cellular stress in an attempt to maintain homeostasis (Kang et al., 2006, Read and Schröder, 2021).

The last cluster, cluster 8, alpha-amino acid biosynthesis, may still be altered due to overall cellular stress as it is an adaptive response that is seen to be altered during the ER stress response, triggered by protein misfolding (Gonen et al., 2019).

A)

color	cluster Id	gene count	description
	Cluster 1	28	- 1. mRNA splicing, via spliceosome 2. Spliceosome
	Cluster 2	11	- 1. Protein folding 2. Unfolded protein binding
	Cluster 3	11	RNA recognition motif domain, and CRD-mediated mRNA stability complex
	Cluster 4	8	Mixed, incl. Preribosome, and DEAD/DEAH box helicase domain
	Cluster 5	7	Nuclear DNA replication
	Cluster 6	6	Formation of the ternary complex, and subsequently, the 43S complex
	Cluster 7	6	- 1. TP53 Regulates Transcription of DNA Repair Genes 2. RNA Polymerase II Transcription Elongation
	Cluster 8	5	Alpha-amino acid biosynthesis
	Cluster 9	4	- 1. Nucleocytoplasmic carrier activity 2. NLS-dependent protein nuclear import complex
	Cluster 10	4	- 1. Supraspliceosomal complex 2. Double-stranded RNA binding motif
	Cluster 11	4	Krueppel-associated box domain binding
	Cluster 12	4	- 1. Protein targeting to mitochondrion 2. Translocation

B)

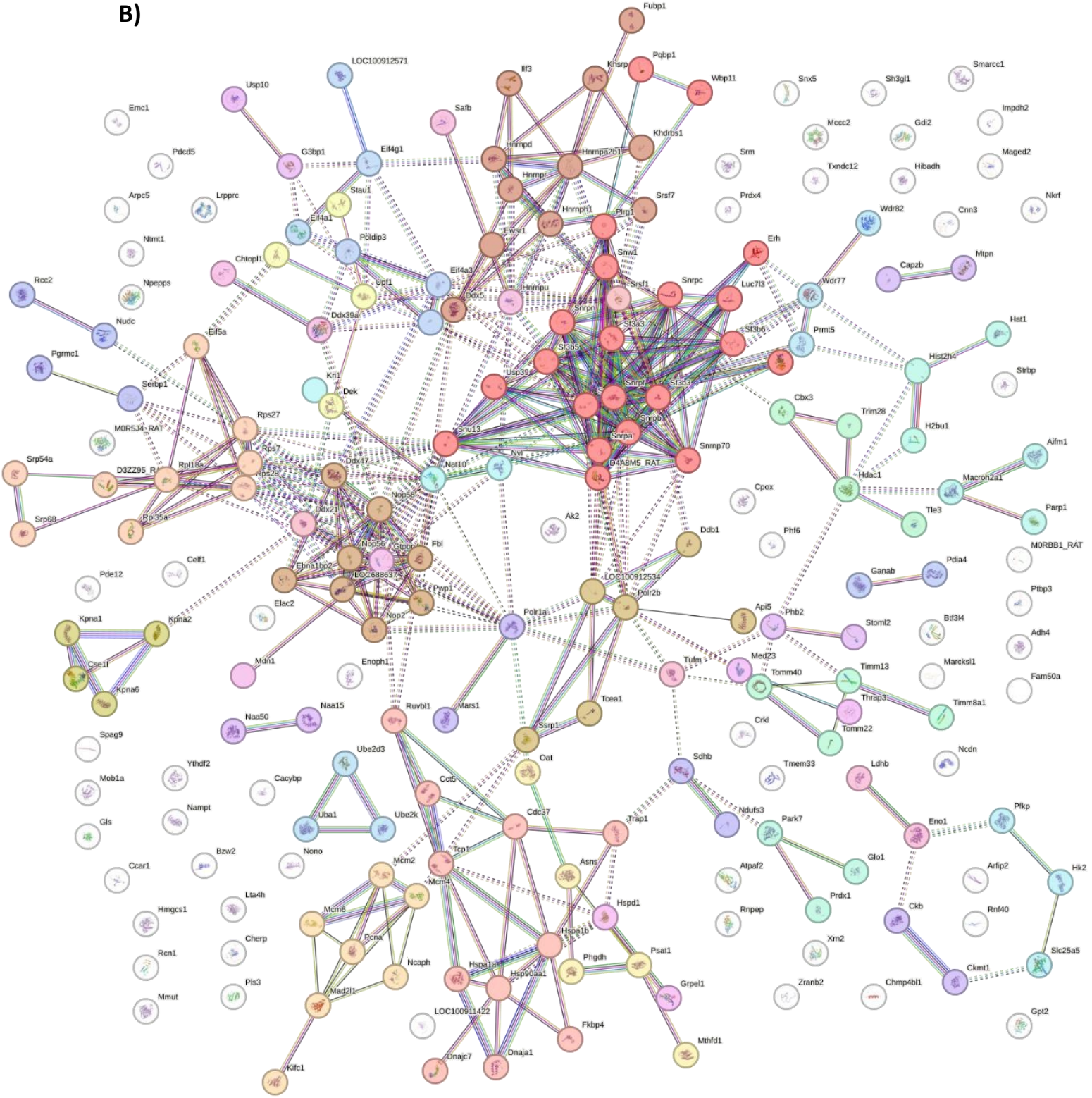
Fubp1
LOC100912571
Ilf3
Khsrp
Pqbp1
Wbp11
Usp10
Safb
Emc1
Hnrnpd
Hnrnpa2b1
Khdrbs1
Pdcd5
G3bp1
Eif4g1
Hnrnpr
Srsf7
Arpc5
Lrpprc
Stau1
Hnrnph1
Plrg1
Eif4a1
Ewsr1
Poldip3
Ntmt1
Chtopl1
Snw1
Rcc2
Npepps
Upf1
Eif4a3
Srsf1
Snrpc
Luc7l3
Ddx5
Hnrnpu
Nudc
Ddx39a
Snrpn
Sf3a3
Eif5a
Sf3b5
Sf3b6
Prmt5
Pgrmc1
Usp39
Snrpf
Sf3b4
Serbp1
Kri1
Dek
Rps27
Snrpb
M0R5J4_RAT
Snu13
Snrpa
Snrnp70
Srp54a
Rps7
Nyl1
D4A8M5_RAT
D3ZZ95_RAT
Rpl18a
Ddx47
Nat10
Rps26
Nop56
Srp68
Ddx21
Rpl35a
Gtpbp4
Fbl
Ebna1bp2
LOC688637
Pwp1
Celf1
Pde12
Elac2
Nop2
Ddb1
LOC100912534
Polr2b
Polr1a
Kpna1
Kpna2
Cse1l
Kpna6
Mdn1
Enoph1
Naa50
Naa15
Ruvbl1
Mars1
Tcea1
Ssrp1
Spag9
Ube2d3
Oat
Ythdf2
Mob1a
Cacybp
Cct5
Gls
Nampt
Uba1
Ube2k
Cdc37
Trap1
Bzw2
Nono
Tcp1
Ccar1
Mcm2
Asns
Mcm4
Lta4h
Hmgcs1
Mcm6
Hspd1
Pcna
Hspa1b
Cherp
Rcn1
Ncaph
Psat1
Hspa1a
Phgdh
Pls3
Hsp90aa1
Grpel1
Mad2l1
Mmut
LOC100911422
Fkbp4
Mthfd1
Dnajc7
Dnaja1
Kifc1
Sdhb
Ndufs3
Park7
Glo1
Prdx1
Atpaf2
Rnpep
Xrn2
Zranb2
Chmp4bl1
Ckmt1
Slc25a5
Ckb
Rnf40
Eno1
Pfkp
Hk2
Arfip2
Ldhb
Tmem33
Ncdn
Gpt2
Api5
Phb2
Stoml2
Btf3l4
Adh4
Fam50a
Ptbp3
M0RBB1_RAT
Pdia4
Ganab
Phf6
Tle3
Parp1
Macroh2a1
Aifm1
Hdac1
Cpox
Cbx3
Trim28
H2bu1
Hist2h4
Strbp
Hat1
Wdr77
Capzb
Mtpn
Wdr82
Cnn3
Nkrf
Erh
Srm
Txndc12
Hibadh
Maged2
Mccc2
Gdi2
Impdh2
Snx5
Sh3gl1
Smarcc1
Ak2
Med23
Tomm40
Timm13
Thrap3
Timm8a1
Tomm22
Crkl
Tufm
Marcksl1

Figure 5.14: STRING clustering of up-regulated alterations between Parental and PC12 CSPα deficit CD3 and CD5 cells. A) Tabulation of upregulated clusters altered in the PC12 CSPα deficit CD3 and CD5 cells, with the number of members and cluster description. B) Schematic of STRING Pathway clusters for proteins upregulated in the CSPα-deficient lines.

For the upregulated STRING analysis, 40 clusters were identified, the highest ranked containing 28 proteins, down to only 1 member as such clusters with 3 or fewer members were excluded due to the thought that whilst STRING clusters with few members can be relevant the larger clusters generally offer more robust insights and due to the number of proteins altered it would be more appropriate to focus on larger clusters to help understand distinct characteristics in the dataset (Figure 5.14).

5.3.10.3 Verification of the reported downregulated protein

Western blotting was used to confirm the down and up-regulation of a selection of proteins identified by the label-free proteomics. Proteins were chosen based on their being part of the most enriched clusters from the pathway analysis, or due to being classified as proteins with a shared function as CSPα (in the case of the heat shock proteins) or due to being associated with unexpected GOterms such as translation and splicing factors. CSPα and EEEF1α2 (translational factor) were tested as shown to be downregulated, and HSP90, HSP40 (Heat-shock family proteins), DJ-1 (One of only a few unregulated neuronal proteins) and SRSF3 (Splicing regulator) were tested as being upregulated. Whilst additional proteins should be validated, this selected list was validated due to time constraints and antibodies that were validated for use in PC12 cells.

CSPα immunoreactivity was present at 36 kDa in the parental and the Lenti CRISPR but was undetectable in the CD lines. Whilst the Eukaryotic translation elongation factor 1 alpha-2 (EEF1α2) was detected to be one of the proteins with the greatest downregulation in the CD lines compared to Parental in the label-free proteomics, which was validated by western blotting with strong immunoreactivity in the parental and Lenti CRISPR lines but only faint immunoreactivity in CD3 and unquantifiable expression in CD5. EEF1α2 is involved in protein synthesis, particularly in the transport of tRNAs (Andersen et al., 2003, Voorhees and Ramakrishnan, 2013, Dever et al., 2018). EEF1α2 has been associated with neurodevelopmental disorders, and disruptions in both EEF1α2 and CSP lead to neuronal dysfunction; as such, their functions could intersect during cellular stress (Davies et al., 2020, De Rinaldis et al., 2020, Mohamed and Klann, 2023) (Figure 5.15).

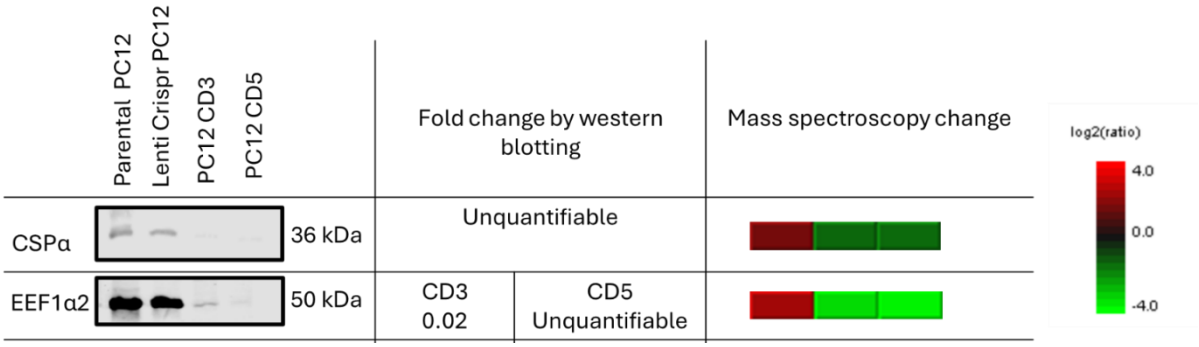

Figure 5.15: Validation of proteins downregulated due to the CSPα CRISPR knockdown in the PC12 cells, determined by Mass spectroscopy Column 1) 20ug of undifferentiated PC12 lysates of Parental, Lenti CRISPR and CD3 and CD5 (40 ug in the case of differentiated Parental and Lenti CRISPR lysate for CSPα) were run on an SDS-PAGE gel and labelled with CSPα and EEF1α2 antibodies by western blotting. Column 2) Loading was normalised to GAPDH or Actin, and changes were quantified. Column 3) log2 (ratio) change determined by mass spectroscopy, N=3.

5.3.10.4 Verification of the reported upregulated proteins

The most enriched upregulated clusters were made up of mRNA splicing and spliceosome factors. Serine/Arginine-rich Splicing Factor 3 (Srsf3), which is involved in RNA splicing and mRNA export, was one of the proteins with the greatest changes determined by the label-free proteomics, and part of the highest-ranked cluster. Srsf3 was blotted for in the Parental, Lenti CRISPR and CSPα-deficient lines. Srsf3 was undetectable in the Parental and Lenti CRISPR lines but was upregulated in both the CD lines with immunoreactivity at 20 kDa (Figure 5.15). There have been no links between CSPα and SRSF3, yet both function to maintain cellular homeostasis (Xiong et al., 2022); as such, it is conceivable that loss of CSPα protein chaperoning ability, leading to cellular stress, could lead to an alteration in splicing factor expression and processes. If other splicing factors were affected in the same way, this may suggest that an upregulation in splicing may, in fact, be a consequence of CSPα loss, but further work would need to be undertaken for this to be confirmed.

The second most upregulated protein cluster was protein folding and unfolded protein binding, of which the Heat shock proteins made up a majority of the class. Whilst CSPα was downregulated, 9 other Heat shock proteins were upregulated. Including both HSP90 and HSP40, which was also observed by Western blot. Potentially suggestive of a compensatory effect of chaperone proteins as observed in other CSPα knockout models.

Neuronal-specific proteins overall were not observed to be upregulated in the CD3 and CD5 lines (Syngo analysis Appendix C.5). However, DJ-1 is one of the only neuronal-specific proteins that was upregulated in the CD lines by proteomics and western blot. It has a role in various cellular processes, including in oxidative stress and mitochondrial function (Junn et al., 2009).

DJ-1 upregulation has been implicated in Parkinson's disease, where it is triggered in response to oxidative stress (Ariga et al., 2013). Blotting for DJ-1 revealed it was undetectable in the Parental and the Lenti CRISPR line but immunoreactivity was present at 22 kDa in the CD3 and CD5 lines (Figure 5.16).

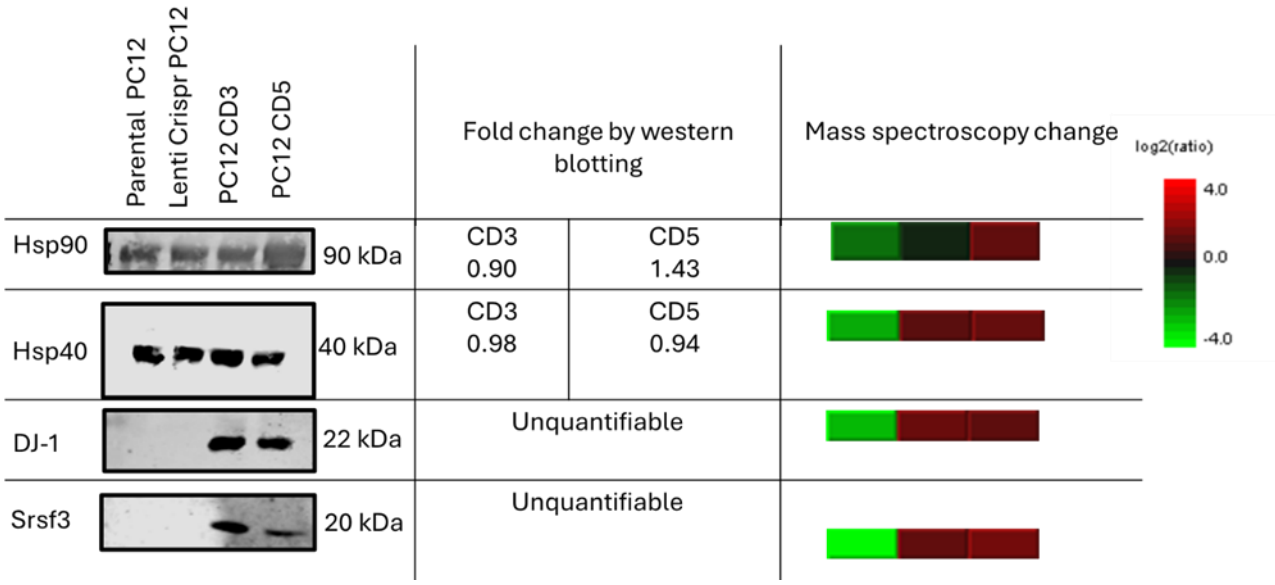

Figure 5.16: Validation of proteins upregulated due to the CSPα CRISPR knockdown in the PC12 cells, determined by Mass spectroscopy Column 1) 20ug of undifferentiated PC12 lysates of Parental, Lenti CRISPR and CD3 and CD5 cells were run on an SDS-PAGE gel and labelled with antibodies by western blotting for upregulated proteins. Column 2) Loading was normalised to GAPDH or Actin, and changes were quantified. Column 3) log2 (ratio) change determined by mass spectroscopy, N=3.

The fact that Parental and Lenti CRISPR appear unaltered in both the down- and upregulated proteins that were blotted for suggests these changes are likely due to the CSPα deficiency and not due to the presence of the CRISPR Cas machinery.

5.4 Discussion

5.4.1 Summary

Here, I have generated two CSPα-deficient PC12 lines using CRISPR Cas technology with both expected and unexpected consequences for cellular proteostasis. In addition to a downregulation in the levels of CSPα and its clients' SNAP-25 and Dynamin-1, it was also observed that cells proliferated at an increased rate and lost their ability to differentiate upon stimulation with neurotrophins. Increased levels of ubiquitination and altered proteostasis were also observed, suggestive of the generation of a stressed cellular state.

Label-free proteomic data obtained from comparison of the Parental and CSPα-deficient cell lines identified changes in the relative expression of 412 proteins. To help refine understanding, I performed bioinformatics and used two approaches 1) GO term enrichment and 2) Network association of the altered proteins. This elucidated biological pathways and mechanisms that are altered in a PC12 CSPα-deficient environment

This revealed both expected and unexpected altered pathways that signatured stress, translation, splicing, regulation of late endosomal to lysosomal transport and regulation of calcium channel activity in the face of the CSPα modulation of cell phenotype. These results are surprising and provide new insights into the additional roles of CSPα. In particular, they associate CSPα with having functional consequences on the proliferating cell state. However, further studies would be required to confirm these findings and determine the cause of the difference observed between these PC12 and other pre-mitotic cell models and CSPα knockout mouse, fly and neuronal models.

5.4.2 Observed changes in phenotype in CSPα-deficient PC12 cells

The generation of two lines from two separate guides that produced the same observed phenotype and the fact that the Lenti CRISPR control is phenotypically the same as the Parental line is reassuring that the changes seen are due to the targeted knockout of CSPα and not an indirect effect of the CRISPR Cas or off-target effects (Section 5.3.3). It was suggested that a possible additional interpretation for the unexpected phenotype changes observed could be due to infection of another cell type. This was investigated by amplifying and sequencing SNAP-25 the knockdown lines (Figure 5.3) with the sequence of both corresponding to the Rat sequence which differs from Human which rules out contamination from lines such as Hela and HEK293 cells. This and the presence of no other Rat cell lines in the facility provides support for the cell lines likely being of PC12 origin.

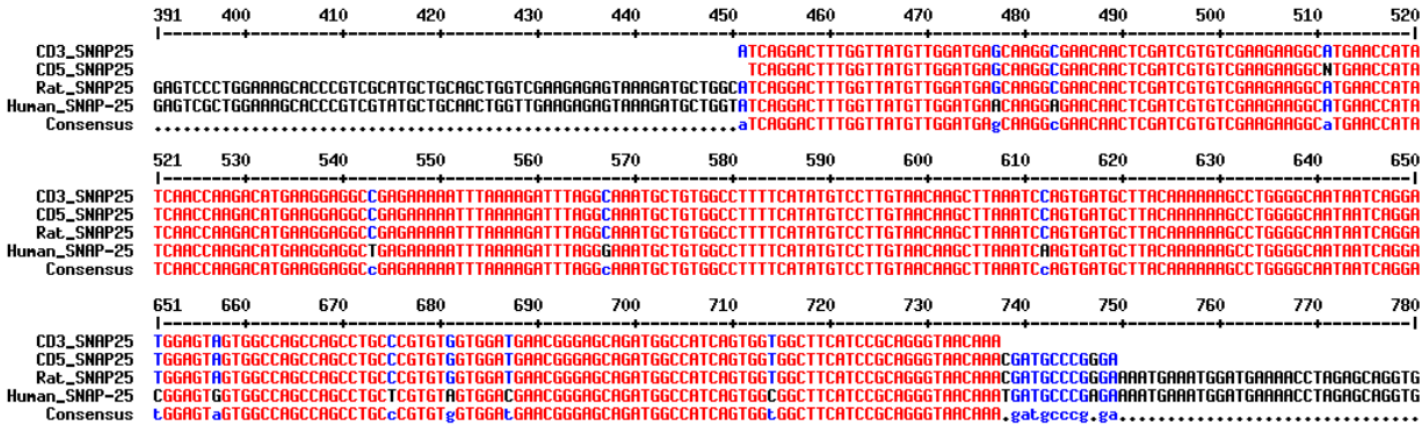

Figure 5.17: Both CD3 and CD5 SNAP-25 sequences align to RAT SNAP-25. A region of SNAP-25 was amplified from both CD3 and CD5 and sent for Sanger sequencing. The sequences were then aligned to both Rat and Human SNAP-25 sequences with both aligning to the Rat sequences with no mismatches (one N-unread base in the case of CD5) but with multiple mismatches compared to the human sequence.

5.4.2.1 Alteration in Trk and EGF receptor expression in CSPα models

The most obvious ways that the controls and the CSPα-deficient cells differ are in their proliferative phenotypes (Figure 5.4) and their lack of ability to differentiate (Figure 5.5). This led to the investigation of Trk and EGF receptor expression levels (Figure 5.6) (Patapoutian and Reichardt, 2001). A reduction in TRK B in the CSPα-deficient model would suggest that not only does CSPα influence presynaptic neurotransmitter release via regulation of SNARE complex assembly, but it may also have a role in neurotrophin signalling or receptor maintenance. This could also be explained by the alteration in endosomal to lysosomal transport (Section 5.3.9), leading to an alteration in the way the TRK and EGF receptors are expressed, recycled and transduce signals (Chen et al., 2005, Moises et al., 22009, Sapmazand Erson-Bensan, 2023).

Blotting for TrkB, total TrK and EGFR in CSPα -/- mouse tissue revealed that in this model, there is no disruption in expression of these receptors. A caveat of this is that in the tissue, not all cell types may express CSPα, so an effect may be less evident. The fact that the expression of Trk and EGF receptors differs between the mouse tissue and in these two CSPα-deficient PC12 lines may be explained by the fact that there is mounting evidence that CSPα has cell-type specific functions (Section 5.3.4, Figure 5.6).

5.4.2.2 Loss of HSP40 proteins affecting the stability of other proteins

HSP40 chaperones have been shown to play a role in regulating the folding and stability of other receptors, such as the hERG Potassium Channels (Walker et al., 2010) and Androgen Receptor (Eftekharzadeh et al., 2019). A loss of CSPα in both this PC12 model and in CSPα -/- mice has been shown to lead to an alteration in the expression of other HSP family members, which could lead to the dysregulation of chaperoning and improper folding of clients (Y.-Q. Zhang et al., 2012).

5.4.2.3 CSPα's role in cellular proliferation

There is precedent for the removal of CSPα affecting cell proliferation in actively dividing cells. CSPα -/- mouse hippocampal radial glia-like (RGL) neural stem cells, postnatally lose quiescence and experience a period of increased proliferation (Nieto-González et al., 2019). Work in culture led to the identification that in the absence of CSPα, led to the hyperactivation of the mechanistic target of rapamycin (mTOR) signalling pathway causing deregulation of neurogenesis (Nieto-González et al., 2019).

Whilst in lung adenocarcinoma, a highly malignant tumour with aberrantly activated EGFR signalling, CSPα acts as an oncogene, whereby overexpression promotes proliferation and migration. CSPα was shown to interact with EGFR via its cystine string domain, enhancing its endocytosis and recycling (Chen et al., 2025) this could potentially help to explain why we observe an increase in EGFR when we knock down CSPα. CSPα also binds to AP2A1, strengthening the EGFR interaction. AP2A1 inhibits proliferation by promoting a senescent state, and its knockdown has been observed to increase the proliferative capacity of cells (Chantachotikul et al., 2025). This is of interest as AP2A1 was noted to be downregulated in the label-free proteomics carried out here and is involved in the recruitment and activation of CSPα client DYN-1 to the site of vesicle formation during clathrin-mediated endocytosis (Fiuza et al., 2017). Finally, AP2 and α-synuclein have been shown to interact, regulating binding to synaptic membranes and it has been hypothesised that malfunction in α-synuclein could lead to a deficit in the initial stages of clathrin-mediated synaptic vesicle endocytosis, which affects synaptic viability (Vargas et al., 2025). This is of interest since mounting evidence links αsynuclein and CSPα (Wu et al., 2023, Caló et al., 2021) and the fact that expression of αsynuclein abolishes the lethality and neurodegeneration in CSPα -/- mice, which has been in part explained by a partial restoration of SNARE complex levels and increased expression of HSC70 and HSP70 (Chandra et al., 2005) but it is feasible there could also be a link to AP2A1, Dyn-1 and clathrin-mediated synaptic vesicle endocytosis.

Whilst the observations of an upregulation of proliferation in the CSPα-deficient PC12 lines were unexpected in the context of CSPα as a presynaptic chaperone. In non-neuronal cell types, our findings, alongside Nieto-González et al demonstrate a cell-autonomous disruption of neurogenesis in the absence of CSPα (As introduced in section 1.5.10). This opens a new avenue to investigate the role of CSPα and highlights a link between receptor maintenance and signalling-dependent cascades resulting in hyperproliferation and a loss of neuronal differentiation upon its loss.

5.4.3 Proteomic investigation into the result of a knockdown of CSPα in the PC12 cells

Whilst 412 proteins were identified as being altered between the Parental and the CSPαdeficient lines (Section 5.3.8), SNAP-25 and TrkB, which were identified as being reduced in the CSPα-deficient lines by western blot, were not identified as being altered in the proteomics (Figures 5.6 and 5.7). There are several potential reasons an expected protein may not be detected in the label-free mass spectroscopy readout. These include factors such as a protein's solubility, stability or amino acid composition; additionally, the size of the digested peptide can affect the ability to be effectively detected (Szabo and Janaky, 2015). Misfolding of proteins can also affect a protein's structure and properties, which can affect its digestion and the detection of the resulting peptide. In the case of SNAP25, palmitoylation, or potentially misfolded or aggregated SNAP-25 in the CSPα-deficient cells may affect the ability to be detected by mass spectroscopy (Greaves et al., 2010, Sharma et al., 2012). For proteins to be included in the label free mass spectroscopy analysis peptides of a certain protein had to be present in both the control (Parental) and the CSPα deficient lines, so there is the possibility that SNAP-25 and the Trks are present in such low levels in the CSPα deficient lines that they were excluded due to the presence of peptides not being above the limit of detection in all conditions.

5.4.3.1 Protein changes in CSPα deficiency determined by label-free proteomics

A total of 412 proteins were altered between the Parental and the CPSα-deficient PC12 cell lines, of which 159 proteins were down-regulated and 253 proteins up-regulated. Although this is a large-scale alteration, it is not without precedent. Work at the transcription level of CSPα knock-out synapses identified 1,772 differentially expressed genes (Wang et al., 2024). In this study, it was noted that there was a downregulation of neuronal clusters and in synapse organisation pathways with a decrease in synaptic density. The analysis here clearly identifies a loss of neuronal phenotype in a distinct context, as the neuronal and synaptic signature is reduced when levels of CSPα are reduced from an already low level in the parental cells. Leading to the loss of differentiation and

downregulation of synaptic signatures observed in the PC12 CD lines (Section 5.3.3, Appendix figure C.5), suggesting neuronal repression.

5.4.3.2 Comparison of proteomic readout with previous CSPα knockout studies

In a proteomic study carried out by Zhang et al in CSPα -/- synapses utilising DIGE (2D fluorescence Difference Gel Electrophoresis) and iTRAQ (Isobaric Tag for Relative and Absolute Quantitation), 1,500 proteins were identified in total. With 37 were downregulated more than 40% (Table 1.2 adapted from Zhang et al., 2012), and 22 proteins were verified by western blot. Of these 22, 13 were also identified as being altered in the label-free proteomics carried out here in the PC12 cells. The most downregulated group of proteins altered was the chaperones, which were also identified as being among the most altered in our proteomics (Section 5.3.10).

This suggests that an upregulation of the stress response is common in response to loss of CSPα in distinct contexts (Zhang et al., 2012).

5.4.3.3 GO term and pathway analysis of up and downregulated proteins in the CSPαdeficient cells relating to an increase in proliferation

The pathways analysis revealed, unexpectedly, that the most upregulated pathways were the regulation of RNA splicing and spliceosome components (Figures 5.13 and 5.14). CSPα is involved in proteostasis and its knockout is likely to cause cellular stress, leading to activation of the UPR and Integrated Stress Response (ISR) pathways, as characterised by an upregulation of ubiquitin-related proteins. These pathways have been shown to induce proliferation and splicing, so it is possible that the splicing component upregulation is the result of activation of cellular stress and proliferation and not directly linked to CSPα. This is further supported by the fact that most of the up-regulated splicing-associated genes identified have been linked to proliferation. Generally, more splicing activity is seen in highly proliferating cell cultures due to splicing playing a role in regulating cell cycle progression (Bradley and Anczukow, 2023).

Alterations in transcription factors were also observed. An enrichment for E2F transcriptional factors in both the up- and down-regulated protein lists is also likely to be linked to the proliferative phenotype observed, since these factors regulate much of the cell cycle progression (Helin, 1998, Ren et al., 2002, DeGregori, 2002).

5.5 Future work

In addition to understanding the molecular CRISPR events in CD3 and attempting to understand the SNAP-25 structures generated in the presence of proteasomal blocker MG-132, as discussed above. Future work could be undertaken to understand the role a lack of CSPα has in cellular stress and PC12 differentiation. This may include attempting to rescue the loss of NGF responsiveness and carrying out further investigations into a potential link between CSPα and modulation and recycling of Trk and EGF receptors.

Chapter 6 General discussion and future directions

The issue of protein misfolding and proteostasis is crucial to cellular function and is often dysregulated in human diseases (Zheng et al., 2016; Cheon, Dean, and Chahrour, 2019). The Cystine string protein-alpha has been well-characterised as a presynaptic co-chaperone, essential for the maintenance of synapses and presynaptic proteostasis (Chandra et al., 2005, Sharma et al., 2012, Sheng and Wu, 2012, Zhang et al., 2012). Here I have investigated CSPα to further our understanding of proteostasis using PC12 cells as a model system.

6.1 Summary of findings

The initial aim of this thesis, largely driven by existing evidence, was to investigate synaptic proteostasis using CSPα and its absence to identify proteins involved in the degradation of SNAP-25. This was done firstly by investigating potential E3 ligases involved in the ubiquitination of SNAP-25. This was achieved via a bioinformatics approach (Chapter 3) and experimentally using BioID protein proximity labelling and Myc immunoprecipitation approaches using a Myc-BioID-SNAP-25 construct as bait (Chapter 4). This identified an interaction between SNAP-25 and the E3 ubiquitin ligase Parkin.

Secondly, generating and characterising a CSPα-deficient PC12 cell model revealed that although the downstream effects on SNAP-25 protein expression were consistent with previously reported outcomes, the CRISPR-mediated knockdown in CSPα resulted in an unexpected dysfunctional differentiation and proliferation in the CSPα-deficient cells (Chapter 5).

Although initiated to investigate how CSPα deficiency couples to synaptic proteostasis, the production and characterisation of two CPSα-deficient PC12 cell lines opened up unexpected questions around molecular changes associated with CSPα deficiency. These provoked experiments utilising label-free proteomics to elucidate the mechanisms behind these unanticipated phenotypic changes. My study identifies a large number of differentially expressed proteins that signatured stress, translation and splicing in the face of the CSPα modulation of cell phenotype. My work coincides with increasing evidence that CSPα has celltype-specific functions that are implicated in proliferation and cancer-related changes that still require further study (Figure 6.3).

6.2 Investigation into candidate E3 ubiquitin ligases suggests an E3 ligase independent interaction between SNAP-25 and Parkin

Whilst it has been well documented that SNAP-25 is ubiquitinated and degraded in the absence of CSPα (Sharma *et al.*, 2012) at the conception of this work, no E3 ligase had been shown to ubiquitinate SNAP-25. As SNAP-25 and the SNARE complex are essential for presynaptic exocytosis, they are targets to inform on the role ubiquitination has at the synapse. We hypothesised that a specific E3 ubiquitin ligase responsible for targeting SNAP-25 for degradation in the absence of CSPα might be identified. Our multi-tiered strategy, incorporating bioinformatic prediction, BioID proximity labelling, and coimmunoprecipitation experiments, revealed evidence supporting a SNAP-25-Parkin protein interaction that seemed to occur independent of Parkin's intrinsic E3-ligase activity.

6.2.1 SNAP-25 and Parkin may interact in an E3 ligase-independent fashion

Parkin is a RING-between-RING E3 ligase (Beasley et al., 2007). Mutations in the gene encoding Parkin are linked to familial Parkinson's disease (Dawson and Dawson, 2010) and it is involved in mitophagy, which is crucial for maintaining mitochondrial integrity (Riley et al., 2013). At the centre of this function is the damage-dependent interaction of Parkin with the protein kinase PINK1(Jin and Youle, 2012, Vincow *et al.*, 2013, Narendra and Youle, 2024). Parkin has other, less well-characterised roles, including a role in activating mitochondrial biogenesis (Shin et al., 2011), regulating lipid metabolism (Kim et al., 2011) and a potential role as a tumour suppressor (Viotti *et al.*, 2014, Rouland *et al.*, 2021, Xu *et al.*, 2014, Shires, Kitsis and Gustafsson, 2017).

In my work, Parkin was first predicted and then evidenced to interact with SNAP-25 (Chapter 3, Section 3.4.2.4). Interestingly, this interaction persisted even in the presence of a catalytically inactive Parkin mutant (C431S) (Section 4.4.12). The C431S mutation is located in the RING2 catalytic domain of Parkin (Iguchi et al., 2013) (Figure 6.1). Parkin enables the ubiquitination of substrates by forming a ubiquitin-thioester bond on Cys-431. C431S impairs substrate ubiquitination by both causing atypical subcellular localisation, characterised by not translocating to the mitochondria following damage, and by irreversibly binding ubiquitin to Ser431 (Iguchi et al., 2013, Zheng and Hunter, 2013). The C431S mutation doesn't diminish Parkin's ability to interact with Pink1, E2 ubiquitin-conjugating enzymes (UbcH7, UbcH8) and substrate protein Mfn2, due to these interactions relying on the non-catalytic domains of Parkin (Zheng and Hunter, 2013, Lazarou et al.,

2013). Suggesting that whilst the mutation blocks ubiquitin transfer, it doesn't affect Parkin's protein-protein interactions with partners or specific substrates.

As the interaction seems to occur independent of an associated ligase activity, it could suggest a potential scaffold or chaperone-like role for Parkin at the presynapse or other cellular compartments that harbour SNAP-25. These finding echoes emerging literature suggesting that Parkin can stabilise protein complexes or act as an adaptor under stress conditions (Iorio, Celenza and Petricca, 2021, Pereira *et al.*, 2023). Although we have not yet investigated Parkin associated SNAP-25 ubiquitination, if an interaction is determined to result in ubiquitination of SNAP-25, it would be a strong candidate for being responsible for the increased SNAP-25 ubiquitination in the CSPα-deficient environment.

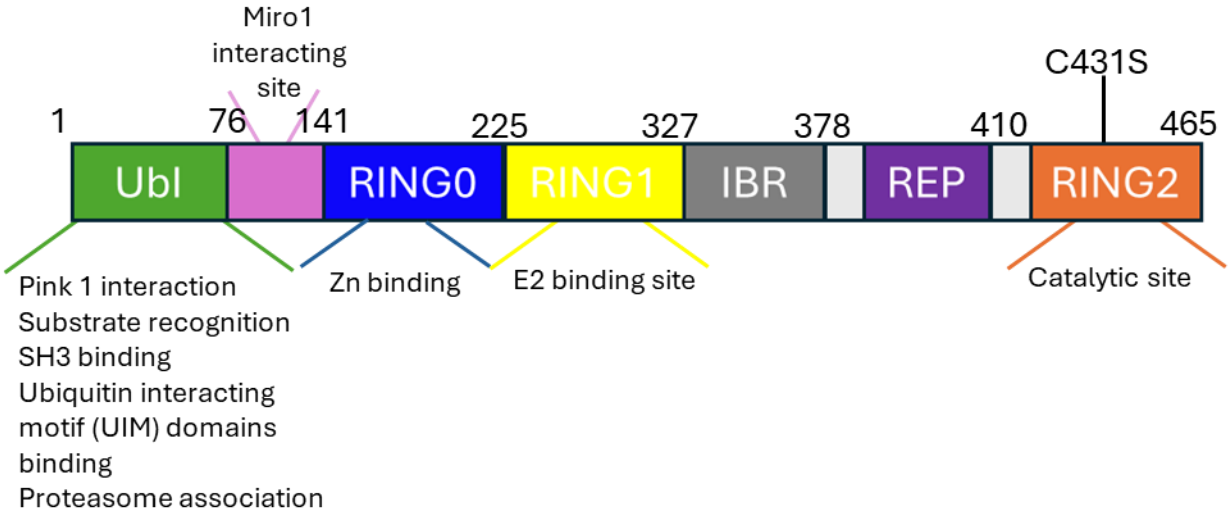

Figure 6.1: Parkin protein domain structure with location of known interactions and functions. Wild-type Parkin domains with C431S mutation highlighted in the Catalytic RING2 domain.

Several E3 ligase proteins have been identified as having additional ubiquitin-independent roles (Table 6.1). In the case of Parkin, it can also act as a scaffold recruiting adaptors to progress mitophagy, and interacts with other proteins such as microtubules, leading to their stabilisation. It also binds to Arrestin, leading to a conformational change, and enhances Arrestin's interaction with another E3 ligase Mdm2 (Yang *et al.*, 2005, Ahmed *et al.*, 2011). Whether Parkin modulates SNAP-25 turnover or interacts in a ubiquitination-independent manner remains to be determined.

Table 6.1: Canonical and ubiquitin-independent functions of E3-ubiquin ligase proteins.

E3 Ligase	Canonical Role	Additional ubiquitinindependent functions	References
Parkin	E3 ligase for mitochondrial proteins in mitophagy	Transcriptional regulation of p53, mitochondrial DNA protection and microtubule stabilisation.	(Müller-Rischart et al., 2013)(Riley et al., 2013b) (da Costa et al., 2009) (Rothfuss et al., 2009)
MDM2	E3 ligase targeting p53	Transcriptional coregulator, RNA-binding molecule, role in ribosomal biogenesis	(Shi and Gu, 2012) (Elenbaas et al., 1996) (Liu et al., 2016)
STUB1	E3 ligase for the ubiquitination and degradation, including FOXP3, RIPK3, tau, Sox2, Oct4, and Nanog	Co-chaperone activity with heat shock proteins	(Chen et al., 2011) (Seo et al., 2016) (Nadel et al., 2023) (Mamun et al., 2022) (Joshi et al., 2016) (Chakraborty and Edkins, 2023)
Cbl family (Cbl, Cbl-b, Cbl-c	Ubiquitin ligases for receptor tyrosine kinases	Act as adaptor proteins in signalling complexes (EGFR, TCR signalling), involved in methylation of RNA	(Tang et al., 2022) (Visser Smit et al., 2009) (Escuder-Rodríguez et al., 2025)
TRIM family	Broad E3 ligase activity in signalling	Transcriptional regulation, chromatin remodelling, and nuclear body organisation	(Hatakeyama, 2017) (Cammas et al., 2012) (Rajsbaum et al., 2014) (Ozato et al., 2008)

HECTD1	HECT E3 ligase	Scaffold function in cytoskeletal dynamics, cell migration and base excision repair in nucleosomes	(Zhang et al., 2024) (Bennett et al., 2020) (Vaughan et al., 2022) (Salas et al., 2023)
FBXW7	E3 ligase targeting cyclin E, c-Myc, Notch	Regulates transcriptional repression and DNA replication checkpoints	(de la Cova, 2023) (Yang et al., 2022) (Giráldez et al., 2014)

6.2.2 Functional implications of a Parkin-SNAP-25 interaction

Both Parkin and SNAP-25 have been well characterised in their specific cellular compartments and have been widely studied in neurodegenerative disorders.

Mitochondrial dysregulation has been linked to a loss of proteostasis (Olivero *et al.*, 2018, Lu and Guo, 2020) Here, my data suggest possible crosstalk between mitochondrial stress pathways and synaptic proteostasis, both of which are known to have important implications in neurodegenerative disorders (Olivero *et al.*, 2018, Jagtap *et al.*, 2023, Bustamante-Barrientos *et al.*, 2023, Klemmensen *et al.*, 2024).

6.2.3 Additional E3 ligases with the potential to ubiquitinate SNAP-25

As discussed in section 3.5.4.2, a recent publication reports that TNFAIP1 ubiquitinates SNAP25 in response to post-operative neuroinflammation (W. Wang et al., 2023). TNFAIP1 a widely expressed inflammatory-associated E3 ligase, was identified as being able to ubiquitinate SNAP-25 in HT22 murine hippocampal neurons and SH-SY5Y cells (Wang et al., 2023). TNFAIP1 conjugates to SNAP-25, leading to K48-linked polyubiquitination of SNAP-25 at K69.

An overexpression of TNFAIP1 reduced HT22 cell viability, with a corresponding accumulation of reactive oxygen species, impaired PINK1/Parkin-dependent mitophagy and suppressed SNAP-25 expression, resulting in caspase-3/GSDME-dependent pyroptosis. Whilst specific knockout of TNFAIP1 led to a restoration in mitophagy, reversed SNAP-25 depletion and reduced pyroptosis (Wang et al., 2023). Not only does this work provide evidence for an E3 ligase that interacts and ubiquitinates SNAP-25, it also suggests a link between E3 ligases, dysregulation of cellular homeostasis, mitophagy and SNAP-25.

As discussed in Chapter 3, TNFAIP1 was one of the proteins predicted to interact with SNAP-25 by Ubibrowser in my bioinformatic pipeline, but was not followed up on due to greater support for other candidates (Section 3.4.2.4). The fact that both TNFAIP1 (W. Wang et al., 2023) and Parkin have evidence to support an interaction with SNAP-25, suggests that Ubibrowser acts as a good starting point to predict E3 ligase-substrate interactions in the case of SNAP-25. This could suggest that other proteins identified by the bioinformatic pipeline in Chapter 3 could also be worth experimentally testing to validate if further SNAP-25-E3 ligase interactions are possible.

In addition to testing interaction with further E3-ligases, the fact that TRIM9 was not identified as being proximal or interacting with SNAP-25 (Chapter 4) here, whilst there is evidence to support interactions in primary neuronal cultures, suggests that interactions of SNAP-25 and E3 ligases can be highly context-dependent. As such, investigations in alternative models may be required to validate interactions and ubiquitination events. As interactions may be missed due to technical features, tagging, or biological or cell-type-specific conditions (Li *et al.*, 2001, Winkle *et al.*, 2014).

6.2.4 The role of mitophagy in the presynaptic compartment

Mitophagy is a selective form of autophagy implicated in the removal of damaged mitochondria (Chu, 2019). Alterations in mitophagy have been implicated in Alzheimer's disease, where amyloid-beta and p-tau inhibit ULK1/TBK1-dependent initiation of mitophagy (Mary et al., 2023). Parkinson's where mutations and reduced expression of PINK1 and Parkin lead to a reduction of labelling of mitochondria for degradation (Liu et al., 2019). In ALS where linked genes including C9orf72 are linked to mitophagy (Evans and Holzbaur, 2019, Lee et al., 2025) and Huntington's diseases, where mutated huntingtin (mHTT) affects mitochondrial dynamics, transport and protein import via OPA1, DRP1, MPTP, TRIM23 and oxidative phosphorylation, which all have a role in mitophagy (Šonský et al., 2021) (Han et al., 2020, Killackey et al., 2020, Banarase et al., 2023, Wang et al., 2022). Emerging literature suggests that the presynapses are hubs of mitophagy for damaged mitochondria in axons, where mitophagy is initiated and the formation of autophagosomes is localised (Lam et al., 2024, Kargbo-Hill et al., 2019, Yang et al., 2022) (Figure 6.2). Defective mitophagy has been shown to lead to the accumulation of Reactive oxygen species which have been shown to induce damage to synaptic proteins (Massaad and Klann, 2011) which suggests that there is the potential for mitophagy to both be a contributing factor and a consequence of the neurodegeneration in the presynaptic compartment set out here.

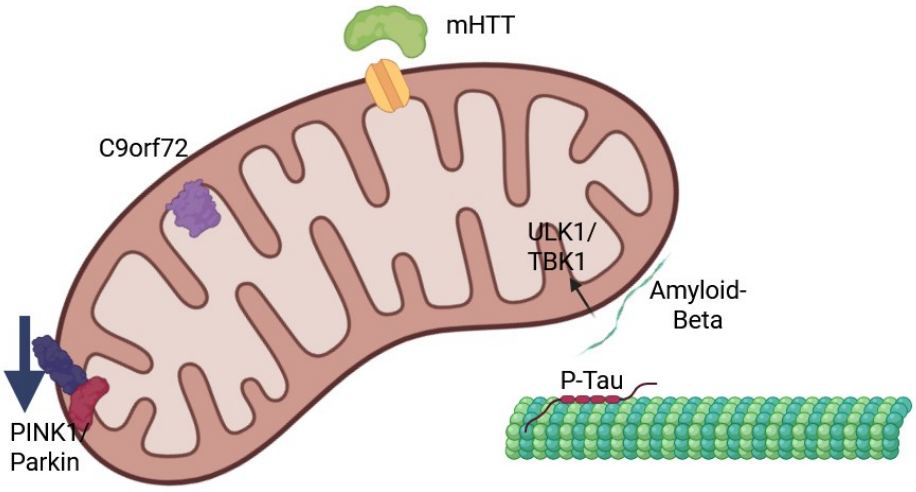

Figure 6.2: The role of dysfunctional mitophagy at the presynapse in neurodegenerative disease.

6.3 Consequences of an absence of CSPα in PC12 cells

As described and discussed in Chapter 5, the deficiency of CSPα in PC12 cells leads to both a decrease in protein levels of SNAP-25 and an unexpected loss of NGF responsiveness with corresponding loss of differentiation ability and a striking increase in proliferation. The lack of differentiation in the face of NGF treatment could be a direct result of the deficiency in CSPα affecting turnover of Trk receptors, as discussed in Section 5.4.2.1, or could be a downstream effect of a downregulation of other proteins in the cell lines (Section 6.3.1).

Whilst CSPα is present in low levels in the undifferentiated PC12 cells (Figure 4.2), the removal here suggests that this small pool has a role either directly or indirectly involved in the development of PC12 neurites, not just the maintenance of exocytosis (Rozas et al., 2012). The choice of PC12 cells over other cell lines and types such as SH-SY5Y cells, IPSc (Induced Pluripotent Stem Cells) or Primary neuronal cultures limits what can be extracted from the model generated here in terms of CSPα's conical role as a pre-synaptic chaperone and its function in neurons but provided a practical model to investigate its role in a rapidly dividing neuronal-like system.

6.3.1 Alterations in several proteins lead to loss of PC12 differentiation

There are other examples of situations where molecularly modified PC12 knockdown cells have also been generated and have lost the ability to differentiate in response to NGF.

PC12 cells express both the TrkA and low-affinity $p75^{NTR}$ receptors for NGF (Hartman *et al.*, 1992, Roux and Barker, 2002, Negrini, D'Alessandro and Meldolesi, 2013). When NGF binds, it causes TrkA dimerisation and autophosphorylation, triggering the MAPK/ERK pathway. PC12 differentiation requires the sustained activation of ERK to activate transcription factor Egr1(Qui and Green, 1992, Friedman and Greene, 1999).

Removal of NGF responsiveness or inhibitors of the MAPK/ERK signalling pathway can disrupt neurite outgrowth (Table 6.2). Alterations in a number of proteins have unexpectedly led to PC12 cells becoming resistant to NGF-triggered differentiation (Table 6.2). Some of the protein alterations directly affected the activity of EGR1, whilst others have not been found to directly affect EGR1 signalling, suggesting that alterations in a number of proteins have the potential to dysregulate the signalling cascade required for PC12 neurite outgrowth.

Both αCaMKII (Ca^{2+}/Calmodulin-Dependent Protein Kinase II) and Rab5 modulation (Table 6.2) have been observed to change the morphology and stop neurite outgrowth in PC12 cells (Massé and Kelly, 1997,Liu *et al.*, 2007), this along with the hint of potential endosomal sorting disruption in my work (Section 5.3.6) and the fact that the two most enriched downregulated GO terms were regulation of late endosome to lysosomal transport and negative regulation of high voltage calcium channel activity (Section 5.3.9) could suggest a potential link between these pathways and neurite outgrowth in PC12 cells.

Table 6.2: PC12 modified lines which have lost the ability to differentiate in response to NGF

Protein alteration	Pathway affected	References
$p75^{NTR}$ repression in PC12-27	Defective NGF signalling due to the absence of $p75^{NTR}$ (lowaffinity NGF receptor) impairs PI3K pathway activation, mTORC2 signalling and neurite outgrowth.	(Negrini et al., 2013)
TrkA-deficient PC12 lines CRISPR TrkA−/− and PC12nnr	Eliminates NGF-induced signalling and neurogenesis	(Loeb et al., 1991) (Testa et al., 2022)
Rap1 pathway components PDZ-GEF1/C3G or Rap1knockdonws	Reduces or abolishes NGF induced neurite formation by disrupting the Rap1 pathway	(Hisata et al., 2007) (Jeon et al., 2010b)

NAB2 overexpression	Cells continue proliferating instead of undergoing growth arrest and neurite outgrowth. Early NGF signalling (e.g., MAPK activation, immediate early gene induction) remains intact, but late response genes such as TGF-β1 and MMP-3 fail to be induced and $p21^{WAF1}$ required for growth	(Qu et al., 1998) (Spolidoro et al., 2020)
	arrest and development of neurites is downregulated	
PTEN overexpression	Leads to a significant downregulation of TrkA and p75, resulting in loss of differentiation and growth arrest	(Musatov et al., 2004)
CDK2 overexpression	Loss of differentiation and an increase in cell growth rate	(Dobashi et al., 1995)
αCaMKII (Ca^{2+}/CalmodulinDependent Protein Kinase II) overexpression	Led to alteration in PC12 morphology whereby cells treated with NGF, flatten and form large growth-cone-like structures but fail to extend neurites.	(Massé and Kelly, 1997)
Rab5 constitutively active (Q79L mutant)	Inhibits NGF-induced neurite outgrowth by blocking activation of TrKA on endosomes	(Liu et al., 2007)

6.3.2 Could loss of differentiation ability in the CSPα-deficient PC12 cells be due to the loss of SNAP-25

SNAP-25 knockdown in PC12 cells has been shown to directly impair exocytosis (Cahill et al., 2006) whilst in NGF-treated PC12 cells SNAP-25 localises to growth cones (Morihara et al., 1999). This, along with observations that alterations in levels of SNAP-25 correlate with an inhibition of

PC12 neurite outgrowth formation, supports the suggestion that a reduction in SNAP-25 levels could inhibit PC12 cells' ability to differentiate.

In models where SNAP-25 is directly reduced or inhibited, PC12 differentiation has been observed to be inhibited. Cleavage of SNAP-25 with botulinum neurotoxin C (BoNT/C) inhibits both PC12 neurite outgrowth and causes collapse of growth cones (Igarashi *et al.*, 1996, Morihara *et al.*, 1999) this has been mechanistically rationalised by the fact that neurite outgrowth requires both membrane addition and targeted exocytosis at the growth cones.
(Kimura et al., 2003).

A PC12 model expressing shRNA targeting SNAP-25, leading to a reduction in its levels to approximately 5% of its normal levels, leads to inhibition of differentiation corresponding to a failure of localised exocytosis (Osen-Sand et al., 1993, Osen-Sand et al., 1996, Cahill, Herring and Fox, 2006). Whilst a Parkin shRNA knockout PC12 line with an accumulation in p21 has a corresponding downregulation of SNAP-25 and an associated loss of differentiation (Park et al., 2017). Conversely, overexpression of SNAP-25 in PC12 cells leads to an increase in the number of neurite outgrowths per cell and an increase in the total length of neurites (Shirasu et al., 2000). The examples here suggest that SNAP-25 influences PC12 cell homeostasis via exocytosis, growth-cone dynamics and potentially via neurite outgrowth.

An over-expression of SNAP-25 supports outgrowth and neurite extension in PC12, hippocampal and cortical neurons (Wu *et al.*, 2011, Tomasoni *et al.*, 2013). A reduction in neurite length is also observed in the neurons from the CSPα-/- mouse, which has a 40% reduction in SNAP-25 due to its misfolding and proteasomal degradation (Sharma et al., 2012a). A further reduction in SNAP-25 levels reduces the formation of neurites and cell survival. SNAP25 knockout is perinatally lethal in mouse models due to an inability to perform evoked synaptic transmission (Washbourne et al., 2002) and whilst primary neurons can be cultured from embryos, impaired neurite outgrowth and branching is observed (Delgado-Martínez et al., 2007). Suggesting that modulating the levels of SNAP-25 both via a reduction in translation and an increased degradation of misfolded SNAP-25 may have a direct effect on signalling and cell state.

The reduction in SNAP-25 levels observed in the CSPα-deficient PC12 cells was quantified as a reduction of 90.5% for CD3 and 99% for CD5 (Section 5.3.5), and similar phenotypic changes are observed as described in this literature which could potentially be suggestive of a role either directly or indirectly for SNAP-25 in PC12 differentiation. Taking this into consideration, the loss of

differentiation ability and loss of NGF responsiveness in the CSPα-deficient lines may be modulated via the observed downregulation of SNAP-25 by an unidentified signalling pathway.

However, as discussed above in (Section 6.3.1), several protein alterations have also been observed to lead to a loss of differentiation, as such loss of differentiation ability could be a consequence of a loss of proteostasis or of cellular stress and further experiments would be required to fully elucidate the mechanism for loss of differentiation ability in the CSPα CD cell lines.

6.4 Cell-type-specific function of CSPα

Whilst the majority of investigations into CSPα have taken place in the context of differentiated neurons or models thereof (Figure 6.3). Recent work investigating CSPα in a range of both pre- and post-mitotic (Figure 6.4) cell states has led to the suggestion that CSPα has additional roles (Fernández-Chacón *et al.*, 2004, Valenzuela-Villatoro *et al.*, 2018, Rosene and Benitez, 2025).

These additional roles highlight the underappreciated function of CSPα that appears to be cell type dependent (Figure 6.3). The neuronal roles of CSPα (summarised in Section 1.5 of the general introduction Chapter 1) are well documented and characterised. CSPα functions include the chaperoning of SNARE protein SNAP-25, a role in the polymerisation of Dyn-1, regulation of G-protein signalling and interaction with calcium ion channels (Zhang et al., 2012, Magga et al., 2000, Bai et al., 2007) (Figure 6.3).

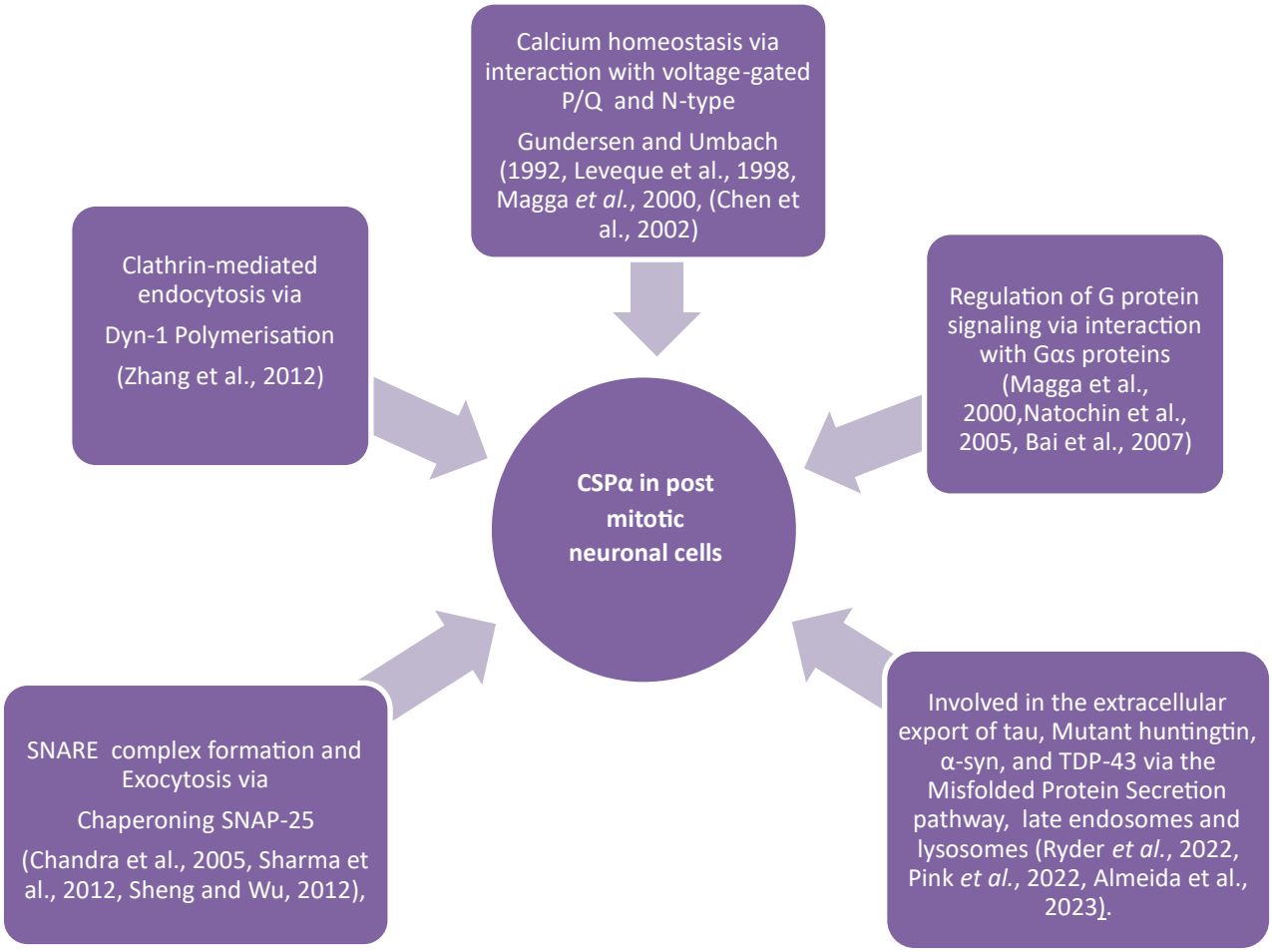

Figure 6.3: Roles of CSPα in neuronal post-mitotic neuronal cell models

Modulation of CSPα in a range of pre-mitotic cell types has led to the identification of roles of CSPα in the pre-mitotic cells, which can be classified as CSPα acting as a co-chaperone on a previously under-represented substrate, acting in a classical trafficking context or acting in a novel non-chaperone-based ways (Figure 6.4). The work undertaken here identifies both potential chaperon and/or trafficking roles of CSPα. Levels of SNAP-25 and Dyn-1 were reduced in the PC12 CSPα-deficient cells as has been previously described in CSPα -/- neuronal models by Chandra et al 2005, Sharma et al 2012, Sheng and Wu 2012 and Zhang et al 2012 (Figure 6.3). Whilst changes in proliferation and differentiation could be supported by work in other CSPα-/- pre-mitotic models. The large change in proteomic signatures alongside the work of Nieto-González et al., 2019 which described changes in the transcriptome of CSPα knockout cells, suggests loss of CSPα may have wide-reaching downstream effects. Whilst this work and both H. Wang et al., 2021, Chen et al., 2025 suggest a role in modulating EGFR downstream signalling effecting rates of proliferation(Figure 6.4). However, here I set out data to support that CSPα may also have a role in the modulation of Trk

receptors, leading to a loss of differentiation which has not been previously identified in any other model, and the large-scale proteomic changes identified in the PC12 model provide future avenues to explore CSPα function away from the synapse.

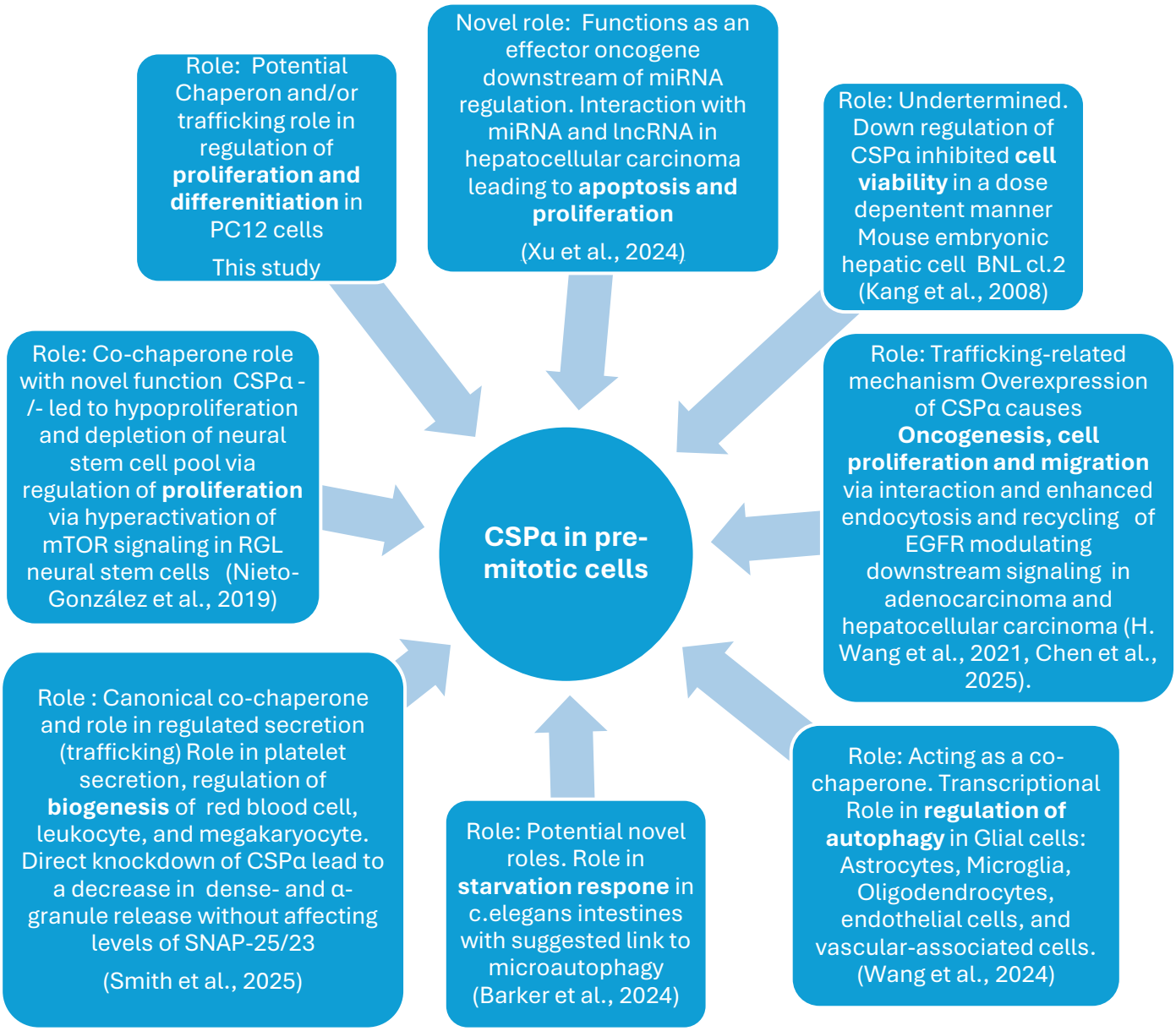

Figure 6.4: Roles of CSPα in non-neuronal pre-mitotic cell lines

6.4.1 A potential model of CSPα-deficiency in PC12 cells

The work undertaken here, alongside other recent work in a range of non-neuronal pre-mitotic cells, highlights that the roles of CSPα are far more diverse than previously thought and highly cell-type specific (Figure 6.4).

6.4.2 Evidence of proteasomal disorder in the CSPα-deficient cell lines suggestive of cellular stress

Overall, Ubiquitination levels were altered between the Parental and the CSPα-deficient cell lines in addition, several ubiquitin-related proteins were altered in the label-free proteomics. Some E3 ubiquitin ligases were increased, whilst hydrolases were down-regulated (Table 5.2). This could suggest that the increase in ubiquitination is not solely due to an increase in ubiquitination but may also be a decrease in de-ubiquitination. This could extend the network of proteins to investigate in the context of dysregulated proteostasis in the absence of CSPα.

My label-free whole-cell proteomics revealed significant alterations in the expression of numerous proteins in CSPα-deficient cells (Appendix C.4 for the full list of altered proteins). These global changes suggest a reprogramming of the cellular proteome and provide candidate pathways through which CSPα might regulate broader aspects of cellular function and homeostasis. For example, shifts in the levels of proteins involved in splicing, transcription factors, or protein quality control components (Figures 5.13 and 5.16) could mediate or compensate for the loss of CSPα activity in the context of cellular stress. This may explain the overall change in cellular phenotype as the burden of stress may modulate proteostasis and have knock on consequences in terms of cellular phenotype.

6.5 Future Work

6.5.1 Characterisation of SNAP-25- E3 ligase Parkin interaction

Having uncovered evidence of a SNAP-25-Parkin interaction within this work, further work would be required to answer three main questions to characterise this interaction. 1 What is the nature of the interaction? Is it direct, indirect, and if direct, what domains are involved in the binding? 2. What are the upstream consequences of the interaction? And 3. Is Parkin the ligase responsible for increased ubiquitination of SNAP-25 in a CSPα-deficient context?

In order to further our understanding of the potential relationship between SNAP-25 and Parkin, ubiquitination studies could be carried out to determine the nature of the interaction. In addition, an attempt to characterise the interacting domains could be interesting in furthering our

understanding of how Parkin interacts with different partners using different domains (Section in chapter 4.4.7).

Functional dissection of the Parkin–SNAP-25 interaction, including whether it impacts SNARE complex assembly or trafficking, or whether an interaction could potentially function in the context of mitochondrial function, would be required to understand the consequences of the interaction.

Finally, it has already been observed that PC12 cells with a Parkin shRNA knockout have a corresponding downregulation of SNAP-25 and a loss of differentiation (Park et al., 2017). If the Parkin-SNAP-25 interaction function was ubiquitin-dependent degradation, this corresponding downregulation of SNAP-25 would be unexpected, potentially providing further support for a potential alternative role of the interaction. It could also be insightful to determine if there is overlap in the pathway altered in the CSPα-deficient PC12 cells generated in this study and the Parkin shRNA knockout PC12 cells, to determine if the mechanisms behind the loss of differentiation can be understood.

6.5.2 CSPα deficiency directs cell phenotype

The generation of the two CSPα-deficient PC12 cell lines has opened up key questions about where and when CSPα may act. It is known to be widely expressed (in the CNS, PNS, Retinal, and secretory cells, as well as in non-neuronal tissues at lower levels) and has roles beyond the classical synaptic vesicle targeting. The production of Isogenic cell lines, as discussed here eliminates the variables of genetic background heterogeneity which is useful for research into the modelling of disease and in genetic research aiding in the unravelling of CSPα's function in post mitotic cells(Haagensen et al., 2016).

Further work would be required to answer three main questions: 1. Does restoring CSPα or SNAP-25 levels lead to a restoration of PC12 differentiation ability and regulation of proliferation? 2. Is induced cellular stress able to prevent PC12 cellular differentiation or is this specific to CSPα? And 3. Does CSPα have a role in the maintenance of plasma membrane receptors?

Attempting rescue experiments of the CSPα-deficiency induced phenotype with the addition of a CSPα construct would dissect the loss of differentiation ability. In addition, the introduction of a SNAP-25 construct to rescue levels of reduced SNAP-25 in the CSPα-deficient background would also provide insight into whether SNAP-25 expression reverses the CSPα-deficient phenotype as observed. As SNAP-25 overexpression in the CSPα knockdown mouse reversed CSPα -/- neurodegeneration in cortical areas with regard to neuron density, synaptic density, apoptosis and

astrogliosis (Sharma *et al.*, 2012). As such, it would be interesting to understand if SNAP-25 rescue can reverse the altered phenotypes observed in the CSPα-deficient PC12 cells also. If the lack of differentiation ability is reduced by SNAP-25 transfection, this could help explain the lack of differentiation in both the CD3 and CD5 lines and also the loss observed in Parkin knockout PC12 lines (Section 6.3.2), which also have a loss of SNAP-25 and differentiation ability (Park et al., 2017).

Secondly, the removal of CSPα both here and in other models produces an alteration in cellular homeostasis in response to cellular stress. This allows the possibility to test if CSPα is acting discretely, producing a downstream signalling cascade leading to the alterations in phenotypes observed. Or if stressed cells treated with drugs or modulators such as VER-155008 and JG98, which inhibit HSP70 or Tunicamycin, which leads to ER stress, would also lead to the change in phenotype in terms of proteomic change, hyperproliferation and loss of differentiation, which here I have characterised here in terms of a CSPα-deficiency. To determine if the intersection of cellular stress at the wrong stage in development could also be responsible for these changes.

Lastly, work to determine if CSPα has a potential role in plasma membrane receptor stabilisation or trafficking would be interesting in both the context of this study and as CSPα has been termed oncogenic due to its implicated involvement in modulating the expression of EGFR in cancerous contexts (H. Wang et al., 2021, Chen et al., 2025). This could involve colocalisation experiments between CSPα and the EGFR and TrK receptors and potentially pulse chase experiments to estimate the half-lives of the receptors in the presence and absence of CSPα.

6.6 Summary and Overall Conclusions

In conclusion, in this thesis, I have met the aims of investigating SNAP-25-E3 ligase and produced and characterised two CSPα-deficient PC12 cell lines.

The observed interaction between SNAP-25 and Parkin, even in the absence of E3 ligase activity, opens new avenues to explore non-canonical roles for E3 ligases in synaptic protein regulation.

Whilst the generation of the CSPα-deficient PC12 cell lines has increased our understanding of the roles CSPα plays beyond the synapse. Together, our findings suggest that CSPα plays a multifaceted role in maintaining homeostasis, not only as a chaperone for specific presynaptic proteins but also as a modulator of broader cellular signalling and differentiation and functions in a cell-type-specific manner.

Appendix A Bioinformatics data

A.1 Identification of E3 ligases that interact with SNAP-25 from the literature-based approach

Appendix A **Table A1.1: Literature results Returned for the identification of E3 ligases associated with SNAP-25 based on PubMed database identification**

SNAP25 ligase	**SNAP25 E3 ligase**	**SNAP25 ubiquitination**
1: Zhang et al 2013 doi:10.1007/s00018-012-1103-5 2: Princely et al 2019 doi:10.1016/j.devcel.2019.03.013. 3: Tsai et al 2010 doi:10.1073/pnas.1008302107. 4: Choe et al. 2007 doi: 10.1523/JNEUROSCI.1408-07.2007. 5: Tsai et al 2017 doi: 10.1073/pnas.1621076114. 6: Winkle et al 2014 doi:10.1083/jcb.201311003. 7: Sen et al 2021 doi: 10.3389/fphar.2021.763950	1: Zhang et al 2012 doi:10.1007/s00018-012-1103-5. 2: Princely et al 2019 doi:10.1016/j.devcel.2019.03.013 3: Park et al 2017 doi: 10.7150/thno.19824. 4: Sen et al. 2021 doi: 10.3389/fphar.2021.763950. 5: Winkle et al 2014 doi:10.1083/jcb.201311003. 6: Tsai et al 2017 Jun .doi: 10.1073/pnas.1621076114. 7: Tai HC, et al 2010 doi: 10.3389/fnmol.2010.00012.	1: Na et al 2012 doi: 10.1021/pr300536k. 2: Shirafuji et al 2017 doi: 10.1267/ahc.17028 3: Princely et al 2019 doi:10.1016/j.devcel.2019.03.013 4: Bodewes et al. 2019 doi: 10.3389/fimmu.2019.00312. 5: Muraoka et al 2021 doi:10.14336/AD.2020.1007. 6: Tizzano et al 2015 Nov Doi: 10.1093/chemse/bjv048. 7: Sadeghi et al. 2021 doi: 10.1038/s41598-021-87555-7.

8: Park et al 2017 doi: 10.7150/thno.19824. 9: Tai et al 2010 doi: 10.3389/fnmol.2010.00012 10: Schubert et al 2011 doi: 10.1002/glia.21190. 11: Jørgensen et al 1997 doi: 10.1006/exnr.1996.6372. 12: Li *et al.*, 2001 Doi:10.1074/jbc.M106141200	8: Choe EA, et al 2007 doi: 10.1523/JNEUROSCI.1408-07.2007.	8: Tsai et al 2017 Jun doi: 10.1073/pnas.1621076114. 9: Shirafuji T, et al 2018 Doi:10.1523/JNEUROSCI.1649-17.2017. 10: Sen et al 2021 doi: 10.3389/fphar.2021.763950. 11: Tsai et al. 2010 doi:10.1073/pnas.1008302107. 12: Park et al. 2017 May doi: 10.7150/thno.19824. PMID: 28656059; 13: Winkle et al 2014 doi:10.1083/jcb.201311003 14: Sharma M, et al 2011 doi: 10.1038/ncb2131. 15: Yiadom et al 2005 doi:10.1016/j.bbrc.2005.07.196.

Appendix A

		16: Tai et al. 2010 doi: 10.3389/fnmol.2010.00012.. 17: Liu 2015 doi: 10.1523/JNEUROSCI.5288-14.2015. 18: Yang et al 2007 Jun doi: 10.1002/cne.21317. PMID: 17447252. 19: Singh et al. 2011 doi: 10.1093/toxsci/kfr115. 20: Zhang et al . 2013 doi:10.1007/s00018-012-1103-5. 21: Latina et al 2018 doi: 10.3389/fncel.2018.00487 22: Honma et al 2017 doi:10.1016/j.archoralbio.2016.10.025. 23: Sherriff et al. 1994 doi: 10.1007/BF00389495. 24: Nibe et al 2009

		doi: 10.1354/vp.08-VP-0156-U-FL. 25: Pullan et al 2006 doi: 10.1016/j.str.2006.01.012. 26: de la Monte et al. doi: 10.3233/JAD-160656. 27: Yee et al 2003 doi: 10.1002/cne.10589. PMID: 12629664. 28: Wilson et al. 2001 doi: 10.1212/wnl.57.4.651. 29: Savioz et al . 2003 doi: 10.1016/s0969- 9961(02)00011-6. 30: Choe et al 2007 doi: 10.1523/JNEUROSCI.1408-07.2007. 31: Sienkiewicz et al. 2000 doi: 10.1046/j.1439-0264.2000.00272.x.

Appendix

E3 ligase filtering from predictions of Ubibrowser

Table A1.2: E3 ligases predicted to interact with SNAP-25 by ubibrowser 1.0 with ranking and evidence used to make the prediction.

Rank	E3	E3 Name	Presence of an enriched domain pair	Presence of E3 recognising domain	Presence of network loops	Ortholog interactions	Enriched GO pair	Confidence level	Confidence score
1	NEDD4	E3 ubiquitin protein ligase NEDD4		●	●		●	HIGH	0.788
2	SOCS5	Suppressor of cytokine signalling 5		●	●		●	MIDDLE	0.719
3	MDM2	E3 ubiquitin protein ligase Mdm2		●	●		●	MIDDLE	0.715
4	STUB1	E3 ubiquitin protein ligase CHIP			●		●	MIDDLE	0.704
5	CBX8	Chromo box protein homolog 8			●		●	MIDDLE	0.695
6	CBL	E3 ubiquitin protein ligase CBL		●	●		●	MIDDLE	0.686

7	PAFAH 1B1	Platelet activating factor acetylhydrol ase IB subunit alpha			●		●	MIDD LE	0.681
8	SMURF 1	E3 ubiquitin protein ligase SMURF1		●	●		●	MIDD LE	0.679
9	SYVN1	E3 ubiquitin protein ligase synoviolin		●	●		●	MIDD LE	0.677
10	NEDD4 L	E3 ubiquitin protein ligase NEDD4-like		●	●		●	MIDD LE	0.677
11	GNB1	Guanine nucleotide binding protein G(I)/G(S)/G(T) subunit beta-1			●		●	MIDD LE	0.675
12	RPH3A L	Rab effector Noc2		●		●	MIDD LE	0.671	
13	SYTL4	Synaptotag min-like protein 4		●		●	MIDD LE	0.667	
14	PCGF2	Polycomb group RING finger protein 2	●		●	LOW	0.665		

Appendix

15	CBX4	E3 SUMO-protein ligase CBX4	●		●	LOW	0.665		
16	BAZ1B	Tyrosine protein kinase BAZ1B			●		●	LOW	0.665
17	HSPA8	Heat shock cognate 71 kDa protein			●		●	LOW	0.653
18	BARD1	BRCA1-associated RING domain protein 1			●		●	LOW	0.649
19	VHL	Von Hippel Lindau disease tumour suppressor		●	●		●	LOW	0.641
20	IBTK	Inhibitor of Bruton tyrosine kinase			●		●	LOW	0.64
21	RING1	E3 ubiquitin protein ligase RING1					●	LOW	0.64
22	MARCH9	E3 ubiquitin protein ligase MARCH9		●			●	LOW	0.633

23	RNF216	E3 ubiquitin protein ligase RNF216		●	●		●	LOW	0.63
24	MNAT1	CDK-activating kinase assembly factor MAT1			●		●	LOW	0.628
25	EP300	Histone acetyltransferase p300			●		●	LOW	0.628
26	CREBBP	CREB-binding protein			●		●	LOW	0.628
27	PML	Protein PML			●		●	LOW	0.626
28	TRIM27	Zinc finger protein RFP			●		●	LOW	0.622
29	RANBP2	E3 SUMO-protein ligase RanBP2			●		●	LOW	0.617
30	TNFAIP1	BTB/POZ domain containing adapter for CUL3mediated RhoA degradation protein 2			●		●	LOW	0.617

Appendix

31	CRYAB	Alpha-crystallin B chain			●		●	LOW	0.617
32	PPIL2	Peptidylprolyl cistrans isomerase-like 2			●		●	LOW	0.617
33	CADPS 2	Calcium dependent secretion activator 2					●	LOW	0.615
34	WDTC1	WD and Tetratrico peptide repeats protein 1					●	LOW	0.615
35	STC1	Stanniocalci n-1					●	LOW	0.615
36	SMURF 2	E3 ubiquitin protein ligase SMURF2		●	●		●	LOW	0.611
37	ASB2	Ankyrin repeat and SOCS box protein 2		●				LOW	0.61
38	PARK2	E3 ubiquitin protein ligase parkin			●		●	LOW	0.609

39	SOCS7	Suppressor of cytokine signalling 7			●		●	LOW	0.609
40	TEP1	Telomerase protein component 1			●		●	LOW	0.605
41	CISH	Cytokine inducible SH2-containing protein			●		●	LOW	0.605
42	UBE3C	Ubiquitin protein ligase E3C		●			●	LOW	0.604
43	FZR1	Fizzy-related protein homolog		●			●	LOW	0.604
44	TTC3	E3 ubiquitin protein ligase TTC3		●			●	LOW	0.604

Appendix

Table A1.3: E3 ligases predicted to interact with SNAP-25 by ubibrowser 2.0, with evidence used to make the prediction.

E3	E3 Name	Species predicted in	Presence of an enriched domain pair	Presence of E3 recognising motif	Presence of network loops	Ortholog interactions	Enriched GO pair	Confidence score
BTRC-1	Fbox/WD repeat containing protein 1A	H.sapiens		●	●		●	0.814
BARD1	BRCA1 Associated RING Domain 1	C.familiaris		●			●	0.8
ARIH1	RBR-type E3 ubiquitin transferase	C.porcellus		●			●	0.793
PRKN	E3 ubiquitin - protein ligase parkin	C.porcellus		●			●	0.793
RC3H2	RING-type E3 ubiquitin transferase	C.porcellus		●			●	0.793
RC3H2	RINGtype E3 ubiquitin transferase	T.guttata		●			●	0.793

ARIH1	E3 ubiquitin - protein ligase arih1	X.tropical is		●			●	0.778

Table A1.4: Sources of information for curation of the DisGeNET gene-disease database

Organisation of DisGeNET gene disease information	**Gene-disease associations sources**
Curated	**UniProt**- database containing information about protein structure and function, GDAs obtained from the humsaver file, and only associations marked as disease included in the DisGeNET database. **PsyGeNET**- Psychiatric disorders gene association Network. Is a resource for exploratory analysis of the genes associated with psychiatric diseases, all included in DisGeNET database. **Orphanet**-reference database for information on rare disease all gene disease associations included Comparative toxico genomics database- CTD (human data) is a manually curated database which focuses on the effects of environmental chemicals on health. Associations marked as marker/mechanism or therapeutic included in DisGeNET database. ClinGen- the clinical genome resource is a resource that defines the clinical relevance of genes all gene-disease associations where included apart from those labelled "refuted"
	Genomics England PanelApp- a database formed of virtual gene panels related to human disorders, all gene-disease associations from this source were used.
Animal models	**RGD Rat genome database-** database of rat genetic and genomic research, associations labelled resistance, no association, or inferred from electronic annotation/sequence/structural similarity and nontraceable authors were excluded. **MGD Mouse Genome Database-** is an integrated genetic, genomic and biological resource database about laboratory mice **CTD Comparative Toxicogenomic database-** mouse and rat database containing gene-disease associations

Appendix

Inferred	**Human Phenotype ontology standardises** vocabulary of phenotype abnormalities, gene_to_phenotype file, imported. **GWAS catalogue and database-** the GWAS catalogue by NHGRI-EBI is a manually curated literature catalogue of genome-wide association studies assaying single nucleotide polymorphism (SNPs). Variant disease associations with p-values <1.0 x10^{-6} were included in the DisGeNET database. **CLINVAR**- Public archive of relationship between medically relevant variants and phenotypes. Imported variant-disease associations with labels including pathogenic, likely pathogenic, risk factor and affects.

Appendix B :BioID development and cloning of constructs

B.1. **Expression of Synaptic and E3 ligase proteins in cellular models**

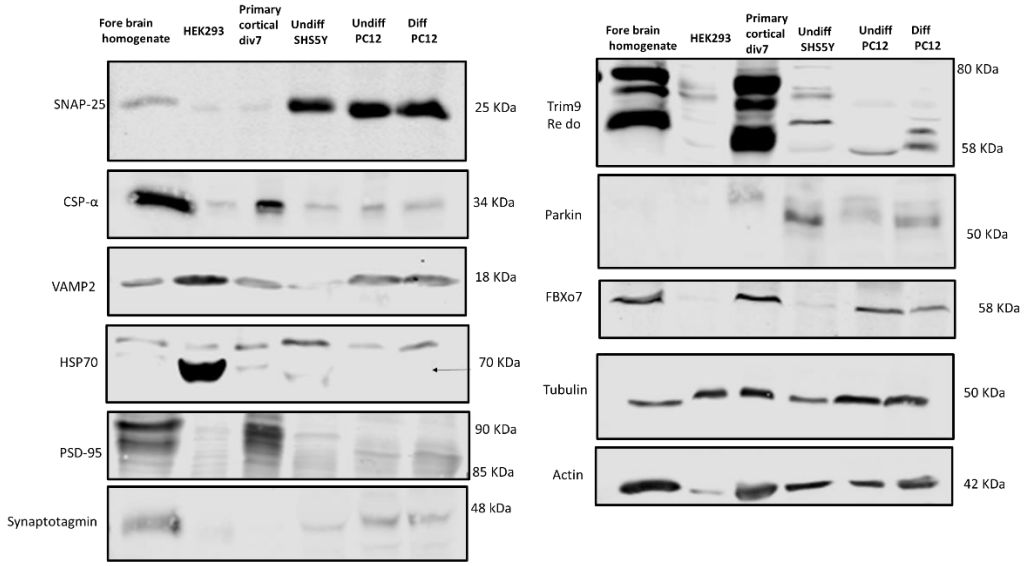

Figure B.1: Expression of Synaptic and E3 ligase proteins in cellular models: **PC12 cells express CSPα and SNAP-25 associated proteins as well as candidate E3 ligases**

Western blot of Mouse forebrain homogenate, HEK293FT, Primary Cortical (Div 7) neurons, SHSy5y (undifferentiated), and Undifferentiated and differentiated PC12 cell lysates probed for CSPα interacting proteins, general synaptic proteins and candidate E3 ligase proteins. Tubulin and actin staining represent probing for housekeeping proteins representative of protein load N=1.

B.1.1 Investigating if Myc-BioID-SNAP-25 can form a SNARE complex.

To ensure that with the addition of the Myc tag and the BioID unit, SNAP-25 was still able to form a SNARE complex with its interacting partners, Syntaxin-1 and VAMP-2, PC12 cells were transfected with Myc-BioID-SNAP-25. The lysates were harvested as described in section 2.9.1 in lysis buffer (Tris pH 7.5 50 mM, NaCl 140 mM, EDTA 2 mM, NP-40 1%, glycerol 10%)) and split into two, with one lysate boiled to dissociate the SDS-resistant SNARE complex and the other left unboiled. These samples were resolved by SDS-PAGE, western blotting and probed for SNAP-25 and Myc immunoreactivity (Appendix Figure B.2).

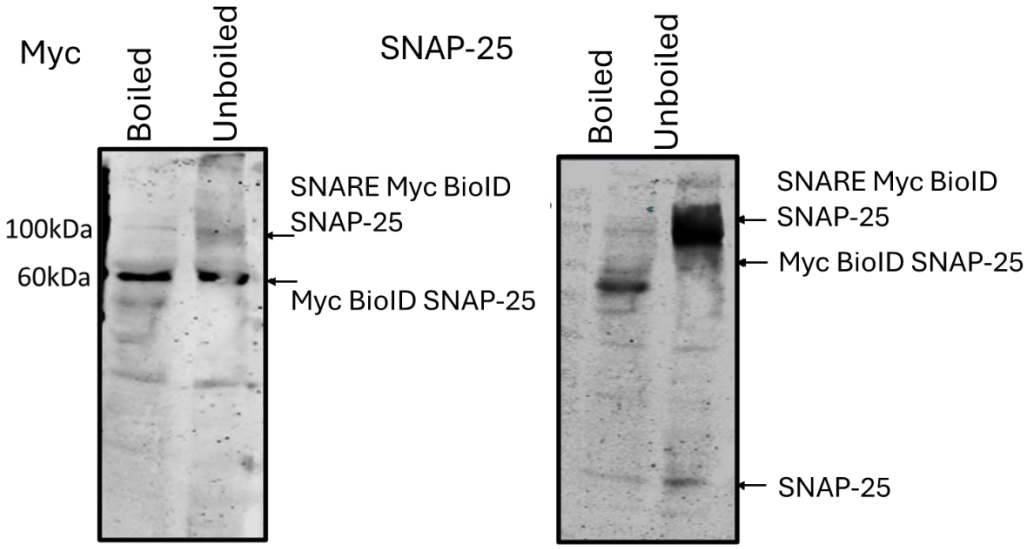

Figure B.2: Myc BioID SNAP-25 forms a SNARE complex in PC12 cells

PC12 cells were transfected with Myc BioID SNAP-25 and lysed 16 hours later. The lysates were untreated (unboiled) or heated at 95C for 5 minutes (boiled) (Assembled SNARE ˚complex) and resolved by SDS PAGE before being immunolabeled with Myc or SNAP-25 antibodies. N=1

Myc immunoreactivity is present at 60 kDa, corresponding to Myc BioID SNAP-25 in the boiled sample. In the unboiled sample, the Myc immunoreactivity is present at 60 kDa, with an additional band at ~100 kDa. The latter high molecular weight immunoreactivity is MycBioID-SNAP-25 in a SNARE complex with VAMP2 and Syntaxin 1. This is consistent with the C-terminal BioID tag not interfering with SNAP-25 propensity to form a SNARE complex.

In the same samples, probed with SNAP-25, SNAP-25 immunoreactivity is present at 25 kDa and 60 kDa. This represents the endogenous and exogenously expressed BioID-tagged SNAP-25. SNAP-25 immunoreactivity in the unboiled sample is abundant at 60 kDa, which is Myc-BioID-SNAP-25, is reduced compared to the boiled sample but the dominant Immunoreactivity is at ~100 kDa, likely corresponding to SNARE complex-associated MycBioID-SNAP-25.

Whilst there is a striking difference regarding incorporation between the immunoreactivity of the Myc and the SNAP-25 in unboiled samples, the presence of immunoreactivity at 100 kDa in both is evidence for the Myc-BioID-SNAP-25 still being able to form a SNARE complex.

B.1.2 Time dependence of cellular biotinylation across varying incubation times

To optimise the biotin incubation time, the Myc-BioID constructs were transfected into HEK239 FT cells. After 24 hours, transfected cultures were incubated with biotin (50 µM) and lysed 16, 18 or 24 hours later. (Roux et al., 2012). These distinct treatments were lysed and resolved by SDS PAGE and probed for streptavidin reactivity (Figure B.3). As before, the most intense labelled reactivity related to immunoreactivity of the size of each construct. In addition, each transfected construct led to a ladder of immunoreactivity bands. There was no clear difference in the levels of cellular biotinylation or the emergence of additional immunoreactivity between 16, 18 and 24 hours. As such, cells were subsequently incubated with biotin for 16 hours in subsequent experiments.

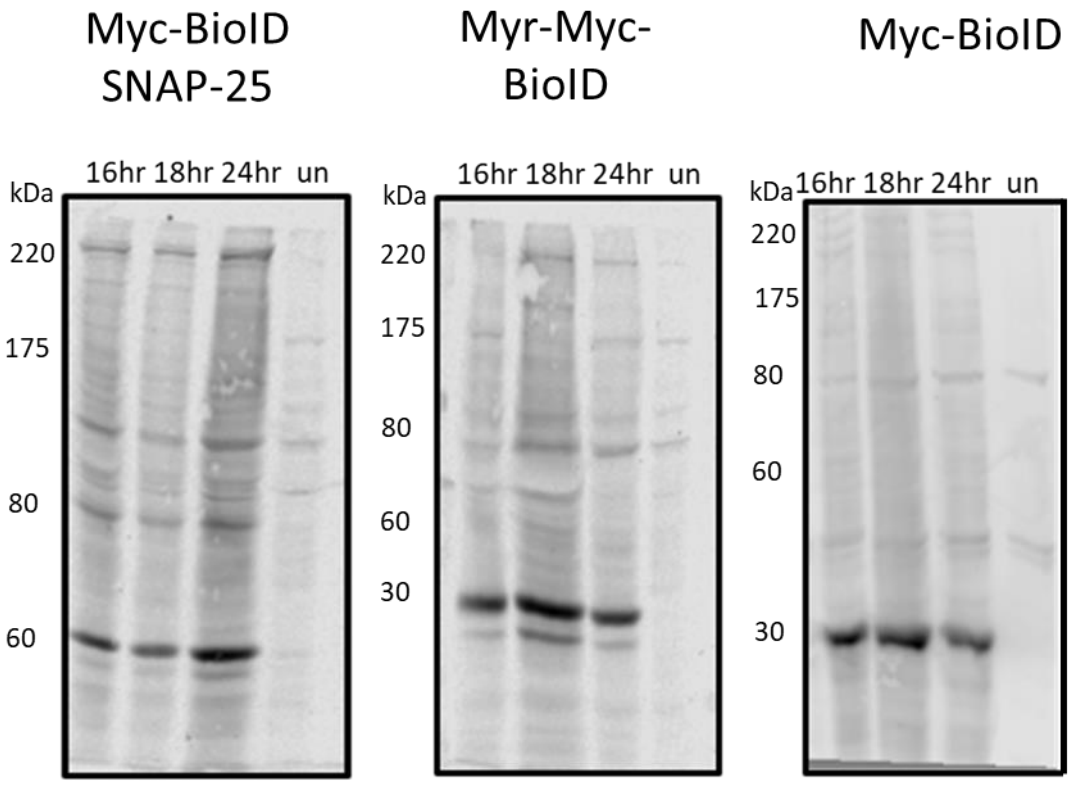

Figure B.3: Time-dependent biotinylation associated with Myc-BioID constructs in HEK293FT cells

HEK293FT cells transfected with Myc-BioID SNAP-25 on the left, Myr-Myc-BioID in the centre and Myc-BioID on the right were incubated with biotin (50 µM) for 16 hrs, 18 hrs and 24 hours before harvesting labelled proteins by lysis. The lysates were resolved by SDS PAGE and labelled via western blotting, using streptavidin to determine if there was a differential in biotinylation between the time points, N=1.

B.1.3 Patterns of biotinylation in proteins extracted from Myc-BioIDtransfected cells reveal construct-selective biotinylation

To determine if the biotinylation between the three discrete constructs was selective, samples were resolved by SDS-PAGE and Western blotted before being incubated with HRPcoupled streptavidin. These streptavidin blots revealed a differential pattern, transfected/ untransfected and with/without biotin (Figure B.4). To investigate the promotion of cellular biotinylation in the absence and presence of exogenous biotin in cells expressing the distinct constructs, streptavidin was used to label biotin via western blot analysis (Figure B.4, B).

As a control, I treated culture wells containing no cells but media with and without biotin for 24 hrs. Although these incubations showed a background of serum proteins (Figure B.4 A and B lanes 1 and 2), there was no contamination of cellular biotinylation. In a treatment of untransfected cells, there was biotinylation of 4 major proteins at 220 kDa, 130 kDa and two bands in the region of 70 kDa. This reflects biotin's appearance within abundant mammalian carboxylases: CoA carboxylase (220 kDa), Pyruvate carboxylase (130 kDa), 3methylcarotonyl CoA Carboxylase (75 kDa) and Propynyl CoA Carboxylase (72 kDa) (Figure 4.8, B indicated with red triangle). Accordingly, the four mammalian carboxylases are present in all the my BioID transfection and represent a clear background contamination.

In addition, each of the constructs generates an additional discrete major biotin-dependent reactivity. The size of which, in each of the independently expressed constructs Myc-BioID (30 kDa), Myr-Myc-BioID (32 kDa) and Myc-BioID-SNAP-25 (60 kDa) (Figure 4.8, B). This reflects self-biotinylation of the BioID fusion constructs and reassures they harbour efficient intrinsic activity. In each of the conditions, transfected with the Myc-BioID constructs, there is evidence of additional biotinylation. This is evidenced by additional streptavidin reactivity when compared to the untransfected control.

In the transfected biotin-fed cultures, there is a visible differential streptavidin reactivity suggestive of the biotin-ligases' biotinylated differential targets (Figure 4.8, B). Suggesting that the additional biotin promotes experimental biotinylation over and above what is possible in the presence of just the biotin present in the media, (Roux et al., 2012).

Overall, these data indicate 1. All three of the Myc-BioID constructs have biotin-ligase reactivity 2. Selective proximity labelling of the distinct fusion constructs is observed.

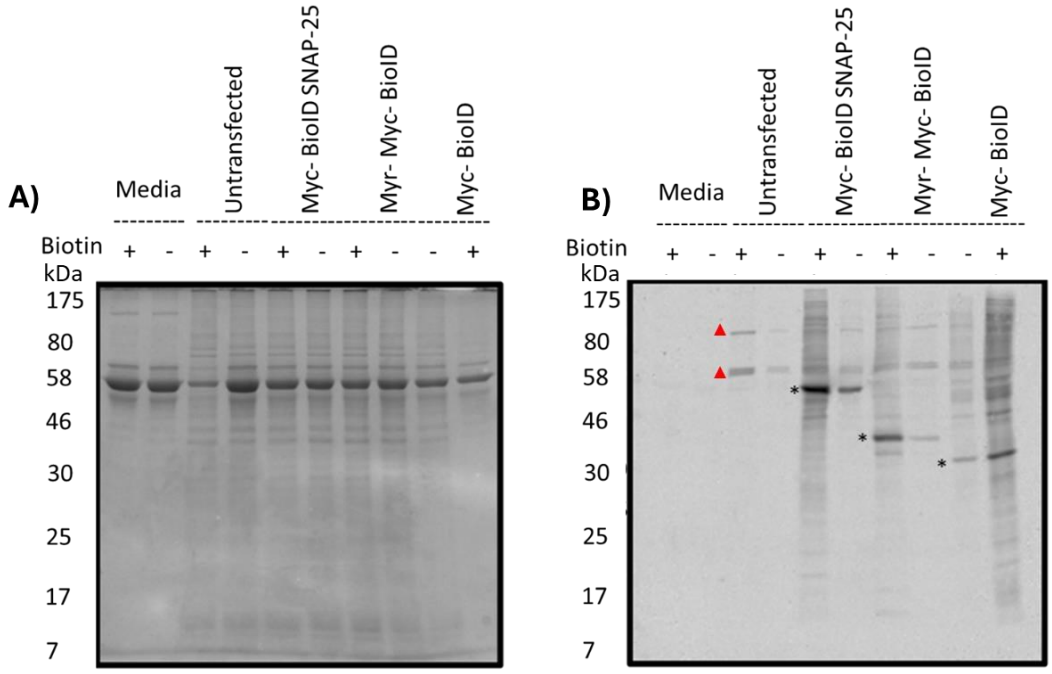

Figure B.4: HEK293FT cells transfected with Myc-BioID biotin ligases effectively biotinylated proteins in the presence of additional biotin supplementation.

A) Commissive for total protein for lysates of media only, untransfected cells or cells transfected with each of the Myc-BioID constructs.

B) Blot for streptavidin reactivity for the detection of biotinylated proteins. * corresponds to reactivity from the expressed Myc-BioID constructs, Δ for the known mammalian biotinylated carboxylases (Chandler and Ballard, 1986, Kirkeby et al., 1993) N=1.

B.1.4 Probing pull-down samples for known interactors of SNAP-25; TRIM9

Once it had been confirmed that the Myc-BioID- SNAP-25 construct could form a SNARE complex, had expected localisation and was active as a biotin ligase and that the pull down methodology was sufficient in extracting biotinylated proteins, an E3 ligase that has been shown to interact with SNAP-25 in other cellular models; TRIM9 was tested to see if it would be biotinylated by the Myc-BioID-SNAP-25 construct and pulled down by the BioID pull down.

The cell lysate and the streptavidin pull-down elution from each of the experimental conditions above were resolved on the same SDS-PAGE gel and labelled with fluorophoreconjugated antibodies by Western blotting. Initially, the samples were probed for streptavidin, then TRIM9 immunoreactivity (Figure 4.12, left). To directly compare the immunoactivity present in each sample.

TRIM9, an E3 ligase which interacts with SNAP-25 in neuronal models, is detectable in HEK293FT cells, albeit at low levels. TRIM9 was tested to see if it was biotinylated and pulled down in the Myc-BioID-SNAP-25 condition, which would indicate it was found in proximity to SNAP-25.

Side-by-side comparison of streptavidin immunoreactivity of each of the conditions allowed for the identification that the streptavidin intensity was strongest in the Myc-BioID sample, then the Myr-Myc-BioID sample, then finally the Myc-Bio-SNAP-25 sample, which would be expected due to the number of proteins accessible to be biotinylated.

The streptavidin immunoreactivity followed the same pattern as described above (Section 4.4.7). In the untransfected control, there were 4 bands present, whilst in the Myc-BioID, MyrMyc-BioID and Myc-BioID-SNAP-25 conditions, there was a laddering pattern in bands both in the lysate and less intense in the eluate.

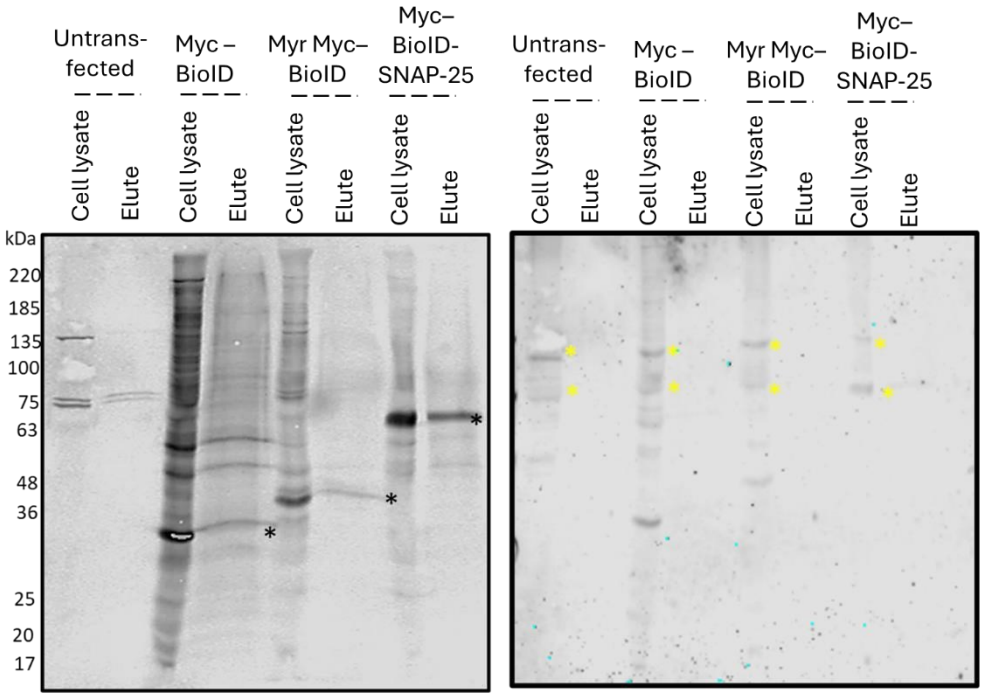

Figure B.5: TRIM9 is not detected by BioID streptavidin pulldown in Myc-BioID-SNAP-25 transfected HEK293FT cells

Cell lysate and elution from untransfected and HEK293FT cells transfected with Myc-BioID, Myr-Myc-BioID and Myc-BioID-SNAP-25 from streptavidin pull-down, stained with Streptavidin IR dye 800 on the left of the panel. Black asterisk marking immunoreactivity for Myc BioID constructs, and on the right immunoreactivity with TRIM9, where the isoforms are highlighted with the Yellow asterisk N=1.

The membrane was reprobed with Myc to confirm that the bands running at the expected molecular weights of each of the constructs were the constructs (Data not shown). These are marked with an asterisk for the band corresponding to each of the constructs in the streptavidin blot (Figure B.5, left).

The Lysate and eluate blots were reprobed with Trim9 (Figure B.5, right). Trim9 immunoreactivity was detected in the cell lysate fraction of all four samples but not in the elute of any. This would be expected for the untransfected, and Myc- and Myr- condition, but the fact that SNAP-25 and Trim9 have been previously shown to interact it would have been hypothesised that TRIM9 would be biotinylated and pulled down in the Myc-BioID-SNAP-25 condition.

B.1.5 Setting up BioID for SNAP-25 in PC12 cells

The BioID pull-down protocol was carried out on lysates from PC12 cells transfected with Myc-BioID-SNAP-25. The sample fractions generated in the pull-down as described in the methods section 2.7.11 were subjected to separation via SDS-PAGE and stained with Coomassie stain to determine the proportion of total protein in each fraction.

The total protein showed that there was protein present in the lysis, supernatant and was depleted in the flow through. No detectable protein was present in the pellet in the washes or the elute fractions. There is depletion in the flow-through staining which suggests some protein is retained by the beads (Figure B.6).

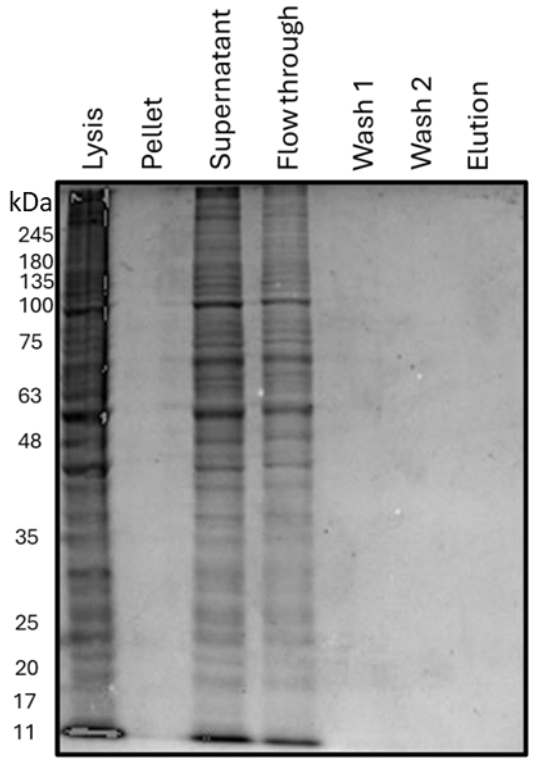

Figure B.6: Total protein is not pulled down in the streptavidin pull-downs

PC12 cells were transfected with Myc BioID SNAP-25, and the lysate was subjected to the streptavidin pull-down protocol. Pull-down fractions were run on a Coomassie gel in order to determine the presence of total protein in each fraction. Protein was detectable in the lysis and supernatant and depleted in the flowthrough, whilst no protein was detectable in the elution for a streptavidin pull-down, suggesting the specificity of pulled-down proteins, N=1.

B.1.6 Secondary only staining of Myc immunoprecipitations

Initially, the Myc pulldown elutions were done with SDS-PAGE sample buffer and boiled without Dithiothreitol (DTT), with DTT being added before the samples were run out on gels. However leaching of chains of the Myc antibody attached to the beads were observed with secondary only probing of the western blot membranes as such the bound proteins were then eluted via an acidic elution with 0.1 M glycine pH 2 then neutralised with tris base pH 8.5 whilst this reduced secondary only immunoreactivity this did not completely remove it which meant detection of proteins with antibodies of the same species (mouse) at 25 kDa, 50 kDa were not possible in the Myc pull downs even after optimisation (Figure B.7).

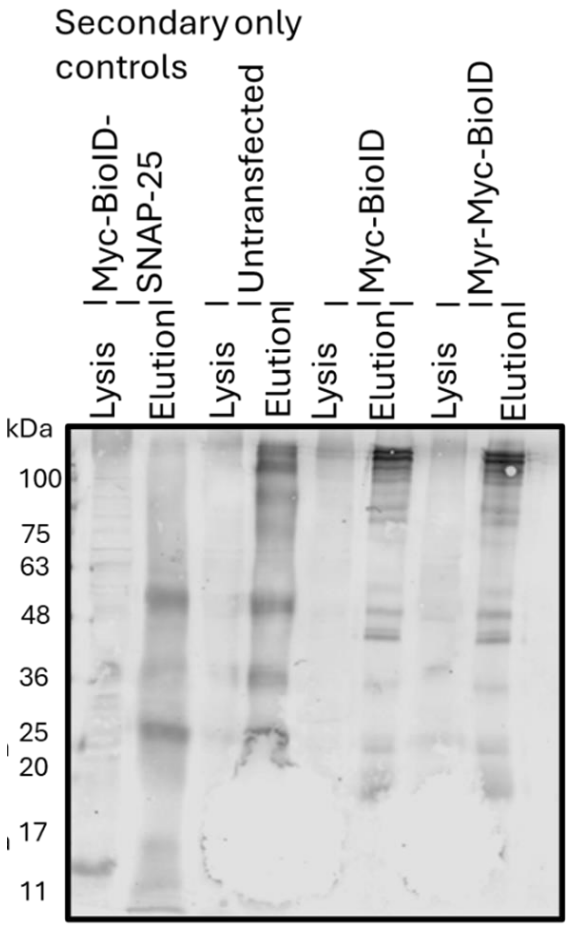

Figure B.7: Non-specific immunoreactivity in elution of Myc-pull downs

A secondary only staining displaying non-specific immunoreactivity in the Myc elution on all conditions in the regions of 25 kDa and 50 kDa.

Appendix C: Generation of CSPα-deficient PC12 cells

C.1 Genomic sequencing attempts

Genomic DNA was extracted from Parental, Lenti CRISPR, CD3 and CD5 PC12 cell lines. Primers were designed to span the regions of the CD3 and CD5 CRISPR lesions (Figure C.1, A). The CD3 primer set let to an amplification of the expected size in the parental, Lenti CRISPR and CD5 but not the CD3 lines. Whilst the CD5 primer pair were able to generate an amplification in all but to a lower intensity in the CD5 line, with the expression of two bands. Using the FWD primer of

the CD3 primer pair and the REV primer of the CD5 set led to the amplification of the expected size in the parental, Lenti CRISPR and in CD5, but no amplification was generated in the CD3 line.

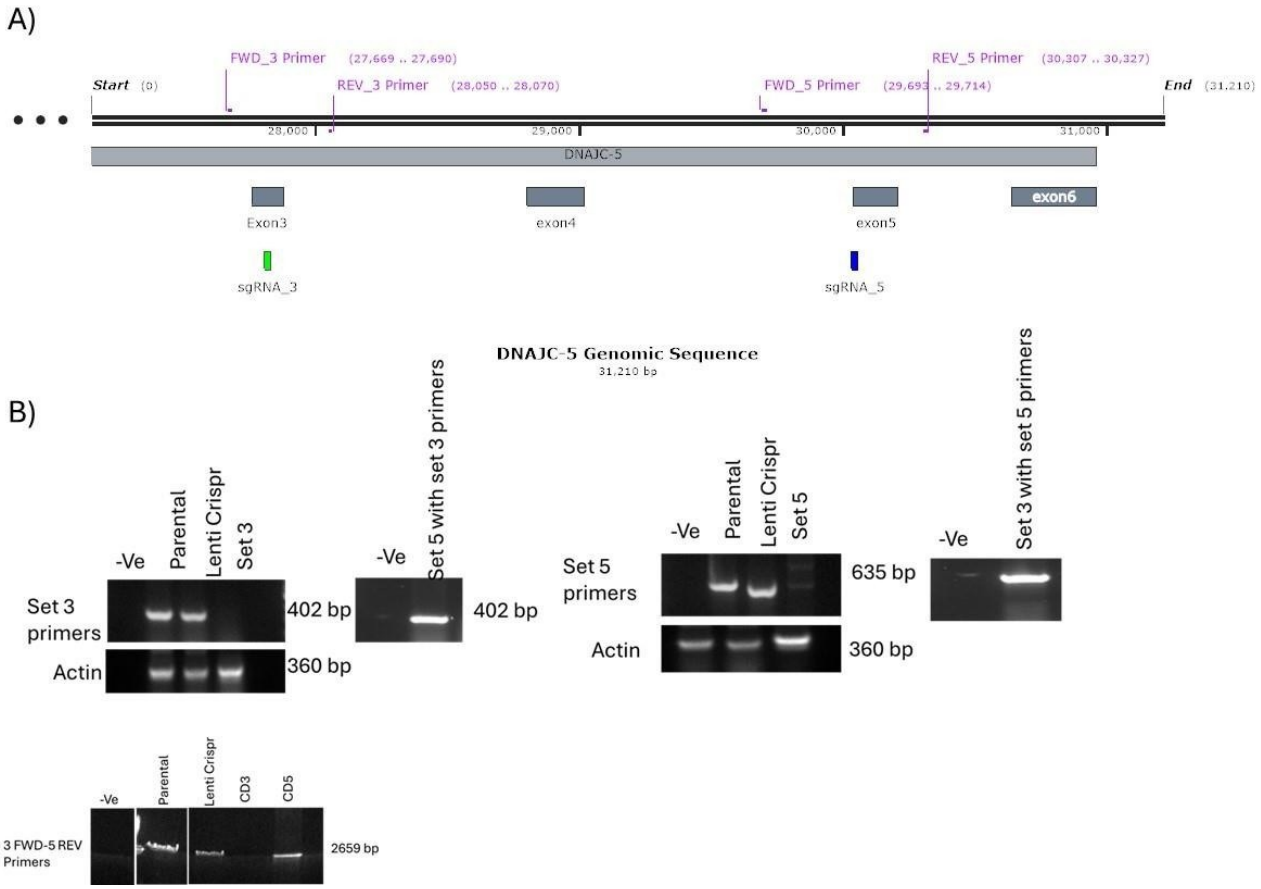

Figure C.1: PCR amplification of CRISPR lesion sites in genomic DNA extracted from control and CSPα-deficient PC12 cell lines. A) Location of primers used to amplify across CRISPR lesions from genomic DNA extracted from Parental, Lenti CRISPR, CD3 and CD5 PC12 cell lines, B) Attempted amplification of CSPα regions with primers depicted in the schematic.

C.2 CD3 cDNA sequencing example

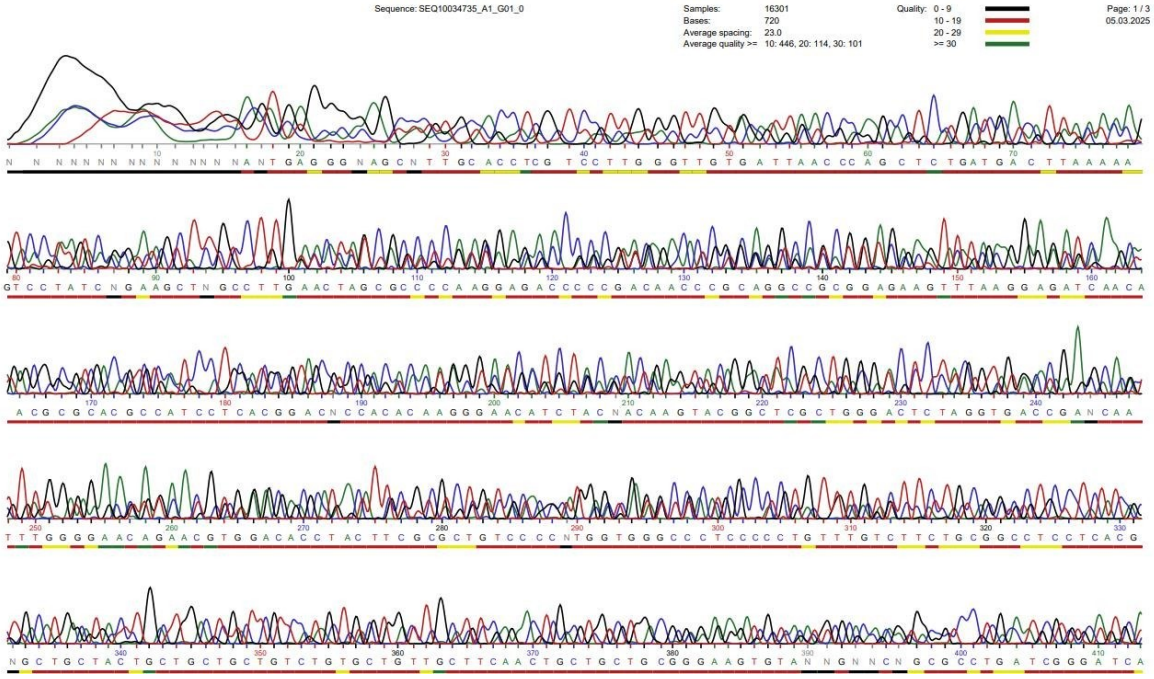

Figure C.2: Example of sequencing of CD3 from cDNA after amplification by PCR, with overlapping sequences.

C.3 Preliminary investigation into alternative protein disposal pathways

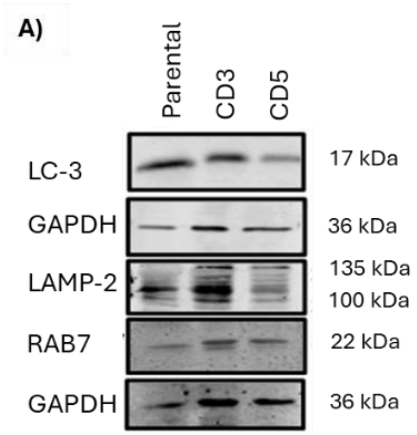

Figure C.3: PC12 CSPα deficient cells lines have no evidence for autophagic origin but evidence of protein disorder A**)** Parental and PC12 CSPα deficit CD3 and CD5 cells lysates 20 µg were resolved by SDS-PAGE and labelled with antibodies by western blotting of proteins involved in protein removal pathways: LC3 (autophagy), LAMP2 (lysosomes) and RAB7 (late endocytic pathway).

C.4 Quantification of protein altered in the cellular lysates submitted for labelfree proteomics

Proteins that were altered in the CSPα-deficient lines were blotted alongside some proteins that had not been observed to change in the samples sent for mass spectroscopy.

CSPα was blotted for in a differentiated parental PC12 sample alongside the undifferentiated parental cell lysates and CD3 and CD5 extracted and sent for proteomics. Exhibiting strong immunoreactivity in the differentiated sample and weak immunoreactivity in the parental line, and no expression in the CD lines.

SNAP-25 is present with strong immunoreactivity at the expected molecular weight in the parental cell lines, but is unquantifiable in the CSPα-deficient lines, as previously observed in the initial blotting when the lines were first generated.

The Dynamin-1 antibody used here (Protein Tech 18205-1-AP) is able to detect both Dynamin-1 and Dynamin-2. In the parental line, two bands are present in all samples; however, in the CSPα-deficient samples, whilst the top band is present in all samples, the lower band is absent in 3 of the 4 CD3 samples and in one of the CD5 samples. In Faire et al, the higher molecular weight polypeptide of the doublet was designated Dynamin 1, with the lower as Dynamin-2 (Faire et al., 1992). Suggesting that in the CSPα deficient lines there may be an effect on both Dynamin-1, which is observed in the CSPα -/- mouse and to a greater extent, Dynamin-2, which has not been reported in other CSPα knockout models. Dynamin-1 is enriched within the brain, localised to the presynaptic terminal, whilst Dynamin-2 has a widespread tissue distribution (Praefcke & McMahon, 2004).

Syntaxin, which was investigated as an interacting partner of SNAP-25, exhibited a decrease of 13% in the CD3 line and a slight increase of 6% in the CD5 line compared to the parental line, suggesting there may be a small effect on other proteins involved in exocytosis.

Trk B follows the same pattern as SNAP-25 present in the parental line, but unquantifiable in the CSPα-deficient lines. Actin and PSD95 are consistent across all samples, suggesting no overall structural loss between the parental and the CSPα-deficient lines, which supports the fact that there is no global change observed in the Coomassie gels (and unshown silverstained SDS-PAGE gels).

Appendix

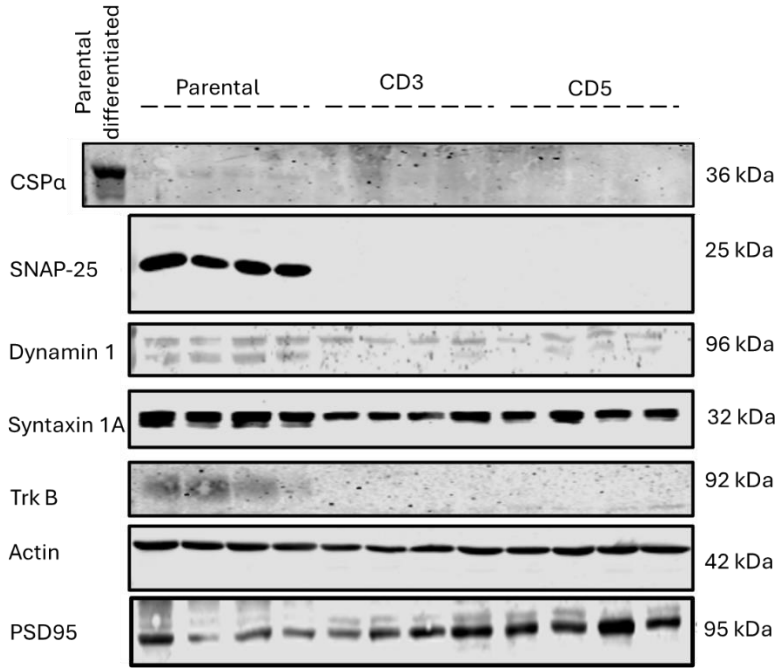

	Quantifiable change	
	CD3	CD5
CSPα	Unquantifiable	
SNAP-25	Unquantifiable	
Dynamin 1	*0.71	0.67*
Syntaxin 1A	0.87	1.06
Trk B	Unquantifiable	
Actin	1.02	1.04
PSD95	1.19	1.24

Figure C.4: Distinct alterations in selective proteins between parental and PC12 CSPαdeficient CD3 and CD5 cells. 20 µg factions of the supernatants that were submitted for mass spectroscopy were run on SDS-PAGE gels and labelled with fluorophore-conjugated antibodies by western blotting for proteins that had been noted to be altered in the lines previously as well as synaptic markers. Change quantified in comparison to parental after normalisation. *covers both upper and lower bands corresponding to Dyn-1 and Dyn-2.

C.5 Alterations in the expression of neuronal-associated proteins

As PC12 cells were used as a neuronal-like model, and it can be noted that phenotypically the CSPα-deficient cells were less neuronal-like than the parental cells, an unbiased approach was undertaken to determine how the synaptic up- and down-regulated protein alterations were using SYNGO. A synaptic gene-ontology evidence-based curated resource for synapse function and gene enrichment studies was used to determine how synapse-like the CSPα-deficient cell lines were.

For each ontology term, SYNGO uses a one-sided Fisher's exact test to compare the terms I input to the selected background set, which was set to rat brain expressed proteins containing 18035 unique genes in total, with 1591 SYNGO annotated genes.

Using SYNGO highlights that there are a lack of synaptic proteins in the CSPα-deficient cells.

Of the downregulated proteins, 38 were mapped to unique SYNGO annotated genes, for which 26 genes had a cellular component annotation with 71 annotations in total (as a gene can have multiple annotations), and 24 had a biological process with 48 annotations

Function terms that were downregulated were categorised into: synaptic assembly, regulation of the post-synapse, regulation of synaptic endocytosis, synaptic vesicle endocytosis, presynaptic modulation of chemical synaptic transmission modulation of chemical synaptic transmission, and regulation of the presynapse.

For up-regulated only two proteins were mapped in SYNGO but upon reviewing these hits it was noted that these proteins were ubiquitous across cell types and as such, were not synaptic-specific proteins.

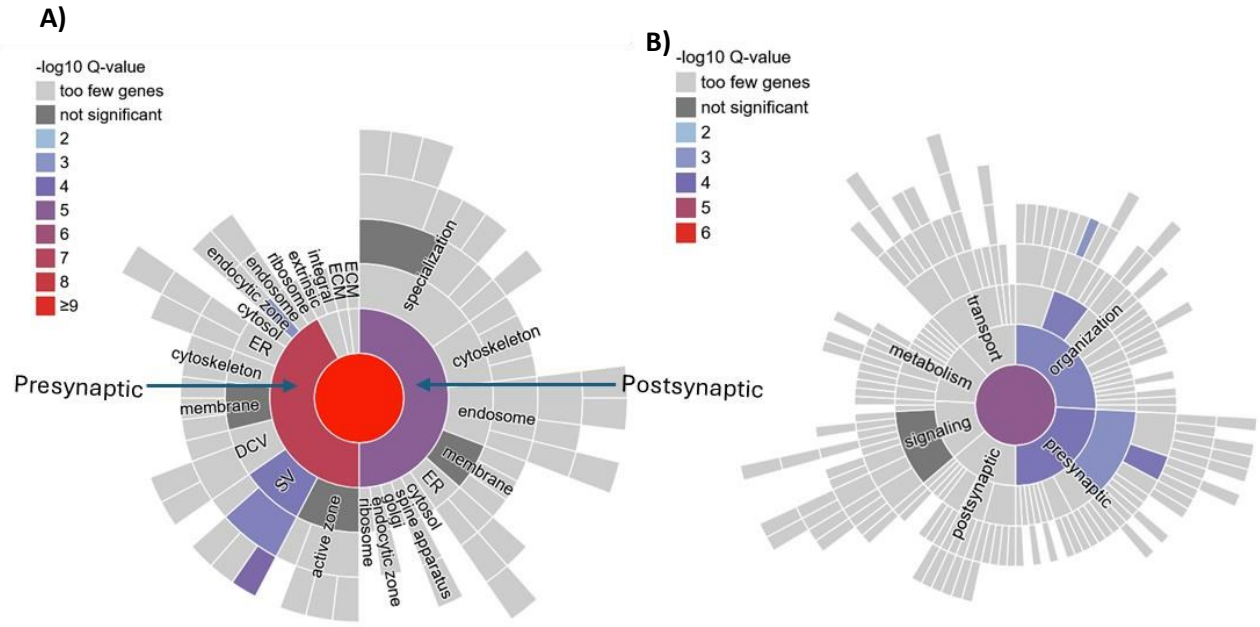

Figure C.5 SYNGO analysis of downregulated proteins enrichment analysis of A) synaptic location and B) synaptic function. Colour coding based on enrichment q- q-values of SYNGO ontology enrichment in the downregulated proteins expressed in the PC12 CSPα deficit CD3 and CD5 cells identified by mass spectroscopy and below a tabulation of the proteins determined to have a neuronal association and how they were determined to be altered in between the parental and CD lines.

C.6 Label-free proteomic readout

Table C1: Proteins down-regulated in the CD3 and CD5 lines identified by label-free proteomics

	Protein Group	Protein ID	Accession	Significance	Coverage (%)	#Peptides	#Unique	PTM	Avg. Mass	Sample Profile	Group Profile	Description
1	60	22565	tr|A0A8L2Q7B9|A0A8L2Q7B9_RAT	200	7	2	2	N	57625			Pyruvate kinase OS=Rattus norvegicus OX=10116 GN=Pkm PE=1 SV=1
2	124	22589	tr|A0A8I6ANE0|A0A8I6ANE0_RAT	200	14	5	5	Y	73161			Dihydropyrimidinase-related protein 2 OS=Rattus norvegicus OX=10116 GN=Dpysl2 PE=1 SV=1
3	227	373	P50398|GDIA_RAT	200	12	4	4	Y	50537			Rab GDP dissociation inhibitor alpha OS=Rattus norvegicus OX=10116 GN=Gdi1 PE=1 SV=1
4	268	22984	tr|A0A8L2Q996|A0A8L2Q996_RAT	200	11	2	2	Y	50620			Elongation factor 1-alpha OS=Rattus norvegicus OX=10116 GN=Eef1a2 PE=3 SV=1
5	268	687	P62632|EF1A2_RAT	200	11	2	2	Y	50454			Elongation factor 1-alpha 2 OS=Rattus norvegicus OX=10116 GN=Eef1a2 PE=1 SV=1
6	277	436	Q07009|CAN2_RAT	200	4	2	2	Y	79919			Calpain-2 catalytic subunit OS=Rattus norvegicus OX=10116 GN=Capn2 PE=1 SV=3
7	342	793	P14173|DDC_RAT	200	4	1	1	N	54053			Aromatic-L-amino-acid decarboxylase OS=Rattus norvegicus OX=10116 GN=Ddc PE=1 SV=1
8	424	23729	tr|F1M6C7|F1M6C7_RAT	200	4	1	1	Y	35628			Heterogeneous nuclear ribonucleoprotein A3-like OS=Rattus norvegicus OX=10116 GN=LOC120096281 PE=1 SV=4
9	437	607	P56574|IDHP_RAT	200	6	2	2	Y	50967			Isocitrate dehydrogenase [NADP], mitochondrial OS=Rattus norvegicus OX=10116 GN=Idh2 PE=1 SV=2
10	453	1133	Q9JHU0|DPYL5_RAT	200	5	2	2	N	61540			Dihydropyrimidinase-related protein 5 OS=Rattus norvegicus OX=10116 GN=Dpysl5 PE=1 SV=1
11	489	1588	P68511|1433F_RAT	200	23	5	5	N	28212			14-3-3 protein eta OS=Rattus norvegicus OX=10116 GN=Ywhah PE=1 SV=2
12	524	779	O35987|NSF1C_RAT	200	20	6	6	N	40680			NSFL1 cofactor p47 OS=Rattus norvegicus OX=10116 GN=Nsfl1c PE=1 SV=1
13	553	22954	tr|A0A8I6AK10|A0A8I6AK10_RAT	200	11	3	3	Y	54550			Fascin OS=Rattus norvegicus OX=10116 GN=Fscn1 PE=3 SV=1
14	625	1348	P61983|1433G_RAT	200	6	1	1	N	28303			14-3-3 protein gamma OS=Rattus norvegicus OX=10116 GN=Ywhag PE=1 SV=2
15	696	3011	Q6XI73|GDIR1_RAT	200	7	2	2	N	23407			Rho GDP-dissociation inhibitor 1 OS=Rattus norvegicus OX=10116 GN=Arhgdia PE=1 SV=1
16	806	2104	P11348|DHPR_RAT	200	13	2	2	Y	25552			Dihydropteridine reductase OS=Rattus norvegicus OX=10116 GN=Qdpr PE=1 SV=1
17	816	1626	Q88989|MDHC_RAT	200	22	5	5	Y	36483			Malate dehydrogenase, cytoplasmic OS=Rattus norvegicus OX=10116 GN=Mdh1 PE=1 SV=3
18	833	1422	Q6QN11|CNDP2_RAT	200	8	2	2	N	52693			Cytosolic non-specific dipeptidase OS=Rattus norvegicus OX=10116 GN=Cndp2 PE=1 SV=1

19	**843**	1861	P41565|IDHG1_RAT	200	11	2	2	Y	42851		Isocitrate dehydrogenase [NAD] subunit gamma 1, mitochondrial OS=Rattus norvegicus OX=10116 GN=Idh3g PE=1 SV=2
20	**844**	1873	P54313|GBB2_RAT	200	9	3	3	Y	37331		Guanine nucleotide-binding protein G(I)/G(S)/G(T) subunit beta-2 OS=Rattus norvegicus OX=10116 GN=Gnb2 PE=1 SV=4
21	**895**	1548	Q99NA5|IDH3A_RAT	200	19	5	5	Y	39614		Isocitrate dehydrogenase [NAD] subunit alpha, mitochondrial OS=Rattus norvegicus OX=10116 GN=Idh3a PE=1 SV=1
22	**895**	23645	tr|F1LNF7|F1LNF7_RAT	200	18	5	5	Y	41434		Isocitrate dehydrogenase [NAD] subunit, mitochondrial OS=Rattus norvegicus OX=10116 GN=Idh3a PE=3 SV=3
23	**909**	23679	tr|A0A0G2K737|A0A0G2K737_RAT	200	43	7	7	Y	32700		Thioredoxin-like 1 OS=Rattus norvegicus OX=10116 GN=Txnl1 PE=1 SV=1
24	**1393**	4780	Q32PX2|AIMP2_RAT	200	3	1	1	N	35443		Aminoacyl tRNA synthase complex-interacting multifunctional protein 2 OS=Rattus norvegicus OX=10116 GN=Aimp2 PE=2 SV=1
25	**1593**	25324	tr|A6J9C6|A6J9C6_RAT	200	12	1	1	N	22094		Biliverdin reductase B OS=Rattus norvegicus OX=10116 GN=Blvrb PE=1 SV=1
26	**266**	477	P04785|PDIA1_RAT	156.54	25	11	11	N	56951		Protein disulfide-isomerase OS=Rattus norvegicus OX=10116 GN=P4hb PE=1 SV=2
27	**2110**	26917	tr|B0K014|B0K014_RAT	156.54	15	2	2	N	23394		D-aminoacyl-tRNA deacylase OS=Rattus norvegicus OX=10116 GN=Dtd1 PE=1 SV=1
28	**2328**	27368	tr|D3ZZR9|D3ZZR9_RAT	153.53	24	3	3	Y	17282		peptidylprolyl isomerase OS=Rattus norvegicus OX=10116 GN=Fkbp2 PE=4 SV=2
29	**3269**	29011	tr|D4A8M5|D4A8M5_RAT	153.53	12	1	1	Y	10834		Small nuclear ribonucleoprotein E OS=Rattus norvegicus OX=10116 GN=Snrpepl2 PE=3 SV=1
30	**975**	24376	Q6ES54|NPL4_RAT	150.51	8	2	2	Y	68056		Nuclear protein localization protein 4 homolog OS=Rattus norvegicus OX=10116 GN=Nploc4 PE=1 SV=3
31	**997**	2394	Q66HG5|TM9S2_RAT	147.5	5	2	2	Y	75586		Transmembrane 9 superfamily member 2 OS=Rattus norvegicus OX=10116 GN=Tm9sf2 PE=2 SV=1
32	**122**	108	Q9ER34|ACON_RAT	145.07	16	7	7	Y	85433		Aconitate hydratase, mitochondrial OS=Rattus norvegicus OX=10116 GN=Aco2 PE=1 SV=2
33	**442**	947	Q5RKI1|IF4A2_RAT	143.11	4	1	1	N	46402		Eukaryotic initiation factor 4A-II OS=Rattus norvegicus OX=10116 GN=Eif4a2 PE=1 SV=1
34	**1755**	25417	tr|A0A8I6AII6|A0A8I6AII6_RAT	142.73	9	1	1	N	23469		small monomeric GTPase OS=Rattus norvegicus OX=10116 GN=Rab5b PE=1 SV=1
35	**235**	1043	P04905|GSTM1_RAT	142.06	6	1	1	N	25914		Glutathione S-transferase Mu 1 OS=Rattus norvegicus OX=10116 GN=Gstm1 PE=1 SV=2

Appendix

36	**1829**	25301	tr|G3V7J2|G3V7J2_RAT	136.71	10	2	2	Y	34385	 Protein activator of interferon induced protein kinase EIF2AK2 OS=Rattus norvegicus OX=10116 GN=Prkra PE=1 SV=1
37	**620**	764	O9Z2L0|VDAC1_RAT	134.66	25	6	6	Y	30756	 Non-selective voltage-gated ion channel VDAC1 OS=Rattus norvegicus OX=10116 GN=Vdac1 PE=1 SV=4
38	**1380**	3214	Q6RUV5|RAC1_RAT	133.57	15	2	2	Y	21450	 Ras-related C3 botulinum toxin substrate 1 OS=Rattus norvegicus OX=10116 GN=Rac1 PE=1 SV=1
39	**1725**	2847	M0RC99|RAB5A_RAT	133.09	24	2	2	Y	23625	 Ras-related protein Rab-5A OS=Rattus norvegicus OX=10116 GN=Rab5a PE=2 SV=1
40	**1725**	24517	tr|A0A8I5ZS76|A0A8I5ZS76_RAT	133.09	24	2	2	Y	23615	 small monomeric GTPase OS=Rattus norvegicus OX=10116 GN=Rab5a PE=1 SV=1
41	**1048**	2538	P15791|KCC2D_RAT	132.57	3	1	1	N	60081	 Calcium/calmodulin-dependent protein kinase type II subunit delta OS=Rattus norvegicus OX=10116 GN=Camk2d PE=1 SV=1
42	**1465**	24472	tr|F1M978|F1M978_RAT	129.31	3	1	1	N	36278	 Inositol-1-monophosphatase OS=Rattus norvegicus OX=10116 GN=Impa1 PE=1 SV=2
43	**925**	1791	P31044|PEBP1_RAT	128.1	14	2	2	N	20801	 Phosphatidylethanolamine-binding protein 1 OS=Rattus norvegicus OX=10116 GN=Pebp1 PE=1 SV=3
44	**1697**	26985	P70550|RAB8B_RAT	125.81	6	1	1	N	23603	 Ras-related protein Rab-8B OS=Rattus norvegicus OX=10116 GN=Rab8b PE=1 SV=1
45	**136**	178	Q4QRB4|TBB3_RAT	124.65	9	2	2	N	50419	 Tubulin beta-3 chain OS=Rattus norvegicus OX=10116 GN=Tubb3 PE=1 SV=1
46	**1190**	4474	Q6PEC4|SKP1_RAT	124.07	26	4	4	N	18672	 S-phase kinase-associated protein 1 OS=Rattus norvegicus OX=10116 GN=Skp1 PE=1 SV=3
47	**673**	1486	P84092|AP2M1_RAT	121.2	21	6	6	Y	49655	 AP-2 complex subunit mu OS=Rattus norvegicus OX=10116 GN=Ap2m1 PE=1 SV=1
48	**234**	523	P00388|NCPR_RAT	117.99	7	3	3	Y	76963	 NADPH--cytochrome P450 reductase OS=Rattus norvegicus OX=10116 GN=Por PE=1 SV=3
49	**1344**	4294	Q6AYP5|CADM1_RAT	116.48	8	2	2	Y	51854	 Cell adhesion molecule 1 OS=Rattus norvegicus OX=10116 GN=Cadm1 PE=1 SV=1
50	**162**	22960	tr|F1M9N9|F1M9N9_RAT	116.02	0	1	1	N	434779	 Ankyrin 2 OS=Rattus norvegicus OX=10116 GN=Ank2 PE=1 SV=4
51	**450**	626	P63004|LIS1_RAT	112.33	25	7	7	Y	46670	 Platelet-activating factor acetylhydrolase IB subunit alpha OS=Rattus norvegicus OX=10116 GN=Pafah1b1 PE=1 SV=2
52	**1893**	61072	tr|A0A8I6GA19|A0A8I6GA19_RAT	110.97	4	1	1	N	47436	 non-specific serine/threonine protein kinase OS=Rattus norvegicus OX=10116 GN=Vrk1 PE=1 SV=1
53	**723**	3469	P0DP31|CALM3_RAT	110.73	52	7	7	Y	16838	 Calmodulin-3 OS=Rattus norvegicus OX=10116 GN=Calm3 PE=1 SV=1
54	**723**	24995	P0DP30|CALM2_RAT	110.73	52	7	7	Y	16838	 Calmodulin-2 OS=Rattus norvegicus OX=10116 GN=Calm2 PE=1 SV=1

55	**723**	24996	P0DP29|CALM1_RAT	110.73	52	7	7	Y	16838	 Calmodulin-1 OS=Rattus norvegicus OX=10116 GN=Calm1 PE=1 SV=1
56	**1111**	2990	Q8K1Q0|NMT1_RAT	107.48	4	1	1	N	56860	 Glycylpeptide N-tetradecanoyltransferase 1 OS=Rattus norvegicus OX=10116 GN=Nmt1 PE=1 SV=1
57	**1111**	24565	tr|A0A8I6ATE4|A0A8I6ATE4_RAT	107.48	4	1	1	N	57227	 Glycylpeptide N-tetradecanoyltransferase OS=Rattus norvegicus OX=10116 GN=Nmt1 PE=1 SV=1
58	**2716**	28583	tr|A6ISV1|A6ISV1_RAT	105.69	7	1	1	N	38540	 Protein phosphatase 1, regulatory (Inhibitor) subunit 8 OS=Rattus norvegicus OX=10116 GN=Ppp1r8 PE=1 SV=1
59	**551**	23625	tr|R9PXU4|R9PXU4_RAT	97.23	12	4	4	Y	54610	 Thioredoxin reductase 1, cytoplasmic OS=Rattus norvegicus OX=10116 GN=Txnrd1 PE=1 SV=3
60	**18**	22615	tr|A0A8I6AG70|A0A8I6AGZ0_RAT	95.63	37	43	43	Y	189019	 Clathrin heavy chain OS=Rattus norvegicus OX=10116 GN=Cltc PE=1 SV=1
61	**556**	1634	Q62991|SCFD1_RAT	95.27	5	2	2	N	72263	 Sec1 family domain-containing protein 1 OS=Rattus norvegicus OX=10116 GN=Scfd1 PE=1 SV=1
62	**2490**	5694	Q9WUI4|CHSP1_RAT	95.18	35	2	2	N	15906	 Calcium-regulated heat stable protein 1 OS=Rattus norvegicus OX=10116 GN=Carhsp1 PE=1 SV=1
63	**1750**	4243	O35263|PA1B3_RAT	94.18	4	1	1	N	25863	 Platelet-activating factor acetylhydrolase IB subunit alpha1 OS=Rattus norvegicus OX=10116 GN=Pafah1b3 PE=1 SV=1
64	**2180**	26206	tr|E9PTV0|E9PTV0_RAT	94.03	6	1	1	Y	22835	 guanylate kinase OS=Rattus norvegicus OX=10116 GN=Guk1 PE=3 SV=3
65	**406**	972	Q9ER24|ATX10_RAT	93.72	4	2	2	Y	53727	 Ataxin-10 OS=Rattus norvegicus OX=10116 GN=Atxn10 PE=1 SV=1
66	**27**	22646	tr|G3V7Q7|G3V7Q7_RAT	92.07	11	13	13	N	188831	 IQ motif containing GTPase activating protein 1 OS=Rattus norvegicus OX=10116 GN=Iqgap1 PE=1 SV=1
67	**680**	2119	Q6QIN3|NT5D2_RAT	91.94	2	1	1	N	63653	 5'-nucleotidase domain-containing protein 2 OS=Rattus norvegicus OX=10116 GN=Nt5dc2 PE=2 SV=2
68	**1068**	24910	tr|A0A8I6AIA8|A0A8I6AIA8_RAT	91.44	8	3	3	Y	62499	Translation initiation factor eIF2B subunit delta OS=Rattus norvegicus OX=10116 GN=Eif2b4 PE=1 SV=1
69	**1068**	3814	Q63186|EI2BD_RAT	91.44	9	3	3	Y	57809	 Translation initiation factor eIF2B subunit delta OS=Rattus norvegicus OX=10116 GN=Eif2b4 PE=2 SV=1
70	**297**	262	Q5RKI0|WDR1_RAT	90.88	10	4	4	Y	66182	 WD repeat-containing protein 1 OS=Rattus norvegicus OX=10116 GN=Wdr1 PE=1 SV=3
71	**1077**	4310	Q9Z2F5|CTBP1_RAT	90.36	12	3	3	Y	46628	 C-terminal-binding protein 1 OS=Rattus norvegicus OX=10116 GN=Ctbp1 PE=1 SV=3
72	**1077**	25884	tr|A0A8I5ZSG1|A0A8I5ZSG1_RAT	90.36	14	3	3	Y	40506	 C-terminal binding protein 1 OS=Rattus norvegicus OX=10116 GN=Ctbp1 PE=1 SV=1

Appendix

73	**1077**	25885	tr|F7FG31|F7FG31_RAT	90.36	13	3	3	Y	42717	 C-terminal binding protein 1 OS=Rattus norvegicus OX=10116 GN=Ctbp1 PE=1 SV=2
74	**1563**	3238	Q6IJ21|SNX3_RAT	89.84	35	3	3	N	18762	 Sorting nexin-3 OS=Rattus norvegicus OX=10116 GN=Snx3 PE=1 SV=1
75	**1005**	24616	tr|A0A0G2K185|A0A0G2K185_RAT	87.71	8	2	2	N	34087	 Arp2/3 complex 34 kDa subunit OS=Rattus norvegicus OX=10116 GN=Arpc2 PE=1 SV=1
76	**1005**	2946	P85970|ARPC2_RAT	87.71	8	2	2	N	34391	 Actin-related protein 2/3 complex subunit 2 OS=Rattus norvegicus OX=10116 GN=Arpc2 PE=1 SV=1
77	**831**	23708	tr|A0A8I6A0A3|A0A8I6A0A3_RAT	87.24	12	3	3	Y	53769	 Glutathione reductase OS=Rattus norvegicus OX=10116 GN=Gsr PE=1 SV=1
78	**1090**	24359	tr|F7FZ84|F7FZ84_RAT	86.08	10	2	2	Y	46609	 Vacuolar protein sorting 4 homolog B OS=Rattus norvegicus OX=10116 GN=Vps4b PE=1 SV=1
79	**1090**	24360	tr|A0A8I6GH80|A0A8I6GH80_RAT	86.08	9	2	2	Y	49451	 vesicle-fusing ATPase OS=Rattus norvegicus OX=10116 GN=Vps4b PE=1 SV=1
80	**1264**	3457	P62959|HINT1_RAT	82.94	21	2	2	Y	13777	 Adenosine 5'-monophosphoramidase HINT1 OS=Rattus norvegicus OX=10116 GN=Hint1 PE=1 SV=5
81	**682**	1184	Q4V7C7|ARP3_RAT	81.05	23	5	5	Y	47357	 Actin-related protein 3 OS=Rattus norvegicus OX=10116 GN=Actr3 PE=1 SV=1
82	**106**	141	Q04462|SYVC_RAT	80.2	9	7	7	Y	140368	 Valine--tRNA ligase OS=Rattus norvegicus OX=10116 GN=Vars1 PE=2 SV=2
83	**30**	31	Q9Z1P2|ACTN1_RAT	79.59	2	1	1	Y	102960	 Alpha-actinin-1 OS=Rattus norvegicus OX=10116 GN=Actn1 PE=1 SV=1
84	**2121**	42148	tr|D3ZHI9|D3ZHI9_RAT	78.19	3	1	1	N	50347	 Serine/threonine-protein phosphatase 2A 56 kDa regulatory subunit OS=Rattus norvegicus OX=10116 GN=Ppp2r5e PE=1 SV=1
85	**1545**	4517	P32089|TXTP_RAT	78.17	4	1	1	N	33835	 Tricarboxylate transport protein, mitochondrial OS=Rattus norvegicus OX=10116 GN=Slc25a1 PE=1 SV=1
86	**1545**	25477	tr|A0A8I6AEC6|A0A8I6AEC6_RAT	78.17	4	1	1	N	32446	 Citrate transport protein OS=Rattus norvegicus OX=10116 GN=Slc25a1 PE=1 SV=1
87	**207**	23082	tr|D4A133|D4A133_RAT	77.49	19	8	8	Y	71401	 H(+)-transporting two-sector ATPase OS=Rattus norvegicus OX=10116 GN=Atp6v1a PE=1 SV=2
88	**53**	125	P06685|AT1A1_RAT	76.86	10	8	8	Y	113054	 Sodium/potassium-transporting ATPase subunit alpha-1 OS=Rattus norvegicus OX=10116 GN=Atp1a1 PE=1 SV=1
89	**1461**	3661	Q9Z118|PTBP3_RAT	76.24	3	1	1	Y	56716	 Polypyrimidine tract-binding protein 3 OS=Rattus norvegicus OX=10116 GN=Ptbp3 PE=2 SV=1
90	**121**	442	Q9JLA3|UGGG1_RAT	76.11	2	2	2	N	176430	 UDP-glucose:glycoprotein glucosyltransferase 1 OS=Rattus norvegicus OX=10116 GN=Uggt1 PE=1 SV=2

91	**495**	23859	tr|F1LQJ7|F1LQJ7_RAT	74.53	2	1	1	N	73697	 phosphoenolpyruvate carboxykinase (GTP) OS=Rattus norvegicus OX=10116 GN=Pck2 PE=1 SV=3
92	**329**	23254	tr|D3ZUY8|D3ZUY8_RAT	74.48	7	5	5	Y	105589	 AP-2 complex subunit alpha OS=Rattus norvegicus OX=10116 GN=Ap2a1 PE=1 SV=2
93	**1486**	25085	tr|A0A0G2K977|A0A0G2K977_RAT	73.94	2	1	1	N	115930	 Golgin A2 OS=Rattus norvegicus OX=10116 GN=Golga2 PE=1 SV=1
94	**1235**	3267	P58405|STRN3_RAT	71.54	5	2	2	N	87111	 Striatin-3 OS=Rattus norvegicus OX=10116 GN=Strn3 PE=1 SV=2
95	**2648**	43578	Q5BJQ6|CSTF1_RAT	70.25	4	1	1	N	48382	 Cleavage stimulation factor subunit 1 OS=Rattus norvegicus OX=10116 GN=Cstf1 PE=2 SV=1
96	**967**	24407	tr|D4A857|D4A857_RAT	69.12	6	4	4	Y	116650	 Importin 9 OS=Rattus norvegicus OX=10116 GN=Ipo9 PE=4 SV=3
97	**1019**	2225	Q35509|RB11B_RAT	68.75	9	2	2	N	24488	 Ras-related protein Rab-11B OS=Rattus norvegicus OX=10116 GN=Rab11b PE=1 SV=4
98	**134**	311	Q4FZT9|PSMD2_RAT	68.39	23	15	15	Y	100188	 26S proteasome non-ATPase regulatory subunit 2 OS=Rattus norvegicus OX=10116 GN=Psmd2 PE=1 SV=1
99	**2432**	28881	tr|D3ZDU5|D3ZDU5_RAT	67.78	9	1	1	N	16027	 Profilin OS=Rattus norvegicus OX=10116 GN=Pfn2 PE=3 SV=1
100	**2432**	9077	Q6EPC6|PROF2_RAT	67.78	10	1	1	N	15002	 Profilin-2 OS=Rattus norvegicus OX=10116 GN=Pfn2 PE=1 SV=3
101	**1102**	3097	Q5HZV9|PP1R7_RAT	66.92	7	2	2	N	41297	 Protein phosphatase 1 regulatory subunit 7 OS=Rattus norvegicus OX=10116 GN=Ppp1r7 PE=1 SV=1
102	**41**	22677	tr|A6JR01|A6JR01_RAT	66.28	19	15	15	Y	141695	 High density lipoprotein binding protein OS=Rattus norvegicus OX=10116 GN=Hdlbp PE=1 SV=1
103	**1514**	3360	O62847|ADDG_RAT	66.05	4	2	2	N	78818	 Gamma-adducin OS=Rattus norvegicus OX=10116 GN=Add3 PE=1 SV=3
104	**1570**	26041	tr|A0A8I5YBE8|A0A8I5YBE8_RAT	64.62	18	4	4	N	34884	 Purine rich element binding protein A OS=Rattus norvegicus OX=10116 GN=Pura PE=1 SV=1
105	**1076**	2986	P84083|ARF5_RAT	64.1	14	2	2	N	20530	 ADP-ribosylation factor 5 OS=Rattus norvegicus OX=10116 GN=Arf5 PE=1 SV=2
106	**2138**	26981	tr|D3ZYH3|D3ZYH3_RAT	63.66	18	2	2	Y	18593	 diphosphoinositol-polyphosphate diphosphatase OS=Rattus norvegicus OX=10116 GN=Nudt11 PE=3 SV=1
107	**1648**	26063	tr|A0A8I5ZRF0|A0A8I5ZRF0_RAT	62.89	15	2	2	N	21511	 Tumor protein D52 OS=Rattus norvegicus OX=10116 GN=Tpd52 PE=1 SV=1
108	**1648**	26150	tr|A0A0G2K865|A0A0G2K865_RAT	62.89	12	2	2	N	26786	 Tumor protein D52 OS=Rattus norvegicus OX=10116 GN=Tpd52 PE=1 SV=2
109	**1688**	2806	O63468|KPRA_RAT	62.62	8	2	2	Y	39436	 Phosphoribosyl pyrophosphate synthase-associated protein 1 OS=Rattus norvegicus OX=10116 GN=Prpsap1 PE=1 SV=1

Appendix

110	**557**	24150	tr|A0A8I8YFS5|A0A8I8YFS5_RAT	62.08	12	4	4	N	56502		Histidine--tRNA ligase, cytoplasmic OS=Rattus norvegicus OX=10116 GN=Hars1 PE=1 SV=1
111	**63**	104	O66X93|SND1_RAT	61.67	12	9	9	Y	101962		Staphylococcal nuclease domain-containing protein 1 OS=Rattus norvegicus OX=10116 GN=Snd1 PE=1 SV=1
112	**2543**	4668	A2RUW1|TOLIP_RAT	61.37	5	1	1	N	30315		Toll-interacting protein OS=Rattus norvegicus OX=10116 GN=Tollip PE=1 SV=1
113	**128**	22958	tr|A0A8I6AUZ1|A0A8I6AUZ1_RAT	59.73	2	2	2	N	108283		Hexokinase-1 OS=Rattus norvegicus OX=10116 GN=Hk1 PE=1 SV=1
114	**306**	22935	tr|G3V8A5|G3V8A5_RAT	59.6	13	8	8	N	91727		Vacuolar protein sorting-associated protein 35 OS=Rattus norvegicus OX=10116 GN=Vps35 PE=1 SV=1
115	**2078**	7278	P63029|TCTP_RAT	59.08	8	1	1	Y	19462		Translationally-controlled tumor protein OS=Rattus norvegicus OX=10116 GN=Tpt1 PE=1 SV=1
116	**1039**	25564	tr|A0A8I6AAH5|A0A8I6AAH5_RAT	58.24	2	1	1	N	106176		O-GlcNAcase OS=Rattus norvegicus OX=10116 GN=Oga PE=1 SV=1
117	**1769**	24670	tr|F2Z3T7|F2Z3T7_RAT	58.15	20	4	4	N	32033		Isochorismatase domain-containing protein 1 OS=Rattus norvegicus OX=10116 GN=Isoc1 PE=1 SV=1
118	**921**	41834	tr|D3ZWA8|D3ZWA8_RAT	57.15	3	1	1	Y	79364		Adaptor protein, phosphotyrosine interacting with PH domain and leucine zipper 1 OS=Rattus norvegicus OX=10116 GN=Appl1 PE=1 SV=4
119	**2661**	42222	Q5HZY0|UBXN4_RAT	54.36	4	1	1	N	56394		UBX domain-containing protein 4 OS=Rattus norvegicus OX=10116 GN=Ubxn4 PE=1 SV=1
120	**491**	952	P07943|ALDR_RAT	54.3	9	2	2	Y	35797		Aldo-keto reductase family 1 member B1 OS=Rattus norvegicus OX=10116 GN=Akr1b1 PE=1 SV=3
121	**1356**	24235	tr|F7FF51|F7FF51_RAT	52.4	20	4	4	Y	39209		Serine/threonine-protein phosphatase 2A activator OS=Rattus norvegicus OX=10116 GN=Ptpa PE=1 SV=1
122	**1463**	24321	tr|A0A8L2QLQ8|A0A8L2QLQ8_RAT	52.23	2	1	1	Y	86292		Amyloid-beta A4 protein OS=Rattus norvegicus OX=10116 GN=App PE=1 SV=1
123	**1463**	24322	P08592|A4_RAT	52.23	2	1	1	Y	86704		Amyloid-beta precursor protein OS=Rattus norvegicus OX=10116 GN=App PE=1 SV=2
124	**414**	716	O09175|AMPB_RAT	50.03	7	3	3	Y	72620		Aminopeptidase B OS=Rattus norvegicus OX=10116 GN=Rnpep PE=1 SV=2
125	**414**	23024	tr|G3V6V1|G3V6V1_RAT	50.03	7	3	3	Y	72689		Arginyl aminopeptidase OS=Rattus norvegicus OX=10116 GN=Rnpep PE=3 SV=1
126	**579**	26713	tr|G3V661|G3V661_RAT	49.29	2	2	2	Y	166740		Bromodomain adjacent to zinc finger domain, 1B OS=Rattus norvegicus OX=10116 GN=Baz1b PE=1 SV=2
127	**1544**	4241	A0JPM9|EIF3J_RAT	48.26	14	3	3	Y	29187		Eukaryotic translation initiation factor 3 subunit J OS=Rattus norvegicus OX=10116 GN=Eif3j PE=1 SV=1

128	**39**	22745	tr|D3ZU13|D3ZU13_RAT	46.49	8	10	10	N	175704		Eukaryotic translation initiation factor 4 gamma 1 OS=Rattus norvegicus OX=10116 GN=Eif4g1 PE=1 SV=1
129	**756**	24098	tr|A0A8L2QJE6|A0A8L2QJE6_RAT	46.01	14	3	3	Y	34939		Omega-amidase NIT2 OS=Rattus norvegicus OX=10116 GN=Nit2 PE=1 SV=1
130	**640**	24270	tr|Q4V8I9|Q4V8I9_RAT	45.76	8	3	3	N	57023		UTP--glucose-1-phosphate uridylyltransferase OS=Rattus norvegicus OX=10116 GN=Ugp2 PE=1 SV=1
131	**588**	2001	Q63355|MYO1C_RAT	45.64	2	2	2	N	119811		Unconventional myosin-Ic OS=Rattus norvegicus OX=10116 GN=Myo1c PE=1 SV=2
132	**398**	22994	tr|D3ZJH9|D3ZJH9_RAT	45.53	7	3	3	N	65352		Malic enzyme OS=Rattus norvegicus OX=10116 GN=Me2 PE=1 SV=1
133	**778**	41829	Q2A121|FTO_RAT	45.24	5	2	2	Y	57972		Alpha-ketoglutarate-dependent dioxygenase FTO OS=Rattus norvegicus OX=10116 GN=Fto PE=2 SV=1
134	**1673**	60918	Q80W92|VAC14_RAT	45.13	2	1	1	N	88068		Protein VAC14 homolog OS=Rattus norvegicus OX=10116 GN=Vac14 PE=1 SV=1
135	**1681**	27299	tr|A0A8I6AFM7|A0A8I6AFM7_RAT	44.79	2	1	1	N	103641		SCY1 like pseudokinase 2 OS=Rattus norvegicus OX=10116 GN=Scyl2 PE=1 SV=1
136	**405**	1784	P09495|TPM4_RAT	44.59	17	3	3	Y	28510		Tropomyosin alpha-4 chain OS=Rattus norvegicus OX=10116 GN=Tpm4 PE=1 SV=3
137	**2396**	61112	tr|G3V818|G3V818_RAT	44.39	4	1	1	N	42322		Parvin, alpha OS=Rattus norvegicus OX=10116 GN=Parva PE=1 SV=1
138	**906**	2244	P24268|CATD_RAT	43	4	1	1	Y	44681		Cathepsin D OS=Rattus norvegicus OX=10116 GN=Ctsd PE=1 SV=1
139	**1711**	5495	P38069|KAD1_RAT	42.59	13	2	2	N	21584		Adenylate kinase isoenzyme 1 OS=Rattus norvegicus OX=10116 GN=Ak1 PE=1 SV=3
140	**221**	515	P24156|THOP1_RAT	42.2	7	4	4	Y	78386		Thimet oligopeptidase OS=Rattus norvegicus OX=10116 GN=Thop1 PE=1 SV=4
141	**1868**	41967	tr|Q6P2A5|Q6P2A5_RAT	42.13	7	1	1	N	25494		GTP:AMP phosphotransferase AK3, mitochondrial OS=Rattus norvegicus OX=10116 GN=Ak3 PE=3 SV=1
142	**1012**	3427	P84079|ARF1_RAT	41.87	20	3	3	Y	20697		ADP-ribosylation factor 1 OS=Rattus norvegicus OX=10116 GN=Arf1 PE=1 SV=2
143	**2493**	6465	O35264|PA1B2_RAT	41.7	22	3	3	Y	25581		Platelet-activating factor acetylhydrolase IB subunit alpha2 OS=Rattus norvegicus OX=10116 GN=Pafah1b2 PE=1 SV=1
144	**1506**	25790	tr|G3V7L8|G3V7L8_RAT	41.46	6	1	1	N	26143		V-type proton ATPase subunit E 1 OS=Rattus norvegicus OX=10116 GN=Atp6v1e1 PE=3 SV=1
145	**2809**	42155	tr|A0A8I6ACK1|A0A8I6ACK1_RAT	40.24	8	1	1	Y	26591		Dynactin subunit 3 OS=Rattus norvegicus OX=10116 GN=Dctn3 PE=1 SV=1
146	**1550**	24956	Q99ML5|PCYOX_RAT	40.12	3	1	1	N	56288		Prenylcysteine oxidase 1 OS=Rattus norvegicus OX=10116 GN=Pcyox1 PE=1 SV=1

Appendix

147	**1392**	3546	P07872|ACOX1_RAT	39.77	3	1	1	N	74679	 Peroxisomal acyl-coenzyme A oxidase 1 OS=Rattus norvegicus OX=10116 GN=Acox1 PE=1 SV=1
148	**1392**	24950	tr|F1LQC1|F1LQC1_RAT	39.77	3	1	1	N	74509	 Acyl-coenzyme A oxidase OS=Rattus norvegicus OX=10116 GN=Acox1 PE=1 SV=3
149	**1497**	2819	O6PVQ4|MLEC_RAT	39.34	16	4	4	Y	32418	 Malectin OS=Rattus norvegicus OX=10116 GN=Mlec PE=2 SV=1
150	**1500**	3671	Q9Z269|VAPB_RAT	38.64	6	1	1	N	26916	 Vesicle-associated membrane protein-associated protein B OS=Rattus norvegicus OX=10116 GN=Vapb PE=1 SV=3
151	**1644**	3641	Q99N27|SNX1_RAT	38.05	3	1	1	N	59044	 Sorting nexin-1 OS=Rattus norvegicus OX=10116 GN=Snx1 PE=1 SV=1
152	**1207**	28337	tr|F1LN92|F1LN92_RAT	37.95	3	1	1	Y	89352	 AFG3 like matrix AAA peptidase subunit 2 OS=Rattus norvegicus OX=10116 GN=Afg3l2 PE=1 SV=1
153	**2247**	42118	P62775|MTPN_RAT	37.81	8	1	1	Y	12861	 Myotrophin OS=Rattus norvegicus OX=10116 GN=Mtpn PE=1 SV=2
154	**1963**	42229	tr|A0A8I577Z3|A0A8I5ZZ43_RAT	33.15	2	1	1	N	50137	 Endophilin-B2 OS=Rattus norvegicus OX=10116 GN=Sh3glb2 PE=1 SV=1
155	**1341**	2719	P56571|ES1_RAT	31.27	6	1	1	N	28173	 ES1 protein homolog, mitochondrial OS=Rattus norvegicus OX=10116 PE=1 SV=2
156	**274**	961	P49088|ASNS_RAT	29.56	4	2	2	N	64247	 Asparagine synthetase [glutamine-hydrolyzing] OS=Rattus norvegicus OX=10116 GN=Asns PE=2 SV=3
157	**1735**	26409	tr|Q5U214|Q5U214_RAT	26.72	13	2	2	Y	31176	 U1 small nuclear ribonucleoprotein A OS=Rattus norvegicus OX=10116 GN=Snrpa PE=3 SV=1
158	**81**	23055	tr|A0A0U1RS25|A0A0U1RS25_RAT	25.75	24	17	17	Y	123963	 UPF1, RNA helicase and ATPase OS=Rattus norvegicus OX=10116 GN=Upf1 PE=1 SV=1
159	**550**	25812	tr|A0A8I6G5P1|A0A8I6G5P1_RAT	24.89	10	4	4	Y	46099	 Heterogeneous nuclear ribonucleoprotein D-like OS=Rattus norvegicus OX=10116 GN=Hnrnpdl PE=1 SV=1
160	**608**	27865	Q6AYB5|SRP54_RAT	24.6	10	4	4	N	55705	 Signal recognition particle subunit SRP54 OS=Rattus norvegicus OX=10116 GN=Srp54 PE=2 SV=1
161	**516**	26296	tr|G3V752|G3V752_RAT	23.92	4	3	3	Y	115334	 RNA cytidine acetyltransferase OS=Rattus norvegicus OX=10116 GN=Nat10 PE=1 SV=1
162	**657**	24019	tr|A0A0G2KAN7|A0A0G2KAN7_RAT	23.29	3	1	1	N	65838	 glutaminase OS=Rattus norvegicus OX=10116 GN=Gls PE=1 SV=1
163	**995**	61286	tr|G3V727|G3V727_RAT	23.07	3	1	1	N	50989	 RNA helicase OS=Rattus norvegicus OX=10116 GN=Ddx47 PE=1 SV=2
164	**1371**	7163	O6P7Q4|LGUL_RAT	23.02	5	1	1	N	20820	 Lactoylglutathione lyase OS=Rattus norvegicus OX=10116 GN=Glo1 PE=1 SV=3
165	**555**	1792	P17425|HMCS1_RAT	22.82	5	2	2	N	57434	 Hydroxymethylglutaryl-CoA synthase, cytoplasmic OS=Rattus norvegicus OX=10116 GN=Hmgcs1 PE=1

166	**555**	23743	tr|A0A8I6AH54|A0A8I6AH54_RAT	22.82	5	2	2	N	57049	Hydroxymethylglutaryl-CoA synthase OS=Rattus norvegicus OX=10116 GN=Hmgcs1 PE=1 SV=1
167	**1049**	5949	O3B7D0|HEM6_RAT	22.76	5	2	2	N	49278	Oxygen-dependent coproporphyrinogen-III oxidase, mitochondrial OS=Rattus norvegicus OX=10116 GN=Cpox PE=1 SV=1
168	**2072**	27708	tr|A0A8I6A412|A0A8I6A412_RAT	22.74	2	1	1	Y	70688	WD repeat domain 46 OS=Rattus norvegicus OX=10116 GN=Wdr46 PE=1 SV=1
169	**2459**	29280	P29266|3HIDH_RAT	21.27	4	1	1	N	35303	3-hydroxyisobutyrate dehydrogenase, mitochondrial OS=Rattus norvegicus OX=10116 GN=Hibadh PE=1 SV=3
170	**932**	26038	tr|A0A0G2|SG6|A0A0G2|SG6_RAT	21.18	9	2	2	N	25529	Adenylate kinase 2, mitochondrial OS=Rattus norvegicus OX=10116 GN=Ak2 PE=3 SV=1
171	**2655**	6622	P62076|TIM13_RAT	21.15	31	2	2	Y	10458	Mitochondrial import inner membrane translocase subunit Tim13 OS=Rattus norvegicus OX=10116 GN=Timm13 PE=3 SV=1
172	**1127**	25553	tr|B2RZ74|B2RZ74_RAT	20.59	9	3	3	N	52133	U1 small nuclear ribonucleoprotein 70 kDa OS=Rattus norvegicus OX=10116 GN=Snrnp70 PE=1 SV=1
173	**58**	22918	tr|G3V8T4|G3V8T4_RAT	20.46	3	4	4	Y	126941	DNA damage-binding protein 1 OS=Rattus norvegicus OX=10116 GN=Ddb1 PE=1 SV=1

Appendix

Table C.2: Proteins identified to be upregulated in CSPα-deficient lines 3 and 5 quantified by label-free proteomics

Up regulated	Protein Group	Protein ID	Accession	Significance	Coverage (%)	#Peptides	#Unique	PTM	Avg. Mass	Sample Profile	Group Profile	Description
1	**50**	24	P63039|CH60_RAT	200	12	8	8	Y	60956			60 kDa heat shock protein, mitochondrial OS=Rattus norvegicus OX=10116 GN=Hspd1 PE=1 SV=1
2	**59**	965	Q9JIL3|ILF3_RAT	200	17	11	11	Y	95935			Interleukin enhancer-binding factor 3 OS=Rattus norvegicus OX=10116 GN=Ilf3 PE=1 SV=2
3	**62**	1100	P27008|PARP1_RAT	200	13	9	9	Y	112660			Poly [ADP-ribose] polymerase 1 OS=Rattus norvegicus OX=10116 GN=Parp1 PE=1 SV=4
4	**68**	368	Q3B8Q1|DDX21_RAT	200	10	6	6	Y	85966			Nucleolar RNA helicase 2 OS=Rattus norvegicus OX=10116 GN=Ddx21 PE=2 SV=1
5	**80**	22703	tr|A0A8I6ABZ7|A0A8I6ABZ7_RAT	200	12	12	12	Y	150232			RNA helicase OS=Rattus norvegicus OX=10116 GN=Dhx9 PE=1 SV=1
6	**101**	1010	P0DMW0|HS71A_RAT	200	6	3	3	Y	70185			Heat shock 70 kDa protein 1A OS=Rattus norvegicus OX=10116 GN=Hspa1a PE=1 SV=1
7	**101**	1011	P0DMW1|HS71B_RAT	200	6	3	3	Y	70185			Heat shock 70 kDa protein 1B OS=Rattus norvegicus OX=10116 GN=Hspa1b PE=2 SV=1
8	**154**	3881	Q63598|PLST_RAT	200	11	4	4	Y	70680			Plastin-3 OS=Rattus norvegicus OX=10116 GN=Pls3 PE=1 SV=2
9	**194**	23737	tr|A0A8L2UJ37|A0A8L2UJ37_RAT	200	6	4	4	Y	83500			TNF receptor-associated protein 1 OS=Rattus norvegicus OX=10116 GN=Trap1 PE=1 SV=1
10	**194**	1919	Q5XH20|TRAP1_RAT	200	7	4	4	Y	80461			Heat shock protein 75 kDa, mitochondrial OS=Rattus norvegicus OX=10116 GN=Trap1 PE=1 SV=1
11	**222**	23392	tr|Q566E4|Q566E4_RAT	200	14	7	7	Y	70874			Heterogeneous nuclear ribonucleoprotein R OS=Rattus norvegicus OX=10116 GN=Hnrnpr PE=1 SV=1
12	**226**	620	Q9QVC8|FKBP4_RAT	200	19	6	6	Y	51450			Peptidyl-prolyl cis-trans isomerase FKBP4 OS=Rattus norvegicus OX=10116 GN=Fkbp4 PE=1 SV=3
13	**237**	22942	tr|M0R5J4|M0R5J4_RAT	200	7	3	3	Y	47075			phosphopyruvate hydratase OS=Rattus norvegicus OX=10116 GN=Eno1 PE=1 SV=1
14	**237**	643	P04764|ENOA_RAT	200	7	3	3	Y	47128			Alpha-enolase OS=Rattus norvegicus OX=10116 GN=Eno1 PE=1 SV=4
15	**295**	1617	Q6AXS5|SERB1_RAT	200	22	7	7	Y	44754			SERPINE1 mRNA-binding protein 1 OS=Rattus norvegicus OX=10116 GN=Serbp1 PE=1 SV=2
16	**339**	913	P07335|KCRB_RAT	200	35	9	9	Y	42725			Creatine kinase B-type OS=Rattus norvegicus OX=10116 GN=Ckb PE=1 SV=2
17	**340**	1127	P60123|RUVB1_RAT	200	42	13	13	Y	50214			RuvB-like 1 OS=Rattus norvegicus OX=10116 GN=Ruvbl1 PE=1 SV=1
18	**346**	23163	tr|F1LNF1|F1LNF1_RAT	200	25	5	5	Y	37430			Heterogeneous nuclear ribonucleoproteins A2/B1 OS=Rattus norvegicus OX=10116 GN=Hnrnpa2b1 PE=1 SV=2

Appendix

19	**354**	23627	tr|A0A8I6AEH8|A0A8I6AEH8_RAT	200	10	7	7	N	76655			Protein disulfide-isomerase OS=Rattus norvegicus OX=10116 GN=Pdia4 PE=1 SV=1
20	**354**	23635	tr|G3V6T7|G3V6T7_RAT	200	10	7	7	N	72748			Protein disulfide-isomerase A4 OS=Rattus norvegicus OX=10116 GN=Pdia4 PE=3 SV=1
21	**366**	2634	P42123|LDHB_RAT	200	15	4	4	N	36612			L-lactate dehydrogenase B chain OS=Rattus norvegicus OX=10116 GN=Ldhb PE=1 SV=2
22	**494**	24031	tr|A0A8I6GKM0|A0A8I6GKM0_RAT	200	32	10	10	Y	40510			Interleukin enhancer binding factor 2 OS=Rattus norvegicus OX=10116 GN=Ilf2 PE=1 SV=1
23	**545**	1817	O08651|SERA_RAT	200	17	7	7	Y	56493			D-3-phosphoglycerate dehydrogenase OS=Rattus norvegicus OX=10116 GN=Phgdh PE=1 SV=3
24	**558**	26213	tr|A0A8I6A5U6|A0A8I6A5U6_RAT	200	18	4	4	Y	38611			RNA-binding protein Luc7-like OS=Rattus norvegicus OX=10116 GN=Luc7l2 PE=1 SV=1
25	**672**	24837	tr|A0A0G2K931|A0A0G2K931_RAT	200	12	4	4	N	40599			Phosphoserine aminotransferase OS=Rattus norvegicus OX=10116 GN=Psat1 PE=1 SV=2
26	**738**	24940	tr|A0A0G2K7K2|A0A0G2K7K2_RAT	200	3	1	1	Y	66134			Apoptosis inducing factor, mitochondria associated 1 OS=Rattus norvegicus OX=10116 GN=Aifm1 PE=1 SV=1
27	**749**	23865	tr|A0A8I6AQI0|A0A8I6AQI0_RAT	200	24	6	6	Y	54870			RB binding protein 4, chromatin remodeling factor OS=Rattus norvegicus OX=10116 GN=Rbbp7 PE=1 SV=1
28	**749**	23927	tr|A6ISI2|A6ISI2_RAT	200	28	6	6	Y	47656			RB binding protein 4, chromatin remodeling factor OS=Rattus norvegicus OX=10116 GN=Rbbp4 PE=1 SV=1
29	**785**	25173	tr|A0A8I6APW4|A0A8I6APW4_RAT	200	17	2	2	Y	11540			Tubulin-specific chaperone A OS=Rattus norvegicus OX=10116 GN=Tbca PE=1 SV=1
30	**797**	26696	Q8CJB9|BRE1B_RAT	200	2	1	1	N	113841			E3 ubiquitin-protein ligase BRE1B OS=Rattus norvegicus OX=10116 GN=Rnf40 PE=1 SV=1
31	**797**	26697	tr|A0A8L2UK73|A0A8L2UK73_RAT	200	2	1	1	N	114290			E3 ubiquitin protein ligase OS=Rattus norvegicus OX=10116 GN=Rnf40 PE=1 SV=1
32	**828**	25849	tr|A0A8I5ZMN7|A0A8I5ZMN7_RAT	200	3	1	1	N	45983			Regulator of chromosome condensation OS=Rattus norvegicus OX=10116 GN=Rcc1 PE=1 SV=1
33	**838**	25867	tr|M0RBQ5|M0RBQ5_RAT	200	8	2	2	N	13908			Histone H2B OS=Rattus norvegicus OX=10116 GN=H2bu1 PE=3 SV=1
34	**870**	25746	tr|A0A0G2JVA2|A0A0G2JVA2_RAT	200	19	4	4	N	35182			Heterogeneous nuclear ribonucleoprotein H3 OS=Rattus norvegicus OX=10116 GN=Hnrnph3 PE=4 SV=1
35	**1219**	27157	tr|E9PU11|E9PU11_RAT	200	3	1	1	Y	61848			YTH domain-containing family protein OS=Rattus norvegicus OX=10116 GN=Ythdf2 PE=1 SV=4
36	**1391**	61217	tr|A0A8I6G4I5|A0A8I6G4I5_RAT	200	3	1	1	N	68696			G-rich RNA sequence binding factor 1 OS=Rattus norvegicus OX=10116 GN=Grsf1 PE=1 SV=1

Appendix

37	**1415**	27159	tr|A0A8I5ZWZ6|A0A8I5ZWZ6_RAT	200	16	3	3	Y	27649			Ribosome assembly factor mrt4 OS=Rattus norvegicus OX=10116 GN=Mrto4 PE=3 SV=1
38	**1494**	61085	O4FZT0|STML2_RAT	200	11	2	2	N	38414			Stomatin-like protein 2, mitochondrial OS=Rattus norvegicus OX=10116 GN=Stoml2 PE=1 SV=1
39	**1883**	26999	tr|A0A8I6G7F4|A0A8I6G7F4_RAT	200	30	3	3	N	13675			Endosulfine alpha OS=Rattus norvegicus OX=10116 GN=Ensa PE=1 SV=1
40		5056	Q4QR85|MEP50_RAT	200	4	1	1	Y	37076			Methylosome protein WDR77 OS=Rattus norvegicus OX=10116 GN=Wdr77 PE=1 SV=1
41	**2059**	27720	tr|Q5M920|Q5M920_RAT	200	4	1	1	N	34745			EBNA1 binding protein 2 OS=Rattus norvegicus OX=10116 GN=Ebna1bp2 PE=1 SV=1
42	**2067**	6265	Q9EPH2|MRP_RAT	200	11	2	2	N	19847			MARCKS-related protein OS=Rattus norvegicus OX=10116 GN=Marcksl1 PE=2 SV=3
43	**2130**	6921	Q498E0|TXD12_RAT	200	9	1	1	N	19019			Thioredoxin domain-containing protein 12 OS=Rattus norvegicus OX=10116 GN=Txndc12 PE=2 SV=2
44	**2879**	43536	D3ZCL3|RU1C_RAT	200	19	2	2	Y	17364			U1 small nuclear ribonucleoprotein C OS=Rattus norvegicus OX=10116 GN=Snrpc PE=3 SV=1
45	**195**	22934	tr|A8CMB8|A8CMB8_RAT	156.54	6	4	4	Y	92815			DNA replication licensing factor MCM6 OS=Rattus norvegicus OX=10116 GN=Mcm6 PE=1 SV=1
46	**193**	23490	tr|Q4KM71|Q4KM71_RAT	153.53	18	11	11	N	75487			Splicing factor proline and glutamine rich OS=Rattus norvegicus OX=10116 GN=Sfpq PE=1 SV=1
47	**448**	23495	tr|A0A8I6ALC1|A0A8I6ALC1_RAT	153.53	16	5	5	N	38804			Heterogeneous nuclear ribonucleoprotein A1 OS=Rattus norvegicus OX=10116 GN=Hnrnpa1 PE=4 SV=1
48	**603**	1264	P04182|OAT_RAT	153.53	17	5	5	Y	48333			Ornithine aminotransferase, mitochondrial OS=Rattus norvegicus OX=10116 GN=Oat PE=1 SV=1
49	**3269**	29011	tr|D4A8M5|D4A8M5_RAT	153.53	12	1	1	Y	10834			Small nuclear ribonucleoprotein E OS=Rattus norvegicus OX=10116 GN=Snrpepl2 PE=3 SV=1
50	**965**	23898	tr|A0A8L2QUA0|A0A8L2QUA0_RAT	148.75	2	1	1	N	75871			Kinesin-like protein OS=Rattus norvegicus OX=10116 GN=Kifc1 PE=3 SV=1
51	**965**	2151	Q5XI63|KIFC1_RAT	148.75	2	1	1	N	76141			Kinesin-like protein KIFC1 OS=Rattus norvegicus OX=10116 GN=Kifc1 PE=2 SV=1
52	**2508**	26883	tr|A6KNE7|A6KNE7_RAT	148.08	38	4	4	N	13282			Small nuclear ribonucleoprotein Sm D1 OS=Rattus norvegicus OX=10116 GN=Snrpd1 PE=1 SV=1
53	**196**	2567	Q5FVM4|NONO_RAT	146.54	15	7	7	Y	54925			Non-POU domain-containing octamer-binding protein OS=Rattus norvegicus OX=10116 GN=Nono PE=1 SV=3

54	**1120**	42042	tr|F1LT58|F1LT58_RAT	146.12	4	1	1	N	60366			Importin subunit alpha OS=Rattus norvegicus OX=10116 GN=Kpna6 PE=1 SV=4
55	**1317**	26628	tr|D4A720|D4A720_RAT	140.51	8	2	2	Y	26023			Serine and arginine rich splicing factor 7 OS=Rattus norvegicus OX=10116 GN=Srsf7 PE=1 SV=2
56	**216**	23046	tr|A0A8I6A206|A0A8I6A206_RAT	140.3	14	11	11	N	77095			Nucleolin OS=Rattus norvegicus OX=10116 GN=Ncl PE=1 SV=1
57	**2144**	27255	P55720|NH2L1_RAT	137.19	34	5	5	Y	14174			NHP2-like protein 1 OS=Rattus norvegicus OX=10116 GN=Snu13 PE=2 SV=4
58	**774**	26154	tr|G3V8B8|G3V8B8_RAT	135.17	9	3	3	Y	55045			DnaJ heat shock protein family (Hsp40) member C7 OS=Rattus norvegicus OX=10116 GN=Dnajc7 PE=4 SV=3
59	**2814**	42424	Q5RJX0|NTM1A_RAT	132.29	10	2	2	Y	25464			N-terminal Xaa-Pro-Lys N-methyltransferase 1 OS=Rattus norvegicus OX=10116 GN=Ntmt1 PE=2 SV=3
60	**1182**	5822	P63164|RSMN_RAT	130.83	15	4	4	Y	24614			Small nuclear ribonucleoprotein-associated protein N OS=Rattus norvegicus OX=10116 GN=Snrpn PE=1 SV=1
61	**1182**	5987	P17136|RSMB_RAT	130.83	16	4	4	Y	23656			Small nuclear ribonucleoprotein-associated protein B OS=Rattus norvegicus OX=10116 GN=Snrpb PE=2 SV=2
62	**1182**	26518	tr|A0A8I6GLH2|A0A8I6GLH2_RAT	130.83	16	4	4	Y	23312			Small nuclear ribonucleoprotein-associated protein OS=Rattus norvegicus OX=10116 GN=Snrpb PE=3 SV=1
63	**569**	1098	Q63716|PRDX1_RAT	130.48	38	8	8	N	22109			Peroxiredoxin-1 OS=Rattus norvegicus OX=10116 GN=Prdx1 PE=1 SV=1
64	**1011**	2999	Q9Z0V5|PRDX4_RAT	130.02	26	4	4	Y	31007			Peroxiredoxin-4 OS=Rattus norvegicus OX=10116 GN=Prdx4 PE=2 SV=1
65	**1011**	24478	tr|A0A8I6AL33|A0A8I6AL33_RAT	130.02	28	4	4	Y	28476			thioredoxin-dependent peroxiredoxin OS=Rattus norvegicus OX=10116 GN=Prdx4 PE=1 SV=1
66	**991**	4626	Q5M939|HAT1_RAT	128.42	9	3	3	Y	49241			Histone acetyltransferase type B catalytic subunit OS=Rattus norvegicus OX=10116 GN=Hat1 PE=2 SV=1
67	**610**	2264	P22509|FBRL_RAT	123.6	27	7	7	N	34222			rRNA 2'-O-methyltransferase fibrillarin OS=Rattus norvegicus OX=10116 GN=Fbl PE=1 SV=2
68	**610**	24094	tr|A0A8L2IJK98|A0A8L2IJK98_RAT	123.6	27	7	7	N	34564			Fibrillarin OS=Rattus norvegicus OX=10116 GN=Fbl PE=1 SV=1
69	**1536**	61033	tr|A0A0G2JXS2|A0A0G2JXS2_RAT	121.04	2	1	1	Y	81317			Protein KRI1 homolog OS=Rattus norvegicus OX=10116 GN=Kri1 PE=3 SV=2
70	**435**	24876	tr|Q4KLK7|Q4KLK7_RAT	118.78	8	4	4	Y	65400			Nucleolar protein 56 OS=Rattus norvegicus OX=10116 GN=Nop56 PE=1 SV=1

Appendix

71	**505**	23834	tr|F1LVV4|F1LVV4_RAT	117.49	15	5	5	Y	56027			Regulator of chromosome condensation 2 OS=Rattus norvegicus OX=10116 GN=Rcc2 PE=1 SV=2
72	**710**	3575	Q9JI54|HNRPD_RAT	113.13	15	4	4	Y	38218			Heterogeneous nuclear ribonucleoprotein D0 OS=Rattus norvegicus OX=10116 GN=Hnrnpd PE=1 SV=2
73	**1683**	29552	tr|D4A8M7|D4A8M7_RAT	112.29	3	1	1	Y	82135			Condensin complex subunit 2 OS=Rattus norvegicus OX=10116 GN=Ncaph PE=1 SV=3
74	**1893**	61071	tr|A0A8I6AIR3|A0A8I6AIR3_RAT	110.97	4	1	1	N	46443			non-specific serine/threonine protein kinase OS=Rattus norvegicus OX=10116 GN=Vrk1 PE=1 SV=1
75	**1765**	61607	tr|D3ZQV8|D3ZQV8_RAT	108.64	4	1	1	Y	41097			PHD finger protein 6 OS=Rattus norvegicus OX=10116 GN=Phf6 PE=1 SV=1
76	**2563**	42285	tr|D4A5T1|D4A5T1_RAT	106.66	10	1	1	N	10119			Splicing factor 3B subunit 5 OS=Rattus norvegicus OX=10116 GN=Sf3b5 PE=3 SV=1
77	**2716**	28583	tr|A6ISV1|A6ISV1_RAT	105.69	7	1	1	N	38540			Protein phosphatase 1, regulatory (Inhibitor) subunit 8 OS=Rattus norvegicus OX=10116 GN=Ppp1r8 PE=1 SV=1
78	**734**	3334	Q3T1J1|IF5A1_RAT	105.68	11	3	3	N	16832			Eukaryotic translation initiatio factor 5A-1 OS=Rattus norvegicus OX=10116 GN=Eif5a PE=1 SV=3
79	**734**	24892	tr|A0A8L2QBS3|A0A8L2QBS3_RAT	105.68	10	3	3	N	17986			Eukaryotic translation initiatio factor 5A OS=Rattus norvegicus OX=10116 GN=Eif5a PE=1 SV=1
80	**142**	23320	tr|D3ZP96|D3ZP96_RAT	104.76	20	13	13	Y	102143			DNA replication licensing factor MCM2 OS=Rattus norvegicus OX=10116 GN=Mcm2 PE=1 SV=2
81	**1314**	11798	O35095|NCDN_RAT	103.49	2	1	1	N	78923			Neurochondrin OS=Rattus norvegicus OX=10116 GN=Ncdn PE=1 SV=2
82	**1813**	30022	tr|A0A8I6AND0|A0A8I6AND0_RAT	103.02	3	2	2	N	85818			Dolichyl-diphosphooligosaccharide--protein glycosyltransferase subunit STT3A OS=Rattus norvegicus OX=10116 GN=Stt3a PE=1 SV=1
83	**2199**	61021	tr|M0RDD7|M0RDD7_RAT	100.27	10	1	1	N	22881			Chromatin target of PRMT1-lik 1 OS=Rattus norvegicus OX=10116 GN=Chtopl1 PE=4 SV=2
84	**832**	41949	Q63692|CDC37_RAT	99.61	7	2	2	N	44510			Hsp90 co-chaperone Cdc37 OS=Rattus norvegicus OX=10116 GN=Cdc37 PE=1 SV=2
85	**1866**	30046	tr|M0R9D4|M0R9D4_RAT	98.58	7	2	2	N	21707			High mobility group box 3 OS=Rattus norvegicus OX=10116 GN=Hmgb3 PE=1 SV=1
86	**960**	27929	tr|A0A8L2ULJ1|A0A8L2ULJ1_RAT	98.21	2	1	1	N	83445			Elongation factor G, mitochondrial OS=Rattus norvegicus OX=10116 GN=Gfm1 PE=1 SV=1
87	**1053**	2796	Q8CGS5|RNZ2_RAT	96.82	1	1	1	Y	92340			Zinc phosphodiesterase ELAC protein 2 OS=Rattus norvegicus OX=10116 GN=Elac2 PE=1 SV=1

88	**386**	1684	Q9QZ86|NOP58_RAT	96.46	18	7	7	Y	60071			Nucleolar protein 58 OS=Rattus norvegicus OX=10116 GN=Nop58 PE=1 SV=1
89	**386**	23692	tr|A0A8I5ZV87|A0A8I5ZV87_RAT	96.46	18	7	7	Y	59810			NOP58 ribonucleoprotein OS=Rattus norvegicus OX=10116 GN=Nop58 PE=1 SV=1
90	**1824**	28147	Q6AXQ5|PDE12_RAT	96.2	3	1	1	N	67176			2',5'-phosphodiesterase 12 OS=Rattus norvegicus OX=10116 GN=Pde12 PE=2 SV=1
91	**287**	1026	Q3B8Q2|IF4A3_RAT	95.82	4	2	2	N	46841			Eukaryotic initiation factor 4A-III OS=Rattus norvegicus OX=10116 GN=Eif4a3 PE=1 SV=1
92	**2555**	26948	tr|D4AAT4|D4AAT4_RAT	94.63	49	3	3	Y	9725			Sm protein F OS=Rattus norvegicus OX=10116 GN=Snrpf PE=3 SV=1
93	**2461**	30110	tr|G3V678|G3V678_RAT	94.54	19	2	2	N	17143			DNA-directed RNA polymerases I, II, and III subunit RPABC3 OS=Rattus norvegicus OX=10116 GN=Polr2h PE=1 SV=1
94	**476**	42020	tr|A0A0G2K762|A0A0G2K762_RAT	94.3	8	4	4	N	71128			ATP binding cassette subfamily F member 2 OS=Rattus norvegicus OX=10116 GN=Abcf2 PE=1 SV=1
95	**1770**	25810	tr|D3ZUB0|D3ZUB0_RAT	93.79	14	2	2	N	38090			Reticulocalbin 1 OS=Rattus norvegicus OX=10116 GN=Rcn1 PE=3 SV=1
96	**440**	23101	tr|G3V9Q3|G3V9Q3_RAT	93.39	20	5	5	Y	48265			Heterogeneous nuclear ribonucleoprotein H1 OS=Rattus norvegicus OX=10116 GN=Hnrnph1 PE=1 SV=3
97	**245**	23573	tr|B2GUX3|B2GUX3_RAT	92.97	12	6	6	Y	82466			DNA replication licensing factor MCM5 OS=Rattus norvegicus OX=10116 GN=Mcm5 PE=1 SV=1
98	**1808**	26378	tr|D3ZFB2|D3ZFB2_RAT	92.55	7	2	2	N	58424			Luc7-like protein OS=Rattus norvegicus OX=10116 GN=Luc7l3 PE=1 SV=1
99	**252**	23091	tr|F7ELS2|F7ELS2_RAT	92.38	5	3	3	N	61744			T-complex protein 1 subunit zeta OS=Rattus norvegicus OX=10116 GN=Cct6a PE=1 SV=1
100	**952**	5679	P63036|DNJA1_RAT	91.9	31	7	7	Y	44868			DnaJ homolog subfamily A member 1 OS=Rattus norvegicus OX=10116 GN=Dnaja1 PE=1 SV=1
101	**117**	513	P27653|C1TC_RAT	91.48	6	5	5	N	100996			C-1-tetrahydrofolate synthase, cytoplasmic OS=Rattus norvegicus OX=10116 GN=Mthfd1 PE=1 SV=3
102	**230**	698	P85834|EFTU_RAT	90.25	19	8	8	N	49522			Elongation factor Tu, mitochondrial OS=Rattus norvegicus OX=10116 GN=Tufm PE=1 SV=1
103	**2408**	6981	P04646|RL35A_RAT	89.79	21	3	3	N	12554			Large ribosomal subunit protein eL33 OS=Rattus norvegicus OX=10116 GN=Rpl35a PE=1 SV=1
104	**206**	691	Q32PX7|FUBP1_RAT	88.91	27	11	11	Y	67197			Far upstream element-binding protein 1 OS=Rattus norvegicus OX=10116 GN=Fubp1 PE=1 SV=1
105	**123**	218	P28480|TCPA_RAT	88.44	41	20	20	Y	60360			T-complex protein 1 subunit alpha OS=Rattus norvegicus OX=10116 GN=Tcp1 PE=1 SV=1

Appendix

106	**1092**	24849	tr|Q99MI5|Q99MI5_RAT	87.09	13	3	3	Y	33997			Spermidine synthase OS=Rattus norvegicus OX=10116 GN=Srm PE=1 SV=1
107	**309**	3996	P27881|HXK2_RAT	84.96	8	5	5	Y	102544			Hexokinase-2 OS=Rattus norvegicus OX=10116 GN=Hk2 PE=1 SV=1
108	**118**	24623	tr|A0ABI5ZJ57|A0A8I5ZJ57_RAT	83.82	12	8	8	Y	119866			FACT complex subunit OS=Rattus norvegicus OX=10116 GN=Supt16h PE=3 SV=1
109	**1466**	25443	tr|A0A0G2IZA2|A0A0G2IZA2_RAT	83.77	17	3	3	N	25812			GrpE protein homolog OS=Rattus norvegicus OX=10116 GN=Grpel1 PE=1 SV=1
110	**1466**	4292	P97576|GRPE1_RAT	83.77	18	3	3	N	24297			GrpE protein homolog 1, mitochondrial OS=Rattus norvegicus OX=10116 GN=Grpel1 PE=1 SV=2
111	**1985**	29081	tr|D3ZG43|D3ZG43_RAT	82.92	10	2	2	N	30226			NADH dehydrogenase [ubiquinone] iron-sulfur protein 3, mitochondrial OS=Rattus norvegicus OX=10116 GN=Ndufs3 PE=3 SV=1
112	**554**	25567	tr|B1WC49|B1WC49_RAT	82.34	18	7	7	Y	56785			Apoptosis inhibitor 5 OS=Rattus norvegicus OX=10116 GN=Api5 PE=1 SV=1
113	**1651**	26686	tr|A0ABL2QDL7|A0A8L2QDL7_RAT	82.11	2	1	1	N	73706			Nucleolar and coiled-body phosphoprotein 1 OS=Rattus norvegicus OX=10116 GN=Nolc1 PE=1 SV=1
114	**132**	724	Q99PF5|FUBP2_RAT	81.76	18	10	10	Y	74227			Far upstream element-binding protein 2 OS=Rattus norvegicus OX=10116 GN=Khsrp PE=1 SV=1
115	**132**	23074	tr|M0R961|M0R961_RAT	81.76	18	10	10	Y	74213			KH-type splicing regulatory protein OS=Rattus norvegicus OX=10116 GN=Khsrp PE=1 SV=1
116	**1511**	27331	tr|D4A1H8|D4A1H8_RAT	80.19	3	1	1	N	55810			PWP1 homolog, endonuclein OS=Rattus norvegicus OX=10116 GN=Pwp1 PE=1 SV=1
117	**1118**	25909	Q4QQW4|HDAC1_RAT	79.76	12	3	3	Y	55093			Histone deacetylase 1 OS=Rattus norvegicus OX=10116 GN=Hdac1 PE=1 SV=1
118	**536**	1546	Q5XIG8|STRAP_RAT	79.1	33	8	8	Y	38456			Serine-threonine kinase receptor-associated protein OS=Rattus norvegicus OX=10116 GN=Strap PE=1 SV=1
119	**112**	480	Q6IMY8|HNRPU_RAT	78.87	1	1	1	N	87733			Heterogeneous nuclear ribonucleoprotein U OS=Rattus norvegicus OX=10116 GN=Hnrnpu PE=1 SV=1
120	**54**	22853	tr|F1LM33|F1LM33_RAT	78.71	2	3	3	N	157404			Leucine-rich pentatricopeptide repeat containing OS=Rattus norvegicus OX=10116 GN=Lrpprc PE=1 SV=3
121	**1363**	26239	tr|M0R907|M0R907_RAT	78.66	40	3	3	Y	13916			Small nuclear ribonucleoprotein Sm D3 OS=Rattus norvegicus OX=10116 GN=Snrpd3 PE=3 SV=1
122	**1679**	25973	tr|Q9ET50|Q9ET50_RAT	78.17	5	2	2	N	54802			Staufen double-stranded RNA binding protein 1 OS=Rattus norvegicus OX=10116 GN=Stau1 PE=1 SV=1

123	**731**	24361	tr|A0A8L2Q0U6|A0A8L2Q0U6_RAT	77.82	6	1	1	Y	37924			Pyrroline-5-carboxylate reductase OS=Rattus norvegicus OX=10116 GN=Pycr2 PE=1 SV=1
124	**695**	30726	Q9WTT7|5MP1_RAT	77.65	5	1	1	N	48049			eIF5-mimic protein 1 OS=Rattus norvegicus OX=10116 GN=Bzw2 PE=1 SV=1
125	**466**	24754	tr|G3V8Y5|G3V8Y5_RAT	77.21	9	6	6	N	133896			DNA-directed RNA polymerase subunit beta OS=Rattus norvegicus OX=10116 GN=Polr2b PE=3 SV=1
126	**2682**	42941	tr|G3V9M8|G3V9M8_RAT	76.66	5	1	1	N	40210			Family with sequence similarity 50, member A OS=Rattus norvegicus OX=10116 GN=Fam50a PE=4 SV=1
127	**1166**	26739	tr|D4ACW1|D4ACW1_RAT	76.36	4	2	2	Y	85385			NOP2 nucleolar protein OS=Rattus norvegicus OX=10116 GN=Nop2 PE=1 SV=3
128	**1461**	3661	Q9Z118|PTBP3_RAT	76.24	3	1	1	Y	56716			Polypyrimidine tract-binding protein 3 OS=Rattus norvegicus OX=10116 GN=Ptbp3 PE=2 SV=1
129	**1516**	3604	Q5U2U2|CRKL_RAT	76.22	18	4	4	Y	33865			Crk-like protein OS=Rattus norvegicus OX=10116 GN=Crkl PE=1 SV=1
130	**173**	22891	tr|F1M9V7|F1M9V7_RAT	76.18	24	16	16	N	103344			Aminopeptidase OS=Rattus norvegicus OX=10116 GN=Npepps PE=1 SV=1
131	**1094**	26741	tr|Q5RJK5|Q5RJK5_RAT	74.7	21	4	4	Y	20811			Chromobox 3 OS=Rattus norvegicus OX=10116 GN=Cbx3 PE=1 SV=1
132	**701**	23980	Q5M7V8|TR150_RAT	74.28	4	3	3	N	108252			Thyroid hormone receptor-associated protein 3 OS=Rattus norvegicus OX=10116 GN=Thrap3 PE=1 SV=1
133	**751**	2503	Q02874|H2AY_RAT	73.2	5	2	2	N	39040			Core histone macro-H2A.1 OS=Rattus norvegicus OX=10116 GN=Macroh2a1 PE=1 SV=5
134	**751**	24319	tr|A0A140TAB4|A0A140TAB4_RAT	73.2	5	2	2	N	39199			Core histone macro-H2A OS=Rattus norvegicus OX=10116 GN=Macroh2a1 PE=1 SV=2
135	**184**	23145	tr|D3ZPB0|D3ZPB0_RAT	72.59	12	10	10	Y	110214			Exportin-2 OS=Rattus norvegicus OX=10116 GN=Cse1l PE=3 SV=1
136	**370**	23696	tr|D3ZYS7|D3ZYS7_RAT	72.21	22	6	6	N	51787			G3BP stress granule assembly factor 1 OS=Rattus norvegicus OX=10116 GN=G3bp1 PE=1 SV=1
137	**826**	3918	Q4KLL0|TCEA1_RAT	72.03	18	4	4	Y	33894			Transcription elongation factor A protein 1 OS=Rattus norvegicus OX=10116 GN=Tcea1 PE=1 SV=1
138	**826**	25240	tr|A0A8L2Q4Y0|A0A8L2Q4Y0_RAT	72.03	18	4	4	Y	34019			Transcription elongation factor OS=Rattus norvegicus OX=10116 GN=Tcea1 PE=3 SV=1
139	**3250**	9876	Q9WVA1|TIM8A_RAT	71.78	11	1	1	Y	11042			Mitochondrial import inner membrane translocase subunit Tim8 A OS=Rattus norvegicus OX=10116 GN=Timm8a PE=1 SV=1
140	**635**	4899	Q5XIH7|PHB2_RAT	71.21	31	8	8	N	33312			Prohibitin-2 OS=Rattus norvegicus OX=10116 GN=Phb2 PE=1 SV=1
141	**2558**	27180	Q71TY3|RS27_RAT	70.77	14	2	2	N	9461			Small ribosomal subunit protein eS27 OS=Rattus

Appendix

142	**704**	24787	tr|D4A9L2|D4A9L2_RAT	70.49	33	7	7	Y	27745			Serine/arginine-rich splicing factor 1 OS=Rattus norvegicus OX=10116 GN=Srsf1 PE=1 SV=1
143	**285**	23629	tr|A0A8I5ZME8|A0A8I5ZME8_RAT	68.98	19	8	8	N	63726			Poly(U)-binding-splicing factor PUF60 OS=Rattus norvegicus OX=10116 GN=Puf60 PE=1 SV=1
144	**2509**	26893	tr|B2RYQ5|B2RYQ5_RAT	68.62	38	3	3	Y	12259			Enhancer of rudimentary homolog OS=Rattus norvegicus OX=10116 GN=Erh PE=3 SV=1
145	**2694**	6641	P62859|RS28_RAT	68.37	46	3	3	Y	7841			Small ribosomal subunit protein eS28 OS=Rattus norvegicus OX=10116 GN=Rps28 PE=1 SV=1
146	**1986**	31107	tr|D4A3I4|D4A3I4_RAT	68.03	19	2	2	N	17271			Transcription factor BTF3 OS=Rattus norvegicus OX=10116 GN=Btf3l4 PE=3 SV=1
147	**1464**	24422	tr|Q5BJT9|Q5BJT9_RAT	67.85	19	4	4	Y	46962			Creatine kinase U-type, mitochondrial OS=Rattus norvegicus OX=10116 GN=Ckmt1 PE=1 SV=1
148	**98**	447	Q68FQ0|TCPE_RAT	67.72	29	16	16	Y	59537			T-complex protein 1 subunit epsilon OS=Rattus norvegicus OX=10116 GN=Cct5 PE=1 SV=1
149	**32**	21	P82995|HS90A_RAT	67.63	26	19	19	Y	84815			Heat shock protein HSP 90-alpha OS=Rattus norvegicus OX=10116 GN=Hsp90aa1 PE=1 SV=3
150	**1768**	5689	Q75Q41|TOM22_RAT	66.82	27	3	3	N	15491			Mitochondrial import receptor subunit TOM22 homolog OS=Rattus norvegicus OX=10116 GN=Tomm22 PE=1 SV=1
151	**318**	875	Q09073|ADT2_RAT	66.6	8	3	3	Y	32901			ADP/ATP translocase 2 OS=Rattus norvegicus OX=10116 GN=Slc25a5 PE=1 SV=3
152	**1467**	25635	tr|A0A8I6GEL5|A0A8I6GEL5_RAT	66	32	5	5	N	23954			40S ribosomal protein S7 OS=Rattus norvegicus OX=10116 GN=Rps7 PE=1 SV=1
153	**1467**	4500	P62083|RS7_RAT	66	35	5	5	N	22127			Small ribosomal subunit protein eS7 OS=Rattus norvegicus OX=10116 GN=Rps7 PE=1 SV=1
154	**1559**	61034	Q27W01|RBM8A_RAT	65.65	32	4	4	Y	19889			RNA-binding protein 8A OS=Rattus norvegicus OX=10116 GN=Rbm8a PE=1 SV=1
155	**824**	3737	P62804|H4_RAT	65.41	53	9	9	Y	11367			Histone H4 OS=Rattus norvegicus OX=10116 GN=H4c2 PE=1 SV=2
156	**165**	22854	tr|Q6P3V8|Q6P3V8_RAT	65.37	30	12	12	Y	46154			Eukaryotic initiation factor 4A-I OS=Rattus norvegicus OX=10116 GN=Eif4a1 PE=3 SV=1
157	**445**	24064	tr|B2RYI2|B2RYI2_RAT	64.67	12	5	5	Y	70492			Signal recognition particle subunit SRP68 OS=Rattus norvegicus OX=10116 GN=Srp68 PE=3 SV=1
158	**2460**	30032	tr|D3ZTW7|D3ZTW7_RAT	64	4	1	1	N	34192			ATP synthase mitochondrial F1 complex assembly factor 2 OS=Rattus norvegicus OX=10116 GN=Atpaf2 PE=3 SV=1
159	**201**	382	Q08629|TIF1B_RAT	63.65	17	10	10	Y	88956			Transcription intermediary factor 1-beta OS=Rattus norvegicus OX=10116 GN=Trim28 PE=1 SV=2

160	**1822**	26882	tr|M0RBB3|M0RBB3_RAT	62.66	23	4	4	N	27027			Aly/REF export factor OS=Rattus norvegicus OX=10116 GN=Alyref PE=4 SV=3
161	**1361**	25682	tr|D4A5Y6|D4A5Y6_RAT	62.44	49	7	7	Y	19301			N-alpha-acetyltransferase 50 OS=Rattus norvegicus OX=10116 GN=Naa50 PE=3 SV=1
162	**1862**	27344	tr|D3ZZ95|D3ZZ95_RAT	62.24	30	3	3	Y	12410			60S ribosomal protein L36 OS=Rattus norvegicus OX=10116 GN=Rpl36l3 PE=1 SV=1
163	**506**	1749	Q63525|NUDC_RAT	61.76	13	4	4	N	38412			Nuclear migration protein nudC OS=Rattus norvegicus OX=10116 GN=Nudc PE=1 SV=1
164	**506**	23712	tr|A0A0G2K0V8|A0A0G2K0V8_RAT	61.76	14	4	4	N	36808			Nuclear distribution C, dynein complex regulator OS=Rattus norvegicus OX=10116 GN=Nudc PE=1 SV=2
165	**308**	1089	P30349|LKHA4_RAT	60.5	14	6	6	Y	69089			Leukotriene A-4 hydrolase OS=Rattus norvegicus OX=10116 GN=Lta4h PE=1 SV=3
166	**644**	27030	P55266|DSRAD_RAT	60.41	2	1	1	Y	129911			Double-stranded RNA-specific adenosine deaminase OS=Rattus norvegicus OX=10116 GN=Adar PE=1 SV=1
167	**422**	24020	tr|M0RBF0|M0RBF0_RAT	60.11	3	1	1	Y	104294			Scaffold attachment factor B OS=Rattus norvegicus OX=10116 GN=Safb PE=1 SV=2
168	**401**	22980	tr|D3ZAN3|D3ZAN3_RAT	59.98	9	6	6	N	90573			Glucosidase II alpha subunit OS=Rattus norvegicus OX=10116 GN=Ganab PE=1 SV=1
169	**2502**	26055	tr|M0R835|M0R835_RAT	59.68	32	3	3	Y	14794			Splicing factor 3B, subunit 6 OS=Rattus norvegicus OX=10116 GN=Sf3b6 PE=1 SV=3
170	**980**	1955	Q6AYK6|CYBP_RAT	57.97	16	4	4	Y	26541			Calcyclin-binding protein OS=Rattus norvegicus OX=10116 GN=Cacybp PE=1 SV=1
171	**43**	22825	tr|E9PT66|E9PT66_RAT	57.82	18	15	15	Y	135550			Splicing factor 3B subunit 3 OS=Rattus norvegicus OX=10116 GN=Sf3b3 PE=1 SV=2
172	**1178**	2548	P62718|RL18A_RAT	57.7	12	2	2	Y	20732			Large ribosomal subunit protein eL20 OS=Rattus norvegicus OX=10116 GN=Rpl18a PE=1 SV=1
173	**541**	25467	tr|D3ZDD7|D3ZDD7_RAT	57.67	2	1	1	N	73725			Spermatid perinuclear RNA-binding protein OS=Rattus norvegicus OX=10116 GN=Strbp PE=4 SV=1
174	**1632**	25046	tr|B1WC50|B1WC50_RAT	56.55	14	6	6	Y	68331			EWS RNA-binding protein 1 OS=Rattus norvegicus OX=10116 GN=Ewsr1 PE=3 SV=1
175	**1920**	42794	Q6AY65|ARFP2_RAT	55.75	5	1	1	N	37773			Arfaptin-2 OS=Rattus norvegicus OX=10116 GN=Arfip2 PE=2 SV=1
176	**829**	3944	Q80Z29|NAMPT_RAT	55.36	14	4	4	N	55438			Nicotinamide phosphoribosyltransferase OS=Rattus norvegicus OX=10116 GN=Nampt PE=1 SV=1
177	**1771**	25825	tr|G3V8F5|G3V8F5_RAT	55.15	11	3	3	N	37920			Mitochondrial import receptor subunit TOM40 homolog OS=Rattus norvegicus OX=10116 GN=Tomm40 PE=3 SV=1

Appendix

178	**1738**	27476	tr|M0R565|M0R565_RAT	55.05	9	2	2	N	35280			WD repeat domain 82 OS=Rattus norvegicus OX=10116 GN=Wdr82 PE=1 SV=3
179	**863**	42254	tr|Q3B7U1|Q3B7U1_RAT	54.3	2	1	1	N	65754			MAGE family member D2 OS=Rattus norvegicus OX=10116 GN=Maged2 PE=1 SV=1
180	**482**	25440	tr|D4A0E8|D4A0E8_RAT	54.26	9	6	6	Y	72695			Protein arginine N-methyltransferase 5 OS=Rattus norvegicus OX=10116 GN=Prmt5 PE=3 SV=1
181	**584**	26501	tr|A0A0H2UHZ4|A0A0H2UHZ4_RAT	54.01	18	4	4	N	36281			Zinc finger Ran-binding domain-containing protein 2 OS=Rattus norvegicus OX=10116 GN=Zranb2 PE=1 SV=2
182	**602**	25741	tr|D3ZJU5|D3ZJU5_RAT	53.76	1	1	1	N	120503			SWI/SNF related, matrix associated, actin dependent regulator of chromatin, subfamily c, member 1 OS=Rattus norvegicus OX=10116 GN=Smarcc1 PE=1 SV=1
183	**250**	789	E9PU28|IMDH2_RAT	53.3	28	10	10	Y	55815			Inosine-5'-monophosphate dehydrogenase 2 OS=Rattus norvegicus OX=10116 GN=Impdh2 PE=1 SV=1
184	**1927**	25117	tr|D4ADF5|D4ADF5_RAT	53.18	38	4	4	N	14204			Programmed cell death 5 OS=Rattus norvegicus OX=10116 GN=Pdcd5 PE=1 SV=1
185	**1407**	27536	Q5488|RPA1_RAT	52.1	1	1	1	Y	194191			DNA-directed RNA polymerase I subunit RPA1 OS=Rattus norvegicus OX=10116 GN=Polr1a PE=1 SV=1
186	**2321**	7495	Q4KLF8|ARPC5_RAT	51.06	31	2	2	Y	16320			Actin-related protein 2/3 complex subunit 5 OS=Rattus norvegicus OX=10116 GN=Arpc5 PE=1 SV=3
187	**232**	565	P50399|GDIB_RAT	50.94	18	6	6	Y	50537			Rab GDP dissociation inhibitor beta OS=Rattus norvegicus OX=10116 GN=Gdi2 PE=1 SV=2
188	**477**	1675	Q5XI32|CAPZB_RAT	50.76	39	9	9	Y	30629			F-actin-capping protein subunit beta OS=Rattus norvegicus OX=10116 GN=Capzb PE=1 SV=1
189	**259**	593	P47860|PFKAP_RAT	50.65	2	1	1	Y	85720			ATP-dependent 6-phosphofructokinase, platelet type OS=Rattus norvegicus OX=10116 GN=Pfkp PE=1 SV=2
190	**259**	22883	tr|A0A8I5ZYA2|A0A8I5ZYA2_RAT	50.65	2	1	1	Y	80431			6-phosphofructokinase OS=Rattus norvegicus OX=10116 GN=Pfkp PE=1 SV=1
191	**414**	716	O09175|AMPB_RAT	50.03	7	3	3	Y	72620			Aminopeptidase B OS=Rattus norvegicus OX=10116 GN=Rnpep PE=1 SV=2
192	**414**	23024	tr|G3V6V1|G3V6V1_RAT	50.03	7	3	3	Y	72689			Arginyl aminopeptidase OS=Rattus norvegicus OX=10116 GN=Rnpep PE=3 SV=1
193	**74**	22713	tr|A0A8I6A0A2|A0A8I6A0A2_RAT	49.81	3	6	6	N	293233			Serine/arginine repetitive matrix 2 OS=Rattus norvegicus OX=10116 GN=Srrm2 PE=1 SV=1
194	**2355**	43367	Q9Z142|TMM33_RAT	49.21	5	1	1	N	27983			Transmembrane protein 33 OS=Rattus norvegicus OX=10116 GN=Tmem33 PE=2 SV=1

195	**2324**	8338	Q6PCT5|PQBP1_RAT	49.21	17	2	2	N	30529			Polyglutamine-binding protein 1 OS=Rattus norvegicus OX=10116 GN=Pqbp1 PE=2 SV=1
196	**992**	25829	tr|A0A8I5Y7K9|A0A8I5Y7K9_RAT	49.18	4	2	2	N	77615			Metadherin OS=Rattus norvegicus OX=10116 GN=Mtdh PE=4 SV=1
197	**204**	22921	tr|D3Z941|D3Z941_RAT	49.01	7	5	5	Y	101582			Methionine--tRNA ligase, cytoplasmic OS=Rattus norvegicus OX=10116 GN=Mars1 PE=1 SV=1
198	**2511**	27280	tr|D4A9Z8|D4A9Z8_RAT	48.69	7	1	1	N	25109			Chromatin modifying protein 4B-like 1 OS=Rattus norvegicus OX=10116 GN=Chmp4bl1 PE=3 SV=1
199	**89**	22848	tr|Q6AYI1|Q6AYI1_RAT	48.67	25	14	14	Y	69239			Probable ATP-dependent RNA helicase DDX5 OS=Rattus norvegicus OX=10116 GN=Ddx5 PE=1 SV=1
200	**1304**	3449	P70580|PGRC1_RAT	48.09	8	2	2	N	21598			Membrane-associated progesterone receptor component 1 OS=Rattus norvegicus OX=10116 GN=Pgrmc1 PE=1 SV=3
201	**332**	25491	tr|A0A8I6AL58|A0A8I6AL58_RAT	47.6	2	2	2	Y	246089			Ankyrin repeat domain 17 OS=Rattus norvegicus OX=10116 GN=Ankrd17 PE=1 SV=1
202	**1984**	28021	tr|A0A8I6A5J2|A0A8I6A5J2_RAT	47.15	3	1	1	N	67513			Pre-mRNA 3'-end-processing factor FIP1 OS=Rattus norvegicus OX=10116 GN=Fip1l1 PE=1 SV=1
203	**56**	115	Q5U300|UBA1_RAT	47.14	14	10	10	Y	117788			Ubiquitin-like modifier-activating enzyme 1 OS=Rattus norvegicus OX=10116 GN=Uba1 PE=1 SV=1
204	**861**	24880	tr|Q7TQ90|Q7TQ90_RAT	46.81	6	3	3	Y	93847			Alcohol dehydrogenase class-3 OS=Rattus norvegicus OX=10116 GN=Adh4 PE=1 SV=1
205	**39**	22745	tr|D3ZU13|D3ZU13_RAT	46.49	8	10	10	N	175704			Eukaryotic translation initiation factor 4 gamma 1 OS=Rattus norvegicus OX=10116 GN=Eif4g1 PE=1 SV=1
206	**39**	22747	tr|M0RD03|M0RD03_RAT	46.49	8	10	10	N	180218			Eukaryotic translation initiation factor 4 gamma 1 OS=Rattus norvegicus OX=10116 GN=Eif4g1 PE=1 SV=2
207	**1074**	29236	tr|F1MA04|F1MA04_RAT	45.96	2	1	1	N	99408			WD repeat domain 36 OS=Rattus norvegicus OX=10116 GN=Wdr36 PE=1 SV=4
208	**269**	25259	tr|D3ZD89|D3ZD89_RAT	45.83	9	5	5	Y	101010			N(alpha)-acetyltransferase 15, NatA auxiliary subunit OS=Rattus norvegicus OX=10116 GN=Naa15 PE=1 SV=2
209	**2111**	27133	tr|A0A8I5ZMG4|A0A8I5ZMG4_RAT	45.82	9	2	2	N	28299			Thioredoxin-dependent peroxide reductase, mitochondrial OS=Rattus norvegicus OX=10116 GN=Prdx3 PE=3 SV=1
210	**2185**	27164	tr|A0A8I6GJ49|A0A8I6GJ49_RAT	45.11	26	4	4	Y	16272			Eukaryotic translation initiation factor 4C OS=Rattus norvegicus OX=10116 GN=Eif1ax PE=1 SV=1

Appendix

211	**2185**	27165	tr|A0A8I6A8I7|A0A8I6A8I7_RAT	45.11	25	4	4	Y	16676			Eukaryotic translation initiation factor 4C OS=Rattus norvegicus OX=10116 GN=Eif1ax PE=1 SV=1
212	**1181**	4272	Q5XIT9|MCCB_RAT	44.97	6	2	2	Y	61517			Methylcrotonoyl-CoA carboxylase beta chain, mitochondrial OS=Rattus norvegicus OX=10116 GN=Mccc2 PE=2 SV=1
213	**1943**	61238	tr|A0A8I6GAM2|A0A8I6GAM2_RAT	44.37	8	1	1	N	24497			Small nuclear ribonucleoprotein polypeptide B2 OS=Rattus norvegicus OX=10116 GN=Snrpb2 PE=1 SV=1
214	**1305**	7172	Q91V33|KHDR1_RAT	44.19	3	1	1	N	48315			KH domain-containing, RNA-binding, signal transduction-associated protein 1 OS=Rattus norvegicus OX=10116 GN=Khdrbs1 PE=1 SV=1
215	**517**	1658	P04961|PCNA_RAT	44.05	44	9	9	Y	28749			Proliferating cell nuclear antigen OS=Rattus norvegicus OX=10116 GN=Pcna PE=1 SV=1
216	**439**	3857	Q04931|SSRP1_RAT	43.98	14	8	8	Y	80915			FACT complex subunit SSRP1 OS=Rattus norvegicus OX=10116 GN=Ssrp1 PE=1 SV=2
217	**439**	25162	tr|A0A8L2R8I0|A0A8L2R8I0_RAT	43.98	13	8	8	Y	91414			FACT complex subunit SSRP1 OS=Rattus norvegicus OX=10116 GN=Ssrp1 PE=1 SV=1
218	**156**	23083	tr|G3V681|G3V681_RAT	43.84	2	1	1	N	96571			DNA replication licensing factor MCM4 OS=Rattus norvegicus OX=10116 GN=Mcm4 PE=1 SV=1
219	**1495**	61596	tr|D3ZKG1|D3ZKG1_RAT	43.62	2	1	1	N	92036			Methylmalonyl-CoA mutase, mitochondrial OS=Rattus norvegicus OX=10116 GN=Mmut PE=1 SV=2
220	**1290**	61057	tr|D3ZTY9|D3ZTY9_RAT	42.75	2	1	1	N	94447			Nuclear VCP-like OS=Rattus norvegicus OX=10116 GN=Nvl PE=1 SV=1
221	**1554**	26273	tr|A0A8I5YBZ5|A0A8I5YBZ5_RAT	42.55	12	2	2	N	31401			Calponin OS=Rattus norvegicus OX=10116 GN=Cnn3 PE=1 SV=1
222	**1554**	5131	P37397|CNN3_RAT	42.55	10	2	2	N	36435			Calponin-3 OS=Rattus norvegicus OX=10116 GN=Cnn3 PE=1 SV=1
223	**337**	864	Q5XJ21|DX39A_RAT	40.14	7	3	3	Y	49110			ATP-dependent RNA helicase DDX39A OS=Rattus norvegicus OX=10116 GN=Ddx39a PE=2 SV=1
224	**337**	23159	tr|A0A8I5ZVU6|A0A8I5ZVU6_RAT	40.14	7	3	3	Y	51174			RNA helicase OS=Rattus norvegicus OX=10116 GN=Ddx39a PE=1 SV=1
225	**1701**	28941	tr|D3ZXS8|D3ZXS8_RAT	39.82	27	3	3	N	15810			E2 ubiquitin-conjugating enzyme OS=Rattus norvegicus OX=10116 GN=Ube2k PE=4 SV=2
226	**1908**	27306	tr|A0A8I6AL51|A0A8I6AL51_RAT	39.37	3	1	1	Y	51980			CUGBP, Elav-like family member 1 OS=Rattus norvegicus OX=10116 GN=Celf1 PE=1 SV=1
227	**1908**	42465	Q4QQT3|CELF1_RAT	39.37	3	1	1	Y	52205			CUGBP Elav-like family member 1 OS=Rattus norvegicus OX=10116 GN=Celf1 PE=2 SV=1

228	**1338**	42236	tr|A0A8I5ZNN2|A0A8I5ZNN2_RAT	39.34	2	1	1	N	82269			TLE family member 3, transcriptional corepressor OS=Rattus norvegicus OX=10116 GN=Tle3 PE=1 SV=1
229	**1338**	42237	Q9JIT3|TLE3_RAT	39.34	2	1	1	N	82644			Transducin-like enhancer protein 3 OS=Rattus norvegicus OX=10116 GN=Tle3 PE=1 SV=1
230	**2145**	27556	tr|A0A8I6A2P1|A0A8I6A2P1_RAT	38.77	4	1	1	N	24461			Serine and arginine rich splicing factor 3 OS=Rattus norvegicus OX=10116 GN=Srsf3 PE=3 SV=1
231	**2145**	27554	tr|A0A8I5ZSN8|A0A8I5ZSN8_RAT	38.77	7	1	1	N	14518			RRM domain-containing protein OS=Rattus norvegicus OX=10116 GN=AABR07026797.1 PE=3 SV=1
232	**492**	23530	tr|Q6P6T9|Q6P6T9_RAT	37.98	3	1	1	N	57837			Importin subunit alpha OS=Rattus norvegicus OX=10116 GN=Kpna2 PE=1 SV=1
233	**2247**	42118	P62775|MTPN_RAT	37.81	8	1	1	Y	12861			Myotrophin OS=Rattus norvegicus OX=10116 GN=Mtpn PE=1 SV=2
234	**739**	26354	tr|D4A8G7|D4A8G7_RAT	37.38	14	4	4	N	61464			SNW domain-containing protein 1 OS=Rattus norvegicus OX=10116 GN=Snw1 PE=1 SV=1
235	**2203**	42328	tr|D4A1V7|D4A1V7_RAT	36.67	14	3	3	N	25349			MOB kinase activator 1B OS=Rattus norvegicus OX=10116 GN=Mob1b PE=4 SV=2
236	**2203**	100473	Q3T1J9|MOB1A_RAT	36.67	14	3	3	N	25080			MOB kinase activator 1A OS=Rattus norvegicus OX=10116 GN=Mob1a PE=2 SV=3
237	**1872**	3397	Q5I0D7|PEPD_RAT	35.97	5	2	2	Y	54751			Xaa-Pro dipeptidase OS=Rattus norvegicus OX=10116 GN=Pepd PE=2 SV=1
238	**1197**	41904	Q3KR59|UBP10_RAT	35.95	6	3	3	N	87311			Ubiquitin carboxyl-terminal hydrolase 10 OS=Rattus norvegicus OX=10116 GN=Usp10 PE=1 SV=1
239	**1417**	81298	Q5EB59|MED23_RAT	35.79	2	2	2	N	156231			Mediator of RNA polymerase II transcription subunit 23 OS=Rattus norvegicus OX=10116 GN=Med23 PE=2 SV=2
240	**321**	29760	tr|F7FMI3|F7FMI3_RAT	35.42	3	1	1	N	88723			Cullin 1 OS=Rattus norvegicus OX=10116 GN=Cul1 PE=1 SV=1
241	**1502**	5098	P83953|IMA5_RAT	35.23	4	1	1	N	60137			Importin subunit alpha-5 OS=Rattus norvegicus OX=10116 GN=Kpna1 PE=1 SV=1
242	**1502**	26051	tr|Q56R20|Q56R20_RAT	35.23	4	1	1	N	60197			Importin subunit alpha OS=Rattus norvegicus OX=10116 GN=Kpna1 PE=3 SV=1
243	**2055**	42226	B1H267|SNX5_RAT	34.86	7	2	2	Y	46793			Sorting nexin-5 OS=Rattus norvegicus OX=10116 GN=Snx5 PE=1 SV=1
244	**501**	25145	tr|E9PSJ4|E9PSJ4_RAT	34.64	2	2	2	N	146442			Sperm associated antigen 9 OS=Rattus norvegicus OX=10116 GN=Spag9 PE=1 SV=3
245	**1237**	25332	tr|D3ZAX5|D3ZAX5_RAT	34.12	2	2	2	Y	107180			Calcium homeostasis endoplasmic reticulum protein OS=Rattus norvegicus OX=10116 GN=Cherp PE=1 SV=3

Appendix

246	**935**	32257	tr|M0R623|M0R623_RAT	34.06	2	1	1	N	74152			Nucleolar GTP-binding protein 1 OS=Rattus norvegicus OX=10116 GN=Gtpbp4 PE=1 SV=2
247	**1612**	26457	P21913|SDHB_RAT	33.96	4	1	1	N	31830			Succinate dehydrogenase [ubiquinone] iron-sulfur subunit, mitochondrial OS=Rattus norvegicus OX=10116 GN=Sdhb PE=2 SV=2
248	**877**	26814	tr|D4A2P1|D4A2P1_RAT	33.84	1	1	1	N	133101			Cell division cycle and apoptosis regulator 1 OS=Rattus norvegicus OX=10116 GN=Ccar1 PE=1 SV=3
249	**564**	24132	tr|D4A994|D4A994_RAT	33.69	5	4	4	N	111185			ER membrane protein complex subunit 1 OS=Rattus norvegicus OX=10116 GN=Emc1 PE=1 SV=1
250	**1631**	6860	Q35964|SH3G1_RAT	33.47	5	1	1	N	41492			Endophilin-A2 OS=Rattus norvegicus OX=10116 GN=Sh3gl1 PE=1 SV=1
251	**699**	34988	tr|A0A0U1RRZ3|A0A0U1RRZ3_RAT	32.88	2	1	1	N	88420			NFKB repressing factor OS=Rattus norvegicus OX=10116 GN=Nkrf PE=3 SV=3
252	**1962**	29250	Q5PQQ2|WBP11_RAT	32.83	2	1	1	N	69996			WW domain-binding protein 11 OS=Rattus norvegicus OX=10116 GN=Wbp11 PE=1 SV=1
253	**1555**	27503	tr|B2GV41|B2GV41_RAT	32.59	6	2	2	N	65245			ubiquitinyl hydrolase 1 OS=Rattus norvegicus OX=10116 GN=Usp39 PE=1 SV=1
254	**1894**	81316	tr|A0A8I5Y176|A0A8I5Y176_RAT	32.54	2	1	1	N	75692			Ran-binding protein 9 OS=Rattus norvegicus OX=10116 GN=Ranbp9 PE=1 SV=1
255	**459**	28245	tr|A0A0G2K9L9|A0A0G2K9L9_RAT	32.35	0	1	1	N	630068			Midasin OS=Rattus norvegicus OX=10116 GN=Mdn1 PE=1 SV=2
256	**590**	24357	tr|Q4KLI7|Q4KLI7_RAT	31.7	22	8	8	Y	58842			Splicing factor 3a, subunit 3 OS=Rattus norvegicus OX=10116 GN=Sf3a3 PE=1 SV=1
257	**605**	3163	Q6AXS3|DEK_RAT	30.89	6	2	2	Y	42892			Protein DEK OS=Rattus norvegicus OX=10116 GN=Dek PE=1 SV=1
258	**605**	24753	tr|A0A8I6A9D8|A0A8I6A9D8_RAT	30.89	6	2	2	Y	44266			DEK proto-oncogene OS=Rattus norvegicus OX=10116 GN=Dek PE=1 SV=1
259	**1248**	3192	Q88767|PARK7_RAT	30.43	4	1	1	N	19974			Parkinson disease protein 7 homolog OS=Rattus norvegicus OX=10116 GN=Park7 PE=1 SV=1
260	**2805**	29376	tr|D4ACM2|D4ACM2_RAT	29.99	8	1	1	N	23539			Mitotic arrest deficient 2 like 1 OS=Rattus norvegicus OX=10116 GN=Mad2l1 PE=3 SV=1
261	**274**	961	P49088|ASNS_RAT	29.56	4	2	2	N	64247			Asparagine synthetase [glutamine-hydrolyzing] OS=Rattus norvegicus OX=10116 GN=Asns PE=2 SV=3
262	**2527**	42564	Q5PPH0|ENOPH_RAT	29.52	13	2	2	Y	28875			Enolase-phosphatase E1 OS=Rattus norvegicus OX=10116 GN=Enoph1 PE=2 SV=1
263	**2689**	61443	tr|A0A0G2JVB4|A0A0G2JVB4_RAT	29.24	3	1	1	Y	60289			alanine transaminase OS=Rattus norvegicus OX=10116 GN=Gpt2 PE=1 SV=1

264	**796**	24301	tr|D4A914|D4A914_RAT	28.91	7	4	4	Y	108647			5'-3' exoribonuclease OS=Rattus norvegicus OX=10116 GN=Xrn2 PE=1 SV=3
265	**996**	2376	Q8WUC8|PLRG1_RAT	27.92	4	1	1	Y	57189			Pleiotropic regulator 1 OS=Rattus norvegicus OX=10116 GN=Plrg1 PE=2 SV=1
266	**1476**	42607	tr|A0A0G2IXM5|A0A0G2IXM5_RAT	27.73	3	1	1	N	44264			DNA polymerase delta interacting protein 3 OS=Rattus norvegicus OX=10116 GN=Poldip3 PE=1 SV=2
267	**1735**	26409	tr|Q5U214|Q5U214_RAT	26.72	13	2	2	Y	31176			U1 small nuclear ribonucleoprotein A OS=Rattus norvegicus OX=10116 GN=Snrpa PE=3 SV=1
268	**81**	23055	tr|A0A0U1RS25|A0A0U1RS25_RAT	25.75	24	17	17	Y	123953			UPF1, RNA helicase and ATPase OS=Rattus norvegicus OX=10116 GN=Upf1 PE=1 SV=1
269	**550**	25812	tr|A0A8I6G5P1|A0A8I6G5P1_RAT	24.89	10	4	4	Y	46099			Heterogeneous nuclear ribonucleoprotein D-like OS=Rattus norvegicus OX=10116 GN=Hnrnpdl PE=1 SV=1
270	**608**	27865	O6AYB5|SRP54_RAT	24.6	10	4	4	N	55705			Signal recognition particle subunit SRP54 OS=Rattus norvegicus OX=10116 GN=Srp54 PE=2 SV=1
271	**516**	26296	tr|G3V752|G3V752_RAT	23.92	4	3	3	Y	115334			RNA cytidine acetyltransferase OS=Rattus norvegicus OX=10116 GN=Nat10 PE=1 SV=1
272	**657**	24019	tr|A0A0G2KAN7|A0A0G2KAN7_RAT	23.29	3	1	1	N	65838			glutaminase OS=Rattus norvegicus OX=10116 GN=Gls PE=1 SV=1
273	**995**	61286	tr|G3V727|G3V727_RAT	23.07	3	1	1	N	50989			RNA helicase OS=Rattus norvegicus OX=10116 GN=Ddx47 PE=1 SV=2
274	**1371**	7163	O6P7Q4|LGUL_RAT	23.02	5	1	1	N	20820			Lactoylglutathione lyase OS=Rattus norvegicus OX=10116 GN=Glo1 PE=1 SV=3
275	**555**	1792	P17425|HMCS1_RAT	22.82	5	2	2	N	57434			Hydroxymethylglutaryl-CoA synthase, cytoplasmic OS=Rattus norvegicus OX=10116 GN=Hmgcs1 PE=1 SV=1
276	**1049**	5949	Q3B7D0|HEM6_RAT	22.76	5	2	2	N	49278			Oxygen-dependent coproporphyrinogen-III oxidase, mitochondrial OS=Rattus norvegicus OX=10116 GN=Cpox PE=1 SV=1
277	**2072**	27708	tr|A0A8I6A412|A0A8I6A412_RAT	22.74	2	1	1	Y	70688			WD repeat domain 46 OS=Rattus norvegicus OX=10116 GN=Wdr46 PE=1 SV=1
278	**2459**	29280	P29266|3HIDH_RAT	21.27	4	1	1	N	35303			3-hydroxyisobutyrate dehydrogenase, mitochondrial OS=Rattus norvegicus OX=10116 GN=Hibadh PE=1 SV=3
279	**932**	26038	tr|A0A0G2ISG6|A0A0G2ISG6_RAT	21.18	9	2	2	N	25529			Adenylate kinase 2, mitochondrial OS=Rattus norvegicus OX=10116 GN=Ak2 PE=3 SV=1
280	**2655**	6622	P62076|TIM13_RAT	21.15	31	2	2	Y	10458			Mitochondrial import inner membrane translocase subunit Tim13 OS=Rattus norvegicus OX=10116 GN=Timm13 PE=3 SV=1

Appendix

281	**1127**	25553	tr|B2RZ74|B2RZ74_RAT	20.59	9	3	3	N	52133			U1 small nuclear ribonucleoprotein 70 kDa OS=Rattus norvegicus OX=10116 GN=Snrnp70 PE=1 SV=1
282	**58**	22918	tr|G3V8T4|G3V8T4_RAT	20.46	3	4	4	Y	126941			DNA damage-binding protein 1 OS=Rattus norvegicus OX=10116 GN=Ddb1 PE=1 SV=1
283	**3172**	11694	P61078|UB2D3_RAT	20.1	7	1	1	N	16687			Ubiquitin-conjugating enzyme E2 D3 OS=Rattus norvegicus OX=10116 GN=Ube2d3 PE=2 SV=1

Bibliography

Ahmed, M.R., Zhan, X., Song, X., Kook, S., Gurevich, V.V., Gurevich, E.V., 2011. Ubiquitin ligase parkin promotes Mdm2-arrestin interaction but inhibits arrestin ubiquitination. Biochemistry 50, 3749–3763. https://doi.org/10.1021/bi200175q

Ainslie, A., Huiting, W., Barazzuol, L., Bergink, S., n.d. Genome instability and loss of protein homeostasis: converging paths to neurodegeneration? Open Biol. 11, 200296. https://doi.org/10.1098/rsob.200296

Akutsu, M., Dikic, I., Bremm, A., 2016. Ubiquitin chain diversity at a glance. J. Cell Sci. 129, 875–880. https://doi.org/10.1242/jcs.183954

AlAbdi, L., Desbois, M., Rusnac, D.-V., Sulaiman, R.A., Rosenfeld, J.A., Lalani, S., Murdock, D.R., Burrage, L.C., Undiagnosed Diseases Network, Billie Au, P.Y., Towner, S., Wilson, W.G., Wong, L., Brunet, T., Strobl-Wildemann, G., Burton, J.E., Hoganson, G., McWalter, K., Begtrup, A., Zarate, Y.A., Christensen, E.L., Opperman, K.J., Giles, A.C., Helaby, R., Kania, A., Zheng, N., Grill, B., Alkuraya, F.S., 2023. Loss-of-function variants in MYCBP2 cause neurobehavioural phenotypes and corpus callosum defects. Brain 146, 1373–1387. https://doi.org/10.1093/brain/awac364

Almeida, L.G.N. de, Armstrong, V., Dufour, A., Braun, J.E.A., 2023. Cysteine String Protein alpha in Extracellular Vesicle Subtypes: a Proteomic Analysis. https://doi.org/10.1101/2023.12.13.571333

Alvarez-Castelao, B., Schuman, E.M., 2015. The Regulation of Synaptic Protein Turnover. J. Biol. Chem. 290, 28623–28630. https://doi.org/10.1074/jbc.R115.657130

Ambrozkiewicz, M.C., Borisova, E., Schwark, M., Ripamonti, S., Schaub, T., Smorodchenko, A., Weber, A.I., Rhee, H.J., Altas, B., Yilmaz, R., Mueller, S., Piepkorn, L., Horan, S.T., Straussberg, R., Zaqout, S., Jahn, O., Dere, E., Rosário, M., Boehm-Sturm, P., Borck, G., Willig, K.I., Rhee, J., Tarabykin, V., Kawabe, H., 2021. The murine ortholog of Kaufman oculocerebrofacial syndrome protein Ube3b regulates synapse number by ubiquitinating Ppp3cc. Mol. Psychiatry 26, 1980– 1995. https://doi.org/10.1038/s41380-020-0714-8

Amy W. Lin and Heng-Ye Man, 2013. Ubiquitination of Neurotransmitter Receptors and Postsynaptic Scaffolding Proteins - PMC [WWW Document]. URL https://www.ncbi.nlm.nih.gov/pmc/articles/PMC3574743/ (accessed 10.31.22).

Anand, S., Samuel, M., Ang, C.-S., Keerthikumar, S., Mathivanan, S., 2017a. Label-Based and Label-Free Strategies for Protein Quantitation. Methods Mol. Biol. Clifton NJ 1549, 31–43. https://doi.org/10.1007/978-1-4939-6740-7_4

Anand, S., Samuel, M., Ang, C.-S., Keerthikumar, S., Mathivanan, S., 2017b. Label-Based and Label-Free Strategies for Protein Quantitation. Methods Mol. Biol. Clifton NJ 1549, 31–43. https://doi.org/10.1007/978-1-4939-6740-7_4

Anders, C., Niewoehner, O., Duerst, A., Jinek, M., 2014. Structural basis of PAM-dependent target DNA recognition by the Cas9 endonuclease. Nature 513, 569–573. https://doi.org/10.1038/nature13579

Andersen, G.R., Nissen, P., Nyborg, J., 2003. Elongation factors in protein biosynthesis. Trends

Bibliography

Biochem. Sci. 28, 434–441. https://doi.org/10.1016/S0968-0004(03)00162-2

Andrews, P.S., Schneider, S., Yang, E., Michaels, M., Chen, H., Tang, J., Emkey, R., 2010. Identification of substrates of SMURF1 ubiquitin ligase activity utilizing protein microarrays. Assay Drug Dev. Technol. 8, 471–487. https://doi.org/10.1089/adt.2009.0264

Anfinsen, C.B., Haber, E., Sela, M., White, F.H., 1961. THE KINETICS OF FORMATION OF NATIVE RIBONUCLEASE DURING OXIDATION OF THE REDUCED POLYPEPTIDE CHAIN. Proc. Natl. Acad. Sci. 47, 1309–1314. https://doi.org/10.1073/pnas.47.9.1309

Antonucci, F., Corradini, I., Fossati, G., Tomasoni, R., Menna, E., Matteoli, M., 2016. SNAP-25, a Known Presynaptic Protein with Emerging Postsynaptic Functions. Front. Synaptic Neurosci. 8.

Arabi, A., Ullah, K., Branca, R.M.M., Johansson, J., Bandarra, D., Haneklaus, M., Fu, J., Ariës, I., Nilsson, P., Den Boer, M.L., Pokrovskaja, K., Grandér, D., Xiao, G., Rocha, S., Lehtiö, J., Sangfelt, O., 2012. Proteomic screen reveals Fbw7 as a modulator of the NF-κB pathway. Nat. Commun. 3, 976. https://doi.org/10.1038/ncomms1975

Aragón, E., Goerner, N., Xi, Q., Gomes, T., Gao, S., Massagué, J., Macias, M.J., 2012. Structural Basis for the Versatile Interactions of Smad7 with Regulator WW Domains in TGF-β Pathways. Structure 20, 1726–1736. https://doi.org/10.1016/j.str.2012.07.014

Araki, S., Tamori, Y., Kawanishi, M., Shinoda, H., Masugi, J., Mori, H., Niki, T., Okazawa, H., Kubota, T., Kasuga, M., 1997. Inhibition of the Binding of SNAP-23 to Syntaxin 4 by Munc18c. Biochem. Biophys. Res. Commun. 234, 257–262. https://doi.org/10.1006/bbrc.1997.6560

Ariga, H., Takahashi-Niki, K., Kato, I., Maita, H., Niki, T., Iguchi-Ariga, S.M.M., 2013. Neuroprotective Function of DJ-1 in Parkinson's Disease. Oxid. Med. Cell. Longev. 2013, 683920. https://doi.org/10.1155/2013/683920

Asmar, A.J., Abrams, S.R., Hsin, J., Collins, J.C., Yazejian, R.M., Wu, Y., Cho, J., Doyle, A.D., Cinthala, S., Simon, M., van Jaarsveld, R.H., Beck, D.B., Kerosuo, L., Werner, A., 2023. A ubiquitin-based effector-to-inhibitor switch coordinates early brain, craniofacial, and skin development. Nat. Commun. 14, 4499. https://doi.org/10.1038/s41467-023-40223-y

Bae, J.R., Kim, S.H., 2017. Synapses in neurodegenerative diseases. BMB Rep. 50, 237–246. https://doi.org/10.5483/BMBRep.2017.50.5.038

Bai, L., Swayne, L.A., Braun, J.E.A., 2007. The CSPα/G protein complex in PC12 cells. Biochem. Biophys. Res. Commun. 352, 123–129. https://doi.org/10.1016/j.bbrc.2006.10.178

Bark, I.C., Hahn, K.M., Ryabinin, A.E., Wilson, M.C., 1995. Differential expression of SNAP-25 protein isoforms during divergent vesicle fusion events of neural development. Proc. Natl. Acad. Sci. U. S. A. 92, 1510–1514. https://doi.org/10.1073/pnas.92.5.1510

Barker, E., Morgan, A., Barclay, J.W., 2024. Tissue distribution of cysteine string protein/DNAJC5 in C. elegans analysed by CRISPR/Cas9-mediated tagging of endogenous DNJ-14. Cell Tissue Res. 396, 41–55. https://doi.org/10.1007/s00441-024-03875-w

Banarase, T.A., Sammeta, S.S., Wankhede, N.L., Mangrulkar, S.V., Rahangdale, S.R., Aglawe, M.M., Taksande, B.G., Upaganlawar, A.B., Umekar, M.J., Kale, M.B., 2023. Mitophagy regulation in aging and neurodegenerative disease. Biophys. Rev. 15, 239–255. https://doi.org/10.1007/s12551-023-01057-6

Beasley, S.A., Hristova, V.A., Shaw, G.S., 2007. Structure of the Parkin in-between-ring domain provides insights for E3-ligase dysfunction in autosomal recessive Parkinson's disease. Proc. Natl. Acad. Sci. 104, 3095–3100. https://doi.org/10.1073/pnas.0610548104

Bell, E.W., Schwartz, J.H., Freddolino, P.L., Zhang, Y., 2022. PEPPI: Whole-proteome Proteinprotein Interaction Prediction through Structure and Sequence Similarity, Functional Association, and Machine Learning. J. Mol. Biol., Computation Resources for Molecular Biology 434, 167530. https://doi.org/10.1016/j.jmb.2022.167530

Bennett, E.J., Rush, J., Gygi, S.P., Harper, J.W., 2010. Dynamics of Cullin-RING Ubiquitin Ligase Network Revealed by Systematic Quantitative Proteomics. Cell 143, 951–965. https://doi.org/10.1016/j.cell.2010.11.017

Bennett, L., Madders, E.C.E.T., Parsons, J.L., 2020. HECTD1 promotes base excision repair in nucleosomes through chromatin remodelling. Nucleic Acids Res. 48, 1301–1313. https://doi.org/10.1093/nar/gkz1129

Berti, C., Messali, S., Ballabio, A., Reymond, A., Meroni, G., 2002. TRIM9 is specifically expressed in the embryonic and adult nervous system. Mech. Dev. 113, 159–162. https://doi.org/10.1016/S0925-4773(02)00013-8

Biamonti, G., Caceres, J.F., 2009. Cellular stress and RNA splicing. Trends Biochem. Sci. 34, 146–153. https://doi.org/10.1016/j.tibs.2008.11.004

Birendra Kc, null, May, D.G., Benson, B.V., Kim, D.I., Shivega, W.G., Ali, M.H., Faustino, R.S., Campos, A.R., Roux, K.J., 2017. VRK2A is an A-type lamin-dependent nuclear envelope kinase that phosphorylates BAF. Mol. Biol. Cell 28, 2241–2250. https://doi.org/10.1091/mbc.E17-030138

Blatch, G.L., Lässle, M., 1999. The tetratricopeptide repeat: a structural motif mediating protein-protein interactions. BioEssays News Rev. Mol. Cell. Dev. Biol. 21, 932–939. https://doi.org/10.1002/(SICI)1521-1878(199911)21:11<932::AID-BIES5>3.0.CO;2-N

Bobby, R., Medini, K., Neudecker, P., Lee, T.V., Brimble, M.A., McDonald, F.J., Lott, J.S., Dingley, A.J., 2013. Structure and dynamics of human Nedd4-1 WW3 in complex with the αENaC PY motif. Biochim. Biophys. Acta BBA - Proteins Proteomics 1834, 1632–1641. https://doi.org/10.1016/j.bbapap.2013.04.031

Bollag, R.J., Watdman, A.S., Liskay, R.M., 1989. HOMOLOGOUS RECOMBINATION IN MAMMALIAN CELLS. Annu. Rev. Genet. 23, 199–225. https://doi.org/10.1146/annurev.ge.23.120189.001215

Boonstra, J., Rijken, P., Humbel, B., Cremers, F., Verkleij, A., van Bergen en Henegouwen, P., 1995. The epidermal growth factor. Cell Biol. Int. 19, 413–430. https://doi.org/10.1006/cbir.1995.1086

Bibliography

Bousman, C.A., Chana, G., Glatt, S.J., Chandler, S.D., Lucero, G.R., Tatro, E., May, T., Lohr, J.B., Kremen, W.S., Tsuang, M.T., Everall, I.P., 2010. Preliminary Evidence of Ubiquitin Proteasome System Dysregulation in Schizophrenia and Bipolar Disorder: Convergent Pathway Analysis Findings from Two Independent Samples. Am. J. Med. Genet. Part B Neuropsychiatr. Genet. Off. Publ. Int. Soc. Psychiatr. Genet. 0, 494–502. https://doi.org/10.1002/ajmg.b.31006

Bradley, R.K., Anczukow, O., 2023. RNA splicing dysregulation and the hallmarks of cancer. Nat. Rev. Cancer 23, 135–155. https://doi.org/10.1038/s41568-022-00541-7

Branon, T.C., Bosch, J.A., Sanchez, A.D., Udeshi, N.D., Svinkina, T., Carr, S.A., Feldman, J.L., Perrimon, N., Ting, A.Y., 2018. Efficient proximity labeling in living cells and organisms with TurboID. Nat. Biotechnol. 36, 880–887. https://doi.org/10.1038/nbt.4201

Braun, J.E.A., Wilbanks, S.M., Scheller, R.H., 1996. The Cysteine String Secretory Vesicle Protein Activates Hsc70 ATPase *. J. Biol. Chem. 271, 25989–25993. https://doi.org/10.1074/jbc.271.42.25989

Brudvig, J.J., Cain, J.T., Schmidt-Grimminger, G.G., Stumpo, D.J., Roux, K.J., Blackshear, P.J., Weimer, J.M., 2018. MARCKS Is Necessary for Netrin-DCC Signaling and Corpus Callosum Formation. Mol. Neurobiol. 55, 8388–8402. https://doi.org/10.1007/s12035-018-0990-3

Burande, C.F., Heuzé, M.L., Lamsoul, I., Monsarrat, B., Uttenweiler-Joseph, S., Lutz, P.G., 2009. A Label-free Quantitative Proteomics Strategy to Identify E3 Ubiquitin Ligase Substrates Targeted to Proteasome Degradation*. Mol. Cell. Proteomics 8, 1719–1727. https://doi.org/10.1074/mcp.M800410-MCP200

Burgoyne, R.D., Morgan, A., 2015. Cysteine string protein (CSP) and its role in preventing neurodegeneration. Semin. Cell Dev. Biol. 40, 153–159. https://doi.org/10.1016/j.semcdb.2015.03.008

Bustamante-Barrientos, F.A., Luque-Campos, N., Araya, M.J., Lara-Barba, E., de Solminihac, J., Pradenas, C., Molina, L., Herrera-Luna, Y., Utreras-Mendoza, Y., Elizondo-Vega, R., Vega-Letter, A.M., Luz-Crawford, P., 2023. Mitochondrial dysfunction in neurodegenerative disorders: Potential therapeutic application of mitochondrial transfer to central nervous system-residing cells. J. Transl. Med. 21, 613. https://doi.org/10.1186/s12967-023-04493-w

Cahill, A.L., Herring, B.E., Fox, A.P., 2006. Stable silencing of SNAP-25 in PC12 cells by RNA interference. BMC Neurosci. 7, 9. https://doi.org/10.1186/1471-2202-7-9

Callis, J., 2014. The Ubiquitination Machinery of the Ubiquitin System. Arab. Book Am. Soc. Plant Biol. 12, e0174. https://doi.org/10.1199/tab.0174

Caló, L., Hidari, E., Wegrzynowicz, M., Dalley, J.W., Schneider, B.L., Podgajna, M., Anichtchik, O., Carlson, E., Klenerman, D., Spillantini, M.G., 2021. CSPα reduces aggregates and rescues striatal dopamine release in α-synuclein transgenic mice. Brain 144, 1661–1669. https://doi.org/10.1093/brain/awab076

Cammas, F., Khetchoumian, K., Chambon, P., Losson, R., 2012. TRIM involvement in transcriptional regulation. Adv. Exp. Med. Biol. 770, 59–76. https://doi.org/10.1007/978-1-46145398-7_5

Campbell, D.S., Holt, C.E., 2001. Chemotropic responses of retinal growth cones mediated by rapid local protein synthesis and degradation. Neuron 32, 1013–1026. https://doi.org/10.1016/s0896-6273(01)00551-7

Caplan, A.J., 2003. What is a co-chaperone? Cell Stress Chaperones 8, 105–107.

Chakraborty, A., Edkins, A.L., 2023. CHIP: A Co-chaperone for Degradation by the Proteasome and Lysosome. Subcell. Biochem. 101, 351–387. https://doi.org/10.1007/978-3-031-147401_12

Chamberlain, L.H., Burgoyne, R.D., 1998. The cysteine-string domain of the secretory vesicle cysteine-string protein is required for membrane targeting. Biochem. J. 335, 205–209.

Chamberlain, L.H., Burgoyne, R.D., 1996. Identification of a Novel Cysteine String Protein

Variant and Expression of Cysteine String Proteins in Non-neuronal Cells (∗). J. Biol. Chem. 271,

7320–7323. https://doi.org/10.1074/jbc.271.13.7320

Chamberlain, L.H., Burgoyne, R.D., Gould, G.W., 2001. SNARE proteins are highly enriched in lipid rafts in PC12 cells: Implications for the spatial control of exocytosis. Proc. Natl. Acad. Sci. 98, 5619–5624. https://doi.org/10.1073/pnas.091502398

Chanaday, N.L., Cousin, M.A., Milosevic, I., Watanabe, S., Morgan, J.R., 2019. The Synaptic

Vesicle Cycle Revisited: New Insights into the Modes and Mechanisms. J. Neurosci. 39, 8209–

8216. https://doi.org/10.1523/JNEUROSCI.1158-19.2019

Chandler, C.S., Ballard, F.J., 1986. Multiple biotin-containing proteins in 3T3-L1 cells. Biochem.

J. 237, 123–130. https://doi.org/10.1042/bj2370123

Chandra, S., Gallardo, G., Fernández-Chacón, R., Schlüter, O.M., Südhof, T.C., 2005. Alphasynuclein cooperates with CSPalpha in preventing neurodegeneration. Cell 123, 383–396. https://doi.org/10.1016/j.cell.2005.09.028

Chang, H.H.Y., Pannunzio, N.R., Adachi, N., Lieber, M.R., 2017. Non-homologous DNA end joining and alternative pathways to double-strand break repair. Nat. Rev. Mol. Cell Biol. 18, 495–506. https://doi.org/10.1038/nrm.2017.48

Chang, Y.-F., Cheng, C.-M., Chang, L.-K., Jong, Y.-J., Yuo, C.-Y., 2006. The F-box protein Fbxo7 interacts with human inhibitor of apoptosis protein cIAP1 and promotes cIAP1 ubiquitination. Biochem. Biophys. Res. Commun. 342, 1022–1026. https://doi.org/10.1016/j.bbrc.2006.02.061

Chantachotikul, P., Liu, S., Furukawa, K., Deguchi, S., 2025. AP2A1 modulates cell states between senescence and rejuvenation. Cell. Signal. 127, 111616. https://doi.org/10.1016/j.cellsig.2025.111616

Chaugule, V.K., Burchell, L., Barber, K.R., Sidhu, A., Leslie, S.J., Shaw, G.S., Walden, H., 2011.

Autoregulation of Parkin activity through its ubiquitin-like domain. EMBO J. 30, 2853–2867. https://doi.org/10.1038/emboj.2011.204

Bibliography

Chen, C., Xu, L., Chen, L., Zhai, Z., Cheng, M., Luo, S., Wang, H., 2025. DNAJC5 facilitates the proliferation and migration of lung adenocarcinoma cells by augmenting EGFR trafficking. Commun. Biol. 8, 757. https://doi.org/10.1038/s42003-025-08191-9

Chen, D., Tang, J.-X., Li, B., Hou, L., Wang, X., Kang, L., 2018. CRISPR/Cas9-mediated genome editing induces exon skipping by complete or stochastic altering splicing in the migratory locust. BMC Biotechnol. 18, 60. https://doi.org/10.1186/s12896-018-0465-7

Chen, T.-C., Lin, K.-T., Chen, C.-H., Lee, S.-A., Lee, P.-Y., Liu, Y.-W., Kuo, Y.-L., Wang, F.-S., Lai, J.-M., Huang, C.-Y.F., 2014. Using an in situ proximity ligation assay to systematically profile endogenous protein-protein interactions in a pathway network. J. Proteome Res. 13, 5339– 5346. https://doi.org/10.1021/pr5002737

Chen, Y.A., Scales, S.J., Duvvuri, V., Murthy, M., Patel, S.M., Schulman, H., Scheller, R.H., 2001.

Calcium Regulation of Exocytosis in PC12 Cells*. J. Biol. Chem. 276, 26680–26687. https://doi.org/10.1074/jbc.M103522200

Chen, Z., Li1, Z., Lin, F., Yao, Z., Greene, M., Li, B., 2011. IdentifICATION OF E3 ubiquitin ligase STUB1 as a negative regulator of FOXP3. BMC Proc. 5, P84.

Chen, Z.-Y., Ieraci, A., Tanowitz, M., Lee, F.S., 2005. A Novel Endocytic Recycling Signal

Distinguishes Biological Responses of Trk Neurotrophin Receptors. Mol. Biol. Cell 16, 5761–

5772. https://doi.org/10.1091/mbc.e05-07-0651

Cheon, S., Dean, M., Chahrour, M., 2019a. The ubiquitin proteasome pathway in neuropsychiatric disorders. Neurobiol. Learn. Mem., Behavioral Analyses of Animal Models of Intellectual and Developmental Disabilities 165, 106791. https://doi.org/10.1016/j.nlm.2018.01.012

Cheon, S., Kaur, K., Nijem, N., Tuncay, I.O., Kumar, P., Dean, M., Juusola, J., Guillen-Sacoto,

M.J., Bedoukian, E., Ierardi-Curto, L., Kaplan, P., Schaefer, G.B., Mishra, P., Chahrour, M.H., 2019b. The ubiquitin ligase UBE3B, disrupted in intellectual disability and absent speech, regulates metabolic pathways by targeting BCKDK. Proc. Natl. Acad. Sci. 116, 3662–3667. https://doi.org/10.1073/pnas.1818751116

Chin, L.-S., Vavalle, J.P., Li, L., 2002a. Staring, a Novel E3 Ubiquitin-Protein Ligase That Targets Syntaxin 1 for Degradation*. J. Biol. Chem. 277, 35071–35079. https://doi.org/10.1074/jbc.M203300200

Chin, L.-S., Vavalle, J.P., Li, L., 2002b. Staring, a Novel E3 Ubiquitin-Protein Ligase That Targets Syntaxin 1 for Degradation*. J. Biol. Chem. 277, 35071–35079. https://doi.org/10.1074/jbc.M203300200

Chiti, F., Dobson, C.M., 2006. Protein Misfolding, Functional Amyloid, and Human Disease.

Annu. Rev. Biochem. 75, 333–366. https://doi.org/10.1146/annurev.biochem.75.101304.123901

Choe, E.-A., Liao, L., Zhou, J.-Y., Cheng, D., Duong, D.M., Jin, P., Tsai, L.-H., Peng, J., 2007. Neuronal morphogenesis is regulated by the interplay between cyclin-dependent kinase 5 and the ubiquitin ligase mind bomb 1. J. Neurosci. Off. J. Soc. Neurosci. 27, 9503–9512. https://doi.org/10.1523/JNEUROSCI.1408-07.2007

Chojnowski, A., Sobota, R.M., Ong, P.F., Xie, W., Wong, X., Dreesen, O., Burke, B., Stewart, C.L.,

2018. 2C-BioID: An Advanced Two Component BioID System for Precision Mapping of Protein

Interactomes. iScience 10, 40–52. https://doi.org/10.1016/j.isci.2018.11.023

Christianson, J.C., Green, W.N., 2004. Regulation of nicotinic receptor expression by the ubiquitin-proteasome system. EMBO J. 23, 4156–4165. https://doi.org/10.1038/sj.emboj.7600436

Chu, C.T., 2019. Mechanisms of selective autophagy and mitophagy: Implications for neurodegenerative diseases. Neurobiol. Dis. 122, 23–34. https://doi.org/10.1016/j.nbd.2018.07.015

Chung, K.K., Zhang, Y., Lim, K.L., Tanaka, Y., Huang, H., Gao, J., Ross, C.A., Dawson, V.L., Dawson, T.M., 2001. Parkin ubiquitinates the alpha-synuclein-interacting protein, synphilin-1: implications for Lewy-body formation in Parkinson disease. Nat. Med. 7, 1144–1150. https://doi.org/10.1038/nm1001-1144

Cianfrocco MA, Wong M, Youn C, Wagner R, Leschziner AE., 2017. COSMIC2 – A science gateway for cryo-electron microscopy [WWW Document]. URL https://figshare.com/articles/journal_contribution/COSMIC2_A_science_gateway_for_cryoelectron_microscopy/5481430?file=9479707 (accessed 6.2.25).

Ciechanover, A., Schwartz, A.L., 1998. The ubiquitin-proteasome pathway: The complexity and myriad functions of proteins death. Proc. Natl. Acad. Sci. U. S. A. 95, 2727–2730.

Clausen, L., Abildgaard, A.B., Gersing, S.K., Stein, A., Lindorff-Larsen, K., Hartmann-Petersen, R., 2019. Chapter Two - Protein stability and degradation in health and disease, in: Donev, R. (Ed.), Advances in Protein Chemistry and Structural Biology, Molecular Chaperones in Human Disorders. Academic Press, pp. 61–83. https://doi.org/10.1016/bs.apcsb.2018.09.002

Clausen, L., Voutsinos, V., Cagiada, M., Johansson, K.E., Grønbæk-Thygesen, M., Nariya, S., Powell, R.L., Have, M.K.N., Oestergaard, V.H., Stein, A., Fowler, D.M., Lindorff-Larsen, K., Hartmann-Petersen, R., 2024. A mutational atlas for Parkin proteostasis. Nat. Commun. 15, 1541. https://doi.org/10.1038/s41467-024-45829-4

Colledge, M., Snyder, E.M., Crozier, R.A., Soderling, J.A., Jin, Y., Langeberg, L.K., Lu, H., Bear, M.F., Scott, J.D., 2003. Ubiquitination Regulates PSD-95 Degradation and AMPA Receptor Surface Expression. Neuron 40, 595–607. https://doi.org/10.1016/S0896-6273(03)00687-1

Cookson, M.R., Lockhart, P.J., McLendon, C., O'Farrell, C., Schlossmacher, M., Farrer, M.J., 2003. RING finger 1 mutations in Parkin produce altered localization of the protein. Hum. Mol. Genet. 12, 2957–2965. https://doi.org/10.1093/hmg/ddg328

Cooper, G.M., 2000. Protein Folding and Processing. Cell Mol. Approach 2nd Ed.

Coppola, T., Gundersen, C., 1996. Widespread expression of human cysteine string proteins. FEBS Lett. 391, 269–272. https://doi.org/10.1016/0014-5793(96)00750-8

Bibliography

Coyaud, E., Mis, M., Laurent, E.M.N., Dunham, W.H., Couzens, A.L., Robitaille, M., Gingras, A.-

C., Angers, S., Raught, B., 2015. BioID-based Identification of Skp Cullin F-box (SCF)β-TrCP1/2 E3 Ligase Substrates. Mol. Cell. Proteomics MCP 14, 1781–1795. https://doi.org/10.1074/mcp.M114.045658

Cronan, J.E., 2005. Targeted and proximity-dependent promiscuous protein biotinylation by a mutant Escherichia coli biotin protein ligase. J. Nutr. Biochem. 16, 416–418. https://doi.org/10.1016/j.jnutbio.2005.03.017

Cui, H., Shi, Q., Macarios, C.M., Schimmel, P., 2024. Metabolic regulation of mRNA splicing.

Trends Cell Biol. 34, 756–770. https://doi.org/10.1016/j.tcb.2024.02.002

Cui, M., Cheng, C., Zhang, L., 2022. High-throughput proteomics: a methodological minireview. Lab. Investig. J. Tech. Methods Pathol. 102, 1170–1181. https://doi.org/10.1038/s41374-022-00830-7

da Costa, C.A., Sunyach, C., Giaime, E., West, A., Corti, O., Brice, A., Safe, S., Abou-Sleiman, P.M., Wood, N.W., Takahashi, H., Goldberg, M.S., Shen, J., Checler, F., 2009. Transcriptional repression of p53 by parkin and impairment by mutations associated with autosomal recessive juvenile Parkinson's disease. Nat. Cell Biol. 11, 1370–1375. https://doi.org/10.1038/ncb1981

da Fonseca, P.C.A., Kong, E.H., Zhang, Z., Schreiber, A., Williams, M.A., Morris, E.P., Barford, D., 2011. Structures of APC/CCdh1 with substrates identify Cdh1 and Apc10 as the D-box coreceptor. Nature 470, 274–278. https://doi.org/10.1038/nature09625

Davies, F.C.J., Hope, J.E., McLachlan, F., Marshall, G.F., Kaminioti-Dumont, L., Qarkaxhija, V., Nunez, F., Dando, O., Smith, C., Wood, E., MacDonald, J., Hardt, O., Abbott, C.M., 2020. Recapitulation of the EEF1A2 D252H neurodevelopmental disorder-causing missense mutation in mice reveals a toxic gain of function. Hum. Mol. Genet. 29, 1592–1606. https://doi.org/10.1093/hmg/ddaa042

Dawson, T.M., Dawson, V.L., 2010. The Role of Parkin in Familial and Sporadic Parkinson's Disease. Mov. Disord. Off. J. Mov. Disord. Soc. 25, S32–S39. https://doi.org/10.1002/mds.22798

de la Cova, C.C., 2023. The Highs and Lows of FBXW7: New Insights into Substrate Affinity in Disease and Development. Cells 12, 2141. https://doi.org/10.3390/cells12172141

De Rinaldis, M., Giorda, R., Trabacca, A., 2020. Mild epileptic phenotype associates with de novo *eef1a2* mutation: Case report and review. Brain Dev. 42, 77–82. https://doi.org/10.1016/j.braindev.2019.08.001

Dechant, G., Rodríguez-Tébar, A., Barde, Y.A., 1994. Neurotrophin receptors. Prog. Neurobiol.

42, 347–352. https://doi.org/10.1016/0301-0082(94)90075-2

DeGregori, J., 2002. The genetics of the E2F family of transcription factors: shared functions and unique roles. Biochim. Biophys. Acta BBA - Rev. Cancer 1602, 131–150. https://doi.org/10.1016/S0304-419X(02)00051-3

Delgado-Martínez, I., Nehring, R.B., Sørensen, J.B., 2007. Differential Abilities of SNAP-25 Homologs to Support Neuronal Function. J. Neurosci. 27, 9380–9391. https://doi.org/10.1523/JNEUROSCI.5092-06.2007

Deng, J., Koutras, C., Donnelier, J., Alshehri, M., Fotouhi, M., Girard, M., Casha, S., McPherson,

P.S., Robbins, S.M., Braun, J.E.A., 2017. Neurons Export Extracellular Vesicles Enriched in Cysteine String Protein and Misfolded Protein Cargo. Sci. Rep. 7, 956. https://doi.org/10.1038/s41598-017-01115-6

Deshaies, R.J., Joazeiro, C.A.P., 2009. RING domain E3 ubiquitin ligases. Annu. Rev. Biochem. 78, 399–434. https://doi.org/10.1146/annurev.biochem.78.101807.093809

Dever, T.E., Dinman, J.D., Green, R., 2018. Translation Elongation and Recoding in Eukaryotes. Cold Spring Harb. Perspect. Biol. 10, a032649. https://doi.org/10.1101/cshperspect.a032649

Di Domenico, F., Coccia, R., Cocciolo, A., Murphy, M.P., Cenini, G., Head, E., Butterfield, D.A., Giorgi, A., Schinina, M.E., Mancuso, C., Cini, C., Perluigi, M., 2013. Impairment of proteostasis network in Down syndrome prior to the development of Alzheimer's disease neuropathology: Redox proteomics analysis of human brain. Biochim. Biophys. Acta 1832, 1249–1259. https://doi.org/10.1016/j.bbadis.2013.04.013

DiAntonio, A., Haghighi, A.P., Portman, S.L., Lee, J.D., Amaranto, A.M., Goodman, C.S., 2001. Ubiquitination-dependent mechanisms regulate synaptic growth and function. Nature 412, 449–452. https://doi.org/10.1038/35086595

Dindot, S.V., Antalffy, B.A., Bhattacharjee, M.B., Beaudet, A.L., 2008. The Angelman syndrome ubiquitin ligase localizes to the synapse and nucleus, and maternal deficiency results in abnormal dendritic spine morphology. Hum. Mol. Genet. 17, 111–118. https://doi.org/10.1093/hmg/ddm288

Ding, M., Chao, D., Wang, G., Shen, K., 2007. Spatial regulation of an E3 ubiquitin ligase directs selective synapse elimination. Science 317, 947–951. https://doi.org/10.1126/science.1145727
Dobashi, Y., Kudoh, T., Matsumine, A., Toyoshima, K., Akiyama, T., 1995. Constitutive Overexpression of CDK2 Inhibits Neuronal Differentiation of Rat Pheochromocytoma PC12 Cells (*). J. Biol. Chem. 270, 23031–23037. https://doi.org/10.1074/jbc.270.39.23031

Doench, J.G., Fusi, N., Sullender, M., Hegde, M., Vaimberg, E.W., Donovan, K.F., Smith, I., Tothova, Z., Wilen, C., Orchard, R., Virgin, H.W., Listgarten, J., Root, D.E., 2016. Optimized sgRNA design to maximize activity and minimize off-target effects of CRISPR-Cas9. Nat. Biotechnol. 34, 184–191. https://doi.org/10.1038/nbt.3437

Dp, H., Dr, S., D, N., Sm, P., 2003. The autosomal recessive juvenile Parkinson disease gene product, parkin, interacts with and ubiquitinates synaptotagmin XI. Hum. Mol. Genet. 12. https://doi.org/10.1093/hmg/ddg269

Ds, D., Y, L., Rj, B., 1999. An ethanol-sensitive variant of the PC12 neuronal cell line: sensitivity to alcohol is associated with increased cell adhesion and decreased glucose accumulation. J. Cell. Physiol. 178. https://doi.org/10.1002/(SICI)1097-4652(199901)178:1<93::AIDJCP12>3.0.CO;2-U

Du, M.-G., Liu, F., Chang, Y., Tong, S., Liu, W., Chen, Y.-J., Xie, P., 2021. Neddylation modification of the U3 snoRNA-binding protein RRP9 by Smurf1 promotes tumorigenesis. J. Biol. Chem. 297, 101307. https://doi.org/10.1016/j.jbc.2021.101307

Bibliography

Duda, D.M., Olszewski, J.L., Schuermann, J.P., Kurinov, I., Miller, D.J., Nourse, A., Alpi, A.F., Schulman, B.A., 2013. Structure of HHARI, a RING-IBR-RING ubiquitin ligase: autoinhibition of an Ariadne-family E3 and insights into ligation mechanism. Struct. Lond. Engl. 1993 21, 1030– 1041. https://doi.org/10.1016/j.str.2013.04.019

Eagleman, D.E., Zhu, J., Liu, D.-C., Seimetz, J., Kalsotra, A., Tsai, N.-P., 2021. Unbiased proteomic screening identifies a novel role for the E3 ubiquitin ligase Nedd4-2 in translational suppression during ER stress. J. Neurochem. 157, 1809–1820. https://doi.org/10.1111/jnc.15219 ebi.ac.uk/QuickGO/targetset/ParkinsonsUK-UCL, n.d.

Eftekharzadeh, B., Banduseela, V.C., Chiesa, G., Martínez-Cristóbal, P., Rauch, J.N., Nath, S.R.,

Schwarz, D.M.C., Shao, H., Marin-Argany, M., Di Sanza, C., Giorgetti, E., Yu, Z., Pierattelli, R.,

Felli, I.C., Brun-Heath, I., García, J., Nebreda, Á.R., Gestwicki, J.E., Lieberman, A.P., Salvatella,

X., 2019. Hsp70 and Hsp40 inhibit an inter-domain interaction necessary for transcriptional activity in the androgen receptor. Nat. Commun. 10, 3562. https://doi.org/10.1038/s41467-01911594-y

Ehlers, M.D., 2003. Activity level controls postsynaptic composition and signaling via the ubiquitin-proteasome system. Nat. Neurosci. 6, 231–242. https://doi.org/10.1038/nn1013

Eisenhaber, B., Chumak, N., Eisenhaber, F., Hauser, M.-T., 2007. The ring between ring fingers

(RBR) protein family. Genome Biol. 8, 209. https://doi.org/10.1186/gb-2007-8-3-209

Elenbaas, B., Dobbelstein, M., Roth, J., Shenk, T., Levine, A.J., 1996. The MDM2 oncoprotein binds specifically to RNA through its RING finger domain. Mol. Med. 2, 439–451.

EMBL-EBI, n.d. Confidence scores in AlphaFold-Multimer | AlphaFold. URL https://www.ebi.ac.uk/training/online/courses/alphafold/inputs-and-outputs/evaluatingalphafolds-predicted-structures-using-confidence-scores/confidence-scores-in-alphafoldmultimer/ (accessed 4.4.25).

Engel, T., Lucas, J.J., Henshall, D.C., 2017. Targeting the proteasome in epilepsy. Oncotarget 8,

45042–45043. https://doi.org/10.18632/oncotarget.18418

Erdem-Eraslan, L., Gao, Y., Kloosterhof, N.K., Atlasi, Y., Demmers, J., Sacchetti, A., Kros, J.M., Sillevis Smitt, P., Aerts, J., French, P.J., 2015. Mutation specific functions of EGFR result in a mutation-specific downstream pathway activation. Eur. J. Cancer Oxf. Engl. 1990 51, 893–903. https://doi.org/10.1016/j.ejca.2015.02.006

Erpapazoglou, Z., Walker, O., Haguenauer-Tsapis, R., 2014. Versatile Roles of K63-Linked Ubiquitin Chains in Trafficking. Cells 3, 1027–1088. https://doi.org/10.3390/cells3041027

Escobedo, A., Gomes, T., Aragón, E., Martín-Malpartida, P., Ruiz, L., Macias, M.J., 2014.

Structural Basis of the Activation and Degradation Mechanisms of the E3 Ubiquitin Ligase

Nedd4L. Structure 22, 1446–1457. https://doi.org/10.1016/j.str.2014.08.016

Escuder-Rodríguez, J.-J., Rodríguez-Alonso, A., Jove, L., Quiroga, M., Alfonsín, G., Figueroa, A.,

2025. Beyond destruction: emerging roles of the E3 ubiquitin ligase Hakai. Cell. Mol. Biol. Lett.

30, 9. https://doi.org/10.1186/s11658-025-00693-y

Evans, G.J.O., Morgan, A., Burgoyne, R.D., 2003. Tying Everything Together: The Multiple Roles of Cysteine String Protein (CSP) in Regulated Exocytosis. Traffic 4, 653–659. https://doi.org/10.1034/j.1600-0854.2003.00127.x

Evans, C.S., Holzbaur, E.L.F., 2019. Autophagy and Mitophagy in ALS. Neurobiol. Dis. 122, 35–40. https://doi.org/10.1016/j.nbd.2018.07.005

F. CORPET, 1988. Multiple sequence alignment with hierarchical clustering. Nucl Acids Res 16, 10881–10890.

Faire, K., Trent, F., Tepper, J.M., Bonder, E.M., 1992. Analysis of dynamin isoforms in mammalian brain: dynamin-1 expression is spatially and temporally regulated during postnatal development. Proc. Natl. Acad. Sci. U. S. A. 89, 8376–8380. https://doi.org/10.1073/pnas.89.17.8376

Faitg, J., Lacefield, C., Davey, T., White, K., Laws, R., Kosmidis, S., Reeve, A.K., Kandel, E.R., Vincent, A.E., Picard, M., 2021. 3D neuronal mitochondrial morphology in axons, dendrites, and somata of the aging mouse hippocampus. Cell Rep. 36, 109509. https://doi.org/10.1016/j.celrep.2021.109509

Fasshauer, D., Sutton, R.B., Brunger, A.T., Jahn, R., 1998. Conserved structural features of the synaptic fusion complex: SNARE proteins reclassified as Q- and R-SNAREs. Proc. Natl. Acad. Sci. 95, 15781–15786. https://doi.org/10.1073/pnas.95.26.15781

Fenech, E.J., Lari, F., Charles, P.D., Fischer, R., Laétitia-Thézénas, M., Bagola, K., Paton, A.W., Paton, J.C., Gyrd-Hansen, M., Kessler, B.M., Christianson, J.C., 2020. Interaction mapping of endoplasmic reticulum ubiquitin ligases identifies modulators of innate immune signalling. eLife 9, e57306. https://doi.org/10.7554/eLife.57306

Ferguson, S.M., Brasnjo, G., Hayashi, M., Wölfel, M., Collesi, C., Giovedi, S., Raimondi, A., Gong, L.-W., Ariel, P., Paradise, S., O'Toole, E., Flavell, R., Cremona, O., Miesenböck, G., Ryan, T.A., De Camilli, P., 2007. A Selective Activity-Dependent Requirement for Dynamin 1 in Synaptic Vesicle Endocytosis. Science 316, 570–574. https://doi.org/10.1126/science.1140621

Fernández-Chacón, R., Wölfel, M., Nishimune, H., Tabares, L., Schmitz, F., Castellano-Muñoz, M., Rosenmund, C., Montesinos, M.L., Sanes, J.R., Schneggenburger, R., Südhof, T.C., 2004. The Synaptic Vesicle Protein CSPα Prevents Presynaptic Degeneration. Neuron 42, 237–251. https://doi.org/10.1016/S0896-6273(04)00190-4

Fesce, R., Grohovaz, F., Valtorta, F., Meldolesi, J., 1994. Neurotransmitter release: fusion or "kiss-and-run"? Trends Cell Biol. 4, 1–4. https://doi.org/10.1016/0962-8924(94)90025-6

Fields, S., Song, O., 1989. A novel genetic system to detect protein-protein interactions. Nature 340, 245–246. https://doi.org/10.1038/340245a0

Fiuza, M., Rostosky, C.M., Parkinson, G.T., Bygrave, A.M., Halemani, N., Baptista, M., Milosevic, I., Hanley, J.G., 2017. PICK1 regulates AMPA receptor endocytosis via direct interactions with AP2 α-appendage and dynamin. J. Cell Biol. 216, 3323–3338. https://doi.org/10.1083/jcb.201701034

Fontaine, S.N., Zheng, D., Sabbagh, J.J., Martin, M.D., Chaput, D., Darling, A., Trotter, J.H.,

Bibliography

Stothert, A.R., Nordhues, B.A., Lussier, A., Baker, J., Shelton, L., Kahn, M., Blair, L.J., Stevens Jr, S.M., Dickey, C.A., 2016. DnaJ/Hsc70 chaperone complexes control the extracellular release of neurodegenerative-associated proteins. EMBO J. 35, 1537–1549. https://doi.org/10.15252/embj.201593489

Fortea, J., Zaman, S.H., Hartley, S., Rafii, M.S., Head, E., Carmona-Iragui, M., 2021. Alzheimer's disease associated with Down syndrome: a genetic form of dementia. Lancet Neurol. 20, 930– 942. https://doi.org/10.1016/S1474-4422(21)00245-3

Fossati, G., Morini, R., Corradini, I., Antonucci, F., Trepte, P., Edry, E., Sharma, V., Papale, A.,

Pozzi, D., Defilippi, P., Meier, J.C., Brambilla, R., Turco, E., Rosenblum, K., Wanker, E.E., Ziv, N.E., Menna, E., Matteoli, M., 2015. Reduced SNAP-25 increases PSD-95 mobility and impairs spine morphogenesis. Cell Death Differ. 22, 1425–1436. https://doi.org/10.1038/cdd.2014.227

Friedman, W.J., Greene, L.A., 1999. Neurotrophin signaling via Trks and p75. Exp. Cell Res. 253,

131–142. https://doi.org/10.1006/excr.1999.4705

Gallo, R., Rai, A.K., McIntyre, A.B.R., Meyer, K., Pelkmans, L., 2023. DYRK3 enables secretory trafficking by maintaining the liquid-like state of ER exit sites. Dev. Cell 58, 1880-1897.e11. https://doi.org/10.1016/j.devcel.2023.08.005

García-Junco-Clemente, P., Cantero, G., Gómez-Sánchez, L., Linares-Clemente, P., MartínezLópez, J.A., Luján, R., Fernández-Chacón, R., 2010. Cysteine string protein-alpha prevents activity-dependent degeneration in GABAergic synapses. J. Neurosci. Off. J. Soc. Neurosci. 30, 7377–7391. https://doi.org/10.1523/JNEUROSCI.0924-10.2010

Germini, D., Tsfasman, T., Zakharova, V.V., Sjakste, N., Lipinski, M., Vassetzky, Y., 2018. A

Comparison of Techniques to Evaluate the Effectiveness of Genome Editing. Trends Biotechnol.

36, 147–159. https://doi.org/10.1016/j.tibtech.2017.10.008

Giráldez, S., Herrero-Ruiz, J., Mora-Santos, M., Japón, M.Á., Tortolero, M., Romero, F., 2014. SCFFBXW7α modulates the intra-S-phase DNA-damage checkpoint by regulating Polo like kinase-1 stability. Oncotarget 5, 4370–4383. https://doi.org/10.18632/oncotarget.2021 Glessner, J.T., Wang, K., Cai, G., Korvatska, O., Kim, C.E., Wood, S., Zhang, H., Estes, A., Brune,

C.W., Bradfield, J.P., Imielinski, M., Frackelton, E.C., Reichert, J., Crawford, E.L., Munson, J.,

Sleiman, P.M.A., Chiavacci, R., Annaiah, K., Thomas, K., Hou, C., Glaberson, W., Flory, J.,

Otieno, F., Garris, M., Soorya, L., Klei, L., Piven, J., Meyer, K.J., Anagnostou, E., Sakurai, T.,

Game, R.M., Rudd, D.S., Zurawiecki, D., McDougle, C.J., Davis, L.K., Miller, J., Posey, D.J.,

Michaels, S., Kolevzon, A., Silverman, J.M., Bernier, R., Levy, S.E., Schultz, R.T., Dawson, G.,

Owley, T., McMahon, W.M., Wassink, T.H., Sweeney, J.A., Nurnberger, J.I., Coon, H., Sutcliffe,

J.S., Minshew, N.J., Grant, S.F.A., Bucan, M., Cook, E.H., Buxbaum, J.D., Devlin, B.,

Schellenberg, G.D., Hakonarson, H., 2009. Autism genome-wide copy number variation reveals ubiquitin and neuronal genes. Nature 459, 569–573. https://doi.org/10.1038/nature07953

Goda, Y., 1997. SNAREs and regulated vesicle exocytosis. Proc. Natl. Acad. Sci. U. S. A. 94, 769–772.

Golkowski, M., Lius, A., Sapre, T., Lau, H.-T., Moreno, T., Maly, D.J., Ong, S.-E., 2023.

Multiplexed kinase interactome profiling quantifies cellular network activity and plasticity. Mol. Cell 83, 803-818.e8. https://doi.org/10.1016/j.molcel.2023.01.015

Gonen, N., Meller, A., Sabath, N., Shalgi, R., 2019. Amino Acid Biosynthesis Regulation during Endoplasmic Reticulum Stress Is Coupled to Protein Expression Demands. iScience 19, 204–213. https://doi.org/10.1016/j.isci.2019.07.022

Gonzalo, S., Greentree, W.K., Linder, M.E., 1999. SNAP-25 Is Targeted to the Plasma Membrane through a Novel Membrane-binding Domain*. J. Biol. Chem. 274, 21313–21318. https://doi.org/10.1074/jbc.274.30.21313

Gorenberg, E.L., Chandra, S.S., 2017. The Role of Co-chaperones in Synaptic Proteostasis and Neurodegenerative Disease. Front. Neurosci. 11, 248. https://doi.org/10.3389/fnins.2017.00248

Greaves, J., Gorleku, O.A., Salaun, C., Chamberlain, L.H., 2010. Palmitoylation of the SNAP25 Protein Family. J. Biol. Chem. 285, 24629–24638. https://doi.org/10.1074/jbc.M110.119289

Greene, L.A., Tischler, A.S., 1976. Establishment of a noradrenergic clonal line of rat adrenal pheochromocytoma cells which respond to nerve growth factor. Proc. Natl. Acad. Sci. U. S. A. 73, 2424–2428. https://doi.org/10.1073/pnas.73.7.2424

Greer, P.L., Hanayama, R., Bloodgood, B.L., Mardinly, A.R., Lipton, D.M., Flavell, S.W., Kim, T.-K., Griffith, E.C., Waldon, Z., Maehr, R., Ploegh, H.L., Chowdhury, S., Worley, P.F., Steen, J., Greenberg, M.E., 2010. The Angelman Syndrome Protein Ube3A Regulates Synapse Development by Ubiquitinating Arc. Cell 140, 704–716. https://doi.org/10.1016/j.cell.2010.01.026

Grice, G.L., Lobb, I.T., Weekes, M.P., Gygi, S.P., Antrobus, R., Nathan, J.A., 2015. The Proteasome Distinguishes between Heterotypic and Homotypic Lysine-11-Linked Polyubiquitin Chains. Cell Rep. 12, 545–553. https://doi.org/10.1016/j.celrep.2015.06.061

Grill, B., Bienvenut, W.V., Brown, H.M., Ackley, B.D., Quadroni, M., Jin, Y., 2007. C. elegans RPM-1 Regulates Axon Termination and Synaptogenesis through the Rab GEF GLO-4 and the Rab GTPase GLO-1. Neuron 55, 587–601. https://doi.org/10.1016/j.neuron.2007.07.009

Groll, M., Heinemeyer, W., Jäger, S., Ullrich, T., Bochtler, M., Wolf, D.H., Huber, R., 1999. The catalytic sites of 20S proteasomes and their role in subunit maturation: A mutational and crystallographic study. Proc. Natl. Acad. Sci. 96, 10976–10983. https://doi.org/10.1073/pnas.96.20.10976

Gundersen, C.B., 2020. Cysteine string proteins. Prog. Neurobiol. 188, 101758. https://doi.org/10.1016/j.pneurobio.2020.101758

Gundersen, C.B., Mastrogiacomo, A., Umbach, J.A., 1995. Cysteine-string proteins as templates for membrane fusion: models of synaptic vesicle exocytosis. J. Theor. Biol. 172, 269– 277. https://doi.org/10.1006/jtbi.1995.0023

Bibliography

Gundersen, C.B., Umbach, J.A., 2013. Synaptotagmins 1 and 2 as mediators of rapid exocytosis at nerve terminals: The dyad hypothesis. J. Theor. Biol. 332, 149–160. https://doi.org/10.1016/j.jtbi.2013.04.029

Guo, N., Peng, Z., 2013. MG132, a proteasome inhibitor, induces apoptosis in tumor cells. Asia Pac. J. Clin. Oncol. 9, 6–11. https://doi.org/10.1111/j.1743-7563.2012.01535.x

Haas, K.F., Broadie, K., 2008. Roles of ubiquitination at the synapse. Biochim. Biophys. Acta 1779, 495–506. https://doi.org/10.1016/j.bbagrm.2007.12.010

Hagai, T., Levy, Y., 2010. Ubiquitin not only serves as a tag but also assists degradation by inducing protein unfolding. Proc. Natl. Acad. Sci. U. S. A. 107, 2001–2006. https://doi.org/10.1073/pnas.0912335107

Haglund, K., Dikic, I., 2005. Ubiquitylation and cell signaling. EMBO J. 24, 3353–3359. https://doi.org/10.1038/sj.emboj.7600808

Hall, B., Cho, A., Limaye, A., Cho, K., Khillan, J., Kulkarni, A.B., 2018. Genome Editing in Mice Using CRISPR/Cas9 Technology. Curr. Protoc. Cell Biol. 81, e57. https://doi.org/10.1002/cpcb.57

Han, S., Jeong, Y.Y., Sheshadri, P., Su, X., Cai, Q., 2020. Mitophagy regulates integrity of mitochondria at synapses and is critical for synaptic maintenance. EMBO Rep. 21, e49801. https://doi.org/10.15252/embr.201949801

Harris, R., Yang, M., Schmidt, C., Royet, C., Singh, S., Natarajan, A., Morris, M., Frezza, C., Laman, H., 2022. Fbxo7 promotes Cdk6 activity to inhibit PFKP and glycolysis in T cells. J. Cell Biol. 221, e202203095. https://doi.org/10.1083/jcb.202203095

Hart, T., Chandrashekhar, M., Aregger, M., Steinhart, Z., Brown, K.R., MacLeod, G., Mis, M., Zimmermann, M., Fradet-Turcotte, A., Sun, S., Mero, P., Dirks, P., Sidhu, S., Roth, F.P., Rissland, O.S., Durocher, D., Angers, S., Moffat, J., 2015. High-Resolution CRISPR Screens Reveal Fitness Genes and Genotype-Specific Cancer Liabilities. Cell 163, 1515–1526. https://doi.org/10.1016/j.cell.2015.11.015

Hartman, D.S., McCormack, M., Schubenel, R., Hertel, C., 1992. Multiple trkA proteins in PC12 cells bind NGF with a slow association rate. J. Biol. Chem. 267, 24516–24522. https://doi.org/10.1016/S0021-9258(18)35795-8

Hatakeyama, S., 2017. TRIM Family Proteins: Roles in Autophagy, Immunity, and Carcinogenesis. Trends Biochem. Sci. 42, 297–311. https://doi.org/10.1016/j.tibs.2017.01.002

Hatakeyama, S., Nakayama, K.I., 2003. U-box proteins as a new family of ubiquitin ligases. Biochem. Biophys. Res. Commun. 302, 635–645. https://doi.org/10.1016/s0006291x(03)00245-6

Havugimana, P.C., Goel, R.K., Phanse, S., Youssef, A., Padhorny, D., Kotelnikov, S., Kozakov, D., Emili, A., 2022. Scalable multiplex co-fractionation/mass spectrometry platform for accelerated protein interactome discovery. Nat. Commun. 13, 4043. https://doi.org/10.1038/s41467-022-31809-z

Heard, D.S., Tuttle, C.S.L., Lautenschlager, N.T., Maier, A.B., 2018. Repurposing ProteostasisModifying Drugs to Prevent or Treat Age-Related Dementia: A Systematic Review. Front. Physiol.

9, 1520. https://doi.org/10.3389/fphys.2018.01520

Hegele, A., Kamburov, A., Grossmann, A., Sourlis, C., Wowro, S., Weimann, M., Will, C.L., Pena, V., Lührmann, R., Stelzl, U., 2012. Dynamic protein-protein interaction wiring of the human spliceosome. Mol. Cell 45, 567–580. https://doi.org/10.1016/j.molcel.2011.12.034

Hein, M.Y., Hubner, N.C., Poser, I., Cox, J., Nagaraj, N., Toyoda, Y., Gak, I.A., Weisswange, I., Mansfeld, J., Buchholz, F., Hyman, A.A., Mann, M., 2015. A human interactome in three quantitative dimensions organized by stoichiometries and abundances. Cell 163, 712–723. https://doi.org/10.1016/j.cell.2015.09.053

Helin, K., 1998. Regulation of cell proliferation by the E2F transcription factors. Curr. Opin. Genet. Dev. 8, 28–35. https://doi.org/10.1016/s0959-437x(98)80058-0

Heuser, J.E., Reese, T.S., 1973. EVIDENCE FOR RECYCLING OF SYNAPTIC VESICLE MEMBRANE DURING TRANSMITTER RELEASE AT THE FROG NEUROMUSCULAR JUNCTION. J. Cell Biol. 57, 315–344. https://doi.org/10.1083/jcb.57.2.315

Hicke, L., 2001. Protein regulation by monoubiquitin. Nat. Rev. Mol. Cell Biol. 2, 195–201. https://doi.org/10.1038/35056583

Hisata, S., Sakisaka, T., Baba, T., Yamada, T., Aoki, K., Matsuda, M., Takai, Y., 2007. Rap1-PDZGEF1 interacts with a neurotrophin receptor at late endosomes, leading to sustained activation of Rap1 and ERK and neurite outgrowth. J. Cell Biol. 178, 843–860. https://doi.org/10.1083/jcb.200610073

Holderith, N., Lorincz, A., Katona, G., Rózsa, B., Kulik, A., Watanabe, M., Nusser, Z., 2012. Release probability of hippocampal glutamatergic terminals scales with the size of the active zone. Nat. Neurosci. 15, 988–997. https://doi.org/10.1038/nn.3137

Holt, M., Varoqueaux, F., Wiederhold, K., Takamori, S., Urlaub, H., Fasshauer, D., Jahn, R., 2006. Identification of SNAP-47, a Novel Qbc-SNARE with Ubiquitous Expression. J. Biol. Chem. 281, 17076–17083. https://doi.org/10.1074/jbc.M513838200

Hornbeck, P.V., Kornhauser, J.M., Tkachev, S., Zhang, B., Skrzypek, E., Murray, B., Latham, V., Sullivan, M., 2012. PhosphoSitePlus: a comprehensive resource for investigating the structure and function of experimentally determined post-translational modifications in man and mouse. Nucleic Acids Res. 40, D261–D270. https://doi.org/10.1093/nar/gkr1122

Hsu, J.-M., Lee, Y.-C.G., Yu, C.-T.R., Huang, C.-Y.F., 2004. Fbx7 Functions in the SCF Complex Regulating Cdk1-Cyclin B-phosphorylated Hepatoma Up-regulated Protein (HURP) Proteolysis by a Proline-rich Region *. J. Biol. Chem. 279, 32592–32602. https://doi.org/10.1074/jbc.M404950200

Hu, C., Ahmed, M., Melia, T.J., Söllner, T.H., Mayer, T., Rothman, J.E., 2003. Fusion of Cells by Flipped SNAREs. Science 300, 1745–1749. https://doi.org/10.1126/science.1084909

Hu, X., Pickering, E.H., Hall, S.K., Naik, S., Liu, Y.C., Soares, H., Katz, E., Paciga, S.A., Liu, W., Aisen, P.S., Bales, K.R., Samad, T.A., John, S.L., 2011. Genome-wide association study identifies multiple novel loci associated with disease progression in subjects with mild cognitive impairment. Transl. Psychiatry 1, e54–e54. https://doi.org/10.1038/tp.2011.50

Bibliography

Hunter, T., 2007. The Age of Crosstalk: Phosphorylation, Ubiquitination, and Beyond. Mol. Cell 28, 730–738. https://doi.org/10.1016/j.molcel.2007.11.019

Hussain, S., Ringsevjen, H., Schupp, M., Hvalby, Ø., Sørensen, J.B., Jensen, V., Davanger, S., 2019. A possible postsynaptic role for SNAP-25 in hippocampal synapses. Brain Struct. Funct. 224, 521–532. https://doi.org/10.1007/s00429-018-1782-2

Hüttenhain, R., Xu, J., Burton, L.A., Gordon, D.E., Hultquist, J.F., Johnson, J.R., Satkamp, L., Hiatt, J., Rhee, D.Y., Baek, K., Crosby, D.C., Frankel, A.D., Marson, A., Harper, J.W., Alpi, A.F., Schulman, B.A., Gross, J.D., Krogan, N.J., 2019. ARIH2 Is a Vif-Dependent Regulator of CUL5Mediated APOBEC3G Degradation in HIV Infection. Cell Host Microbe 26, 86-99.e7. https://doi.org/10.1016/j.chom.2019.05.008

Huttlin, E.L., Bruckner, R.J., Navarrete-Perea, J., Cannon, J.R., Baltier, K., Gebreab, F., Gygi, M.P., Thornock, A., Zarraga, G., Tam, S., Szpyt, J., Gassaway, B.M., Panov, A., Parzen, H., Fu, S., Golbazi, A., Maenpaa, E., Stricker, K., Guha Thakurta, S., Zhang, T., Rad, R., Pan, J., Nusinow, D.P., Paulo, J.A., Schweppe, D.K., Vaites, L.P., Harper, J.W., Gygi, S.P., 2021. Dual proteomescale networks reveal cell-specific remodeling of the human interactome. Cell 184, 30223040.e28. https://doi.org/10.1016/j.cell.2021.04.011

Huttlin, E.L., Ting, L., Bruckner, R.J., Gebreab, F., Gygi, M.P., Szpyt, J., Tam, S., Zarraga, G., Colby, G., Baltier, K., Dong, R., Guarani, V., Vaites, L.P., Ordureau, A., Rad, R., Erickson, B.K., Wühr, M., Chick, J., Zhai, B., Kolippakkam, D., Mintseris, J., Obar, R.A., Harris, T., ArtavanisTsakonas, S., Sowa, M.E., De Camilli, P., Paulo, J.A., Harper, J.W., Gygi, S.P., 2015. The BioPlex Network: A Systematic Exploration of the Human Interactome. Cell 162, 425–440. https://doi.org/10.1016/j.cell.2015.06.043

Igarashi, M., Kozaki, S., Terakawa, S., Kawano, S., Ide, C., Komiya, Y., 1996. Growth cone collapse and inhibition of neurite growth by Botulinum neurotoxin C1: a t-SNARE is involved in axonal growth. J. Cell Biol. 134, 205–215. https://doi.org/10.1083/jcb.134.1.205

Iguchi, M., Kujuro, Y., Okatsu, K., Koyano, F., Kosako, H., Kimura, M., Suzuki, N., Uchiyama, S., Tanaka, K., Matsuda, N., 2013. Parkin-catalyzed Ubiquitin-Ester Transfer Is Triggered by PINK1dependent Phosphorylation. J. Biol. Chem. 288, 22019–22032. https://doi.org/10.1074/jbc.M113.467530

Imai, Y., Soda, M., Hatakeyama, S., Akagi, T., Hashikawa, T., Nakayama, K.-I., Takahashi, R., 2002. CHIP Is Associated with Parkin, a Gene Responsible for Familial Parkinson's Disease, and Enhances Its Ubiquitin Ligase Activity. Mol. Cell 10, 55–67. https://doi.org/10.1016/S10972765(02)00583-X

Iorio, R., Celenza, G., Petricca, S., 2021. Mitophagy: Molecular Mechanisms, New Concepts on Parkin Activation and the Emerging Role of AMPK/ULK1 Axis. Cells 11, 30. https://doi.org/10.3390/cells11010030

Ishikawa, K., Nash, S.R., Nishimune, A., Neki, A., Kaneko, S., Nakanishi, S., 1999. Competitive interaction of Seven in absentia homolog-1A and Ca2+/calmodulin with the cytoplasmic tail of group 1 metabotropic glutamate receptors. Genes Cells 4, 381–390. https://doi.org/10.1046/j.1365-2443.1999.00269.x

Ito, T., Young, M.J., Li, R., Jain, S., Wernitznig, A., Krill-Burger, J.M., Lemke, C.T., Monducci, D., Rodriguez, D.J., Chang, L., Dutta, S., Pal, D., Paolella, B.R., Rothberg, M.V., Root, D.E., Johannessen, C.M., Parida, L., Getz, G., Vazquez, F., Doench, J.G., Zamanighomi, M., Sellers, W.R., 2021. Paralog knockout profiling identifies DUSP4 and DUSP6 as a digenic dependence in MAPK pathway-driven cancers. Nat. Genet. 53, 1664–1672. https://doi.org/10.1038/s41588021-00967-z

Iwasaki, Y., Ishikawa, M., Okada, N., Koizumi, S., 1997. Induction of a distinct morphology and signal transduction in TrkB/PC12 cells by nerve growth factor and brain-derived neurotrophic factor. J. Neurochem. 68, 927–934. https://doi.org/10.1046/j.1471-4159.1997.68030927.x

Jaenicke, R., n.d. Protein Stability and Protein Folding, in: Ciba Foundation Symposium 161 - Protein Conformation. John Wiley & Sons, Ltd, pp. 206–221. https://doi.org/10.1002/9780470514146.ch13

Jagtap, Y.A., Kumar, P., Kinger, S., Dubey, A.R., Choudhary, A., Gutti, R.K., Singh, S., Jha, H.C., Poluri, K.M., Mishra, A., 2023. Disturb mitochondrial associated proteostasis: Neurodegeneration and imperfect ageing. Front. Cell Dev. Biol. 11, 1146564. https://doi.org/10.3389/fcell.2023.1146564

Jahn, R., Cafiso, D.C., Tamm, L.K., 2024. Mechanisms of SNARE proteins in membrane fusion. Nat. Rev. Mol. Cell Biol. 25, 101–118. https://doi.org/10.1038/s41580-023-00668-x

Jasin, M., Rothstein, R., 2013a. Repair of strand breaks by homologous recombination. Cold Spring Harb. Perspect. Biol. 5, a012740. https://doi.org/10.1101/cshperspect.a012740

Jasin, M., Rothstein, R., 2013b. Repair of strand breaks by homologous recombination. Cold Spring Harb. Perspect. Biol. 5, a012740. https://doi.org/10.1101/cshperspect.a012740

Jeon, C.-Y., Jin, J.-K., Koh, Y.-H., Chun, W., Choi, I.-G., Kown, H.-J., Kim, Y.-S., Park, J.-B., 2010a. Neurites from PC12 cells are connected to each other by synapse-like structures. Synap. N. Y. N 64, 765–772. https://doi.org/10.1002/syn.20789

Jeon, C.-Y., Kim, H.-J., Lee, J.-Y., Kim, J., Kim, S.-C., Park, J.-B., 2010b. p190RhoGAP and Rapdependent RhoGAP (ARAP3) inactivate RhoA in response to nerve growth factor leading to neurite outgrowth from PC12 cells. Exp. Mol. Med. 42, 335–344. https://doi.org/10.3858/emm.2010.42.5.035

Jiang, H., Jiang, Q., Feng, J., 2004. Parkin Increases Dopamine Uptake by Enhancing the Cell Surface Expression of Dopamine Transporter*. J. Biol. Chem. 279, 54380–54386. https://doi.org/10.1074/jbc.M409282200

Jiang, Y., Beaudet, A.L., 2004. Human disorders of ubiquitination and proteasomal degradation. Curr. Opin. Pediatr. 16, 419–426. https://doi.org/10.1097/01.mop.0000133634.79661.cd

Jin, S.M., Youle, R.J., 2012. PINK1- and Parkin-mediated mitophagy at a glance. J. Cell Sci. 125, 795–799. https://doi.org/10.1242/jcs.093849

Bibliography

Jinek, M., Chylinski, K., Fonfara, I., Hauer, M., Doudna, J.A., Charpentier, E., 2012. A programmable dual-RNA-guided DNA endonuclease in adaptive bacterial immunity. Science 337, 816–821. https://doi.org/10.1126/science.1225829

Jones, R.B., Gordus, A., Krall, J.A., MacBeath, G., 2006. A quantitative protein interaction network for the ErbB receptors using protein microarrays. Nature 439, 168–174. https://doi.org/10.1038/nature04177

Joshi, V., Amanullah, A., Upadhyay, A., Mishra, R., Kumar, A., Mishra, A., 2016. A Decade of

Boon or Burden: What Has the CHIP Ever Done for Cellular Protein Quality Control Mechanism Implicated in Neurodegeneration and Aging? Front. Mol. Neurosci. 9, 93. https://doi.org/10.3389/fnmol.2016.00093

Jumper, J., Evans, R., Pritzel, A., Green, T., Figurnov, M., Ronneberger, O., Tunyasuvunakool, K.,

Bates, R., Žídek, A., Potapenko, A., Bridgland, A., Meyer, C., Kohl, S.A.A., Ballard, A.J., Cowie,

A., Romera-Paredes, B., Nikolov, S., Jain, R., Adler, J., Back, T., Petersen, S., Reiman, D.,

Clancy, E., Zielinski, M., Steinegger, M., Pacholska, M., Berghammer, T., Bodenstein, S., Silver, D., Vinyals, O., Senior, A.W., Kavukcuoglu, K., Kohli, P., Hassabis, D., 2021. Highly accurate protein structure prediction with AlphaFold. Nature 596, 583–589. https://doi.org/10.1038/s41586-021-03819-2

Junn, E., Jang, W.H., Zhao, X., Jeong, B.S., Mouradian, M.M., 2009. Mitochondrial Localization of DJ-1 Leads to Enhanced Neuroprotection. J. Neurosci. Res. 87, 123. https://doi.org/10.1002/jnr.21831

Kádková, A., Radecke, J., Sørensen, J.B., 2019. The SNAP-25 Protein Family. Neuroscience, SNARE Proteins: A Long Journey of Science in Brain Health and Disease 420, 50–71. https://doi.org/10.1016/j.neuroscience.2018.09.020

Kang, J., Chung, K.C., 2015. The F-box protein FBXO7 positively regulates bone morphogenetic protein-mediated signaling through Lys-63-specific ubiquitination of neurotrophin receptorinteracting MAGE (NRAGE). Cell. Mol. Life Sci. 72, 181–195. https://doi.org/10.1007/s00018014-1665-5

Kang, J.S., Yum, Y.N., Han, E., Kim, J.H., Lee, E.M., Ryu, D.Y., Kim, Y.H., Yang, S.H., Kim, S.H., Park, S.N., 2008. Evaluation of Potential Biomarkers for Thioacetamide-induced Hepatotoxicity using siRNA. Biomol. Ther. 16, 197–202. https://doi.org/10.4062/biomolther.2008.16.3.197

Kang, S.-W., Rane, N.S., Kim, S.J., Garrison, J.L., Taunton, J., Hegde, R.S., 2006. SubstrateSpecific Translocational Attenuation during ER Stress Defines a Pre-Emptive Quality Control Pathway. Cell 127, 999–1013. https://doi.org/10.1016/j.cell.2006.10.032

Kao, S., Jaiswal, R.K., Kolch, W., Landreth, G.E., 2001. Identification of the Mechanisms Regulating the Differential Activation of the MAPK Cascade by Epidermal Growth Factor and Nerve Growth Factor in PC12 Cells*. J. Biol. Chem. 276, 18169–18177. https://doi.org/10.1074/jbc.M008870200

Kapulkin, W.J., Hiester, B.G., Link, C.D., 2005. Compensatory regulation among ER chaperones in C. elegans. FEBS Lett. 579, 3063–3068. https://doi.org/10.1016/j.febslet.2005.04.062 Kawabe, H., Neeb, A., Dimova, K., Young, S.M., Takeda, M., Katsurabayashi, S., Mitkovski, M.,

Kargbo-Hill, S.E., Kauffman, K.J., Krout, M., Richmond, J.E., Melia, T.J., Colón-Ramos, D.A., 2019. Maturation and Clearance of Autophagosomes in Neurons Depends on a Specific Cysteine Protease Isoform, ATG-4.2. Dev. Cell 49, 251-266.e8. https://doi.org/10.1016/j.devcel.2019.02.013

Malakhova, O.A., Zhang, D.-E., Umikawa, M., Kariya, K., Goebbels, S., Nave, K.-A., Rosenmund,

C., Jahn, O., Rhee, J., Brose, N., 2010. Regulation of Rap2A by the Ubiquitin Ligase Nedd4-1 Controls Neurite Development. Neuron 65, 358–372. https://doi.org/10.1016/j.neuron.2010.01.007

Kawabe, H., Stegmüller, J., 2021a. The role of E3 ubiquitin ligases in synapse function in the healthy and diseased brain. Mol. Cell. Neurosci. 112, 103602. https://doi.org/10.1016/j.mcn.2021.103602

Kawabe, H., Stegmüller, J., 2021b. The role of E3 ubiquitin ligases in synapse function in the healthy and diseased brain. Mol. Cell. Neurosci. 112, 103602. https://doi.org/10.1016/j.mcn.2021.103602

Khan, M., Youn, J.-Y., Gingras, A.-C., Subramaniam, R., Desveaux, D., 2018. In planta proximity dependent biotin identification (BioID). Sci. Rep. 8, 9212. https://doi.org/10.1038/s41598-01827500-3

Kido, K., Yamanaka, S., Nakano, S., Motani, K., Shinohara, S., Nozawa, A., Kosako, H., Ito, S., Sawasaki, T., 2020. AirID, a novel proximity biotinylation enzyme, for analysis of protein-protein interactions. eLife 9, e54983. https://doi.org/10.7554/eLife.54983

Killackey, S.A., Philpott, D.J., Girardin, S.E., 2020. Mitophagy pathways in health and disease. J. Cell Biol. 219, e202004029. https://doi.org/10.1083/jcb.202004029

Kim, A.H., Puram, S.V., Bilimoria, P.M., Ikeuchi, Y., Keough, S., Wong, M., Rowitch, D., Bonni, A.,

2009. A Centrosomal Cdc20-APC Pathway Controls Dendrite Morphogenesis in Postmitotic

Neurons. Cell 136, 322–336. https://doi.org/10.1016/j.cell.2008.11.050

Kim, D.I., Birendra, K.C., Zhu, W., Motamedchaboki, K., Doye, V., Roux, K.J., 2014. Probing nuclear pore complex architecture with proximity-dependent biotinylation. Proc. Natl. Acad. Sci. U. S. A. 111, E2453-2461. https://doi.org/10.1073/pnas.1406459111

Kim, D.I., Jensen, S.C., Noble, K.A., Kc, B., Roux, K.H., Motamedchaboki, K., Roux, K.J., 2016. An improved smaller biotin ligase for BioID proximity labeling. Mol. Biol. Cell 27, 1188–1196. https://doi.org/10.1091/mbc.E15-12-0844

Kim, D.I., Roux, K.J., 2016. Filling the void: Proximity-based labeling of proteins in living cells.

Trends Cell Biol. 26, 804–817. https://doi.org/10.1016/j.tcb.2016.09.004

Kim, K., Wi, S., Seo, J.H., Pyo, S., Cho, S.-R., 2021. Reduced Interaction of Aggregated αSynuclein and VAMP2 by Environmental Enrichment Alleviates Hyperactivity and Anxiety in a Model of Parkinson's Disease. Genes 12, 392. https://doi.org/10.3390/genes12030392

Kim, K.-Y., Stevens, M.V., Akter, M.H., Rusk, S.E., Huang, R.J., Cohen, A., Noguchi, A., Springer,

D., Bocharov, A.V., Eggerman, T.L., Suen, D.-F., Youle, R.J., Amar, M., Remaley, A.T., Sack,

M.N., 2011. Parkin is a lipid-responsive regulator of fat uptake in mice and mutant human cells.

J. Clin. Invest. 121, 3701–3712. https://doi.org/10.1172/JCI44736

Kim, M.-S., Kang, K.-K., Cho, Y.-G., 2021. Molecular and Functional Analysis of U-box E3 Ubiquitin Ligase Gene Family in Rice (Oryza sativa). Int. J. Mol. Sci. 22, 12088. https://doi.org/10.3390/ijms222112088

Kim, S.-H., Shin, D.H., Choi, I.-G., Schulze-Gahmen, U., Chen, S., Kim, R., 2003. Structurebased functional inference in structural genomics. J. Struct. Funct. Genomics 4, 129–135. https://doi.org/10.1023/A:1026200610644

Kimura, K., Mizoguchi, A., Ide, C., 2003. Regulation of Growth Cone Extension by SNARE Proteins. J. Histochem. Cytochem. 51, 429–433. https://doi.org/10.1177/002215540305100404

Kirkeby, S., Moe, D., Bøg-Hansen, T.C., van Noorden, C.J., 1993. Biotin carboxylases in mitochondria and the cytosol from skeletal and cardiac muscle as detected by avidin binding. Histochemistry 100, 415–421. https://doi.org/10.1007/BF00267821

Kisselev, A.F., Akopian, T.N., Woo, K.M., Goldberg, A.L., 1999. The Sizes of Peptides Generated from Protein by Mammalian 26 and 20 S Proteasomes: IMPLICATIONS FOR UNDERSTANDING THE DEGRADATIVE MECHANISM AND ANTIGEN PRESENTATION *. J. Biol. Chem. 274, 3363–3371. https://doi.org/10.1074/jbc.274.6.3363

Kitada, T., Asakawa, S., Hattori, N., Matsumine, H., Yamamura, Y., Minoshima, S., Yokochi, M., Mizuno, Y., Shimizu, N., 1998. Mutations in the parkin gene cause autosomal recessive juvenile parkinsonism. Nature 392, 605–608. https://doi.org/10.1038/33416

Klemmensen, M.M., Borrowman, S.H., Pearce, C., Pyles, B., Chandra, B., 2024. Mitochondrial dysfunction in neurodegenerative disorders. Neurotherapeutics 21, e00292. https://doi.org/10.1016/j.neurot.2023.10.002

Konishi, Y., Stegmüller, J., Matsuda, T., Bonni, S., Bonni, A., 2004. Cdh1-APC Controls Axonal Growth and Patterning in the Mammalian Brain. Science 303, 1026–1030. https://doi.org/10.1126/science.1093712

Koopmans, F., van Nierop, P., Andres-Alonso, M., Byrnes, A., Cijsouw, T., Coba, M.P., Cornelisse, L.N., Farrell, R.J., Goldschmidt, H.L., Howrigan, D.P., Hussain, N.K., Imig, C., de Jong, A.P.H., Jung, H., Kohansalnodehi, M., Kramarz, B., Lipstein, N., Lovering, R.C., MacGillavry, H., Mariano, V., Mi, H., Ninov, M., Osumi-Sutherland, D., Pielot, R., Smalla, K.-H., Tang, H., Tashman, K., Toonen, R.F.G., Verpelli, C., Reig-Viader, R., Watanabe, K., van Weering, J., Achsel, T., Ashrafi, G., Asi, N., Brown, T.C., De Camilli, P., Feuermann, M., Foulger, R.E., Gaudet, P., Joglekar, A., Kanellopoulos, A., Malenka, R., Nicoll, R.A., Pulido, C., de Juan-Sanz, J., Sheng, M., Südhof, T.C., Tilgner, H.U., Bagni, C., Bayés, À., Biederer, T., Brose, N., Chua, J.J.E., Dieterich, D.C., Gundelfinger, E.D., Hoogenraad, C., Huganir, R.L., Jahn, R., Kaeser, P.S., Kim, E., Kreutz, M.R., McPherson, P.S., Neale, B.M., O'Connor, V., Posthuma, D., Ryan, T.A., Sala, C., Feng, G., Hyman, S.E., Thomas, P.D., Smit, A.B., Verhage, M., 2019. SynGO: An Evidence-Based, Expert-Curated Knowledge Base for the Synapse. Neuron 103, 217-234.e4. https://doi.org/10.1016/j.neuron.2019.05.002

Koyano, F., Yamano, K., Kosako, H., Tanaka, K., Matsuda, N., 2019. Parkin recruitment to impaired mitochondria for nonselective ubiquitylation is facilitated by MITOL. J. Biol. Chem. 294, 10300–10314. https://doi.org/10.1074/jbc.RA118.006302

Kubo, S., Kitami, T., Noda, S., Shimura, H., Uchiyama, Y., Asakawa, S., Minoshima, S., Shimizu, N., Mizuno, Y., Hattori, N., 2001. Parkin is associated with cellular vesicles. J. Neurochem. 78, 42–54. https://doi.org/10.1046/j.1471-4159.2001.00364.x

Kuiken, H.J., Egan, D.A., Laman, H., Bernards, R., Beijersbergen, R.L., Dirac, A.M., 2012. Identification of F-box only protein 7 as a negative regulator of NF-kappaB signalling. J. Cell. Mol. Med. 16, 2140–2149. https://doi.org/10.1111/j.1582-4934.2012.01524.x

Kulkarni, A., Preeti, K., Tryphena, K.P., Srivastava, S., Singh, S.B., Khatri, D.K., 2023. Proteostasis in Parkinson's disease: Recent development and possible implication in diagnosis and therapeutics. Ageing Res. Rev. 84, 101816. https://doi.org/10.1016/j.arr.2022.101816

Kulkarni, P., Porter, L., Chou, T.-F., Chong, S., Chiti, F., Schafer, J.W., Mohanty, A., Ramisetty, S., Onuchic, J.N., Tuite, M., Uversky, V.N., Weninger, K.R., Koonin, E.V., Orban, J., Salgia, R., 2025. Evolving concepts of the protein universe. iScience 28, 112012. https://doi.org/10.1016/j.isci.2025.112012

Kwak, Y.-D., Wang, B., Li, J.J., Wang, R., Deng, Q., Diao, S., Chen, Y., Xu, R., Masliah, E., Xu, H., Sung, J.-J., Liao, F.-F., 2012. Upregulation of the E3 ligase NEDD4-1 by oxidative stress degrades IGF-1 receptor protein in neurodegeneration. J. Neurosci. Off. J. Soc. Neurosci. 32, 10971– 10981. https://doi.org/10.1523/JNEUROSCI.1836-12.2012

L, F., F, M., Bg, C., N, L., Wj, G., Ea, F., 2002. Parkin and CASK/LIN-2 associate via a PDZmediated interaction and are co-localized in lipid rafts and postsynaptic densities in brain. J. Biol. Chem. 277. https://doi.org/10.1074/jbc.M109806200

Lambrughi, M., Maiani, E., Aykac Fas, B., Shaw, G.S., Kragelund, B.B., Lindorff-Larsen, K., Teilum, K., Invernizzi, G., Papaleo, E., 2021. Ubiquitin Interacting Motifs: Duality Between Structured and Disordered Motifs. Front. Mol. Biosci. 8.

Lam, W.K., Lindblom, R.S.J., Milky, B., Mazzachi, P., Hadian-Jazi, M., Küng, C., Khuu, G., Uoselis, L., Nguyen, T.N., Skulsuppaisarn, M., Saunders, T.L., Schmidt, M.F., Dewson, G., Fogel, A.I., Bardy, C., Lazarou, M., 2024. Presynapses are mitophagy pit stops that prevent axon degeneration. https://doi.org/10.1101/2024.09.09.611943

Lau, C.G., Takayasu, Y., Rodenas-Ruano, A., Paternain, A.V., Lerma, J., Bennett, M.V.L., Zukin, R.S., 2010. SNAP-25 is a target of protein kinase C phosphorylation critical to NMDA receptor trafficking. J. Neurosci. Off. J. Soc. Neurosci. 30, 242–254. https://doi.org/10.1523/JNEUROSCI.4933-08.2010

Lau, C.-H., Tin, C., Suh, Y., 2020. CRISPR-based strategies for targeted transgene knock-in and gene correction. Fac. Rev. 9, 20. https://doi.org/10.12703/r/9-20

Lazarou, M., Narendra, D.P., Jin, S.M., Tekle, E., Banerjee, S., Youle, R.J., 2013a. PINK1 drives Parkin self-association and HECT-like E3 activity upstream of mitochondrial binding. J. Cell Biol. 200, 163–172. https://doi.org/10.1083/jcb.201210111

Lazarou, M., Narendra, D.P., Jin, S.M., Tekle, E., Banerjee, S., Youle, R.J., 2013b. PINK1 drives

Parkin self-association and HECT-like E3 activity upstream of mitochondrial binding. J. Cell Biol. 200, 163–172. https://doi.org/10.1083/jcb.201210111

Leal, C.P., Borjini, N., Guzmán, E.G., Clemente, P.G.-J., Chacón, R.F., 2023. THE CO-CHAPERONE CSPA/DNAJC5 PREVENTS PRESYNAPTIC DEGENERATION IN PURKINJE CELLS BY A CELL-AUTONOMOUS MECHANISM. IBRO Neurosci. Rep. 15, S216–S217. https://doi.org/10.1016/j.ibneur.2023.08.347

Lebedeva, O., Poberezhniy, D., Novosadova, E., Gerasimova, T., Novosadova, L., Arsenyeva, E., Stepanenko, E., Shimchenko, D., Volovikov, E., Anufrieva, K., Illarioshkin, S., Lagarkova, M., Grivennikov, I., Tarantul, V., Nenasheva, V., 2023. Overexpression of Parkin in the Neuronal Progenitor Cells from a Patient with Parkinson's Disease Shifts the Transcriptome Towards the Normal State. Mol. Neurobiol. 60, 3522–3533. https://doi.org/10.1007/s12035-023-03293-z

Lecker, S.H., Goldberg, A.L., Mitch, W.E., 2006. Protein Degradation by the Ubiquitin– Proteasome Pathway in Normal and Disease States. J. Am. Soc. Nephrol. 17, 1807–1819. https://doi.org/10.1681/ASN.2006010083

Lee, D.H., Goldberg, A.L., 1998. Proteasome inhibitors: valuable new tools for cell biologists. Trends Cell Biol. 8, 397–403. https://doi.org/10.1016/s0962-8924(98)01346-4

Lee, J.A.K., Granger, S., Roome, K., Allen, S.P., Ferraiuolo, L., Shaw, P.J., Mortiboys, H., 2025. C9orf72-ALS mutation drives mitophagy impairments in iNeurons. https://doi.org/10.1101/2025.02.28.640849

Lee, J., Xu, Y., Saidi, L., Xu, M., Zinsmaier, K., Ye, Y., 2023. Abnormal triaging of misfolded proteins by adult neuronal ceroid lipofuscinosis-associated DNAJC5/CSPα mutants causes lipofuscin accumulation. Autophagy 19, 204–223. https://doi.org/10.1080/15548627.2022.2065618

Lee, J., Xu, Y., Ye, Y., 2022. Safeguarding Lysosomal Homeostasis by DNAJC5/CSPα-Mediated Unconventional Protein Secretion and Endosomal Microautophagy. Front. Cell Dev. Biol. 10. https://doi.org/10.3389/fcell.2022.906453

Lee, J.H., Ahn, H.H., Kim, K.S., Lee, J.Y., Kim, M.S., Lee, B., Khang, G., Lee, H.B., 2008. Polyethyleneimine-mediated gene delivery into rat pheochromocytoma PC-12 cells. J. Tissue Eng. Regen. Med. 2, 288–295. https://doi.org/10.1002/term.94

Leveque, C., Pupier, S., Marqueze, B., Geslin, L., Kataoka, M., Takahashi, M., Waard, M.D., Seagar, M., 1998. Interaction of Cysteine String Proteins with the α1A Subunit of the P/Q-type Calcium Channel *. J. Biol. Chem. 273, 13488–13492. https://doi.org/10.1074/jbc.273.22.13488

Li, H., Kulkarni, G., Wadsworth, W.G., 2008. RPM-1, a Caenorhabditis elegans Protein That Functions in Presynaptic Differentiation, Negatively Regulates Axon Outgrowth by Controlling SAX-3/robo and UNC-5/UNC5 Activity. J. Neurosci. 28, 3595–3603. https://doi.org/10.1523/JNEUROSCI.5536-07.2008

Li, W., Bengtson, M.H., Ulbrich, A., Matsuda, A., Reddy, V.A., Orth, A., Chanda, S.K., Batalov, S.,

Joazeiro, C.A.P., 2008. Genome-wide and functional annotation of human E3 ubiquitin ligases identifies MULAN, a mitochondrial E3 that regulates the organelle's dynamics and signaling. PloS One 3, e1487. https://doi.org/10.1371/journal.pone.0001487

Li, W., Yao, A., Zhi, H., Kaur, K., Zhu, Y., Jia, M., Zhao, H., Wang, Q., Jin, S., Zhao, G., Xiong, Z.-Q.,

Zhang, Y.Q., 2016. Angelman Syndrome Protein Ube3a Regulates Synaptic Growth and Endocytosis by Inhibiting BMP Signaling in Drosophila. PLoS Genet. 12, e1006062. https://doi.org/10.1371/journal.pgen.1006062

Li, W., Ye, Y., 2008. Polyubiquitin chains: functions, structures, and mechanisms. Cell. Mol. Life Sci. CMLS 65, 2397–2406. https://doi.org/10.1007/s00018-008-8090-6

Li, Yankun, Chin, L.-S., Weigel, C., Li, L., 2001. Spring, a Novel RING Finger Protein That Regulates Synaptic Vesicle Exocytosis *. J. Biol. Chem. 276, 40824–40833. https://doi.org/10.1074/jbc.M106141200

Li, Y., Chin, L.S., Weigel, C., Li, L., 2001. Spring, a novel RING finger protein that regulates synaptic vesicle exocytosis. J. Biol. Chem. 276, 40824–40833. https://doi.org/10.1074/jbc.M106141200

Li, Y., Xie, P., Lu, L., Wang, J., Diao, L., Liu, Z., Guo, F., He, Y., Liu, Y., Huang, Q., Liang, H., Li, D., He, F., 2017. An integrated bioinformatics platform for investigating the human E3 ubiquitin ligase-substrate interaction network. Nat. Commun. 8, 347. https://doi.org/10.1038/s41467017-00299-9

Liberek, K., Lewandowska, A., Ziętkiewicz, S., 2008. Chaperones in control of protein disaggregation. EMBO J. 27, 328–335. https://doi.org/10.1038/sj.emboj.7601970

Liu, C., Zhang, L., Liu, H., Cheng, K., 2017. Delivery Strategies of the CRISPR-Cas9 Gene-Editing

System for Therapeutic Applications. J. Control. Release Off. J. Control. Release Soc. 266, 17–

26. https://doi.org/10.1016/j.jconrel.2017.09.012

Liu, J., Lamb, D., Chou, M.M., Liu, Y.-J., Li, G., 2007. Nerve Growth Factor-mediated Neurite Outgrowth via Regulation of Rab5. Mol. Biol. Cell 18, 1375–1384. https://doi.org/10.1091/mbc.E06-08-0725

Liu, J., Liu, W., Li, R., Yang, H., 2019. Mitophagy in Parkinson's Disease: From Pathogenesis to Treatment. Cells 8, 712. https://doi.org/10.3390/cells8070712

Liu, Q.Y., Lei, J.X., Sikorska, M., Liu, R., 2008. A novel brain-enriched E3 ubiquitin ligase RNF182 is up regulated in the brains of Alzheimer's patients and targets ATP6V0C for degradation. Mol. Neurodegener. 3, 4. https://doi.org/10.1186/1750-1326-3-4

Liu, Y., Deisenroth, C., Zhang, Y., 2016. RP-MDM2-p53 Pathway: Linking Ribosomal Biogenesis and Tumor Surveillance. Trends Cancer 2, 191–204. https://doi.org/10.1016/j.trecan.2016.03.002

Loch, C.M., Eddins, M.J., Strickler, J.E., 2011. Protein Microarrays for the Identification of Praja1 E3 Ubiquitin Ligase Substrates. Cell Biochem. Biophys. 60, 127–135. https://doi.org/10.1007/s12013-011-9180-x

Loeb, D.M., Maragos, J., Martin-Zanca, D., Chao, M.V., Parada, L.F., Greene, L.A., 1991. The trk proto-oncogene rescues NGF responsiveness in mutant NGF-nonresponsive PC12 cell lines. Cell 66, 961–966. https://doi.org/10.1016/0092-8674(91)90441-z

Bibliography

Long, S., Brown, K.M., Sibley, L.D., 2018. CRISPR-mediated Tagging with BirA Allows Proximity Labeling in Toxoplasma gondii. Bio-Protoc. 8, e2768. https://doi.org/10.21769/BioProtoc.2768

López-Begines, S., Borjini, N., Lavado-Roldán, Á., Mesa-Cruz, C., Mavillard, F., Wiersma, V.I., Rubio-Pastor, F., Tumini, E., Paradela-Leal, C., Chiclana-Valcárcel, M.L., Aguado, C., Luján, R., Scheper, W., Nieto-González, J.L., Fernández-Chacón, R., 2025. Neuronal lipofuscinosis caused by Kufs disease/CLN4 DNAJC5 mutations but not by a CSPα/DNAJC5 deficiency. Sci. Adv. 11, eads3393. https://doi.org/10.1126/sciadv.ads3393

Lopez-Ortega, E., Ruiz, R., Tabares, L., 2017. CSPα, a Molecular Co-chaperone Essential for Short and Long-Term Synaptic Maintenance. Front. Neurosci. 11, 39. https://doi.org/10.3389/fnins.2017.00039

Lo Surdo, P., Iannuccelli, M., Contino, S., Castagnoli, L., Licata, L., Cesareni, G., Perfetto, L., 2023. SIGNOR 3.0, the SIGnaling network open resource 3.0: 2022 update. Nucleic Acids Res. 51, D631–D637. https://doi.org/10.1093/nar/gkac883

Lu, B., Guo, S., 2020. Mechanisms Linking Mitochondrial Dysfunction and Proteostasis Failure. Trends Cell Biol. 30, 317–328. https://doi.org/10.1016/j.tcb.2020.01.008

Mabbitt, P.D., Loreto, A., Déry, M.-A., Fletcher, A.J., Stanley, M., Pao, K.-C., Wood, N.T., Coleman, M.P., Virdee, S., 2020. Structural basis for RING-Cys-Relay E3 Ligase Activity and its Role in Axon Integrity. Nat. Chem. Biol. 16, 1227–1236. https://doi.org/10.1038/s41589-0200598-6

Magga, J.M., Jarvis, S.E., Arnot, M.I., Zamponi, G.W., Braun, J.E., 2000. Cysteine string protein regulates G protein modulation of N-type calcium channels. Neuron 28, 195–204. https://doi.org/10.1016/s0896-6273(00)00096-9

Maillet, S., Fernandez, J., Decourcelle, M., El Koulali, K., Blanchet, F.P., Arhel, N.J., Maarifi, G., Nisole, S., 2020. Daxx Inhibits HIV-1 Reverse Transcription and Uncoating in a SUMO-Dependent Manner. Viruses 12, 636. https://doi.org/10.3390/v12060636

Mamun, M.M.A., Khan, M.R., Zhu, Y., Zhang, Y., Zhou, S., Xu, R., Bukhari, I., Thorne, R.F., Li, J., Zhang, X.D., Liu, G., Chen, S., Wu, M., Song, X., 2022. Stub1 maintains proteostasis of master transcription factors in embryonic stem cells. Cell Rep. 39, 110919. https://doi.org/10.1016/j.celrep.2022.110919

Marshall, R.S., Vierstra, R.D., 2019. Dynamic Regulation of the 26S Proteasome: From Synthesis to Degradation. Front. Mol. Biosci. 6.

Martinez, A., Lectez, B., Ramirez, J., Popp, O., Sutherland, J.D., Urbé, S., Dittmar, G., Clague, M.J., Mayor, U., 2017. Quantitative proteomic analysis of Parkin substrates in Drosophila neurons. Mol. Neurodegener. 12, 29. https://doi.org/10.1186/s13024-017-0170-3

Martínez-Noël, G., Luck, K., Kühnle, S., Desbuleux, A., Szajner, P., Galligan, J.T., Rodriguez, D., Zheng, L., Boyland, K., Leclere, F., Zhong, Q., Hill, D.E., Vidal, M., Howley, P.M., 2018. Network analysis of UBE3A/E6AP-associated proteins provides connections to several distinct cellular processes. J. Mol. Biol. 430, 1024–1050. https://doi.org/10.1016/j.jmb.2018.01.021

Martin-Moutot, N., Charvin, N., Leveque, C., Sato, K., Nishiki, T., Kozaki, S., Takahashi, M., Seagar, M., 1996. Interaction of SNARE Complexes with P/Q-type Calcium Channels in Rat Cerebellar Synaptosomes (∗). J. Biol. Chem. 271, 6567–6570. https://doi.org/10.1074/jbc.271.12.6567

Massé, T., Kelly, P.T., 1997. Overexpression of Ca2+/Calmodulin-Dependent Protein Kinase II in PC12 Cells Alters Cell Growth, Morphology, and Nerve Growth Factor-Induced Differentiation. J. Neurosci. 17, 924–931. https://doi.org/10.1523/JNEUROSCI.17-03-00924.1997

Mayer, M.P., Bukau, B., 2005. Hsp70 chaperones: Cellular functions and molecular mechanism. Cell. Mol. Life Sci. 62, 670–684. https://doi.org/10.1007/s00018-004-4464-6 Mechold, U., Gilbert, C., Ogryzko, V., 2005. Codon optimization of the BirA enzyme gene leads to higher expression and an improved efficiency of biotinylation of target proteins in mammalian cells. J. Biotechnol. 116, 245–249. https://doi.org/10.1016/j.jbiotec.2004.12.003

Mei Zhu, , Giuseppe P. Cortese and Clarissa L. Waites, 2018. Parkinson's disease-linked Parkin mutations impair glutamatergic signaling in hippocampal neurons. BMC Biol.

Menon, S., Boyer, N.P., Winkle, C.C., McClain, L.M., Hanlin, C.C., Pandey, D., Rothenfußer, S.,

Taylor, A.M., Gupton, S.L., 2015. The E3 Ubiquitin Ligase TRIM9 Is a Filopodia Off Switch Required for Netrin-Dependent Axon Guidance. Dev. Cell 35, 698–712. https://doi.org/10.1016/j.devcel.2015.11.022

Menon, S., Goldfarb, D., Ho, C.T., Cloer, E.W., Boyer, N.P., Hardie, C., Bock, A.J., Johnson, E.C., Anil, J., Major, M.B., Gupton, S.L., 2021. The TRIM9/TRIM67 neuronal interactome reveals novel activators of morphogenesis. Mol. Biol. Cell 32, 314–330. https://doi.org/10.1091/mbc.E20-100622

Mary, A., Eysert, F., Checler, F., Chami, M., 2023. Mitophagy in Alzheimer's disease: Molecular defects and therapeutic approaches. Mol. Psychiatry 28, 202–216. https://doi.org/10.1038/s41380-022-01631-6

Massaad, C.A., Klann, E., 2011. Reactive Oxygen Species in the Regulation of Synaptic Plasticity and Memory. Antioxid. Redox Signal. 14, 2013–2054. https://doi.org/10.1089/ars.2010.3208

Metzger, M.B., Pruneda, J.N., Klevit, R.E., Weissman, A.M., 2014. RING-type E3 ligases: Master manipulators of E2 ubiquitin-conjugating enzymes and ubiquitination. Biochim. Biophys. Acta 1843, 47–60. https://doi.org/10.1016/j.bbamcr.2013.05.026

Milone, M.C., O'Doherty, U., 2018. Clinical use of lentiviral vectors. Leukemia 32, 1529–1541. https://doi.org/10.1038/s41375-018-0106-0

Minichiello, L., Casagranda, F., Tatche, R.S., Stucky, C.L., Postigo, A., Lewin, G.R., Davies, A.M., Klein, R., 1998. Point Mutation in *trkB* Causes Loss of NT4-Dependent Neurons without Major Effects on Diverse BDNF Responses. Neuron 21, 335–345. https://doi.org/10.1016/S08966273(00)80543-7

Mohamed, M.S., Klann, E., 2023. Autism- and epilepsy-associated EEF1A2 mutations lead to translational dysfunction and altered actin bundling. Proc. Natl. Acad. Sci. 120, e2307704120. https://doi.org/10.1073/pnas.2307704120

Mohrmann, R., de Wit, H., Verhage, M., Neher, E., Sørensen, J.B., 2010. Fast Vesicle Fusion in Living Cells Requires at Least Three SNARE Complexes. Science 330, 502–505. https://doi.org/10.1126/science.1193134

Moises, T., Wüller, S., Saxena, S., Senderek, J., Weis, J., Krüttgen, A., 2009. Proteasomal inhibition alters the trafficking of the neurotrophin receptor TrkA. Biochem. Biophys. Res. Commun. 387, 360–364. https://doi.org/10.1016/j.bbrc.2009.07.032

Moore, D.J., West, A.B., Dikeman, D.A., Dawson, V.L., Dawson, T.M., 2008. Parkin mediates the degradation-independent ubiquitination of Hsp70. J. Neurochem. 105, 1806–1819. https://doi.org/10.1111/j.1471-4159.2008.05261.x

Morandell, J., Schwarz, L.A., Basilico, B., Tasciyan, S., Dimchev, G., Nicolas, A., Sommer, C.,

Kreuzinger, C., Dotter, C.P., Knaus, L.S., Dobler, Z., Cacci, E., Schur, F.K.M., Danzl, J.G., Novarino, G., 2021. Cul3 regulates cytoskeleton protein homeostasis and cell migration during a critical window of brain development. Nat. Commun. 12, 3058. https://doi.org/10.1038/s41467-021-23123-x

Morihara, T., Mizoguchi, A., Takahashi, M., Kozaki, S., Tsujihara, T., Kawano, S., Shirasu, M., Ohmukai, T., Kitada, M., Kimura, K., Okajima, S., Tamai, K., Hirasawa, Y., Ide, C., 1999. Distribution of synaptosomal-associated protein 25 in nerve growth cones and reduction of neurite outgrowth by botulinum neurotoxin A without altering growth cone morphology in dorsal root ganglion neurons and PC-12 cells. Neuroscience 91, 695–706. https://doi.org/10.1016/s0306-4522(98)00671-x

Mou, H., Smith, J.L., Peng, L., Yin, H., Moore, J., Zhang, X.-O., Song, C.-Q., Sheel, A., Wu, Q.,

Ozata, D.M., Li, Y., Anderson, D.G., Emerson, C.P., Sontheimer, E.J., Moore, M.J., Weng, Z., Xue, W., 2017. CRISPR/Cas9-mediated genome editing induces exon skipping by alternative splicing or exon deletion. Genome Biol. 18, 108. https://doi.org/10.1186/s13059-017-1237-8

Mouatt-Prigent, A., Muriel, M.-P., Gu, W.-J., El Hachimi, K.H., Lücking, C.B., Brice, A., Hirsch, E.C., 2004. Ultrastructural localization of parkin in the rat brainstem, thalamus and basal ganglia. J. Neural Transm. Vienna Austria 1996 111, 1209–1218. https://doi.org/10.1007/s00702-004-0144-9

Mouri, A., Sasaki, A., Watanabe, K., Sogawa, C., Kitayama, S., Mamiya, T., Miyamoto, Y., Yamada, K., Noda, Y., Nabeshima, T., 2012. MAGE-D1 Regulates Expression of Depression-Like Behavior through Serotonin Transporter Ubiquitylation. J. Neurosci. 32, 4562–4580. https://doi.org/10.1523/JNEUROSCI.6458-11.2012

Moxin Wu, Manqing Zhang, Xiaoping Yin, Kai Chen, Zhijian Hu, Qin Zhou, Xianming Cao, Zhiying Chen,and Dan Liu, 2021. The role of pathological tau in synaptic dysfunction in Alzheimer's diseases - PMC. Transl Neurodegener. https://doi.org/10.1186/s40035-021-00270-1

Mulcahy, B., Ibbett, P., Holden-Dye, L., O'Connor, V., 2019. The Caenorhabditis elegans cysteine-string protein homologue DNJ-14 is dispensable for neuromuscular junction maintenance across ageing. J. Exp. Biol. 222, jeb205450. https://doi.org/10.1242/jeb.205450

Müller-Rischart, A.K., Pilsl, A., Beaudette, P., Patra, M., Hadian, K., Funke, M., Peis, R., Deinlein,

A., Schweimer, C., Kuhn, P.-H., Lichtenthaler, S.F., Motori, E., Hrelia, S., Wurst, W., Trümbach, D., Langer, T., Krappmann, D., Dittmar, G., Tatzelt, J., Winklhofer, K.F., 2013. The E3 ligase parkin maintains mitochondrial integrity by increasing linear ubiquitination of NEMO. Mol. Cell 49, 908–921. https://doi.org/10.1016/j.molcel.2013.01.036

Münster-Wandowski, A., Heilmann, H., Bolduan, F., Trimbuch, T., Yanagawa, Y., Vida, I., 2017. Distinct Localization of SNAP47 Protein in GABAergic and Glutamatergic Neurons in the Mouse and the Rat Hippocampus. Front. Neuroanat. 11, 56. https://doi.org/10.3389/fnana.2017.00056

Musatov, S., Roberts, J., Brooks, A.I., Pena, J., Betchen, S., Pfaff, D.W., Kaplitt, M.G., 2004.

Inhibition of neuronal phenotype by PTEN in PC12 cells. Proc. Natl. Acad. Sci. U. S. A. 101, 3627–3631. https://doi.org/10.1073/pnas.0308289101

MyGene.info | Gene Annotation as a Service. [WWW Document], n.d. . MyGene.info. URL http://MyGene.info/ (accessed 5.28.25).

Nadel, C.M., Thwin, A.C., Callahan, M., Lee, K., Connelly, E., Craik, C.S., Southworth, D.R., Gestwicki, J.E., 2023. The E3 Ubiquitin Ligase, CHIP/STUB1, Inhibits Aggregation of Phosphorylated Proteoforms of Microtubule-associated Protein Tau (MAPT). J. Mol. Biol. 435, 168026. https://doi.org/10.1016/j.jmb.2023.168026

Nakata, K., Abrams, B., Grill, B., Goncharov, A., Huang, X., Chisholm, A.D., Jin, Y., 2005. Regulation of a DLK-1 and p38 MAP kinase pathway by the ubiquitin ligase RPM-1 is required for presynaptic development. Cell 120, 407–420. https://doi.org/10.1016/j.cell.2004.12.017

Narendra, D., Tanaka, A., Suen, D.-F., Youle, R.J., 2008. Parkin is recruited selectively to impaired mitochondria and promotes their autophagy. J. Cell Biol. 183, 795–803. https://doi.org/10.1083/jcb.200809125

Narendra, D.P., Youle, R.J., 2024. The role of PINK1–Parkin in mitochondrial quality control. Nat. Cell Biol. 26, 1639–1651. https://doi.org/10.1038/s41556-024-01513-9

Naro, C., Bielli, P., Pagliarini, V., Sette, C., 2015. The interplay between DNA damage response and RNA processing: the unexpected role of splicing factors as gatekeepers of genome stability. Front. Genet. 6, 142. https://doi.org/10.3389/fgene.2015.00142

Natochin, M., Campbell, T.N., Barren, B., Miller, L.C., Hameed, S., Artemyev, N.O., Braun, J.E.A., 2005. Characterization of the G alpha(s) regulator cysteine string protein. J. Biol. Chem. 280, 30236–30241. https://doi.org/10.1074/jbc.M500722200

Negrini, S., D'Alessandro, R., Meldolesi, J., 2013. NGF signaling in PC12 cells: the cooperation of p75NTR with TrkA is needed for the activation of both mTORC2 and the PI3K signalling cascade. Biol. Open 2, 855–866. https://doi.org/10.1242/bio.20135116

Nelson, D.E., Randle, S.J., Laman, H., 2013. Beyond ubiquitination: the atypical functions of Fbxo7 and other F-box proteins. Open Biol. 3, 130131. https://doi.org/10.1098/rsob.130131

Nguyen, H.C., Wang, W., Xiong, Y., 2017. Cullin-RING E3 Ubiquitin Ligases: Bridges to Destruction. Subcell. Biochem. 83, 323–347. https://doi.org/10.1007/978-3-319-46503-6_12

Nieto-González, J.L., Gómez-Sánchez, L., Mavillard, F., Linares-Clemente, P., Rivero, M.C., Valenzuela-Villatoro, M., Muñoz-Bravo, J.L., Pardal, R., Fernández-Chacón, R., 2019. Loss of postnatal quiescence of neural stem cells through mTOR activation upon genetic removal of cysteine string protein-α. Proc. Natl. Acad. Sci. 116, 8000–8009. https://doi.org/10.1073/pnas.1817183116

O'Connor, H.F., Huibregtse, J.M., 2017. Enzyme-Substrate Relationships in the Ubiquitin System: Approaches for Identifying Substrates of Ubiquitin Ligases. Cell. Mol. Life Sci. CMLS

74, 3363–3375. https://doi.org/10.1007/s00018-017-2529-6

Oh, E., Mark, K.G., Mocciaro, A., Watson, E.R., Prabu, J.R., Cha, D.D., Kampmann, M., Gamarra, N., Zhou, C.Y., Rape, M., 2020. Gene expression and cell identity controlled by anaphasepromoting complex. Nature 579, 136–140. https://doi.org/10.1038/s41586-020-2034-1

Ohi, M.D., Vander Kooi, C.W., Rosenberg, J.A., Chazin, W.J., Gould, K.L., 2003. Structural insights into the U-box, a domain associated with multi-ubiquitination. Nat. Struct. Biol. 10, 250–255. https://doi.org/10.1038/nsb906

Olivero, P., Lozano, C., Sotomayor-Zárate, R., Meza-Concha, N., Arancibia, M., Córdova, C.,

González-Arriagada, W., Ramírez-Barrantes, R., Marchant, I., 2018. Proteostasis and

Mitochondrial Role on Psychiatric and Neurodegenerative Disorders: Current Perspectives.

Neural Plast. 2018, 6798712. https://doi.org/10.1155/2018/6798712

Osen-Sand, A., Catsicas, M., Staple, J.K., Jones, K.A., Ayala, G., Knowles, J., Grenningloh, G., Catsicas, S., 1993. Inhibition of axonal growth by SNAP-25 antisense oligonucleotides in vitro and in vivo. Nature 364, 445–448. https://doi.org/10.1038/364445a0

Osen-Sand, A., Staple, J.K., Naldi, E., Schiavo, G., Rossetto, O., Petitpierre, S., Malgaroli, A., Montecucco, C., Catsicas, S., 1996. Common and distinct fusion proteins in axonal growth and transmitter release. J. Comp. Neurol. 367, 222–234. https://doi.org/10.1002/(SICI)10969861(19960401)367:2<222::AID-CNE5>3.0.CO;2-7

Otto, H., Hanson, P.I., Jahn, R., 1997. Assembly and disassembly of a ternary complex of synaptobrevin, syntaxin, and SNAP-25 in the membrane of synaptic vesicles. Proc. Natl. Acad. Sci. 94, 6197–6201. https://doi.org/10.1073/pnas.94.12.6197

Oughtred, R., Rust, J., Chang, C., Breitkreutz, B., Stark, C., Willems, A., Boucher, L., Leung, G.,

Kolas, N., Zhang, F., Dolma, S., Coulombe-Huntington, J., Chatr-aryamontri, A., Dolinski, K., Tyers, M., 2021. The BioGRID database: A comprehensive biomedical resource of curated protein, genetic, and chemical interactions. Protein Sci. Publ. Protein Soc. 30, 187–200. https://doi.org/10.1002/pro.3978

Ozato, K., Shin, D.-M., Chang, T.-H., Morse, H.C., 2008. TRIM family proteins and their emerging roles in innate immunity. Nat. Rev. Immunol. 8, 849–860. https://doi.org/10.1038/nri2413

Pang, L., Sawada, T., Decker, S.J., Saltiel, A.R., 1995. Inhibition of MAP kinase kinase blocks the differentiation of PC-12 cells induced by nerve growth factor. J. Biol. Chem. 270, 13585–13588. https://doi.org/10.1074/jbc.270.23.13585

Pao, K.-C., Wood, N.T., Knebel, A., Rafie, K., Stanley, M., Mabbitt, P.D., Sundaramoorthy, R.,

Hofmann, K., van Aalten, D.M.F., Virdee, S., 2018. Activity-based E3 ligase profiling uncovers an

E3 ligase with esterification activity. Nature 556, 381–385. https://doi.org/10.1038/s41586-0180026-1

Park, M.H., Lee, H.-J., Lee, H.L., Son, D.J., Ju, J.H., Hyun, B.K., Jung, S.H., Song, J.-K., Lee, D.H.,

Hwang, C.J., Han, S.B., Kim, S., Hong, J.T., 2017. Parkin Knockout Inhibits Neuronal Development via Regulation of Proteasomal Degradation of p21. Theranostics 7, 2033–2045. https://doi.org/10.7150/thno.19824

Patapoutian, A., Reichardt, L.F., 2001. Trk receptors: mediators of neurotrophin action. Curr. Opin. Neurobiol. 11, 272–280. https://doi.org/10.1016/s0959-4388(00)00208-7

PC-12 [WWW Document], n.d. URL https://www.culturecollections.org.uk/nop/product/pc-12 (accessed 6.5.25).

Pereira, S.L., Grossmann, D., Delcambre, S., Hermann, A., Grünewald, A., 2023. Novel insights into Parkin-mediated mitochondrial dysfunction and neuroinflammation in Parkinson's disease. Curr. Opin. Neurobiol. 80, 102720. https://doi.org/10.1016/j.conb.2023.102720

Persaud, A., Alberts, P., Amsen, E.M., Xiong, X., Wasmuth, J., Saadon, Z., Fladd, C., Parkinson, J., Rotin, D., 2009. Comparison of substrate specificity of the ubiquitin ligases Nedd4 and Nedd4-2 using proteome arrays. Mol. Syst. Biol. 5, 333. https://doi.org/10.1038/msb.2009.85

Pfeiffer, C.T., Paulo, J.A., Gygi, S.P., Rockman, H.A., 2022. Proximity labeling for investigating protein-protein interactions. Methods Cell Biol. 169, 237–266. https://doi.org/10.1016/bs.mcb.2021.12.006

Pickart, C.M., 2001. Mechanisms Underlying Ubiquitination. Annu. Rev. Biochem. 70, 503–533. https://doi.org/10.1146/annurev.biochem.70.1.503

Pickart, C.M., Eddins, M.J., 2004. Ubiquitin: structures, functions, mechanisms. Biochim. Biophys. Acta BBA - Mol. Cell Res., The Ubiquitin-Proteasome System 1695, 55–72. https://doi.org/10.1016/j.bbamcr.2004.09.019

Pierce, N.W., Kleiger, G., Shan, S., Deshaies, R.J., 2009. Detection of sequential polyubiquitylation on a millisecond timescale. Nature 462, 615–619. https://doi.org/10.1038/nature08595

Pinto, M.J., Tomé, D., Almeida, R.D., 2021. The Ubiquitinated Axon: Local Control of Axon Development and Function by Ubiquitin. J. Neurosci. 41, 2796–2813. https://doi.org/10.1523/JNEUROSCI.2251-20.2021

Plechanovová, A., Jaffray, E., Tatham, M.H., Naismith, J.H., Hay, R.T., 2012. Structure of a RING E3 ligase and ubiquitin-loaded E2 primed for catalysis. Nature 489, 115–120. https://doi.org/10.1038/nature11376

Pokhrel, S., Devi, S., Gestwicki, J.E., 2025. Chaperone-dependent and chaperone-independent functions of carboxylate clamp tetratricopeptide repeat (CC-TPR) proteins. Trends Biochem. Sci. 50, 121–133. https://doi.org/10.1016/j.tibs.2024.11.004

Potjewyd, F.M., Axtman, A.D., 2021. Exploration of Aberrant E3 Ligases Implicated in Alzheimer's Disease and Development of Chemical Tools to Modulate Their Function. Front. Cell. Neurosci. 15, 768655. https://doi.org/10.3389/fncel.2021.768655

Qi, S., O'Hayre, M., Gutkind, J.S., Hurley, J.H., 2014. Structural and Biochemical Basis for Ubiquitin Ligase Recruitment by Arrestin-related Domain-containing Protein-3 (ARRDC3) *. J. Biol. Chem. 289, 4743–4752. https://doi.org/10.1074/jbc.M113.527473

Bibliography

Qian, H., Zhang, Y., Wu, B., Wu, S., You, S., Zhang, N., Sun, Y., 2020. Structure and Function of HECT E3 Ubiquitin Ligases and their Role in Oxidative Stress. J. Transl. Intern. Med. 8, 71–79. https://doi.org/10.2478/jtim-2020-0012

Qiu, L., Joazeiro, C., Fang, N., Wang, H.-Y., Elly, C., Altman, Y., Fang, D., Hunter, T., Liu, Y.-C.,

2000. Recognition and Ubiquitination of Notch by Itch, a Hect-type E3 Ubiquitin Ligase*. J. Biol. Chem. 275, 35734–35737. https://doi.org/10.1074/jbc.M007300200

Qu, Z., Wolfraim, L.A., Svaren, J., Ehrengruber, M.U., Davidson, N., Milbrandt, J., 1998. The

Transcriptional Corepressor NAB2 Inhibits NGF-induced Differentiation of PC12 Cells. J. Cell

Biol. 142, 1075–1082. https://doi.org/10.1083/jcb.142.4.1075

Qui, M.S., Green, S.H., 1992. PC12 cell neuronal differentiation is associated with prolonged p21ras activity and consequent prolonged ERK activity. Neuron 9, 705–717. https://doi.org/10.1016/0896-6273(92)90033-a

Suryadinata, R., Holien, J., Yang, G., Parker, M., Papalea, E., Šarčević, B., 2013. Molecular and structural insight into lysine selection on substrate and ubiquitin lysine 48 by the ubiquitin-conjugating enzyme Cdc34. Cell Cycle Georget. Tex 12. https://doi.org/10.4161/cc.24818

Radivojac, P., Vacic, V., Haynes, C., Cocklin, R.R., Mohan, A., Heyen, J.W., Goebl, M.G.,

Iakoucheva, L.M., 2010. Identification, Analysis and Prediction of Protein Ubiquitination Sites.

Proteins 78, 365–380. https://doi.org/10.1002/prot.22555

Raisch, J., Dubois, M.-L., Groleau, M., Lévesque, D., Burger, T., Jurkovic, C.-M., Brailly, R.,

Marbach, G., McKenna, A., Barrette, C., Jacques, P.-É., Boisvert, F.-M., 2023. Pulse-SILAC and Interactomics Reveal Distinct DDB1-CUL4-Associated Factors, Cellular Functions, and Protein Substrates. Mol. Cell. Proteomics MCP 22, 100644. https://doi.org/10.1016/j.mcpro.2023.100644

Rajsbaum, R., García-Sastre, A., Versteeg, G.A., 2014. TRIMmunity: The roles of the TRIM E3ubiquitin ligase family in innate antiviral immunity. J. Mol. Biol. 426, 1265–1284. https://doi.org/10.1016/j.jmb.2013.12.005

Ran, F.A., Hsu, P.D., Wright, J., Agarwala, V., Scott, D.A., Zhang, F., 2013. Genome engineering using the CRISPR-Cas9 system. Nat. Protoc. 8, 2281–2308. https://doi.org/10.1038/nprot.2013.143

Rao, V.S., Srinivas, K., Sujini, G.N., Kumar, G.N.S., 2014. Protein-Protein Interaction Detection:

Methods and Analysis. Int. J. Proteomics 2014, 147648. https://doi.org/10.1155/2014/147648

RCSB PDB - Structure Pairwise Alignment Tool [WWW Document], 11 FEB 2022. URL https://www.rcsb.org/alignment (accessed 11.2.22).

Read, A., Schröder, M., 2021. The Unfolded Protein Response: An Overview. Biology 10, 384. https://doi.org/10.3390/biology10050384

Reits, E., Neijssen, J., Herberts, C., Benckhuijsen, W., Janssen, L., Drijfhout, J.W., Neefjes, J.,

2004. A Major Role for TPPII in Trimming Proteasomal Degradation Products for MHC Class I

Antigen Presentation. Immunity 20, 495–506. https://doi.org/10.1016/S1074-7613(04)00074-3

Ren, B., Cam, H., Takahashi, Y., Volkert, T., Terragni, J., Young, R.A., Dynlacht, B.D., 2002. E2F integrates cell cycle progression with DNA repair, replication, and G2/M checkpoints. Genes Dev. 16, 245–256. https://doi.org/10.1101/gad.949802

Reymond, A., Meroni, G., Fantozzi, A., Merla, G., Cairo, S., Luzi, L., Riganelli, D., Zanaria, E., Messali, S., Cainarca, S., Guffanti, A., Minucci, S., Pelicci, P.G., Ballabio, A., 2001. The tripartite motif family identifies cell compartments. EMBO J. 20, 2140–2151. https://doi.org/10.1093/emboj/20.9.2140

Riley, B.E., Lougheed, J.C., Callaway, K., Velasquez, M., Brecht, E., Nguyen, L., Shaler, T.,

Walker, D., Yang, Y., Regnstrom, K., Diep, L., Zhang, Z., Chiou, S., Bova, M., Artis, D.R., Yao, N., Baker, J., Yednock, T., Johnston, J.A., 2013a. Structure and function of Parkin E3 ubiquitin ligase reveals aspects of RING and HECT ligases. Nat. Commun. 4, 1982. https://doi.org/10.1038/ncomms2982

Riley, B.E., Lougheed, J.C., Callaway, K., Velasquez, M., Brecht, E., Nguyen, L., Shaler, T.,

Walker, D., Yang, Y., Regnstrom, K., Diep, L., Zhang, Z., Chiou, S., Bova, M., Artis, D.R., Yao, N., Baker, J., Yednock, T., Johnston, J.A., 2013b. Structure and function of Parkin E3 ubiquitin ligase reveals aspects of RING and HECT ligases. Nat. Commun. 4, 1982. https://doi.org/10.1038/ncomms2982

Ronai, Z.A., 2016. Monoubiquitination in proteasomal degradation. Proc. Natl. Acad. Sci. 113,

8894–8896. https://doi.org/10.1073/pnas.1610186113

Roodveldt, C., Outeiro, T.F., Braun, J.E.A., 2017. Editorial: Molecular Chaperones and Neurodegeneration. Front. Neurosci. 11.

Rosene, M.J., Benitez, B.A., 2025. Cysteine string protein α and a link between rare and common neurodegenerative dementias. Npj Dement. 1, 15. https://doi.org/10.1038/s44400025-00016-0

Rothfuss, O., Fischer, H., Hasegawa, T., Maisel, M., Leitner, P., Miesel, F., Sharma, M., Bornemann, A., Berg, D., Gasser, T., Patenge, N., 2009. Parkin protects mitochondrial genome integrity and supports mitochondrial DNA repair. Hum. Mol. Genet. 18, 3832–3850. https://doi.org/10.1093/hmg/ddp327

Rotin, D., Kumar, S., 2009. Physiological functions of the HECT family of ubiquitin ligases. Nat.

Rev. Mol. Cell Biol. 10, 398–409. https://doi.org/10.1038/nrm2690

Rouland, L., Duplan, E., Ramos dos Santos, L., Bernardin, A., Katula, K.S., Manfioletti, G., Idbaih, A., Checler, F., Alves da Costa, C., 2021. Therapeutic potential of parkin as a tumor suppressor via transcriptional control of cyclins in glioblastoma cell and animal models. Theranostics 11, 10047–10063. https://doi.org/10.7150/thno.57549

Roux, K.J., Kim, D.I., Raida, M., Burke, B., 2012. A promiscuous biotin ligase fusion protein identifies proximal and interacting proteins in mammalian cells. J. Cell Biol. 196, 801–810. https://doi.org/10.1083/jcb.201112098

Roux, P.P., Barker, P.A., 2002. Neurotrophin signaling through the p75 neurotrophin receptor.

Prog. Neurobiol. 67, 203–233. https://doi.org/10.1016/S0301-0082(02)00016-3

Bibliography

Rozas, J.L., Gómez-Sánchez, L., Mircheski, J., Linares-Clemente, P., Nieto-González, J.L., Vázquez, M.E., Luján, R., Fernández-Chacón, R., 2012. Motorneurons Require Cysteine String Protein-α to Maintain the Readily Releasable Vesicular Pool and Synaptic Vesicle Recycling. Neuron 74, 151–165. https://doi.org/10.1016/j.neuron.2012.02.019

Rubio, M.D., Wood, K., Haroutunian, V., Meador-Woodruff, J.H., 2013. Dysfunction of the Ubiquitin Proteasome and Ubiquitin-Like Systems in Schizophrenia. Neuropsychopharmacology 38, 1910–1920. https://doi.org/10.1038/npp.2013.84

Rude Voldborg, B., Damstrup, L., Spang-Thomsen, M., Skovgaard Poulsen, H., 1997. Epidermal growth factor receptor (EGFR) and EGFR mutations, function and possible role in clinical trials. Ann. Oncol. 8, 1197–1206. https://doi.org/10.1023/A:1008209720526

Ruiz, R., Casañas, J.J., Südhof, T.C., Tabares, L., 2008. Cysteine string protein-alpha is essential for the high calcium sensitivity of exocytosis in a vertebrate synapse. Eur. J. Neurosci. 27, 3118– 3131. https://doi.org/10.1111/j.1460-9568.2008.06301.x

Rupawala, H., Shah, K., Davies, C., Rose, J., Colom-Cadena, M., Peng, X., Granat, L., Aljuhani, M., Mizuno, K., Troakes, C., Perez-Nievas, B.G., Morgan, A., So, P.-W., Hortobagyi, T., SpiresJones, T.L., Noble, W., Giese, K.P., 2022. Cysteine string protein alpha accumulates with early pre-synaptic dysfunction in Alzheimer's disease. Brain Commun. 4, fcac192. https://doi.org/10.1093/braincomms/fcac192

Ryan, M., Lockstone, H., Huffaker, S., Wayland, M., Webster, M., Bahn, S., n.d. Gene expression analysis of bipolar disorder reveals downregulation of the ubiquitin cycle and alterations in synaptic genes. Mol. Psychiatry 14.

Ryan, T.A., Phillips, E.O., Collier, C.L., JB Robinson, A., Routledge, D., Wood, R.E., Assar, E.A., Tumbarello, D.A., 2020. Tollip coordinates Parkin-dependent trafficking of mitochondrialderived vesicles. EMBO J. 39, e102539. https://doi.org/10.15252/embj.2019102539 Sadowski, M., Sarcevic, B., 2010. Mechanisms of mono- and poly-ubiquitination: Ubiquitination specificity depends on compatibility between the E2 catalytic core and amino acid residues proximal to the lysine. Cell Div. 5, 19. https://doi.org/10.1186/1747-1028-5-19

Saibil, H., 2013. Chaperone machines for protein folding, unfolding and disaggregation. Nat. Rev. Mol. Cell Biol. 14, 630–642. https://doi.org/10.1038/nrm3658

Salas, J., Garcia, A., Zora, V., Dornbush, S., Mousa-Ibrahim, F., Fogg, H., Gromley, Z., Gromley, A., 2023. Centriolin interacts with HectD1 in a cell cycle dependent manner. BMC Res. Notes 16, 375. https://doi.org/10.1186/s13104-023-06670-y

Salaün, C., Gould, G.W., Chamberlain, L.H., 2005a. The SNARE proteins SNAP-25 and SNAP-23 display different affinities for lipid rafts in PC12 cells. Regulation by distinct cysteine-rich domains. J. Biol. Chem. 280, 1236–1240. https://doi.org/10.1074/jbc.M410674200

Salaün, C., Gould, G.W., Chamberlain, L.H., 2005b. The SNARE Proteins SNAP-25 and SNAP-23 Display Different Affinities for Lipid Rafts in PC12 Cells: REGULATION BY DISTINCT CYSTEINE-RICH DOMAINS*. J. Biol. Chem. 280, 1236–1240. https://doi.org/10.1074/jbc.M410674200

Sap, K.A., Reits, E.A., 2020. Strategies to Investigate Ubiquitination in Huntington's Disease.

Front. Chem. 8, 485. https://doi.org/10.3389/fchem.2020.00485

Sapmaz, A., Erson-Bensan, A.E., 2023. EGFR endocytosis: more than meets the eye.
Oncotarget 14, 297–301. https://doi.org/10.18632/oncotarget.28400

Saric, T., Graef, C.I., Goldberg, A.L., 2004. Pathway for Degradation of Peptides Generated by
Proteasomes: A KEY ROLE FOR THIMET OLIGOPEPTIDASE AND OTHER METALLOPEPTIDASES *.
J. Biol. Chem. 279, 46723–46732. https://doi.org/10.1074/jbc.M406537200

Sarraf, S.A., Raman, M., Guarani-Pereira, V., Sowa, M.E., Huttlin, E.L., Gygi, S.P., Harper, J.W., 2013. Landscape of the PARKIN-dependent ubiquitylome in response to mitochondrial depolarization. Nature 496, 372–376. https://doi.org/10.1038/nature12043

Sassone, J., Serratto, G., Valtorta, F., Silani, V., Passafaro, M., Ciammola, A., 2017. The synaptic function of parkin. Brain 140, 2265–2272. https://doi.org/10.1093/brain/awx006

Schindelin, J., Arganda-Carreras, I., Frise, E., Kaynig, V., Longair, M., Pietzsch, T., Preibisch, S.,
Rueden, C., Saalfeld, S., Schmid, B., Tinevez, J.-Y., White, D.J., Hartenstein, V., Eliceiri, K., Tomancak, P., Cardona, A., 2012. Fiji: an open-source platform for biological-image analysis.
Nat. Methods 9, 676–682. https://doi.org/10.1038/nmeth.2019

Schmitz, F., Tabares, L., Khimich, D., Strenzke, N., de la Villa-Polo, P., Castellano-Muñoz, M., Bulankina, A., Moser, T., Fernández-Chacón, R., Südhof, T.C., 2006. CSPalpha-deficiency causes massive and rapid photoreceptor degeneration. Proc. Natl. Acad. Sci. U. S. A. 103, 2926–2931. https://doi.org/10.1073/pnas.0510060103

Schopp, I.M., Amaya Ramirez, C.C., Debeljak, J., Kreibich, E., Skribbe, M., Wild, K., Béthune, J.,
2017. Split-BioID a conditional proteomics approach to monitor the composition of spatiotemporally defined protein complexes. Nat. Commun. 8, 15690. https://doi.org/10.1038/ncomms15690

Schweitzer, A., Aufderheide, A., Rudack, T., Beck, F., Pfeifer, G., Plitzko, J.M., Sakata, E., Schulten, K., Förster, F., Baumeister, W., 2016. Structure of the human 26S proteasome at a resolution of 3.9 Å. Proc. Natl. Acad. Sci. 113, 7816–7821. https://doi.org/10.1073/pnas.1608050113

Scott, C.C., Furuya, W., Trimble, W.S., Grinstein, S., 2003. Activation of Store-operated Calcium Channels: ASSESSMENT OF THE ROLE OF SNARE-MEDIATED VESICULAR TRANSPORT*. J. Biol. Chem. 278, 30534–30539. https://doi.org/10.1074/jbc.M304718200

Sears, R.M., May, D.G., Roux, K.J., 2019. BioID as a Tool for Protein-Proximity Labeling in Living
Cells. Methods Mol. Biol. Clifton NJ 2012, 299–313. https://doi.org/10.1007/978-1-4939-95462_15

Selak, S., Paternain, A.V., Aller, I.M., Picó, E., Rivera, R., Lerma, J., 2009. A Role for SNAP25 in Internalization of Kainate Receptors and Synaptic Plasticity. Neuron 63, 357–371. https://doi.org/10.1016/j.neuron.2009.07.017

Seo, J., Lee, E.-W., Sung, H., Seong, D., Dondelinger, Y., Shin, J., Jeong, M., Lee, H.-K., Kim, J.H., Han, S.Y., Lee, C., Seong, J.K., Vandenabeele, P., Song, J., 2016. CHIP controls necroptosis through

ubiquitylation- and lysosome-dependent degradation of RIPK3. Nat. Cell Biol. 18, 291– 302. https://doi.org/10.1038/ncb3314

Sharma, A., Mannan, A., Singh, T.G., 2025. Rethinking Parkinson's: The role of proteostasis networks and autophagy in disease progression. Mol. Cell. Neurosci. 134, 104023. https://doi.org/10.1016/j.mcn.2025.104023

Sharma, M., Burré, J., Bronk, P., Zhang, Y., Xu, W., Südhof, T.C., 2012a. CSPα knockout causes neurodegeneration by impairing SNAP-25 function. EMBO J. 31, 829–841. https://doi.org/10.1038/emboj.2011.467

Sharma, M., Burré, J., Bronk, P., Zhang, Y., Xu, W., Südhof, T.C., 2012b. CSPα knockout causes neurodegeneration by impairing SNAP-25 function. EMBO J. 31, 829–841. https://doi.org/10.1038/emboj.2011.467

Sharma, M., Burré, J., Bronk, P., Zhang, Y., Xu, W., Südhof, T.C., 2012c. CSPα knockout causes neurodegeneration by impairing SNAP-25 function. EMBO J. 31, 829–841. https://doi.org/10.1038/emboj.2011.467

Sharma, M., Burré, J., Südhof, T.C., 2012d. Proteasome Inhibition Alleviates SNARE-Dependent Neurodegeneration. Sci. Transl. Med. 4, 147ra113-147ra113. https://doi.org/10.1126/scitranslmed.3004028

Sharma, M., Burré, J., Südhof, T.C., 2011. CSPα promotes SNARE-complex assembly by chaperoning SNAP-25 during synaptic activity. Nat. Cell Biol. 13, 30–39. https://doi.org/10.1038/ncb2131

Sheehan, P., Zhu, M., Beskow, A., Vollmer, C., Waites, C.L., 2016. Activity-Dependent Degradation of Synaptic Vesicle Proteins Requires Rab35 and the ESCRT Pathway. J. Neurosci. 36, 8668–8686. https://doi.org/10.1523/JNEUROSCI.0725-16.2016

Sheng, Z.-H., Rettig, J., Cook, T., Catterall, W.A., 1996. Calcium-dependent interaction of Ntype calcium channels with the synaptic core complex. Nature 379, 451–454. https://doi.org/10.1038/379451a0

Shi, D., Gu, W., 2012. Dual Roles of MDM2 in the Regulation of p53. Genes Cancer 3, 240–248. https://doi.org/10.1177/1947601912455199

Shimojo, M., Courchet, J., Pieraut, S., Torabi-Rander, N., Sando, R., Polleux, F., Maximov, A., 2015. SNAREs Controlling Vesicular Release of BDNF and Development of Callosal Axons. Cell Rep. 11, 1054–1066. https://doi.org/10.1016/j.celrep.2015.04.032

Shimura, H., Schlossmacher, M.G., Hattori, N., Frosch, M.P., Trockenbacher, A., Schneider, R., Mizuno, Y., Kosik, K.S., Selkoe, D.J., 2001. Ubiquitination of a new form of alpha-synuclein by parkin from human brain: implications for Parkinson's disease. Science 293, 263–269. https://doi.org/10.1126/science.1060627

Shin, J.-H., Ko, H.S., Kang, H., Lee, Y., Lee, Y.-I., Pletinkova, O., Troconso, J.C., Dawson, V.L., Dawson, T.M., 2011. PARIS (ZNF746) repression of PGC-1α contributes to neurodegeneration in Parkinson's disease. Cell 144, 689–702. https://doi.org/10.1016/j.cell.2011.02.010

Shirasaki, D.I., Greiner, E.R., Al-Ramahi, I., Gray, M., Boontheung, P., Geschwind, D.H., Botas, J., Coppola, G., Horvath, S., Loo, J.A., Yang, X.W., 2012. Network Organization of the Huntingtin Proteomic Interactome in Mammalian Brain. Neuron 75, 41–57. https://doi.org/10.1016/j.neuron.2012.05.024

Shirasu, M., Kimura, K., Kataoka, M., Takahashi, M., Okajima, S., Kawaguchi, S., Hirasawa, Y., Ide, C., Mizoguchi, A., 2000. VAMP-2 promotes neurite elongation and SNAP-25A increases neurite sprouting in PC12 cells. Neurosci. Res. 37, 265–275. https://doi.org/10.1016/S01680102(00)00125-5

Shires, S.E., Kitsis, R.N., Gustafsson, Å.B., 2017. Beyond Mitophagy: The Diversity and Complexity of Parkin Function. Circ. Res. 120, 1234–1236. https://doi.org/10.1161/CIRCRESAHA.116.310179

Sin, O., Nollen, E.A.A., 2015. Regulation of protein homeostasis in neurodegenerative diseases: the role of coding and non-coding genes. Cell. Mol. Life Sci. 72, 4027–4047. https://doi.org/10.1007/s00018-015-1985-0

Smith, A.N., Alfar, H.R., Joshi, S., Coenen, D.M., Lykins, J.T., Becker, I.C., Dong, B.E., Chanzu,

H., Peng, C., Prakhya, K.S., Omali, L.A.N., Pokrovskaya, I.D., Storrie, B., Italiano, J.E., Jr, Whiteheart, S.W., 2025. Uncovering the Role of the Hsp40 Family Member, Cysteine String Protein-α, in Mouse Platelets. Blood Adv. bloodadvances.2024014870. https://doi.org/10.1182/bloodadvances.2024014870

Smithies, O., Gregg, R.G., Boggs, S.S., Koralewski, M.A., Kucherlapati, R.S., 1985. Insertion of

DNA sequences into the human chromosomal β-globin locus by homologous recombination.

Nature 317, 230–234. https://doi.org/10.1038/317230a0

Snyder, N.A., Silva, G.M., 2021. Deubiquitinating enzymes (DUBs): Regulation, homeostasis, and oxidative stress response. J. Biol. Chem. 297, 101077. https://doi.org/10.1016/j.jbc.2021.101077

Song, L., Luo, Z.-Q., 2019. Post-translational regulation of ubiquitin signaling. J. Cell Biol. 218,

1776–1786. https://doi.org/10.1083/jcb.201902074

Song, M., Hakala, K., Weintraub, S.T., Shiio, Y., 2011. Quantitative proteomic identification of the BRCA1 ubiquitination substrates. J. Proteome Res. 10, 5191–5198. https://doi.org/10.1021/pr200662b

Song, P., Krainc, D., 2024a. Diverse Functions of Parkin in Midbrain Dopaminergic Neurons. Mov. Disord. 39, 1282–1288. https://doi.org/10.1002/mds.29890

Song, P., Krainc, D., 2024b. Diverse Functions of Parkin in Midbrain Dopaminergic Neurons.

Mov. Disord. 39, 1282–1288. https://doi.org/10.1002/mds.29890

Song, P., Trajkovic, K., Tsunemi, T., Krainc, D., 2016. Parkin Modulates Endosomal Organization and Function of the Endo-Lysosomal Pathway. J. Neurosci. Off. J. Soc. Neurosci. 36, 2425– 2437. https://doi.org/10.1523/JNEUROSCI.2569-15.2016

Šonský, I., Vodička, P., Vodičková Kepková, K., Hansíková, H., 2021. Mitophagy in Huntington's disease. Neurochem. Int. 149, 105147. https://doi.org/10.1016/j.neuint.2021.105147

Bibliography

Sousa, R., Lafer, E.M., 2015. The role of molecular chaperones in clathrin mediated vesicular trafficking. Front. Mol. Biosci. 2. https://doi.org/10.3389/fmolb.2015.00026

Spagnol, V., Oliveira, C.A.B., Randle, S.J., Passos, P.M.S., Correia, C.R.S.T.B., Simaroli, N.B., Oliveira, J.S., Mevissen, T.E.T., Medeiros, A.C., Gomes, M.D., Komander, D., Laman, H., Teixeira, F.R., 2021. The E3 ubiquitin ligase SCF(Fbxo7) mediates proteasomal degradation of UXT isoform 2 (UXT-V2) to inhibit the NF-κB signaling pathway. Biochim. Biophys. Acta BBA - Gen. Subj. 1865, 129754. https://doi.org/10.1016/j.bbagen.2020.129754

Speese, S.D., Trotta, N., Rodesch, C.K., Aravamudan, B., Broadie, K., 2003. The ubiquitin proteasome system acutely regulates presynaptic protein turnover and synaptic efficacy. Curr. Biol. CB 13, 899–910. https://doi.org/10.1016/s0960-9822(03)00338-5

Spolidoro, S., Cunningham, M., King, G., Correia, A., Couto, R., Perez, A., Adams, K., 2020. Using CRISPR/Cas9 to Investigate the Role of Egr1 and NAB2 in Neuronal Differentiation of PC12 Cells. FASEB J. 34, 1–1. https://doi.org/10.1096/fasebj.2020.34.s1.04119

Spratt, D.E., Walden, H., Shaw, G.S., 2014. RBR E3 ubiquitin ligases: new structures, new insights, new questions. Biochem. J. 458, 421–437. https://doi.org/10.1042/BJ20140006

Steegmaier, M., Yang, B., Yoo, J.-S., Huang, B., Shen, M., Yu, S., Luo, Y., Scheller, R.H., 1998. Three Novel Proteins of the Syntaxin/SNAP-25 Family*. J. Biol. Chem. 273, 34171–34179. https://doi.org/10.1074/jbc.273.51.34171

Steffan, J.S., Agrawal, N., Pallos, J., Rockabrand, E., Trotman, L.C., Slepko, N., Illes, K., Lukacsovich, T., Zhu, Y.-Z., Cattaneo, E., Pandolfi, P.P., Thompson, L.M., Marsh, J.L., 2004. SUMO Modification of Huntingtin and Huntington's Disease Pathology. Science 304, 100–104. https://doi.org/10.1126/science.1092194

Stieglitz, B., Morris-Davies, A.C., Koliopoulos, M.G., Christodoulou, E., Rittinger, K., 2012. LUBAC synthesizes linear ubiquitin chains via a thioester intermediate. EMBO Rep. 13, 840–846. https://doi.org/10.1038/embor.2012.105

Storey, J.M., Storey, K.B., 2023. Chaperone proteins: universal roles in surviving environmental stress. Cell Stress Chaperones, Organisms in a Changing Environment 28, 455–466. https://doi.org/10.1007/s12192-022-01312-x

Sugiyama, T., Nishitoh, H., 2024. Neurodegenerative diseases associated with the disruption of proteostasis and their therapeutic strategies using chemical chaperones. J. Biochem. (Tokyo) 176, 179–186. https://doi.org/10.1093/jb/mvae048

Sun, J., Zhu, G., Liu, Y., Standley, S., Ji, A., Tunuguntla, R., Wang, Y., Claus, C., Luo, L., Baudry, M., Bi, X., 2015. UBE3A regulates synaptic plasticity and learning and memory by controlling SK2 channel endocytosis. Cell Rep. 12, 449–461. https://doi.org/10.1016/j.celrep.2015.06.023

Sutton, R.B., Fasshauer, D., Jahn, R., Brunger, A.T., 1998. Crystal structure of a SNARE complex involved in synaptic exocytosis at 2.4 Å resolution. Nature 395, 347–353. https://doi.org/10.1038/26412

Szabo, Z., Janaky, T., 2015. Challenges and developments in protein identification using mass spectrometry. TrAC Trends Anal. Chem. 69, 76–87. https://doi.org/10.1016/j.trac.2015.03.007

Szklarczyk, D., Kirsch, R., Koutrouli, M., Nastou, K., Mehryary, F., Hachilif, R., Gable, A.L., Fang, T., Doncheva, N.T., Pyysalo, S., Bork, P., Jensen, L.J., von Mering, C., 2023. The STRING database in 2023: protein-protein association networks and functional enrichment analyses for any sequenced genome of interest. Nucleic Acids Res. 51, D638–D646. https://doi.org/10.1093/nar/gkac1000

Szulc, N.A., Stefaniak, F., Piechota, M., Soszyńska, A., Piórkowska, G., Cappannini, A., Bujnicki, J.M., Maniaci, C., Pokrzywa, W., 2024. DEGRONOPEDIA: a web server for proteome-wide inspection of degrons. Nucleic Acids Res. 52, W221–W232. https://doi.org/10.1093/nar/gkae238

Tang, R., Langdon, W.Y., Zhang, J., 2022. Negative regulation of receptor tyrosine kinases by ubiquitination: Key roles of the Cbl family of E3 ubiquitin ligases. Front. Endocrinol. 13, 971162. https://doi.org/10.3389/fendo.2022.971162

Tanji, K., Kamitani, T., Mori, F., Kakita, A., Takahashi, H., Wakabayashi, K., 2010. TRIM9, a novel brain-specific E3 ubiquitin ligase, is repressed in the brain of Parkinson's disease and dementia with Lewy bodies. Neurobiol. Dis. 38, 210–218. https://doi.org/10.1016/j.nbd.2010.01.007

Tao-Cheng, J.H., Dosemeci, A., Bressler, J.P., Brightman, M.W., Simpson, D.L., 1995. Characterization of synaptic vesicles and related neuronal features in nerve growth factor and ras oncogene differentiated PC12 cells. J. Neurosci. Res. 42, 323–334. https://doi.org/10.1002/jnr.490420306

Tao-Cheng, J.-H., Du, J., McBain, C.J., 2000. Snap-25 is polarized to axons and abundant along the axolemma: an immunogold study of intact neurons. J. Neurocytol. 29, 67–77. https://doi.org/10.1023/A:1007168231323

Taoufik, E., Kouroupi, G., Zygogianni, O., Matsas, R., 2018. Synaptic dysfunction in neurodegenerative and neurodevelopmental diseases: an overview of induced pluripotent stem-cell-based disease models. Open Biol. 8, 180138. https://doi.org/10.1098/rsob.180138

Tarjányi, O., Berta, G., Harci, A., Bacsa, E.B., Stark, B., Pap, M., Szeberényi, J., Sétáló, G., 2013. The role of Src protein in the process formation of PC12 cells induced by the proteasome inhibitor MG-132. Neurochem. Int. 63, 413–422. https://doi.org/10.1016/j.neuint.2013.07.008

Tarjányi, O., Haerer, J., Vecsernyés, M., Berta, G., Stayer-Harci, A., Balogh, B., Farkas, K., Boldizsár, F., Szeberényi, J., Sétáló, G., 2022. Prolonged treatment with the proteasome inhibitor MG-132 induces apoptosis in PC12 rat pheochromocytoma cells. Sci. Rep. 12, 5808. https://doi.org/10.1038/s41598-022-09763-z

Teixeira, F.R., Randle, S.J., Patel, S.P., Mevissen, T.E.T., Zenkeviciute, G., Koide, T., Komander, D., Laman, H., 2016a. Gsk3β and Tomm20 are substrates of the SCFFbxo7/PARK15 ubiquitin ligase associated with Parkinson's disease. Biochem. J. 473, 3563–3580. https://doi.org/10.1042/BCJ20160387

Teixeira, F.R., Randle, S.J., Patel, S.P., Mevissen, T.E.T., Zenkeviciute, G., Koide, T., Komander, D., Laman, H., 2016b. Gsk3β and Tomm20 are substrates of the SCFFbxo7/PARK15 ubiquitin ligase

associated with Parkinson's disease. Biochem. J. 473, 3563–3580. https://doi.org/10.1042/BCJ20160387

Testa, G., Mainardi, M., Vannini, E., Pancrazi, L., Cattaneo, A., Costa, M., 2022. Disentangling the signaling complexity of nerve growth factor receptors by CRISPR/Cas9. FASEB J. 36, e22498. https://doi.org/10.1096/fj.202101760RR

Thibaudeau, T.A., Smith, D.M., 2019. A Practical Review of Proteasome Pharmacology.

Pharmacol. Rev. 71, 170–197. https://doi.org/10.1124/pr.117.015370

Tiwari, S.S., d'Orange, M., Troakes, C., Shurovi, B.N., Engmann, O., Noble, W., Hortobágyi, T., Giese, K.P., 2015. Evidence that the presynaptic vesicle protein CSPalpha is a key player in synaptic degeneration and protection in Alzheimer's disease. Mol. Brain 8, 6. https://doi.org/10.1186/s13041-015-0096-z

Tobaben, S., Varoqueaux, F., Brose, N., Stahl, B., Meyer, G., 2003. A Brain-specific Isoform of

Small Glutamine-rich Tetratricopeptide Repeat-containing Protein Binds to Hsc70 and the Cysteine String Protein*. J. Biol. Chem. 278, 38376–38383. https://doi.org/10.1074/jbc.M301558200

Toft-Bertelsen, T.L., Ziomkiewicz, I., Houy, S., Pinheiro, P.S., Sørensen, J.B., 2016. Regulation of

Ca2+ channels by SNAP-25 via recruitment of syntaxin-1 from plasma membrane clusters. Mol.

Biol. Cell 27, 3329–3341. https://doi.org/10.1091/mbc.E16-03-0184

Tomasoni, R., Repetto, D., Morini, R., Elia, C., Gardoni, F., Di Luca, M., Turco, E., Defilippi, P., Matteoli, M., 2013a. SNAP-25 regulates spine formation through postsynaptic binding to p140Cap. Nat. Commun. 4, 2136. https://doi.org/10.1038/ncomms3136

Tomasoni, R., Repetto, D., Morini, R., Elia, C., Gardoni, F., Di Luca, M., Turco, E., Defilippi, P., Matteoli, M., 2013b. SNAP-25 regulates spine formation through postsynaptic binding to p140Cap. Nat. Commun. 4, 2136. https://doi.org/10.1038/ncomms3136

Tramutola, A., Di Domenico, F., Barone, E., Arena, A., Giorgi, A., di Francesco, L., Schininà, M.E., Coccia, R., Head, E., Butterfield, D.A., Perluigi, M., 2017. Polyubiquitinylation Profile in Down Syndrome Brain Before and After the Development of Alzheimer Neuropathology. Antioxid. Redox Signal. 26, 280–298. https://doi.org/10.1089/ars.2016.6686

Trepte, P., Kruse, S., Kostova, S., Hoffmann, S., Buntru, A., Tempelmeier, A., Secker, C., Diez, L., Schulz, A., Klockmeier, K., Zenkner, M., Golusik, S., Rau, K., Schnoegl, S., Garner, C.C., Wanker, E.E., 2018. LuTHy: a double-readout bioluminescence-based two-hybrid technology for quantitative mapping of protein-protein interactions in mammalian cells. Mol. Syst. Biol. 14, e8071. https://doi.org/10.15252/msb.20178071

Tseng, C.-S., Chao, Y.-W., Liu, Y.-H., Huang, Y.-S., Chao, H.-W., 2023. Dysregulated proteostasis network in neuronal diseases. Front. Cell Dev. Biol. 11, 1075215. https://doi.org/10.3389/fcell.2023.1075215

Upadhyay, A., Joshi, V., Amanullah, A., Mishra, R., Arora, N., Prasad, A., Mishra, A., 2017. E3 Ubiquitin Ligases Neurobiological Mechanisms: Development to Degeneration. Front. Mol. Neurosci. 10, 151. https://doi.org/10.3389/fnmol.2017.00151

Urfer, R., Tsoulfas, P., Soppet, D., Escandón, E., Parada, L.F., Presta, L.G., 1994. The binding epitopes of neurotrophin-3 to its receptors trkC and gp75 and the design of a multifunctional human neurotrophin. EMBO J. 13, 5896–5909. https://doi.org/10.1002/j.14602075.1994.tb06935.x

Valenzuela-Villatoro, M., García-Junco-Clemente, P., Nieto-González, J.L., Fernández-Chacón, R., 2018. Presynaptic neurodegeneration: CSP-α/DNAJC5 at the synaptic vesicle cycle and beyond. Curr. Opin. Physiol., Neuromuscular Junctions 4, 65–69. https://doi.org/10.1016/j.cophys.2018.06.001

van Roessel, P., Elliott, D.A., Robinson, I.M., Prokop, A., Brand, A.H., 2004. Independent regulation of synaptic size and activity by the anaphase-promoting complex. Cell 119, 707–718. https://doi.org/10.1016/j.cell.2004.11.028

Vargas, K.J., Wallace, J.N., Mooney, I., Owen, D.J., Morgan, J.R., 2025. α-Synuclein interacts directly with AP2 and regulates its binding to synaptic membranes. J. Biol. Chem. 301, 108502. https://doi.org/10.1016/j.jbc.2025.108502

Varshavsky, A., 2012. The Ubiquitin System, an Immense Realm. Annu. Rev. Biochem. 81, 167–176. https://doi.org/10.1146/annurev-biochem-051910-094049

Vaughan, N., Scholz, N., Lindon, C., Licchesi, J.D.F., 2022. The E3 ubiquitin ligase HECTD1 contributes to cell proliferation through an effect on mitosis. Sci. Rep. 12, 13160. https://doi.org/10.1038/s41598-022-16965-y

Verma, K., Verma, M., Chaphalkar, A., Chakraborty, K., 2021. Recent advances in understanding the role of proteostasis. Fac. Rev. 10, 72. https://doi.org/10.12703/r/10-72

Vincow, E.S., Merrihew, G., Thomas, R.E., Shulman, N.J., Beyer, R.P., MacCoss, M.J., Pallanck, L.J., 2013. The PINK1–Parkin pathway promotes both mitophagy and selective respiratory chain turnover in vivo. Proc. Natl. Acad. Sci. 110, 6400–6405. https://doi.org/10.1073/pnas.1221132110

Vingill, S., Brockelt, D., Lancelin, C., Tatenhorst, L., Dontcheva, G., Preisinger, C., Schwedhelm-Domeyer, N., Joseph, S., Mitkovski, M., Goebbels, S., Nave, K., Schulz, J.B., Marquardt, T., Lingor, P., Stegmüller, J., 2016. Loss of FBXO7 (PARK15) results in reduced proteasome activity and models a parkinsonism-like phenotype in mice. EMBO J. 35, 2008–2025. https://doi.org/10.15252/embj.201593585

Viotti, J., Duplan, E., Caillava, C., Condat, J., Goiran, T., Giordano, C., Marie, Y., Idbaih, A., Delattre, J.-Y., Honnorat, J., Checler, F., Alves da Costa, C., 2014. Glioma tumor grade correlates with parkin depletion in mutant p53-linked tumors and results from loss of function of p53 transcriptional activity. Oncogene 33, 1764–1775. https://doi.org/10.1038/onc.2013.124

Visser Smit, G.D., Place, T.L., Cole, S.L., Clausen, K.A., Vemuganti, S., Zhang, G., Koland, J.G., Lill, N.L., 2009. Cbl Controls EGFR Fate by Regulating Early Endosome Fusion. Sci. Signal. 2, ra86–ra86. https://doi.org/10.1126/scisignal.2000217

Vogel, K., Cabaniols, J.-P., Roche, P.A., 2000. Targeting of SNAP-25 to Membranes Is Mediated by Its Association with the Target SNARE Syntaxin. J. Biol. Chem. 275, 2959–2965. https://doi.org/10.1074/jbc.275.4.2959

Vogel, K., Roche, P.A., 1999. SNAP-23 and SNAP-25 Are Palmitoylatedin Vivo. Biochem. Biophys. Res. Commun. 258, 407–410. https://doi.org/10.1006/bbrc.1999.0652

Bibliography

Voges, D., Zwickl, P., Baumeister, W., 1999. The 26S proteasome: a molecular machine designed for controlled proteolysis. Annu. Rev. Biochem. 68, 1015–1068. https://doi.org/10.1146/annurev.biochem.68.1.1015

Voorhees, R.M., Ramakrishnan, V., 2013. Structural basis of the translational elongation cycle. Annu. Rev. Biochem. 82, 203–236. https://doi.org/10.1146/annurev-biochem-113009-092313

Walch-Solimena, C., Blasi, J., Edelmann, L., Chapman, E.R., von Mollard, G.F., Jahn, R., 1995. The t-SNAREs syntaxin 1 and SNAP-25 are present on organelles that participate in synaptic vesicle recycling. J. Cell Biol. 128, 637–645. https://doi.org/10.1083/jcb.128.4.637

Walden, H., Martinez-Torres, R.J., 2012. Regulation of Parkin E3 ubiquitin ligase activity. Cell. Mol. Life Sci. CMLS 69, 3053–3067. https://doi.org/10.1007/s00018-012-0978-5

Walker, V.E., Wong, M.J.H., Atanasiu, R., Hantouche, C., Young, J.C., Shrier, A., 2010. Hsp40 chaperones promote degradation of the HERG potassium channel. J. Biol. Chem. 285, 3319–3329. https://doi.org/10.1074/jbc.M109.024000

Walter, P., Ron, D., 2011. The Unfolded Protein Response: From Stress Pathway to Homeostatic Regulation. Science 334, 1081–1086. https://doi.org/10.1126/science.1209038

Wang, C., Kang, X., Zhou, L., Chai, Z., Wu, Q., Huang, R., Xu, H., Hu, M., Sun, X., Sun, S., Li, J., Jiao, R., Zuo, P., Zheng, L., Yue, Z., Zhou, Z., 2018. Synaptotagmin-11 is a critical mediator of parkin-linked neurotoxicity and Parkinson's disease-like pathology. Nat. Commun. 9, 81. https://doi.org/10.1038/s41467-017-02593-y

Wang, Q., Xue, H., Yue, Y., Hao, S., Huang, S.-H., Zhang, Z., 2022. Role of mitophagy in the neurodegenerative diseases and its pharmacological advances: A review. Front. Mol. Neurosci. 15. https://doi.org/10.3389/fnmol.2022.1014251

Wang, G., Liu, X., Wang, K., Gao, Y., Li, G., Baptista-Hon, D.T., Yang, X.H., Xue, K., Tai, W.H., Jiang, Z., Cheng, L., Fok, M., Lau, J.Y.-N., Yang, S., Lu, L., Zhang, P., Zhang, K., 2023. Deeplearning-enabled protein–protein interaction analysis for prediction of SARS-CoV-2 infectivity and variant evolution. Nat. Med. 29, 2007–2018. https://doi.org/10.1038/s41591-023-02483-5

Wang, H., Luo, J., Tian, X., Xu, L., Zhai, Z., Cheng, M., Chen, L., Luo, S., 2021. DNAJC5 promotes hepatocellular carcinoma cells proliferation though regulating SKP2 mediated p27 degradation. Biochim. Biophys. Acta Mol. Cell Res. 1868, 118994. https://doi.org/10.1016/j.bbamcr.2021.118994

Wang, J., Joseph, S., Vingill, S., Dere, E., Tatenhorst, L., Ronnenberg, A., Lingor, P., Preisinger, C., Ehrenreich, H., Schulz, J.B., Stegmüller, J., 2023. Loss of the parkinsonism-associated protein FBXO7 in glutamatergic forebrain neurons in mice leads to abnormal motor behavior and synaptic defects. J. Neurochem. 167, 296–317. https://doi.org/10.1111/jnc.15962

Wang, J.Y., Doudna, J.A., 2023. CRISPR technology: A decade of genome editing is only the beginning. Science 379, eadd8643. https://doi.org/10.1126/science.add8643

Wang, N., Zhu, B., Allnutt, M.A., Grijalva, R.M., Zhao, H., Chandra, S.S., 2024. Decoding transcriptomic signatures of cysteine string protein alpha–mediated synapse maintenance. Proc. Natl. Acad. Sci. 121, e2320064121. https://doi.org/10.1073/pnas.2320064121

Wang, W., Gao, W., Gong, P., Song, W., Bu, X., Hou, J., Zhang, L., Zhao, B., 2023. Neuronalspecific TNFAIP1 ablation attenuates postoperative cognitive dysfunction via targeting SNAP25 for K48-linked ubiquitination. Cell Commun. Signal. 21, 356. https://doi.org/10.1186/s12964023-01390-z

Wang, X., Li, Y., He, M., Kong, X., Jiang, P., Liu, X., Diao, L., Zhang, X., Li, H., Ling, X., Xia, S., Liu,

Z., Liu, Y., Cui, C.-P., Wang, Y., Tang, L., Zhang, L., He, F., Li, D., 2022. UbiBrowser 2.0: a comprehensive resource for proteome-wide known and predicted ubiquitin

ligase/deubiquitinase-substrate interactions in eukaryotic species. Nucleic Acids Res. 50, D719–D728. https://doi.org/10.1093/nar/gkab962

Wang, X.S., Cotton, T.R., Trevelyan, S.J., Richardson, L.W., Lee, W.T., Silke, J., Lechtenberg, B.C., 2023. The unifying catalytic mechanism of the RING-between-RING E3 ubiquitin ligase family. Nat. Commun. 14, 168. https://doi.org/10.1038/s41467-023-35871-z

Washbourne, P., Thompson, P.M., Carta, M., Costa, E.T., Mathews, J.R., Lopez-Benditó, G., Molnár, Z., Becher, M.W., Valenzuela, C.F., Partridge, L.D., Wilson, M.C., 2002. Genetic ablation of the t-SNARE SNAP-25 distinguishes mechanisms of neuroexocytosis. Nat. Neurosci. 5, 19–26. https://doi.org/10.1038/nn783

Weiss, N., Hameed, S., Fernández-Fernández, J.M., Fablet, K., Karmazinova, M., Poillot, C.,

Proft, J., Chen, L., Bidaud, I., Monteil, A., Huc-Brandt, S., Lacinova, L., Lory, P., Zamponi, G.W., De Waard, M., 2012. A Cav3.2/Syntaxin-1A Signaling Complex Controls T-type Channel Activity and Low-threshold Exocytosis*. J. Biol. Chem. 287, 2810–2818. https://doi.org/10.1074/jbc.M111.290882

Westerink, R.H.S., Ewing, A.G., 2008. The PC12 cell as model for neurosecretion. Acta Physiol.

Oxf. Engl. 192, 273–285. https://doi.org/10.1111/j.1748-1716.2007.01805.x

Wheat, A., Yu, C., Wang, X., Burke, A.M., Chemmama, I.E., Kaake, R.M., Baker, P., Rychnovsky, S.D., Yang, J., Huang, L., 2021. Protein interaction landscapes revealed by advanced in vivo cross-linking-mass spectrometry. Proc. Natl. Acad. Sci. U. S. A. 118, e2023360118. https://doi.org/10.1073/pnas.2023360118

Wiatrak, B., Kubis-Kubiak, A., Piwowar, A., Barg, E., 2020. PC12 Cell Line: Cell Types, Coating of Culture Vessels, Differentiation and Other Culture Conditions. Cells 9, 958. https://doi.org/10.3390/cells9040958

Wickramasinghe, V.O., Venkitaraman, A.R., 2016. RNA processing and genome stability: cause and consequence. Mol. Cell 61, 496–505. https://doi.org/10.1016/j.molcel.2016.02.001

Wiesmann, C., Ultsch, M.H., Bass, S.H., de Vos, A.M., 1999. Crystal structure of nerve growth factor in complex with the ligand-binding domain of the TrkA receptor. Nature 401, 184–188. https://doi.org/10.1038/43705

Willeumier, K., Pulst, S.M., Schweizer, F.E., 2006. Proteasome inhibition triggers activitydependent increase in the size of the recycling vesicle pool in cultured hippocampal neurons. J. Neurosci. Off. J. Soc. Neurosci. 26, 11333–11341. https://doi.org/10.1523/JNEUROSCI.168406.2006

Williams, E.T., Glauser, L., Tsika, E., Jiang, H., Islam, S., Moore, D.J., 2018. Parkin mediates the ubiquitination of VPS35 and modulates retromer-dependent endosomal sorting. Hum. Mol. Genet. 27, 3189–3205. https://doi.org/10.1093/hmg/ddy224

Winkle, C.C., Gupton, S.L., 2016. Chapter Four - Membrane Trafficking in Neuronal

Development: Ins and Outs of Neural Connectivity, in: Jeon, K.W. (Ed.), International Review of

Cell and Molecular Biology, International Review of Cell and Molecular Biology. Academic

Press, pp. 247–280. https://doi.org/10.1016/bs.ircmb.2015.10.003

Winkle, C.C., McClain, L.M., Valtschanoff, J.G., Park, C.S., Maglione, C., Gupton, S.L., 2014a. A novel Netrin-1–sensitive mechanism promotes local SNARE-mediated exocytosis during axon branching. J. Cell Biol. 205, 217–232. https://doi.org/10.1083/jcb.201311003

Winkle, C.C., McClain, L.M., Valtschanoff, J.G., Park, C.S., Maglione, C., Gupton, S.L., 2014b. A novel Netrin-1-sensitive mechanism promotes local SNARE-mediated exocytosis during axon branching. J. Cell Biol. 205, 217–232. https://doi.org/10.1083/jcb.201311003

Winston, J.T., Koepp, D.M., Zhu, C., Elledge, S.J., Harper, J.W., 1999. A family of mammalian Fbox proteins. Curr. Biol. CB 9, 1180–1182. https://doi.org/10.1016/S0960-9822(00)80021-4

Wiser, O., Trus, M., Hernández, A., Renström, E., Barg, S., Rorsman, P., Atlas, D., 1999. The voltage sensitive Lc-type Ca2+ channel is functionally coupled to the exocytotic machinery. Proc. Natl. Acad. Sci. 96, 248–253. https://doi.org/10.1073/pnas.96.1.248

Wong, M.-L., Dong, C., Maestre-Mesa, J., Licinio, J., 2008. Polymorphisms in inflammationrelated genes are associated with susceptibility to major depression and antidepressant response. Mol. Psychiatry 13, 800–812. https://doi.org/10.1038/mp.2008.59

Wu, C.-S., Lin, J.-T., Chien, C.-L., Chang, W.-C., Lai, H.-L., Chang, C.-P., Chern, Y., 2011. Type VI Adenylyl Cyclase Regulates Neurite Extension by Binding to Snapin and Snap25 ▿ . Mol. Cell. Biol. 31, 4874–4886. https://doi.org/10.1128/MCB.05593-11

Wu, S., Hernandez Villegas, N.C., Sirkis, D.W., Thomas-Wright, I., Wade-Martins, R., Schekman, R., 2023. Unconventional secretion of α-synuclein mediated by palmitoylated DNAJC5 oligomers. eLife 12, e85837. https://doi.org/10.7554/eLife.85837

Xiong, J., Chen, Y., Wang, W., Sun, J., 2022. Biological function and molecular mechanism of SRSF3 in cancer and beyond. Oncol. Lett. 23, 21. https://doi.org/10.3892/ol.2021.13139

Xu, G., Jaffrey, S.R., 2011. The new landscape of protein ubiquitination. Nat. Biotechnol. 29, 1098–1100. https://doi.org/10.1038/nbt.2061

Xu, H., Shen, P., Fang, J., Jiang, J., Shi, Y., Xu, P., Jiang, R., Wang, Z., 2024. LINC00624 affects hepatocellular carcinoma proliferation and apoptosis through the miR-342-3p/DNAJC5 axis. J. Biochem. Mol. Toxicol. 38, e23650. https://doi.org/10.1002/jbt.23650

Xu, L., Lin, D., Yin, D., Koeffler, H.P., 2014. An emerging role of PARK2 in cancer. J. Mol. Med. Berl. Ger. 92, 31–42. https://doi.org/10.1007/s00109-013-1107-0

Xu, Y., Cui, L., Dibello, A., Wang, L., Lee, J., Saidi, L., Lee, J.-G., Ye, Y., 2018a. DNAJC5 facilitates USP19-dependent unconventional secretion of misfolded cytosolic proteins. Cell Discov. 4, 1–18. https://doi.org/10.1038/s41421-018-0012-7

Xu, Y., Cui, L., Dibello, A., Wang, L., Lee, J., Saidi, L., Lee, J.-G., Ye, Y., 2018b. DNAJC5 facilitates USP19-dependent unconventional secretion of misfolded cytosolic proteins. Cell Discov. 4, 11. https://doi.org/10.1038/s41421-018-0012-7

Yang, F., Jiang, Q., Zhao, J., Ren, Y., Sutton, M.D., Feng, J., 2005. Parkin stabilizes microtubules through strong binding mediated by three independent domains. J. Biol. Chem. 280, 17154– 17162. https://doi.org/10.1074/jbc.M500843200

Yang, H., Ren, S., Yu, S., Pan, H., Li, T., Ge, S., Zhang, J., Xia, N., 2020. Methods Favoring

Homology-Directed Repair Choice in Response to CRISPR/Cas9 Induced-Double Strand Breaks. Int. J. Mol. Sci. 21, 6461. https://doi.org/10.3390/ijms21186461

Yang, Q., Zhao, J., Chen, D., Wang, Y., 2021. E3 ubiquitin ligases: styles, structures and functions. Mol. Biomed. 2, 23. https://doi.org/10.1186/s43556-021-00043-2

Yang, S., Park, D., Manning, L., Kargbo-Hill, S.E., Cao, M., Xuan, Z., Gonzalez, I., Dong, Y., Clark, B., Shao, L., Okeke, I., Almoril-Porras, A., Bai, J., De Camilli, P., Colón-Ramos, D.A., 2022. Presynaptic autophagy is coupled to the synaptic vesicle cycle via ATG-9. Neuron 110, 824-840.e10. https://doi.org/10.1016/j.neuron.2021.12.031

Yang, S.Y., Hayer, K.E., Fazelinia, H., Spruce, L.A., Asnani, M., Black, K.L., Naqvi, A.S., Pillai, V., Barash, Y., Elenitoba-Johnson, K.S.J., Thomas-Tikhonenko, A., 2022. FBXW7β isoform drives transcriptional activation of the proinflammatory TNF cluster in human pro-B cells. Blood Adv. 7, 1077–1091. https://doi.org/10.1182/bloodadvances.2022007910

Yao, I., Takagi, H., Ageta, H., Kahyo, T., Sato, S., Hatanaka, K., Fukuda, Y., Chiba, T., Morone, N.,

Yuasa, S., Inokuchi, K., Ohtsuka, T., MacGregor, G.R., Tanaka, K., Setou, M., 2007. SCRAPPER Dependent Ubiquitination of Active Zone Protein RIM1 Regulates Synaptic Vesicle Release. Cell 130, 943–957. https://doi.org/10.1016/j.cell.2007.06.052

Yoon, T.-Y., Munson, M., 2018. SNARE complex assembly and disassembly. Curr. Biol. 28,

R397–R401. https://doi.org/10.1016/j.cub.2018.01.005

Youn, J.-Y., Dunham, W.H., Hong, S.J., Knight, J.D.R., Bashkurov, M., Chen, G.I., Bagci, H.,

Rathod, B., MacLeod, G., Eng, S.W.M., Angers, S., Morris, Q., Fabian, M., Côté, J.-F., Gingras, A.C., 2018. High-Density Proximity Mapping Reveals the Subcellular Organization of mRNAAssociated Granules and Bodies. Mol. Cell 69, 517-532.e11. https://doi.org/10.1016/j.molcel.2017.12.020

Young, J.C., 2010. Mechanisms of the Hsp70 chaperone system. Biochem. Cell Biol. Biochim.

Biol. Cell. 88, 291–300. https://doi.org/10.1139/o09-175

Zarrinpar, A., Lim, W.A., 2000. Converging on proline: the mechanism of WW domain peptide recognition. Nat. Struct. Biol. 7, 3.

Zhang, J., Xin, L., Shan, B., Chen, W., Xie, M., Yuen, D., Zhang, W., Zhang, Z., Lajoie, G.A., Ma, B., 2012. PEAKS DB: de novo sequencing assisted database search for sensitive and accurate peptide identification. Mol. Cell. Proteomics MCP 11, M111.010587. https://doi.org/10.1074/mcp.M111.010587

Zhang, J., Xin, Y., Ling, X., Liang, H., Zhang, L., Fang, C., Ma, J., 2024. Nucleoporin 93, a new substrate of the E3 ubiquitin protein ligase HECTD1, promotes esophageal squamous cell carcinoma progression. Hum. Cell 37, 245–257. https://doi.org/10.1007/s13577-023-01005-2

Zhang, Q., Fu, Y., Thakur, C., Bi, Z., Wadgaonkar, P., Qiu, Y., Xu, L., Rice, M., Zhang, W., Almutairy, B., Chen, F., 2020. CRISPR-Cas9 gene editing causes alternative splicing of the targeting mRNA. Biochem. Biophys. Res. Commun. 528, 54–61. https://doi.org/10.1016/j.bbrc.2020.04.145

Zhang, R., Malinverni, D., Cyr, D.M., Rios, P.D.L., Nillegoda, N.B., 2023. J-domain protein chaperone circuits in proteostasis and disease. Trends Cell Biol. 33, 30–47. https://doi.org/10.1016/j.tcb.2022.05.004

Zhang, X., Kim-Miller, M.J., Fukuda, M., Kowalchyk, J.A., Martin, T.F.J., 2002. Ca2+-dependent synaptotagmin binding to SNAP-25 is essential for Ca2+-triggered exocytosis. Neuron 34, 599– 611. https://doi.org/10.1016/s0896-6273(02)00671-2

Zhang, Y., Gao, J., Chung, K.K., Huang, H., Dawson, V.L., Dawson, T.M., 2000. Parkin functions as an E2-dependent ubiquitin- protein ligase and promotes the degradation of the synaptic vesicle-associated protein, CDCrel-1. Proc. Natl. Acad. Sci. U. S. A. 97, 13354–13359. https://doi.org/10.1073/pnas.240347797

Zhang, Yi, Gao, J., Chung, K.K.K., Huang, H., Dawson, V.L., Dawson, T.M., 2000. Parkin functions as an E2-dependent ubiquitin– protein ligase and promotes the degradation of the synaptic vesicle-associated protein, CDCrel-1. Proc. Natl. Acad. Sci. U. S. A. 97, 13354–13359.

Zhang, Y.-Q., Henderson, M.X., Colangelo, C.M., Ginsberg, S.D., Bruce, C., Wu, T., Chandra,

S.S., 2012. Identification of CSPα Clients Reveals a Role in Dynamin 1 Regulation. Neuron 74,

136–150. https://doi.org/10.1016/j.neuron.2012.01.029

Zhang, Z., Wang, D., Sun, T., Xu, J., Chiang, H.-C., Shin, W., Wu, L.-G., 2013. The SNARE

Proteins SNAP25 and Synaptobrevin Are Involved in Endocytosis at Hippocampal Synapses. J.

Neurosci. 33, 9169–9175. https://doi.org/10.1523/JNEUROSCI.0301-13.2013

Zheng, Q., Huang, T., Zhang, L., Zhou, Y., Luo, H., Xu, H., Wang, X., 2016. Dysregulation of Ubiquitin-Proteasome System in Neurodegenerative Diseases. Front. Aging Neurosci. 8.

Zheng, X., Hunter, T., 2013. Parkin mitochondrial translocation is achieved through a novel catalytic activity coupled mechanism. Cell Res. 23, 886–897. https://doi.org/10.1038/cr.2013.66

Zheng, Z., Lauritzen, J.S., Perlman, E., Robinson, C.G., Nichols, M., Milkie, D., Torrens, O., Price,

J., Fisher, C.B., Sharifi, N., Calle-Schuler, S.A., Kmecova, L., Ali, I.J., Karsh, B., Trautman, E.T.,

Bogovic, J.A., Hanslovsky, P., Jefferis, G.S.X.E., Kazhdan, M., Khairy, K., Saalfeld, S., Fetter,

R.D., Bock, D.D., 2018. A Complete Electron Microscopy Volume of the Brain of Adult

Drosophila melanogaster. Cell 174, 730-743.e22. https://doi.org/10.1016/j.cell.2018.06.019

Zhong, Y., Li, J., Ye, M., Jin, X., 2023. The characteristics of FBXO7 and its role in human diseases. Gene 851, 146972. https://doi.org/10.1016/j.gene.2022.146972

Zhou, Q., Lai, Y., Bacaj, T., Zhao, M., Lyubimov, A.Y., Uervirojnangkoorn, M., Zeldin, O.B.,

Brewster, A.S., Sauter, N.K., Cohen, A.E., Soltis, S.M., Alonso-Mori, R., Chollet, M., Lemke, H.T., Pfuetzner, R.A., Choi, U.B., Weis, W.I., Diao, J., Südhof, T.C., Brunger, A.T., 2015. Architecture of the Synaptotagmin-SNARE Machinery for Neuronal Exocytosis. Nature 525, 62–67. https://doi.org/10.1038/nature14975

Zhou, T., Xu, B., Que, H., Lin, Q., Lv, S., Liu, S., 2006. Neurons derived from PC12 cells have the potential to develop synapses with primary neurons from rat cortex. Acta Neurobiol. Exp. (Warsz.) 66, 105–112. https://doi.org/10.55782/ane-2006-1596

Zhou, Z.D., Sathiyamoorthy, S., Angeles, D.C., Tan, E.K., 2016. Linking F-box protein 7 and parkin to neuronal degeneration in Parkinson's disease (PD). Mol. Brain 9, 41. https://doi.org/10.1186/s13041-016-0218-2

Zhu, W., Smith, J.W., Huang, C.-M., 2010. Mass Spectrometry-Based Label-Free Quantitative

Proteomics. BioMed Res. Int. 2010, 840518. https://doi.org/10.1155/2010/840518

Zinsmaier, K.E., Hofbauer, A., Heimbeck, G., Pflugfelder, G.O., Buchner, S., Buchner, E., 1990.

A Cysteine-String Protein is Expressed in Retina and Brain of *Drosophila*. J. Neurogenet. 7, 15– 29. https://doi.org/10.3109/01677069009084150